**THÈSE DE DOCTORAT
DE L'UNIVERSITÉ PIERRE ET MARIE CURIE**

et de l'École Doctorale de Physique en Île-de-France

réalisée à
l'Institut d'Astrophysique de Paris

Light propagation in inhomogeneous and anisotropic cosmologies

présentée par

Pierre FLEURY

et soutenue publiquement le 2 novembre 2015

devant le jury composé de

Pr	Ruth DURRER	Rapportrice
Pr	Pedro FERREIRA	Rapporteur
Pr	Michael JOYCE	Examinateur
Dr	David LANGLOIS	Examinateur
Dr	Reynald PAIN	Examinateur
Dr	Éric GOURGOULHON	Invité
Dr	Jean-Philippe UZAN	Directeur de thèse

À la mémoire d'Olivier Jean-Marie.

Remerciements

M ES premiers remerciements vont à mon directeur de thèse, Jean-Philippe Uzan, d'abord pour m'avoir donné l'opportunité de travailler sur un sujet passionnant, et ensuite pour m'avoir guidé au cours de ces trois années. Si je préfère parler de guide, c'est parce que, pour mon plus grand bonheur, tu n'as jamais été directif envers moi ; je te sais particulièrement gré de cette confiance que tu m'as accordée dès les premiers mois. J'ai beaucoup appris grâce à toi, en physique bien sûr mais pas seulement, car dans ton univers la musique, la théâtre, le cinéma, la bande-dessinée et tant de choses encore gravitent autour des sciences. J'espère moi aussi atteindre, un jour, une si belle virialisation. Bien qu'il me faille à présent quitter le nid(AP), je sais que nous aurons encore beaucoup d'occasions d'échanger et de travailler ensemble. Je m'en réjouis.

Ma reconnaissance va ensuite à mon « grand frère », Cyril Pitrou, qui fut presque un second encadrant pour moi, qu'il s'agît de science pure ou de chose plus prosaïques. J'ai énormément apprécié chaque occasion de travailler avec toi, j'aime ta façon très géométrique de raisonner et j'admire la vivacité et la précision de ton esprit. Vivement que nous écrivions un livre ensemble ! Merci aussi pour tes décryptages politiques et économiques : à l'instar de Jean-Philippe, tu m'as démontré par l'exemple qu'un véritable intellectuel ne peut pas, ne doit pas, se cantonner à une seule discipline. Enfin, je n'oublie pas la méticulosité avec laquelle tu as corrigé les moindres erreurs phonétiques et déplacements d'accents lors de mes présentations en anglais. Compte sur moi pour te renvoyer l'ascenseur.

I wish to address special thanks to my other close collaborators. À Hélène Dupuy d'abord : cela a été un réel plaisir de travailler avec toi dès notre stage de master en binôme. Merci surtout d'avoir bien voulu dédier une partie non négligeable de ta première année de thèse pour m'aider à clore ce projet que nous avions commencé ensemble. Après tout, il le valait bien ! A Juan Pablo Beltrán, fue un gran placer conocerte y trabajar contigo. Muchas gracias por haber compartido un poco de tu país: desde los patacones hasta Guatavita, me encantó todo. À Julien Larena, enfin, merci pour ta sympathie si immédiate et si sincère, je suis heureux à l'idée que notre collaboration ne fait que commencer.

Je souhaite bien sûr exprimer ma gratitude envers les rapporteurs, Ruth Durrer et Pedro Ferreira, car je suis bien conscient que l'évaluation d'un texte de 300 pages représente une tâche très chronophage, ainsi qu'envers les examinateurs et invité, Michael Joyce, David Langlois, Reynald Pain et Éric Gourgoulhon. Je suis honoré de voir mon travail jugé par un comité d'une si grande qualité.

Je remercie également les membres de l'IAP que j'ai eu le plaisir de rencontrer et de côtoyer pendant ces trois ans : Patrick Boissé, Frédéric Daigne, Robert Mochkovitch, Pasquier Noterdaeme et Elisabeth Vangioni au troisième étage ; Luc Blanchet, Gilles Esposito-Farèse, Guillaume Faye, Patrick Peter et Sébastien Renaux-Petel au sein du $\mathcal{GR}\varepsilon\mathbb{C}\mathcal{O}$. À Guillaume, merci de ta gestion exemplaire du trésor, et de partager aussi spontanément tes idées ou connaissances, parfois surprenantes, souvent longues à raconter, mais toujours passionnantes ! À Sébastien, merci pour ton amitié, et pour ce super-pouvoir

que tu as de mettre immédiatement à l'aise toute personne avec qui tu échanges ne serait-ce que quelques mots. C'est une qualité très précieuse que tu partages avec Gilles.

Grâce à la confiance que m'ont accordé Jacques Chauveau, Nicolas Treps et Philippe Thomen, cette thèse a aussi eu une composante d'enseignement passionnante ; je les en remercie. Je salue par ailleurs Charles Antoine, Mathieu Bertin et Remi Geiger pour leur accueil chaleureux au sein de l'équipe de Quanta et Relativité, et pour avoir supporté mon perfectionnisme sur les sujets de TD.

Esta tesis no habría sido tan enriquecedora sin los dos viajes extraordinarios a Colombia, que fueron posibles gracias al intercambio iniciado por Yeinzon Rodríguez. Agradezco también a todos los que me recibieron de manera tan calurosa, y me hicieron descubrir un país tan fascinante como magnífico, en particular a César Valenzuela y a Juan Pablo Beltrán. Y cómo no acordarme de la salsa Caleña!

I have given a few seminars across Europe during my thesis. This has always been a nice and stimulating experience, but it would not have been so without those who kindly devoted a bit of their time to take care of me when I was visiting their institutes. For this, I thank a lot Miguel Zumalacárregui, Andrew Jaffe, Nathalie Schwaiger, Vincent Vennin, Thibaut Louis, Johannes Noller, Thomas Buchert, Pierre Salati, Björn Hermann, Giovanni Marozzi, Ruth Durrer, Sami Nurmi, Syksy Räsänen, Viraj Sanghai, and Timothy Clifton.

Ces trois années aurait été tellement plus fades, tellement moins stimulantes, et tellement moins drôles sans vous tous : les doctorants ! Alba, Alice, Caterina, Charlotte, Clément, Clotilde, Erwan, Federico, Flavien, Florent, Guillaume D. et Guillaume P., Hayley, Hélène, Jean, Jean-Baptiste, Julia, Laura, Maxime, Mélanie, Nicolas C. et Nicolas M., Rebekka, Sandrine, Sébastien, Sylvain, Thomas, Tilman, Vincent B. et Vincent V. et enfin Vivien ; nombre d'entre vous sont aujourd'hui des amis plus que des collègues, et ce n'est que pour garder une taille raisonnable à ces remerciements que je me retiens d'écrire dix lignes sur chacun. Nos YMCA autant que nos pauses café ont indéniablement compté parmi les moments les plus essentiels de mon passage à l'IAP. Mais il n'est pas question que j'oublie ceux qui n'ont pas eu la chance d'effectuer leur thèse dans le meilleur institut d'astrophysique *du monde*[1], et que j'ai (malgré tout) eu beaucoup de plaisir à rencontrer, les uns aux Houches : Agnès, Anais, Mathilde, Julian, Linda, Tico et Thibaut ; les autres à Elbereth, dans des séminaires divers et variés, ou simplement autour d'un verre à la Butte aux Cailles : Alexis, Benjamin, Jibril et Marta. Je sais que nous nous recroiserons, car après tout notre monde est homéomorphe à $\mathbb{S}_2$, et cette idée me plaît.

Une thèse marque la fin de longues études, et il serait illusoire de nier l'influence que certains professeurs de physique ont pu avoir sur mes choix d'orientation. Dès mes premiers pas dans cette discipline jusqu'à l'ENS de Lyon, j'ai eu la chance d'être accompagné par des enseignants qui m'ont sans cesse incité à donner le meilleur de moi-même, par l'admiration qu'ils m'inspiraient. Ce fut le cas d'Olivier Calvosa, Martine Brenier, Éric Brottier, Philippe Cren, François Gieres, Henning Samtleben, Pierre Salati, et surtout d'Olivier Jean-Marie. C'est en grande partie grâce à cet enseignant hors-pair que je suis arrivé jusqu'ici. Je lui dois ma rigueur et ma pédagogie. Cette thèse est dédiée à sa mémoire ; puisse-t-elle vivre dans chaque graine de scientifique qu'il a semée au cours de sa vie.

Les remerciements d'une thèse ne sont, à mon sens, pas le lieu pour exposer sa vie personnelle. C'est une excuse bien commode, car je ne saurais trouver de mots assez justes pour exprimer toute la gratitude et l'affection que j'éprouve envers ma famille. C'est ce même mélange de pudeur et de maladresse qui me fera taire le nom de celle avec qui j'ai partagé ma vie pendant ces quelques années, et à qui je dois tant.

---

[1] Dixit Joe Silk et Pedro Ferreira. Des gens très bien.

Contents

Introduction

2^{015} has seen the very appropriate conjunction of the international year of light and the centenary of Einstein's general theory of relativity; it would have been difficult to find a better occasion for presenting a thesis dedicated to the propagation of light in cosmology. The paradigmatic revolution that represented general relativity one hundred years ago indeed deeply changed our vision of the Universe, setting the foundations of modern cosmology. Since then, this discipline grew and lived, becoming an entire field of research. Physical phenomena that were formerly considered unmeasurable, such as gravitational lensing, or whose very existence was ignored, such as the cosmic microwave background radiation, became powerful cosmological probes, and have now reached an unprecedented level of precision.

In contrast with this increasing accuracy of observations—which had us enter into the so-called *precision era* of cosmology—, the theoretical framework currently used to interpret the associated data is remarkably simple. In fact, for most practical purposes, it has barely changed since the pioneering works of Friedmann and Lemaître in the 1920s. There was however no reason for such a change, since to date the Friedmann-Lemaître cosmological model, based on the assumption that the Universe is spatially homogeneous and isotropic, has shamelessly passed all observational tests. Of course, the Universe is not *strictly* homogeneous, especially on small scales, but it seems that such an inhomogeneity does not need to be taken into account when interpreting cosmological observations.

The tremendous success of the homogeneous and isotropic model is particularly striking if we consider the case of distance measurements. On astronomical and cosmological scales, distances are mostly measured by comparing the apparent size or luminosity of a light source with its intrinsic size or luminous power. Consequently, such measurements rely on the good understanding of light propagation through the cosmos, in particular the way light beams are focused by matter lying between the sources and us. The point is that current observations involve beams with extremely different sizes: from less than a microarcsecond for supernova observation, to a few degrees with baryon acoustic oscillation experiments, in terms of angular aperture. Depending on the observations at stake, light is thus expected to experience a completely different Universe. Yet the Friedmann-Lemaître model arises as *one model to fit them all.*

Why, and to which extent, such a simplistic model can be considered a good approximation for interpreting cosmological observations? If not, how to go beyond the assumptions of perfect homogeneity and isotropy? are the fundamental questions which motivated the present thesis. I chose to divide this dissertation in four parts, the first two being dedicated to fundamentals, while the last two report the original research that I have performed during the last three years. More precisely, in Part I, I introduce the laws governing light propagation in curved spacetime, from a relativist's point of view. The presentation is intended to be modern and pedagogical, with a few novel elements absent from textbooks. Part II is dedicated to standard cosmology: after having presented the Friedmann-Lemaître

model and the standard perturbation theory about it, I review the current observational status, emphasizing the precise points on which the understanding of light propagation through the Universe is required, and where the standard model is used. Part III is the heart of this thesis, it is devoted to the analysis of the effect of small-scale structures on the interpretation of observations, in particular the Hubble diagram of supernovae. I demonstrate that this effect may be non-negligible given the accuracy reached by current and future measurements, and I propose a new theoretical framework for addressing this issue. Finally, Part IV deals with two works related to cosmology beyond perfect isotropy. Besides, elements of differential geometry and general relativity can be found in Appendix.

The research reported in this dissertation has been done in collaboration with several colleagues, and led to the following articles:

1. P. Fleury, H. Dupuy, and J.-P. Uzan *Interpretation of the Hubble diagram in a nonhomogeneous universe.* Phys. Rev. D 87, 123526 (2013), [arXiv:1302.5308].

2. P. Fleury, H. Dupuy, and J.-P. Uzan. *Can all cosmological observations be accurately interpreted with a unique geometry?* Phys. Rev. Lett. 111, 091302 (2013), [arXiv:1304.7791]. This letter has been highlighted by the science popularisation website Phys.org.

3. P. Fleury. *Swiss-cheese models and the Dyer-Roeder approximation.* JCAP06(2014)054, [arXiv:1402.3123].

4. P. Fleury, J. P. Beltrán Almeida, C. Pitrou, and J.-P. Uzan. *On the stability and causality of scalar-vector theories.* JCAP11(2014)043, [arXiv:1406.6254]

5. P. Fleury, C. Pitrou, and J.-P. Uzan. *Light propagation in a homogeneous and anisotropic universe.* Phys. Rev. D 91, 043511, [arXiv:1410.8473].

6. P. Fleury, J. Larena, and J.-P. Uzan. *The theory of stochastic cosmological lensing.* Accepted for publication in JCAP. [arXiv:1508.07903].

Conventions, notations, and acronyms

Units. Numerical results are mostly given in terms of units of the International System. In abstract calculations, we adopt the usual relativistic convention of $c = 1$, so that lengths and times have the same dimension.

Differential geometry. We follow the conventions of Misner, Thorne, Wheeler [1]. In particular, the signature of spacetime's metric is taken to be $(-+++)$. We use Einstein's summation rule over repeated indices, the range of the sum being dictated by the nature of the indices (see Table 1). As often as possible, we dedicate indices of the beginning of the alphabet to components over orthonormal bases.

Notations. See Table 1 for a list of the recurrent symbols used in this dissertation. As often in the relativity literature, vectors and tensors are identified with their components over an arbitrary coordinate basis (e.g. $\boldsymbol{u}$ will be equivalently denoted u^μ). Partial derivatives and covariant derivatives with respect to, e.g. coordinate x^μ are abridged as

$$\frac{\partial f}{\partial x^\mu} \equiv \partial_\mu f \equiv f_{,\mu} \tag{1}$$

$$\nabla_{\partial/\partial x^\mu} f \equiv \nabla_\mu f = f_{;\mu} \tag{2}$$

for any function or tensor f.

Sets of indices are symmetrised and antisymmetrised according to

$$T_{(\mu_1 \ldots \mu_n)} \equiv \frac{1}{n!} \sum_{\sigma \in S_n} T_{\sigma(\mu_1 \ldots \mu_n)} \tag{3}$$

$$T_{[\mu_1 \ldots \mu_n]} \equiv \frac{1}{n!} \sum_{\sigma \in S_n} \varepsilon(\sigma) \, T_{\sigma(\mu_1 \ldots \mu_n)}, \tag{4}$$

for any tensor or subtensor $\boldsymbol{T}$, where S_n denotes the set of all permutations σ of n elements, and $\varepsilon(\sigma)$ is the signature of σ, i.e. $+1$ or -1 depending of whether it consists of an even or odd number of transpositions, respectively. In particular,

$$T_{(\mu\nu)} \equiv \frac{1}{2} \left(T_{\mu\nu} + T_{\nu\mu} \right), \qquad T_{[\mu\nu]} \equiv \frac{1}{2} \left(T_{\mu\nu} - T_{\nu\mu} \right). \tag{5}$$

Acronyms. They will be defined when used for the first time. See also Table 2.

Notation	Description
$\equiv$	definition
$\overset{*}{=}$	equality in a given coordinate system
bold symbols $\boldsymbol{A}$, $\boldsymbol{g}$, $\boldsymbol{\mathcal{D}}$, …	vectors, tensors, and matrices
greek indices $\alpha, \beta, \ldots \mu, \nu, \ldots$	run from 0 to 3
lowercase latin indices $a, b, \ldots, i, j, \ldots$	run from 1 to 3
uppercase latin indices $A, B, \ldots, I, J, \ldots$	run from 1 to 2
$\mathrm{d}\Omega^2 \equiv \mathrm{d}\theta^2 + \sin^2\theta \mathrm{d}\varphi^2$	infinitesimal solid angle in spherical coordinates
$[\mu\nu\rho\sigma]$	permutation symbol with $[0123] = 1$
$\varepsilon_{\mu\nu\rho\sigma} \equiv \sqrt{-g}[\mu\nu\rho\sigma]$	Levi-Civita tensor
$\mathcal{L}_{\boldsymbol{V}}$	Lie derivative along vector $\boldsymbol{V}$
$\boldsymbol{\xi}$	Killing vector, or separation vector
∇, D	covariant derivatives
$\Gamma^{\rho}{}_{\mu\nu}$	connection coefficients
$R^{\mu}{}_{\nu\rho\sigma}$	curvature tensor
$R_{\mu\nu}, R$	Ricci tensor, scalar
$E_{\mu\nu}$	Einstein tensor
Σ	hypersurface
$\perp_{\mu\nu}$	induced metric on a hypersurface
$\mathscr{L}$	worldline
$\boldsymbol{u}$	four-velocity
τ	proper time
$\boldsymbol{k}$	wave four-vector
v	affine parameter along null geodesics
S, O	source, observation events
$(\boldsymbol{s}_A)_{A=1,2}$	Sachs (screen) basis
$S_{\mu\nu}$	screen projector
$\boldsymbol{\mathcal{R}}$	optical tidal matrix
$\mathscr{R}, \mathscr{W}$	Ricci, Weyl lensing scalars
$\boldsymbol{\mathcal{W}}$	Wronski matrix
$\boldsymbol{\mathcal{D}}$	Jacobi matrix
$\boldsymbol{\mathcal{A}}$	amplification matrix
$\boldsymbol{\mathcal{S}}$	deformation rate matrix
θ, σ	null expansion rate, null shear rate
t	cosmic time
a	cosmic scale factor
η	conformal time, with $\mathrm{d}t = a\mathrm{d}\eta$
$H \equiv a^{-1}\mathrm{d}a/\mathrm{d}t$	Hubble expansion rate
$\mathcal{H} \equiv a^{-1}\mathrm{d}a/\mathrm{d}\eta = aH$	conformal Hubble expansion rate
Ω_x	cosmological parameter associated with x
$\delta = \delta\rho/\bar{\rho}$	density contrast
δ_{D}	Dirac distribution
$f, \alpha, \bar{\alpha}$	smoothness parameter
$M_{\odot}$	Solar mass

Table 1 Description of the main notations used in this thesis.

Acronym	Signification
BAO	Baryon Acoustic Oscillation
BOSS	Baryon Oscillation Spectroscopic Survey
c.c.	complex conjugate
CFHT(LenS)	Canada-France-Hawaii-Telescope (Lensing Survey)
CMB	Cosmic Microwave Background
COSMOGRAIL	COsmological MOnitoring of GRAvItational Lenses
FL	Friedmann-Lemaître
GR	General Relativity
HST	Hubble Space Telescope
JLA	Joint Lightcurve Analysis
(K)DR	(Kantowski)-Dyer-Roeder
ΛCDM	Λ Cold Dark Matter
LRG	Luminous Red Galaxy
LSST	Large Synoptic Survey Telescope
LTB	Lemaître-Tolman-Bondi
MLCS	Multicolour Light Curve Shape
RS	Rees-Sciama
SALT	Spectral Adaptive Lightcurve Template
SDSS	Sloan Digital Sky Survey
SNLS	SuperNova Legacy Survey
SC	Swiss Cheese
SL	Strong gravitational Lensing
SN(e)(Ia)	(Type Ia) SuperNova(e)
(I)SW	(Integrated) Sachs-Wolfe
VLBI	Very Long Baseline Interferometry
WFIRST	Wide-Field InfraRed Survey Telescope
WL	Weak gravitational Lensing
WMAP	Wilkinson Microwave Anisotropy Probe

Table 2   List of acronyms and their signification.

PART I

GEOMETRIC OPTICS IN CURVED SPACETIME

From electromagnetism to geometric optics

I N 1860, Maxwell unified electricity, magnetism, and light in a single physical theory, thus providing foundations for the phenomenological laws of geometric optics formulated earlier by Euclid, Newton, Snell, Descartes, or Fermat. Because it is quite naturally extended in the presence of gravity, described by Einstein's general relativity, Maxwell's theory not only teaches us about the nature of light, it also tells us how its propagation is affected by gravitational fields. This first chapter is a journey from standard Maxwell's electromagnetism to gravitational lensing, in which we review in details how gravity is able to modify the path of light, but also its frequency, energy, and polarisation.

Contents

1.1 Electromagnetism

Maxwell's theory of electromagnetism is naturally formulated in Minkowski spacetime, the structure of which it historically revealed, leading to the development of special, and later general, relativity. This section aims at reminding this standard formulation and describing its extension in the presence of gravity. Because our main purpose is the analysis of electromagnetic waves, we will only consider here Maxwell's theory in electric vacuum, that is in the absence of electric charges and currents; see Ref. [2] for details about the coupling between electromagnetism and matter.

1.1.1 In Minkowski spacetime

In Maxwell's theory of electromagnetism, the fundamental object is a vector field $\boldsymbol{A}$, which represents the four-vector potential from which derives the electromagnetic field. The latter is encoded into the Faraday tensor $\boldsymbol{F}$ defined as the field strength of $\boldsymbol{A}$, i.e.

$$F_{\mu\nu} \equiv \partial_\mu A_\nu - \partial_\nu A_\mu. \tag{1.1}$$

This definition ensures that the *intrinsic* Maxwell equations $\partial_{[\mu} F_{\nu\rho]} = 0$ are satisfied. The dynamics of the electromagnetic field is then described by an action principle, the Maxwell action being

$$S_{\mathrm{M}}[\boldsymbol{A}] = -\frac{1}{16\pi} \int_{\mathcal{M}} \mathrm{d}^4 x \, F^{\mu\nu} F_{\mu\nu} \qquad \text{(flat spacetime)}, \tag{1.2}$$

where $\mathcal{M}$ denotes the spacetime manifold. The $1/16\pi$ prefactor in S_{EM} indicates that we work in the Gaussian system of units, in which the electric and magnetic fields have the same dimension; see e.g. Ref. [2] for a detailed correspondence between Gaussian units and the units of the International System.

In classical electromagnetism, the four-vector potential $\boldsymbol{A}$ is not observable, contrary to its field strength $\boldsymbol{F}$, directly related to the force that the electromagnetic field applies on charged particles[1]. From the definition (1.1) of $F_{\mu\nu}$, we see that the potential $\boldsymbol{A}$ from which it derives is not unique; any *gauge transformation*

$$A_\mu \mapsto A_\mu + \partial_\mu s, \tag{1.3}$$

where s is a scalar quantity, indeed leaves $F_{\mu\nu}$ unchanged. The action (1.2) is thus also unaffected by (1.3): Maxwell's theory is gauge invariant. As any symmetry in the action, gauge invariance is associated via Noether theorem [4,5] with the conservation of a physical quantity, which in this case is the vector $Q^\nu \equiv \partial_\mu F^{\mu\nu}$. When matter is (minimally) coupled to the electromagnetic field, this is equivalent to the conservation of electric charge.

In the absence of any electric source, the four-vector potential $\boldsymbol{A}$ only appears in S_{EM}; stationarity of the latter with respect to variations of the former thus leads to the equations of motion

$$0 = 4\pi \frac{\delta S_{\mathrm{M}}}{\delta A_\nu} = \partial_\mu F^{\mu\nu} \qquad \text{(flat spacetime)}, \tag{1.4}$$

---

[1]In quantum mechanics, however, the vector potential influences the phase of the wavefunction of charged particles [3], in a way that depends on their path. Such an effect, named after Aharonov and Bohm, is experimentally accessible via interferometry, and is used in Superconducting Quantum Interference Devices (SQIDs) to measure magnetic fluxes.

which represent the *extrinsic* Maxwell equations in vacuum. When we additionally impose the Lorenz gauge condition $\partial_\mu A^\mu = 0$, the extrinsic Maxwell equations (1.4) take the form of a simple wave equation

$$\Box A_\mu = 0 \qquad \text{(flat spacetime)}, \tag{1.5}$$

where $\Box \equiv \partial^\nu \partial_\nu$ is the d'Alembertian operator in flat spacetime.

1.1.2 In curved spacetime

Let us now examine how the laws of electromagnetism are affected by the presence of gravity, that we will assume to be described by Einstein's general theory of relativity. Because the dynamics of the gravitational field is not the topic of this chapter, we will not address it here, but we refer the reader to the appendix A for a summary of the notations, conventions, physical quantities, and concepts of general relativity that we will use throughout this thesis.

Minimally coupled electrodynamics

As stated by Einstein's equivalence principle, the laws of non-gravitational physics must be locally the same in the presence or in the absence of gravitation, provided they are worked out in a freely falling frame. Hence, a theory of electromagnetism in curved spacetime must give back the Lagrangian density of Eq. (1.2) about any event E of $\mathcal{M}$, provided it is written using, e.g., Gaussian normal coordinates, for which $g_{\mu\nu}(E) \mapsto \eta_{\mu\nu}$ and $\Gamma^\rho{}_{\mu\nu}(E) \mapsto 0$.

Besides, since curvature cannot be eliminated by any coordinate transformation, we deduce that any direct coupling in the action between A_μ and the Riemann tensor (or higher derivatives of the metric) would violate Einstein's equivalence principle as stated above. Imposing this principle then results into the *minimal coupling prescription* for making curved-spacetime laws from flat-spacetimes laws: starting from the action in Minkowski spacetime,

1. Replace the coordinate volume element $\mathrm{d}^4 x$ by the covariant volume element $\sqrt{-g}\,\mathrm{d}^4 x$, where g denotes the determinant of spacetime's metric. This quantity is defined with respect to the *covariant* components $g_{\mu\nu}$ of the metric,

$$g \equiv \frac{1}{4!} \left[\alpha\beta\gamma\delta\right] \left[\mu\nu\rho\sigma\right] g_{\alpha\mu}\, g_{\beta\nu}\, g_{\gamma\rho}\, g_{\delta\sigma} \qquad \text{(sum on all indices)} \tag{1.6}$$

where $[\alpha\beta\gamma\delta]$ is the completely antisymmetric permutation symbol, with the convention $[0123] = 1$.

2. Replace partial derivatives ∂_μ by covariant derivatives ∇_μ.

Applying the minimal coupling prescription to the Maxwell action (1.2) leads to the standard action of electromagnetism in curved spacetime

$$\boxed{S_{\mathrm{M}}[\boldsymbol{A}, \boldsymbol{g}] = -\frac{1}{16\pi} \int_{\mathcal{M}} \mathrm{d}^4 x\, \sqrt{-g}\, F^{\mu\nu} F_{\mu\nu},} \tag{1.7}$$

where the Faraday tensor now reads $F_{\mu\nu} = \nabla_\mu A_\nu - \nabla_\nu A_\mu$, which turns out to be equal to its expression in flat spacetime (with partial derivatives), provided spacetime geometry is torsion free as assumed in GR.

The equations of motion deriving from the stationarity of S_{EM} are now

$$0 = 4\pi \frac{\delta S_{\text{EM}}}{\delta A_\nu} = \frac{1}{\sqrt{-g}} \partial_\mu \left(\sqrt{-g}\, F^{\mu\nu} \right) = \nabla_\mu F^{\mu\nu}, \tag{1.8}$$

which can be rewritten in terms of the four-vector potential as

$$0 = \nabla_\mu F^{\mu\nu} \tag{1.9}$$

$$= \nabla_\mu \nabla^\mu A^\nu - \nabla_\mu \nabla^\nu A^\mu \tag{1.10}$$

$$= \nabla_\mu \nabla^\mu A^\nu - \nabla^\nu \nabla_\mu A^\mu - R^\mu{}_{\rho\mu}{}^\nu A^\rho, \tag{1.11}$$

where the Riemann tensor appeared due to the commutation of two covariant derivatives; imposing in addition the general-relativistic form of the Lorenz gauge $\nabla_\mu A^\mu = 0$, finally yields

$$\boxed{\Box A_\mu - R^\nu_\mu A_\nu = 0,} \tag{1.12}$$

with the covariant d'Alembertian $\Box \equiv \nabla^\nu \nabla_\nu$ and the Ricci tensor $R_{\mu\nu} \equiv R^\rho{}_{\mu\rho\nu}$. It is interesting here to note the importance of applying the minimal coupling prescription *in the action* rather than in the equations of motion; indeed if we had replaced ∂_ν by ∇_ν directly in Eq. (1.5), then we would have missed the Ricci curvature term that appears in Eq. (1.12).

The presence of covariant derivatives in $\Box$ and of the Ricci tensor in Eq. (1.12) clearly indicates that spacetime geometry affects the electromagnetic field. Note that the converse is also true, since the electromagnetic field has energy and momentum, encoded into its stress-energy tensor

$$T_{\mu\nu}^{\text{EM}} \equiv \frac{-2}{\sqrt{-g}} \frac{\delta S_{\text{M}}}{\delta g^{\mu\nu}} = \frac{1}{4\pi} \left[F_{\mu\rho} F_\nu{}^\rho - \frac{1}{4} (F^{\rho\sigma} F_{\rho\sigma}) g_{\mu\nu} \right], \tag{1.13}$$

which is a source of gravity in the Einstein field equations. It is a significant difference, that it is worth emphasizing, between Newtonian gravity in which mass is the only form of energy to gravitate, and general relativity in which all forms of energy have the ability to curve spacetime; in Einstein's theory, even photons attract each others!

Beyond minimal coupling?

If one relaxes the assumption of minimal coupling between the vector field A_μ and spacetime geometry, then various terms involving spacetime curvature can appear in the action, e.g. $R_{\mu\nu\rho\sigma} F^{\mu\nu} F^{\rho\sigma}$, $R_{\mu\nu} A^\mu A^\nu$, $R F^{\mu\nu} F_{\mu\nu}$, etc. Such couplings turn out to be generically unhealthy [6], by generating Hamiltonian instabilities or, since they are already second-order derivatives of the metric, third-order derivatives in the equations of motion; the presence of a bare $\boldsymbol{A}$ also potentially violates the gauge-invariance of the electromagnetic sector, which implies the nonconservation of electric charge if $\boldsymbol{A}$ is minimally coupled to matter.

There is however at least one exception. In a very technical article [7], Horndeski proved that if a theory which couples a vector field $\boldsymbol{A}$ to spacetime geometry (i) derives from an action principle involving $\boldsymbol{A}$ and $\boldsymbol{g}$; (ii) generates second-order equations of motion; (iii) conserves the electric charge; and (iv) reduces to standard electromagnetism in flat spacetime, then its action reads

$$S_{\text{H}}[\boldsymbol{A}, \boldsymbol{g}] = S_{\text{EH}}[g_{\mu\nu}] + S_{\text{M}}[A_\mu, g_{\mu\nu}] + \frac{\ell^2}{16\pi} \int \mathrm{d}^4 x \sqrt{-g}\, L^{\mu\nu\rho\sigma} F_{\mu\nu} F_{\rho\sigma} \tag{1.14}$$

where the first term is the Einstein-Hilbert action (see appendix A), the second term is the Maxwell action as seen in the previous paragraph, and the last term is the only nonminimal coupling term that is allowed by the above four assumptions. The $L^{\mu\nu\rho\sigma}$ tensor is defined by

$$L^{\mu\nu\rho\sigma} \equiv -\frac{1}{2}\varepsilon^{\mu\nu\alpha\beta}\varepsilon^{\rho\sigma\gamma\delta}R_{\alpha\beta\gamma\delta} \tag{1.15}$$

$$= 2R^{\mu\nu\rho\sigma} + 4\left(R^{\mu[\sigma}g^{\rho]\nu} + R^{\nu[\sigma}g^{\rho]\mu}\right) + 2Rg^{\mu[\rho}g^{\sigma]\nu}, \tag{1.16}$$

it enjoys the same symmetries as the Riemann tensor, and is divergence free (i.e. $\nabla_\mu L^{\mu\nu\rho\sigma} = 0$). The coupling constant ℓ, which has the dimension of a length, physically represents the typical curvature radius scale below which this theory would significantly deviate from minimally coupled electromagnetism. The sign of this new term in Eq. (1.14) ensures the Hamiltonian stability of the theory [8].

Due to its non-trivial coupling between electromagnetism and gravity, Horndeski's vector-tensor theory is expected to present a rich phenomenology beyond the standard Einstein-Maxwell framework, such as photon-graviton oscillations, varying speed of light, gravitational birefringence and optical activity, etc.

1.1.3 Electric and magnetic fields

Let us close this section on pure electromagnetism by indicating how to disentangle electric and magnetic fields from the Faraday tensor $\boldsymbol{F}$. In a special-relativistic context, if $F_{\mu\nu}$ is written as a matrix whose μ, ν respectively label the lines and columns, then

$$[F_{\mu\nu}] = \begin{bmatrix} 0 & -E_1 & -E_2 & -E_3 \\ E_1 & 0 & B_3 & -B_2 \\ E_2 & -B_3 & 0 & B_1 \\ E_3 & B_2 & -B_1 & 0 \end{bmatrix} \qquad \text{(flat spacetime)}, \tag{1.17}$$

where E_i and B_i are the components of the electric and magnetic fields. This comes from an identification between (i) the definition of the Faraday tensor $F_{\mu\nu} = \partial_\mu A_\nu - \partial_\nu A_\mu$, and (ii) the relation linking fields and potentials, usually written as $\vec{E} = -\vec{\nabla}V - \partial_t\vec{A}$ and $\vec{B} = \vec{\nabla} \times \vec{A}$, with $(A^\mu) = (V, \vec{A})$. As parts of an order-two tensor, $\vec{E}$ and $\vec{B}$ are not, properly speaking, vectors: they are *observer dependent*, and thus transform in a non-trivial way under Lorentz boosts.

Let $\boldsymbol{u}$ be the four-velocity of an experimentalist (with $u^\mu u_\mu = -1$) who wishes to characterise the electric and magnetic parts of $\boldsymbol{F}$ in her rest frame. By definition, the components of the Faraday tensor over an orthonormal tetrad representing such a frame must take the form of Eq. (1.17). One can therefore define the electric and magnetic fields $(\boldsymbol{E}, \boldsymbol{B})$ as purely spatial vectors, i.e.

$$u_\mu E^\mu = u_\mu B^\mu = 0, \tag{1.18}$$

such that

$$\boxed{F_{\mu\nu} = 2u_{[\mu}E_{\nu]} + \varepsilon_{\mu\nu\rho\sigma}u^\rho B^\sigma,} \tag{1.19}$$

where we have introduced the *Levi-Civita tensor*

$$\varepsilon_{\mu\nu\rho\sigma} \equiv \sqrt{-g}\,[\mu\nu\rho\sigma] \tag{1.20}$$

following the convention of Ref. [9]. Note that, given the definition of the metric determinant g, the completely contravariant counterpart of Eq. (1.20) is $\varepsilon^{\mu\nu\rho\sigma} = -[\mu\nu\rho\sigma]/\sqrt{-g}$. By inverting Eq. (1.19) one obtains the expressions of the electric and magnetic fields:

$$E^\mu = u_\nu F^{\mu\nu}, \tag{1.21}$$

$$B^\mu = -u_\nu \tilde{F}^{\mu\nu}, \tag{1.22}$$

where $\tilde{F}_{\mu\nu} = \varepsilon_{\mu\nu\rho\sigma} F^{\rho\sigma}/2$ is the *Hodge dual* of the Faraday two-form. It enjoys a decomposition similar to Eq. (1.19), as $\tilde{F}_{\mu\nu} = -2u_{[\mu}B_{\nu]} + \varepsilon_{\mu\nu\rho\sigma}u^\rho E^\sigma$. Summarising, the Hodge duality turns $\boldsymbol{E}$ into $-\boldsymbol{B}$ and $\boldsymbol{B}$ into $\boldsymbol{E}$.

These two quantities can also be used to rewrite the electromagnetic stress-energy tensor $T_{\mu\nu}^{\text{EM}}$ in a way that makes its interpretation in terms of energy, energy flux, pressure, etc. easier. Introducing Eq. (1.19) into Eq. (1.13) one indeed obtains

$$T_{\mu\nu}^{\text{EM}} = \rho\, u_\mu u_\nu + 2u_{(\mu}\Pi_{\nu)} + p \perp_{\mu\nu} + \Pi_{\mu\nu}, \tag{1.23}$$

where we introduced the spatial part of the metric $\perp_{\mu\nu} = u_\mu u_\nu + g_{\mu\nu}$, while

$$\rho \equiv \frac{E^2 + B^2}{8\pi} \qquad (X^2 \equiv X^\mu X_\mu), \tag{1.24}$$

$$p \equiv \frac{\rho}{3}, \tag{1.25}$$

$$\Pi_\nu \equiv \frac{u^\mu \varepsilon_{\mu\nu\rho\sigma} E^\rho B^\sigma}{4\pi}, \tag{1.26}$$

$$\Pi_{\mu\nu} = 2p \perp_{\mu\nu} - \frac{E_\mu E_\nu + B_\mu B_\nu}{4\pi}, \tag{1.27}$$

are respectively the energy density, isotropic radiation pressure, Poynting vector, and anisotropic stress of the electromagnetic field. Both the Poynting vector and the anisotropic stress are purely spatial ($\Pi_\mu u^\mu = 0$, $\Pi_{\mu\nu}u^\mu = 0$), and the latter is trace free ($\Pi_\mu^\mu = 0$).

1.2   Light rays in geometric optics

In this section, we introduce what will be the framework for all the remainder of this thesis, namely geometric optics. After having discussed the underlying assumptions—the eikonal approximation—, we examine how the Maxwell equations in curved spacetime govern the propagation of electromagnetic waves in this regime, and analyse some features of their trajectories.

1.2.1   The geometric optics regime

An ansatz for electromagnetic waves

The geometric optics framework is conveniently discussed when one considers the following ansatz for the vector four-potential of an electromagnetic wave,

$$\boldsymbol{A} = \boldsymbol{a}\mathrm{e}^{\mathrm{i}\phi} + \text{c.c.}, \tag{1.28}$$

where $\boldsymbol{a}$, ϕ respectively stand for the wave's amplitude and the phase. While the latter is real by definition, the former can be complex in general; here nevertheless *we assume*

that a_μ is real, i.e. we restrict our study to *linearly polarised* waves. This assumption can actually be made without any loss of generality: thanks to the linearity of the Maxwell equations (1.12), any elliptically polarised wave is indeed the superposition of two linearly polarised ones.

To the wave (1.28) can be associated a *wave four-vector* defined as the gradient of the phase,

$$k_\mu \equiv \partial_\mu \phi, \qquad (1.29)$$

which thus represents the local direction of propagation of the wave through spacetime. Note that the Lorenz gauge condition already imposes conditions on $\boldsymbol{a}$ and $\boldsymbol{k}$, namely

$$0 = \nabla_\mu A^\mu = (\nabla_\mu a^\mu + \mathrm{i} k_\mu a^\mu)\,\mathrm{e}^{\mathrm{i}\phi} + \text{c.c.} \qquad (1.30)$$

whose real and imaginary parts respectively imply

$$\nabla_\mu a^\mu = 0, \qquad k_\mu a^\mu = 0. \qquad (1.31)$$

Such a wave is therefore *transverse*, in the sense that its directions of excitation and propagation are orthogonal.

The eikonal approximation

Geometric optics corresponds to a regime for which the genuinely undulatory properties of light are irrelevant, so that it behaves as a stream of classical point particles: well-defined trajectories and no interference nor diffraction phenomena. In flat spacetime, such a situation is achieved when the phase of the electromagnetic wave varies much faster than its amplitude, i.e.

$$\partial \phi \gg a^{-1}\partial a, \qquad (1.32)$$

which is known as the *eikonal approximation*.

In the presence of gravity, however, the approximation requires an additional assumption since another spatio-temporal scale enters into the game: spacetime curvature itself. In order for the undulatory phenomena not to be affected by this additional element, the phase of the electromagnetic wave must evolve on scales much smaller than the typical spacetime curvature radius ℓ_c, i.e.

$$\partial \phi \gg \ell_\mathrm{c}^{-1}, \qquad (1.33)$$

where ℓ_c^{-1} must be understood as the square-root of a typical component of the Riemann curvature tensor. Assumption (1.33) is therefore the second part of the eikonal approximation in curved spacetime [1].

Let us examine the restrictiveness of (1.33) in terms of the wavelength λ—which is indeed the typical evolution scale of ϕ—on two examples. In a cosmological context, the typical curvature radius is given by the inverse of the expansion rate $\ell_\mathrm{c} \sim c/H \sim 4\,\mathrm{Gpc}$ today (that is essentially the size of the observable Universe) or $\sim 0.2\,\mathrm{Mpc}$ at the epoch of recombination; hence $\lambda \ll \ell_\mathrm{c}$ is not particularly restrictive in this context. In the vicinity of a spherically symmetric massive object, ℓ_c can be evaluated using the Kretschmann scalar[2] K as $\ell_\mathrm{c} \sim K^{-1/4} \sim \sqrt{r^3/r_\mathrm{S}}$, where r_S denotes the Schwarzshild radius of the object, and r the coordinate distance to it. On the surface of Earth, this implies $\lambda \ll 2\,\mathrm{AU}$, while on the horizon of a stellar black hole it leads to $\lambda \ll 3\,\mathrm{km}$. Only in the latter—rather extreme—case, a part of the radio domain does not satisfy the eikonal approximation.

---

[2]The Kretschmann scalar is defined as the contraction of the Riemann tensor with itself, $K \equiv R^{\mu\nu\rho\sigma} R_{\mu\nu\rho\sigma}$, and is useful to investigate the properties of the complete spacetime curvature, rather than restricting to the Ricci scalar which, for example, is useless in vacuum.

The Maxwell equations in geometric optics

Inserting the ansatz (1.28) for $\boldsymbol{A}$ into the Maxwell equations (1.12) gives

$$\Box a^\mu - (k^\nu k_\nu)a^\mu - R^\mu_\nu a^\nu + \mathrm{i}\left(2k^\nu\nabla_\nu a^\mu + a^\mu\nabla_\nu k^\nu\right) = 0. \tag{1.34}$$

The real part of Eq. (1.34) implies $(k^\nu k_\nu)a^\mu = \Box a^\mu - R^\mu_\nu a^\nu$, but the eikonal approximation indicates that the left-hand side is much larger than the right-hand side; both must therefore vanish identically for the situation to be acceptable. Putting it together with the imaginary part of Eq. (1.34) results into the propagation equations of electromagnetic waves in the geometric optics regime:

$$k^\mu k_\mu = 0, \tag{1.35}$$

$$k^\nu\nabla_\nu a^\mu + \frac{1}{2}(\nabla_\nu k^\nu)a^\mu = 0. \tag{1.36}$$

The first one (1.35) is the dispersion relation, while the second one (1.36) contains both photon conservation and the evolution equation of polarisation, as we shall see respectively in § 1.3.2 and § 1.3.3.

The eikonal approximation also leads to a familiar structure for the trio (k^μ, E^μ, B^μ). The Faraday tensor indeed reads $F_{\mu\nu} = 2\mathrm{i}k_{[\mu}A_{\nu]} + \text{c.c.}$ at leading order, so that $E_\mu = 2\mathrm{i}u^\nu k_{[\mu}A_{\nu]} + \text{c.c.}$ and $B_\mu = \mathrm{i}u^\nu\varepsilon_{\nu\mu\rho\sigma}k^\rho A^\sigma + \text{c.c.}$, whence

$$k^\mu E_\mu = k^\mu B_\mu = E^\mu B_\mu = 0, \tag{1.37}$$

which express the wave's transversality in terms of its electric and magnetic fields.

1.2.2   Photons follow null geodesics

We now focus on the trajectory followed by electromagnetic waves. Start with taking the gradient of the dispersion relation $k^\nu k_\nu = 0$,

$$0 = \nabla_\mu(k^\nu k_\nu) = 2k^\nu\nabla_\mu k_\nu. \tag{1.38}$$

Because k_ν is defined itself as the gradient of the phase ϕ, the indices of $\nabla_\mu k_\nu$ can be inverted due to the symmetry of the Christoffel coefficients,

$$\nabla_\mu k_\nu = \nabla_\mu\partial_\nu\phi = \partial_\mu\partial_\nu\phi - \Gamma^\rho_{\mu\nu}\partial_\rho\phi,$$

and the above equation takes the familiar form

$$k^\nu\nabla_\nu k^\mu = 0. \tag{1.39}$$

The integral curves of the vector field k^μ—the curves to which k^μ is everywhere tangent—are therefore *null geodesics*, since they satisfy the geodesic equation[3] (1.39) and their

---

[3]It is interesting to note here that the geodesic equation emerges as a consequence of the null condition $k^\mu k_\mu = 0$, and it would be tempting to conclude that any null curve is a geodesic. This is actually the case *only if its tangent vector is a gradient*, as this property of k^μ was a crucial ingredient in the derivation. A counterexample is easily constructed in Minkowski spacetime; consider the curve defined as $x = r\cos(ct/r)$, $y = r\sin(ct/r)$, which corresponds to a circular motion—a helicoid in spacetime—of radius r at velocity c. Its tangent vector $(u^\mu) = [1, -c\sin(ct/r), c\cos(ct/r), 0]$ is clearly null, but it is not a geodesic.

tangent vectors are null (1.35). Such curves, that we shall call light rays in the following[4], can be interpreted as the worldlines of photons, referring to the Einstein-de Broglie duality between waves and particles, according to which the momentum of a photon is $p^\mu = \hbar k^\mu$, where $\hbar \equiv h/(2\pi)$ denotes the reduced Planck constant.

A parameter v along a given light ray is naturally defined through its tangent vector by

$$k^\mu \equiv \frac{\mathrm{d}x^\mu}{\mathrm{d}v}, \tag{1.40}$$

which tells us that a small variation $\mathrm{d}v$ of parameter v corresponds to the small displacement $\mathrm{d}x^\mu = k^\mu \mathrm{d}v$ along the ray. The geodesic equation (1.39) then reads, in terms of v,

$$0 = \frac{\mathrm{D}k^\mu}{\mathrm{d}v} \equiv \frac{\mathrm{d}k^\mu}{\mathrm{d}v} + \Gamma^\mu{}_{\nu\rho} k^\nu k^\rho = \frac{\mathrm{d}^2 x^\mu}{\mathrm{d}v^2} + \Gamma^\mu{}_{\nu\rho} \frac{\mathrm{d}x^\nu}{\mathrm{d}v} \frac{\mathrm{d}x^\rho}{\mathrm{d}v}, \tag{1.41}$$

where $\mathrm{D}/\mathrm{d}v$ denotes the *covariant derivative* with respect to v. The particular form (1.41) of the geodesic equation, where $\mathrm{D}k^\mu/\mathrm{d}v$ completely vanishes instead of just being proportional to k^μ, indicates that v is not any parameter along the curve but an *affine parameter* (see e.g. Ref. [9] for further details). Any affine transformation $v \mapsto av + b$ indeed preserves the form of Eq. (1.41). The physical meaning of v, which has been introduced so far as a mathematical object, will be discussed in § 1.3.1.

1.2.3 Conformal invariance

Null geodesics turn out to enjoy a particular symmetry that they do not share with their timelike or spacelike equivalents, namely the invariance under conformal transformations of the metric. This property can be stated as the following theorem.

Theorem. Let $\boldsymbol{g}$ and $\tilde{\boldsymbol{g}}$ be two metric tensors for a same spacetime manifold $\mathcal{M}$ described with an arbitrary coordinate system $\{x^\mu\}_{\mu=0\ldots3}$, related by a *conformal transformation*:

$$g_{\mu\nu}(x^\rho) = \Omega^2(x^\rho) \tilde{g}_{\mu\nu}(x^\rho), \tag{1.42}$$

where Ω is an arbitrary scalar function on $\mathcal{M}$. If a curve γ is a null geodesic for $\boldsymbol{g}$, then it is also a null geodesic for $\tilde{\boldsymbol{g}}$. Moreover, if v is an affine parameter of γ for $\boldsymbol{g}$, then any $\tilde{v}$ so that $\mathrm{d}v = \Omega^2 \mathrm{d}\tilde{v}$ is an affine parameter of γ for $\tilde{\boldsymbol{g}}$.

The above property is practically very useful when there exists a conformal transformation such that $\tilde{g}_{\mu\nu}$ is much simpler than $g_{\mu\nu}$; the analysis of light propagation is then more easily performed in terms $\tilde{g}_{\mu\nu}$, while its counterpart in $g_{\mu\nu}$ can be recovered by a systematic procedure (see § 5.1.1 for a complete dictionary and an example). Besides practical calculations, conformal invariance also immediately explains the failure of Nordstrøm's theory of gravitation [10, 11], proposed in 1912—three years before Einstein's general relativity. In this theory, as reformulated by Einstein and Fokker in 1914, spacetime's geometry is conformally flat: its metric reads $g_{\mu\nu} = \exp(2\Phi)\eta_{\mu\nu}$, where $\eta_{\mu\nu}$ denotes the Minkowski metric and Φ corresponds to the Newtonian potential in the weak-field regime. Because of the conformal invariance of null geodesics, Nordstrøm's gravity thus predicts no gravitational deflection of light, and is therefore ruled out by observations.

---

[4]Albeit in their classical definition, light rays are rather the spatial projections of null geodesics.

Proof of the theorem

Suppose that γ is a null geodesic affinely parametrised by $x^\mu(v)$, so that its tangent vector $k^\mu \equiv \mathrm{d}x^\mu/\mathrm{d}v$ satisfies $\mathrm{D}k^\mu/\mathrm{d}v = 0$. Then consider the same curve γ but parametrised by $\tilde{v}$, with $\mathrm{d}v = \Omega^2 \mathrm{d}\tilde{v}$; the associated tangent vector reads $\tilde{k}^\mu \equiv \mathrm{d}x^\mu/\mathrm{d}\tilde{v} = \Omega^2 k^\mu$. The covariant derivative

$$\frac{\tilde{\mathrm{D}}\tilde{k}^\mu}{\mathrm{d}\tilde{v}} \equiv \tilde{k}^\nu \tilde{\nabla}_\nu \tilde{k}^\mu = \tilde{k}^\nu \partial_\nu \tilde{k}^\mu + \tilde{\Gamma}^\mu{}_{\nu\rho} \tilde{k}^\nu \tilde{k}^\rho \tag{1.43}$$

can be rewritten using the following correspondence between the Christoffel coefficients of $\tilde{\boldsymbol{g}}$ and $\boldsymbol{g}$:

$$\tilde{\Gamma}^\mu{}_{\nu\rho} \equiv \frac{1}{2} \tilde{g}^{\mu\sigma} \left(\partial_\nu \tilde{g}_{\sigma\rho} + \partial_\rho \tilde{g}_{\sigma\nu} - \partial_\sigma \tilde{g}_{\nu\rho} \right) \tag{1.44}$$

$$= \Gamma^\mu{}_{\nu\rho} - 2\delta^\mu_{(\nu}\partial_{\rho)} \ln \Omega + g_{\nu\rho} g^{\mu\sigma} \partial_\sigma \ln \Omega, \tag{1.45}$$

so that

$$\frac{\tilde{\mathrm{D}}\tilde{k}^\mu}{\mathrm{d}\tilde{v}} = \Omega^4 \left[\frac{\mathrm{D}k^\mu}{\mathrm{d}v} + (k^\nu k_\nu) g^{\mu\sigma} \partial_\sigma \ln \Omega \right] = 0, \tag{1.46}$$

which concludes the proof.

Microscopic or emergent symmetry?

It is tempting to see in the conformal invariance of lightcones a consequence of the conformal invariance of electromagnetism. Indeed, the Maxwell action (1.7) is unchanged by the transformation (1.42) of the metric, without the need of any transformation of the vector field $\boldsymbol{A}$, it was therefore expected to find such a symmetry for the propagation of light. However, this rationale only holds in four dimensions, since in dimension d,

$$S_{\mathrm{M}}[\boldsymbol{A}, \tilde{\boldsymbol{g}}] \equiv \int \mathrm{d}^d x \, \sqrt{-\tilde{g}} \, \tilde{g}^{\mu\rho} \tilde{g}^{\nu\sigma} F_{\mu\nu} F_{\rho\sigma} \tag{1.47}$$

$$= \int \mathrm{d}^d x \, \sqrt{-g} \, \Omega^{d-4} g^{\mu\rho} g^{\nu\sigma} F_{\mu\nu} F_{\rho\sigma} \tag{1.48}$$

$$\neq S_{\mathrm{M}}[\boldsymbol{A}, \boldsymbol{g}] \qquad \text{if } d \neq 4, \tag{1.49}$$

while the conformal invariance of null geodesics is fully general, regardless of the dimension—as it was not involved in the proof of the previous paragraph. Yet photons do follow null geodesics, even for $d \neq 4$, since the dimension was not involved in the derivation of § 1.2.2 either.

This paradoxical situation suggests that, in general, conformal invariance must emerge somewhere on the way from electromagnetism to geometric optics. It can be understood by considering the equation of motion for $\boldsymbol{A}$ which derives from the action (1.48),

$$\Box A_\mu - R^\nu_\mu A_\nu + (d-4) F^\nu{}_\mu \partial_\nu \ln \Omega = 0, \tag{1.50}$$

where last term makes Eq. (1.50) differ from the Maxwell equations (1.12), and thus spoils conformal invariance. This new term is however proportional to $\partial \ln \Omega \sim \ell_\Omega^{-1}$, where ℓ_Ω denotes the typical evolution scale of Ω. Similar terms turn out to appear in the transformation of the Ricci tensor between the metrics $\boldsymbol{g}$ and $\tilde{\boldsymbol{g}}$ (see e.g. Ref. [12] for details), so that ℓ_Ω^{-2} can be considered a contribution to spacetime curvature. Hence, by virtue of the eikonal approximation, the last term of (1.50) can be neglected, and conformal invariance is approximately recovered.

The conformal invariance of lightcones is therefore an *emergent* symmetry in general, which accidentally coincides with a fundamental symmetry of electromagnetism in four dimensions.

1.2.4 Conserved quantities

In many situations of interest, spacetime geometry itself enjoys some symmetries, which implies the existence of conserved quantities for its geodesics. Mathematically speaking, such a symmetry is defined by the existence of a Killing vector $\boldsymbol{\xi}$ along which the (Lie) derivative of the metric vanishes [5, 9]:

$$\mathcal{L}_{\boldsymbol{\xi}} \boldsymbol{g} = \boldsymbol{0}. \tag{1.51}$$

In terms of components, the above equation reads

$$0 = \xi^{\rho} \partial_{\rho} g_{\mu\nu} + \partial_{\mu} \xi^{\rho} g_{\rho\nu} + \partial_{\nu} \xi^{\rho} g_{\rho\mu} \tag{1.52}$$

$$= \xi^{\rho} \nabla_{\rho} g_{\mu\nu} + \nabla_{\mu} \xi^{\rho} g_{\rho\nu} + \nabla_{\nu} \xi^{\rho} g_{\rho\mu} \tag{1.53}$$

$$= 2 \nabla_{(\mu} \xi_{\nu)}; \tag{1.54}$$

the tensor $\nabla_{\mu} \xi_{\nu}$ is thus antisymmetric if $\boldsymbol{\xi}$ is a Killing vector. This property implies that its scalar product with the wave-four vector is a constant of motion, since

$$\frac{\mathrm{d}(k^{\mu} \xi_{\mu})}{\mathrm{d}v} = k^{\mu} k^{\nu} \nabla_{\nu} \xi_{\mu} \tag{1.55}$$

$$= 2 k^{\mu} k^{\nu} \nabla_{(\nu} \xi_{\mu)} \tag{1.56}$$

$$= 0. \tag{1.57}$$

A spacetime with N Killing vectors $(\boldsymbol{\xi}_i)_{i=1\ldots N}$ thus generates in principle N constants $C_i \equiv \xi_i^{\mu} k_{\mu}$ along any geodesic motion. The above calculations are indeed true for any geodesic (timelike, spacelike or null).

1.2.5 Fermat's principle

While both timelike and spacelike geodesics enjoy a intuitive geometrical meaning in terms of extremalisation of the associated proper time or length, null geodesics are a priori harder to interpret this way, because the line element $\mathrm{d}s^2$ between two neighbouring events of any null curve vanishes, by definition. It is thus unclear what extremalising such an always zero function is supposed to mean.

Yet there exists a similar characterisation of null geodesics, reminiscent of classical Fermat's principle (see e.g. [13, 14]) which essentially states that light always follows the quickest way between two points. In a general relativistic context, this can be formulated as the following theorem, illustrated in Fig. 1.1.

Theorem. [15, 16] Let S be an arbitrary event (light emission) and consider a null curve $\bar{\gamma}$ connecting S to the worldline $\mathscr{L}$ of an observer. Call O the intersection between $\bar{\gamma}$ and $\mathscr{L}$ (observation event), and τ_O the proper time measured by the observer at O, with respect to an arbitrary origin. Then $\bar{\gamma}$ is a null geodesic if and only if τ_O extremises the arrival times τ of all the *null* curves γ connecting S to $\mathscr{L}$ which slightly deviate from $\bar{\gamma}$.

Let us now prove this theorem. Our demonstration is partially inspired from Ref. [17], pp. 101-102, though we tried to propose a more intuitive formulation of the converse part. In all that follows, we respectively denote with $\bar{x}^{\mu}(v)$ and $x^{\mu}(v) \equiv \bar{x}^{\mu}(v) + \delta x^{\mu}(v)$ parametrisations of the neighbouring null curves $\bar{\gamma}$ and γ; the associated tangent vectors are defined by $\bar{k}^{\mu} \equiv \mathrm{d}\bar{x}^{\mu}/\mathrm{d}v$ and $k^{\mu} \equiv \mathrm{d}x^{\mu}/\mathrm{d}v$. As an infinitesimal quantity, $\delta x^{\mu}(v)$ can be considered a vector field along $\bar{\gamma}$; we assume that its values at the events S and O read

$$\delta x_S^{\mu} = 0, \qquad \delta x_O^{\mu} = u_O^{\mu} \delta\tau, \tag{1.58}$$
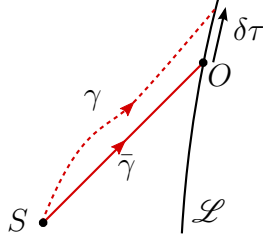
Figure 1.1 Relativistic Fermat's principle. The null curve $\bar{\gamma}$ is a geodesic iff τ_O is a local extremum of arrival times, i.e. $\delta\tau = 0$ for any null curve γ slightly differing from $\bar{\gamma}$.

where u_O^μ is the four-velocity of the observer at O. These assumptions mean that both $\bar{\gamma}$ and γ emerge from S, and cross $\mathscr{L}$ with a relative delay $\delta\tau$.

Finally, since the (covariant) derivative of δx^μ with respect to v reads $\mathrm{D}\delta x^\mu/\mathrm{d}v = k^\mu - \bar{k}^\mu \equiv \delta k^\mu$, a consequence of the nullity of γ is then

$$k^\mu k_\mu = 2\bar{k}^\mu \delta k_\mu = 0, \tag{1.59}$$

at first order in δk^μ.

$\bar{\gamma}$ geodesic $\Longrightarrow \delta\tau = 0$

Suppose that $\bar{\gamma}$ is a null geodesic affinely parametrised by v (without loss of generality), we then have

$$\frac{\mathrm{d}}{\mathrm{d}v}\left(\bar{k}_\mu \delta x^\mu\right) = \frac{\mathrm{D}\bar{k}^\mu}{\mathrm{d}v}\delta x^\mu + \bar{k}^\mu \delta k_\mu = 0, \tag{1.60}$$

where both terms in the middle are zero because of, respectively, the geodesic equation (1.41), and Eq. (1.59). We conclude that $\bar{k}_\mu \delta x^\mu$ is a constant all along $\bar{\gamma}$, which moreover vanishes because $\delta x_S^\mu = 0$, hence

$$0 = (\bar{k}_\mu \delta x^\mu)_O = (\bar{k}_\mu u^\mu)_O \delta\tau, \tag{1.61}$$

that is $\delta\tau = 0$ since the null vector $\bar{\boldsymbol{k}}_O$ and the timelike vector $\boldsymbol{u}_O$ cannot be orthogonal to each other.

$\bar{\gamma}$ geodesic $\Longleftarrow \delta\tau = 0$

Proving this converse assertion requires a more constructive approach. Let $\{\boldsymbol{e}_\alpha\}_{\alpha=0\ldots3}$ be a tetrad field so that $\boldsymbol{e}_0(O) \equiv \boldsymbol{u}_O$, and parallely transported along $\bar{\gamma}$ from O to S. This procedure basically generates a family of fictive observers with four-velocities $\boldsymbol{e}_0(v)$ along $\bar{\gamma}$, as illustrated in Fig. 1.2.

Suppose each of these observers selects an arbitrary *spatial* position $\{\delta x^a\}_{a=1\ldots3}$ in his rest frame—i.e., with respect to the local tetrad $\{\boldsymbol{e}_\alpha(v)\}$—so that the $\delta x^a(v)$ are smooth, and consider the worldline γ of a particle that would interpolate all those spatial positions at the speed of light. By construction, γ is therefore a null curve, and its deviation with respect to $\bar{\gamma}$ is

$$\delta x^\mu = \delta x^0 e_0^\mu + \delta x^a e_a^\mu, \tag{1.62}$$

where the value of δx^0 is imposed δx^a via the speed-of-light condition, i.e. $\bar{k}^\alpha \delta k_\alpha = 0$ in tetrad components. When integrated from S to O, this condition implies

$$\delta\tau = \delta x_O^0 = \int_S^O \mathrm{d}v\, \frac{\bar{k}_a \delta k^a}{\bar{k}_0} = -\int_S^O \frac{\mathrm{d}}{\mathrm{d}v}\left(\frac{\bar{k}_a}{\bar{k}_0}\right)\delta x^a \tag{1.63}$$
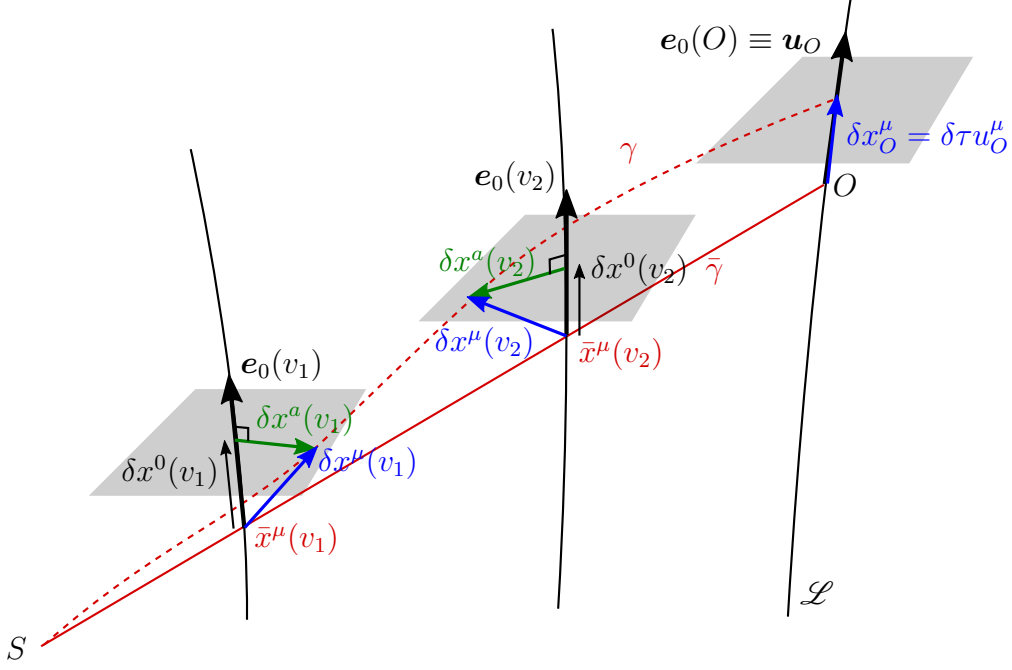
Figure 1.2 Geometry of the proof of (the converse of) Fermat's principle. The four-velocity u_O^μ of the observer at O is parallely transported along $\bar{\gamma}$ to generate a vector field $e_0(v)$, interpreted as the four-velocity of fictive observers (two of them are represented, at v_1 and v_2). The null curve γ is defined as the trajectory of a particle moving at the speed of light which is detected at spatial positions $\delta x^a(v)$ by each of the fictive observers. This imposes the delay $\delta x^0(v)$ of this particle with respect to the one following $\bar{\gamma}$, and thus the complete separation $\delta x^\mu = \delta x^0 e_0^\mu + \delta x^a e_a^\mu$ between γ and $\bar{\gamma}$.

after an integration by parts.

Now if $\delta\tau = 0$ for any null curve γ in the vicinity of $\bar{\gamma}$, then Eq. (1.63) implies

$$\frac{\mathrm{d}}{\mathrm{d}v}\left(\frac{\bar{k}_a}{\bar{k}_0}\right) = 0, \tag{1.64}$$

because the $\delta x^a(v)$ were arbitrary fields. Besides, using $\bar{k}_\alpha \equiv \bar{k}_\mu e_\alpha^\mu$ and the fact that the tetrad field $\{e_\alpha\}$ is parallely transported along $\bar{\gamma}$ ($\mathrm{D}e_\alpha/\mathrm{d}v = \mathbf{0}$), we can rewrite Eq. (1.64) as

$$e_a^\mu\left(\frac{\mathrm{D}\bar{k}_\mu}{\mathrm{d}v} - \frac{\bar{k}_\mu}{\bar{k}_0}\frac{\mathrm{d}\bar{k}_0}{\mathrm{d}v}\right) = 0, \tag{1.65}$$

so that the expression between parentheses vanishes, since its projection over e_0 is also clearly zero. The null curve $\bar{\gamma}$ is therefore a geodesic as its tangent vector remains parallel to itself. One can also recover the affinely parametrised geodesic equation using e.g. the parameter w such that $\mathrm{d}v = \bar{k}_0\mathrm{d}w$ instead of v.

1.3   Observables of an electromagnetic wave

So far, we have investigated the propagation of light from a four-dimensional, fully covariant, point of view. In this section, on the contrary, we examine the properties of electromagnetic waves which are actually observable, and therefore observer-dependent by definition. We chose to divide them into three categories: the kinematical observables (§ 1.3.1), associated

with light's trajectory and frequency; the energetical observables (§ 1.3.2); and finally polarisation (§ 1.3.3).

1.3.1 Kinematics

The 3+1 decomposition of the wave vector

In the rest frame of an observer with four-velocity $\boldsymbol{u}$, the electric field associated with a wave $\boldsymbol{A} = \boldsymbol{a}e^{i\phi} + \text{c.c.}$ oscillates with an angular frequency ω defined as the (absolute value of the) rate of change of the phase ϕ. If τ denotes the proper time of this observer, we thus have

$$\omega \equiv \left| \frac{\mathrm{d}\phi}{\mathrm{d}\tau} \right| = |u^\mu \partial_\mu \phi| = -u^\mu k_\mu, \tag{1.66}$$

where the minus sign comes from the fact that we consider $\boldsymbol{k}$ as being future oriented, i.e. $k^0 > 0$ in any coordinate system. The frequency ν is related to ω via the usual relation $\omega = 2\pi\nu$.

Besides frequency, the wave is also characterised, in the frame of the observer, by its direction of propagation, that is the opposite of the direction in which the observer must look to actually detect the wave. It can be defined as being parallel to the spatial gradient of the phase,

$$d^\mu \propto \perp^{\mu\nu} \partial_\nu \phi \equiv (g^{\mu\nu} + u^\mu u^\nu) k_\nu, \tag{1.67}$$

where $\perp$ denotes the projector on the observer's local space. In the above equation, we used a proportionality symbol $\propto$ instead of an equality, because we also want $\boldsymbol{d}$ to be a unit vector; it is actually easy to check that the norm of $\perp^\mu_\nu k^\nu$ is ω, so that the right-hand side of Eq. (1.67) must be divided by ω.

The above definitions finally lead to the so-called 3+1 decomposition of the wave four-vector, illustrated in Fig. 1.3,
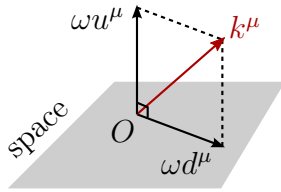
$$\boxed{\boldsymbol{k} = \omega \left(\boldsymbol{u} + \boldsymbol{d} \right),} \tag{1.68}$$

Figure 1.3 Decomposition of the wave four-vector.

with the orthonormality relations

$$u^\mu u_\mu = -1, \qquad d^\mu d_\mu = 1, \qquad u^\mu d_\mu = 0. \tag{1.69}$$

Physical meaning of the affine parameter

The 3+1 decomposition (1.68) of the wave four-vector with respect to a given observer provides a simple physical interpretation for the affine parameter v. Between v and $v + \mathrm{d}v$, the displacement of a photon through spacetime is given by $\mathrm{d}x^\mu = k^\mu \mathrm{d}v$. Hence, in the frame of the observer, the photon travels over a distance

$$\mathrm{d}\ell \equiv d_\mu \mathrm{d}x^\mu = d_\mu k^\mu \mathrm{d}v = \omega \mathrm{d}v, \tag{1.70}$$

which gives to $\mathrm{d}v$ its meaning. Equivalently, $\omega \mathrm{d}v$ can be interpreted as the time lapse $\mathrm{d}\tau$ measured by the observer between the events $x^\mu(v)$ and $x^\mu(v + \mathrm{d}v)$, but it is somehow harder to visualise than the corresponding travel distance.

The redshift and its interpretation

The relative difference between the frequency emitted by a source, ω_S, and the one actually measured by an observer, ω_O, is quantified by the redshift z as

$$1 + z \equiv \frac{\omega_S}{\omega_O} = \frac{(u^\mu k_\mu)_S}{(u^\mu k_\mu)_O}. \tag{1.71}$$

Because the expression of z involves both the four-velocities and the wave four-vectors at the source and observation events (respectively S and O), there is a fundamental degeneracy in its interpretation—is it a Doppler effect due to their relative velocity, or an Einstein effect due to, e.g., gravitational dilation of time?

This turns out to be a bad question in general, for its answer is *coordinate dependent.* We are indeed always free to pick a *comoving* coordinate system (see Fig. 1.4), with respect to which both the source and the observer are at rest, $u_S^i \overset{*}{=} u_O^i \overset{*}{=} 0$, so that any difference between ω_S and ω_O would be due to $k_\mu^O \overset{*}{\neq} k_\mu^S$. In such a case, z shall be interpreted as a gravitational redshift. Besides, we could also make the opposite choice and pick an *observational* coordinate system, such that now $k_\alpha^O \overset{*}{=} k_\alpha^S$; any redshift would then be attributed to $u_O^\alpha \overset{*}{\neq} u_S^\alpha$, and interpreted as a Doppler effect.
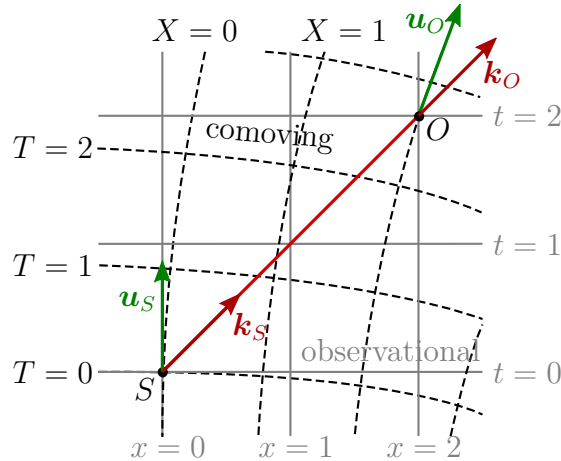
Figure 1.4   Illustration of the coordinate dependence of the interpretation of the redshift. With comoving coordinates (T, X)—black, dashed—only the components of the wave four-vector differ between S and O: z is interpreted as a gravitational redshift. With observational coordinates (t, x)—grey, solid—only the components of the four-velocity of the source and the observer differ: z is interpreted as a Doppler effect.

The point I try to make here is that there is fundamentally no preferred interpretation for the redshift of an observed signal[5]. In a cosmological context [19] for instance, it is *not* more sensible to attribute the redshift of remote galaxies to a stretching of wavelengths, due to the expansion of the Universe, than to a Doppler effect due to their recession velocities. They are just two different points of view on a same physical phenomenon[6].

---

[5]See however Ref. [18] for a case against this conclusion.

[6]This does not mean that the expansion of the Universe can be modelled by the motion of test particles in a Minkowski spacetime. See e.g. Ref. [20] for a thought experiment illustrating the difference between both situations.

Observational notion of relative velocity

Pushing further the above reasoning, the redshift allows us to define a very general notion of velocity of a light source as seen by an observer. It is essentially the velocity $\vec{V}$ that the observer would associate to the source by applying the special-relativistic Doppler formula

$$1 + z = \frac{1 - \vec{d} \cdot \vec{V}}{1 - V^2}, \tag{1.72}$$

where $-\vec{d}$ is an Euclidean unit vector materialising the observer's line of sight.

It can seem very artificial, but there is actually a fully covariant way of constructing such this velocity (see Fig. 1.5). Let γ be a light ray connecting a source S to an observer O, affinely parametrised by v, and define the four-vector $\boldsymbol{U}_S(v)$ as the parallel transportation of the source's four-velocity $\boldsymbol{u}_S$ from S to O along γ,

$$\frac{\mathrm{D}U_S^\mu}{\mathrm{d}v} = 0 \qquad \text{with} \qquad U_S^\mu(v_S) = u_S^\mu, \tag{1.73}$$

Since both $\boldsymbol{U}_S^\mu$ and $\boldsymbol{k}$ are parallel transported along γ, their scalar product $U^\mu k_\mu$ is a constant along this geodesic; in particular $U_S^\mu(v_O)k_\mu^O = U_S^\mu(v_S)k_\mu^S = u_S^\mu k_\mu^S = -\omega_S$, the redshift can therefore be written as

$$1 + z = \frac{U_S^\mu(v_O)k_\mu^O}{u_O^\mu k_\mu^O}. \tag{1.74}$$

If we work at O in the observer's frame, for which $u_O^\mu \overset{*}{=} (1, \vec{0})$, $k_O^\mu \overset{*}{=} \omega_O(1, \vec{d})$, then $U_S^\mu(v_O) \overset{*}{=} (1, \vec{V})/\sqrt{1 - V^2}$ in general, so that Eq. (1.74) is equivalent to Eq. (1.72). This construction is orginally due to Synge [21].
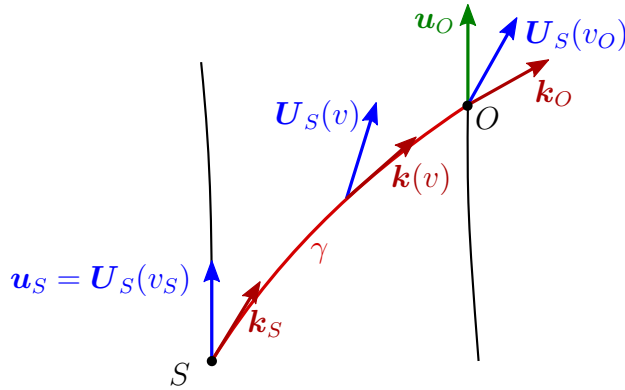
Figure 1.5 Defining an observational notion of relative velocity. The four-vector $\boldsymbol{U}_S(v)$ is constructed by parallel-transporting $\boldsymbol{u}_S$ from S to O along the null geodesic γ connecting them. The resulting vector $\boldsymbol{U}_S(v_O)$ at O represents the four–velocity of the source as seen by the observer: the observed redshift is computed from it by applying the special-relativistic formula (1.72).

Let us give two concrete examples of this *Synge velocity*. In homogeneous cosmology, where spacetime is described by the Friedmann-Lemaître geometry (see Chap. 4), the recession velocity of a comoving source with respect to a comoving observer reads $V = (a_O^2 - a_S^2)/(a_O^2 + a_S^2)$, where $a_E \equiv a(t_E)$ denotes the scale factor at the cosmic time t_E of the event E. Note that for $t_O \gtrsim t_S$ we recover the Hubble law $V \approx H_0(t_O - t_S)$.

In the vicinity of non-rotating body of mass M, where spacetime is described by the Schwarzschild geometry, the recession Doppler velocity between a source at r_S and an observer at $r_O > r_S$ with the same angular coordinates is $V = (A_S - A_O)/(A_S + A_O)$, where $A(r) \equiv 1 - 2GM/r$. If $r_S \to 2GM$, i.e. if the massive body is a black hole whose horizon is approached by the source, then V approaches the speed of light.

1.3.2 Energetics and photon conservation

As already mentioned in § 1.1.2 and § 1.1.3, any electromagnetic field possesses energy and momentum, whose various components are encoded in the decomposition (1.23) of its stress-energy tensor. In the special case of an electromagnetic wave of the form $\boldsymbol{A} = \boldsymbol{a}e^{i\phi} + \text{c.c.}$, the energy density ρ and the Poynting vector $\boldsymbol{\Pi}$—which represents the energy flux density, or momentum density—read

$$\rho \equiv \frac{E^2 + B^2}{8\pi} = \frac{\omega^2 a^2 \sin^2\phi}{\pi}, \tag{1.75}$$

$$\Pi_\mu \equiv \frac{u^\nu \varepsilon_{\nu\mu\rho\sigma} E^\rho B^\sigma}{4\pi} = \rho\, d_\mu, \tag{1.76}$$

with $a^2 \equiv a^\mu a_\mu \geq 0$, as ensured by the Lorenz gauge $k^\mu a_\mu = 0$ together with the dispersion relation $k^\mu k_\mu = 0$, and $\boldsymbol{d}$ is the unit vector in the direction of propagation introduced in Eq. (1.68).

In practice, experiments are not sensitive to the detailed time evolution of such quantities, but rather to their average over a certain integration time $\Delta\tau \gg \omega^{-1}$. For instance, the luminous power P associated with an electromagnetic wave is the time average of the flux of the Poynting vector over the detector surface

$$P(\tau) \equiv \iint_{\text{detect.}} \mathrm{d}^2\Sigma_\mu \int_\tau^{\tau+\Delta\tau} \mathrm{d}t\; \Pi^\mu = \iint_{\text{detect.}} \mathrm{d}^2\Sigma_\mu d^\mu \langle\rho\rangle, \tag{1.77}$$

where $\langle\ldots\rangle$ denotes (proper) time averaging. From Eq. (1.75) we get $\langle\rho\rangle = \omega^2 a^2/(2\pi)$ for the mean energy density of the electromagnetic wave. Note that, by virtue of Eq. (1.77), $\langle\rho\rangle$ also represent the power per unit area, that is, the luminous intensity I detected by the observer.

If we now adopt a corpuscular description of light, i.e. if we consider the electromagnetic wave as a photon stream, then the mean energy density can be written as $\langle\rho\rangle = n \times \hbar\omega$, where n denotes the number of photons per unit volume within the wave. Similarly, because the Poynting vector is the momentum density of the wave, it reads $\langle\boldsymbol{\Pi}\rangle = n \times \hbar\omega\boldsymbol{d}$ in terms of photons. These considerations naturally drive us to define the *photon flux density* associated with the wave as

$$\boldsymbol{j} \equiv \frac{\langle\rho\rangle\,\boldsymbol{u} + \langle\boldsymbol{\Pi}\rangle}{\hbar\omega} = \frac{a^2}{2\pi\hbar}\,\boldsymbol{k}. \tag{1.78}$$

Note that thanks to the above second equality, $\boldsymbol{j}$ is a real four-vector in the sense that it is *observer-independent*, contrary to ρ, $\boldsymbol{\Pi}$, or the photon number density given by $n = -u^\mu j_\mu$.

Going back to the propagation equations for electromagnetic waves, the contraction of Eq. (1.36) with $\boldsymbol{a}$ immediately leads to a continuity equation

$$\boxed{\nabla_\mu j^\mu = 0,} \tag{1.79}$$

which translates photon number conservation. Of course, this law is only valid in vacuum, or at least in the absence of coupling between matter and the electromagnetic field, since in the latter case photons can potentially be emitted of absorbed, which would generate a source term in Eq. (1.79).

1.3.3 Polarisation

In terms of the vector potential

So far we have only exploited the information that Eq. (1.36) provides about the norm of the wave amplitude $\boldsymbol{a}$, but it actually also drives the evolution of its direction. Let us assume that $a^2 \neq 0$ (else the wave has no energy, i.e. does not exist at all), and define the unit potential polarisation vector as

$$\boldsymbol{\alpha} \equiv \frac{\boldsymbol{a}}{\sqrt{a^2}}. \tag{1.80}$$

Inserting $a^\mu = \sqrt{a^2}\alpha^\mu$ in Eq. (1.36), we get

$$0 = \sqrt{a^2}\, k^\nu \nabla_\nu \alpha^\mu + \frac{\alpha^\mu}{2\sqrt{a^2}} \nabla_\nu(a^2 k^\nu). \tag{1.81}$$

In the second term we recognise the divergence of the photon flux density $2\pi\hbar\nabla_\nu j^\nu$, which vanishes by virtue of photon conservation as seen in the previous paragraph, so that finally

$$\boxed{\frac{\mathrm{D}\boldsymbol{\alpha}}{\mathrm{d}v} = 0.} \tag{1.82}$$

The potential polarisation vector is thus parallely transported along the light ray.

In terms of the electric field

Albeit very convenient for a covariant description of polarisation, the vector potential is not directly measurable. In practice, polarisation is rather characterised by the behaviour of the electric field, but since the latter is observer-dependent, we can already suspect that parallel transportation, satisfied for $\boldsymbol{\alpha}$, will not hold here. Defining the electric field all along the wave's worldline γ indeed requires to define a family of observers, i.e. a field of four-velocities $\boldsymbol{u}$, which has no reason to be parallel-transported along γ. This issue becomes evident when one calculates the covariant derivative of $E^\mu = 2\mathrm{i}u_\nu k^{[\mu}A^{\nu]} + \text{c.c.}$ along γ,

$$\frac{\mathrm{D}E^\mu}{\mathrm{d}v} = -\frac{1}{2}(\nabla_\nu k^\nu)E^\mu + \left[2\mathrm{i}k^{[\mu}A^{\nu]}\frac{\mathrm{D}u_\nu}{\mathrm{d}v} + \text{c.c.}\right], \tag{1.83}$$

where we see that the second term, which prevents $\mathrm{D}\boldsymbol{E}/\mathrm{d}v$ from being proportional to $\boldsymbol{E}$, and thus prevents the electric polarisation vector

$$\boldsymbol{\epsilon} \equiv \frac{\boldsymbol{E}}{\sqrt{E^2}} \tag{1.84}$$

from being parallely transported, precisely encodes the deviation from parallel transportation of $\boldsymbol{u}$ along γ.

Yet the electric polarisation partially inherits the propagation properties of $\boldsymbol{\alpha}$; it is actually parallel-transported *as much as possible*, while keeping orthogonal to both $\boldsymbol{u}$ and $\boldsymbol{d}$.

Such a notion can be formalised by defining the projector on the two-plane orthogonal to those vectors,

$$S^\mu_\nu \equiv \delta^\mu_\nu + u^\mu u_\nu - d^\mu d_\nu, \tag{1.85}$$

that we shall call *screen projector*, since the plane it projects on materialises a spatial ($\perp \boldsymbol{u}$) screen, orthogonal to the observer's line of sight $\boldsymbol{d}$. The electric polarisation then reads

$$\boxed{S^\mu_\nu \frac{\mathrm{D}\epsilon^\nu}{\mathrm{d}v} = 0.} \tag{1.86}$$

Let us now prove Eq. (1.86). First, because $u^\mu E_\mu = 0 = k^\mu E_\mu$, we also have $d^\mu E_\mu = 0$, so that $E^\mu = S^\mu_\nu E^\nu$ (the electric field belongs to the screen plane). Plugging-in the relation between E^μ and A^μ yields

$$E^\rho = S^\rho_\mu \, 2\mathrm{i}u_\nu k^{[\mu} A^{\nu]} + \text{c.c.} = \mathrm{i}\omega S^\rho_\mu A^\mu + \text{c.c.}, \tag{1.87}$$

where we used $S^\mu_\nu k^\nu = 0$. The screen projection Eq. (1.83) thus reads

$$S^\rho_\mu \frac{\mathrm{D}E^\mu}{\mathrm{d}v} = \left(-\frac{1}{2}\nabla_\nu k^\nu + \frac{1}{\omega}\frac{\mathrm{d}\omega}{\mathrm{d}v} \right) E^\rho. \tag{1.88}$$

The above equation can then be contracted with E_ρ in order to get an equation governing E^2; combining the latter with the former finally gives Eq. (1.86). Note that the same calculations could have been done with the magnetic field instead of the electric field.

Light beams

O**BSERVATIONS** in astronomy and cosmology often rely on the measurement of the apparent size, shape, and luminosity of distant light sources. Such notions cannot be described from a single light ray, a single geodesic, but rather require a collection of rays—a light beam—which connect each point of the extended source to the observer. If the rays remain close enough to each other, then their collective behaviour can be studied as a whole, and the beam considered an object in itself. This chapter is dedicated to the laws governing the propagation of such narrow light beams, and their connection with observables. In particular, we introduce the two fundamental tools of the gravitational lensing theory, namely the Jacobi matrix and the optical scalars, which will be crucial for discussing the various observable notions of distance in Chap. 3.

Contents

2.1 Description of a light beam

In this section, we show how the covariant description of light beams (§ 2.1.1), which is indeed the most natural way they are defined, can be turned to a more observation-oriented description. This requires to introduce a notion of screen (§ 2.1.2) on which observers can project the beam and characterise its shape and extension. We will show in particular that such morphological properties are actually observer independent. Their evolution with light propagation will finally be discussed in § 2.1.3.

2.1.1 Covariant approach

We define a light beam as a set of light rays which *all intersect at one event*, the lightcone of which they belong to. Depending on the physical situation that one wishes to address, this event can either represent light emission S from which the rays emerge, or light reception O towards which they converge. In this chapter, without loss of generality, we will consider the second option.

Intrinsic coordinate system and basis

Geometrically speaking, a light beam is thus modelled by a bundle of null geodesic with a vertex point. Its structure therefore only requires three coordinates to be explored (see Fig. 2.1). One is naturally chosen to be an affine parameter v along each individual geodesic within the bundle. The other two $(y^I)_{I=1,2}$ can be thought of as labels for the geodesics, such as angular coordinates on the observer's celestial sphere [22]. To this coordinate system is canonically associated a vector basis formed by

$$\boldsymbol{k} \equiv \frac{\partial}{\partial v}, \qquad \boldsymbol{e}_I \equiv \frac{\partial}{\partial y^I}. \tag{2.1}$$

Since all the geodesics of the bundle intersect at O, it is natural to affect to this event a common value v_O (often set to zero) of their affine parametrisation: $v = v_O \Leftrightarrow O$. This choice implies that the coordinate system (v, y^I) is singular at O—just like spherical coordinates are singular at their origin—in particular the vectors $\boldsymbol{e}_I$ vanish at O. Consider indeed any two neighbouring rays $v \mapsto x^\mu(v, y^I)$ and $v \mapsto x^\mu(v, y^I + \delta y^I)$; because they intersect at v_O, we have

$$0 = x^\mu(v_O, y^I + \delta y^I) - x^\mu(v_O, y^I) = e_I^\mu(O)\delta y^I, \tag{2.2}$$

which implies $e_I^\mu(O) = 0$ since δy^I is arbitrary.

A second consequence of the existence of a vertex point in the geodesic bundle is the orthogonality of $\boldsymbol{k}$ and $\boldsymbol{e}_I$. Proving this property requires to note that $(\boldsymbol{k}, \boldsymbol{e}_1, \boldsymbol{e}_2)$ is not any vector set but a *coordinate basis* (or *holonomous basis*), which means that the Lie brackets $[\boldsymbol{k}, \boldsymbol{e}_I]$ and $[\boldsymbol{e}_I, \boldsymbol{e}_J]$ must vanish [3]. In terms of components, $[\boldsymbol{k}, \boldsymbol{e}_I] = \boldsymbol{0}$ reads

$$0 = k^\nu \partial_\nu e_I^\mu - e_I^\nu \partial_\nu k^\mu = k^\nu \nabla_\nu e_I^\mu - e_I^\nu \nabla_\nu k^\mu; \tag{2.3}$$

it follows that

$$\frac{\partial}{\partial v}(e_I^\mu k_\mu) = k_\mu k^\nu \nabla_\nu e_I^\mu \qquad \text{since } k^\nu \nabla_\nu k_\mu = 0 \tag{2.4}$$

$$= k_\mu e_I^\nu \nabla_\nu k^\mu \qquad \text{because of Eq. (2.3)} \tag{2.5}$$

$$= \frac{1}{2} e_I^\nu \nabla_\nu (k_\mu k^\mu) \tag{2.6}$$

$$= 0 \qquad \text{as } \boldsymbol{k} \text{ is null.} \tag{2.7}$$

So the scalar product $e_I^\mu k_\mu$ does not depend on v, whence

$$e_I^\mu k_\mu = (e_I^\mu k_\mu)_O = 0. \tag{2.8}$$

Physically speaking, this means that the phase ϕ of the electromagnetic wave represented by the beam is the same for two events separated by $dx^\mu = e_I^\mu dy^I$, since for such a displacement $d\phi = k_\mu dx^\mu = 0$. The wave four-vector $\boldsymbol{k}$ being also orthogonal to itself, we conclude that any displacement $dx^\mu = k^\mu dv + e_I^\mu dy^I$ within the beam keeps ϕ unchanged: the beam entirely belongs to a $\phi = \text{cst}$-hypersurface, which defines the lightcone of O.
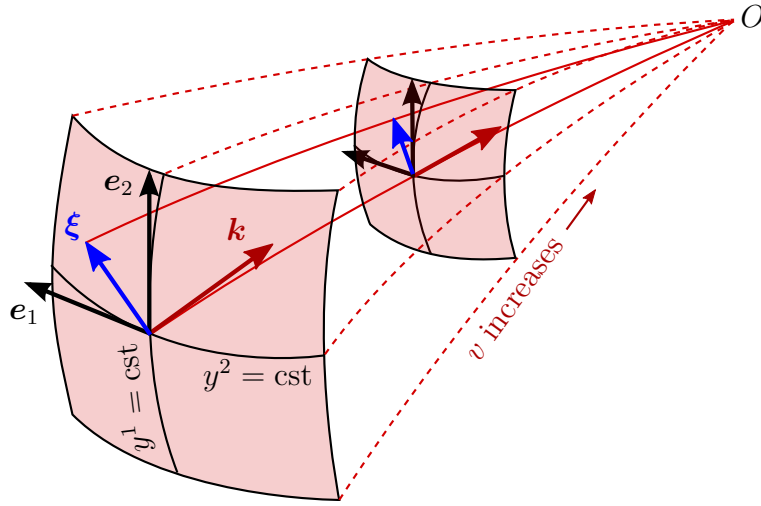
Figure 2.1 Schematic representation of a light beam converging at O, with its coordinate system (v, y^1, y^2) and the associated basis $(\boldsymbol{k}, \boldsymbol{e}_1, \boldsymbol{e}_2)$. Red lines (solid and dashed) represent light rays within the beam; the separation $\boldsymbol{\xi}$ between two of them is indicated in blue. Red surfaces are iso-v; horizontal or vertical black lines are respectively the intersection between iso-y^1 or iso-y^2 surfaces and iso-v surfaces.

Separation vector

The relative behaviour of two neighbouring rays, respectively labelled by y^I and $y^I + \delta y^I$, is usually described by their *separation vector* (or connecting vector)

$$\xi^\mu(v, y^I, y^I + \delta y^I) \equiv x^\mu(v, y^I + \delta y^I) - x^\mu(v, y^I) = e_I^\mu \delta y^I. \tag{2.9}$$

As a linear combination of the $\boldsymbol{e}_I$, $\boldsymbol{\xi}$ inherits all their properties, namely

$$\xi_O^\mu = 0, \tag{2.10}$$

$$k^\nu \nabla_\nu \xi^\mu = \xi^\nu \nabla_\nu k^\mu, \tag{2.11}$$

$$\xi^\mu k_\mu = 0, \tag{2.12}$$

which will turn out to be particularly useful for the remainder of this chapter.

Geodesic deviation equation

The fact that $\boldsymbol{\xi}$ is the separation between two geodesics imposes its evolution with v. Taking the gradient of the geodesic equation in the direction of $\boldsymbol{\xi}$, we indeed have

$$0 = \xi^\rho \nabla_\rho (k^\nu \nabla_\nu k^\mu) \tag{2.13}$$

$$= (\xi^\rho \nabla_\rho k^\nu)(\nabla_\nu k^\mu) + \xi^\rho k^\nu \nabla_\rho \nabla_\nu k^\mu \tag{2.14}$$

$$= (k^\rho \nabla_\rho \xi^\nu)(\nabla_\nu k^\mu) + \xi^\rho k^\nu \nabla_\nu \nabla_\rho k^\mu - \xi^\rho k^\nu R^\mu{}_{\sigma\nu\rho} k^\sigma \tag{2.15}$$

$$= k^\rho \nabla_\rho (\xi^\nu \nabla_\nu k^\mu) - R^\mu{}_{\sigma\nu\rho} k^\sigma k^\nu \xi^\rho \tag{2.16}$$

where, in Eq. (2.15), we used Eq. (2.11) to exchange the roles of $\boldsymbol{\xi}$ and $\boldsymbol{k}$ in the first term, and the definition of the Riemann tensor to exchange ∇_ρ and ∇_ν in the second term. Using again Eq. (2.3), we can rewrite the first term of Eq. (2.16) as $k^\rho \nabla_\rho k^\nu \nabla_\nu \xi^\mu$, which is nothing but the second covariant derivative of $\boldsymbol{\xi}$ with respect to v; the result is known as the *geodesic deviation equation*

$$\boxed{\frac{\mathrm{D}^2 \xi^\mu}{\mathrm{d}v^2} = R^\mu{}_{\sigma\nu\rho} k^\sigma k^\nu \xi^\rho.} \tag{2.17}$$

This equation surely provides the best geometrical interpretation of curvature, as the quantity which rules the relative acceleration between neighbouring geodesic motions. Note that Eq. (2.17) also applies to timelike and spacelike geodesics.

2.1.2 Screen space

From now on, we restrict to *infinitesimal light beams*, within which any two rays are close enough for their relative behaviour to be well-described by their separation vector $\boldsymbol{\xi}$. This vector is then the key tool for the analysis of a beam's morphology, but its relation to actually observable quantities requires to introduce a notion of screen.

Defining a screen

Consider an observer with four-velocity $\boldsymbol{u}$ whose worldline intersects the beam at an event E different from O. Since in general $e^\mu_I(E) \neq 0$, the beam has a nonzero extension around E. In order to characterise its morphology, the observer shall project it on a screen, defined as a two-dimensional spatial ($\perp \boldsymbol{u}$) plane, and chosen to be orthogonal to the local line-of-sight ($\perp \boldsymbol{d}$).

The relative position, on the screen, of the two light spots associated with two rays separated by ξ^μ, is then

$$\xi^\mu_\perp \equiv S^\mu_\nu \xi^\nu, \tag{2.18}$$

where the screen projector is defined by

$$S^{\mu\nu} \equiv g^{\mu\nu} + u^\mu u^\nu - d^\mu d^\nu, \tag{2.19}$$

and indeed coincides with the one introduced in § 1.3.3.

The beam's morphology is frame independent

Consider a set of any three rays $\gamma_{1,2,3}$ within the beam, the last two being respectively separated from the first one by $\boldsymbol{\xi}$ and $\boldsymbol{\zeta}$, as depicted in Fig. 2.2. The scalar product of their screen projection is then

$$\xi_\perp^\mu \zeta_\mu^\perp = \ell_{12} \ell_{13} \cos \vartheta, \tag{2.20}$$

where ℓ_{ij} stands for the (proper) distance between the spots i and j, while ϑ is the angle between the segments relating 1 to 2 and 1 to 3.
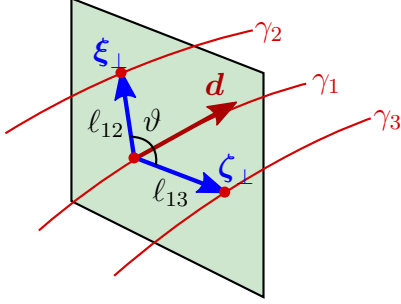
Figure 2.2 Relative position, on an observer's screen, of the three light spots associated with the three rays $\gamma_{1,2,3}$.

The orthogonality between $\boldsymbol{\xi}$ and $\boldsymbol{k}$ (2.12) allows us to rewrite Eq. (2.18) as

$$\xi_\perp^\mu = \xi^\mu + \frac{\xi^\nu u_\nu}{\omega} k^\mu. \tag{2.21}$$

and the analog relation for $\zeta_\perp^\mu$, so that

$$\boxed{\xi_\perp^\mu \zeta_\mu^\perp = \xi^\mu \zeta_\mu.} \tag{2.22}$$

Therefore, the scalar product $\xi_\perp^\mu \zeta_\mu^\perp$ does not depend on $\boldsymbol{u}$, and so do the lengths ℓ_{12}, ℓ_{13} (the above rationale can be done with $\boldsymbol{\xi} = \boldsymbol{\zeta}$), and the angle ϑ. We conclude that *the morphology of an infinitesimal light beam is an intrinsic property, neither its size nor its shape depend on the frame in which they are measured.* Let us emphasize that this property is valid for measurements of lengths and angles on a screen by an experimentalist located at a point where the beam has a nonzero extension. It does *not* apply to the observer situated at O, where the beam converges. In particular, the relativistic aberration effects that will be discussed in § 3.2.3 are precisely due to the fact that angles measured by an observer at O depend on its four-velocity.

The Sachs basis

For the purpose of characterising the morphology of a beam, it is convenient to introduce an orthonormal basis $(\boldsymbol{s}_A)_{A=1,2}$ for the screen. By definition, its vectors must satisfy

$$s_A^\mu u_\mu = s_A^\mu d_\mu = 0, \qquad s_A^\mu s_{B\mu} = \delta_{AB}, \tag{2.23}$$

which also implies $s_A^\mu k_\mu = 0$ since $k^\mu = \omega(u^\mu + d^\mu)$. The screen projector is naturally decomposed in terms of this basis as

$$S^{\mu\nu} = \delta^{AB} s_A^\mu s_B^\nu. \tag{2.24}$$

Suppose that a family of observers, lying all along the beam and thus defining a four-velocity field $\boldsymbol{u}(v)$, want to compare the patterns they observe on their respective

screen. Each of them can define a basis $(\boldsymbol{s}_A)_{A=1,2}(v)$ according to the requirements (2.23), but these requirements do not specify any orientation—the bases of two different observers could be arbitrarily rotated with respect to each other.

In order for the orientation of the patterns on the screens to be tractable, the screen vectors $\boldsymbol{s}_A(v)$ should be parallely transported along the beam. However, just like for polarisation (§ 1.3.3), a complete parallel transportation is forbidden if $\boldsymbol{u}(v)$ is not, because $\boldsymbol{s}_A$ and $\boldsymbol{u}$ must keep orthogonal to each other. The solution is again a partial parallel transportation, in the sense of

$$S^\mu_\nu \frac{\mathrm{D}s^\nu_A}{\mathrm{d}v} = 0. \tag{2.25}$$

Vector $\dot{\boldsymbol{s}}_A$, where a dot denotes the covariant derivative $\mathrm{D}/\mathrm{d}v$, can thus be decomposed as $\dot{\boldsymbol{s}}_A = \alpha\boldsymbol{u} + \beta\boldsymbol{d}$. Furthermore, since $k_\mu s^\mu_A = 0$ and $\dot{\boldsymbol{k}} = \boldsymbol{0}$ (geodesic equation), we also have $k_\mu \dot{s}^\mu_A = 0$, which implies $\alpha = \beta$; in other words,

$$\dot{\boldsymbol{s}}_A \propto \boldsymbol{k}. \tag{2.26}$$

The above relation, together with $\dot{\boldsymbol{k}} = \boldsymbol{0}$, then implies that any nth-order covariant derivative of $\boldsymbol{s}_A$ along $\boldsymbol{k}$ is parallel to $\boldsymbol{k}$.

In many references on gravitational lensing theory (e.g. Refs. [17, 23]), the authors take advantage of observer independence of the beam's morphology and assume, without loss of generality, that $\boldsymbol{u}(v)$ is actually parallely transported along the beam, hence so are the $\boldsymbol{s}_A(v)$. With this additional requirement, $(\boldsymbol{s}_1, \boldsymbol{s}_2)$ is called the *Sachs basis*. We choose here not to make this assumption and work with a generic $\boldsymbol{u}(v)$ field. We will however use the same terminology for simplicity.

An advantage of our choice is that our Sachs basis enjoys a simple physical interpretation. The transportation law (2.25) is indeed reminiscent of the electric polarisation vector $\boldsymbol{\epsilon}$ defined in § 1.3.3, and we can make the following identification:

$$\boldsymbol{s}_1 = \boldsymbol{\epsilon}, \qquad \boldsymbol{s}_2 = \boldsymbol{\beta}, \tag{2.27}$$

where $\boldsymbol{\beta}$ is the magnetic analog of $\boldsymbol{\epsilon}$; the Sachs vectors then indicate the directions of oscillation of the electric and magnetic fields of a given photon within the beam. Of course, any global isometry between $(\boldsymbol{s}_1, \boldsymbol{s}_2)$ and $(\boldsymbol{\epsilon}, \boldsymbol{\beta})$ is allowed as well. Note also that the identification (2.27) does not hold if other physical phenomena besides gravitation affect polarisation, such as optically active matter or Faraday rotation in the presence of strong background magnetic fields.

2.1.3 Propagation in screen space

We now want to investigate the consequences of the geodesic deviation equation (2.17) on the evolution, with v, of the beam's morphology. For that purpose, it is natural to focus on the components of $\boldsymbol{\xi}$ on the Sachs basis, defined by

$$\xi_A \equiv s^\mu_A \xi_\mu = s^\mu_A \xi^\perp_\mu, \tag{2.28}$$

and therefore such that

$$\boldsymbol{\xi}_\perp = \xi^A \boldsymbol{s}_A. \tag{2.29}$$

Note that the position of indices $A, B, C \ldots$ does not matter (here $\xi^A = \xi_A$) as they are raised and lowered by δ_{AB}.

The Sachs vector equation

An evolution equation for ξ_A, directly inherited from the geodesic deviation equation, can be derived the following way. We first decompose its second derivative with respect to v thanks to the Leibnitz rule,

$$\ddot{\xi}_A = \ddot{\xi}_\mu s_A^\mu + 2\dot{\xi}_\mu \dot{s}_A^\mu + \xi_\mu \ddot{s}_A^\mu, \tag{2.30}$$

where, again, a dot denotes a covariant derivative $\mathrm{D}/\mathrm{d}v$. We have seen in the previous paragraph that both $\dot{s}_A$ and $\ddot{s}_A$ are parallel to k; the orthogonality of k and ξ then implies that the last two terms in the right-hand side of Eq. (2.30) vanish identically. Inserting Eq. (2.17) in the first one therefore leads to

$$\ddot{\xi}_A = R_{\mu\nu\rho\sigma} s_A^\mu k^\nu k^\rho \xi^\sigma. \tag{2.31}$$

Finally, using $\xi^\sigma = \xi_\perp^\sigma + (\xi^\nu u_\nu/\omega)k^\sigma$, and the antisymmetry of the Riemann tensor under $\rho \leftrightarrow \sigma$, we obtain the *Sachs vector equation*

$$\boxed{\frac{\mathrm{d}^2\xi^A}{\mathrm{d}v^2} = \mathcal{R}_B^A \xi^B,} \tag{2.32}$$

in which the left-hand side involves a simple (not covariant) derivative, because ξ_A is actually a scalar, and where we introduced the *optical tidal matrix*

$$\mathcal{R}_{AB} \equiv R_{\mu\nu\rho\sigma} s_A^\mu k^\nu k^\rho s_B^\sigma. \tag{2.33}$$

Because the Riemann tensor is invariant under the exchange of the first pair of indices with second one, the optical tidal matrix is *symmetric* $\mathcal{R}_{AB} = \mathcal{R}_{BA}$, which justifies a posteriori the notation $\mathcal{R}_B^A$ in Eq. (2.32).

Ricci and Weyl lensing

As any 2×2 matrix, $\mathcal{R}$ can be decomposed into a pure-trace part and a trace-free part. This decomposition turns out to fit very well with the decomposition of the Riemann tensor as

$$R_{\mu\nu\rho\sigma} = R_{\mu[\rho}g_{\sigma]\nu} - R_{\nu[\rho}g_{\sigma]\mu} - \frac{1}{3}R\, g_{\mu[\rho}g_{\sigma]\nu} + C_{\mu\nu\rho\sigma}, \tag{2.34}$$

where $C_{\mu\nu\rho\sigma}$ denotes the Weyl (or conformal curvature) tensor; it has the same symmetries as the Riemann tensor, and it is trace free, in the sense that $C^\mu{}_{\nu\mu\sigma} = 0$. Inserting this decomposition in the definition (2.33), and using the orthogonality relations involving k^μ, s_A^μ, we get

$$\mathcal{R}_{AB} = -\frac{1}{2}R_{\mu\nu}k^\mu k^\nu\, \delta_{AB} + C_{\mu\nu\rho\sigma} s_A^\mu k^\nu k^\rho s_B^\sigma, \tag{2.35}$$

whose last term is a trace-free matrix, indeed

$$\delta^{AB}C_{\mu\nu\rho\sigma} s_A^\mu k^\nu k^\rho s_B^\sigma = C_{\mu\nu\rho\sigma}k^\nu k^\rho S^{\mu\sigma} \tag{2.36}$$

$$= C_{\mu\nu\rho\sigma}k^\nu k^\rho(u^\mu u^\sigma - d^\mu d^\sigma) \tag{2.37}$$

$$= \omega^2(C_{\mu\nu\rho\sigma}d^\nu d^\rho u^\mu u^\sigma - C_{\mu\nu\rho\sigma}u^\nu u^\rho d^\mu d^\sigma) \tag{2.38}$$

$$= 0, \tag{2.39}$$

where we used that the Weyl tensor is trace free in the second line, and its symmetries in the third and fourth lines.

The optical tidal matrix therefore takes the simple form

$$\boldsymbol{\mathcal{R}} = \begin{pmatrix} \mathscr{R} & 0 \\ 0 & \mathscr{R} \end{pmatrix} + \begin{pmatrix} -\mathrm{Re}\,\mathscr{W} & \mathrm{Im}\,\mathscr{W} \\ \mathrm{Im}\,\mathscr{W} & \mathrm{Re}\,\mathscr{W} \end{pmatrix} \tag{2.40}$$

which involves the Ricci lensing and Weyl lensing scalars, respectively defined by

$$\mathscr{R} \equiv -\frac{1}{2} R_{\mu\nu} k^\mu k^\nu, \tag{2.41}$$

$$\mathscr{W} \equiv -\frac{1}{2} C_{\mu\nu\rho\sigma} (s_1^\mu - \mathrm{i} s_2^\mu) k^\nu k^\rho (s_1^\sigma - \mathrm{i} s_2^\sigma). \tag{2.42}$$

Physical interpretation

The decomposition (2.40) of $\boldsymbol{\mathcal{R}}$ is useful to qualitatively understand the physics of gravitational lensing. It is indeed clear that Ricci and Weyl curvatures affect the beam's geometry in different ways:

- Suppose that only $\mathscr{R}$ is at work, then the separation ξ_A between any two light spots on a screen evolves as $\ddot{\xi}_A = \mathscr{R}\xi_A$ as the beam propagates. Ricci lensing thus induces a *homothetic transformation* of the beam's pattern.

- The Weyl lensing matrix, on the contrary, has two different eigenvalues $\mp|\mathscr{W}|$, whose eigendirections are respectively rotated by β and $\beta + \pi/2$, with $\mathscr{W} = |\mathscr{W}|\mathrm{e}^{-2\mathrm{i}\beta}$, with respect to the Sachs basis. The separation vectors $\xi_A^\pm$ aligned with those directions thus evolve as $\ddot{\xi}_A^\pm = \pm|\mathscr{W}|\xi_A^\pm$, so that the beam's shape gets elongated in the first direction and contracted in the second one. Weyl lensing thus tends to *shear* light beams.

Ricci and Weyl curvatures have distinct physical origins. On the one hand, the Ricci tensor is directly to matter's *local* density of energy and momentum via the Einstein equation $R_{\mu\nu} - Rg_{\mu\nu}/2 + \Lambda g_{\mu\nu} = 8\pi G T_{\mu\nu}$, which implies

$$\mathscr{R} = -4\pi G T_{\mu\nu} k^\mu k^\nu \leq 0 \tag{2.43}$$

under the null energy condition. In the case of a perfect fluid with rest-frame energy density ρ and pressure p, the stress-energy tensor reads $T_{\mu\nu} = (\rho + p)u_\mu u_\nu + pg_{\mu\nu}$, and the above relation becomes simply $\mathscr{R} = -4\pi G(\rho + p)\omega^2$. *Ricci lensing thus tells us how a light beam is focused by the matter it encloses.* Note by the way that the cosmological constant does not have any focusing effect, like any other form of matter equivalent to a perfect fluid with $p = -\rho$.

The Weyl tensor, on the other hand, describes the *nonlocal* effects of gravity. The simplest examples are the tidal forces created around a massive body, but gravitational waves or frame dragging are also gravitational phenomena encoded in the Weyl tensor. Hence, unlike Ricci lensing, *Weyl lensing is mostly due to matter lying outside the beam.* This fits quite well with our Newtonian intuition: a mass inside the beam attracts all the rays towards it, generating convergence, while a mass outside shears it by tidal effects.

Self focusing

Let us close this section by a remark on the potential ability of light beams to focus themselves. As mentioned in § 1.1.2, light indeed possesses energy and momentum, whose

contribution to Ricci focusing reads

$$\mathscr{R}_{\text{self}} \equiv -4\pi G\, T_{\mu\nu}^{\text{beam}} k^\mu k^\nu = -16\pi G I \omega^2, \tag{2.44}$$

where I is the luminous intensity (power per unit area) of the beam, also equal to its energy density ρ_{beam}. This quantity is not a constant during light propagation, the energy being diluted over the growing wavefront and redshifted. If the light source has an absolute luminosity (power) L, the observed intensity goes like $I = L/(4\pi D_{\text{L}}^2)$, where D_{L} denotes the *luminosity distance* from the source to the observer—see Chap. 3 for more details about distances in curved spacetime.

The amplitude of self focusing can be evaluated by comparing it to the cosmic Ricci focusing $\mathscr{R}_{\text{cosm}} \equiv -4\pi G\rho_{\text{m}}\omega^2$, associated with the mean matter density $\rho_{\text{m}} = 2.8 \times 10^{-27}(1+z)^3 \,\text{kg/m}^3$ in the Universe. We get

$$\frac{\mathscr{R}_{\text{self}}}{\mathscr{R}_{\text{cosm}}} = \frac{1.7 \times 10^{-6}}{(1+z)^3} \frac{L}{L_\odot} \left(\frac{1\,\text{pc}}{D_{\text{L}}}\right)^2, \tag{2.45}$$

where $L_\odot = 3.8 \times 10^{26}\,\text{W}$ is the solar luminosity. For stellar sources, this is therefore a very small number; but for much brighter sources such as quasars, with a typical luminosity of $L \sim 10^{40}\,\text{W} \sim 10^{14} L_\odot$, self focusing turns out to dominate over cosmic focusing as far as $D_{\text{L}} < 10\,\text{kpc}$. This effect makes very luminous sources appear even brighter than they already are.

2.2 The Jacobi matrix

The comparison between the physical morphology of a source and how it appears to an observer is the heart of gravitational lensing experiments. The Jacobi matrix, which we introduce in this section, precisely contains this information.

2.2.1 Definition and interpretation

Wronski matrix

The Sachs vector equation (2.32) is a second-order *linear* differential equation, which satisfies the Cauchy-Lipshitz conditions if we assume that $\mathcal{R}_{AB}(v)$ is smooth. Hence there is a linear one-to-one and onto relation between any solution of Eq. (2.32) and its initial conditions; in other words, there exists a 4×4 invertible matrix $\boldsymbol{\mathcal{W}}$ such that

$$\begin{pmatrix} \xi_1 \\ \xi_2 \\ \dot{\xi}_1 \\ \dot{\xi}_2 \end{pmatrix}(v_2) = \boldsymbol{\mathcal{W}}(v_2 \leftarrow v_1) \begin{pmatrix} \xi_1 \\ \xi_2 \\ \dot{\xi}_1 \\ \dot{\xi}_2 \end{pmatrix}(v_1). \tag{2.46}$$

We shall call $\boldsymbol{\mathcal{W}}$ the *Wronski matrix* of the Sachs equation[1]. The notation $v_2 \leftarrow v_1$, which indicates that Eq. (2.32) is integrated from v_1 to v_2, is useful for expressing the elementary

---

[1] In a mathematically rigorous way, $\boldsymbol{\mathcal{W}}(v \leftarrow v_0)$ is the Wronski matrix associated with a fundamental system of solutions $(\boldsymbol{M}_1, \boldsymbol{M}_2)$ of the matrix equation $\ddot{\boldsymbol{M}} = \boldsymbol{\mathcal{R}}\boldsymbol{M}$, with initial conditions $\boldsymbol{M}_1(v_0) = \dot{\boldsymbol{M}}_2(v_0) = \mathbf{1}_2$ and $\dot{\boldsymbol{M}}_1(v_0) = \boldsymbol{M}_2(v_0) = \mathbf{0}_2$

properties of $\boldsymbol{W}$ implied by its very definition, namely

$$\boldsymbol{W}(v_3 \leftarrow v_1) = \boldsymbol{W}(v_3 \leftarrow v_2)\boldsymbol{W}(v_2 \leftarrow v_1), \tag{2.47}$$

$$\boldsymbol{W}(v_2 \leftarrow v_1) = [\boldsymbol{W}(v_1 \leftarrow v_2)]^{-1}. \tag{2.48}$$

Its propagation equation, inherited from Eq. (2.32), reads

$$\frac{\partial}{\partial v_2}\boldsymbol{W}(v_2 \leftarrow v_1) = \begin{pmatrix} \boldsymbol{0}_2 & \boldsymbol{1}_2 \\ \boldsymbol{\mathcal{R}}(v_2) & \boldsymbol{0}_2 \end{pmatrix}\boldsymbol{W}(v_2 \leftarrow v_1), \tag{2.49}$$

with initial condition $\boldsymbol{W}(v_1 \leftarrow v_1) = \boldsymbol{1}_4$, and where $\boldsymbol{0}_n$, $\boldsymbol{1}_n$ respectively denote the $n \times n$ zero and unity matrices. This Cauchy problem is formally solved by

$$\boldsymbol{W}(v_2 \leftarrow v_1) = \mathrm{Vexp}\int_{v_1}^{v_2} \begin{pmatrix} \boldsymbol{0}_2 & \boldsymbol{1}_2 \\ \boldsymbol{\mathcal{R}}(v) & \boldsymbol{0}_2 \end{pmatrix}\mathrm{d}v, \tag{2.50}$$

where Vexp is the affine-parameter ordered exponential defined, for any matrix-valued function $\boldsymbol{M}(v)$, by

$$\mathrm{Vexp}\int_{v_1}^{v_2} \boldsymbol{M}(v)\mathrm{d}v \equiv \sum_{n=0}^{\infty} \int_{v_1}^{v_2} \mathrm{d}w_1 \int_{v_0}^{w_1} \mathrm{d}w_2 \ldots \int_{v_0}^{w_{n-1}} \mathrm{d}w_n \; \boldsymbol{M}(w_1)\boldsymbol{M}(w_2)\ldots\boldsymbol{M}(w_n). \tag{2.51}$$

This expression reduces to a regular exponential if, for all v, v', $\boldsymbol{M}(v)$ commutes with $\boldsymbol{M}(v')$. In the case of Eq. (2.50), this occurs if, and only if, $\boldsymbol{\mathcal{R}}(v)$ is a constant.

Because of its "Chasles relation" (2.47), the Wronski matrix is a very convenient tool for solving the Sachs equation (2.32) piecewise, as the junction between various pieces of solution is simply achieved by matrix multiplications. This is indeed the reason why the Wronski matrix was introduced independently by Ref. [24] (not under this name) and by the author of this thesis in Ref. [25], in order to deal with light propagation in Swiss-cheese models (see Chap. 6). In most cases, however, only a 2×2 part of $\boldsymbol{W}$ is really useful, as we will see below.

Jacobi matrix

If we choose the initial conditions for the integration of the Sachs equation to be a vertex point of the light beam (here the observation event O), then by definition $\xi_A(v_O) = 0$, and Eq. (2.46) indicates that $\xi_A(v \neq v_O)$ is related to $\dot{\xi}_A(v_O)$ as

$$\boxed{\xi^A(v) = \mathcal{D}^A{}_B(v \leftarrow v_O)\frac{\mathrm{d}\xi^B}{\mathrm{d}v}(v_O),} \tag{2.52}$$

where $\boldsymbol{\mathcal{D}}(v \leftarrow v_O)$ is the 2×2 top-right block of $\boldsymbol{W}(v \leftarrow v_O)$; it is called *Jacobi matrix* for reasons that shall become clearer below.

In § 1.3.1 of the previous chapter, we have seen that an increase $\mathrm{d}v$ of the affine parameter corresponds, in the rest frame of arbitrary observer, to a displacement $\mathrm{d}\ell/\omega$ of the photon. It follows, as depicted in Fig. 2.3, that the derivative $\dot{\xi}^B(v_O)$ involved in the definition (2.52) of $\boldsymbol{\mathcal{D}}$ reads

$$\frac{\mathrm{d}\xi^B}{\mathrm{d}v}\bigg|_O = \omega_O \frac{\mathrm{d}\xi^B}{\mathrm{d}\ell}\bigg|_O = -\omega_O\theta_O^B, \tag{2.53}$$
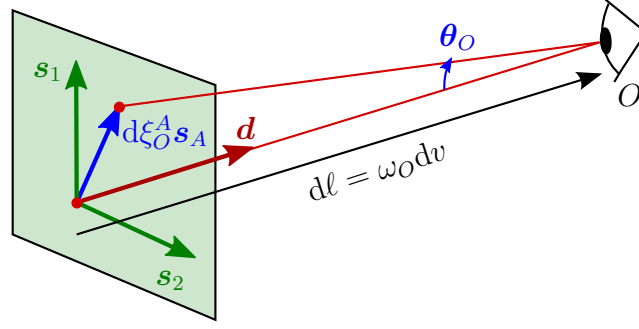
Figure 2.3 The vector $\dot{\xi}_O^A \boldsymbol{s}_A$ at O is directly proportional to the observed angular separation $\boldsymbol{\theta}_O = \theta_O^A \boldsymbol{s}_A$ between the rays, since $\theta^A = \mathrm{d}\xi^A/\mathrm{d}\ell$.

where $\theta_O^B \ll 1$ denotes the angular separation, on the observer's celestial sphere, between the two images associated with two rays separated by $\boldsymbol{\xi}$. The minus sign on the right-hand side is due to the fact that k^μ is future oriented, so that $\mathrm{d}\ell$ is positive for a displacement towards the future, whereas θ_O^B is more naturally defined from a past-oriented displacement.

In light of the identification (2.53), the matrix $\boldsymbol{\mathcal{D}}(S \leftarrow O)$ corresponding to the integration of the Sachs equation from the observation event O to the source event S can be written as

$$\mathcal{D}^A{}_B(S \leftarrow O) = -\frac{1}{\omega_O} \frac{\partial \xi_S^A}{\partial \theta_O^B}. \tag{2.54}$$

We conclude that, modulo the normalisation factor $-1/\omega_O$, $\boldsymbol{\mathcal{D}}(S \leftarrow O)$ indeed represents the Jacobi matrix of the map $\{\theta_O^A\} \mapsto \{\xi_S^A\}$, which relates the positions of images on the observer's celestial sphere to the physical separations of the associated sources. As such, $\boldsymbol{\mathcal{D}}(S \leftarrow O)$ encodes all the gravitational distortions of the image of a very small light source.

2.2.2 Decompositions

General case

The Jacobi matrix $\boldsymbol{\mathcal{D}}(S \leftarrow O)$ can be decomposed in a way that emphasize the geometrical transformations between the observed image and the actual source—whose intrinsic morphology cannot be observed. First note that its determinant is, still modulo a frequency factor, the Jacobian of $\{\theta_O^A\} \mapsto \{\xi_S^A\}$, that is, the ratio between the physical area of the source A_S and its apparent angular size (observed solid angle) Ω_O, both assumed to be infinitesimal quantities. In other words,

$$\det(\omega_O \boldsymbol{\mathcal{D}}) = \frac{A_S}{\Omega_O} \equiv D_{\mathrm{A}}^2, \tag{2.55}$$

where we anticipated on Chap. 3, § 3.2.3 identifying the above ratio with the square of the angular diameter distance D_{A} between the source and the observer.

As any 2×2 matrix, $\boldsymbol{\mathcal{D}}/\sqrt{\det \boldsymbol{\mathcal{D}}}$ can be written as the product $\boldsymbol{RS}$ of a rotation matrix $\boldsymbol{R}$ and a symmetric matrix $\boldsymbol{S}$. Moreover, since its determinant is unity, we can write $\boldsymbol{S}$ as the exponential of traceless symmetric matrix. The resulting decomposition of the Jacobi matrix thus reads

$$\boldsymbol{\mathcal{D}} = -\frac{D_{\mathrm{A}}}{\omega_O} \begin{pmatrix} \cos\psi & -\sin\psi \\ \sin\psi & \cos\psi \end{pmatrix} \exp \begin{pmatrix} -\gamma_1 & \gamma_2 \\ \gamma_2 & \gamma_1 \end{pmatrix}. \tag{2.56}$$

A further step consists in diagonalising the exponential matrix; it is convenient for that purpose to define $\gamma \geq 0$ and φ such that $\gamma_1 + \mathrm{i}\gamma_2 = \gamma \mathrm{e}^{-2\mathrm{i}\varphi}$, leading to

$$\exp \begin{pmatrix} -\gamma_1 & \gamma_2 \\ \gamma_2 & \gamma_1 \end{pmatrix} = \begin{pmatrix} \cos\varphi & -\sin\varphi \\ \sin\varphi & \cos\varphi \end{pmatrix} \begin{pmatrix} \mathrm{e}^{-\gamma} & 0 \\ 0 & \mathrm{e}^{\gamma} \end{pmatrix} \begin{pmatrix} \cos\varphi & \sin\varphi \\ -\sin\varphi & \cos\varphi \end{pmatrix}. \tag{2.57}$$

The various quantities involved in the above decomposition must be interpreted the following way (see Fig. 2.4). Starting from an observed image, the intrinsic properties of the source are reconstructed by successively:

1. contracting and expanding the image by factors $\mathrm{e}^{-\gamma}$ and e^{γ}, respectively, in the directions

$$\boldsymbol{s}_- \equiv \cos\varphi \boldsymbol{s}_1 + \sin\varphi \boldsymbol{s}_2, \tag{2.58}$$

$$\boldsymbol{s}_+ \equiv -\sin\varphi \boldsymbol{s}_1 + \cos\varphi \boldsymbol{s}_2, \tag{2.59}$$

this *shear* operation preserves the area of the image;

2. rotating anticlockwise the result by the angle ψ;

3. translating angles into physical distances by multiplying them with D_{A}.

The changes of orientation of the image with respect to its source—induced by shear (2.) and rotation (3.)—are a priori not measurable, because it is a priori impossible to know what is the intrinsic orientation of the source. Nevertheless, for a source of polarised light, whose shape is aligned with the direction of polarisation (e.g. in quasar jets), such effects can become observable because they generically break the alignment between polarisation—materialised by the Sachs basis—and the image's shape.

Perturbative case

In a number of practical situations, the lensing effects encoded in the Jacobi matrix result from small perturbations of the spacetime geometry, with respect to a background which generates no shear nor rotation of images (Friedmann-Lemaître or Minkowski), i.e. for which $\overline{\boldsymbol{\mathcal{D}}} = -\bar{D}_{\mathrm{A}}/\omega_O \mathbf{1}_2$. In such cases, the general decomposition (2.56) can be expanded at order 1 in the deformation scalars $\gamma_1, \gamma_2, \psi \ll 1$, and in the *convergence*

$$\kappa \equiv \frac{\bar{D}_{\mathrm{A}} - D_{\mathrm{A}}}{\bar{D}_{\mathrm{A}}} \ll 1, \tag{2.60}$$

under the form

$$\boldsymbol{\mathcal{D}} = \boldsymbol{\mathcal{A}}\overline{\boldsymbol{\mathcal{D}}} + \ldots, \tag{2.61}$$

where the *amplification* (or *magnification*) matrix reads

$$\boldsymbol{\mathcal{A}} \equiv \begin{pmatrix} 1 - \kappa - \gamma_1 & \gamma_2 - \psi \\ \gamma_2 + \psi & 1 - \kappa + \gamma_1 \end{pmatrix}. \tag{2.62}$$

In fact, we will see in § 2.3.2 that if $\gamma \ll 1$, then $\psi \sim \gamma^2$ and can thus be neglected in the above first-order expansion. This is the reason why the amplification matrix is usually considered symmetric in the weak-lensing literature [17, 26].

In principle, it is possible to use a decomposition of the form (2.62) even for finite deformations, but the quantities $\kappa, \gamma, \psi \sim 1$ then differ from the ones defined in Eqs. (2.56),
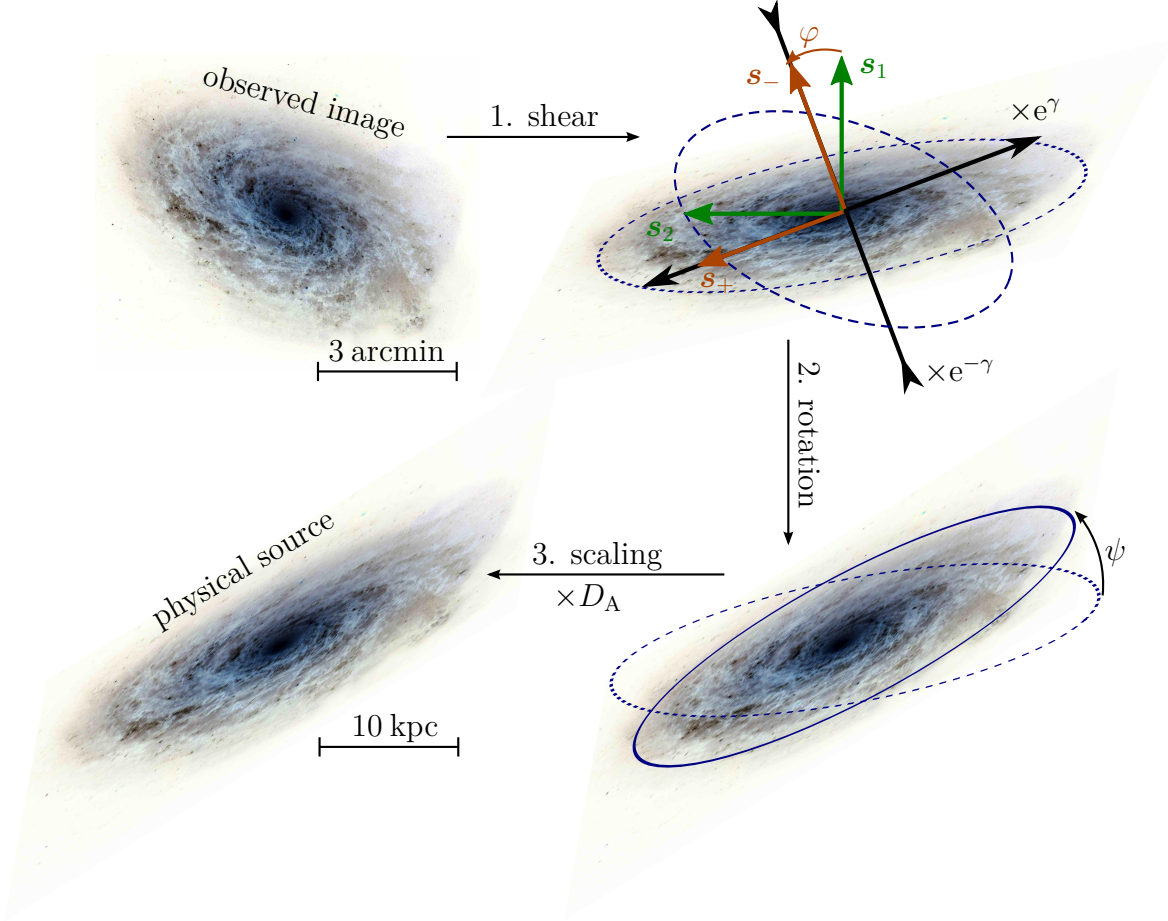
Figure 2.4 Transformations of an image due to gravitational lensing, as encoded in the decomposition (2.56) of the Jacobi matrix. In this example, the angular distance between the source galaxy and the observer is $D_{\mathrm{A}} = 10\,\mathrm{kpc}/3\,\mathrm{arcmin} \approx 1\,\mathrm{Mpc}$.

(2.60), and thus lose their geometrical meaning. For instance, the relative correction to the angular distance is, in that case, no longer equal to the convergence, but rather to

$$\frac{\bar{D}_{\mathrm{A}} - D_{\mathrm{A}}}{\bar{D}_{\mathrm{A}}} = 1 - \frac{1}{\sqrt{\mu}}, \tag{2.63}$$

where the *magnification* μ reads

$$\mu \equiv \frac{1}{\det \boldsymbol{\mathcal{A}}} = \frac{1}{(1-\kappa)^2 - \gamma^2 + \psi^2}. \tag{2.64}$$

Note by the way that the conventional name "magnification matrix" for $\boldsymbol{\mathcal{A}}$ is somewhat misleading, and would be more adapted to $\boldsymbol{\mathcal{A}}^{-1}$. It is precisely this loss of geometrical interpretation for the commonly used κ, γ, ψ which led the author of this thesis to propose the more generally sensitive decomposition (2.56).

Let us finally mention that a perturbative expansion of the form (2.61) can also be performed with respect to a background with nonzero shear and rotation—e.g. for weak lensing in a perturbed Bianchi I universe [27, 28]—but the expression (2.62) of $\boldsymbol{\mathcal{A}}$ needs to be slightly adapted to account for it.

2.2.3   Evolution

Formally, the evolution of the Jacobi matrix with v is entirely determined by simply extracting the 2×2 top-right block of the Wronski matrix given by Eq. (2.50). However, affine-parameter ordered exponentials are not particularly easy to handle, and thus of limited interest for practical calculations.

Jacobi matrix equation

An evolution equation for $\boldsymbol{D}$ only is directly obtained by taking the second derivative of its definition (2.52) and inserting the Sachs equation (2.32), which yields

$$\boxed{\frac{\partial^2}{\partial v^2}\boldsymbol{D}(v \leftarrow v_O) = \boldsymbol{R}(v)\boldsymbol{D}(v \leftarrow v_O),}$$
(2.65)

that we will refer to as the *Jacobi matrix equation*, and abridge as $\ddot{\boldsymbol{D}} = \boldsymbol{R}\boldsymbol{D}$, where it is understood that a dot stands for a derivative with respect to the *final* affine parameter v of $\boldsymbol{D}(v \leftarrow v_O)$.

The initial conditions ($v = v_O$) for the differential equation (2.65) derive from the very definition (2.52) of the Jacobi matrix, and read

$$\boldsymbol{D}(v_O \leftarrow v_O) = \boldsymbol{0}_2,$$
(2.66)

$$\dot{\boldsymbol{D}}(v_O \leftarrow v_O) = \boldsymbol{1}_2.$$
(2.67)

The set of Eqs. (2.65), (2.66), and (2.67) thus completely characterises the evolution of the Jacobi matrix with v.

Etherington's reciprocity law

We have seen in Eq. (2.48) that the Wronski matrix enjoys a simple reciprocity law: inverting the initial and final conditions simply turns $\boldsymbol{W}$ into its inverse. There exist a similar relation for the Jacobi matrix, known as Etherington's reciprocity law [29], but contrary to the former, the latter does not trivially follow from a definition: it relies on the specific equation (2.65) governing the evolution of $\boldsymbol{D}$.

Following Refs. [23, 30], we consider two solutions $v \mapsto \boldsymbol{D}(v \leftarrow v_1)$ and $v \mapsto \boldsymbol{D}(v \leftarrow v_2)$ of the Jacobi matrix equation, and define

$$\boldsymbol{C}(v) \equiv \dot{\boldsymbol{D}}^{\mathrm{T}}(v \leftarrow v_1)\boldsymbol{D}(v \leftarrow v_2) - \boldsymbol{D}^{\mathrm{T}}(v \leftarrow v_1)\dot{\boldsymbol{D}}(v \leftarrow v_2),$$
(2.68)

where $^{\mathrm{T}}$ denotes matrix transposition. The symmetry of the optical tidal matrix $\boldsymbol{R}^{\mathrm{T}} = \boldsymbol{R}$ implies that $\boldsymbol{C}$ *is a constant*; in particular, $\boldsymbol{C}(v_1) = \boldsymbol{C}(v_2)$ implies

$$\boxed{\boldsymbol{D}(v_1 \leftarrow v_2) = -\boldsymbol{D}^{\mathrm{T}}(v_2 \leftarrow v_1)}$$
(2.69)

by virtue of Eqs. (2.66), (2.67). A particular consequence of the above relation is that inverting v_1 and v_2 leaves the determinant of the Jacobi matrix unchanged:

$$\det \boldsymbol{D}(v_1 \leftarrow v_2) = \det \boldsymbol{D}(v_2 \leftarrow v_1),$$
(2.70)

which will allow us to derive the duality relation between the angular and luminosity distances in Chap. 3.

2.3 The optical scalars

The propagation equations for light beams can be reformulated in terms of their deformation rates, also known as the optical scalars. This formulation has the advantage of exhibiting even more clearly the respective roles of Ricci or Weyl curvatures, and allows one to derive the so-called focusing theorem.

2.3.1 Definitions

From the Jacobi matrix

Since the deformations of a light beam are described by the Jacobi matrix, the associated deformation *rates* are naturally defined by its logarithmic derivative with respect to the affine parameter; we thus introduce the *deformation rate matrix*

$$\boxed{\boldsymbol{\mathcal{S}} \equiv \dot{\boldsymbol{\mathcal{D}}}\boldsymbol{\mathcal{D}}^{-1}} \qquad \text{i.e.} \qquad \mathcal{S}^A{}_B \equiv \frac{\partial \dot{\xi}^A}{\partial \xi^B}. \tag{2.71}$$

The conservation law (2.68) applied for $v_1 = v_2$ (hence $\boldsymbol{C} = \boldsymbol{0}_2$) reads

$$\boldsymbol{0}_2 = \boldsymbol{\mathcal{D}}^{\mathrm{T}}\boldsymbol{\mathcal{S}}^{\mathrm{T}}\boldsymbol{\mathcal{D}} - \boldsymbol{\mathcal{D}}^{\mathrm{T}}\boldsymbol{\mathcal{S}}\boldsymbol{\mathcal{D}} \tag{2.72}$$

which, if we assume $\det \boldsymbol{\mathcal{D}} \neq 0$, implies that $\boldsymbol{\mathcal{S}}$ *is a symmetric matrix.*

Decomposing $\boldsymbol{\mathcal{S}}$ into its pure-trace and trace-free parts then yields

$$\boldsymbol{\mathcal{S}} = \begin{pmatrix} \theta & 0 \\ 0 & \theta \end{pmatrix} + \begin{pmatrix} -\sigma_1 & \sigma_2 \\ \sigma_2 & \sigma_1 \end{pmatrix}, \tag{2.73}$$

where θ and $\sigma \equiv \sigma_1 + \mathrm{i}\sigma_2$ are the *optical scalars*; they are called respectively the beam's expansion rate and shear rate, for reasons that shall become clearer in § 2.3.2. Note that, despite its notation, this θ must not be confused with an angle, both θ and σ have the dimension of $[v]^{-1}$.

From the gradient of the wave four-vector

Alternatively, one can define the deformation rate matrix $\boldsymbol{\mathcal{S}}$, and thus the optical scalars θ, σ, via

$$\boxed{\mathcal{S}_{AB} = s_A^\mu s_B^\nu \nabla_\mu k_\nu.} \tag{2.74}$$

Let us show that this definition is indeed equivalent to the previous one (2.71),

$$\dot{\xi}_A \equiv k^\mu \nabla_\mu (s_A^\nu \xi_\nu) \tag{2.75}$$

$$= s_A^\nu k^\mu \nabla_\mu \xi_\nu \qquad \text{since } \dot{s}_A^\mu \propto k^\mu \perp s_A^\mu \tag{2.76}$$

$$= s_A^\nu \xi^\mu \nabla_\mu k_\nu \qquad \text{because of Eq. (2.11)} \tag{2.77}$$

$$= s_A^\nu \xi_\perp^\mu \nabla_\mu k_\nu \qquad \text{as } k^\mu \nabla_\mu k_\nu = 0 \tag{2.78}$$

$$= s_A^\nu \xi^B s_B^\mu \nabla_\mu k_\nu, \tag{2.79}$$

whose derivative with respect to ξ^B indeed leads to the expression (2.74), modulo an inversion of the indices $\mu \leftrightarrow \nu$, which is allowed since $\nabla_\mu k_\nu$ is a symmetric tensor. This property, which comes from the fact that k_μ is the gradient of the wave's phase, is an alternative proof for the symmetry of $\boldsymbol{\mathcal{S}}$.

More generally, the tensor $\nabla_\mu k_\nu$ can be decomposed over the four-dimensional orthonormal basis $(u^\mu, d^\mu, s_1^\mu, s_2^\mu)$ according to

$$\nabla_\mu k_\nu = \mathcal{S}_{AB} s_\mu^A s_\nu^B - 2\omega^{-1} S_{(\mu}^\rho k_{\nu)} u^\sigma \nabla_\rho k_\sigma + \omega^{-2} k_\mu k_\nu u^\rho u^\sigma \nabla_\rho k_\sigma, \tag{2.80}$$

which can be derived starting from $\nabla_\mu k_\nu = \delta_\mu^\rho \delta_\nu^\sigma \nabla_\rho k_\sigma$, with $\delta_\mu^\rho = S_\mu^\rho + d_\mu d^\rho - u_\mu u^\rho$, and using $k^\mu k_\mu = 0 = k^\nu \nabla_\nu k_\mu$. Taking the trace of Eq. (2.80) then yields

$$\boxed{\nabla_\mu k^\mu = \mathrm{tr}\boldsymbol{\mathcal{S}} = 2\theta,} \tag{2.81}$$

while the trace of its square gives

$$\boxed{(\nabla_\mu k_\nu)(\nabla^\mu k^\nu) = \mathrm{tr}(\boldsymbol{\mathcal{S}}^2) = 2(\theta^2 + |\sigma^2|).} \tag{2.82}$$

The quantities θ and $|\sigma|^2$ are thus fully covariant quantities, which reflects the frame independence of the beam's morphology.

2.3.2   Geometrical interpretation

Expansion rate

The physical cross-sectional area of a light beam is defined as

$$A \equiv \int_{\text{beam}} \mathrm{d}\xi^1 \mathrm{d}\xi^2 = \int_{\text{beam}} \det \boldsymbol{\mathcal{D}} \, \mathrm{d}\dot{\xi}_O^1 \mathrm{d}\dot{\xi}_O^2. \tag{2.83}$$

For an infinitesimal light beam, $\boldsymbol{\mathcal{D}}$ can be considered constant in the above integral, and the evolution rate of A with the affine parameter reads

$$\frac{\dot{A}}{A} = \frac{1}{\det \boldsymbol{\mathcal{D}}} \frac{\mathrm{d}(\det \boldsymbol{\mathcal{D}})}{\mathrm{d}v} = \mathrm{tr}(\dot{\boldsymbol{\mathcal{D}}} \boldsymbol{\mathcal{D}}^{-1}) \equiv \mathrm{tr}\boldsymbol{\mathcal{S}}, \tag{2.84}$$

whence

$$\boxed{\theta = \frac{1}{2A} \frac{\mathrm{d}A}{\mathrm{d}v} = \frac{1}{D_\text{A}} \frac{\mathrm{d}D_\text{A}}{\mathrm{d}v},} \tag{2.85}$$

where we reintroduced the angular diameter distance $D_\text{A} \propto \sqrt{A}$. The quantity 2θ therefore represents the evolution rate of the beam's area.

Shear rate

Consider two light rays separated by $\boldsymbol{\xi}$. The distance ℓ between the associated light spots on the local screen reads

$$\ell^2 \equiv \xi_\perp^\mu \xi_\mu^\perp = \xi^A \xi_A = \mathcal{D}^A{}_B \mathcal{D}_{AC} \, \dot{\xi}_O^B \dot{\xi}_O^C, \tag{2.86}$$

and since $(\mathrm{d}\boldsymbol{\mathcal{D}}^\mathrm{T} \boldsymbol{\mathcal{D}})/\mathrm{d}v = 2\boldsymbol{\mathcal{D}}^\mathrm{T} \boldsymbol{\mathcal{S}} \boldsymbol{\mathcal{D}}$, we conclude that the evolution rate of ℓ reads

$$\frac{1}{\ell} \frac{\mathrm{d}\ell}{\mathrm{d}v} = \frac{\xi^A \mathcal{S}_{AB} \xi^B}{\xi^A \xi_A} = \theta - |\sigma| \cos 2\iota, \tag{2.87}$$

where ι denotes here the angle between (ξ^A) and the eigendirection of $\boldsymbol{S}$ associated with the eigenvalue $\theta - |\sigma|$. The quantity $\dot{\ell}/\ell$ thus belongs to the interval $[\theta - |\sigma|\,, \theta + |\sigma|]$, which gives $|\sigma|$ its geometrical meaning:

$$\boxed{2\,|\sigma| = \left(\frac{1}{\ell}\frac{\mathrm{d}\ell}{\mathrm{d}v}\right)_{\mathrm{max}} - \left(\frac{1}{\ell}\frac{\mathrm{d}\ell}{\mathrm{d}v}\right)_{\mathrm{min}}} \tag{2.88}$$

is the rate of stretching of the light beam. Note by the way the alternative expression for the expansion rate, $2\theta = (\dot{\ell}/\ell)_{\mathrm{max}} + (\dot{\ell}/\ell)_{\mathrm{min}}$.

Relation with the deformation scalars

We have just seen that the expansion rate θ is related to D_{A} via Eq. (2.85). Similarly, there exist relations between the shear rate σ, the net shear γ, its direction φ, and the rotation angle ψ, which can be derived by inserting the decomposition (2.56) of $\boldsymbol{\mathcal{D}}$ in the definition (2.71) of $\boldsymbol{S}$. The result is explicitly

$$\boldsymbol{S} = \frac{\dot{D}_{\mathrm{A}}}{D_{\mathrm{A}}}\begin{pmatrix} 1 & 0 \\ 0 & 1 \end{pmatrix} + (\dot{\psi} + \dot{\varphi})\begin{pmatrix} 0 & -1 \\ 1 & 0 \end{pmatrix} + \dot{\gamma}\begin{pmatrix} -\cos 2(\psi + \varphi) & -\sin 2(\psi + \varphi) \\ -\sin 2(\psi + \varphi) & \cos 2(\psi + \varphi) \end{pmatrix}$$
$$+ \dot{\varphi}\begin{pmatrix} \sin 2(\psi + \varphi)\sinh 2\gamma & \cosh 2\gamma - \cos 2(\psi + \varphi)\sinh 2\gamma \\ -\cosh 2\gamma - \cos 2(\psi + \varphi)\sinh 2\gamma & -\sin 2(\psi + \varphi)\sinh 2\gamma \end{pmatrix}, \tag{2.89}$$

which, after regrouping the trace, trace-free symmetric, and antisymmetric parts, and identifying with Eq. (2.73), indeed confirms Eq. (2.85) and yields

$$\boxed{\begin{aligned} \sigma &= (\dot{\gamma} - \mathrm{i}\dot{\varphi}\sinh 2\gamma)\,\mathrm{e}^{-2\mathrm{i}(\psi + \varphi)}, \\ 0 &= \dot{\psi} - 2\dot{\varphi}\sinh^2 \gamma. \end{aligned}} \tag{2.90} \tag{2.91}$$

An alternative expression for σ can also be derived by combining Eqs. (2.90), (2.91), and reads

$$\sigma = \frac{1}{2\cosh 2\gamma}\frac{\mathrm{d}}{\mathrm{d}v}\left[\mathrm{e}^{-2\mathrm{i}(\psi + \varphi)}\sinh 2\gamma\right]. \tag{2.92}$$

In the weak-lensing case ($\gamma \ll 1$), Eq. (2.91) implies that $\psi \sim \gamma^2$ is a second-order quantity and can be neglected. Besides, Eq. (2.92) becomes

$$\sigma \approx \frac{\mathrm{d}}{\mathrm{d}v}\left(\gamma \mathrm{e}^{-2\mathrm{i}\varphi}\right). \tag{2.93}$$

The geometrical interpretation of Eq. (2.90) is more easily discussed if we introduce the angle α such that $\sigma = |\sigma|\,\mathrm{e}^{-2\mathrm{i}\alpha}$; moving the phase term $\mathrm{e}^{2\mathrm{i}(\psi + \varphi)}$ to the left-hand side of Eq. (2.90) and taking the real and imaginary parts then gives

$$|\sigma|\cos 2(\varphi + \psi - \alpha) = \dot{\gamma}, \tag{2.94}$$
$$|\sigma|\sin 2(\varphi + \psi - \alpha) = -\dot{\varphi}\sinh 2\gamma, \tag{2.95}$$

which tell us how the shear rate works on an already sheared image, depending on their relative orientation. On the one hand, as already illustrated in Fig. 2.4, $\varphi + \psi$ is the angle between $\boldsymbol{s}_1$ (resp. $\boldsymbol{s}_2$) and the direction in which the beam has been effectively contracted (resp. expanded). On the other hand, α is the angle between $\boldsymbol{s}_1$ (resp. $\boldsymbol{s}_2$) along which the beam undergoes minimum (resp. maximum) elongation *rate* $\dot{\ell}/\ell$. The following three situations, depicted in Fig. 2.5 are then easily understood:

1. If $\alpha = \psi + \varphi$, then the stretching described by σ occurs precisely in the same direction along which the beam is already stretched. Its deformation is then amplified, without any change of its orientation: $\dot{\gamma} = |\sigma|$, $\dot{\varphi} = \dot{\psi} = 0$.

2. If $\alpha = \psi + \varphi + \pi/2$, it is the contrary of the above, elongation occurs in the direction for which the beam is contracted, and vice versa. The deformation thus tends to attenuate, $\dot{\gamma} = -|\sigma|$, $\dot{\varphi} = \dot{\psi} = 0$.

3. If $\alpha = \psi + \varphi + \pi/4$, we have an interesting situation for which the shear rate actually generates no distortion of the beam ($\dot{\gamma} = 0$). The pattern displayed on the screen thus conserves its degree of deformation, but the direction in which the latter occurs changes according to $\dot{\varphi} = |\sigma| / \sinh 2\gamma$. It also undergoes a global rotation according to $\dot{\psi} = 2\dot{\varphi} \sinh^2 \gamma = |\sigma| \tanh \gamma$.
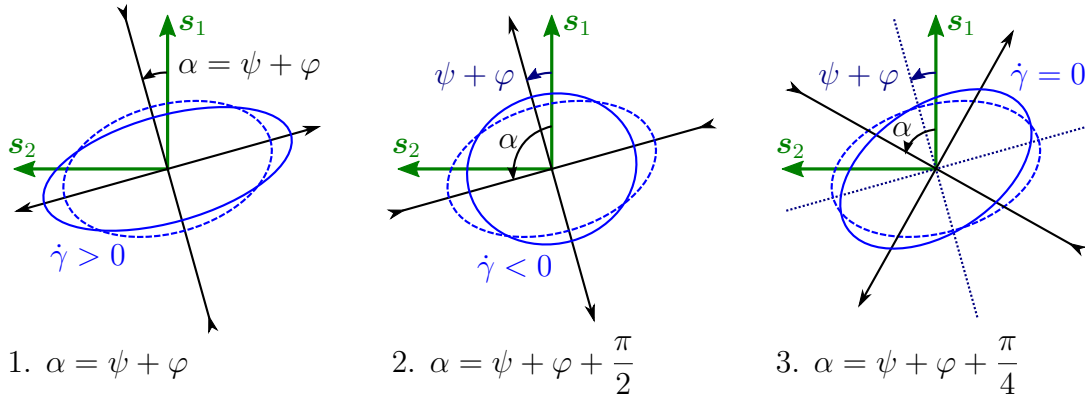

1. $\alpha = \psi + \varphi$ 2. $\alpha = \psi + \varphi + \dfrac{\pi}{2}$ 3. $\alpha = \psi + \varphi + \dfrac{\pi}{4}$

Figure 2.5 Illustration of the effect of the shear rate σ for the three configurations discussed in the text. Blue ellipses represent the cross-sectional shape of an initially circular light beam, for two successive values of the affine parameter: v (dashed) and $v + \delta v$ (solid). Black arrows indicate the eigendirection of the shear rate matrix.

2.3.3 Evolution

Sachs scalar equations

Besides the geometrical meaning of its components, the deformation rate matrix $\boldsymbol{S}$ can be considered a *Riccati variable* associated with $\boldsymbol{D}$, since its allows one to trade the second-order linear Jacobi matrix equation (2.65) for a first-order nonlinear Riccati equation

$$\dot{\boldsymbol{S}} + \boldsymbol{S}^2 = \boldsymbol{R}, \qquad (2.96)$$

that one easily obtain by taking the derivative of $\boldsymbol{S}$ and replacing $\ddot{\boldsymbol{D}}$ by $\boldsymbol{R}\boldsymbol{D}$. Inserting the decomposition (2.73) of $\boldsymbol{S}$ then leads to the *Sachs scalar equations*

$$\boxed{\begin{aligned} \dot{\theta} + \theta^2 + |\sigma|^2 &= \mathscr{R}, \\ \dot{\sigma} + 2\theta\sigma &= \mathscr{W}. \end{aligned}} \qquad \begin{aligned} &(2.97) \\ &(2.98) \end{aligned}$$

They confirm the discussion of § 2.1.3 regarding the respective role of Ricci and Weyl tensors in gravitational lensing, as $\mathscr{R}$ stands for the source of convergence (antiexpansion), while $\mathscr{W}$ is a source of shear. Note however the presence of $|\sigma|^2$ in Eq. (2.97), which adds to the focusing effect of $\mathscr{R}$ and therefore makes Weyl lensing an *indirect* source of convergence. This property is far from being obvious if one works within the Jacobi matrix formalism only.

Initial conditions

Due to the initial condition $\boldsymbol{\mathcal{D}}(v_O \leftarrow v_O) = \mathbf{0}_2$ for the Jacobi matrix, the deformation matrix $\boldsymbol{\mathcal{S}} \equiv \dot{\boldsymbol{\mathcal{D}}} \boldsymbol{\mathcal{D}}^{-1}$ diverges at O, and so do in principle the optical scalars θ, σ. This divergence can be analysed from the Taylor series of the Jacobi matrix in the vicinity of v_O, that is

$$\boldsymbol{\mathcal{D}}(v \leftarrow v_O) = (v - v_O)\mathbf{1}_2 + \frac{(v - v_O)^3}{3!} \boldsymbol{\mathcal{R}}_O + \mathcal{O}(v - v_O)^4, \tag{2.99}$$

hence

$$\boldsymbol{\mathcal{S}} = \left[\mathbf{1}_2 + \mathcal{O}(v - v_O)^2 \right] \left[(v - v_O)\mathbf{1}_2 + \mathcal{O}(v - v_O)^3 \right]^{-1} \tag{2.100}$$

$$= (v - v_O)^{-1}\mathbf{1}_2 + \mathcal{O}(v - v_O). \tag{2.101}$$

The deformation matrix therefore has a simple pole at O, which moreover only concerns its trace part (expansion rate). In other words, the initial conditions for the optical scalars are

$$\theta = (v - v_O)^{-1} + \mathcal{O}(v - v_O), \tag{2.102}$$

$$\sigma = \mathcal{O}(v - v_O). \tag{2.103}$$

The initial divergence of θ makes it inconvenient for numerical calculations. It is preferable, in practice, to use directly the area A of the beam, or the angular distance D_{A}, as in the equations exhibited hereafter.

Focusing theorem

Replacing θ by $(\mathrm{d}\sqrt{A}/\mathrm{d}v)/\sqrt{A}$ in the first Sachs scalar equation (2.97) leads to the following evolution equation for the beam's area A, known as the *focusing theorem*,

$$\boxed{\frac{\mathrm{d}^2\sqrt{A}}{\mathrm{d}v^2} = \left(\mathscr{R} - |\sigma|^2 \right) \sqrt{A} \leq 0,} \tag{2.104}$$

where we used $\mathscr{R} \leq 0$, as ensured by the null energy condition (see § 2.1.3). Note that, by virtue of Eq. (2.85), $\sqrt{A}$ could also have been replaced by the angular distance D_{A} in the above. A similar introduction of D_{A} in Eq. (2.98) then leads to the following reformulation of the Sachs scalar equations

$$\frac{\mathrm{d}^2 D_{\mathrm{A}}}{\mathrm{d}v^2} = \left(\mathscr{R} - |\sigma|^2 \right) D_{\mathrm{A}}, \tag{2.105}$$

$$\frac{\mathrm{d} D_{\mathrm{A}}^2 \sigma}{\mathrm{d}v} = D_{\mathrm{A}}^2 \mathscr{W}, \tag{2.106}$$

which enjoy a better behaviour at O than the original ones, and are therefore more adapted to numerical calculations of $D_{\mathrm{A}}(v)$.

Physically speaking, the focusing theorem tells us that $\sqrt{A}$ cannot increase more than linearly with v, and that *any* gravitational effect tends to focus the beam. This seems to imply that there exist no divergent gravitational lenses. Yet that is wrong in general: for example, a beam going through the interior of a matter circle *is* defocused. The point is that the focusing theorem is true for *infinitesimal* light beams only. If this assumption is relaxed, if the beam has a finite extension, then its rays no longer have the same direction of propagation, and their separations no longer belong to the same screen space, etc. It is precisely the existence of a collection of different screen spaces within a finite beam that can make it locally focused and globally defocused.

Distances

T HE greatest achievement of the theory of relativity is certainly the unification of the concepts of space and time, which implies in particular that the notion of spatial distance is fundamentally ambiguous. Yet astronomy—hence, to some extent, cosmology—is all about distance measurements, which encourages us to try to generalise the notion of distance in a relativistic context, rather than abandoning it. We here review a number of attempts to address this issue, both from purely theoretical and observational points of view. Throughout this chapter, at least ten different well-defined and well-motivated notions of distance are presented.

Contents

3.1 Defining distances

In this section, we expose several theoretical constructions for characterising spatial distances in relativity. The first difficulty being to artificially disentangle space from time, we start by investigating the issue in the context of special relativity (§ 3.1.1), where we show that distances can be univocally defined. The conclusion is nevertheless drastically different if we allow observers to be noninertial, or spacetime to be curved (§ 3.1.2).

3.1.1 In special relativity

We suppose in all this subsection that spacetime geometry is described by the Minkowski metric, and we use an *inertial* coordinate system $\{x^\alpha\}$ for which its components read $\boldsymbol{g}(\boldsymbol{\partial}_\alpha, \boldsymbol{\partial}_\beta) = \eta_{\alpha\beta} \equiv [\mathrm{diag}(-1, 1, 1, 1)]_{\alpha\beta}$.

Distance between two events

Let A and B be two events with coordinates $x^\alpha_{A,B}$. Their *spatio-temporal* separation is defined as the norm of the four-vector[1] $\boldsymbol{AB}$ connecting them, that is

$$\Delta s^2(A, B) \equiv \boldsymbol{g}(\boldsymbol{AB}, \boldsymbol{AB}) = \eta_{\alpha\beta} \Delta x^\alpha \Delta x^\beta, \tag{3.1}$$

with $\Delta x^\alpha \equiv x^\alpha_B - x^\alpha_A$. This separation is timelike, null, or spacelike respectively for $\Delta s^2 < 0$, $\Delta s^2 = 0$, or $\Delta s^2 > 0$ respectively. In the third case, it can be interpreted as the square of the spatial distance between A and B,

$$\boxed{D(A, B) \equiv \sqrt{\Delta s^2(A, B)}.} \tag{3.2}$$

As originally shown in Ref. [31], this notion of distance can also be expressed in terms of time measurements only. Consider an arbitrary inertial observer whose worldline $\mathscr{L}$ passes through A. Without loss of generality, we assume the coordinate system $\{x^\alpha\}$ to be adapted to this observer, in particular $x^0 = t$ is her proper time, and t_A is the date of A in her rest frame. We define two events $E, R \in \mathscr{L}$ from the construction depicted in Fig. 3.1a: the observer emits a photon at E, which is reflected at B back to the observer, who finally receives it at R. We call t_E, t_R the corresponding dates.

This construction implies that both the four-vectors $\boldsymbol{EB}$ and $\boldsymbol{BR}$ are null, because proportional to the emitted and reflected wave four-vectors. From $\boldsymbol{EB} = \boldsymbol{EA} + \boldsymbol{AB}$ we deduce

$$0 = \boldsymbol{g}(\boldsymbol{EB}, \boldsymbol{EB}) \tag{3.3}$$
$$= \boldsymbol{g}(\boldsymbol{EA}, \boldsymbol{EA}) + \boldsymbol{g}(\boldsymbol{EA}, \boldsymbol{AB}) + \boldsymbol{g}(\boldsymbol{AB}, \boldsymbol{AB}) \tag{3.4}$$
$$= -(t_A - t_E)^2 + (t_A - t_E)\,\boldsymbol{g}(\boldsymbol{\partial}_t, \boldsymbol{AB}) + \boldsymbol{g}(\boldsymbol{AB}, \boldsymbol{AB}), \tag{3.5}$$

where we used $\boldsymbol{EA} = (t_A - t_E)\boldsymbol{\partial}_t$ and $\boldsymbol{g}(\boldsymbol{\partial}_t, \boldsymbol{\partial}_t) = -1$; the same calculation with $\boldsymbol{BR} = \boldsymbol{BA} + \boldsymbol{AR}$ then yields

$$0 = -(t_R - t_A)^2 - (t_R - t_A)\,\boldsymbol{g}(\boldsymbol{\partial}_t, \boldsymbol{AB}) + \boldsymbol{g}(\boldsymbol{AB}, \boldsymbol{AB}). \tag{3.6}$$

---

[1]This notion of four-vector connecting two arbitrary events is meaningless in general, but Minkowski spacetime is an exception.

Combining Eqs. (3.5), (3.6) to eliminate the scalar product between $\boldsymbol{\partial}_t$ and $\boldsymbol{AB}$, we finally obtain

$$\boldsymbol{g}(\boldsymbol{AB}, \boldsymbol{AB}) = (t_A - t_E)(t_R - t_A), \tag{3.7}$$

which is positive iff $t_A \in [t_E, t_R]$, that is, as expected, iff A lies outside the lightcone of B. When this condition is fulfilled, the above relation yields the *Synge formula* [32] for the distance between two events

$$\boxed{D(A, B) = \sqrt{(t_A - t_E)(t_R - t_A)}.} \tag{3.8}$$

Although it involves here the proper time of a particular observer, $D(A, B)$ is by definition a Lorentz-invariant quantity, thus any inertial observer can calculate $D(A, B)$ using the Synge formula.

Observer independence is, however, the reason why $D(A, B)$ actually fails in describing what we usually call a spatial distance. For example, the couple of events corresponding to (A) the emission of a photon by this text, and (B) its reception by your eye, has $D(A, B) = 0$ by definition. Yet the text does not touch your eye, hopefully. The reason for such a failure is that the natural questions associated with spatial distances concern the distance between an event and an worldline (how far is this supernova explosion from us?) or between two worldlines (how far is this text from your eye?), rather than the distance between two events.

Distance between an event and an inertial observer

Let $\mathscr{L}$ be the worldline of an inertial observer and B an arbitrary event. The distance $D(\mathscr{L}, B)$ between them is naturally defined as $D(A^*, B)$, such that $A^* \in \mathscr{L}$ and B are *simultaneous* in the observer's frame. The notion of simultaneity invoked here admits three equivalent definitions in special relativity:

1. $t_{A^*} = t_B$ in an inertial coordinate system associated with $\mathscr{L}$.

2. $t_R - t_{A^*} = t_{A^*} - t_E$, where $E, R \in \mathscr{L}$ are, as in the previous paragraph, the emission and reception by the observer of a photon reflected at B. This definition is known as the Einstein-Poincaré simultaneity criterion [33, 34].

3. $\boldsymbol{g}(\boldsymbol{A^*B}, \boldsymbol{\partial}_t) = 0$.

Therefore

$$D(\mathscr{L}, B) \equiv D(A^*, B) = \delta_{ab} x_B^a x_B^b = \frac{t_R - t_E}{2}, \tag{3.9}$$

where we have chosen $\mathscr{L}$ as the origin of spatial coordinates $\{x^a\}_{a=1\ldots3}$ in the penultimate expression, while the last one have been obtained from the Synge formula (3.8) by replacing t_A by $t_{A^*} = (t_E + t_R)/2$. By virtue of the same Synge formula, it is easy to check that $D(\mathscr{L}, B)$ is also the maximal distance between B and any event of the observer's worldline,

$$D(\mathscr{L}, B) = \max_{A \in \mathscr{L}} D(A, B), \tag{3.10}$$

provided this quantity exists.

Another possible characterisation of $D(\mathscr{L}, B)$ relies on the affine parametrisation of null geodesics connecting B with $\mathscr{L}$. We have seen in § 1.3.1 that the affine parameter v indeed represents the distance travelled by light, modulo a frequency factor. Here the geodesic
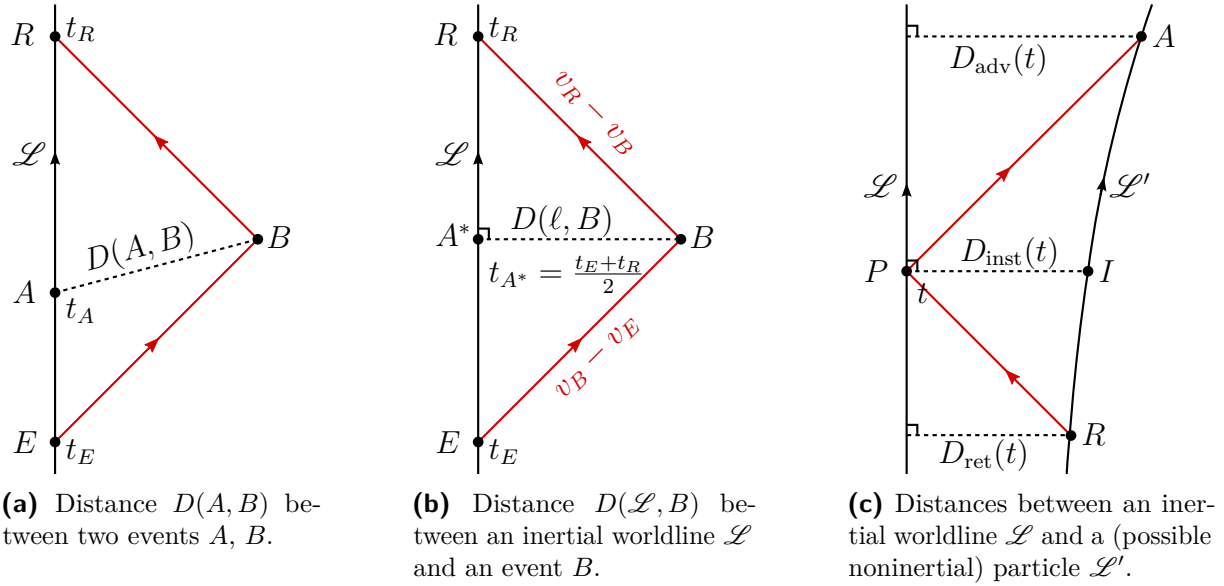
(a) Distance $D(A, B)$ between two events A, B.

(b) Distance $D(\mathscr{L}, B)$ between an inertial worldline $\mathscr{L}$ and an event B.

(c) Distances between an inertial worldline $\mathscr{L}$ and a (possible noninertial) particle $\mathscr{L}'$.

Figure 3.1   Defining distances in special relativity.

equation is easily solved, e.g. from B to R, leading in particular to $k^t = \text{cst} = \omega_R$, where ω_R is the cyclic frequency measured by the observer at R. In other words, $\mathrm{d}t/\mathrm{d}v = \omega_R$, which we immediately integrate as $\omega_R(v_R - v_B) = t_R - t_B = D(\mathscr{L}, B)$. We could also have chosen to integrate along the past ray (from E to B), and get $\omega_E(v_B - v_E) = t_B - t_E = D(\mathscr{L}, B)$ as well.

Summarising, the special-relativistic distance between a worldline and an event is univocally defined, because

$$D(\mathscr{L}, B) = \max_{A \in \mathscr{L}} D(A, B) = \omega_R(v_R - v_B) = \frac{t_R - t_E}{2}, \tag{3.11}$$

though each expression actually corresponds to a different geometrical construction.

Distance between a particle and an inertial observer

Consider a (possibly noninertial) particle following a worldline $\mathscr{L}'$. The distance between this particle and the inertial observer following $\mathscr{L}$ is, in general, a time-dependent quantity, because of their relative motion. There are three possible definitions for this distance represented in Fig. 3.1c: let P be an event on $\mathscr{L}$ and t the associated date in the observer's frame,

- the *instantaneous distance* is $D_{\text{inst}}(t) \equiv D(\mathscr{L}, I)$, where $I \in \mathscr{L}'$ and P are simultaneous in the observer's frame;

- the *retarded distance* reads $D_{\text{ret}}(t) \equiv D(\mathscr{L}, R)$, where $R \in \mathscr{L}'$ is the emission of a photon received at P—it is the notion of distance involved, e.g., in special-relativistic electrodynamics [2]; and finally

- the *advanced distance* is $D_{\text{adv}}(t) \equiv D(\mathscr{L}, A)$, where $A \in \mathscr{L}'$ is the reception of a photon emitted at P.

They all differ, except when they are constant.

3.1.2 In general relativity

In curved spacetime, or for non-inertial observers in Minkowski spacetime, the previous reasonings still apply locally, i.e. for small distances compared to (i) spacetime's curvature radii, and (ii) the inverse of the observer's acceleration. In the previous chapters, we tacitly took advantage of this property to univocally invoke physical distances—e.g. between two light spots on a screen—when they were infinitesimal. When they are not, many constructions which coincide locally turn out to differ globally.

Distance between two events

Let A, B be two events, and assume that they are connected by a unique geodesic $\mathscr{G}$ affinely parametrised by λ, as represented in Fig. 3.2. In mathematical terms, B is said to lie in a normal neighbourhood of A, and conversely. A natural extension of the spatio-temporal separation Δs^2 defined in § 3.1.1 to the general-relativistic case is then given by (twice) *Synge's worldfunction*

$$\sigma(A, B) \equiv \frac{1}{2}(\lambda_B - \lambda_A) \int_A^B t^\mu t_\mu \, \mathrm{d}\lambda, \tag{3.12}$$

where $t^\mu \equiv \mathrm{d}x^\mu/\mathrm{d}\lambda$ is the tangent vector to $\mathscr{G}$ associated with λ. The geodesic equation $\mathrm{D}\boldsymbol{t}/\mathrm{d}\lambda = \boldsymbol{0}$ implies that $t^\mu t_\mu$ is a constant along $\mathscr{G}$, so $\sigma(A, B) = (\lambda_B - \lambda_A)^2 t^\mu t_\mu/2$. Just like $\Delta s^2(A, B)$ in special relativity, the sign of $\sigma(A, B)$ dictates the nature of $\mathscr{G}$:

- $\sigma(A, B) < 0 \Leftrightarrow \mathscr{G}$ is timelike. In this case, the affine parameter λ can be chosen as the proper time τ along $\mathscr{G}$, so that $t^\mu t_\mu = -1$, and $\sigma(A, B) = -(\tau_B - \tau_A)^2/2$.

- $\sigma(A, B) = 0 \Leftrightarrow \mathscr{G}$ is null.

- $\sigma(A, B) > 0 \Leftrightarrow \mathscr{G}$ is spacelike. If we choose an affine parameter $\lambda = s$ such that $t^\mu t_\mu = 1$, then $\sigma(A, B) = (s_B - s_A)^2/2$.

In the last case, we conclude that

$$\boxed{D(A, B) \equiv \sqrt{2\sigma(A, B)} = |s_B - s_A|} \tag{3.13}$$

generalises the special-relativistic notion of spatial distance between two events. There is however no equivalent of the Synge formula (3.8) in general relativity, in the sense that a quantity of the form $\sqrt{(\tau_A - \tau_E)(\tau_R - \tau_A)}$—where τ is the proper time of an observer whose worldline $\mathscr{L}$ contains A, and $E, R \in \mathscr{L}$ are the emission and the reception of a photon reflected at B—is observer dependent and does not coincide with Eq. (3.13).
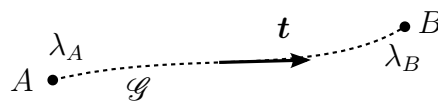

Figure 3.2 Geodesic $\mathscr{G}$ linking two events A, B, and its tangent vector $t^\mu = \mathrm{d}x^\mu/\mathrm{d}\lambda$.

Distances between an event and an observer

Let $\mathscr{L}$ be the worldline of a possibly noninertial observer and B an event. A straightforward generalisation of the special-relativistic distance $D(\mathscr{L}, B)$, that we shall call *spatial-geodesic distance*, is

$$D_{\mathrm{S}}(\mathscr{L}, B) \equiv \max_{A \in \mathscr{L}} D(A, B), \tag{3.14}$$

where $D(A, B)$ is now given by Eq. (3.13). An equivalent definition for the same quantity, whose construction is depicted in Fig. 3.3a, is the following: find the assumed-to-be unique spacelike geodesic $\mathscr{G}^*$ starting from B and intersecting $\mathscr{L}$ orthogonally; call A^* their intersection; then $D_{\mathrm{S}}(\mathscr{L}, B) = D(A^*, B)$. Note the similarity with the construction of Fermi normal coordinates in the vicinity of a timelike geodesic [9].

The equivalence between both definitions follows from the properties of Synge's world-function. One shows [35] that if the event A is displaced by $\delta x_A^\mu = u_A^\mu \delta\tau$ along $\mathscr{L}$, where $\boldsymbol{u}_A$ denotes the four-velocity of the observer at A, then $\sigma(A, B)$ changes by

$$\delta\sigma = (\lambda_B - \lambda_A)\,(t^\mu u_\mu)_A \delta\tau. \tag{3.15}$$

We conclude that $\sigma(A, B)$ is stationary with respect to displacements of A along $\mathscr{L}$ iff the geodesic $\mathscr{G}$ along which it is computed is orthogonal to $\mathscr{L}$. Moreover, this stationary point is a maximum if we suppose that it is unique, i.e., if we suppose that only one geodesic $\mathscr{G}^*$ connects B and $\mathscr{L}$ orthogonally. Indeed, $\sigma(A, B)$ is positive if A lies between the intersections E and R of $\mathscr{L}$ with the lightcone of B [see Fig. 3.3a] where it vanishes. Hence a unique stationary point between them must be a maximum.

Besides distances, the above construction also defines a notion of simultaneity: $A^* \in \mathscr{L}$ and B are *spatial-geodesic simultaneous* for the observer iff the geodesic $\mathscr{G}^*$ connecting them is orthogonal to $\mathscr{L}$ at A^*. Contrary to the special-relativistic case, this prescription for simultaneity does not necessarily coincide with the Einstein-Poincaré criterion: $\tau_R - \tau_{A^*}$ and $\tau_{A^*} - \tau_E$, where E and R are defined as before, are different in general. However, the equality can be shown to approximately hold, up to second order in $D_{\mathrm{S}}(A, B)$, if $\mathscr{L}$ is a timelike geodesic.

We thus expect from constructions based on light rays to define distinct notions of distance between $\mathscr{L}$ and B. For example, the *radar distance* defined as half the duration of light's round trip from $\mathscr{L}$ to B,

$$D_{\mathrm{R}}(\mathscr{L}, B) \equiv \frac{\tau_R - \tau_E}{2}, \tag{3.16}$$

has no reason to be equal to D_{S}. Similarly, a *null-geodesic distance*, relying on the affine parametrisation of a null geodesic connecting B to $\mathscr{L}$, e.g.,

$$D_{\mathrm{N}}(\mathscr{L}, B) \equiv \omega_R(v_R - v_B), \tag{3.17}$$

generically differs from both D_{S} and D_{R}. It could also have been defined as $\omega_E(v_B - v_E)$ leading to a fourth distinct distance.

A last option for connecting an event to a worldline consists in relying on a particular foliation of spacetime by spacelike hypersurfaces. Suppose $\mathcal{M} = \bigcup \Sigma_t$, where t is a label for the hypersurfaces Σ_t. Spacetime's metric $\boldsymbol{g}$ induces on each of them an intrinsic metric $\boldsymbol{h}(t) = \boldsymbol{g}|_{\Sigma_t}$. The associated Levi-Civita connection then allows us to define $\boldsymbol{h}$-geodesics on Σ_t which are not, in general, $\boldsymbol{g}$-geodesics of $\mathcal{M}$. A *foliation-based distance* $D_{\mathrm{F}}(\mathscr{L}, B)$

(a) Distances based on geodesics.
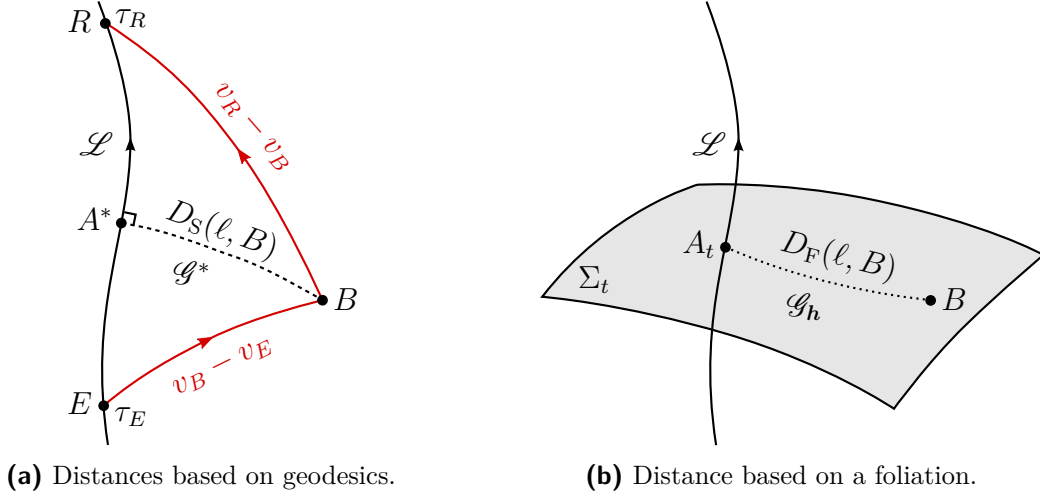

(b) Distance based on a foliation.

Figure 3.3 Defining distances between a worldline $\mathscr{L}$ and an event B in general relativity.

between $\mathscr{L}$ and B can be constructed the following way, illustrated in Fig. 3.3b: (i) identify the hypersurface Σ_t such that $B \in \Sigma_t$; (ii) call $A_t \equiv \mathscr{L} \cap \Sigma_t$ and $\mathscr{G}_{\boldsymbol{h}}$ the $\boldsymbol{h}$-geodesic of Σ_t connecting A_t with B; (iii) define

$$D_{\mathrm{F}}(\mathscr{L}, B) \equiv D_{\boldsymbol{h}}(A_t, B) = \sqrt{2\sigma_{\boldsymbol{h}}(A_t, B)}, \tag{3.18}$$

where $\sigma_{\boldsymbol{h}}$ is Synge's worldfunction for the manifold Σ_t equipped with $\boldsymbol{h}(t)$.

This procedure can seem quite natural for spacetimes which admit a preferred foliation, for example to exhibit their stationarity (Schwarzschild, Reissner-Nordstrøm, Kerr, Majumdar-Papapetrou, etc.), or their homogeneity[2] (Friedmann-Lemaître, Bianchi); however, for D_{F} to locally coincide with the other notions of distance, the foliation must be orthogonal to the observer's worldline $\mathscr{L}$. A way to construct such a foliation in *any* spacetime consists in using the Einstein-Poincaré criterion: for any event $A \in \mathscr{L}$, the set of all B which are Einstein-Poincaré simultaneous with A indeed form a hypersurface which is orthogonal to $\mathscr{L}$.

Distance between a particle and an observer

Like in special relativity, the instantaneous, retarded, and advanced distances between an observer following $\mathscr{L}$ and a particle following $\mathscr{L}'$ can be constructed from each of the event-worldline distances exposed in the previous paragraph. The associated prescriptions for simultaneity can be used for defining the event $I \in \mathscr{L}'$ simultaneous to a given $P \in \mathscr{L}$, in the case of the instantaneous distance.

3.2 Measuring distances

In the previous section, we have demonstrated the ambiguity of the notion of spatial distance in general relativity by proposing half a dozen theoretically well-motivated

---

[2]In cosmology, the D_{F} associated with the foliation of spacetime by homogeneous hypersurfaces is usually referred to as the physical distance, not because it is more physical than D_{S}, D_{N}, or D_{R}, but rather to distinguish it from the comoving (or conformal) distance. It is also the notion of distance which is implicitly chosen in, e.g., Buchert's approach to the backreaction issue [36].

definitions for it. However, none of them is actually observable—except the radar distance, but it is practically very limited. In the present section, we thus adopt a complementary approach, reviewing the main observables used to measure distances in astronomy and cosmology, and the different notions of distance they define. Table 3.1 provides a summary of what follows, together with some orders of magnitude.

observable	distance	applicability	range	precision
time	radar D_{R}	Solar system	AU	10^{-11}
angle	parallax D_{P}	Milky way	kpc	1-10%
	angular D_{A}	extragalactic	Gpc	10-50% (clusters)
				5% (BAO)
intensity	luminosity D_{L}	extragalactic	10 Mpc	5% (Cepheids)
			Gpc	20% (SNe)

Table 3.1 Summary of the observable notions of distance in astronomy and cosmology, with their domains of applicability, and orders of magnitude for their maximum range and current level of precision. The precision on D_{R} refers to the Viking Earth-Mars distance measurement [37]; on D_{P} to the objectives of the Gaia mission [38]; on D_{A} to galaxy-cluster distances measured from the X-ray emission/SZ effect [39], or to the BAO scale with BOSS [40]; finally the precisions on D_{L} for Cepheids and SNe are based respectively on Refs. [41] and [42].

3.2.1 Radar distance

Already defined in Eq. (3.16) of the previous section, the radar distance D_{R} corresponds to half the duration of a light signal's round trip between the observer and its target, as measured in the observer's frame.

This method is of daily use for short-distance measurements on the Earth, but it is not adapted to astronomy as it requires high-reflexivity objects. As such, it is limited to distance measurements within the Solar system. A notable example is the Earth-Moon distance, thanks to the five retroreflector arrays installed by the US missions Apollo 11, 14, 15, and Soviet missions Luna 17, 21. The associated Lunar Laser Ranging experiments have determined the radar distance to the Moon with a precision on the order of the centimetre, that is, enough to carry tests of the equivalence principle and Lorentz invariance [43–46]. The radar distances to Venus, Mars, and Cassini have also been used to measure the Shapiro time delay, which is a standard test of GR in the Solar system [1].

The radar distance is also involved in gravitational wave detection experiments, such as the ground interferometers LIGO [47], VIRGO [48], and the future space mission eLISA [49]. All three are based on the same principle: as a gravitational wave propagates through the interferometer, the *radar length* of each arm is affected differently, inducing a phase difference between light signals propagating inside, and therefore a characteristic interference signal.

3.2.2 Parallax distance

Definition

Parallax is the apparent displacement of a light source caused by a displacement of its observer. The larger the distance between them, the smaller the parallax, so that a

measurement of the apparent motion of the source by the observer, together with the knowledge of its own actual motion, is a method for measuring distances. For simplicity, we restrict here to the case where the observer's motion is orthogonal to the line of sight (see Fig. 3.4); the *parallax distance* is then

$$D_\mathrm{P} \equiv \sqrt{\frac{A_O}{\Omega_O}},$$ (3.19)

where A_O is the physical area of the observer's trajectory and $\Omega_O \ll 1$ is the solid angle occupied by the apparent trajectory of the source on the observer's celestial sphere.
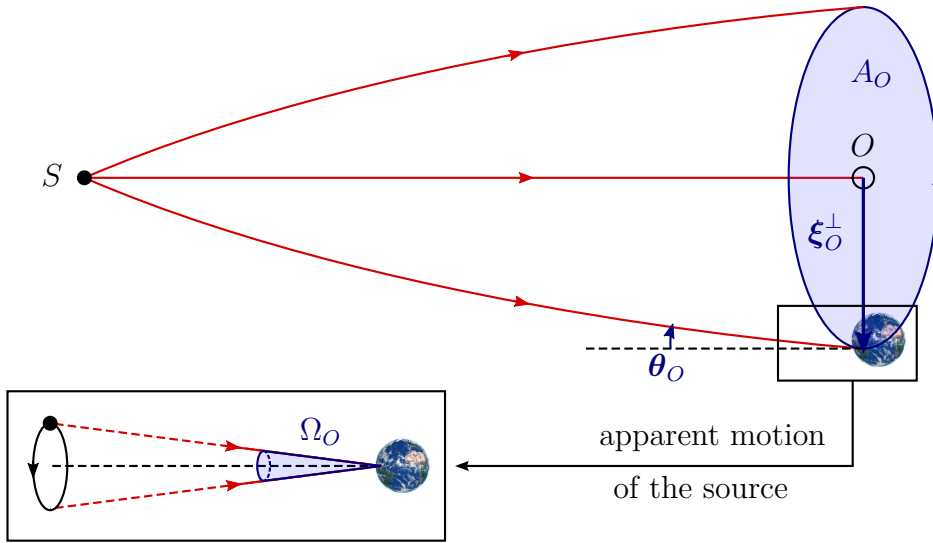

Figure 3.4 Solar parallax. The revolution of the Earth around the Sun induces an apparent motion of the source on the observer's celestial sphere. The solid angle Ω_O corresponding to this apparent motion is smaller as the source is farther. The parallax distance is obtained by comparing Ω_O with the area A_O of the observer's motion—here $A_O = \pi(\mathrm{AU})^2$—according to $D_\mathrm{P}^2 \equiv A_O/\Omega_O$. We chose to depict a beam with some focusing, which tends to *increase* D_P.

In astronomy, solar parallax—due to the revolution of the Earth around the Sun—is the most common technique for determining the distance of stars within the Milky Way. It gave birth to the *parsec* unit, defined as the distance such that a source has a solar parallax of one arcsecond. The European astrometry satellite Hipparcos [50], launched in 1989, measured the parallax of 2.5 millions stars. It has been replaced in 2013 by Gaia [38], which is expected to deliver a catalogue of 1 billion stars, with a precision of 20–200 μas on their parallax. This level of precision is the best that we can achieve today, even with Very Long Baseline Interferometry (VLBI) whose resolution is on the order 1 mas, setting the current limit on parallax distance measurements to $D_\mathrm{P} < 10$ kpc.

Theoretical expression

Let us relate the definition (3.19) of the parallax distance to the properties of a light beam connecting the source to the observer. For that purpose, consider the beam delimited by all the rays emerging from S and reaching a possible position of the Earth on its trajectory around the Sun, as depicted in Fig. 3.4. Let O be, for example, the intersection between the beam with the Sun's worldline. Note that, contrary to the convention adopted in

Chap. 2, this beam has a vertex at S and a nonzero extension around O. The ecliptic plane then plays the role of screen space at O.

On the one hand, the area A_O of the Earth's trajectory is clearly identified with the area $d^2\xi_O^A$ of the beam at O, with ξ_O^A the components of the separation vector $\boldsymbol{\xi}$ over the Sachs basis at O. On the other hand, $\Omega_O = \omega_O^{-2} d^2\dot{\xi}_O^A$, where ω_O is the observed frequency since, as discussed in § 2.2.1, $\omega^{-1}|\dot{\xi}^A|$ represents the angle between two rays separated by $\boldsymbol{\xi}$. We conclude that

$$D_{\mathrm{P}}^2 = \frac{d^2\xi_O^A}{\omega_O^{-2}d^2\dot{\xi}_O^A} = \frac{\omega_O^2}{\det \boldsymbol{S}(O \leftarrow S)}, \tag{3.20}$$

by definition (2.71) of the deformation rate matrix $\boldsymbol{S}$. The parallax distance can therefore be expressed in terms of the optical scalars as

$$\boxed{D_{\mathrm{P}} = \frac{\omega_O}{\sqrt{\theta^2 - |\sigma|^2}},} \tag{3.21}$$

where θ and σ correspond to $\boldsymbol{S}(O \leftarrow S)$, i.e. to an integration of the Sachs equation from the source to the observer. Note that our expression (3.21) differs from the one given in Ref. [51] and used in Ref. [52], in which the shear rate $|\sigma|^2$ has been neglected.

Since D_{P} is an decreasing function of θ^2 and an increasing function of $|\sigma|^2$, the Sachs scalar equations (2.97), (2.98) imply that any gravitational lensing effect tends to *increase* the parallax distance.

3.2.3   Angular diameter distance

Definition

The notion of angular diameter distance, or area distance[3] is based on the fact that a given object appears smaller as it lies farther form us. It is defined by

$$\boxed{D_{\mathrm{A}} \equiv \sqrt{\frac{A_S}{\Omega_O}},} \tag{3.22}$$

where A_S is the physical area of the light source, and $\Omega_O \ll 1$ its apparent angular size for the observer, as depicted in Fig. 3.5.

The difficulty of measuring angular distances in astronomy is that it requires standard rulers, i.e. sources whose size is known, or at least can be calibrated by independent experiments. An important example in cosmology is the Baryon Acoustic Oscillation (BAO) scale, which corresponds to the maximum distance travelled by a sound wave in the primordial Universe. It can be extracted from the analysis of the anisotropies of the Cosmic Microwave Background (CMB), and in the distribution of galaxies. The angular diameter distance is also naturally involved in strong gravitational lensing and time delays experiments.

---

[3]Angular diameter distance and area distance can actually be considered two slightly different notion [23]. Strictly speaking, the former is a comparison between the proper and apparent diameter of the source, which thus depends on its orientation if some shear is at work. The area distance do not suffer from this ambiguity.
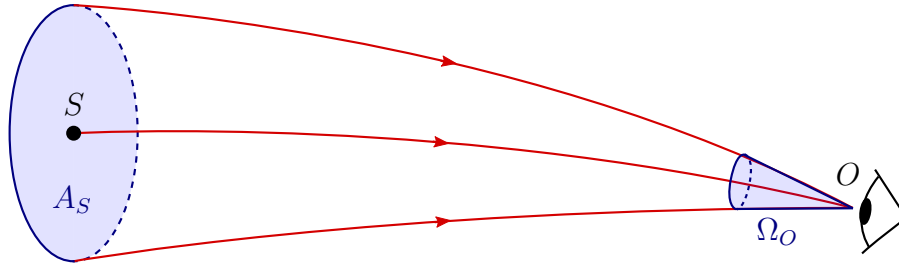
Figure 3.5 The angular diameter distance, or area distance, is obtained by comparing the actual and apparent sizes of a light source, according to $D_\mathrm{A}^2 = A_S/\Omega_O$.

Theoretical expression

The angular diameter distance is directly related to the determinant of the Jacobi matrix (see § 2.2.1) via

$$D_\mathrm{A} = \omega_O\sqrt{\det \boldsymbol{\mathcal{D}}(v_S \leftarrow v_O)}. \tag{3.23}$$

The notation $v_S \leftarrow v_O$ indicates that the Jacobi matrix equation (2.65) must be solved from the observation event O, where all the rays converge, to the source event S.

By comparing Eqs. (3.21) and Eq. (3.23), we immediately deduce that $D_\mathrm{A} \neq D_\mathrm{P}$ in general. If an observer performs two experiments to measure his distance to a light source, the first one using the solar parallax and the second one using the angular-diameter method, the results will generically disagree. In particular, the focusing theorem derived in § 2.3.3 implies that any gravitational effect tends to *reduce* D_A, contrary to D_P.

In the gravitational lensing literature, it is customary to set the observed frequency ω_O to one—which can be considered a particular choice of units for frequencies—in order to simplify Eq. (3.23). However, keeping explicitly ω_O in the expression of D_A has a significant pedagogical advantage: it allows one to easily understand (i) aberration effects, and (ii) the relation between the angular diameter distance and the luminosity distance, defined in § 3.2.4.

Aberration effects

Because the cross-sectional area of a light beam is frame independent (see § 2.1.2), the source's area A_S involved in the definition (3.22) of the angular distance does not depend on the source's four-velocity $\boldsymbol{u}_S$. On the contrary, the observer angular size Ω_O does depend on $\boldsymbol{u}_O$ in general. We thus expect D_A to be independent from the source's velocity, but to be affected by the observer's velocity.

These dependences are evident in Eq. (3.23). The Jacobi matrix is indeed independent from any four-velocity, as it is driven by the optical tidal matrix $\boldsymbol{\mathcal{R}}$, independent of the frame in which the screen space is defined. Besides, the ω_O term exhibits a $\boldsymbol{u}_O$-dependence of D_A, which is responsible for *aberration* effects. If the observer moves towards the source, ω_O increases and the source thus appears smaller (i.e. farther, D_A is larger) to her, than if she were receding from it. The same phenomenon potentially occurs if the observer lies within a stronger gravitational field—hence increasing ω_O—though it also potentially affects the Jacobi matrix.

3.2.4 Luminosity distance

Definition

A light source not only appears smaller but also fainter as it lies farther from the observer. In a nonrelativistic picture, if the source has isotropic light emission, then the energy δE it emits during a short period of time δt is homogeneously distributed on a spherical shell (the photosphere) with a surface density $\delta E/(4\pi r^2)$, where r is the shell's radius which increases as light propagates. An observer located at r_O thus receives an energy per unit time and area equal to $\delta E/(4\pi r_O^2)/\delta t$. This motivates the following definition for the *luminosity distance*:

$$D_{\mathrm{L}} = \sqrt{\frac{L_S}{4\pi I_O}}, \tag{3.24}$$

where L_S denotes the intrinsic luminosity of the source, that is, the total luminous power it emits in all directions; I_O is the observed luminous intensity, defined as $I_O \equiv P_O/A_O$, where A_O is the area of the observer's detector, and P_O the luminous power measured by this detector. The relevant geometry is represented in Fig. 3.6.
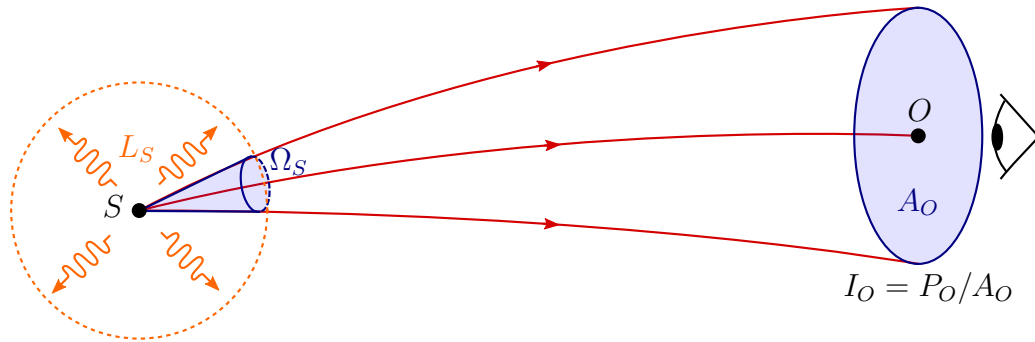

Figure 3.6 The luminosity distance is defined from the ratio between the intrinsic luminosity (total emission power) L_S of the source and the observed luminous intensity $I_O \equiv P_O/A_O$, where P_O is the power detected at O by a small detector of area A_O. Ω_S denotes the angular aperture, in the source's frame, of the beam intercepted by the observer. The relevant picture is thus reversed compared to the angular distance's, since the vertex of the beam is here S rather than O, like for the parallax.

In astronomy, the luminosity distance is often used under a logarithmic form called *distance modulus*, and defined as

$$\mu_{\mathrm{L}} = 5 \log \left(\frac{D_{\mathrm{L}}}{10 \,\mathrm{pc}} \right). \tag{3.25}$$

It is the most used notion of distance in practice, as it applies to extra-galactic sources contrary to the parallax, and to unresolved sources contrary to the angular diameter distance. Nevertheless, similarly to the latter, any direct measurement of D_{L} requires sources whose intrinsic luminosity L_S is known, or can be inferred from other observations: the so-called *standard(-isable) candles*.

A good example is provided by *Cepheid variables*, which are pulsating stars whose luminosity oscillates with a period correlated with its mean [53, 54]. Once calibrated, typically with auxiliary parallax distance measurements, this relation can then be used to deduce the intrinsic luminosity of any Cepheid variable from a measurement of its

period. Type Ia supernovae (SNeIa), which are mostly thought to originate from binary systems where a white dwarf reaches its Chandrasekhar mass by accreting matter from its companion—though the nature of progenitors is still debated [55]—, are also good standard-isable candles, as there exists a relation between the duration of the explosion and its peak luminosity [56]. In cosmology, they are used to plot the *Hubble diagram* from which key information on the expansion history of the Universe can be extracted (see Chap. 5). Recently, a Hubble diagram has been constructed from quasars [57], by exploiting a relation between their X-ray and UV luminosities. Because they are orders-of-magnitude brighter than supernovae, quasars have the advantage of providing a much deeper Hubble diagram, up to $z = 6$.

Future detections of gravitational waves are also expected to provide excellent measurements of the luminosity distance to their sources [58, 59]. Indeed, gravitational waves follow null geodesics just like electromagnetic waves, hence all the notions defined for the latter apply to the former as well. In addition, theoretical analyses of the signal generated by an inspiraling binary system of compact objects (neutrons stars, black holes, etc.) show that its phase gives access to the mass of the objects, i.e. to the gravitational luminosity of the system. For that reason, binary systems of compact objects have been nicknamed *standard sirens*—the gravitational analog of standard candles. They have, compared to supernovae, the significant advantage of relying on well-controlled theoretical predictions, and should therefore be less plagued by systematics.

Distance duality relation

The similarity of the pictures that we used to define angular and luminosity distances (compare Figs. 3.5, 3.6) strongly suggests that they are not independent notions. This expectation can be made more explicit by reexpressing D_L as a function of the geometrical quantities Ω_S, A_O. Consider the fraction of all the photons emitted during a short time interval $\delta\tau_S$ in the source's frame which can be received by the observer's detector. By definition, there are

$$\delta N = \frac{L_S}{\hbar\omega_S} \times \delta\tau_S \times \frac{\Omega_S}{4\pi} \tag{3.26}$$

such photons. *Assuming that none of them is absorbed* by some interaction with matter on its way to the observer, and according to the photon conservation law derived in § 1.3.2, we also have

$$\delta N = \frac{I_O}{\hbar\omega_O} \times \delta\tau_O \times A_O, \tag{3.27}$$

where $\delta\tau_O$ is the time interval, in the observer's frame, corresponding to the reception of all these photons. Note that the ratio between $\delta\tau_O/\delta\tau_S$ is the same as the ratio between the observed and emitted periods of a light signal, in other words

$$\frac{\delta\tau_O}{\delta\tau_S} = \frac{\omega_S}{\omega_O} = 1 + z, \tag{3.28}$$

so that

$$D_L \equiv \sqrt{\frac{L_S}{4\pi I_O}} = (1 + z)\sqrt{\frac{A_O}{\Omega_S}}. \tag{3.29}$$

It is then tempting to recognise the angular distance in the right-hand side of Eq. (3.29), except that the roles of S and O are inverted compared to the definition (3.22) of D_A.

This can nevertheless be solved by

$$\sqrt{\frac{A_O}{\Omega_S}}\sqrt{\frac{\Omega_O}{A_S}} = \frac{\omega_S\sqrt{\det \boldsymbol{\mathcal{D}}(v_O \leftarrow v_S)}}{\omega_O\sqrt{\det \boldsymbol{\mathcal{D}}(v_S \leftarrow v_O)}} = 1 + z, \tag{3.30}$$

where we have used the consequence (2.70) of Etherington's reciprocity law, which states that the determinant of the Jacobi matrix is invariant under the exchange of its arguments. The *distance duality relation* finally reads

$$\boxed{D_{\mathrm{L}} = (1 + z)^2 D_{\mathrm{A}}.} \tag{3.31}$$

The origin of the redshift factor $(1 + z)^2$ can be summarised as $2 = 1/2 + 1/2 + 1$. The first $1/2$ comes from the fact that the energies of emitted and received photons differ; the second $1/2$ is due time dilation between the source and the observer; and finally the 1 originates from the exchange of the roles of S and O in Figs. 3.5, 3.6. The latter can be seen as a comparative aberration effect, which for the angular distance occurs at O, whereas for the luminosity distance it occurs at S.

Equation (3.31) holds for any spacetime, as long as any physical process capable of violating photon conservation is negligible. Note also that strict GR is not even necessary, in the sense that the dynamics of the metric has no impact on the distance duality law. It therefore remains valid for Nordstrøm's gravity, $f(R)$, ..., provided electromagnetism is still minimally coupled to the metric. A counterexample is the Horndeski vector-tensor theory mentioned in § 1.1.2.

Observational tests of the distance duality relation thus potentially provide constraints on the transparency of the Universe (photon conservation) and on some potential departures from GR. A method based on the X-ray emission and the Sunyaev-Zel'dovich effect in galaxy clusters was proposed in Ref. [60], and concluded that $(1 + z)^2 D_{\mathrm{A}}/D_{\mathrm{L}} = 0.93^{+0.05}_{-0.04}$, suggesting no significant violation of the distance duality relation. Besides, it has recently been shown by Ref. [61] that any violation of Etherington's reciprocity law—in particular of its consequence (3.30)—would induce spectral distortions in the observed CMB. Such violations cannot exceed 0.01%.

PART II

STANDARD COSMOLOGY AND OBSERVATIONS

<div style="text-align: right;">CHAPTER 4</div>

The standard cosmological spacetimes

C OSMOLOGY has today an impressively successful standard model. Discussing the reasons of such a success is central to this thesis, which cannot be done without presenting the model itself. In this first chapter dedicated to standard cosmology, we introduce the spacetime geometries used to describe the Universe on large scales: first the purely homogeneous and isotropic Friedmann-Lemaître model, with the cosmic history reconstructed from it; then the perturbation theory relaxing the strict assumptions of homogeneity and isotropy, whose limitations will also be discussed.

Contents

4.1   Homogeneous and isotropic cosmologies

Observing our Universe, in particular through the cosmic microwave background, reveals that its properties are almost identical whatever the direction we look at. This fact, together with the *Copernican principle*, according to which we do not occupy a special place in the cosmos, led cosmologists to model the Universe as statistically spatially homogeneous and isotropic, a hypothesis known as the *cosmological principle*. This section examines the consequences of the simplest application of this principle: strictly homogeneous and isotropic cosmologies.

4.1.1   The Friedmann-Lemaître geometry

The first proposal of a spacetime geometry satisfying the cosmological principle was formulated in 1917 with Einstein's static Universe [62]. Einstein's approach was then generalised, allowing for the possibility of an evolving cosmos, independently by Friedmann in 1922 [63], and Lemaître in 1927 [64] who also predicted the redshift of receding galaxies *before* its observation by Hubble [65] in 1929. The work of Friedmann was noticed by Robertson in 1929 [66], followed by Walker. In the 1930s, both of them analysed in great details [67–70] the properties of the metric discovered by Friedmann and Lemaître, which we shall call FL metric throughout this thesis.

Coordinate systems and metric

Suppose spacetime can be foliated by a family of spacelike hypersurfaces $\{\Sigma_t\}$ whose intrinsic geometry is homogeneous and isotropic. Their label, t, is naturally used as a time coordinate; each hypersurface Σ_{t_0} of the foliation is thus characterised by the simple equation $t = t_0$, and the one-form associated with its normal vector $\boldsymbol{n}$ satisfies

$$n_\mu \mathrm{d}x^\mu \propto \mathrm{d}t, \tag{4.1}$$

which implies $0 = n_i = \boldsymbol{g}(\boldsymbol{n}, \boldsymbol{\partial}_i)$. In other words, whatever the choice of the other three coordinates $\{x^i\}_{i=1\dots3}$, the associated vector fields $\boldsymbol{\partial}_i$ are tangent to Σ_t. A convenient setting then consists in imposing that the $x^i = \mathrm{cst}$ curves are orthogonal to the foliation, i.e. $\boldsymbol{\partial}_t \propto \boldsymbol{n}$. This means that the metric has no shift: $g_{ti} = 0$ (see Fig. 4.1). Finally, the assumed homogeneity of the geometry of Σ_t allows us to rescale the coordinate t so that $g_{tt} = \boldsymbol{g}(\boldsymbol{\partial}_t, \boldsymbol{\partial}_t) = -1$ everywhere. The metric, expressed in terms of the resulting coordinate system (t, x^i)—called *synchronous*—, reads

$$\mathrm{d}s^2 = -\mathrm{d}t^2 + g_{ij}\mathrm{d}x^i\mathrm{d}x^j. \tag{4.2}$$

In the context of cosmology, the coordinate t is called *cosmic time*.

   The homogeneity and isotropy assumptions for Σ_t can be shown [12] to impose the following form of the spatial metric:

$$g_{ij} = a^2(t)\gamma_{ij}(x^k)\mathrm{d}x^i\mathrm{d}x^j, \tag{4.3}$$

where $a(t) \geq 0$ is called the *scale factor*, and γ_{ij} denotes the intrinsic metric of Σ_t (as within any Σ_t, the scale factor can be absorbed by a coordinate transformation). The high level of symmetry of γ_{ij} imply that its Riemann tensor reads

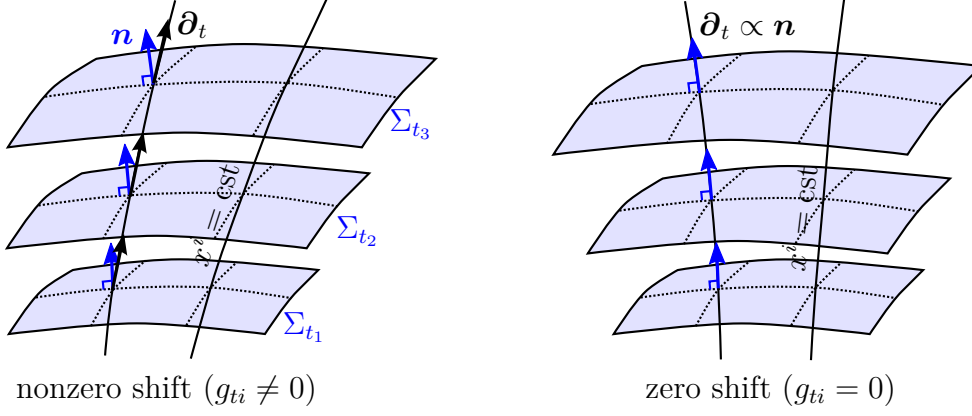$$^3R_{ijk\ell} = 2K\gamma_{k[i}\gamma_{j]\ell}, \tag{4.4}$$

Figure 4.1 Given a foliation $\{\Sigma_t\}$ of spacetime, the coordinate systems $\{x^i\}$ of the hypersurfaces are generally shifted with respect to each other: the $x^i = \text{cst}$ curves are not orthogonal to the hypersurfaces. In this case $g_{ti} = \boldsymbol{g}(\boldsymbol{\partial}_t, \boldsymbol{\partial}_i) \neq 0$.

where K is a constant of dimension L^{-2} called spatial curvature parameter. The cases $K < 0$, $K = 0$, and $K > 0$ respectively correspond to hyperbolic, Euclidean, and spherical foliations. Explicit forms of the metric γ_{ij} can be written using various spherical-like coordinate systems, such as

$$\gamma_{ij}\mathrm{d}x^i\mathrm{d}x^j = \left(\frac{1}{1 + K\varrho^2/4}\right)^2 \left(\mathrm{d}\varrho^2 + \varrho^2\mathrm{d}\Omega^2\right) \tag{4.5}$$

$$= \frac{\mathrm{d}r^2}{1 - Kr^2} + r^2\mathrm{d}\Omega^2, \tag{4.6}$$

$$= \mathrm{d}\chi^2 + f_K^2(\chi)\,\mathrm{d}\Omega^2, \tag{4.7}$$

with $\mathrm{d}\Omega^2 \equiv \mathrm{d}\theta^2 + \sin^2\theta\,\mathrm{d}\varphi^2$, and where the radial coordinates ϱ, r, χ are related by

$$\frac{\varrho}{1 + K\varrho^2/4} = r = f_K(\chi) \equiv \begin{cases} \dfrac{\sinh(\sqrt{-K}\chi)}{\sqrt{-K}} & \text{if } K < 0, \\ \chi & \text{if } K = 0, \\ \dfrac{\sin(\sqrt{K}\chi)}{\sqrt{K}} & \text{if } K > 0. \end{cases} \tag{4.8}$$

The foliation-based distance D_F (see § 3.1.2) between the worldline $\chi = 0$ and the event (t, x^i) is easily checked to be $a(t)\chi$ which leads us to call χ the *conformal radial distance*. Besides, within a given spatial section Σ_t the proper area of a $\chi = \text{cst}$ sphere is $4\pi a^2(t)f_K^2(\chi) = 4\pi a^2(t)r^2$, hence r represents the *conformal areal radius* of the sphere. The last radial coordinate ϱ has no specific interpretation, but it is adapted to the introduction of Cartesian-like coordinates $x \equiv \varrho\sin\theta\cos\varphi$, $y \equiv \varrho\sin\theta\sin\varphi$, $z \equiv \varrho\cos\theta$, since $\mathrm{d}\varrho^2 + \varrho^2\mathrm{d}\Omega^2 = \mathrm{d}x^2 + \mathrm{d}y^2 + \mathrm{d}z^2$.

It is often convenient to introduce the *conformal time* η defined from cosmic time by $\mathrm{d}t = a\,\mathrm{d}\eta$, in order to completely factorise the scale factor in the expression of the metric,

$$\mathrm{d}s^2 = a^2(\eta)\left(-\mathrm{d}\eta^2 + \gamma_{ij}\mathrm{d}x^i\mathrm{d}x^j\right). \tag{4.9}$$

Geometrical properties

Table 4.1 summarises all the geometrical quantities (Christoffel symbols, curvatures, etc.) associated with the FL spacetime, for two different choices for the x^0-coordinate: cosmic

time t or conformal time η. We introduced the evolution rates of the scale factor

$$H \equiv \frac{1}{a}\frac{\mathrm{d}a}{\mathrm{d}t} \equiv \frac{\dot{a}}{a}, \qquad \mathcal{H} \equiv \frac{1}{a}\frac{\mathrm{d}a}{\mathrm{d}\eta} \equiv \frac{a'}{a} = aH, \tag{4.10}$$

respectively called the *Hubble expansion rate* and conformal Hubble expansion rate, for reasons that shall become clearer below. We see from Table 4.1 that the FL spacetime admits three typical curvature scales, namely $\mathcal{H}^2$, $\mathcal{H}'$, and K.

Interestingly, since its Weyl tensor vanishes, the FL geometry is *conformally flat*. This property is obvious if $K = 0$, as the metric then reads $\mathrm{d}s^2 = a^2\eta_{\mu\nu}\mathrm{d}x^\mu\mathrm{d}x^\nu$, so that the conformal factor is simply a^2; for $K \neq 0$ the underlying conformal transformation is more complicated, in particular it is no longer homogeneous [71].

	$x^0 = t$	$x^0 = \eta$
Metric	$\mathrm{d}s^2 = -\mathrm{d}t^2 + a^2(t)\gamma_{ij}\mathrm{d}x^i\mathrm{d}x^j$	$\mathrm{d}s^2 = a^2(\eta)\left(-\mathrm{d}\eta^2 + \gamma_{ij}\mathrm{d}x^i\mathrm{d}x^j\right)$
Christoffel symbols	$\Gamma^0{}_{ij} = Hg_{ij}$ $\Gamma^i{}_{0j} = H\delta^i_j \qquad \Gamma^i{}_{jk} = {}^3\Gamma^i{}_{jk}$	$\Gamma^0{}_{00} = \mathcal{H} \qquad \Gamma^0{}_{ij} = \mathcal{H}\gamma_{ij}$ $\Gamma^i{}_{0j} = \mathcal{H}\delta^i_j \qquad \Gamma^i{}_{jk} = {}^3\Gamma^i{}_{jk}$
Riemann tensor	$R^0{}_{i0j} = \frac{\ddot{a}}{a}g_{ij} \qquad R^i{}_{0j0} = -\frac{\ddot{a}}{a}\delta^i_j$ $R^i{}_{jk\ell} = 2\left(H^2 + \frac{K}{a^2}\right)\delta^i_{[k}g_{\ell]j}$	$R^0{}_{i0j} = \mathcal{H}'\gamma_{ij} \qquad R^i{}_{0j0} = -\mathcal{H}'\delta^i_j$ $R^i{}_{jk\ell} = 2(\mathcal{H}^2 + K)\delta^i_{[k}\gamma_{\ell]j}$
Kretschmann scalar	$\mathcal{K} = 12\left[\left(\frac{\ddot{a}}{a}\right)^2 + \left(H^2 + \frac{K}{a^2}\right)^2\right] = \frac{12}{a^4}\left[(\mathcal{H}')^2 + (\mathcal{H}^2 + K)^2\right]$	
Ricci tensor	$R_{00} = -\frac{3\ddot{a}}{a}$ $R_{ij} = \left(\frac{\ddot{a}}{a} + 2H^2 + \frac{2K}{a^2}\right)g_{ij}$	$R_{00} = -3\mathcal{H}'$ $R_{ij} = (\mathcal{H}' + 2\mathcal{H}^2 + 2K)\gamma_{ij}$
Ricci scalar	$R = 6\left(\frac{\ddot{a}}{a} + H^2 + \frac{K}{a^2}\right) = \frac{6}{a^2}(\mathcal{H}' + \mathcal{H}^2 + K)$	
Weyl tensor	$C_{\mu\nu\rho\sigma} = 0$	
	$E_{00} = 3\left(H^2 + \frac{K}{a^2}\right)$ $E_{ij} = -\left(\frac{2\ddot{a}}{a} + H^2 + \frac{K}{a^2}\right)g_{ij}$	$E_{00} = 3(\mathcal{H}^2 + K)$ $E_{ij} = -(2\mathcal{H}' + \mathcal{H}^2 + K)\gamma_{ij}$

Table 4.1 Geometry of the FL spacetime for two different choices of the time coordinate: t or η. A dot and a prime respectively denote a derivative with respect to t and η, with the relation $X' = a\dot{X}$. The associated evolution rates for a are $H \equiv \dot{a}/a$ and $\mathcal{H} \equiv a'/a = aH$. The notation ${}^3\Gamma^i{}_{jk}$ stands for the Christoffel symbols associated with the three-dimensional metric γ_{ij}. We recall that the Kretshmann scalar is defined by $\mathcal{K} \equiv R^{\mu\nu\rho\sigma}R_{\mu\nu\rho\sigma}$.

Fundamental observers, cosmic expansion

Let us now turn to the physical interpretation of the FL geometry. First note that the curves defined by $x^i =$ cst are timelike geodesics, as easily shown by checking that the associated four-velocity $u^\mu = \delta_t^\mu$ satisfies $\dot{u}^\mu + \Gamma^\mu{}_{\nu\rho} u^\nu u^\rho = 0$. These curves thus correspond to the worldlines of free-falling observers, called *fundamental observers*, whose proper time is cosmic time t. The spatial coordinates $\{x^i\}$ can also be viewed as Lagrangian, or *comoving*, coordinates for the fundamental observers.

The kinematics of the fundamental geodesic flow can be described using Fermi normal coordinates around, e.g., the worldline $\mathscr{L}_0$ defined by $x^i = 0$. A possible choice is

$$\tau \equiv t + \frac{H}{2}\,[a(t)r]^2, \tag{4.11}$$

$$D \equiv a(t)r, \tag{4.12}$$

in terms of which the metric is indeed Minkowskian, up to terms on the order of curv. $\times D^2$,

$$\mathrm{d}s^2 = (-1 + 3H^2D^2 + \dot{H}D^2 + \ldots)\mathrm{d}\tau^2 + (1 + H^2D^2 + \ldots)\mathrm{d}D^2 + D^2\mathrm{d}\Omega^2 + \ldots \tag{4.13}$$

In the vicinity of $r = 0$, the quantity $D = a(t)r$ is thus a good notion of physical distance[1]. We conclude that a particle following the neighbouring fundamental geodesic $\mathscr{L}_r$, with comoving coordinate r, moves radially with respect to $\mathscr{L}_0$, with a velocity $v = \mathrm{d}D/\mathrm{d}\tau = \dot{a}r = HD$ as measured in the observer's frame. Because the origin of the spatial coordinate system is arbitrary, the previous reasoning equally applies to the vicinity of any fundamental observer. The cases $H \leq 0$ or $H \geq 0$ therefore correspond respectively to a contracting or expanding universe, in which fundamental observers are all approaching or receding from each other. In 1929, the observation of nearby galaxies by Hubble [65] revealed that our Universe lies in the second case. It also established empirically the relation $v = HD$, called the *Hubble law* in the honour of its discoverer.

4.1.2 Dynamics of cosmic expansion

The dynamics of the scale factor, hence of cosmic expansion, is governed by the matter content of the Universe via the Einstein equation. Before we analyse their specific consequences, let us first discuss the description of matter in cosmology.

Description of matter

For matter to respect the assumptions of homogeneity and isotropy, its stress-energy tensor must read

$$T_{\mu\nu} = \rho(t)\,u_\mu u_\nu + p(t) \perp_{\mu\nu}, \tag{4.14}$$

identified with a homogeneous perfect fluid[2] following the fundamental geodesic flow, with $\boldsymbol{u} = \boldsymbol{\partial}_t$, and whose energy density ρ and isotropic pressure p do not depend on spatial coordinates; $\perp_{\mu\nu} \equiv g_{\mu\nu} + u_\mu u_\nu$ denotes the projector on spatial sections $t =$ cst, hence $\perp_{\mu 0} = 0$ and $\perp_{ij} = g_{ij}$ here. The form (4.14) of $T_{\mu\nu}$ forbids, for instance, the presence of a

---

[1]All the worldline-event distances defined in the previous chapter coincide with D up to curvature terms. Note that we could have replaced r by χ in the expression of D, since both quantities differ by terms on the order of $K\chi^2$.

[2]A perfect fluid is an idealised fluid model with no viscosity, anisotropic stress, or diffusive heat transport.

cosmic electromagnetic field which, as we will see in Chap. 9, generically creates anisotropy. Nevertheless, the superposition of a large number of electromagnetic fields with random polarisations, i.e. a gas of photons, is allowed.

The cosmological fluid described by the stress-energy tensor (4.14) is in principle made of several species s, so that we must write

$$\rho = \sum_s \rho_s, \qquad p = \sum_s p_s. \tag{4.15}$$

Each species is characterised by its equation-of-state parameter w, defined as the ratio between its pressure and its energy density

$$w_s \equiv \frac{p_s}{\rho_s}, \tag{4.16}$$

or in other words, the ratio between (two thirds of) its microscopic kinetic energy and its total energy. For example, a nonrelativistic perfect gas of point particles with mass m at a temperature T has

$$w_{\mathrm{gas}} = \frac{k_{\mathrm{B}} T}{mc^2} = 9.20 \times 10^{-11} \left(\frac{T}{100 \ \mathrm{K}} \right) \left(\frac{m_{\mathrm{p}}}{m} \right), \tag{4.17}$$

where $k_{\mathrm{B}} = 1.38 \times 10^{-23}$ J/K is the Boltzmann constant, and $m_{\mathrm{p}} = 938 \ \mathrm{MeV}/c^2$ is the proton mass; w_{gas} is thus a very small quantity, except at very high temperatures, for which the gas becomes relativistic. The other end of the spectrum is ultrarelativistic matter, i.e. radiation, for which we have already seen in § 1.1.3 that $w_{\mathrm{rad}} = 1/3$. The effective equation-of-state parameter for the cosmological fluid can be written as

$$w \equiv \frac{p}{\rho} = \sum_s f_s w_s, \qquad \text{with} \quad f_{\mathrm{s}} \equiv \frac{\rho_s}{\rho}; \tag{4.18}$$

it approaches 0 when the total energy is dominated by nonrelativistic matter (baryons, dark matter), and 1/3 when dominated by radiation (photons, neutrinos).

The conservation of total matter's energy $\nabla_\mu T^{\mu 0} = 0$ leads to the following constraint for the time evolution of ρ

$$\boxed{\dot\rho + 3H(1+w)\rho = 0,} \tag{4.19}$$

while the conservation of total momentum $\nabla_\mu T^{\mu i} = 0$ is here trivially satisfied.

The Friedmann equations

The Einstein equation, including a cosmological constant and using the stress-energy tensor (4.14) on the right-hand side leads to the two *Friedmann equations* governing the dynamics of cosmic expansion

$$\boxed{\begin{aligned} H^2 &= \frac{8\pi G}{3}\rho - \frac{K}{a^2} + \frac{\Lambda}{3}, \\[2mm] \frac{\ddot a}{a} &= -\frac{4\pi G}{3}(1 + 3w)\rho + \frac{\Lambda}{3}. \end{aligned}}$$

$$\tag{4.20}$$
$$\tag{4.21}$$

Because of the link between the conservation of energy-momentum and the Bianchi identity, Eq. (4.19) is not independent from the Friedmann equations, more precisely $\mathrm{d}(4.20)/\mathrm{d}t - 2 \times (4.21) \Leftrightarrow (4.19)$.

The first Friedmann equation (4.20) shows that, at any time, the cosmic expansion rate has three distinct contributions: matter's energy density, spatial curvature, and cosmological constant. Their relative weight is usually quantified by introducing the associated *cosmological parameters*

$$\Omega_{\rm m} \equiv \frac{8\pi G \rho}{3H^2}, \qquad \Omega_K \equiv \frac{-K}{a^2 H^2}, \qquad \Omega_\Lambda \equiv \frac{\Lambda}{3H^2}, \tag{4.22}$$

whose sum is 1 by virtue of Eq. (4.20). In the case where $\Omega_{\rm m} \gg \Omega_K, \Omega_\Lambda$, and assuming that matter's energy density is dominated by its nonrelativistic ($w = 0$) or ultrarelativistic ($w = 1/3$) component, we find from Eq. (4.19)

$$\rho \propto \begin{cases} a^{-3} & \text{if } w = 0 \\ a^{-4} & \text{if } w = 1/3 \end{cases}. \tag{4.23}$$

Equation (4.20) is then integrated as

$$a \propto \begin{cases} t^{2/3} \propto \eta^2 & \text{if } w = 0 \\ t^{1/2} \propto \eta & \text{if } w = 1/3 \end{cases}. \tag{4.24}$$

Another interesting case is $\Omega_K \ll \Omega_{\rm m}, \Omega_\Lambda > 0$, with $w = 0$, which yields

$$a(t) \propto \sinh^{2/3}\left(\frac{\sqrt{3\Lambda}}{2} t\right). \tag{4.25}$$

This solution coincides with $a \propto t^{2/3}$ in the limit $\Lambda \to 0$; on the contrary, when the cosmological constant dominates over the contribution of matter we get $a(t) \propto \exp(t\sqrt{\Lambda/3}) = \exp(Ht)$, the expansion rate being a constant in this case.

Possible sources of accelerated expansion

The last case is an example of accelerated expansion ($\ddot{a} > 0$), driven by a positive cosmological constant. As clearly shown by the second Friedmann equation (4.21), standard matter is generally unable to produce such an acceleration—which fits with our Newtonian intuition that gravity is an attractive force—unless its energy density is negative, or $w < -1/3$. The first possibility is excluded by stability requirements; the second one would mean that matter has negative pressure, which cannot happen with standard matter since pressure is proportional to kinetic energy, hence always positive. However, such a behaviour can be *mimicked* by a quantum field[3], the simplest example being a scalar.

Consider a scalar field ϕ minimally coupled with spacetime geometry, and self interacting through a potential $V(\phi)$. The associated action reads

$$S_{\rm sf}[\phi, \boldsymbol{g}] = \int_{\mathcal{M}} {\rm d}^4 x \, \sqrt{-g} \left[-\frac{1}{2}\partial_\mu \phi \, \partial^\mu \phi - V(\phi) \right], \tag{4.26}$$

and the corresponding stress-energy tensor is

$$T_{\mu\nu}^{\rm sf} \equiv \frac{-2}{\sqrt{-g}} \frac{\delta S_{\rm sf}}{\delta g^{\mu\nu}} = \partial_\mu \phi \, \partial_\nu \phi - \frac{1}{2}(\partial^\rho \phi \, \partial_\rho \phi) \, g_{\mu\nu} - V(\phi) g_{\mu\nu}. \tag{4.27}$$

---

[3]Quantisation is actually not required here, but an action of the form (4.26) is motivated by quantum field theory.

Suppose this field is homogeneous on spatial sections $t = \text{cst}$, then $\partial_\mu \phi = -\dot\phi\, u_\mu$ and the above stress-energy tensor takes the form

$$T_{\mu\nu}^{\text{sf}} = \left(\frac{\dot\phi^2}{2} + V \right) u_\mu u_\nu + \left(\frac{\dot\phi^2}{2} - V \right) \perp_{\mu\nu}, \qquad (4.28)$$

readily identified with Eq. (4.14). A homogeneous scalar field thus behaves similarly to a perfect fluid with equation-of-state parameter

$$w_{\text{sf}} = \frac{\dot\phi^2 - 2V(\phi)}{\dot\phi^2 + 2V(\phi)}, \qquad (4.29)$$

which can be negative, and even reach -1 if the field evolves very slowly compared to the amplitude of its potential, $\dot\phi^2 \ll V(\phi)$. In this extreme case, it is similar to the cosmological constant, $T_{\mu\nu}^{\text{hsf}} = -V g_{\mu\nu}$.

As will be discussed in § 4.1.3, our Universe seems to have experienced two eras of accelerated expansion: an early-time one known as *inflation*, and a recent one. Both can be driven by a scalar field—respectively called *inflaton* and *quintessence* [72]—but there are in fact many other mechanisms capable of producing acceleration, gathered in the denomination of *dark energy* [73] in the late-time case. A noncomprehensive list includes:

- The presence of **exotic matter**, either minimally coupled to gravity, such as quintessence and Chaplygin gas [74], or nonminimally coupled such as chameleons [75], Galileons, Horndeski theories [76] and beyond [77,78]. Models involving nonminimally coupled fields can also be viewed as

- **modified theories of gravity** [79], more precisely scalar-tensor theories, which also contain $f(R)$ actions [80]. Other theories beyond GR include bimetric and massive gravities [81], Lorentz-violating models like Einstein-æther gravity [82], etc.

- In a more conservative way, acceleration could be due to the **backreaction** of inhomogeneities on the average cosmic expansion [83–85] (see also § 4.2.3).

Another possibility is that acceleration is apparent, due to a misinterpretation of our observations. Two scenarios—though now ruled out as viable explanations of dark energy—can be cited:

- A strong absorption of the photons emitted by SNe, or their oscillations with axions [86], which would explain their overdimming (see § 5.3.1) by violating the distance-duality relation. The photon-axion oscillation model has been eliminated by taking into account the effects intergalactic plasma [87]. Besides, the violations of the distance duality relation compatible with observations [60] are not sufficient to explain SN data without the need of dark energy.

- A second option consists in violating the Copernical principle, by assuming that we lie at the centre of a huge void [88] (modelled e.g. by the Lemaître-Tolman-Bondi metric) expanding faster than the homogeneous Universe. This possibility is nevertheless highly constrained by observations related to CMB scattering (see Ref. [89] and references therein), and would therefore require a unnatural level of fine tuning.

4.1.3 Content and history of our Universe

The cosmological parameters of our Universe, whose geometry is assumed to be well modelled by the FL metric, have been measured with an increasing precision over the last decades. Most observations agree [90] on the following value for today's expansion rate [91]

$$H_0 = 67.74 \pm 0.46 \,\text{km/s/Mpc}, \tag{4.30}$$

often written as $H_0 = h \times 100 \,\text{km/s/Mpc}$, and with the *concordance set* of cosmological parameters [91]

$$\Omega_{\text{m0}} = 0.3089 \pm 0.0062, \qquad \Omega_{K0} = 0.0008^{+0.0040}_{-0.0039}, \qquad \Omega_{\Lambda 0} = 0.6911 \pm 0.0062, \tag{4.31}$$

where a subscript zero conventionally denotes today's value of a quantity. The mean matter density in today's Universe is therefore $\rho_{\text{m0}} \sim 3 \times 10^{-27} \,\text{kg/m}^3$. Among this matter content, only one sixth is made of quarks and nonrelativistic leptons—abusively called *baryonic matter* in cosmology, as leptons and mesons do not contribute significantly to the total amount—with $\Omega_{\text{b0}} h^2 = 0.02230 \pm 0.00014$ [91], while radiation—photons and neutrinos—represent much less, $\Omega_{\text{r0}} \sim 10^{-4}$. The actual nature of the remainder is unknown, except that it is nonrelativistic and does not seem to interact with normal matter; it has in particular no electromagnetic signature, and therefore has been denominated (cold) *dark matter* [92]. The resulting cosmological model, in which spacetime is described by the FL geometry, whose dynamics is dictated by General Relativity with a cosmological constant, and where five sixth of the material content today is made of noninteracting and nonrelativistic dark matter, is known as Λ-Cold-Dark-Matter (ΛCDM).

Let us close this section with a brief history of our Universe, as inferred in the ΛCDM framework and summarised in Fig. 4.2. First of all, following the Friedmannian dynamics backwards in time[4] shows that a singularity, namely $a = 0$, occurs in a finite-time past. If this so-called *Big Bang* singularity is taken as the origin of cosmic time, then today corresponds to $t_0 = 13.81 \,\text{Gyr}$. During the first $\sim 10^{-32}\,\text{s}$ after the Planck era ($t \sim 10^{-35}\,\text{s}$), our Universe is thought to have experienced a first period of accelerated expansion, *cosmic inflation*, during which distances have increased by a factor e^N, where $N > 60$ is the number of *e*-folds characterising the duration of inflation. Originally introduced as a solution to the flatness and horizon problems of the Hot-Big-Bang model [93–95], inflation now fully belongs to standard cosmology; see however Refs. [96, 97] for alterinflationarist theories. Although hundreds of inflationary models have been proposed and tested against observations [98], the most popular ones involve a single scalar field (the inflaton), whose slight inhomogeneities, due quantum fluctuations, have been the seeds of the structures that we observe today. The end of inflation is followed by a *reheating* phase, during which the inflaton decays into particles of the standard model of particle physics. Nevertheless, the underlying mechanisms are still poorly constrained by observations [99].

After reheating, the Universe is made of a dense quark and lepton plasma. As the temperature drops due to expansion, hadrons are formed, followed by light atomic nuclei (essentially deuterium, helium, and lithium): this is *primordial nucleosynthesis* (from $k_{\text{B}}T \sim 150 \,\text{MeV}$ to $\sim 50 \,\text{keV}$). At the end of this period, the scale factor reads $a_0/a_{\text{n}} = 5 \times 10^7$, and the expansion dynamics is still by far dominated by radiation. However, as seen in Eq. (4.23), the energy density of radiation decreases faster than the one of nonrelativistic matter, and both contributions become comparable ($\Omega_{\text{r}} \sim \Omega_{\text{m}}$) for

---

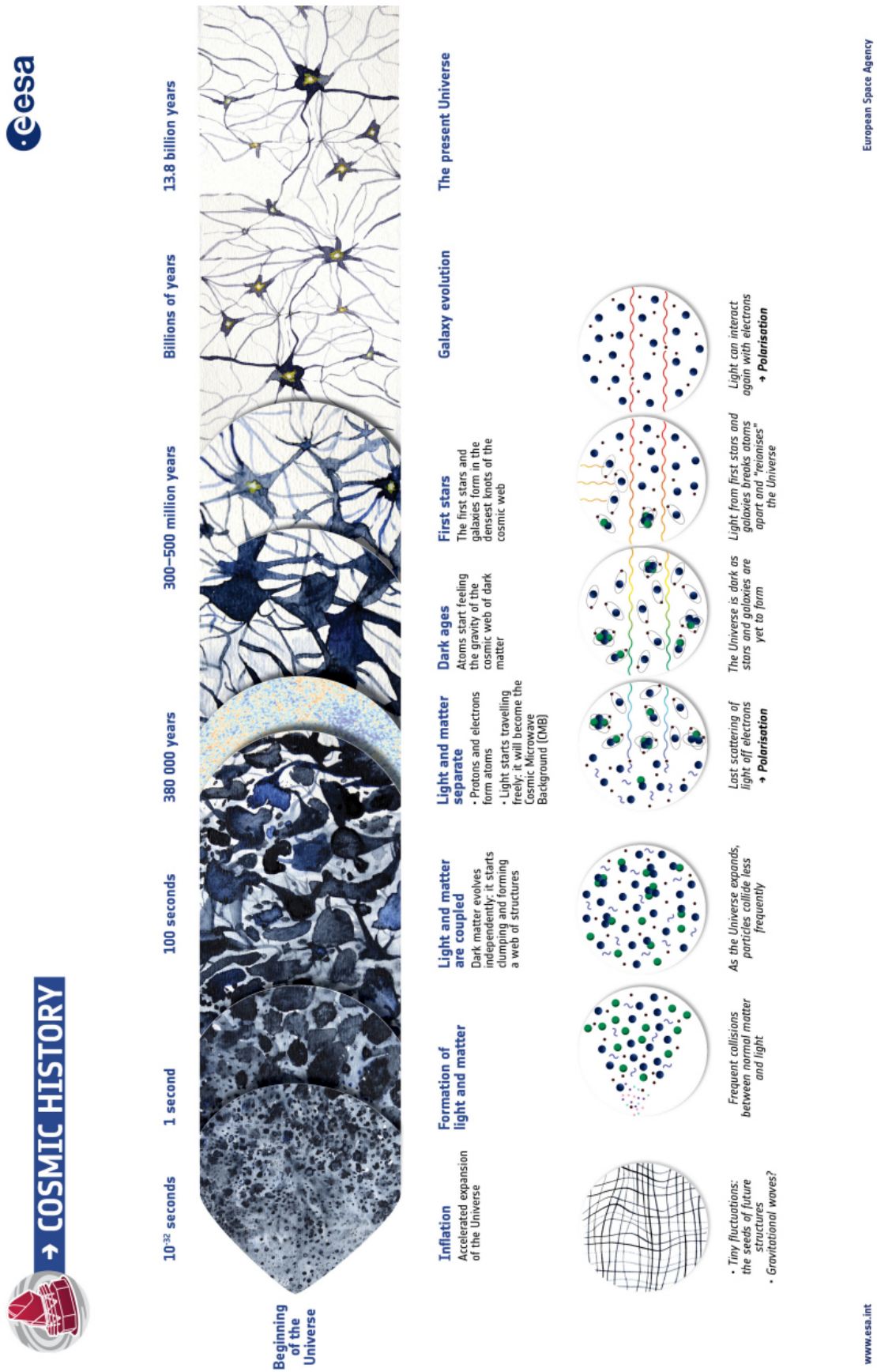[4]and extrapolating it to energy scales where current physical theories are expected to break down

Figure 4.2 A brief history of our Universe, in terms of cosmic time t. Image courtesy of ESA.

$a_0/a_{\rm eq} = \Omega_{\rm m0}/\Omega_{\rm r0} \approx 3400$. This *equality* represents the transition between the radiation and matter eras, i.e. between the two expansion laws of Eq. (4.24). At this stage, however, the photon fluid is still dense and energetic enough to maintain matter ionised. For $a_0/a_* = 1100$ ($k_{\rm B}T_* \sim 0.3\,{\rm eV}$), this condition is no longer fulfilled, and the *recombination* of atomic nuclei and electrons into atoms occurs, followed by the *decoupling* between photons and electrons: the Universe becomes neutral and transparent. The light released at that epoch is observed today under the form of a cosmic microwave background (CMB).

After recombination, the Universe remains neutral for a few hundreds of millions of years (the *dark ages*), during which structures form via gravitational accretion. On small scales, some matter clumps collapse and get hot enough to activate the fusion of hydrogen into helium, giving birth to the first stars. The light they emit induces a *reionisation* of the Universe ($a_0/a_{\rm re} \approx 12$). The next billions of years are then characterised by the formation and evolution of galaxies on small scales; and by the apparition of a large-scale cosmic web [100], where voids (from 10 to 150 Mpc) are separated by walls and filaments. The cosmological constant starts to dominate over matter's energy density for $a_0/a_{\rm ded} \approx 1.3$, leading to an acceleration of cosmic expansion well described by Eq. (4.25).

4.2 Linear perturbation theory

Our own existence, on a planet orbiting around a star, within a galaxy belonging to a supercluster, indicates that the Universe is not perfectly homogeneous, but rather presents structures over a wide variety of scales, the largest one being the cosmic web, whose typical inhomogeneity scale is ~ 100 Mpc today. A possible strategy for modelling this departure from strict homogeneity and isotropy consists in introducing small perturbations to FL geometry. In this section—essentially based on textbook [101], though much less complete—we summarise the main features of the cosmological perturbation theory at linear order.

4.2.1 Perturbed quantities

The scalar-vector-tensor decomposition

Before discussing the standard perturbation scheme, let us introduce the scalar-vector-tensor (SVT) decomposition of spatial vectors and tensors. Let $\boldsymbol{V}$ be a vector tangent to a spatial hypersurface Σ_t equipped with the metric $\boldsymbol{\gamma}(t)$. It can be uniquely decomposed into a gradient part and a curl (divergent-free) part as

$$V_i = \partial_i V + \hat{V}_i, \qquad \text{with} \quad {\rm D}_i \hat{V}^i = 0, \tag{4.32}$$

where $\mathbf{D}$ denotes the covariant derivative associated with the Levi-Civita connection of $\boldsymbol{\gamma}(t)$. The 3 degrees of freedom (dofs) of $\boldsymbol{V}$ are thus split into 1 scalar dof plus $3-1=2$ vector dofs. Note that, in all this section, *the indices $i, j, \ldots$ are raised and lowered by γ^{ij} and γ_{ij}, and a hat will always denote a divergence-free quantity.*

Similarly, any rank-two symmetric tensor $\boldsymbol{T} \in {\rm T}\Sigma_t \otimes {\rm T}\Sigma_t$ can be decomposed as

$$T_{ij} = {\rm D}_i {\rm D}_j T_1 + T_2\,\gamma_{ij} + {\rm D}_{(i}\hat{T}_{j)} + \hat{T}_{ij}, \qquad \text{with} \quad {\rm D}_i \hat{T}^i = {\rm D}_i \hat{T}^{ij} = \hat{T}^i_i = 0, \tag{4.33}$$

which spreads the 6 dofs of $\boldsymbol{T}$ into 2 scalar dofs, $3-1=2$ vector dofs, and $6-3-1=2$ tensor dofs. Such decompositions will be particularly convenient for the cosmological perturbation theory, because the scalar, vector, and tensor components will turn out to decouple from each other at linear order.

Perturbed metric

The cosmological perturbation theory consists in modelling the full spacetime metric $\boldsymbol{g}$ as approximately equal to the FL metric $\bar{\boldsymbol{g}}$—hereafter, a bar denotes an unperturbed, background quantity—from which it differs by a small perturbation $\delta\boldsymbol{g}$. The general expression for this perturbed metric is thus

$$\mathrm{d}s^2 = (\bar{g}_{\mu\nu} + \delta g_{\mu\nu})\,\mathrm{d}x^\mu\mathrm{d}x^\nu \tag{4.34}$$
$$= a^2(\eta)\left[-(1+2A)\mathrm{d}\eta^2 + 2B_i\mathrm{d}x^i\mathrm{d}\eta + (\gamma_{ij} + 2C_{ij})\mathrm{d}x^i\mathrm{d}x^j\right], \tag{4.35}$$

where $A, B_i, C_{ij} \ll 1$. All three are functions of the spacetime coordinates (η, x^k). Mathematically speaking, they are respectively a scalar, a vector and a tensor with respect to the spatial hypersurfaces Σ_t equipped with the background spatial metric $\boldsymbol{\gamma}$. As such, B_i and C_{ij} can be decomposed according to the SVT scheme as

$$B_i = \mathrm{D}_i B + \hat{B}_i \tag{4.36}$$
$$C_{ij} = \mathrm{D}_i\mathrm{D}_j C_1 + C_2\gamma_{ij} + \mathrm{D}_{(i}\hat{C}_{j)} + \hat{C}_{ij} \tag{4.37}$$

with the conventional requirements on hatted quantities. Among the 10 dofs of the set $\{A, B_i, C_{ij}\}$, 4 are spurious, because associated with the detailed coordinate mapping between the background and perturbed spacetimes (see e.g. Chap. 5 of Ref. [101] for details). This issue is known as the *gauge freedom* of the cosmological perturbation theory. The remaining $10-4=6$ dofs can be encoded into the following gauge-invariant quantities

$$\Phi \equiv A + \mathcal{H}(B - C_1') + (B - C_1')', \tag{4.38}$$
$$\Psi \equiv -C_2 - \mathcal{H}(B - C_1'), \tag{4.39}$$
$$\hat{\Omega}_i \equiv \hat{B}_i - (\hat{C}_i)', \tag{4.40}$$
$$\hat{C}_{ij}. \tag{4.41}$$

As in classical electrodynamics, the gauge can be fixed by imposing some conditions on the gauge fields (here A, B_i, C_{ij}). A few interesting choices exist, we here choose to work in the so-called Poisson (or Newtonian or longitudinal) gauge, for which

$$B = C_1 = \hat{C}_i = 0, \tag{4.42}$$

so that the metric can be completely written in terms of gauge-invariant quantities as

$$\boxed{\mathrm{d}s^2 = a^2(\eta)\left[-(1+2\Phi)\mathrm{d}\eta^2 + 2\hat{\Omega}_i\mathrm{d}x^i\mathrm{d}\eta + (1-2\Psi)\gamma_{ij}\mathrm{d}x^i\mathrm{d}x^j + \hat{C}_{ij}\mathrm{d}x^i\mathrm{d}x^j\right].} \tag{4.43}$$

Note that there are some variations in what is called Newtonian gauge in the literature; for instance, in Ref. [101] $\hat{B}_i$ is set to zero, while $\hat{C}_i$ is nonzero in general. The perturbations of geometrical quantities (Christoffel symbols, curvatures,...) associated with the metric (4.43) can be found in the Appendix C of Ref. [101].

Physically speaking, (i) the scalars Φ, Ψ, called the Bardeen potentials, are analogous to the Newtonian gravitational potential; (ii) the vector perturbation Ω_i is a gravitomagnetic term producing inertial-frame dragging, analogously to the $g_{t\phi}$ component of the Kerr geometry [102]; while (iii) the tensor perturbation $\hat{C}_{ij}$ represents gravitational waves.

Perturbed stress-energy tensor

The perturbations of spacetime's geometry are sourced by inhomogeneities of the distribution of matter. We here make the simplifying assumptions that the perturbed cosmological fluid (i) consists of one species; and (ii) can still be modelled by a perfect fluid. The associated perturbed stress-energy tensor thus reads

$$T_{\mu\nu} = \bar{T}_{\mu\nu} + \delta T_{\mu\nu} \tag{4.44}$$
$$= (\rho + p)u_\mu u_\nu + p\, g_{\mu\nu}. \tag{4.45}$$

While these assumptions are wrong in general, they are sufficient to model matter during the (dark-)matter-dominated and dark-energy-dominated eras, where matter's anisotropic stress is negligible.

Decomposing each quantity q of Eq. (4.45) as $\bar{q} + \delta q$ yields

$$\delta T_{\mu\nu} = (\delta\rho + \delta p)\bar{u}_\mu \bar{u}_\nu + 2(\bar{\rho} + \bar{p})\bar{u}_{(\mu}\delta u_{\nu)} + \bar{p}\,\delta g_{\mu\nu}. \tag{4.46}$$

The conventional normalisations of the background and perturbed flows $\bar{u}^\mu$ and u^μ, namely

$$\bar{g}_{\mu\nu}\bar{u}^\mu \bar{u}^\nu = g_{\mu\nu} u^\mu u^\nu = -1 \tag{4.47}$$

imply at first order

$$2g_{\mu\nu}\bar{u}^\mu \delta u^\nu + \delta g_{\mu\nu}\bar{u}^\mu \bar{u}^\nu = 0 \qquad \text{i.e.} \qquad \delta u^0 = -\frac{\Phi}{a}, \tag{4.48}$$

where it is understood that a 0th component refers to a component with respect to ∂_η. As for the spatial components of the perturbation of the four-velocity, they can be written as $\delta u^i = a^{-1}v^i$, where the vector $v^i \partial_i$ belongs to $\mathrm{T}\Sigma_t$—like the vector perturbation of the metric—and can thus be decomposed as

$$v_i = \partial_i v + \hat{v}_i. \tag{4.49}$$

These perturbation of matter's stress-energy tensor is also subject to gauge freedom, and it can be shown that the following combinations

$$\delta\rho_\mathrm{P} \equiv \delta\rho + \bar{\rho}'(B - C_1'), \tag{4.50}$$
$$\delta p_\mathrm{P} \equiv \delta p + \bar{p}'(B - C_1'), \tag{4.51}$$
$$\Upsilon = v + C_1, \tag{4.52}$$
$$\hat{\Upsilon}_i = \hat{v}_i + \hat{C}_i, \tag{4.53}$$

which coincide with $\delta\rho, \delta p, v, \hat{v}_i$ respectively in the Poisson gauge ($B = C_1 = \hat{C}_i = 0$), are gauge invariant.

Because the cosmological fluid is assumed to contain a single matter species, its pressure and energy density are univocally related, through $p = w\rho$. As a consequence, their perturbations are related as well; in particular, the ratio

$$\frac{\delta p}{\delta\rho} = \frac{\mathrm{d}p}{\mathrm{d}\rho} = w + \rho\frac{\mathrm{d}w}{\mathrm{d}\rho} \equiv c_\mathrm{s}^2 \tag{4.54}$$

defines the *sound velocity* c_s, i.e. the velocity of adiabatic pressure waves within the fluid. For $w = \mathrm{cst}$, we thus have $c_\mathrm{s}^2 = w$. Note that c_s^2 is gauge invariant, since

$$\frac{\delta p_\mathrm{N}}{\delta\rho_\mathrm{N}} = \frac{\delta p + \bar{p}'(B - C_1')}{\delta\rho + \bar{\rho}'(B - C_1')} = \frac{c_\mathrm{s}^2\delta\rho + c_\mathrm{s}^2\bar{\rho}'(B - C_1')}{\delta\rho + \bar{\rho}'(B - C_1')} = c_\mathrm{s}^2 \tag{4.55}$$

at first order in perturbations.

4.2.2   Evolution of perturbations

Let us now focus on the evolution equations for the metric and matter perturbations. As previously mentioned, the equations of motion naturally separate into a decoupled set of scalar, vector, and tensor modes.

Einstein's equation

The *tensor modes* of the Einstein's equation yields

$$\hat{C}_{ij}'' + 2\mathcal{H}\,\hat{C}_{ij}' + (2K - \Delta)\hat{C}_{ij} = 0, \tag{4.56}$$

with $\Delta \equiv \gamma^{ij}\mathrm{D}_i\mathrm{D}_j$; it is analogous to a wave equation with friction $(2\mathcal{H}\hat{C}_{ij}')$ in a harmonic potential with stiffness $2K$. During the matter- and radiation-dominated eras, Eq. (4.56) can be solved in Fourier space thanks to Bessel functions. The amplitude of $\hat{C}_{ij}$ turns out to decrease with $k\eta$, and is therefore negligible on small scales and at late times.

The *vector modes* satisfy the following constraint and evolution equations:

$$(\Delta + 2K)\hat{\Omega}_i = -16\pi G\bar{\rho}a^2(1+w)\hat{\Upsilon}_i \tag{4.57}$$

$$\hat{\Omega}_i' + 2\mathcal{H}\hat{\Omega}_i = 0. \tag{4.58}$$

From the second one, we deduce that $\hat{\Omega}_i \propto a^{-2}$, the vector perturbation of the metric is damped in an expanding Universe, and can therefore be neglected in late-time cosmology.

Finally, the *scalar modes* of Einstein's equation read

$$(\Delta + 3K)\Psi = 4\pi Ga^2\left(\delta\rho_\mathrm{P} + \bar{\rho}'\Upsilon\right) \tag{4.59}$$

$$\Psi - \Phi = 0 \tag{4.60}$$

$$\Psi' + \mathcal{H}\Phi = -4\pi G\bar{\rho}(1+w)\Upsilon \tag{4.61}$$

$$\Psi'' + 3\mathcal{H}(1+c_\mathrm{s}^2)\Psi' + \left[2\mathcal{H}' + (\mathcal{H}^2 - K)(1+3c_\mathrm{s}^2)\right]\Psi - c_\mathrm{s}^2\Delta\Psi = 0 \tag{4.62}$$

Note the similarity between Eq. (4.59) and the Poisson equation of Newtonian gravitation. The second term on its right-hand side, $\bar{\rho}'\Upsilon$, is related to the perturbation of the fluid's velocity, it can be understood as a kinetic energy term which, contrary to the Newtonian case, gravitates just as mass does.

Conservation of energy and momentum

The conservation of the fluid's energy and momentum, encoded in the equation $\nabla_\mu T^{\mu\nu} = 0$, also leads to a set of equations for the vector and scalar modes of matter perturbations. The *vector mode*, on the one hand, satisfies

$$\hat{\Upsilon}_i' + \mathcal{H}(1 - 3c_\mathrm{s}^2)\hat{\Upsilon}_i = 0. \tag{4.63}$$

When the sound velocity c_s is nonrelativistic $(c_\mathrm{s}^2 \ll 1)$, then $\hat{\Upsilon}_i \propto a^{-1}$. On the other hand, the *scalar modes* are governed by

$$\delta_\mathrm{P}' + 3\mathcal{H}(c_\mathrm{s}^2 - w)\delta_\mathrm{P} = -(1+w)(\Delta\Upsilon - 3\Psi') \tag{4.64}$$

$$\Upsilon' + \mathcal{H}(1 - 3c_\mathrm{s}^2)\Upsilon = -\Phi - \frac{c_\mathrm{s}^2}{1+w}\,\delta_\mathrm{P} \tag{4.65}$$

where we introduced the *density contrast*

$$\delta \equiv \frac{\delta\rho}{\bar{\rho}}, \tag{4.66}$$

which, here, is worked out in the Poisson gauge and thus denoted δ_{P}. Equation (4.64) is analogous to the conservation of mass in fluid dynamics, while Eq. (4.65) is similar to a integral of the Euler equation. Note that, just like in the unperturbed FL case, the evolution equations for matter and spacetime's metric are not independent from each other. For instance, inserting (4.58) into d(4.57)/dη yields (4.63). In the set of all the scalar equations, only four are independent (three if we directly replace Ψ by Φ).

Newtonian regime

Let us focus on the late-time Universe, where the cosmological fluid essentially consists of a pressureless matter, so that we can take $w = c_{\mathrm{s}}^2 = 0$ in all the above equations. Besides, as previously mentioned, vector and tensor perturbations decrease with cosmic expansion, so that we can neglect them at late times for any reasonable initial condition, the metric therefore reads

$$\mathrm{d}s^2 = a^2(\eta)\left[-(1+2\Phi)\mathrm{d}\eta^2 + (1-2\Phi)\gamma_{ij}\mathrm{d}x^i\mathrm{d}x^j\right] \tag{4.67}$$

in that regime.

If we consider relatively small scales (compared to $\mathcal{H}^{-1}$), then the spatial derivatives of the perturbations completely dominate over the background quantities, in particular, in Eq. (4.59) $\Delta\Phi \gg 3K\Phi$, and

$$\frac{\delta\rho_{\mathrm{P}}}{\bar{\rho}'\Upsilon} \sim \frac{\delta_{\mathrm{P}}}{\mathcal{H}\Upsilon} \sim \frac{\delta_{\mathrm{P}}}{\Phi} \sim \frac{\Delta\Phi}{\mathcal{H}^2\Phi} \ll 1, \tag{4.68}$$

where we used successively Eqs. (4.19), (4.65), and (4.59). The resulting system of evolution equations reads

$$\boxed{\Delta\Phi = 4\pi G a^2 \bar{\rho}\delta,} \tag{4.69}$$
$$\boxed{\delta' = -\Delta\Upsilon,} \tag{4.70}$$
$$\boxed{\Upsilon' + \mathcal{H}\Upsilon = -\Phi,} \tag{4.71}$$

which is identical to the Euler-Poisson system of Newtonian cosmology. Note that we have dropped the index P of the density contrast δ, because in this regime the discrepancies due to a gauge choice vanish (for δ, but not for the metric perturbations). This is no longer true when Hubble-scale perturbations are at stake—see e.g. Fig. 5.6 of Ref. [101].

Equations (4.70) and (4.71) can be combined to get

$$\delta'' + \mathcal{H}\delta' = 4\pi G\bar{\rho}\delta, \tag{4.72}$$

which rules the evolution of δ only. It is straightforward to check that, during the matter-dominated era ($a \propto \eta^2$), Eq. (4.72) admits a growing solution D_+ and a damping solution D_- such that

$$D_+ \propto \eta^2 \propto a, \qquad D_- \propto \eta^{-3} \propto a^{-3/2}, \tag{4.73}$$

and over which the general solution can be decomposed as

$$\delta(\eta, x^k) = D_+(\eta \leftarrow \eta_{\mathrm{ini}})\delta_+(\eta_{\mathrm{ini}}, x^k) + D_-(\eta \leftarrow \eta_{\mathrm{ini}})\delta_-(\eta_{\mathrm{ini}}, x^k). \tag{4.74}$$

If the initial time is much later than matter-radiation equality, then the decaying mode can be neglected, and the density contrast becomes proportional to its initial condition $\delta(\eta, x^k) \approx D_+(\eta \leftarrow \eta_{\rm ini})\delta(\eta_{\rm ini}, x^k)$. The major part of structure formation occurs during the matter era, since the cosmological constant (or dark energy) starts to dominate at very late times, which justifies the relevance of the expressions (4.73) for $D_\pm$. The growing mode can however be modified to allow for the effect of Λ as [103]

$$D_+ \propto {}_2F_1\left[1, \frac{1}{3}; \frac{11}{6}; -\sinh^2\left(\frac{\sqrt{3\Lambda}}{2}t\right)\right]\sinh^{2/3}\left(\frac{\sqrt{3\Lambda}}{2}t\right) \tag{4.75}$$

$$\stackrel{\rm fit}{\approx} \frac{5}{2}\frac{a\Omega_{\rm m}}{\Omega_{\rm m}^{4/7} - \Omega_\Lambda + (1 - \Omega_{\rm m} + 2)(1 + \Omega_\Lambda/70)}. \tag{4.76}$$

Transfer function

The evolution equations being (by construction) linear, they are conveniently worked out in Fourier space. From now on, we suppose for simplicity that $K = 0$—a choice also motivated by observations—, so that the spatial metric is Euclidean, $\gamma_{ij} = \delta_{ij}$. Any quantity $Q(\eta, x^i)$ can then be decomposed into Fourier modes according to the convention

$$Q(\eta, x^i) = \int \frac{{\rm d}^3k}{(2\pi)^3}\, {\rm e}^{{\rm i}k_j x^j}\tilde{Q}(\eta, k_i), \tag{4.77}$$

$$\tilde{Q}(\eta, k_i) \equiv \int {\rm d}^3x\, {\rm e}^{-{\rm i}k_j x^j}Q(\eta, x^i). \tag{4.78}$$

The partial differential equations governing the evolution of perturbations thus become systems of independent ordinary differential equations (with respect to η) for each mode $\vec{k}$ of each quantity, which is therefore linearly related to its initial conditions. Regarding the scalar potential Φ in particular, it is customary to introduce the transfer function

$$T(\eta \leftarrow \eta_{\rm ini}, k_i) \equiv \frac{\tilde{\Phi}(\eta, k_i)}{\tilde{\Phi}(\eta_{\rm ini}, k_i)}, \tag{4.79}$$

which depends on the cosmological parameters.

4.2.3 Limits of the linear perturbation theory

Correlation function and power spectrum

Because the inhomogeneity of the Universe is believed to origin from the primordial quantum fluctuations of the inflaton, any comparison between theoretical predictions and observations must rely on statistics—in particular, the statistics of matter's density contrast δ. A central object, for that purpose, is the *correlation function*

$$\xi(\eta; x^i, y^i) \equiv \left\langle \delta(\eta, x^i)\delta(\eta, y^i)\right\rangle, \tag{4.80}$$

which quantifies the statistical similarity between $\delta(\eta, x^i)$ and $\delta(\eta, y^i)$. A positive correlation indicates that if the region around x^i is overdense (resp. underdense), then the region around y^i is likely to be overdense (resp. underdense). A negative correlation (anticorrelation) indicates the opposite situation.

The assumptions of statistical homogeneity and isotropy of our Universe, based on the cosmological principle, imply that ξ can only depend on the distance[5] between x^i and y^i,

$$\xi(\eta; x^i, y^i) = \xi(\eta; |x^i - y^i|). \tag{4.81}$$

As a consequence, the Fourier transform of ξ with respect to both x and y reads

$$\tilde{\xi}(\eta; k_i, l_i) \equiv \left\langle \tilde{\delta}(\eta, k_i) \, \tilde{\delta}(\eta, l_i) \right\rangle \tag{4.82}$$

$$= (2\pi)^3 \delta_{\mathrm{D}}(k_i + l_i) \, P_\delta(\eta; |k_i|), \tag{4.83}$$

where δ_{D} denotes the Dirac distribution, and where we introduced the matter *power spectrum P*, defined as

$$P(\eta; k) = \int \mathrm{d}^3 x \, \mathrm{e}^{\mathrm{i}k_j x^j} \xi(\eta; |x^i|) = 4\pi \int_0^\infty r^2 \mathrm{d}r \, \frac{\sin kr}{kr} \, \xi(\eta; r). \tag{4.84}$$

Analogous quantities can be defined for the other quantities of interest, in particular for the scalar potential Φ, whose evolution is described by the transfer function defined in Eq. (4.79), so that

$$P_\Phi(\eta; k) = T^2(\eta \leftarrow \eta_{\mathrm{ini}}, k) P_\Phi(\eta_{\mathrm{ini}}; k). \tag{4.85}$$

Figure 4.3 compares the observed power spectrum with theoretical predictions, in particular the linear perturbation theory (dashed line). We see that the latter fails at reproducing the actual behaviour of $P(k)$ on scales smaller than $10\,\mathrm{Mpc}/h$ ($k > 0.1h\,\mathrm{Mpc}$), where the nonlinearities of self-gravitating fluid dynamics become significant. On such scales, theoretical models must rely on advanced perturbative techniques [104] or *N*-body simulations (e.g. Ref. [105]).

Refinements

Besides nonlinearities at small scales, let us mention a few possible refinements for standard perturbation theory in general. Among the simplifying assumptions that we made in the present section, the crudest is the single-fluid approximation, which may be valid at late time but certainly not, e.g., at the epoch of recombination. A more precise approach considers the cosmological fluid as made of several species—see e.g. Ref. [101] for the detailed treatment of two fluids (dark matter and radiation). Nevertheless, a fluid description is not capable of modelling precisely the matter-matter and radiation-matter interactions, which rather require kinetic theory and the Boltzmann equation [107]. The presence of massive neutrinos also potentially affect the formation of the large-scale structure; this issue has been investigated, e.g., in Refs. [108–110].

Backreaction and related issues

By definition, the whole formalism developed in this section assumes that spacetime geometry is well approximated by the FL metric, i.e., that perturbations are small. While it should be valid on very large scales—i.e. typically for the description of the cosmic web, where substructures are somehow smeared out—such a perturbative approach is nevertheless highly questionable on small scales. For instance, the density contrast δ corresponding to a galaxy is $\rho_{\mathrm{gal}}/\rho_0 \sim 10^4 \gg 1$, which cannot be considered a small perturbation; the associated formalism thus should not be extrapolated to those scales.

---

[5]We here refer to distances within a spatial hypersurface, i.e. Euclidean distances as we set $K = 0$.
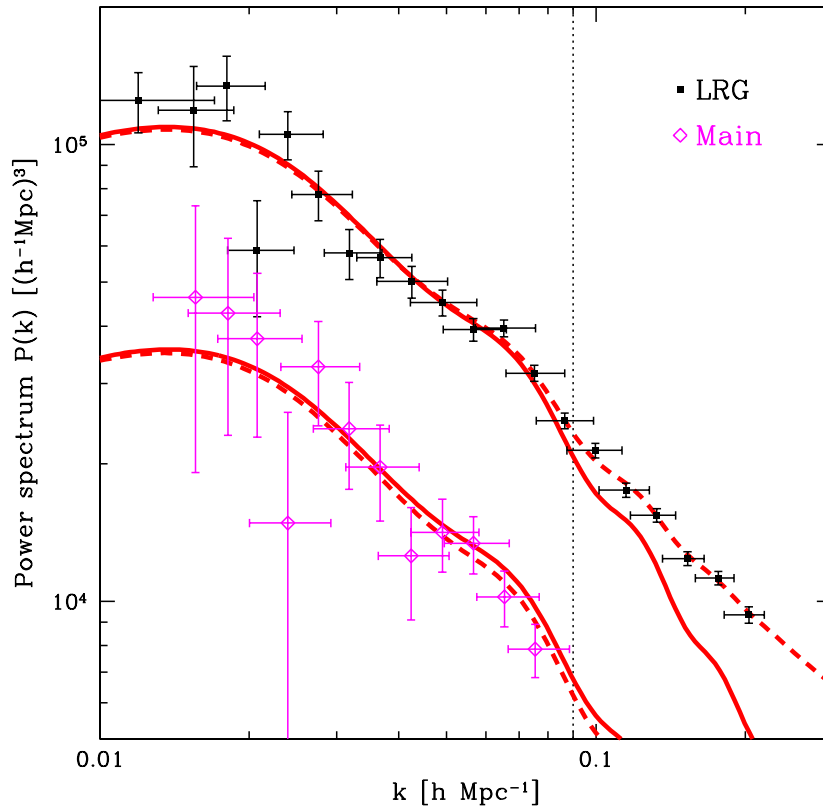
Figure 4.3 Matter power spectra measured from the luminous red galaxy (LRG) sample and the main galaxy sample of the Sloan Digital Sky Survey (SDSS). Red solid lines indicate the predictions of the linear perturbation theory, while red dashed lines include nonlinear corrections. From Ref. [106].

While the perturbative dynamics clearly breaks down on small scales, it can be argued that the form (4.67) of the metric still holds, except in the vicinity of very compact object such as neutron stars or black holes, because the density contrast δ is a second derivative of the metric perturbation Φ, therefore it can be very large with Φ remaining small. This argument is reinforced by the fact that Eq. (4.67) is essentially a metric formulation of Newtonian gravity, which turns out to be very successful at describing gravitating systems on small scales, far from compact objects. This question of how well is the Universe modelled by the FL metric is still an open question, and was recently the subject of a lively debate in Refs. [111–113].

It could be argued that cosmology does not a priori aim at describing the Universe on small scales. Just like geometric optics in dielectric media does not require to describe the interactions between each photon of the ray with each quark of each atom of each molecule of the medium, but rather relies on a continuous approximation, cosmology should not have to care about each star, or each dark matter halo to get a satisfactory description of the cosmos. There are however two significant differences between cosmology and this example of optics in media.

First, cosmology is mainly based on gravitation, which, if described by the general theory of relativity, is *nonlinear* contrary to electromagnetism. Linearity indeed facilitates smoothing procedures: suppose $\langle\ldots\rangle$ denotes a coarse-graining operator, then, in electromagnetism, the coarse-grained four-vector potential $\langle\boldsymbol{A}\rangle$ is governed by the Maxwell

equation with a coarse-grained four-current $\langle \boldsymbol{J} \rangle$, since

$$\boldsymbol{\nabla}^2 \langle \boldsymbol{A} \rangle = \left\langle \boldsymbol{\nabla}^2 \boldsymbol{A} \right\rangle = 4\pi \langle \boldsymbol{J} \rangle \,. \tag{4.86}$$

On the contrary, in gravitation the Riemann curvature, and thus the Einstein tensor, is highly nonlinear with respect to the metric $\boldsymbol{g}$, as it involves its inverse. It follows [30] that

$$\boldsymbol{E}[\langle \boldsymbol{g} \rangle] \neq \langle \boldsymbol{E}[\boldsymbol{g}] \rangle = 8\pi G \langle \boldsymbol{T} \rangle \,; \tag{4.87}$$

in other words, the procedures corresponding to (i) coarse graining a solution $\boldsymbol{g}$ of the Einstein equation driven by $\boldsymbol{T}$, or (ii) solving the Einstein equation driven by a coarse-grained $\langle \boldsymbol{T} \rangle$, yield different results. In cosmology, we ideally would like to perform (i), but the FL approach consists in (ii), the resulting Friedmann equations thus potentially predict a wrong dynamics for cosmic expansion. Contrary to electromagnetism, the small scales which are smeared out in cosmology can effectively reemerge in the large-scale dynamics. This issue, known as *backreaction*, has been proposed in the late 1990s as an explanation of the recent acceleration of cosmic expansion without the need of dark energy [114].

A second—though related—difference between gravitation and any other physical theory concerns the coarse-graining procedure itself. In a theory of macroscopic electromagnetism, for instance, the coarse-graining operator and the target of this operator (the electromagnetic field) are independent. In macroscopic gravitation, on the contrary, the metric is involved in the coarse-graining procedure (since it defines physical lengths and times) while being its target. This issue, together with the mathematical question of defining covariant averages in curved spacetime, has been addressed in Ref. [115], and summarised in Ref. [116] in a more cosmology-oriented way.

Relativistic effects in cosmology, including backreaction, have recently stimulated various works, both from the numerical [117, 118] and analytical points of view, such as the timescape scenario [85]; traceless backreaction [119], a Lagrangian perturbation theory based on a relativistic Zel'dovich approximation [120–122], an effective-cosmological-fluid theory [123],... As emphasized by Ref. [112], no definite conclusions on the amplitude of backreaction phenomena can be drawn so far.

The issues raised here concern the way we model the *dynamics* of cosmic expansion: How, given a realistic inhomogeneous distribution of matter in the Universe, does the latter evolve on large scales? Such a question however only represents half the way towards a fully relativistic description of the cosmos. The other half concerns *kinematics*—in particular optics: How does light propagates through a realistic model of the Universe? How can we allow for a realistic distribution of matter when interpreting cosmological observations? These questions are the main concerns of the present thesis. In the next chapter, we will present the answers proposed by standard cosmology, and then focus on alternatives in Part III.

Observations in standard cosmology

ALMOST all cosmological measurements rely, so far, on the observation of distant light sources, such as galaxies, supernovae, or quasars, in a wide range of wavelengths. Interpreting these observations, that is, extracting from them information about the structure and dynamics of the Universe, thus requires to know its optical properties. In this second chapter dedicated to standard cosmology, we present the answers provided by the Friedmann-Lemaître model and by the standard perturbation theory. We then review a number of cosmological observations with the constraints they impose on some cosmological parameters. Their surprising level of agreement, despite the fact that they involve totally different scales, finally leads us to discuss the motivations of this thesis.

Contents

5.1 Optics in homogeneous and isotropic cosmologies

This first section is dedicated to light propagation in Friedmann-Lemaître cosmologies. We first introduce a method for simplifying the underlying calculations, based on the invariance of lightcones under conformal transformations, and then use it to solve explicitly the null geodesic equations and calculate the lensing Jacobi matrix.

5.1.1 The conformal trick

As demonstrated in § 1.2.3, null geodesics are invariant under conformal transformations of spacetime's metric. This property can be conveniently exploited to simplify the analysis of light propagation in cosmology, since both the unperturbed and perturbed FL metrics take the form

$$\boldsymbol{g} = a^2(\eta)\,\tilde{\boldsymbol{g}}, \tag{5.1}$$

with, in the unperturbed case[1],

$$\tilde{g}_{\mu\nu}\mathrm{d}x^\mu\mathrm{d}x^\nu = -\mathrm{d}\eta^2 + \mathrm{d}\chi^2 + f_K^2(\chi)\left(\mathrm{d}\theta^2 + \sin^2\theta\,\mathrm{d}\varphi^2\right), \tag{5.2}$$

which does not depend on η. From a purely technical point of view, it is much simpler to analyse light propagation in terms of $\tilde{\boldsymbol{g}}$, getting rid of the geometrical terms due to the time evolution of a, and then recover all the lensing quantities for $\boldsymbol{g}$ thanks to the dictionary given in Table 5.1. *This dictionary is completely general*, in the sense that it applies for any metric and any conformal factor a; in particular, the latter could depend on all spacetime coordinates. It was used for instance in Ref. [124]—which belongs to the present thesis, see Chap. 8—in order to simplify the analysis of light propagation in anisotropic cosmologies of the Bianchi I kind.

Before applying it to the FL spacetime, let us comment a few entries of the conformal dictionary. Most relations are actually direct consequences of the definitions of the quantities at stake, in particular $\boldsymbol{\xi} = \tilde{\boldsymbol{\xi}}$ is due to the fact that the definition (2.9) of the separation vector does not involve the metric, but only the coordinates of null geodesics. On the contrary, $\boldsymbol{u} = a^{-1}\tilde{\boldsymbol{u}}$ is a *choice*, made here for simplicity, because the four-velocities of sources and observers are independent from the laws of light propagation. The correspondence between the Sachs bases follows from this choice, and from their normalisation conditions. One can also check that, with this correspondence, the partial parallel transport requirement (2.25) for $\boldsymbol{s}_A$ is satisfied iff it is for $\tilde{\boldsymbol{s}}_A$,

$$S_\nu^\mu\frac{\mathrm{D}s_A^\nu}{\mathrm{d}v} = 0 \iff \tilde{S}_\nu^\mu\frac{\widetilde{\mathrm{D}}\tilde{s}_A^\nu}{\mathrm{d}\tilde{v}} = 0. \tag{5.3}$$

5.1.2 Light rays

Without loss of generality, we choose the observation event O (here and now) to be the centre $\chi = 0$ of the spatial coordinate system. As mentioned in the previous chapter, in

---

[1]This conformal transformation is somehow incomplete for $K \neq 0$, in the sense that it does not fully take advantage of the conformal flatness of the FL geometry: there indeed exists a conformal factor $\Omega(x^\mu)$ such that $\boldsymbol{g} = \Omega^2\boldsymbol{f}$ where $\boldsymbol{f}$ is the Minkowski metric [71]. However, as we will see below, factorising a^2 out already simplifies enough the calculations.

Quantity	Correspondence
metric	$g_{\mu\nu} = a^2 \tilde{g}_{\mu\nu} \qquad g^{\mu\nu} = a^{-2}\tilde{g}^{\mu\nu}$
affine parameter	$\mathrm{d}v = a^2 \mathrm{d}\tilde{v}$
wave four-vector	$k^\mu = a^{-2}\tilde{k}^\mu \qquad k_\mu = \tilde{k}_\mu$
four-velocity	$u^\mu = a^{-1}\tilde{u}^\mu \qquad u_\mu = a\tilde{u}_\mu$
frequency	$\omega = a^{-1}\tilde{\omega}$
redshift	$1 + z = a_O a_S^{-1}(1 + \tilde{z})$
propagation direction	$d^\mu = a^{-1}\tilde{d}^\mu \qquad d_\mu = a\tilde{d}_\mu$
screen projector	$S_{\mu\nu} = a^2 \tilde{S}_{\mu\nu} \qquad S^{\mu\nu} = a^{-2}\tilde{S}^{\mu\nu}$
Sachs basis	$s_A^\mu = a^{-1}\tilde{s}_A^\mu \qquad s_\mu^A = a\tilde{s}_\mu^A$
separation four-vector	$\xi^\mu = \tilde{\xi}^\mu \qquad\qquad \xi_\mu = a^2\tilde{\xi}_\mu$
separation in screen space	$\xi_A = a\tilde{\xi}_A$
Jacobi matrix	$\boldsymbol{\mathcal{D}}(S \leftarrow O) = a_S a_O \widetilde{\boldsymbol{\mathcal{D}}}(S \leftarrow O)$
angular distance	$D_{\mathrm{A}} = a_S \widetilde{D}_{\mathrm{A}}$
luminosity distance	$D_{\mathrm{L}} = a_O^2 a_S^{-1} \widetilde{D}_{\mathrm{L}}$
deformation scalars	$\gamma, \varphi, \psi = \tilde{\gamma}, \tilde{\varphi}, \tilde{\psi}$
deformation rate matrix	$\boldsymbol{\mathcal{S}} = \dfrac{1}{a}\dfrac{\mathrm{d}a}{\mathrm{d}v}\mathbf{1}_2 + a^{-2}\widetilde{\boldsymbol{\mathcal{S}}}$
expansion rate	$\theta = \dfrac{1}{a}\dfrac{\mathrm{d}a}{\mathrm{d}v} + a^{-2}\tilde{\theta}$
shear rate	$\sigma = a^{-2}\tilde{\sigma}$

Table 5.1 The conformal dictionary of geometric optics in curved spacetime. All quantities are defined in Chaps. 2, 3. Tilded and untilded four-dimensional vectors and tensors are defined on the same manifold, but not with respect to the same metric: (un)tilded indices μ, ν are raised and lowered, respectively, by the (un)tilded metric.

cosmology, quantities referring to O are conventionally denoted with a zero subscript $_0$, this standard notation will here be equivalent to the $_O$ subscript.

It is straightforward to check that the radial null curves such that

$$\chi = \eta_0 - \eta, \qquad \theta, \varphi = \mathrm{cst} \tag{5.4}$$

satisfy the null geodesic equations for the static metric (5.2), and are therefore null geodesics for $\boldsymbol{g}$ as well. They form the lightcone of O. Note that although the curves (5.4) appear as straight lines in terms of the coordinates (χ, θ, φ), when $K \neq 0$ they are exceptions in the sense that other null geodesics (out of the lightcone of O) do not. Any affine parametrisations of the null curves (5.4) is, with respect to $\tilde{\boldsymbol{g}}$, simply proportional to conformal time $\mathrm{d}\tilde{v} = \tilde{\omega}^{-1}\mathrm{d}\eta$, with $\tilde{\omega} = \tilde{\omega}_0 = \mathrm{cst}$. In other words, $\tilde{k}^\mu = \mathrm{cst}$. We conclude that, with respect to the original metric $\boldsymbol{g}$,

$$k^\mu = \left(\frac{a_0}{a}\right)^2 k_0^\mu, \tag{5.5}$$

where it is understood that $\mu = 0$ would refer to a component with respect to $\boldsymbol{\partial}_\eta$, not $\boldsymbol{\partial}_t$. The frequency measured by a comoving observer at η is thus $\omega = [a_0/a(\eta)]\omega_0$, and the

redshift between emitted light as S and the observed light at O reads

$$1 + z = \frac{a_0}{a_S} \geq 1, \tag{5.6}$$

in agreement with the relation given by Table 5.1, since $\tilde{z} = 0$. By virtue of Eq. (5.4), the redshift is related to the radial coordinate χ of S by $\mathrm{d}z/\mathrm{d}\chi = a_0 H$, integrated as

$$a_0 \chi = \int_0^z \frac{\mathrm{d}\zeta}{H(\zeta)} = \frac{1}{H_0} \int_0^z \mathrm{d}\zeta \, \left[\Omega_{\mathrm{m}0}(1+\zeta)^3 + \Omega_{K0}(1+\zeta)^2 + \Omega_{\Lambda 0}\right]^{-1/2}, \tag{5.7}$$

where we used the first Friedmann equation (4.20) to link H with a, i.e. with z. In homogeneous cosmology, the redshift can thus be considered a kind of distance measurement. Depending on the cosmological parameters, the integral of Eq. (5.7) can be calculated either analytically or numerically.

The observed redshift of a comoving source (with $\chi = \mathrm{cst}$) generally evolves with time. Consider a light signal observed at $t_0 + \mathrm{d}t_0$; to this reception cosmic time corresponds an emission time $t_S + \mathrm{d}t_S$, where $\mathrm{d}t_S = \mathrm{d}t_0/(1+z)$ by the very definition of the redshift. The associated correction to the redshift reads

$$\mathrm{d}(1+z) = \frac{\dot{a}_0 \mathrm{d}t_0}{a_S} - a_0 \frac{\dot{a}_S \mathrm{d}t_S}{a_S^2} \tag{5.8}$$

whence

$$\frac{\mathrm{d}z}{\mathrm{d}t_0} = (1+z)H_0 - H_S. \tag{5.9}$$

This *redshift drift* was first mentioned by Refs. [125,126]. Its theoretical order of magnitude is $\mathrm{d}z/\mathrm{d}t_0 \sim 10^{-11}$ yr^{-1} for $z \sim 1$. Albeit very small, next generation high-resolution spectroscopy experiments, such as the COsmic Dynamics EXperiment (CODEX) [127] proposed for the European Extremely Large Telescope (E-ELT), should be able to measure redshift drifts by the next decades. As forecasted by Ref. [128], such a measurement over 30 years, applied to $z > 2$ quasars, could contribute to observationally distinguish between several models of dark energy.

5.1.3   Light beams

We now investigate the properties of radial light beams. Like for single light rays, we start with the conformal geometry $\tilde{\boldsymbol{g}}$, for which calculations are simpler.

In the conformal geometry

The spatial direction of propagation of radial geodesics (5.4) is $\tilde{\boldsymbol{d}} = -\boldsymbol{\partial}_\chi$. The other two spatial basis vectors being orthogonal to $\tilde{\boldsymbol{d}}$, it is natural to use them for constructing the Sachs basis as

$$\tilde{\boldsymbol{s}}_1 = \frac{-1}{f_K(\chi)} \frac{\partial}{\partial \theta}, \qquad \tilde{\boldsymbol{s}}_2 = \frac{-1}{f_K(\chi) \sin\theta} \frac{\partial}{\partial \varphi}. \tag{5.10}$$

It is straightforward to check that these vectors indeed satisfy the transport condition (5.3). The optical tidal matrix associated with this Sachs basis then reads $\widetilde{\boldsymbol{\mathcal{R}}} = -\tilde{\omega}_0^2 K \, \mathbf{1}_2$, where we used that the frequency $\tilde{\omega}$ measured by comoving observers ($\tilde{\boldsymbol{u}} = \boldsymbol{\partial}_\eta$) is a constant. The full specification of the Sachs basis was actually not necessary to get this result, since the

FL geometry is conformally flat, which implies that the optical tidal matrix $\widetilde{\mathcal{R}}$ has only a Ricci (pure-trace) part $\widetilde{\mathscr{R}}\mathbf{1}_2$, with $\widetilde{\mathscr{R}} = -(1/2)\tilde{R}_{\mu\nu}\tilde{k}^\mu\tilde{k}^\nu = -\tilde{\omega}_0^2 K$. The Jacobi matrix equation

$$\frac{\mathrm{d}^2\widetilde{\mathcal{D}}}{\mathrm{d}\tilde{v}^2} = -\tilde{\omega}_0^2 K\widetilde{\mathcal{D}} \tag{5.11}$$

is then easily solved as

$$\widetilde{\mathcal{D}}(S \leftarrow O) = \tilde{\omega}_0^{-1}f_K(\eta_S - \eta_0)\,\mathbf{1}_2, \tag{5.12}$$

where $\eta_0 - \eta_S$ can be replaced by the conformal radial distance χ_S of the source.

In the original geometry

Recovering all lensing quantities for the original FL metric $\boldsymbol{g}$ is now easily achieved using the dictionary of Table 5.1. In particular, the Jacobi matrix reads

$$\boxed{\boldsymbol{\mathcal{D}}(S \leftarrow O) = -a_S\omega_0^{-1}f_K(\chi_S)\,\mathbf{1}_2.} \tag{5.13}$$

Note that the minus sign is here due to our conventional future orientation of the wave four-vector. As expected, light propagation in the FL spacetime exhibits no shear nor rotation: the Jacobi matrix is directly proportional to the angular diameter distance (see § 2.2.2)

$$D_\mathrm{A} = a_S f_K(\chi_S). \tag{5.14}$$

The above result matches the interpretation of $f_K(\chi) \equiv R$ as a conformal *areal* radius. For a given radial coordinate χ, sources appear larger (closer) as K increases. This, however shall not be interpreted as if spatial curvature had any actual focusing effect. As discussed in § 2.1.3, the *physical* source of focusing is the local density of energy and momentum, due to Ricci focusing, which here reads $\mathscr{R} = -4\pi G(\rho + p)\omega^2$. Spatial curvature only enters into the game via the dynamics of $a(t)$, related to ρ by the Friedmann equations.

In Table 5.2, we summarise the expressions of the other observational notions of distance defined in Chap. 3 in a FL spacetime. Note that, contrary to the angular and luminosity distances, the radar and parallax distances are given as the results of an academic exercise, since they cannot be applied to cosmological distances in practice (see § 3.2). As such, they can nevertheless serve to illustrate the difference between the various observational notions of distance in general relativity.

Distance	Expression
radar	$D_\mathrm{R} = \dfrac{1}{2}\displaystyle\int_{\eta_0 - 2\chi}^{\eta_0} a\,\mathrm{d}\eta$
parallax	$D_\mathrm{P} = \left[H_0 + \dfrac{f_K'(\chi_S)}{a_0 f_K(\chi_S)}\right]^{-1}$
angular	$D_\mathrm{A} = a_S f_K(\chi_S)$
luminosity	$D_\mathrm{L} = a_0^2 a_S^{-1} f_K(\chi_S)$

Table 5.2 Expressions of the observational distances in a FL geometry, for a source with comoving radial coordinate χ. The radar distance is here defined as a retarded distance.

5.2   Optics in perturbation theory

The presence of perturbations with respect to strict homogeneity and isotropy (see § 4.2) modifies the propagation of light compared to the previous results. This section reviews the consequent corrections to light's frequency, beam's morphology, etc. For that purpose, we restrict to the Newtonian regime, where the metric reads

$$ds^2 = a^2(\eta) \left[-(1 + 2\Phi)d\eta^2 + (1 - 2\Phi)\gamma_{ij}dx^i dx^j \right] \tag{5.15}$$

$$= a^2(\eta)(\bar{g}_{\mu\nu} + \delta\tilde{g}_{\mu\nu})dx^\mu dx^\nu \tag{5.16}$$

which, as discussed in § 4.2.2, is a good approximation at late times, and provided large-scale perturbations are not concerned. The first assumption is meaningful because gravitational lensing is mostly due to (i) collapsed structures, or (ii) the cosmic web; both are absent in the primordial Universe, and appear during the matter-dominated era. The second assumption is generally satisfied in gravitational lensing, because the size of the beam dictates the relevant scales.

5.2.1   Perturbation of light rays

We start with the effect of metric perturbation on a single light ray.[2] Like in the previous section, we take advantage of the conformal invariance of null geodesic and work with the conformal metric $\bar{g} + \delta\tilde{g}$. Note that, in order to be perfectly consistent, the conformal background metric should be denoted $\bar{\tilde{g}}$; we here choose to drop the tilde to alleviate notation. In the remainder of this section, a bar thus denotes conformal background quantities, except explicit mention of the contrary.

We consider a background null geodesic $\bar{x}^\mu(\tilde{v})$ and a perturbed null geodesic $x^\mu(\tilde{v}) = \bar{x}^\mu(\tilde{v}) + \delta x^\mu(\tilde{v})$. Both curves are affinely parameterised by the same $\tilde{v}$, which defines the mapping between them: $\delta x^\mu(\tilde{v})$ is the difference between the positions of the perturbed and background geodesics at the same $\tilde{v}$. We also define the associated wave four-vectors as $\tilde{k}^\mu \equiv dx^\mu/d\tilde{v}$, $\bar{k}^\mu \equiv d\bar{x}^\mu/d\tilde{v}$, and $\delta\tilde{k}^\mu \equiv d\delta x^\mu/d\tilde{v} = \tilde{k}^\mu - \bar{k}^\mu$.

The geodesic equations for the background and perturbed geodesics read

$$\frac{d\bar{k}^\mu}{d\tilde{v}} + \bar{\Gamma}^\mu{}_{\nu\rho}\bar{k}^\nu\bar{k}^\rho = 0, \tag{5.17}$$

$$\frac{d\tilde{k}^\mu}{d\tilde{v}} + \tilde{\Gamma}^\mu{}_{\nu\rho}\tilde{k}^\nu\tilde{k}^\rho = 0, \tag{5.18}$$

which, by subtraction, yields at first order

$$\frac{d\delta\tilde{k}^\mu}{d\tilde{v}} + 2\bar{\Gamma}^\mu{}_{\nu\rho}\bar{k}^\nu\delta\tilde{k}^\rho = -\delta\tilde{\Gamma}^\mu{}_{\nu\rho}\bar{k}^\nu\bar{k}^\rho, \tag{5.19}$$

where $\delta\tilde{\Gamma}^\mu{}_{\nu\rho} \equiv \tilde{\Gamma}^\mu{}_{\nu\rho} - \bar{\Gamma}^\mu{}_{\nu\rho}$ denotes the perturbation of the conformal Christoffel symbols.

---

[2]Note of April 2023: I thank Angela Ng for spotting an error in the original version of this paragraph, which is now corrected.

Effect on the frequency

Let us first calculate the effect of perturbations on the observed frequency of the light signal. By definition, we have

$$\tilde{\omega} = -\tilde{u}_\mu \tilde{k}^\mu \tag{5.20}$$

$$= \bar{\omega} + \delta\tilde{k}^0 + \bar{\omega}(\Phi - v_i \bar{d}^i) + \mathcal{O}(2). \tag{5.21}$$

where we have used the decomposition of the perturbation of the four-velocity introduced in § 4.2.1 as $\delta\tilde{\boldsymbol{u}} = -\Phi\boldsymbol{\partial}_\eta + v^i\boldsymbol{\partial}_i$. We see that only the 0th component of $\delta\tilde{\boldsymbol{k}}$ needs to be determined for computing the perturbed frequency.

Since $\bar{\Gamma}^0{}_{\nu\rho} = 0$ (see Table 4.1 with $a = \mathrm{cst}$), the second term on the left-hand side of Eq. (5.19) vanishes for $\mu = 0$. The right-hand side is given by the perturbations to the Christoffel symbols [101]

$$\delta\widetilde{\Gamma}^0{}_{0\mu} = \partial_\mu\Phi, \qquad \delta\widetilde{\Gamma}^0{}_{ij} = -(\partial_0\Phi)\,\gamma_{ij}, \tag{5.22}$$

so that

$$\delta\widetilde{\Gamma}^0{}_{\nu\rho}\bar{k}^\nu\bar{k}^\rho = 2\bar{\omega}\frac{\mathrm{d}\Phi}{\mathrm{d}\bar{v}} - 2\bar{\omega}^2\partial_0\Phi. \tag{5.23}$$

Therefore, for $\mu = 0$, Eq. (5.19) is readily integrated as

$$\left[\delta\tilde{k}^0\right]_S^O = -2\bar{\omega}\left[\Phi\right]_S^O + 2\bar{\omega}^2\int_S^O \mathrm{d}\tilde{v}\,\partial_0\Phi[\eta, \bar{x}^i(\tilde{v})]. \tag{5.24}$$

Finally, we can use the fact that along the background null geodesic, $\mathrm{d}\tilde{v} = \bar{\omega}^{-1}\mathrm{d}\eta$, with $\bar{\omega} = \mathrm{cst}$, and obtain

$$\boxed{\frac{\delta\omega_0}{\omega_0} - \frac{\delta\omega_S}{\omega_S} = \frac{-\delta z}{1+z} = -\left[\Phi + v_i\bar{d}^i\right]_S^O + 2\int_{\eta_S}^{\eta_0} \mathrm{d}\eta\,\partial_0\Phi[\eta, \bar{x}^i(\eta)],} \tag{5.25}$$

where we have reintroduced the frequencies defined with respect to the full perturbed metric. The quantity $v_i\bar{d}^i$ can be considered either with respect to the conformal metric (i.e. $\gamma_{ij}v^i\tilde{d}^j$) or with respect to the full metric (i.e. $g_{ij}v^i d^j$), because both are equal. Note that the integral term on the right-hand side of Eq. (5.25) is not trivially integrated, because the partial derivative ∂_η only hits the first η; in other words, while the integral is a curvilinear integral along the unperturbed null geodesic $\bar{x}^\mu(\eta)$, the derivative is not performed along this geodesic.

Physically speaking, the bracket term on the right-hand side of Eq. (5.25) contains the intuitively expected corrections to the redshift, respectively interpreted as gravitational and Doppler effects with respect to this coordinate system. The gravitational part $[-\Phi]_S^O$ is sometimes referred to as the *Sachs-Wolfe* (SW) effect, while the quantities v_O^i and v_S^i are usually called the observer's and source's *peculiar velocities*, they encode the deviation of their motions with respect to the Hubble flow. They are, of course, gauge dependent. The integral term, contrary to the previous ones, depends on the whole light path from S to O, and is specific to time-dependent perturbations. The corresponding physical phenomenon is either called *integrated Sachs-Wolfe* (ISW) effect [129] or *Rees-Sciama* (RS) effect [130], depending on its physical cause.

First note that, in linear perturbation theory during the matter-dominated era ($\Omega_\mathrm{m} \approx 1$), since $\delta \propto a$, Eq. (4.69) implies that $\partial_\eta\Phi = 0$, so the integrated effect vanishes in this case. There are three possible excursions from this situation:

1. Before the matter era, i.e. during the radiation era. We then talk about the *early* ISW effect. Note that the above calculations cannot be directly applied to this case, since vector, tensor modes, and anisotropic stress cannot be neglected.

2. After the matter era, when the cosmological constant (or dark energy, or spatial curvature) starts to affect the growth of structures. This is the *late* ISW effect. It has first been detected in 2004 by cross-correlating the CMB map of the Wilkinson Microwave Anisotropy Probe (WMAP) with maps of the large-scale structure [131]; since then, the late ISW effect has been exploited in a number of studies to put constraints on dark energy (see e.g. Ref. [132] and references therein). For instance, the recent *Planck* results [133] exclude $\Lambda = 0$ at a 3σ confidence level, from the ISW effect only.

3. In the matter era, but beyond the linear regime. The time-dependence of the gravitational potential then occurs in the vicinity of virialised structures. In this case we talk about the Rees-Sciama effect. We will see in Chap. 6 an explicit example of this phenomenon in Swiss-cheese cosmological models.

Effect on the source's position

We now turn to the spatial part of the perturbed geodesic equation (5.19). The second term on the left-hand side, for $\mu = i$, reads

$$2\bar{\Gamma}^i_{\ \nu\rho}\bar{k}^\nu\delta\tilde{k}^\rho = 2\,^3\Gamma^i_{\ jl}\bar{k}^l\delta\tilde{k}^j = -2\bar{\omega}\frac{f'_K(\chi)}{f_K(\chi)}\left(\delta^i_j - \delta^i_\chi\delta^\chi_j\right)\delta\tilde{k}^j, \tag{5.26}$$

where we used that $\bar{k}^i = -\bar{\omega}\delta^i_\chi$, and that the nonzero Christoffel symbols $^3\Gamma^i_{\ jl}$ of the background spatial metric γ_{ij} such that $l = \chi$ are $^3\Gamma^\theta_{\ \theta\chi} = \,^3\Gamma^\varphi_{\ \varphi\chi} = f'_K(\chi)/f_K(\chi)$. The right-hand side of Eq. (5.19) requires the correction to the Christoffel coefficients

$$\delta\widetilde{\Gamma}^i_{\ 00} = \gamma^{ij}\partial_j\Phi, \qquad \delta\widetilde{\Gamma}^i_{\ j0} = -\delta^i_j\,\partial_0\Phi, \qquad \delta\widetilde{\Gamma}^i_{\ jk} = -2\delta^i_{(j}\partial_{k)}\Phi + \gamma_{jk}\gamma^{il}\partial_l\Phi, \tag{5.27}$$

so that

$$-\delta\tilde{\Gamma}^i_{\ \mu\nu}\bar{k}^\mu\bar{k}^\nu = 2\frac{\mathrm{d}\Phi}{\mathrm{d}\tilde{v}}\bar{k}^i - 2\bar{\omega}^2\gamma^{ij}\partial_j\Phi. \tag{5.28}$$

The resulting differential equation is naturally expressed in terms of $\tilde{v}$. We have seen in the previous paragraph that it can be written in terms of η since $\mathrm{d}\tilde{v} = \bar{\omega}^{-1}\mathrm{d}\eta$; similarly, since at the background level $\mathrm{d}\eta = -\mathrm{d}\chi$, we can translate it as

$$\frac{\mathrm{d}\delta\tilde{k}^i}{\mathrm{d}\chi} + 2\frac{f'_K(\chi)}{f_K(\chi)}\left(\delta^i_j - \delta^i_\chi\delta^\chi_j\right)\delta\tilde{k}^j = 2\frac{\mathrm{d}\Phi}{\mathrm{d}\chi}\bar{k}^i + 2\bar{\omega}\gamma^{ij}\partial_j\Phi. \tag{5.29}$$

Let us focus on the perturbation to the position of the source on the observer's celestial sphere. The problem can be formulated as follows: consider a line of sight $-\bar{\boldsymbol{d}}$, corresponding to the direction $(\bar{\theta}, \bar{\varphi}) \equiv (\bar{\theta}^A)_{A=1,2}$ towards which the observer looks; the deflection of light by Φ implies that the light ray deviates from the radial straight line $\theta^A = \bar{\theta}^A = \mathrm{cst}$, so that the source event S actually has angular coordinates $\bar{\theta}^A + \delta\theta^A$. This new direction corresponds to the direction in which the observer would see the image if light did follow a radial straight line (see Fig. 5.1).
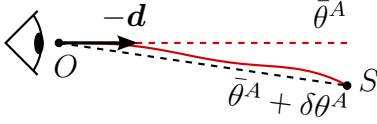
Figure 5.1 Perturbation of the angular coordinates $(\theta^A) = (\theta, \varphi)$ of the source, given an observation direction $-\bar{\boldsymbol{d}}$.

The correction $\delta\theta^A$ is related to the perturbation of the wave four-vector via $\delta\tilde{k}^A = \mathrm{d}\delta\theta^i/\mathrm{d}\tilde{v} = -\bar{\omega}\mathrm{d}\delta\theta^A/\mathrm{d}\chi$. For $i = A$, the first term on the right-hand side of Eq. (5.29) vanishes, because $\bar{k}^i \propto \delta^i_\chi$, and the equation is integrated twice as

$$\delta\theta^A = -2\int_0^\chi \mathrm{d}\chi' \int_0^{\chi'} \mathrm{d}\chi'' \left[\frac{f_K(\chi'')}{f_K(\chi')}\right]^2 \gamma^{AB}\partial_B\Phi[\eta'', \bar{x}^i(\eta'')], \tag{5.30}$$

where it is understood that $\eta'' = \eta_0 - \chi''$, and $\bar{x}^i(\eta'') = (\eta'', \chi'', \bar{\theta}, \bar{\varphi})$ is the unperturbed ray. The properties of the areal function f_K allow us to turn the double integral of Eq. (5.30) into the single integral[3]

$$\boxed{\delta\theta^A = -2\int_0^\chi \mathrm{d}\chi' \frac{f_K(\chi')f_K(\chi - \chi')}{f_K(\chi)} \gamma^{AB}\partial_B\Phi[\eta', \bar{x}^i(\eta')].} \tag{5.33}$$

This formula agrees with the Newtonian intuition according to which particles are deflected by gravitational fields, i.e. by $-\partial\Phi$, modulo a factor two which distinguishes the deflection of light with the deflection of nonrelativistic particles in GR. Note the form of the kernel

$$\frac{f_K(\chi - \chi')f_K(\chi')}{f_K(\chi)} \propto \frac{D_\mathrm{A}(L \leftarrow O)D_\mathrm{A}(S \leftarrow L)}{D_\mathrm{A}(S \leftarrow O)}, \tag{5.34}$$

sometimes called *lensing efficiency*, which peaks for $\chi' = \chi/2$, i.e. when the lens L is such that $D_\mathrm{A}(S \leftarrow L) = D_\mathrm{A}(L \leftarrow O)$. This is a generic characteristic of gravitational lensing: the most important contributions to the net deflection are due to gravitational fields lying halfway between the source and the observer.

5.2.2 Perturbation of light beams

The previous paragraph showed that an inhomogeneous potential Φ tends to deflect light with respect to the purely radial geodesics of the background FL spacetime. Considering now a family of neighbouring light rays, we expect from their differential deflection to distort and focus the underlying beam.

---

[3]A first step consists in changing the integration scheme as

$$\int_0^\chi \mathrm{d}\chi' \int_0^{\chi'} \mathrm{d}\chi'' \, F(\chi', \chi'') = \int_0^\chi \mathrm{d}\chi'' \int_{\chi''}^\chi \mathrm{d}\chi' \, F(\chi', \chi''), \tag{5.31}$$

and then perform the integration with respect to χ',

$$\int_{\chi''}^\chi \frac{\mathrm{d}\chi'}{f_K^2(\chi')} = \left[-\frac{f_K'}{f_K}\right]_\chi^{\chi''} = \frac{1}{f_K(\chi'')f_K(\chi)}[f_K(\chi)f_K'(\chi'') - f_K(\chi'')f_K'(\chi)] = \frac{f_K(\chi - \chi'')}{f_K(\chi'')f_K(\chi)}, \tag{5.32}$$

where we used twice the fact that f_K is either sin or sinh (or the identity). Renaming χ'' as χ' finally gives the result of Eq. (5.33)

Perturbed optical tidal matrix

The sources of focusing and distortions of a light beam are encoded in the optical tidal matrix (see Chap. 2). We keep working in the conformal geometry, and decompose the conformal optical tidal matrix as $\widetilde{\mathcal{R}} = \overline{\mathcal{R}} + \delta\widetilde{\mathcal{R}}$, with $\overline{\mathcal{R}} = -\bar{\omega}^2 K$. Its perturbation

$$\delta\widetilde{\mathcal{R}}_{AB} \equiv \delta\left(R_{\mu\nu\rho\sigma} s_A^\mu k^\nu k^\rho s_B^\sigma\right) \tag{5.35}$$

contains a priori terms of the form $\delta R \bar{s} \bar{k} \bar{k} \bar{s} \propto \delta(\partial^2 g)$, and $\bar{R}\delta s \bar{k} \bar{k} \bar{s}, \bar{R}\bar{s}\delta k \bar{k} \bar{s} \propto \delta(\partial g)$. As discussed at the end of the previous chapter, the perturbations of curvature $\delta(\partial^2 g)$ are generally much larger than the perturbations of lower-order derivatives of the metric. At leading order, we can thus neglect the latters compared to the formers, so that

$$\delta\widetilde{\mathcal{R}}_{AB} \approx \delta\tilde{R}_{\mu\nu\rho\sigma}\bar{s}_A^\mu \bar{k}^\nu \bar{k}^\rho \bar{s}_B^\sigma \qquad \text{neglecting } \bar{R}\delta s \bar{k} \bar{k} \bar{s}, \bar{R}\bar{s}\delta k \bar{k} \bar{s} \tag{5.36}$$

$$\approx -2\delta\tilde{\Gamma}_{\mu\nu[\rho,\sigma]}\bar{s}_A^\mu \bar{k}^\nu \bar{k}^\rho \bar{s}_B^\sigma \qquad \text{neglecting } \overline{\Gamma}\delta\tilde{\Gamma} \tag{5.37}$$

$$= \frac{1}{2}\left(\delta\tilde{g}_{\mu\nu,\rho\sigma} + \delta\tilde{g}_{\rho\sigma,\mu\nu}\right)\bar{s}_A^\mu \bar{s}_B^\nu \bar{k}^\rho \bar{k}^\sigma. \tag{5.38}$$

Similar considerations allow us to write

$$\delta\tilde{g}_{\mu\nu,\rho\sigma}\bar{s}_A^\mu \bar{s}_B^\nu \bar{k}^\rho \bar{k}^\sigma \approx \frac{\mathrm{d}^2}{\mathrm{d}\tilde{v}^2}\left(\delta\tilde{g}_{\mu\nu}\bar{s}_A^\mu \bar{s}_B^\nu\right), \tag{5.39}$$

$$\delta\tilde{g}_{\rho\sigma,\mu\nu}\bar{s}_A^\mu \bar{s}_B^\nu \bar{k}^\rho \bar{k}^\sigma \approx -4\bar{\omega}^2\Phi_{,\mu\nu}\bar{s}_A^\mu \bar{s}_B^\nu, \tag{5.40}$$

which finally leads to

$$\delta\widetilde{\mathcal{R}}_{AB} = -2\bar{\omega}^2\partial_A^\perp\partial_B^\perp\Phi + \frac{\mathrm{d}^2}{\mathrm{d}\tilde{v}^2}\left(\delta\tilde{g}_{\mu\nu}\bar{s}_A^\mu \bar{s}_B^\nu\right) + \mathcal{O}(\partial\tilde{g}) + \mathcal{O}(2). \tag{5.41}$$

In Eq. (5.41), we have introduced transverse derivatives $\partial_A^\perp \equiv \bar{s}_A^\mu \partial_\mu$, such that

$$\partial_A^\perp\partial_B^\perp \equiv \bar{s}_A^\mu \bar{s}_B^\nu \partial_\mu \partial_\nu = \frac{1}{f_K^2(\chi)}\begin{pmatrix} \frac{\partial^2}{\partial\theta^2} & \frac{1}{\sin\theta}\frac{\partial^2}{\partial\theta\partial\varphi} \\ \frac{1}{\sin\theta}\frac{\partial^2}{\partial\theta\partial\varphi} & \frac{1}{\sin^2\theta}\frac{\partial^2}{\partial\varphi^2} \end{pmatrix}. \tag{5.42}$$

Jacobi matrix at linear order

Let us now exploit the perturbed optical tidal matrix to determine the correction to the Jacobi matrix. Still in conformal geometry, we decompose it into a background and a perturbation as $\widetilde{\mathcal{D}} = \overline{\mathcal{D}} + \delta\widetilde{\mathcal{D}}$. At linear order in perturbations, the Jacobi matrix equation (2.65) reads

$$\frac{\mathrm{d}^2\delta\widetilde{\mathcal{D}}}{\mathrm{d}\tilde{v}^2} = \overline{\mathcal{R}}\,\delta\widetilde{\mathcal{D}} + \delta\widetilde{\mathcal{R}}\,\overline{\mathcal{D}}, \tag{5.43}$$

or, in terms of the comoving radial coordinate χ, and replacing the background quantities by their expressions,

$$\frac{\mathrm{d}^2\delta\widetilde{\mathcal{D}}}{\mathrm{d}\chi^2} = -K\,\delta\widetilde{\mathcal{D}} - \bar{\omega}^{-3}f_K(\chi)\,\delta\widetilde{\mathcal{R}}. \tag{5.44}$$

A Green-function method for solving this second-order differential equation then yields

$$\delta\widetilde{\mathcal{D}} = -\int_0^\chi \mathrm{d}\chi'\, f_K(\chi')f_K(\chi-\chi')\,\bar{\omega}^{-3}\delta\widetilde{\mathcal{R}}, \tag{5.45}$$

which is easily checked to be a solution of Eq. (5.44), with initial conditions $\delta\widetilde{\mathcal{D}}_0 = (\mathrm{d}\delta\widetilde{\mathcal{D}}/\mathrm{d}\tilde{v})_0 = \mathbf{0}_2$.

In the expression (5.41) of $\delta\widetilde{\mathcal{R}}$, the total derivative $\mathrm{d}^2(\delta\tilde{g}_{\mu\nu}\bar{s}_A^\mu\bar{s}_B^\nu)/\mathrm{d}\tilde{v}^2$ can be integrated by parts, and yields a term on the order of $K\Phi$, which is much smaller than $\partial^2\Phi$ because the gravitational potential varies on distances much smaller than the background spatial curvature radius. Back to the original perturbed geometry, we thus obtain the following formula for the Jacobi matrix, at first order in cosmological perturbations:

$$\mathcal{D}_{AB}(S \leftarrow O) = -a_S\omega_0^{-1}f_K(\chi)\left\{\delta_{AB} - 2\int_0^\chi \mathrm{d}\chi'\,\frac{f_K(\chi')f_K(\chi-\chi')}{f_K(\chi)}\partial_A^\perp\partial_B^\perp\Phi[\eta',\bar{x}^i(\eta')]\right\},$$

(5.46)

which is a standard textbook result [101, 134].

Inside the braces, we recognise the amplification matrix $\mathcal{A} = \mathcal{D}\overline{\mathcal{D}}^{-1}$ defined in § 2.2.2. Interestingly, this expression of $\mathcal{A}$ could also have been obtained from Eq. (5.30). By definition, this matrix is indeed

$$\mathcal{A}^A{}_B = \frac{\partial\xi^A}{\partial\dot{\xi}_0^C}\frac{\partial\dot{\xi}_0^C}{\partial\xi^B}\bigg|_{\mathrm{FL}} = \frac{\partial\xi^A}{\partial\bar{\xi}^B},$$

(5.47)

where ξ^A and $\bar{\xi}^A$ are defined as follows and depicted in Fig. 5.2. Consider two (very close) directions of observation defined by the angles $(\bar{\theta}_1^A)$ and $(\bar{\theta}_2^A)$. To these directions of observation correspond, for a given radial coordinate χ, two sources S_1 and S_2, whose positions differ whether we consider the perturbed or background spacetime; $\bar{\xi}^A$ (resp. ξ^A) represents the physical separation, in screen space, between the sources in the background (resp. perturbed) spacetime.
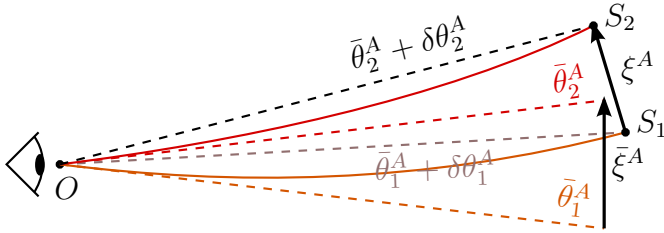

Figure 5.2 Position of two light sources S_1, S_2, associated with the directions of observation $\bar{\theta}_1^A$, $\bar{\theta}_2^A$, and their physical separation in screen space for the background $(\bar{\xi}^A)$ and perturbed (ξ^A) spacetimes.

We assume for simplicity that the system of axes is set so that the directions that we are considering lie in the vicinity of the $\theta = \pi/2$ plane; the physical separation between the points (η, χ, θ_1^A) and (η, χ, θ_2^A) is then simply $a(\eta)f_K(\chi)(\theta_2^A - \theta_1^A)$ (at the background level). In particular, it avoids complications due to the $\sin\theta$ term, always present in the geometry of spherical coordinates. We thus have

$$\xi^A = af_K(\chi)\left[\bar{\theta}_2^A + \delta\theta_2^A - (\bar{\theta}_1^A + \delta\theta_1^A)\right] = \bar{\xi}^A + \frac{\partial\delta\theta^A}{\partial\bar{\theta}^B}\bar{\xi}^B$$

(5.48)

so

$$\mathcal{A}^A{}_B = \delta_B^A + \frac{\partial\delta\theta^A}{\partial\bar{\theta}^B},$$

(5.49)

which, using the expression (5.33) of $\delta\theta^A$, indeed coincides with Eq. (5.46).

Note that the Jacobi and amplification matrices are symmetric here, i.e. at linear order in cosmological perturbations. This agrees with the discussion of § 2.2.2, where we have seen that when Weyl lensing is treated as a perturbation, rotation is a second-order quantity contrary to convergence κ and shear γ, and we can write

$$\boldsymbol{\mathcal{A}} = \begin{pmatrix} 1 - \kappa - \gamma_1 & \gamma_2 \\ \gamma_2 & 1 - \kappa + \gamma_1 \end{pmatrix}. \tag{5.50}$$

Cosmic convergence

The net convergence κ of a light beam due to cosmological perturbations is called *cosmic convergence*. It represents the order-one correction to the observed angular distance of a given light source, compared to the background FL case, and is extracted from the amplification matrix as

$$\kappa \equiv \frac{\bar{D}_{\mathrm{A}} - D_{\mathrm{A}}}{\bar{D}_{\mathrm{A}}} = 1 - \frac{\mathrm{tr}\boldsymbol{\mathcal{A}}}{2}. \tag{5.51}$$

Taking the trace of Eq. (5.46) yields a transverse Laplacian of the gravitational potential

$$\delta^{AB}\partial_A^\perp\partial_B^\perp\Phi = \bar{S}^{\mu\nu}\partial_\mu\partial_\nu\Phi = \Delta\Phi - \partial_\chi^2\Phi, \tag{5.52}$$

where we identified the coordinate Laplacian $\gamma^{ij}\partial_i\partial_i$ with the background covariant Laplacian $\Delta = \gamma^{ij}\bar{\mathrm{D}}_i\bar{\mathrm{D}}_i$, because their difference is on the order of $\bar{\Gamma}\partial\Phi$ which is negligible compared to $\partial^2\Phi$. By virtue of the Poisson equation (4.69), $\Delta\Phi$ can be replaced by $4\pi Ga^2\bar{\rho}\delta$, where δ is matter's density contrast. Besides, the longitudinal derivative $\partial_\chi^2\Phi$ can also be neglected because of the integration[4] with respect to χ', and the convergence finally reads

$$\boxed{\kappa = \frac{3}{2}H_0^2\Omega_{\mathrm{m}0}\int_0^\chi \mathrm{d}\chi'\, \frac{f_K(\chi')f_K(\chi - \chi')}{f_K(\chi)}\frac{\delta[\eta', \bar{x}^i(\eta')]}{a(\eta')},} \tag{5.54}$$

where we assumed that matter is well modelled by a pressureless dust ($w = 0$) in order to write $\bar{\rho} = (a_0/a)^3\bar{\rho}_0$, and introduced the cosmological parameter $\Omega_{\mathrm{m}0} = 8\pi G\bar{\rho}_0/(3H_0^2)$. This expression of κ shows that overdensities ($\delta > 0$) or underdensities ($\delta < 0$) respectively tend to focus and defocus light beams with respect to their background behaviour, in agreement with the effect of *Ricci* focusing $\mathscr{R}$ discussed in Chap. 2. Weyl lensing $\mathscr{W}$ is indeed absent from Eq. (5.54), which could have been derived e.g. from Eq. (2.104) by taking $\sigma = 0$. This no longer true for lensing at second order in perturbations, see e.g. Refs. [135–139].

Besides second-order effects, several first-order contributions have also been neglected to obtain the simple result (5.54). In particular, by identifying the amplification matrix $\boldsymbol{\mathcal{A}}$

---

[4]Contrary to what is sometimes claimed [101, 134], the contribution of $\partial_\chi^2\Phi$ does not trivially vanish after integrating by parts. First note that it is only a *partial* derivative, which cannot be directly integrated by parts, for the same reason that we could not do so for the ISW term in Eq. (5.25). However, since the time evolution of Φ is much slower than its spatial evolution, we can consider $\mathrm{d}\Phi/\mathrm{d}\chi = -\bar{\omega}^{-1}\mathrm{d}\Phi/\mathrm{d}\tilde{v} = \partial_\chi\Phi - \partial_\eta\Phi \approx \partial_\chi\Phi$. A double integration by parts then gives

$$\int_0^\chi \mathrm{d}\chi'\, f_K(\chi')f_K(\chi - \chi')\frac{\mathrm{d}^2\Phi}{\mathrm{d}\chi'^2} = f_K(\chi)\left[\Phi(\chi) - \Phi(0)\right] - 2\int_0^\chi \mathrm{d}\chi'\, f_K'(\chi')f_K'(\chi - \chi')\Phi(\chi'), \tag{5.53}$$

which does not exactly vanish, but can be neglected as it does not contain second-order derivative of Φ any more.

with the expression between braces in Eq. (5.46), we did not take into account the fact that the observed frequency ω_0 is also affected by cosmological perturbations, leading to a Doppler contribution to the amplification matrix. Physically speaking, this a contribution to the convergence corresponds to the aberration effects discussed in § 3.2.3. It can actually be large [140], and generically dominates over deflection effects on short distances [141, 142]. For a more careful derivation of the correction to the convergence, taking into account all the first order contributions, see e.g. in Ref. [143], see also Ref. [144] for calculations which include the effect of vector and tensor modes.

Averaging the expression (5.54) over a large number of sources yields the effective cosmic convergence which only depends on the line of sight

$$\kappa_{\mathrm{eff}} = \frac{3}{2} H_0^2 \Omega_{\mathrm{m0}} \int_0^\infty \mathrm{d}\chi \, g(\chi) f_K(\chi) \frac{\delta[\eta', \bar{x}^i(\eta')]}{a(\eta')}, \tag{5.55}$$

where

$$g(\chi) \equiv \int_\chi^\infty \mathrm{d}\chi' \, p(\chi') \frac{f_K(\chi' - \chi)}{f_K(\chi')} \tag{5.56}$$

is the integrated lensing efficiency, $p(\chi)\mathrm{d}\chi$ being the probability of finding a source within the interval $[\chi, \chi + \mathrm{d}\chi]$. The resulting power spectrum P_κ for κ_{eff}, in the so-called flat-sky approximation[5], together with an analogue of Limber's approximation [145], is related to the matter density power spectrum P_δ as

$$P_\kappa(k) \approx \left(\frac{3}{2} H_0^2 \Omega_{\mathrm{m0}} \right)^2 \int_0^\infty \mathrm{d}\chi \, \frac{g^2(\chi)}{a^2(\eta)} P_\delta \left[\eta, \frac{k}{f_K(\chi)} \right], \tag{5.57}$$

where it is understood that $\eta = \eta(\chi) = \eta_0 - \chi$.

Cosmic shear

Lensing does not only affect the apparent size (or distance) of light sources, but also their shape. Observing the shape of lensed galaxies provides a measurement of this *cosmic shear* effect, which encodes key information on the matter distribution in the Universe. Suppose that we observe remote galaxies, whose intrinsic shape and observed shape are well described by ellipses. The properties of any ellipse $\mathscr{E}$ can be quantified by a complex number $\varepsilon \equiv \varepsilon_1 + \mathrm{i}\varepsilon_2 = |\varepsilon|\mathrm{e}^{-2\mathrm{i}\vartheta}$, which defines the transformation which must be applied to a circle $\mathscr{C}$ to obtain it, according to

$$\mathscr{E} = \exp \begin{pmatrix} -\varepsilon_1 & \varepsilon_2 \\ \varepsilon_2 & \varepsilon_1 \end{pmatrix} \mathscr{C}. \tag{5.58}$$

For a circle $\mathscr{C}$ with unit radius, the ellipse $\mathscr{E}$ has semi-minor axis $b = \mathrm{e}^{-|\varepsilon|}$ along the direction ϑ, and semi-major axis $a = \mathrm{e}^{|\varepsilon|}$ along the orthogonal direction, so that the ellipticity of $\mathscr{E}$ is given by $(a - b)/(a + b) = \tan|\varepsilon|$. Note that the present ε is *not* the complex ellipticity usually defined in this context [26] (though they agree for $|\varepsilon| \ll 1$). Our choice, however, together with the general decomposition of the Jacobi matrix introduced in § 2.2.2, turns out make the following discussion clearer.

---

[5]This approximation consists in computing the Fourier transform of $\kappa_{\mathrm{eff}}(\theta^A)$ as if the angular variables θ^A were Cartesian coordinates, hence neglecting the curvature of the celestial sphere. It is justified by the fact that the correlations between lines of sight with large angular separations are small.

By definition (see § 2.2.1) the source $\mathscr{S}$ is related to the image $\mathscr{I}$ by the Jacobi matrix as $\mathscr{S} = -\omega_O \boldsymbol{\mathcal{D}}(S \leftarrow O)\mathscr{I}$. Normalising $\mathscr{S}$ (resp. $\mathscr{I}$) by its physical size (resp. angular size) results into a unity-area ellipse $\mathscr{E}_{\mathrm{intr}}$ (resp. $\mathscr{E}_{\mathrm{obs}}$) characterising the intrinsic shape of the source (resp. observed shape of the image). These two ellipses are thus related by $\mathscr{E}_{\mathrm{intr}} = (-\boldsymbol{\mathcal{D}}/\sqrt{\det \boldsymbol{\mathcal{D}}})\mathscr{E}_{\mathrm{obs}}$, which, introducing the decomposition (2.56) of $\boldsymbol{\mathcal{D}}$, yields

$$\mathscr{E}_{\mathrm{obs}} = \exp \begin{pmatrix} \gamma_1 & -\gamma_2 \\ -\gamma_2 & -\gamma_1 \end{pmatrix} \begin{pmatrix} \cos\psi & \sin\psi \\ -\sin\psi & \cos\psi \end{pmatrix} \mathscr{E}_{\mathrm{intr}}. \tag{5.59}$$

Now suppose that many galaxies are observed in a small region of the sky, across which $\boldsymbol{\mathcal{D}}$ (hence γ, ψ) can be considered constant. Since the galaxies have in principle random shapes and orientations[6], we have $\langle \mathscr{E}_{\mathrm{intr}} \rangle = \mathscr{C}$, and the ensemble average of the observed ellipses reads

$$\langle \mathscr{E}_{\mathrm{obs}} \rangle = \exp \begin{pmatrix} \gamma_1 & -\gamma_2 \\ -\gamma_2 & -\gamma_1 \end{pmatrix} \mathscr{C}. \tag{5.60}$$

Comparing with Eq. (5.58), we conclude that this average ellipse is characterised by $\bar{\varepsilon}_{\mathrm{obs}} = -\gamma$. The same reasonings apply to the two-point correlation function of the observed galaxy shapes, which thus coincides with shear correlation function.

While the above considerations are fully general, they can be further exploited in the context of cosmological perturbation theory. In the expression (5.46) of the Jacobi matrix, we see that the convergence (trace part) and the shear (trace-free part) both come from derivatives of the same function Φ, so they are not independent from each other. For example, it can be shown that κ and γ have the same angular power spectrum, $P_\kappa = P_\gamma = P_\varepsilon$. In Ref. [148], Kaiser and Squires exploited this property to design an algorithm for reconstructing the convergence, which is not directly observable, from the shear. Observing the shape of galaxies therefore allows one to infer the properties of the density contrast, via the reconstructed convergence.

5.3 Some observations and their interpretation

In the previous sections we have derived the theoretical optical properties of the standard cosmological model. This provide a framework to interpret cosmological observations, i.e., to validate or falsify the model, and to measure its free parameters such as the Ωs. In this section, we briefly review the main current cosmological probes, namely the Hubble diagram of SNe (§ 5.3.1), the CMB (§ 5.3.2), BAO (§ 5.3.3), and mention some other observations in § 5.3.4. For all of them, we will emphasize the crucial character of the relation between distances and redshift for their correct interpretation.

5.3.1 Hubble diagram

The Hubble diagram is, conceptually, the simplest observation to interpret. It consists in plotting the luminosity distance D_{L}, or the distance modulus μ_{L}, of objects with known intrinsic luminosity—the so-called standard-(isable) candles—as a function of their redshift. In cosmology, as discussed in § 3.2.4, type Ia supernovae (SNeIa) are the best candidates.

---

[6]This hypothesis can however be spoiled by the potential trend of galaxies to align each others, or with the cosmic web, due to gravitational interactions [146, 147].

In practice, SNeIa are standardised by the measurement of their lightcurve, that is the evolution of the luminosity of the event with time (which typically lasts from a few weeks to a few months). Most current analyses are based on the assumption that the absolute magnitudes of all SNeIa are comparable, and that their variations can be captured by two parameters X_1 and C, characterising respectively the duration and the colour of the explosion [149]. Together with the observed peak B-band magnitude $m_{\rm B}^\star$ of the SNIa, they allow one to determine its distance modulus according to [42]

$$\mu_{\rm L} = 5 \log_{10} \left(\frac{D_{\rm L}}{10\,{\rm pc}} \right) = m_{\rm B}^\star - (M_{\rm B} - \alpha X_1 + \beta C), \qquad (5.61)$$

where $M_{\rm B}$, α, and β are three nuisance parameters which are fitted simultaneously with the cosmological parameters. The redshift is determined besides by spectroscopic measurements. Figure 5.3 shows the most recent Hubble diagram [42], obtained from the joint lightcurve analysis (JLA) of 740 SNeIa belonging to four different samples: Low-z survey [150], the SDSS-II supernova survey [151], the 3-year data release of the SuperNova Legacy Survey (SNLS) [152], and a few high redshift SNe detected with the Hubble Space Telescope (HST) [153].
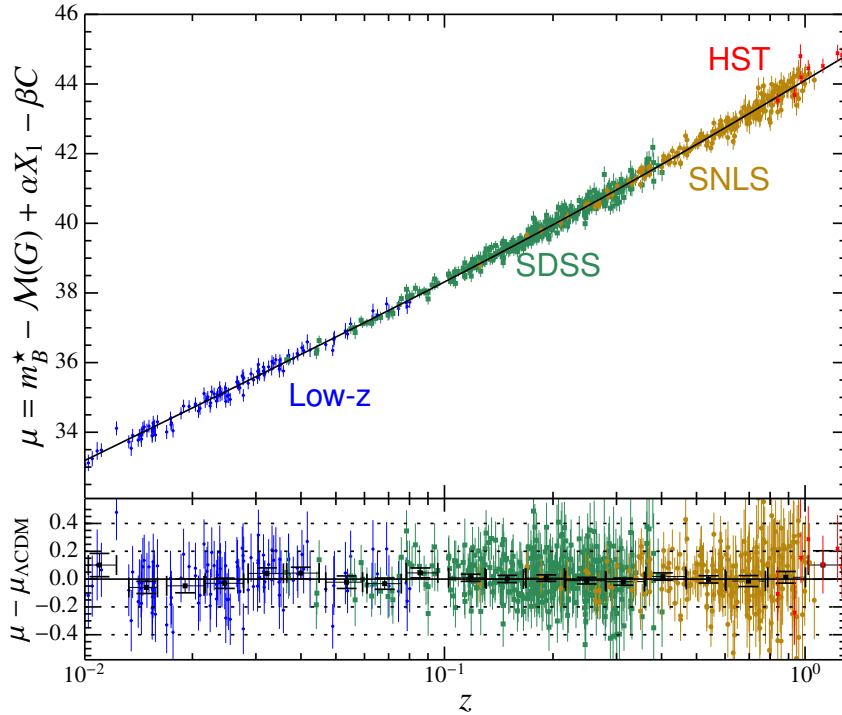

Figure 5.3 A Hubble diagram obtained by the joint lightcurve analysis of 740 SNeIa from four different samples: Low-z, SDSS-II, SNLS3, and HST. The top panel depicts the Hubble diagram itself with the ΛCDM best fit (black line); the bottom panel shows the residuals. From Ref. [42]

In all current analyses of the Hubble diagram, including Ref. [42], the data are interpreted *assuming that light propagates through a perfectly homogeneous and isotropic Universe*, so that the theoretical relation between luminosity distance and redshift to which observations are confronted is

$$D_{\rm L}(z) = a_0(1 + z) f_K \left(\frac{1}{a_0 H_0} \int_0^z {\rm d}\zeta \, \left[\Omega_{\rm m0}(1 + \zeta)^3 + \Omega_{K0}(1 + \zeta)^2 + \Omega_{\Lambda 0} \right]^{-1/2} \right), \quad (5.62)$$
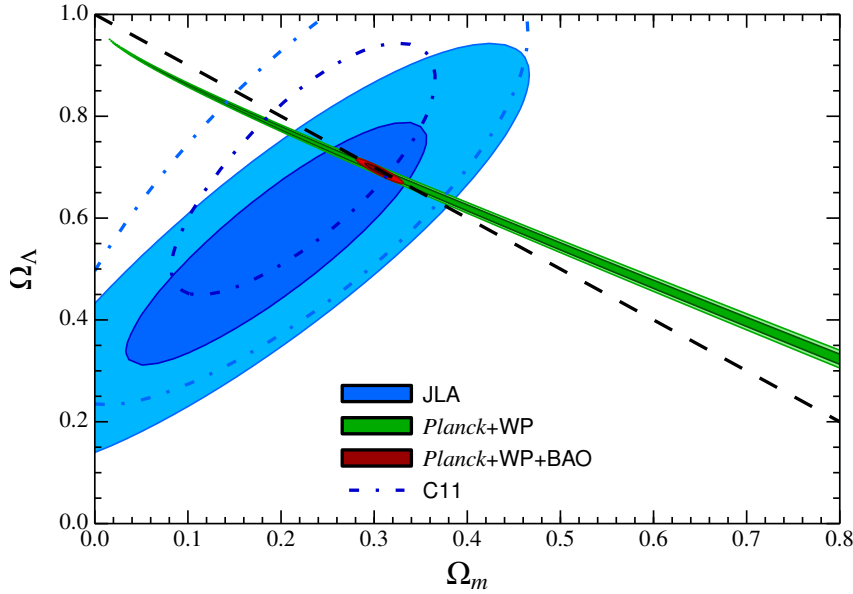
Figure 5.4 Constraints on the cosmological parameters $\Omega_{m0}, \Omega_{\Lambda0}$ obtained from the Hubble diagram of Fig. 5.3 (blue contours), together with other observations: CMB (green), and CMB+BAO (red). The dot-dashed contours corresponds to the constraints from earlier SN data [156]. The dashed line indicates $\Omega_{m0} + \Omega_{\Lambda0} = 1$, i.e. $K = 0$. From Ref. [42]

which is derived from $D_{\mathrm{L}} = (1 + z)^2 D_{\mathrm{A}}$, and with the results of § 5.1. We can see in Fig. 5.3 that this model provides an excellent fit to the data. The resulting constraints on the free parameters $\Omega_{m0}, \Omega_{\Lambda0}$ are displayed in Fig. 5.4, which shows in particular that the absence of dark energy is excluded at a 3σ confidence level. The Hubble diagram of SNeIa is indeed particularly adapted to investigating the existence and properties of dark energy, as it probes the Universe at low redshift, i.e. at late times. This is the reason why SNeIa provided the first evidence of the acceleration of cosmic expansion in the late 1990s [154, 155], a discovery rewarded by the 2011 Nobel Prize.

Physically speaking, the cosmological constant affects SNIa observations in two complementary ways. Consider a source at a given affine-parameter distance v from us. On the one hand, Λ reduces its redshift due to the acceleration of cosmic expansion: if the expansion accelerates, then it was slower in the past, so the recession velocity of a distant object is smaller. In other words, $z_{\Lambda\neq0}(v) < z_{\Lambda=0}(v)$, as confirmed by the fact that, in a FL model,

$$-\omega_0 v = \int_0^z \frac{\mathrm{d}\zeta}{(1 + \zeta)^2 H(\zeta)}, \tag{5.63}$$

which can be derived from $\mathrm{d}z/\mathrm{d}v = \mathrm{d}(a_0/a)/\mathrm{d}v$, using that $\mathrm{d}/\mathrm{d}v = k^t\mathrm{d}/\mathrm{d}t = \omega_0(1+z)\mathrm{d}/\mathrm{d}t$. On the other hand, for a given expansion rate today H_0, the presence of Λ reduces the Universe's matter density (it reduces Ω_{m0}), so it reduces the actual Ricci focusing experienced by light beams, therefore enhancing the observed angular distance: $D_{\mathrm{A}}^{\Lambda=0}(v) > D_{\mathrm{A}}^{\Lambda\neq0}(v)$. As illustrated in Fig. 5.5, these two effects combine so that $D_{\mathrm{A}}^{\Lambda\neq0}(z) > D_{\mathrm{A}}^{\Lambda=0}(z)$, hence $D_{\mathrm{L}}^{\Lambda\neq0}(z) > D_{\mathrm{L}}^{\Lambda=0}(z)$ as well. We conclude that SNe with a given observed z appear dimmer in a Universe with dark energy than without. Of course, it could also be attributed to a negative spatial curvature $K < 0$, which acts similarly to Λ. This is the reason why the constraints of Fig. 5.4 are degenerate in the direction orthogonal to $K = \mathrm{cst}$.

In the context of linear perturbation theory, the use of the background distance-redshift relation (5.62) for modelling the Hubble diagram can be justified by the fact that the
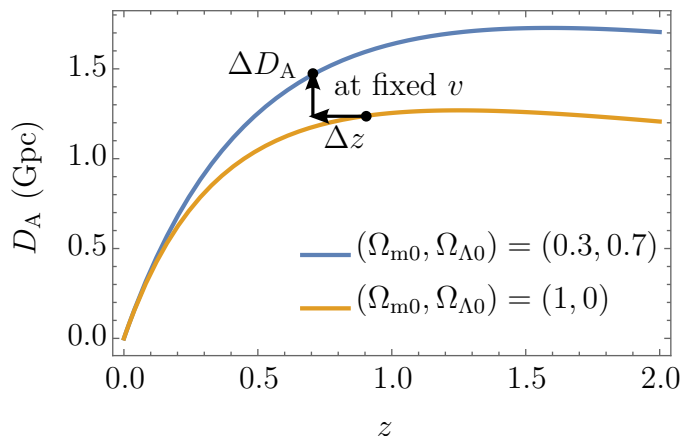
Figure 5.5 For a given observed redshift z, a SN appears farther (smaller and dimmer) through a Universe with dark energy, due to both the acceleration of cosmic expansion and the reduction of Ricci focusing.

corrections are negligible once averaged over many sources. Indeed, regarding the correction to the redshift (5.25), the Doppler contribution vanishes if we suppose that the SNe have random peculiar velocities (see however Ref. [157]), while the SW and ISW/RS effects are anyway very small. As for the cosmic convergence κ, since by definition $\langle \delta \rangle = 0$, we deduce that $\langle \kappa \rangle = 0$ after averaging over the sky.[7] The cosmological perturbations thus do not significantly bias the distance-redshift relation at linear order. However, they are expected to contribute to the scattering of the Hubble diagram: at low redshift because some SNe are more or less redshifted due to their peculiar velocity; at high redshifts because some are magnified and others demagnified. In the analysis of SN data, these effects are taken into account by adding two terms diagonal terms σ_{pec}^2 and σ_{lens}^2 to the covariance matrix of the χ^2. In Ref. [42], for instance, $\sigma_{\mathrm{pec}} = (5 \times 150 \, \mathrm{km/s})/(cz \ln 10)$ and $\sigma_{\mathrm{lens}} = 0.055z$. For comparison, the intrinsic scatter of SN magnitudes is $\sigma_{\mathrm{int}} \sim 0.1$ [156].

If gravitational lensing is worked out at second-order in cosmological perturbations, then the apparent luminosity of the SNe is biased with respect to the background case. This bias remains however very small [141, 159, 161, 162]. This conclusion does not necessarily hold in nonperturbative approaches, in particular when the fluid description of matter in the Universe is abandoned, as we shall see in Part III.

Let us finally mention that, although SNIa observations are often presented as the most model-independent cosmological probes, the accuracy of this claim actually depends on the lightcurve fitter used for processing the data [163]. The results presented here have been obtained with the Spectral Adaptive Lightcurve Template (SALT2) method [164], where the phenomenological parameters α, β are fitted simultaneously with the cosmological parameters. So in this approach, the SN distance moduli themselves are measured by assuming a homogeneous FL model. This method is therefore not completely model-independent, in the sense that alternative cosmological models cannot be consistently tested with these data. An alternative method is the Multicolour Light Curve Shape (MLCS) fitter [165], whose calibration is performed using only low-redshift SNe, where only the linear Hubble law is required. Though more model independent, MLCS has the disadvantage of producing results with larger error bars than SALT2.

---

[7]We here identified three notions of averaging with the notation $\langle \cdots \rangle$: sky averaging, ensemble averaging, and source averaging. Such an assumption is valid as far as only first-order perturbations are at stake, but it breaks down at second order, as discussed in Refs. [158–160].

5.3.2   Cosmic microwave background

A dissertation on cosmology cannot be without mentioning the observation of the CMB, which is certainly the archetype of high-precision cosmological experiments. Its origin, as originally understood by Refs. [166, 167] in 1948, goes back to the early Universe, when the primordial plasma cooled enough for the atomic nuclei to recombine with electrons, forming (mostly) neutral hydrogen atoms. Light thus suddenly stopped being scattered by charged particles, and started propagating freely, following null geodesics. According to the cosmological principle, this happened everywhere at the same (cosmic) time, so that whatever the direction we look at today, we receive such photons coming from some remote place of the Universe where they were released 13.8 billion years ago.

The first experimental evidence for the CMB was accidentally found in 1964 [168], and rewarded by the 1978 Nobel Prize. Since then, considerable efforts were carried out to measure and analyse this primordial radiation with an increasing precision, both with Earth-based and space experiments, such as the COsmic Background Explorer (COBE) [169], the Wilkinson Microwave Anisotropy Probe (WMAP) [170], and lately the *Planck* satellite [171]. The CMB appears today as an almost perfect black body, very well-described by a Planck spectrum of temperature $T_{\mathrm{CMB}} = 2.72548 \pm 0.00057\,\mathrm{K}$ [172], whose peak wavelength is[8] $\lambda_{\mathrm{CMB}} \sim \mathrm{mm}$ (microwave/radio domain). This observed signal corresponds to an emitted Planck spectrum of temperature $k_{\mathrm{B}}T_* \sim 0.3\,\mathrm{eV}$ ($\lambda_* \sim \mathrm{\mu m}$) redshifted by $z_* = 1089.90 \pm 0.23$ [91] due to cosmic expansion.

The CMB is however not perfectly isotropic, and the fluctuations of the observed temperature $\Theta \equiv \delta T / \bar{T} \sim 10\,\mathrm{\mu K}$ (see Fig. 5.6) actually contain a lot of information about the Universe. The origin of the temperature anisotropies can be separated in two categories: (i) primary anisotropies, generated before recombination, and thus related to the physics of inflation and of the primordial plasma; (ii) secondary anisotropies, due to what happens to the CMB photons after their release and before their observation (gravitational lensing, SZ effect in galaxy clusters, etc.) We refer the reader to textbooks [101, 174] for details about the physics and the analysis of the CMB. In the perspective of the present thesis, we choose to restrict to a single important feature of the CMB anisotropies: the acoustic horizon scale.

Assuming statistical isotropy, the covariance of the temperature fluctuation Θ as observed in two directions $\boldsymbol{e}_1$, $\boldsymbol{e}_2$ can be decomposed over Legendre polynomials P_ℓ as

$$\langle \Theta(\boldsymbol{e}_1)\Theta(\boldsymbol{e}_2) \rangle = \sum_{\ell=0}^{\infty} \frac{2\ell+1}{4\pi} C_\ell P_\ell(\boldsymbol{e}_1 \cdot \boldsymbol{e}_2), \tag{5.64}$$

where $\boldsymbol{e}_1 \cdot \boldsymbol{e}_2 = \cos\theta$ denotes the Euclidean scalar product between the unit spatial vectors $\boldsymbol{e}_1$, $\boldsymbol{e}_2$, and θ is the angle between them. Physically speaking, C_ℓ quantifies the correlation between the temperature of two points in the sky separated by an angle $\theta \sim \pi/\ell$. It thus corresponds to an angular power spectrum. Figure 5.7 shows the C_ℓ, or more precisely the $\mathcal{D}_\ell \equiv \ell(\ell+1)C_\ell/2\pi$, as measured by the *Planck* mission.

Among the features of this plot, note the oscillation of $\mathcal{D}_\ell$, with a period of $\Delta\ell_* \approx 300$, indicating a particular correlation between points separated by $\theta_* \approx 0.5\,\mathrm{deg}$. The origin of this correlation lies in the presence of sound waves propagating within the photon/plasma fluid before recombination, sustained by radiation pressure. From its birth at the end of inflation to its disappearance at recombination, such a wave propagates over a distance r_{s} called *sound horizon*. At recombination, two overdensities (or underdensities) are thus

---

[8]According to Wien's displacement law, $\lambda_{\mathrm{peak}}T = b$, with [173] $b = 2.8977729 \times 10^{-3}\,\mathrm{m \cdot K}$.
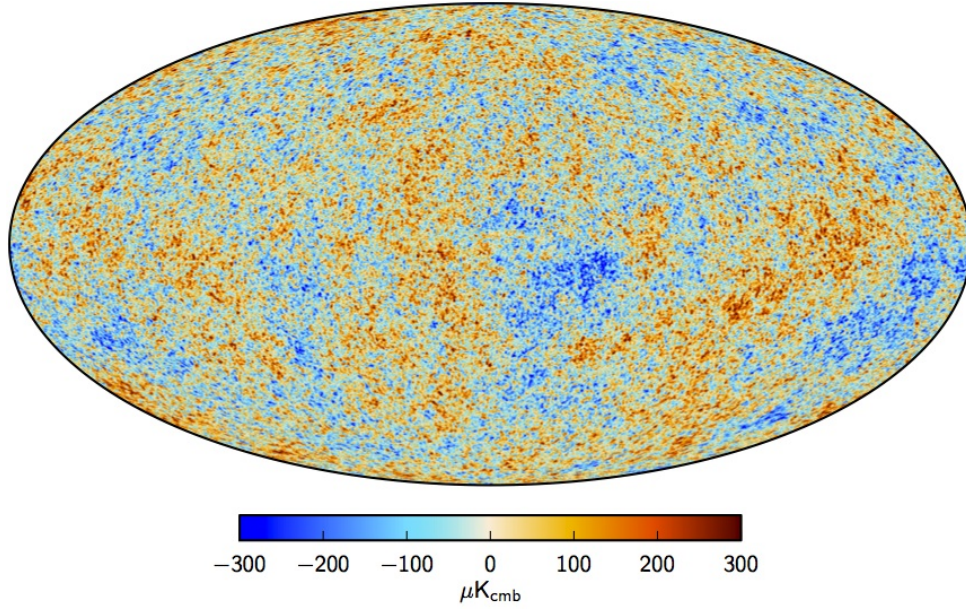
Figure 5.6 Temperature anisotropy of the CMB, as observed by the *Planck* satellite. This map of the whole celestial sphere is obtained by a Mollweide projection. From Ref. [175]
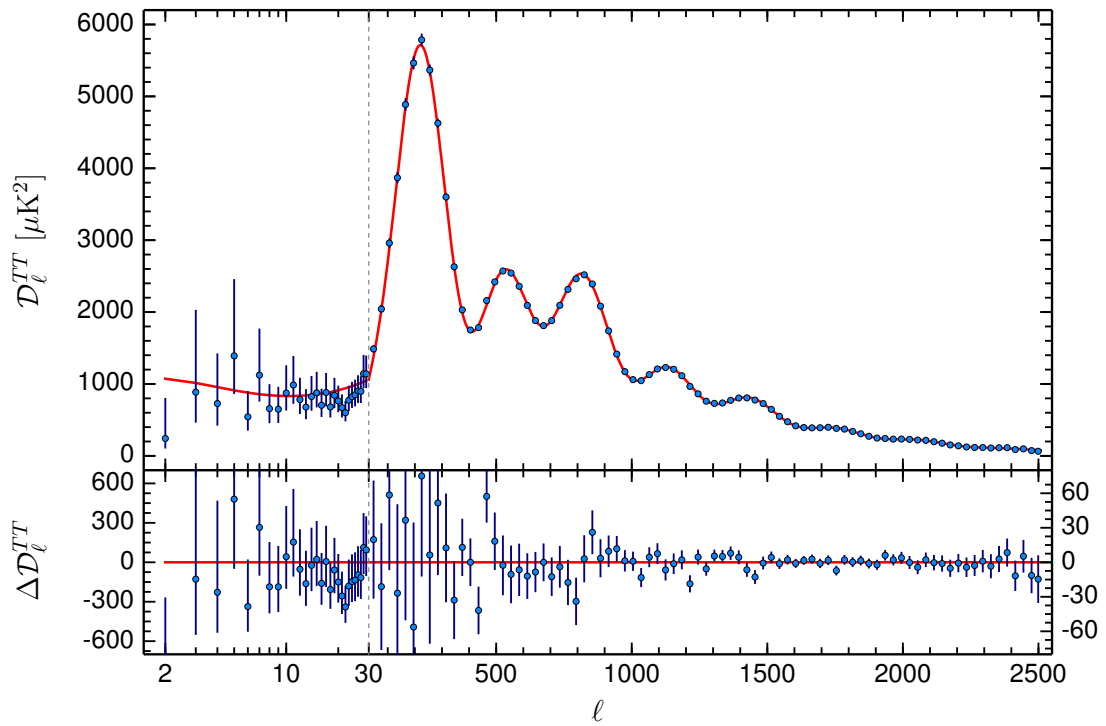

Figure 5.7 Angular power spectrum of the temperature anisotropies of the CMB, as measured by the *Planck* mission. From Ref. [175]

more likely to be separated by r_s. This implies, on the CMB temperature map, that two hot (or cold) points are more likely to be separated by an angle $\theta_* = r_s/D_A$, where D_A is the angular diameter distance from us to the last scattering surface.

While r_s depends on the physics of the primordial plasma, in particular through the density of baryonic matter Ω_{b0}, it requires a model for the angular distance-redshift relation $D_A(z)$ to be connected with the observable quantity θ_*. The situation is similar

to the analysis of the Hubble diagram, where a model for $D_{\mathrm{L}}(z)$ is required, and once again the standard choice is to use the distance-redshift relation of a FL model. Because this relation involves $\Omega_{\mathrm{m}0}$ and $\Omega_{\Lambda0}$, the analysis of the CMB provides constraints on these parameters, as shown in Fig. 5.8. Its degeneracy direction is kindly orthogonal to the one of SNIa constraints, making the combination of both a powerful and accurate measurement of $\Omega_{\mathrm{m}0}, \Omega_{\Lambda0}$. These parameters are not the only ones to be constrained by the CMB, from which can also be extracted crucial information on the amplitude of matter density fluctuations [91], cosmic topology [176], inflation [177], reionisation, etc.
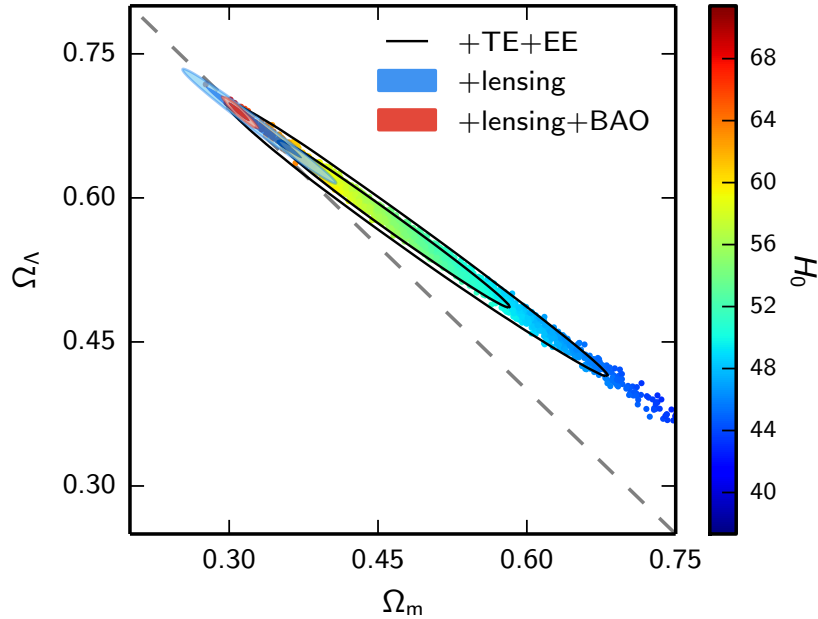

Figure 5.8 Constraints on the cosmological parameters $\Omega_{\mathrm{m}0}, \Omega_{\Lambda0}$, and on the Hubble expansion rate H_0, obtained from the analysis of the CMB. From Ref. [91]

In the standard CMB analyses, gravitational lensing is considered to act essentially as a remapping of anisotropies of the temperature field [178, 179], according to the first-order formula (5.30). This brings an additional contribution to the angular power spectrum C_ℓ, but it does not affect the mean angular distance $D_{\mathrm{A}}(z_*)$ mentioned above, and thus does not lead to any shift in the position of the acoustic peaks. This approach has been questioned recently in Ref. [180], where second-order lensing corrections seemed to affect the average distance to the last-scattering surface by a few percents, a correction which would significantly impact the analysis of the CMB. Almost one year later, however, it was shown independently by Refs. [159, 181] (one of them being coauthored by the very authors of Ref. [180]) that this effect is actually caused by a subtle confusion between source averaging, sky averaging, and ensemble averaging. The distinction between these different ways of averaging physical quantities, and their natural domain of applicability, had been emphasized earlier by Ref. [158]; it now seems to be fully understood [160]. In the end, this debate validated the standard treatment of CMB lensing.

5.3.3 Baryon acoustic oscillation

The acoustic feature present in the CMB corresponds to a rather large scale, which is weakly affected by the gravitational evolution of the Universe between the epoch of

recombination and today—contrary to small-scale inhomogeneities which tend to collapse and lose information about their initial conditions. As a consequence, this correlation has survived within the distribution of baryonic matter in the Universe. In this case, it is referred to as the *Baryon Acoustic Oscillation* signal. Because it only grows with cosmic expansion, the BAO scale (or its comoving counterpart $\chi_{\rm BAO}$) can be considered a cosmic *standard ruler*, by analogy with the notion of standard candle.

From the above reasoning, it is easy to estimate the BAO scale today $r_{\rm d}$ as

$$r_{\rm d} = \frac{a_0}{a_*} r_{\rm s} = (1 + z_*) D_{\rm A}(z_*) \theta_* \approx 150 \, {\rm Mpc} \approx 100 h^{-1} \, {\rm Mpc}, \qquad (5.65)$$

where we used the FL expression of $D_{\rm A}(z)$. The first detection of the BAO signal in today's distribution of matter has been obtained by the Sloan Digital Sky Survey (SDSS), in the two-point correlation function of low-redshift LRGs [182]. To date, the most precise measurement has been realised by the Baryon Oscillation Spectroscopic Survey (BOSS) of SDSS-III [183], with two complementary experiments: (i) a large survey of 1 million galaxies between $0.2 \leq z \leq 0.7$ [184]; (ii) a survey of distant quasars $(2.1 \leq z \leq 3.5)$, and of the intergalactic medium traced by the Lyman-α forest in their spectrum [40]. The corresponding correlation functions are shown in Fig. 5.9, where the BAO signal is evident (7σ confidence level), and in agreement with the order of magnitude obtained above. It is remarkable that this property of the matter distribution can be observed at so different epochs of the Universe: $z = 1090$ (Fig. 5.7), $z = 2.35$, and $z = 0.54$ (Fig. 5.9).

Experiments such as BOSS have the advantage, with respect to CMB observations, of extracting the BAO signal from a three-dimensional distribution rather than from a two-dimensional map. Hence, additionally to the angular correlation scale $\theta_{\rm BAO}$, they yield a redshift correlation scale $\Delta z_{\rm BAO}$ associated with BAOs aligned with the line of sight. Assuming a FL model, these quantities are related to the BAO scale today $r_{\rm d} = a_0 \chi_{\rm BAO}$ as

$$\theta_{\rm BAO} = \frac{a}{a_0} \frac{r_{\rm d}}{D_{\rm A}(z)} = \frac{r_{\rm d}}{(1+z) D_{\rm A}(z)} \qquad (5.66)$$

$$\Delta z_{\rm BAO} = H(z) a_0 \chi_{\rm BAO} = \frac{r_{\rm d}}{D_H(z)}, \qquad (5.67)$$

for observations at redshift z, with $D_H \equiv 1/H$, and where we used Eq. (5.7) for writing $a_0 \Delta\chi = \Delta z / H$. Given a set of cosmological parameters, $\theta_{\rm BAO}$ and $\Delta z_{\rm BAO}$ are therefore precisely related, so that their comparison allows to test the choice of these cosmological parameters, or the validity of the FL model itself. This procedure is known as the *Alcock-Paczyński test* [185]. In Fig. 5.10 are represented the observed values of $D_{\rm A}/r_{\rm d}$, $D_H/r_{\rm d}$, and the consequent constraints on $\Omega_{\rm m0}, \Omega_{\Lambda 0}$ obtained by Ref. [40]. Note that, here again, the standard interpretation of the observed data relies on the FL $D_{\rm A}(z)$ relation.

5.3.4 Other observations

Let us finally mention a few other cosmological probes which, though less emblematic, have become more and more precise over the last years and are now efficient complements to SNIa, CMB, and BAO observations.

Baryon and gas fraction in galaxy clusters

The potential of galaxy clusters as cosmological probes was revealed in the early 1990s, when Ref. [186] seriously challenged the standard paradigm of that time, according to
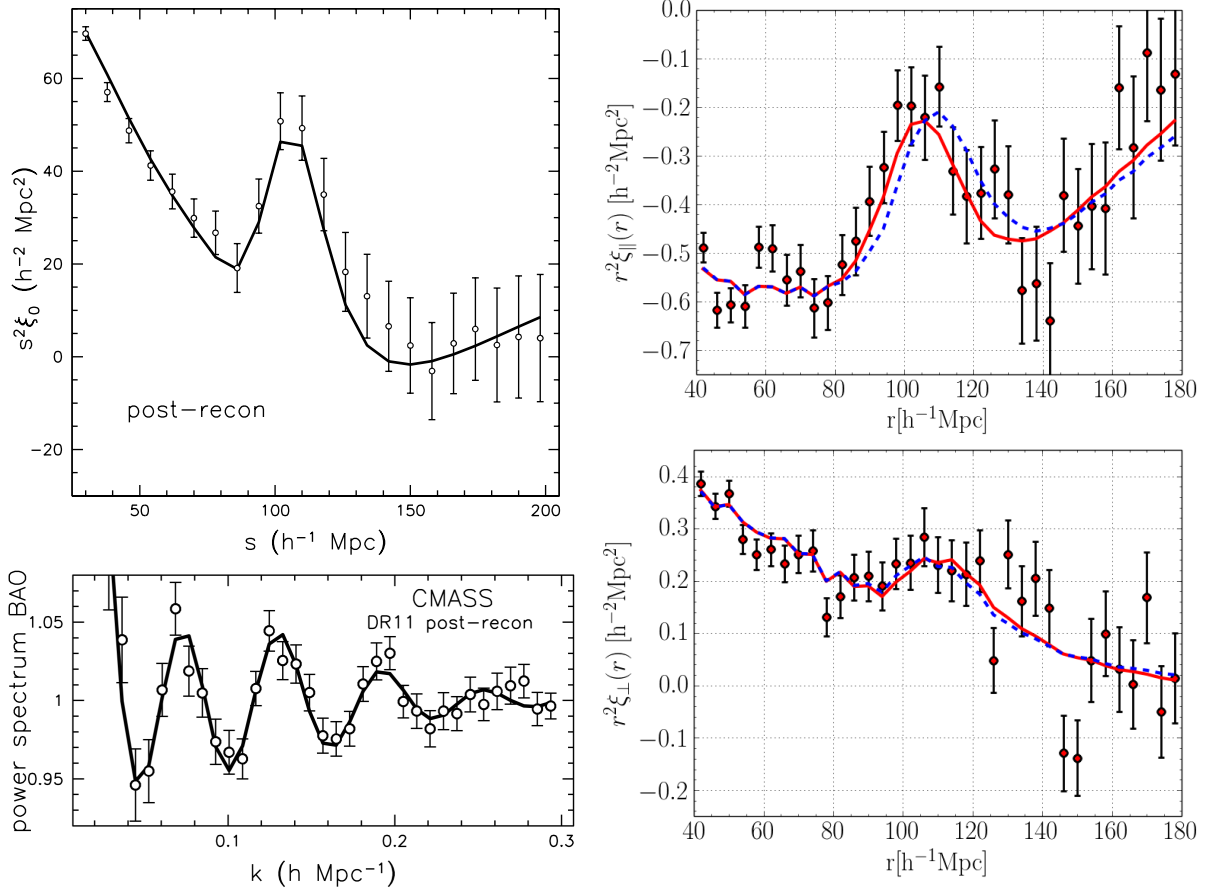
Figure 5.9 *Left panel.* Two-point correlation function (top) and power spectrum (bottom) of the distribution of the BOSS CMASS galaxy sample ($0.2 \leq z \leq 0.7$), as a function of comoving distance s and comoving wavenumber k, respectively. This BAO signal is effectively measured at $z = 0.57$. From Ref. [184]. *Right panel.* Two-point correlation function for objects aligned with the line of sight (top), or orthogonal to the line of sight (bottom), measured with the BOSS quasars ($2.1 \leq z \leq 3.5$) and the intergalactic medium traced by their Lyman-α forest, as a function of comoving distance r. The effective redshift is $z = 2.34$ here. From Ref. [40].

which $\Omega_{\mathrm{m}0} = 1$. By measuring the gas and stellar masses M_{gas}, M_{gal} of the Coma cluster, respectively from its X-ray and B-band luminosities, the authors of Ref. [186] estimated the total baryonic mass $M_{\mathrm{b}} = M_{\mathrm{gal}} + M_{\mathrm{gas}}$ of this cluster and compared it with its total (dynamical) mass M_{tot}. Assuming a ratio $M_{\mathrm{b}}/M_{\mathrm{tot}}$ equal to the mean cosmological baryonic fraction,

$$\frac{M_{\mathrm{b}}}{M_{\mathrm{tot}}} = \frac{\Omega_{\mathrm{b}0}}{\Omega_{\mathrm{m}0}}, \tag{5.68}$$

and using the value of $\Omega_{\mathrm{b}0}$ obtained by analyses of the Big Bang Nucleosynthesis (BBN), they concluded that $\Omega_{\mathrm{m}0} \approx 0.28$ (for $h = 0.7$), a result surprisingly close to the current admitted value. It is worth emphasizing that this discovery occurred *before* the first analyses of the Hubble diagram, which really opened the era of dark energy cosmology.

Three years later, Ref. [187] proposed a more subtle method for constraining cosmological parameters with galaxy clusters. The X-ray data of galaxy clusters are indeed interpreted in such a way that the gas mass fraction extracted from them reads

$$f_{\mathrm{gas}} \equiv \frac{M_{\mathrm{gas}}}{M_{\mathrm{tot}}} = B(z)D_{\mathrm{A}}^{3/2}(z), \tag{5.69}$$
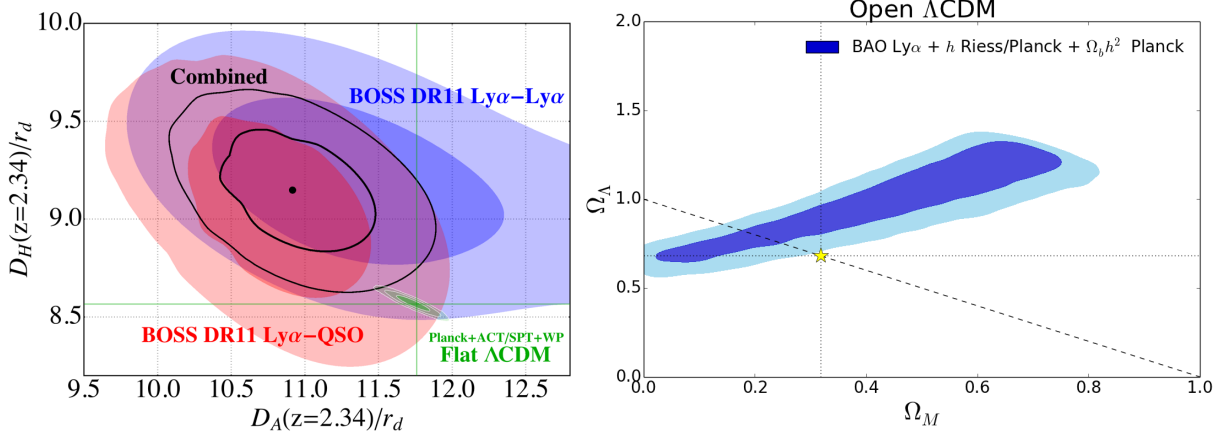
Figure 5.10 *Left panel.* Constraints on the longitudinal and transverse distances D_A/r_d, D_H/r_d at $z = 2.34$ from BAO measured with quasars and intergalactic medium. The green contours indicate the constraints from the CMB in the case of a flat FL model. *Right panel.* Consequent constraints on the cosmological parameters $\Omega_{m0}, \Omega_{\Lambda 0}$. The yellow star indicates the concordance ΛCDM model. From Ref. [40].

where B is independent from the cosmological parameters, so that $D_A(z)$ contains all the cosmological dependence. Assuming that $f_{\rm gas}$ does not depend (on average) on the redshift of the cluster, we conclude that a plot representing the $f_{\rm gas}$ of several clusters as a function of their redshift must be flat. However, it is not the case if a wrong cosmology—or more generally a wrong distance-redshift relation—is assumed for the data analysis. This idea provides a consistency test of the cosmological model, similarly to the comparison between the longitudinal and transverse BAO signal. Though limited by the intrinsic scatter of $f_{\rm gas}$, estimated to be $(7.4 \pm 2.3)\%$ by Ref. [188], this method provides today constraints on $(\Omega_{m0}, \Omega_{\Lambda 0})$ which are competitive with BAO's or SNeIa's (see Fig. 5.11a). We keep emphasizing that, like all the other cosmological probes reviewed so far, the $f_{\rm gas}$ method relies on a particular model for $D_A(z)$, taken to be the FL one.

Weak lensing tomography

We have seen in § 5.2.2 that the observations of the shapes of lensed galaxies gives access to the power spectrum of cosmic convergence, via the one of cosmic shear, as $P_\kappa = P_\gamma = P_\varepsilon$. Besides, the expression (5.57) of P_κ turns out to involve the cosmological parameters in various ways: directly on Ω_{m0} and H_0, and indirectly via both the lensing efficiency and the matter power spectrum P_δ. Measuring the statistics of galaxy ellipticities is therefore a means to constrain the cosmological parameters. As an illustration, Fig. 5.11b shows the constraints on $\Omega_{m0}, \Omega_{\Lambda 0}$ obtained from the two- and three-point correlation functions of cosmic shear, as measured by the Canada France Hawaii Telescope Lensing Survey CFHTLenS [189] in Ref. [190]. These constraints are rather loose compared to ones obtained with other cosmological probes. Weak lensing (WL) is actually much more efficient at constraining σ_8, which is the standard deviation of the matter density fluctuations δ smoothed over a comoving sphere of radius $R \equiv 8h^{-1}$ Mpc,

$$\sigma_8^2 \equiv \left\langle \left[\frac{3}{4\pi R^3} \int_{|x^i| \leq R} {\rm d}^3 x\, \delta(x) \right]^2 \right\rangle = \int_0^\infty \frac{{\rm d}k}{k} \left[\frac{3 j_1(kR)}{kR} \right]^2 P_\delta(k) \sim 1, \qquad (5.70)$$

where j_1 is the order-one spherical Bessel function [191]. This can be understood by the fact that $\Omega_{m0}^2 \sigma_8^2$ essentially sets the amplitude of P_κ, while its dependence in the other
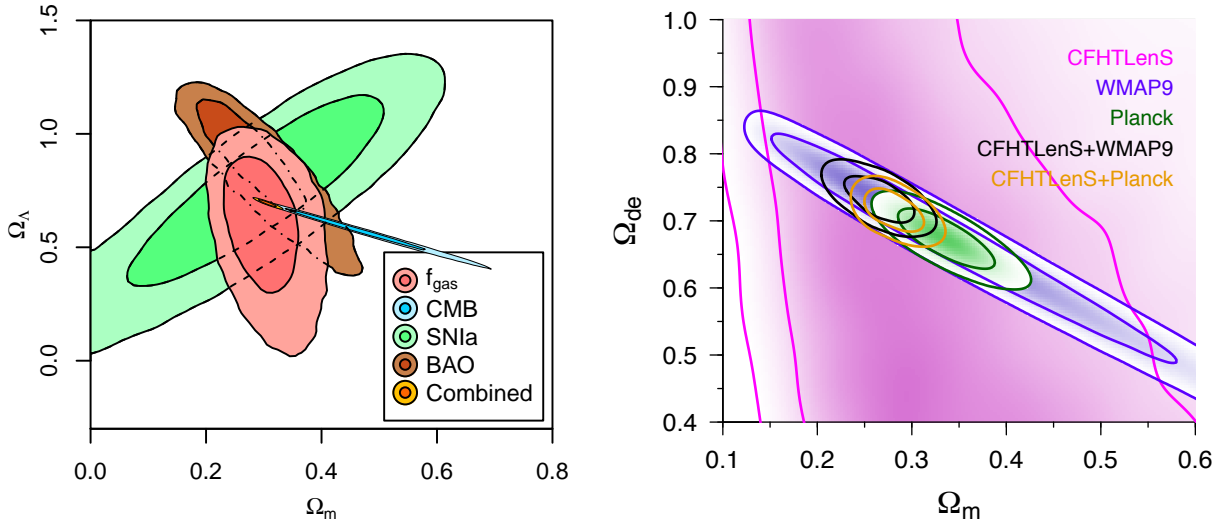
(a) Constraints on $\Omega_{m0}, \Omega_{\Lambda 0}$ by comparing the gas fraction f_{gas} within galaxy clusters at different redshifts. From Ref. [188]

(b) Constraints on $\Omega_{m0}, \Omega_{\Lambda 0}$ imposed by the measured two- and three-point correlation functions of cosmic shear. From Ref. [190]

Figure 5.11 Some cosmological constraints from f_{gas} measurements in galaxy clusters (left panel) or weak-lensing tomography (right panel).

cosmological parameters is weaker.

Alternative methods exploiting weak lensing, e.g. from the shear ratio around galaxy clusters [192], or using higher-order statistical properties such as shear peak counts [193,194], are still under development. They are expected to provide very accurate measurements of the cosmological parameters from future large surveys, such as Euclid [195], or the Wide-Field InfraRed Survey Telescope (WFIRST) [196].

Strong lensing and time delays

When very massive or compact objects lie between a light source and an observer, the deflection they induce can be large enough for allowing light to have several paths from the one to the other. In this regime of *strong gravitational lensing* (SL), the observer can thus see multiple images of a single source (gravitational mirages), or images which are so sheared that they appear as luminous arcs around the lens [17]. The size and shape of these arcs, or the Shapiro time delay between two different images, depend on the properties of the lens, but also on the lensing efficiency factor (5.34), and therefore on the cosmological parameters. Provided one has an accurate model for the lenses, this property can be exploited to constrain the cosmological parameters from strong lensing measurements [197]. This idea has the advantage, with respect to WL, that it can be applied to single objects [198], rather than relying on statistics. Its main limitation, however, concerns the uncertainties on the lens properties. Recently, time delays between multiple images observed by the COSmological MOnitoring of GRAvItational Lenses (COSMOGRAIL) [199] were used to measure $h = 0.800^{+0.058}_{-0.057}$ [200]. Besides, strong lensing measurements were recently exploited to constrain spatial curvature via the distance sum rule Ω_{K0} [201], or the dark-energy equation of state [202].

5.3.5 Discussion

This brief review of the current status of observational cosmology shows that the standard ΛCDM model consistently fits all the data with an impressively high level of precision, given its simplicity. We emphasized that the interpretation of every observation involves the relation between angular (or luminosity) distance and redshift $D_A(z)$, from which generally comes its sensitivity with respect to the cosmological parameters. This relation is always assumed to be the one of a FL spacetime, derived in § 5.1. In other words, *all the distances necessary to interpret cosmological observations are calculated by assuming that light propagates through a perfectly homogeneous and isotropic Universe.* The success of this strong assumption is particularly striking if we compare the scales involved in all these observations, listed in Table 5.3. We see that the typical observed angles, i.e. the typical size of the corresponding light beams, span 12 orders of magnitude. To my knowledge, there exists no model in the whole History of physics whose domain of validity is so wide[9].

The issue raised here must be connected to the laws of geometric optics in curved spacetime presented in Part I. We have seen in Chap. 2 that the evolution of the angular distance is driven by Ricci and Weyl curvatures in quite different ways. Ricci lensing tends to directly reduce D_A by focusing the underlying light beam, while Weyl lensing indirectly reduces it via the beam's shear rate. However, what is considered Ricci or Weyl lensing depends on the size of the beam itself: a distribution of point masses can appear alternatively clumpy or smooth to a beam whose cross-sectional diameter is respectively much smaller or much larger than the typical distance between two point masses. Similarly, our Universe can be considered smooth—Ricci dominated—for the beams involved in BAO observations, but it is certainly very clumpy—Weyl dominated—when SN observations are at stake. This *Ricci-Weyl paradox* of cosmology is central to the present thesis, whose motivation can be summarised by the following question: why is the FL geometry so efficient at interpreting all the cosmological observations? The next part intends to provide elements of answer.

observation	relevant angular scale	typical value (rad)
BAO	BAO scale at $z \sim 0.5, 2$	$10^{-1}, 10^{-2}$
CMB	BAO scale at $z \sim 1000$	10^{-2}
f_{gas}	apparent size of a cluster at $z \sim 0.5$	10^{-3}
SL	Einstein radius of a galaxy on cosmological scales	10^{-4}
WL	apparent size of a galaxy at $z \sim 0.5$	10^{-5}
SNeIa	apparent size of a SN at $z \sim 0.5$	10^{-13}

Table 5.3 Relevant angular size (observed angular aperture) of the light beams involved in various cosmological observations, and their orders of magnitude.

---

[9]One could argue that the validity of quantum electrodynamics has been experimentally verified over more than 11 orders of magnitude, but the latter is more a theory than a model.

PART III

INHOMOGENEITY BEYOND THE FLUID LIMIT

THE question of how the clumpiness of the Universe affects the interpretation of cosmological observations has a long history. It was first raised more than 50 years ago, in 1964, by Zel'dovich in Ref. [203], and by Feynman in a colloquium given at the California Institute of Technology (mentioned e.g. in Ref. [204]). The underlying argument is that, on the very small scales probed by, e.g., the light beam coming from a supernova, a fluid description of the surrounding matter shall not hold in principle, as it is rather concentrated in clumps than smoothly distributed. A typical beam is thus expected to encounter less matter than in a strictly homogeneous model. Then followed a series of seminal articles, both on the Soviet side by Dashevskii & Slysh [205–207], and on the western side by Bertotti [208] and Gunn [204, 209].

While those studies were based on general arguments about geometric optics in an inhomogeneous Universe, Kantowski [210], and later Dyer & Roeder [211–214], relied on an exact solution of the Einstein equation, namely the Swiss-cheese model. This solution, obtained by gluing together the Schwarzschild and FL spacetime—which makes a 'hole' inside the Friedmann-Lemaître 'cheese'—had been originally proposed by Einstein & Straus [215, 216] as a means to model individual stars within the expanding Universe (see Chap. 6 for more details). These analyses yielded in particular a procedure for determining the effective impact of clumpiness on the angular distance-redshift relation, known as the partially-filled beam approximation, or *Dyer-Roeder approximation*, the name of Kantowski being usually—but unfairly—omitted in the literature. In agreement with Zel'dovich's original intuition, this approximation predicts that a typical light beam is defocused with respect to the FL behaviour, and therefore bias distance measurements towards larger values. Such a conclusion was criticized by Weinberg in Ref. [217], who argued on the basis of flux conservation that inhomogeneities should have no mean effect. Although this argument turns out to be inexact, it holds in principle at a very high order of precision (see e.g. Ref. [159, 181] for recent discussions). In practice, however, Weinberg's approach fails at capturing the consequences of: (a) the sparsity of observations—we do not observe an infinity of sources over the whole sky—; and (b) selection effects—some lines of sight can be masked [218]—which were central to the earlier results.

The whole issue has been then progressively left aside, presumably because no observation managed to arbitrate between the various points of view. It was revived in the 2000s within a new cosmological paradigm, in particular with the perspective of explaining the apparent acceleration of cosmic expansion without the need of dark energy. Most analyses, in this case, focused on the impact on observations of the *large-scale* inhomogeneity, relying either on the standard perturbation theory [135–139, 141, 159, 161, 162, 180, 219–225], or on Swiss-cheese models with Lemaître-Tolman-Bondi holes [24, 140, 226–238] or Szekeres [239–242] holes, which typically aim at modelling superclusters or cosmic voids (see also Refs. [243, 244]). Particular efforts were made in Refs. [245–250] in order to connect observables with the backreaction and cosmic averaging problems. In contrast, less attention was paid to the specific issue of clumpiness—with the notable exceptions of Refs. [251–256], where inhomogeneities are treated similarly to the historical Einstein-Straus Swiss-cheese model. It was exhumed by Clarkson et al. [257], who reviewed past and present approaches, emphasizing that no definite answer had been formulated so far.

This latter article motivated the present part of my thesis, which represents roughly three quarters of it—the last quarter concerns anisotropic cosmologies and is the subject of Part IV. It is divided into two chapters, which present two different approaches to the initial question raised by Zel'dovich and Feynman. In Chap. 6, I revisit light propagation in Einstein-Straus Swiss-cheese models with the eyes of modern cosmology. In Chap. 7, I

propose a completely new framework for dealing with lensing on small scales, based on the theory of stochastic processes.

Swiss-cheese cosmologies

THIS chapter is devoted to the analysis of light propagation in the Einstein-Straus Swiss-cheese model. Because it does not rely on a fluid description of matter, this model is indeed particularly adapted to modelling the small-scale inhomogeneity of the Universe, and evaluating its consequences on the interpretation of the Hubble diagram. It consists of three articles, whose main results are summarised in § 6.1. The first two articles, given in § 6.2 and 6.3, were done in collaboration with Hélène Dupuy and Jean-Philippe Uzan; they cover theoretical calculations, cosmological interpretations, and data analysis. The third article, given in § 6.4, contains important theoretical complements on the relation between Swiss-cheese models and the so-called Dyer-Roeder approximation.

Contents

6.1 Summary

The Einstein-Straus Swiss-cheese (hereafter SC) model is constructed from a homogeneous Universe by introducing spherical 'holes', with a point mass at their centres, within the FL 'cheese'. Inside a hole, spacetime geometry is described by the Schwarzschild metric, or the Kottler—also called Schwarzschild-de Sitter—metric in the presence of a nonzero cosmological constant. The boundary of the hole, where the junction between both geometries is performed, is a sphere of constant comoving radius $R_h = f_K(\chi_h)$. For this junction to be smooth, the central mass M must be related to the hole radius via

$$M = \frac{4\pi}{3}\rho(aR_h)^3, \tag{6.1}$$

where ρ is the average cosmic matter density, and a the scale factor. This result can be proven by two methods. In Art. 6.2, we followed the traditional derivation based on the Darmois-Israel junction conditions [258–260], according to which the induced metric and the extrinsic curvature of the junction hypersurface $R = R_h$ must be identical as seen from the interior or from the exterior. In Art. 6.4, I proposed a novel approach where the Kottler metric is first written in terms of free-fall coordinates, similar to the coordinates used by Lemaître for demonstrating the absence of singularity at the horizon of the Schwarzschild geometry [261, 262]. In terms of those coordinates, the Kottler metric takes a form very similar to the FL metric, and the junction is then performed more naturally, because the coordinate system is actually valid both inside and outside the hole.

The analysis of the propagation of single light rays through a SC model reveals that the presence of holes only marginally affects the relation between redshift z and affine parameter v. Corrections are due to a subtle mix between the Shapiro time delay caused by the central mass, and the Rees-Sciama due the fact that, in comoving coordinates, the gravitational potential inside the hole changes with time[1]. In Art. 6.4, I have rigorously proved that the corresponding fractional correction to $1 + z$ is on the order of $r_S/R_h \ll 1$, where $r_S \equiv 2GM$ is the Schwarzschild radius associated with the central mass.

Regarding light *beams*, I introduced in Art. 6.2 a technique based on the lensing Wronski matrix, in order to facilitate both the analytical and numerical treatments of the problem. I carefully rederived in Art. 6.4 the earlier results by Kantowski [210] and Dyer & Roeder [213], and reached the same conclusions: if the masses inside the holes are opaque, with physical radius $r_{phys} \gg r_S$, then Weyl lensing is essentially negligible, while Ricci focusing is reduced by a factor $f \in [0, 1]$, corresponding to the fraction of volume occupied by the FL regions, with respect to the homogeneous case. Note that this *smoothness parameter* is denoted α in Art. 6.4. This tends to bias the distance-redshift relation towards larger distances. I then checked those results numerically. This step required to design a numerical ray-tracing code in SC models. I wrote two different versions of it: the first one, exploited in Art. 6.2, has its holes arranged on a regular compact hexagonal lattice; the second one, exploited in Art. 6.4, has a random distribution of holes, where randomness was implemented by the method of Ref. [251], so that "each ray creates its own universe".

The cosmological consequences of these results were analysed in Arts. 6.2, 6.3 in two complementary ways, detailed below.

---

[1]Alternatively, if one uses the standard Droste coordinates with respect to which the Schwarzschild spacetime is explicitly static, then the radius of the hole grows with cosmic expansion. The gravitational potential experienced by an entering photon is thus lower than when the same photon exits from the hole. The latter thus gains a slight blueshift.

Fitting Mock Hubble diagrams. By randomly throwing rays in a SC model, whose FL regions are characterised by a set of cosmological parameters $\{\Omega\}$, I generated mock catalogues of SNe. The potential error in the interpretation of SN data caused by inhomogeneity was then quantified by fitting the associated Hubble diagrams with the FL distance-redshift relation, i.e. by wrongly assuming that the light of SNe propagated through a homogeneous Universe. The best-fit *apparent* cosmological parameters $\{\bar{\Omega}\}$ turned out to significantly differ from the input ones $\{\Omega\}$. For instance, a SC model constructed from the Einstein-de Sitter universe, i.e. $(\Omega_{m0}, \Omega_{K0}, \Omega_{\Lambda 0}) = (1, 0, 0)$, with $f = 0.26$, would be observed as $(\bar{\Omega}_{m0}, \bar{\Omega}_{K0}, \bar{\Omega}_{\Lambda 0}) = (0.5, 0.8, -0.3)$, or $(0.15, 0, 0.85)$ if spatial curvature is forced to vanish (see Fig. 19 of Art. 6.2). In other words, the light defocusing effect in SC models tends to mimic the effect of a negative spatial curvature, or a cosmological constant. The effect is however too small to explain SN observations without the need of dark energy. Importantly, the discrepancy $\bar{\Omega} - \Omega$ between the inferred and actual cosmological parameters drastically reduces as Λ increases. This can be understood as follows: the cosmological constant being homogeneous, if it dominates the geometry of spacetime then the difference between a SC and the underlying FL universe is not dramatic.

Re-analysing actual SN data. The natural questions arising from the above are: How should we interpret SN data in order to account for the effect of small-scale inhomogeneity? What are the values of the cosmological parameters inferred in this case? To the first question, the natural answer provided by Swiss-cheese models is to use the Kantowski-Dyer-Roeder distance-redshift relation, instead of the FL one, in order to fit the Hubble diagram. Note that this option was already considered by Perlmutter et al. in Ref. [155], in order to check whether inhomogeneity could be the origin of the apparent accelerating expansion. It cannot. We repeated this analysis on a more recent data set, namely the SNLS3 catalogue [156], and found that the smoothness parameter f is not constrained by SN observations. However, fixing a smaller value for f, i.e. increasing the clumpiness of the SC, increases the inferred value of Ω_{m0} from 0.25 ($f = 1$) to 0.3 ($f = 0$). See Fig. 25 of Art. 6.2. That answers the second question. We used this effect in Art. 6.3 to reconcile the constraints on Ω_{m0} obtained by SNLS3 (best-fit value of 0.2) with the one of *Planck* (0.31). Note however that, on the experimental side, recalibrations of the SDSS-II and SNLS lightcurves posterior to our work also managed to reduce this tension, attributed to systematics (see e.g. § 6.6 of Ref. [42]). This conclusion is only partially convincing, since as emphasized in Ref. [163], the calibration of SN lightcurves with the SALT2 method has a degree of model dependence which might force SN data to agree with the FL model.

From this series of works, we shall conclude that nature has somehow been kind with us by making a Universe dominated by the cosmological constant today. Indeed, if on the contrary it were dominated by matter, then the net effect of clumpiness on SN data would be larger, leading to a clear discrepancy between the cosmological parameters measured from the Hubble diagram and the ones measured from other probes, such as CMB or BAO experiments. Nevertheless, Art. 6.3 revealed that, in the era of precision cosmology, such effects may start to become non-negligible.

Interpretation of the Hubble diagram in a nonhomogeneous universe

Pierre Fleury[1,2,*], Hélène Dupuy[1,2,3,†] and Jean-Philippe Uzan[1,2‡]

[1] *Institut d'Astrophysique de Paris, UMR-7095 du CNRS,*
Université Pierre et Marie Curie, 98 bis bd Arago, 75014 Paris, France.
[2] *Sorbonne Universités, Institut Lagrange de Paris, 98 bis bd Arago, 75014 Paris, France.*
[3] *Institut de Physique Théorique, CEA, IPhT, URA 2306 CNRS, F-91191 Gif-sur-Yvette, France.*
(Dated: 24 june 2013)

In the standard cosmological framework, the Hubble diagram is interpreted by assuming that the light emitted by standard candles propagates in a spatially homogeneous and isotropic spacetime. However, the light from "point sources"—such as supernovae—probes the Universe on scales where the homogeneity principle is no longer valid. Inhomogeneities are expected to induce a bias and a dispersion of the Hubble diagram. This is investigated by considering a Swiss-cheese cosmological model, which (1) is an exact solution of the Einstein field equations, (2) is strongly inhomogeneous on small scales, but (3) has the same expansion history as a strictly homogeneous and isotropic universe. By simulating Hubble diagrams in such models, we quantify the influence of inhomogeneities on the measurement of the cosmological parameters. Though significant in general, the effects reduce drastically for a universe dominated by the cosmological constant.

I. INTRODUCTION

The standard physical model of cosmology relies on a solution of general relativity describing a spatially homogeneous and isotropic spacetime, known as the Friedmann-Lemaître (FL) solution (see e.g. Ref. [1]). It is assumed to describe the geometry of our Universe smoothed on large scales. Besides, the use of the perturbation theory allows one to understand the properties of the large scale structure, as well as its growth from initial conditions set by inflation and constrained by the observation of the cosmic microwave background.

While this simple solution of the Einstein field equations, together with the perturbation theory, provides a description of the Universe in agreement with all existing data, it raises many questions on the reason why it actually gives such a good description. In particular, it involves a smoothing scale which is not included in the model itself [2]. This opened a lively debate on the fitting problem [3] (i.e. what is the best-fit FL model to the lumpy Universe?) and on backreaction (i.e. the fact that local inhomogeneities may affect the cosmological dynamics). The amplitude of backreaction is still actively debated [4–6], see Ref. [7] for a critical review.

Regardless of backreaction, the cosmological model assumes that the distribution of matter is continuous (i.e. it assumes that the fluid approximation holds on the scales of interest) both at the background and perturbation levels. Indeed numerical simulations fill part of this gap by dealing with N-body gravitational systems in an expanding space. The fact that matter is not continuously

distributed can however imprint some observations, in particular regarding the propagation of light with narrow beams, as discussed in detail in Ref. [8]. It was argued that such beams, as e.g. for supernova observations, probe the spacetime structure on scales much smaller than those accessible in numerical simulations. The importance of quantifying the effects of inhomogeneities on light propagation was first pointed out by Zel'dovich [9]. Arguing that photons should mostly propagate in vacuum, he designed an "empty beam" approximation, generalized later by Dyer and Roeder as the "partially filled beam" approach [10]. More generally, the early work of Ref. [9] stimulated many studies on this issue [11–25].

The propagation of light in an inhomogeneous universe gives rise to both distortion and magnification induced by gravitational lensing. While most images are demagnified, because most lines of sight probe underdense regions, some are amplified because of strong lensing. Lensing can thus discriminate between a diffuse, smooth component, and the one of a gas of macroscopic, massive objects (this property has been used to probe the nature of dark matter [26–28]). Therefore, it is expected that lensing shall induce a dispersion of the luminosities of the sources, and thus an extra scatter in the Hubble diagram [29]. Indeed, such an effect does also appear at the perturbation level—i.e. with light propagating in a perturbed FL spacetime—and it was investigated in Refs. [30–35]. The dispersion due to the large-scale structure becomes comparable to the intrinsic dispersion for redshifts $z > 1$ [36] but this dispersion can actually be corrected [37–42]. Nevertheless, a considerable fraction of the lensing dispersion arises from sub-arc minute scales, which are not probed by shear maps smoothed on arc minute scales [43]. The typical angular size of the light beam associated with a supernova (SN) is typically of order 10^{-7} arc sec (e.g. for a source of physical size ~ 1 AU at redshift $z \sim 1$),

* fleury@iap.fr
† helene.dupuy@cea.fr
‡ uzan@iap.fr

while the typical observational aperture is of order 1 arc sec. This is smaller than the mean distance between any massive objects.

One can estimate [27] that a gas composed of particles of mass M can be considered diffuse on the scale of the beam of an observed source of size λ_s if $M < 2 \times 10^{-23} M_\odot h^2 \left(\lambda_s / 1\,\mathrm{AU}\right)^3$. In the extreme case for which matter is composed only of macroscopic pointlike objects, then most high-redshift SNeIa would appear fainter than in a universe with the same density distributed smoothly, with some very rare events of magnified SNeIa [27, 44, 45]. This makes explicit the connection between the Hubble diagram and the fluid approximation which underpins its standard interpretation.

The fluid approximation was first tackled in a very innovative work of Lindquist and Wheeler [46], using a Schwarzschild cell method modeling an expanding universe with spherical spatial sections. For simplicity, they used a regular lattice which restricts the possibilities to the most homogeneous topologies of the 3-sphere [47]. It has recently been revisited in Refs. [48] and in Refs. [49] for Euclidean spatial sections. They both constructed the associated Hubble diagrams, but their spacetimes are only approximate solutions of the Einstein field equations. An attempt to describe filaments and voids was also proposed in Ref. [50].

These approaches are conceptually different from the solution we adopt in the present article. We consider an exact solution of the Einstein field equations with strong density fluctuations, but which keeps a well-defined FL averaged behavior. Such conditions are satisfied by the Swiss-cheese model [51]: one starts with a spatially homogeneous and isotropic FL geometry, and then cuts out spherical vacuoles in which individual masses are embedded. Thus, the masses are contained in vacua within a spatially homogeneous fluid-filled cosmos (see bottom panel of Fig. 2). By construction, this exact solution is free from any backreaction: its cosmic dynamics is identical to the one of the underlying FL spacetime.

From the kinematical point of view, Swiss-cheese models allow us to go further than perturbation theory, because not only the density of matter exhibits finite fluctuations, but also the metric itself. Hence, light propagation is expected to be very different in a Swiss-cheese universe compared to its underlying FL model. Moreover, the inhomogeneities of a Swiss cheese are introduced in a way that addresses the so-called "Ricci-Weyl problem." Indeed, the standard FL geometry is characterized by a vanishing Weyl tensor and a nonzero Ricci tensor, while in reality light mostly travels in vacuum, where conversely the Ricci tensor vanishes—apart from the contribution of Λ, which does not focus light—and the Weyl tensor is nonzero (see Fig. 1). A Swiss-cheese model is closer to the latter situation, because the Ricci tensor is zero inside the holes (see Fig. 2). It is therefore hoped to capture the relevant optical properties of the Universe.

In fact, neither a Friedmann-Lemaître model nor a Swiss-cheese model can be considered a realistic descrip-

tion of the Universe. They share the property of being exact solutions of the Einstein equations which satisfy the Copernican principle, either strictly or statistically. Swiss-cheese models can be characterized by an extra-cosmological parameter describing the smoothness of their distribution of matter. Thus, a FL spacetime is nothing but a perfectly smooth Swiss cheese. It is legitimate to investigate to which extent observations can constrain the smoothness cosmological parameter, and therefore to quantify how close to a FL model the actual Universe is.
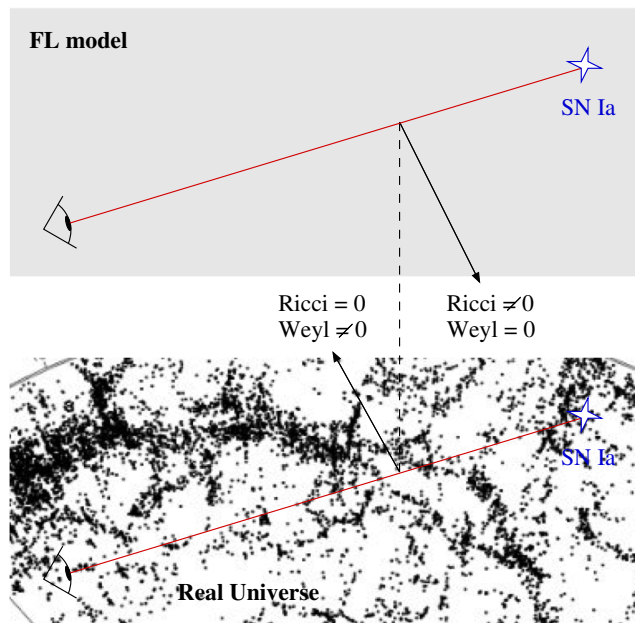

FIG. 1. The standard interpretation of SNe data assumes that light propagates in purely homogeneous and isotropic space (top). However, thin light beams are expected to probe the inhomogeneous nature of the actual Universe (bottom) down to a scale where the continuous limit is no longer valid.

The propagation of light in a Swiss-cheese universe was first investigated by Kantowski [52], and later by Dyer and Roeder [53]. Both concluded that the effect, on the Hubble diagram, of introducing "clumps" of matter was to lower the apparent deceleration parameter. The issue was revived within the backreaction and averaging debates, and the Swiss-cheese models have been extended to allow for more generic distributions of matter inside the holes—instead of just concentrating it at the center—where spacetime geometry is described by the Lemaître-Tolman-Bondi (LTB) solution. The optical properties of such models have been extensively studied (see Refs. [54–62]) to finally conclude that the average luminosity-redshift relation remains unchanged with respect to the purely homogeneous case, contrary to the early results of Refs. [52, 53].

In general, the relevance of "LTB holes" in Swiss-cheese models is justified by the fact that they allow one to reproduce the actual large-scale structure of the Universe (with voids and walls). However, though inhomoge-

FL model

SN Ia

Ricci = 0   Ricci ≠ 0
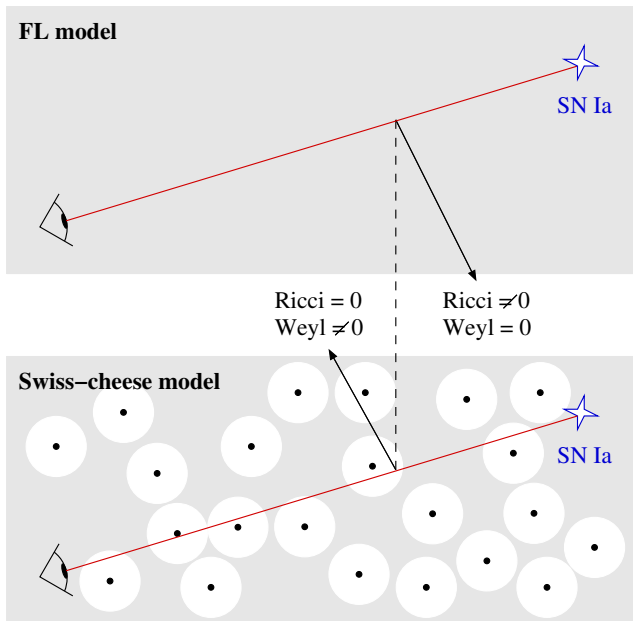Weyl ≠ 0   Weyl = 0

Swiss−cheese model

SN Ia

FIG. 2. Swiss-cheese models (bottom) allow us to model inhomogeneities beyond the continuous limit, while keeping the same dynamics and average properties as the FL model (top).

neous, the distribution of matter in this class of models remains continuous at all scales. On the contrary, the old-fashioned approach with "clumps" of matter inside the holes *breaks the continuous limit*. Hence, it seems more relevant for describing the small-scale structure probed by thin light beams.

In this article, we revisit and update the studies of Refs. [52, 53] within the paradigm of modern cosmology. For that purpose, we first provide a comprehensive study of light propagation in the same class of Swiss-cheese models, including the cosmological constant. By generating mock Hubble diagrams, we then show that the inhomogeneities induce a significant bias in the apparent luminosity-redshift relation, which affects the determination of the cosmological parameters. As we shall see, the effect increases with the fraction of clustered matter but decreases with Λ. For a universe apparently dominated by dark energy, the difference turns out to be small.

The article is organized as follows. Section II describes the construction and mathematical properties of the Swiss-cheese model. In Sec. III, we summarize the laws of light propagation, and introduce a new tool to deal with a patchwork of spacetimes, based on matrix multiplications. In Sec. IV, we apply the laws introduced in Sec. III to Swiss-cheese models and solve the associated equations. The results enable us to investigate the effect of one hole (Sec. V) and of many holes (Sec. VI) on cosmological observables, namely the redshift and the luminosity distance. Finally, the consequences on the determination of the cosmological parameters are presented in Sec. VII.

II. DESCRIPTION OF THE SWISS-CHEESE COSMOLOGICAL MODEL

The construction of Swiss-cheese models is based on the Einstein-Straus method [51] for embedding a point-mass within a homogeneous spacetime (the "cheese"). It consists in cutting off a spherical domain of the cheese and concentrating the matter it contained at the center of the hole. This section presents the spacetime geometries inside and outside a hole (Subsec. II A), and how they are glued together (Subsec. II B).

A. Spacetime patches

1. The "cheese"—Friedmann-Lemaître geometry

Outside the hole, the geometry is described by the standard Friedmann-Lemaître (FL) metric

$$ds^2 = -dT^2 + a^2(T)\left[d\chi^2 + f_K^2(\chi)\,d\Omega^2\right], \qquad (2.1)$$

where a is the scale factor and T is the cosmic time. The function $f_K(\chi)$ depends on the sign of K and thus of the spatial geometry (spherical, Euclidean or hyperbolic),

$$f_K(\chi) = \frac{\sin\sqrt{K}\chi}{\sqrt{K}}, \quad \chi \quad \text{or} \quad \frac{\sinh\sqrt{-K}\chi}{\sqrt{-K}} \qquad (2.2)$$

respectively for $K > 0$, $K = 0$ or $K < 0$. The Einstein field equations imply that the scale factor $a(T)$ satisfies the Friedmann equation

$$H^2 = \frac{8\pi G}{3}\rho - \frac{K}{a^2} + \frac{\Lambda}{3}, \quad \text{with} \quad H \equiv \frac{1}{a}\frac{da}{dT}, \qquad (2.3)$$

and where $\rho = \rho_0 (a_0/a)^3$ is the energy density of a pressureless fluid. A subscript 0 indicates that the quantity is evaluated today. It is convenient to introduce the cosmological parameters

$$\Omega_m = \frac{8\pi G\rho_0}{3H_0^2}, \quad \Omega_K = -\frac{K}{a_0^2 H_0^2}, \quad \Omega_\Lambda = \frac{\Lambda}{3H_0^2}, \quad (2.4)$$

in terms of which the Friedmann equation takes the form

$$\left(\frac{H}{H_0}\right)^2 = \Omega_m\left(\frac{a_0}{a}\right)^3 + \Omega_K\left(\frac{a_0}{a}\right)^2 + \Omega_\Lambda. \qquad (2.5)$$

2. The "hole"—Kottler geometry

Inside the hole, the geometry is described by the extension of the Schwarzschild metric to the case of a nonzero cosmological constant, known as the Kottler solution [63, 64] (see e.g. Ref. [65] for a review). In spherical coordinates (r, θ, φ), it reads

$$ds^2 = -A(r)\,dt^2 + A^{-1}(r)\,dr^2 + r^2 d\Omega^2, \qquad (2.6)$$

$$\text{with} \quad A(r) \equiv 1 - \frac{r_S}{r} - \frac{\Lambda r^2}{3}, \qquad (2.7)$$

and where $r_{\rm S} \equiv 2\,GM$ is the Schwarzschild radius associated with the mass M at the center of the hole. It is easy to check that the above metric describes a static spacetime. The corresponding Killing vector $\xi^\mu = \delta_0^\mu$ has norm $g_{\mu\nu}\xi^\mu\xi^\nu = A(r)$ and is therefore timelike as long as $A > 0$. Hence, there are two cases:

1. If $9(GM)^2\Lambda > 1$, then $A(r) < 0$ for all $r > 0$, so that ξ^μ is spacelike. In this case, the Kottler spacetime contains no static region but it is spatially homogeneous.

2. If $9(GM)^2\Lambda < 1$, then $A(r) > 0$ for r between $r_{\rm b}$ and $r_{\rm c} > r_{\rm b}$ which are the two positive roots of the polynomial $rA(r)$, and correspond respectively to the black hole and cosmological horizons. We have

$$r_{\rm c} = \frac{2}{\sqrt{\Lambda}}\cos\left(\frac{\psi}{3} + \frac{\pi}{3}\right), \qquad (2.8)$$

$$r_{\rm b} = \frac{2}{\sqrt{\Lambda}}\cos\left(\frac{\psi}{3} - \frac{\pi}{3}\right), \qquad (2.9)$$

with $\cos\psi = 3\,GM\sqrt{\Lambda}$, so that

$$r_{\rm S} < r_{\rm b} < \frac{3}{2}\,r_{\rm S} < \frac{1}{\sqrt{\Lambda}} < r_{\rm c} < \frac{3}{\sqrt{\Lambda}}. \qquad (2.10)$$

In the region $r_{\rm b} < r < r_{\rm c}$, the Kottler spacetime is static. Note also that $r = r_{\rm b}$ and $r = r_{\rm c}$ are Killing horizons, since ξ vanishes on these hypersurfaces.

In practice, we use the Kottler solution to describe the vicinity of a gravitationally bound object, such as a galaxy, or a cluster of galaxies. In this context, we have typically $9(GM)^2\Lambda < 10^{-14}$ (see Subsec. V A), so we are in the second case. Moreover, this solution only describes the exterior region of the central object; it is thus valid only for $r > r_{\rm phys}$, where $r_{\rm phys}$ is the physical size of the object. For the cases we are interested in, $r_{\rm phys} \gg r_{\rm b}$, so that there is actually no black-hole horizon.

B. Junction conditions

Any spacetime obtained by gluing together two different geometries, via a hypersurface Σ, is well defined if—and only if—it satisfies the Israel junction conditions [66, 67]: both geometries must induce (a) the same 3-metric, and (b) the same extrinsic curvature on Σ.

The junction hypersurface Σ is the world sheet of a comoving 2-sphere, as imposed by the symmetry of the problem. Hence, it is defined by $\chi = \chi_{\rm h} = {\rm cst}$ in FL coordinates, and by $r = r_{\rm h}(t)$ in Kottler coordinates. Both points of view are depicted in Fig. 3.

In the FL region, the normal vector to the hypersurface is given by $n_\mu^{\rm (FL)} = \delta_\mu^\chi/a$. The 3-metric and the extrinsic curvature induced by the FL geometry are respectively

$$ds_\Sigma^2 = -dT^2 + a^2(T)f_K^2(\chi_{\rm h})\,d\Omega^2, \qquad (2.11)$$

$$K_{ab}^{\rm (FL)}dx^a dx^b = a(T)f_K(\chi_{\rm h})f_K'(\chi_{\rm h})\,d\Omega^2. \qquad (2.12)$$
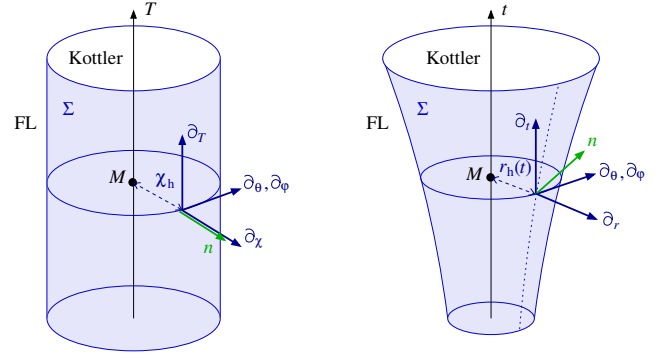

FIG. 3. The junction hypersurface as seen from the FL point of view with equation $\chi = \chi_{\rm h}$ (left); and from the Kottler point of view with equation $r = r_{\rm h}(t)$ (right).

where $(x^a) = (T, \theta, \varphi)$ are natural intrinsic coordinates for Σ. We stress carefully that, in the following and as long as there is no ambiguity, a dot can denote a time derivative with respect to T or t, so that $\dot{a} = da/dT$ and $\dot{r}_{\rm h} = dr_{\rm h}/dt$, while a prime can denote a derivative with respect to χ or r, so that $f_K' = df_K/d\chi$ and $A' = dA/dr$.

The 3-metric induced on Σ by the Kottler geometry is

$$ds^2 = -\kappa^2(t)\,dt^2 + r_{\rm h}^2(t)\,d\Omega^2, \qquad (2.13)$$

where

$$\kappa(t) \equiv \sqrt{\frac{A^2[r_{\rm h}(t)] - \dot{r}_{\rm h}^2(t)}{A[r_{\rm h}(t)]}}. \qquad (2.14)$$

Therefore, the first junction condition implies

$$r_{\rm h}(t) = a(T)f_K(\chi_{\rm h}), \qquad (2.15)$$

$$\frac{dT}{dt} = \kappa(t), \qquad (2.16)$$

which govern the dynamics of the hole boundary, and relate the time coordinates of the FL and Kottler regions.

The extrinsic curvature of Σ induced by the Kottler geometry, but expressed in (x^a) coordinates, reads

$$K_{ab}^{\rm (K)}dx^a dx^b = -\frac{\ddot{r}_{\rm h} + A'(r_{\rm h})\left[3\kappa^2/2 - A(r_{\rm h})\right]}{\kappa^3}\,dT^2 + \frac{r_{\rm h}A(r_{\rm h})}{\kappa}\,d\Omega^2. \qquad (2.17)$$

Hence, the second junction condition is satisfied only if

$$\kappa = \frac{A(r_{\rm h})}{f_K'(\chi_{\rm h})}, \qquad \text{whence} \qquad \frac{dT}{dt} = \frac{A[a(T)f_K(\chi_{\rm h})]}{f_K'(\chi_{\rm h})}. \qquad (2.18)$$

It is straightforward to show that Eq. (2.18), together with the Friedmann equation (2.3), imply that the Kottler and FL regions have the same cosmological constant, and

$$M = \frac{4\pi}{3}\rho\,a^3 f_K^3(\chi_{\rm h}). \qquad (2.19)$$

C. Summary

Given a FL spacetime with pressureless matter and a cosmological constant, $a(T)$ is completely determined from the Friedmann equation. A spherical hole of comoving radius χ_{h}, which contains a constant mass $M = 4\pi\rho a^3 f_K^3(\chi_{\mathrm{h}})/3$ at its center, and whose geometry is described by the Kottler metric, can then be inserted anywhere. The resulting spacetime geometry is an exact solution of the Einstein field equations.

By construction, the clump inside the hole does not backreact on the surrounding FL region. It follows that many such holes can be inserted, as long as they do not overlap. Note that if two holes do not overlap initially, then they will never do so, despite the expansion of the universe, because their boundaries are comoving.

III. PROPAGATION OF LIGHT

A. Light rays

The past light cone of a given observer is a constant phase hypersurface $w = \mathrm{const}$. Its normal vector $k_\mu \equiv \partial_\mu w$ (the wave four-vector) is a null vector satisfying the geodesic equation, and whose integral curves (light rays) are irrotational:

$$k^\mu k_\mu = 0, \quad k^\nu \nabla_\nu k_\mu = 0, \quad \nabla_{[\mu} k_{\nu]} = 0. \qquad (3.1)$$

For an emitter and an observer with respective four-velocities u_{em}^μ and u_{obs}^μ, we define the redshift by

$$1 + z = \frac{u_{\mathrm{em}}^\mu k_\mu(v_{\mathrm{em}})}{u_{\mathrm{obs}}^\mu k_\mu(0)}, \qquad (3.2)$$

where v is an affine parameter along the geodesic, so that $k^\mu = \mathrm{d}x^\mu/\mathrm{d}v$, and $v = 0$ at the observation event. The wave four-vector can always be decomposed into temporal and spatial components,

$$k^\mu = (1+z)(u^\mu - d^\mu), \quad d^\mu u_\mu = 0, \quad d^\mu d_\mu = 1, \quad (3.3)$$

where d^μ denotes the spatial direction of observation. In Eq. (3.3), we have chosen an affine parameter adapted to the observer, in the sense that $2\pi\nu_0 = u_{\mathrm{obs}}^\mu k_\mu(0) = 1$. This convention is used in all the remainder of the article.

B. Light beams

1. Geodesic deviation equation

A light beam is a collection of light rays, that is, a bundle of null geodesics $\{x^\mu(v,\gamma)\}$, where γ labels the curves and v is the affine parameter along them. The relative behavior of two neighboring geodesics $x^\mu(\cdot,\gamma)$ and $x^\mu(\cdot,\gamma+\mathrm{d}\gamma)$ is described by their separation vector

$\xi^\mu \equiv \mathrm{d}x^\mu/\mathrm{d}\gamma$. Hence, this vector encodes the whole information on the size and shape of the bundle.

Having chosen $v = 0$ at the observation event—which is a vertex point of the bundle—ensures that the separation vector field is everywhere orthogonal to the geodesics, $k^\mu\xi_\mu = 0$. In such conditions, the evolution of ξ^μ with v is governed by the geodesic deviation equation

$$k^\alpha k^\beta \nabla_\alpha \nabla_\beta \xi^\mu = R^\mu{}_{\nu\alpha\beta} k^\nu k^\alpha \xi^\beta, \qquad (3.4)$$

where $R^\mu{}_{\nu\alpha\beta}$ is the Riemann tensor.

2. Sachs equation

Consider an observer with four-velocity u^μ. In view of relating ξ^μ to observable quantities, we introduce the Sachs basis $(s_A^\mu)_{A\in\{1,2\}}$, defined as an orthonormal basis of the plane orthogonal to both u^μ and k^μ,

$$s_A^\mu s_{B\mu} = \delta_{AB}, \quad s_A^\mu u_\mu = s_A^\mu k_\mu = 0, \qquad (3.5)$$

and parallel-transported along the geodesic bundle,

$$k^\nu \nabla_\nu s_A^\mu = 0. \qquad (3.6)$$

The plane spanned by (s_1, s_2) can be considered a screen on which the observer projects the light beam. The two-vector of components $\xi_A = \xi_\mu s_A^\mu$ then represents the relative position, on the screen, of the light spots corresponding to two neighboring rays separated by ξ^μ.

The evolution of ξ_A, with light propagation, is determined by projecting the geodesic deviation equation (3.4) on the Sachs basis. The result is known as the Sachs equation [1, 68, 69], and reads

$$\frac{\mathrm{d}^2\xi_A}{\mathrm{d}v^2} = \mathcal{R}_{AB}\,\xi^B, \qquad (3.7)$$

where $\mathcal{R}_{AB} = R_{\mu\nu\alpha\beta} k^\nu k^\alpha s_A^\mu s_B^\beta$ is the screen-projected Riemann tensor, called optical tidal matrix. It is conveniently decomposed into a Ricci term and a Weyl term as

$$(\mathcal{R}_{AB}) = \begin{pmatrix} \Phi_{00} & 0 \\ 0 & \Phi_{00} \end{pmatrix} + \begin{pmatrix} -\mathrm{Re}\,\Psi_0 & \mathrm{Im}\,\Psi_0 \\ \mathrm{Im}\,\Psi_0 & \mathrm{Re}\,\Psi_0 \end{pmatrix} \qquad (3.8)$$

with

$$\Phi_{00} \equiv -\frac{1}{2} R_{\mu\nu} k^\mu k^\nu, \quad \Psi_0 \equiv -\frac{1}{2} C_{\mu\nu\alpha\beta}\,\sigma^\mu k^\nu k^\alpha \sigma^\beta, \quad (3.9)$$

and where $\sigma^\mu \equiv s_1^\mu - \mathrm{i}\,s_2^\mu$.

3. Notions of distance

Since the light beam converges at the observation event, we have $\xi^A(v = 0) = 0$. The linearity of the Sachs equation then implies the existence of a 2×2 matrix $\mathcal{D}^A{}_B$, called Jacobi matrix, such that

$$\xi^A(v) = \mathcal{D}^A{}_B(v) \left(\frac{\mathrm{d}\xi^B}{\mathrm{d}v}\right)_{v=0}. \qquad (3.10)$$

From Eq. (3.7), we immediately deduce that this matrix satisfies the Jacobi matrix equation

$$\frac{\mathrm{d}^2}{\mathrm{d}v^2}\mathcal{D}^A{}_B = \mathcal{R}^A{}_C\,\mathcal{D}^C{}_B, \qquad (3.11)$$

with initial conditions

$$\mathcal{D}^A{}_B(0) = 0, \qquad \frac{\mathrm{d}\mathcal{D}^A{}_B}{\mathrm{d}v}(0) = \delta^A_B. \qquad (3.12)$$

We shall also use the short-hand notation $\boldsymbol{\xi} = (\xi^A)$ and $\boldsymbol{\mathcal{D}} = (\mathcal{D}^A{}_B)$ so that Eq. (3.11) reads $\mathrm{d}^2\boldsymbol{\mathcal{D}}/\mathrm{d}v^2 = \boldsymbol{\mathcal{R}}\cdot\boldsymbol{\mathcal{D}}$, with $\boldsymbol{\mathcal{D}}(0) = 0$ and $\dot{\boldsymbol{\mathcal{D}}}(0) = \mathbf{1}$.

Since the Jacobi matrix relates the shape of a light beam to its "initial" aperture, it is naturally related to the various notions of distance used in astronomy and cosmology. The *angular distance* D_A is defined by comparing the emission cross-sectional area $\mathrm{d}^2S_\mathrm{source}$ of a source to the solid angle $\mathrm{d}\Omega^2_\mathrm{obs}$ under which it is observed,

$$\mathrm{d}^2S_\mathrm{source} = D_\mathrm{A}^2\,\mathrm{d}\Omega^2_\mathrm{obs}. \qquad (3.13)$$

It is related to the Jacobi matrix by

$$D_\mathrm{A} = \sqrt{|\det\boldsymbol{\mathcal{D}}(v_\mathrm{source})|}, \qquad (3.14)$$

where v_source is the affine parameter at emission.

The *luminosity distance* D_L is defined from the ratio between the observed flux F_obs and the intrinsic luminosity L_source of the source, so that

$$L_\mathrm{source} = 4\pi D_\mathrm{L}^2\,F_\mathrm{obs}. \qquad (3.15)$$

It is related to the angular distance by the following distance duality law

$$D_\mathrm{L} = (1+z)^2 D_\mathrm{A}. \qquad (3.16)$$

Hence, the theoretical determination of the luminosity distance relies on the computation of the Jacobi matrix.

C. Solving the Sachs equation piecewise

Since we work in a Swiss-cheese universe, we have to compute the Jacobi matrix for a patchwork of spacetimes. It is tempting, in this context, to calculate the Jacobi matrix for each patch independently, and then try to reconnect them. In fact, such an operation is unnatural, because the very definition of $\boldsymbol{\mathcal{D}}$ imposes that the initial condition is a vertex point of the light beam. Thus, juxtaposing two Jacobi matrices is only possible at a vertex point, which is of course too restrictive for us.

We can solve this problem by extending the Jacobi matrix formalism into a richer structure. This requires us to consider the general solution of Eq. (3.7), for arbitrary initial conditions. Thus, we have

$$\boldsymbol{\xi}(v) = \boldsymbol{\mathcal{C}}(v;v_\mathrm{init})\cdot\boldsymbol{\xi}_{v=v_\mathrm{init}} + \boldsymbol{\mathcal{D}}(v;v_\mathrm{init})\cdot\left.\frac{\mathrm{d}\boldsymbol{\xi}}{\mathrm{d}v}\right|_{v=v_\mathrm{init}} , \quad (3.17)$$

as for any linear second order differential equation, solved from v_init to v. In the following, $\boldsymbol{\mathcal{C}}(v;v_\mathrm{init})$ is referred to as the *scale matrix*. It is easy to check that both the scale and Jacobi matrices satisfy the Jacobi matrix equation (3.11) but with different initial conditions:

$$\boldsymbol{\mathcal{D}}(v_\mathrm{init};v_\mathrm{init}) = \mathbf{0}, \qquad \frac{\mathrm{d}\boldsymbol{\mathcal{D}}}{\mathrm{d}v}(v_\mathrm{init};v_\mathrm{init}) = \mathbf{1}, \quad (3.18)$$

whereas

$$\boldsymbol{\mathcal{C}}(v_\mathrm{init};v_\mathrm{init}) = \mathbf{1}, \qquad \frac{\mathrm{d}\boldsymbol{\mathcal{C}}}{\mathrm{d}v}(v_\mathrm{init};v_\mathrm{init}) = \mathbf{0}. \quad (3.19)$$

The most useful object for our problem turns out to be the 4×4 *Wronski matrix* constructed from $\boldsymbol{\mathcal{C}}$ and $\boldsymbol{\mathcal{D}}$,

$$\boldsymbol{\mathcal{W}}(v;v_\mathrm{init}) \equiv \begin{pmatrix} \boldsymbol{\mathcal{C}}(v;v_\mathrm{init}) & \boldsymbol{\mathcal{D}}(v;v_\mathrm{init}) \\ \frac{\mathrm{d}\boldsymbol{\mathcal{C}}}{\mathrm{d}v}(v;v_\mathrm{init}) & \frac{\mathrm{d}\boldsymbol{\mathcal{D}}}{\mathrm{d}v}(v;v_\mathrm{init}) \end{pmatrix}, \quad (3.20)$$

in terms of which the general solution (3.17) reads

$$\begin{pmatrix} \boldsymbol{\xi} \\ \frac{\mathrm{d}\boldsymbol{\xi}}{\mathrm{d}v} \end{pmatrix}(v) = \boldsymbol{\mathcal{W}}(v;v_\mathrm{init})\cdot\begin{pmatrix} \boldsymbol{\xi} \\ \frac{\mathrm{d}\boldsymbol{\xi}}{\mathrm{d}v} \end{pmatrix}(v_\mathrm{init}). \quad (3.21)$$

It is clear, from Eq. (3.21), that $\boldsymbol{\mathcal{W}}$ satisfies the relation

$$\boldsymbol{\mathcal{W}}(v_1;v_3) = \boldsymbol{\mathcal{W}}(v_1;v_2)\cdot\boldsymbol{\mathcal{W}}(v_2;v_3). \qquad (3.22)$$

Hence, the general solution of the Sachs equation in a Swiss-cheese universe can be obtained by multiplying Wronski matrices, according to

$$\boldsymbol{\mathcal{W}}(v_\mathrm{source};0) = \boldsymbol{\mathcal{W}}_\mathrm{FL}(v_\mathrm{source};v_\mathrm{in}^{(1)})\cdot\boldsymbol{\mathcal{W}}_\mathrm{K}(v_\mathrm{in}^{(1)};v_\mathrm{out}^{(1)})$$
$$\cdot\,\boldsymbol{\mathcal{W}}_\mathrm{FL}(v_\mathrm{out}^{(1)};v_\mathrm{in}^{(2)})\cdots\boldsymbol{\mathcal{W}}_\mathrm{FL}(v_\mathrm{out}^{(N)};0) \quad (3.23)$$

where $\boldsymbol{\mathcal{W}}_\mathrm{FL}$ and $\boldsymbol{\mathcal{W}}_\mathrm{K}$ are the Wronski matrices computed respectively in the FL region and in the Kottler holes; $v_\mathrm{in}^{(i)}$ and $v_\mathrm{out}^{(i)}$ are the values of the affine parameter respectively at the entrance and the exit of the ith hole.

IV. INTEGRATION OF THE GEODESIC AND SACHS EQUATIONS

Consider an observer lying within a FL region, who receives a photon after the latter has crossed a hole. In this section, we determine the light path from entrance to observation by solving the geodesic equation, and we calculate the Wronski matrix for the Sachs equation.

The main geometrical quantities are summarized in Fig. 4. d^μ is the direction of observation as defined in Eq. (3.3). The spatial sections of the FL region can be described either by comoving spherical coordinates (χ,θ,φ) or, when the spatial sections are Euclidean, by comoving Cartesian coordinates (X,Y,Z).
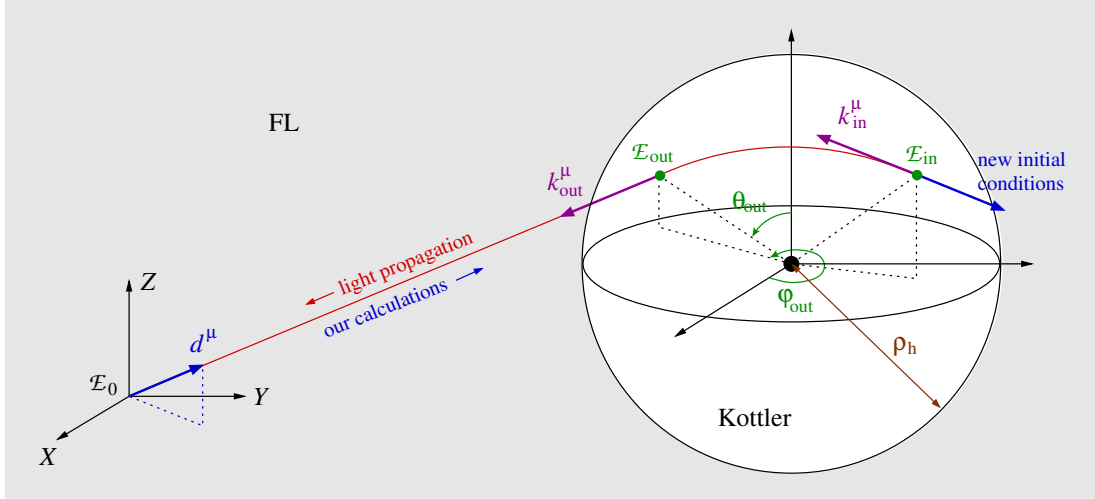
FIG. 4. A light ray propagates alternatively in FL and Kottler regions. The main geometrical quantities defined and used in Sec. IV are depicted in this simplified view of a single hole.

The hole is characterized by its comoving spatial position X_{h}^i, in terms of the FL coordinates, and its mass M, or equivalently its comoving radius ρ_{h}. Note that, contrary to Subsec. II A, it is no longer denoted χ_{h}, in order to avoid confusion with the radial comoving coordinate of the center of the hole.

A photon enters into the hole with wave vector k_{in}^μ, exits from it with wave vector k_{out}^μ, and reaches the observer with wave vector k_0^μ. We respectively denote $\mathcal{E}_{\mathrm{in}}$, $\mathcal{E}_{\mathrm{out}}$ and $\mathcal{E}_0$ the associated events. The coordinates of the first two can be expressed either with respect to FL, e.g. as $(T_{\mathrm{in}}, X_{\mathrm{in}}^i)$ in Cartesian coordinates, or with respect to the hole, e.g. as $(t_{\mathrm{in}}, r_{\mathrm{in}}, \theta_{\mathrm{in}}, \varphi_{\mathrm{in}})$ in the Kottler spherical coordinate system.

Our calculations go backward in time. Starting from $\mathcal{E}_0$, we first determine $\mathcal{E}_{\mathrm{out}}$, $\boldsymbol{\mathcal{W}}_{\mathrm{FL}}(v_{\mathrm{out}}; v_{\mathrm{obs}})$, and second $\mathcal{E}_{\mathrm{in}}$, $\boldsymbol{\mathcal{W}}_{\mathrm{K}}(v_{\mathrm{in}}; v_{\mathrm{out}})$. The same operations can then be repeated starting from $\mathcal{E}_{\mathrm{in}}$ and so on.

A. Friedmann-Lemaître region *(from $\mathcal{E}_0$ to $\mathcal{E}_{\mathrm{out}}$)*

The geometry of the Friedmann-Lemaître region is given by the metric (2.1) which can be rewritten in terms of the conformal time η, defined by $\mathrm{d}\eta = \mathrm{d}T/a(T)$, as

$$\mathrm{d}s^2 = a^2(\eta) \left[-\mathrm{d}\eta^2 + \mathrm{d}\chi^2 + f_K^2(\chi)\,\mathrm{d}\Omega^2 \right]. \qquad (4.1)$$

1. Geodesic equation

If one chooses the center $\chi = 0$ of the FL spherical coordinate system on the worldline of the (comoving) observer, then the geodesic equation is easily solved as

$$\chi(\eta) = \eta_0 - \eta, \quad \theta = \theta_0, \quad \varphi = \varphi_0, \qquad (4.2)$$

which corresponds to a purely radial trajectory. Note however that for a generic origin, this is no longer true. The associated wave vector remains collinear to the observed one, k_0^μ. It is only subject to a redshift induced by the cosmic expansion, so that

$$k^\mu = \left(\frac{a_0}{a} \right)^2 k_0^\mu. \qquad (4.3)$$

We stress that, in Eq. (4.3), $\mu = 0$ refers to components on ∂_η, not on $\partial_T = \partial_\eta/a$.

2. Intersection with the hole

Once the geodesic equation has been solved and the position of the hole has been chosen, we can calculate the intersection $\mathcal{E}_{\mathrm{out}}$ between the light ray and the hole boundary. *In the particular case of a spatially Euclidean FL solution ($K = 0$), the Cartesian coordinates X_{out}^i of $\mathcal{E}_{\mathrm{out}}$ satisfy the simple system of equations*

$$\begin{cases} \delta_{ij} \left(X_{\mathrm{out}}^i - X_{\mathrm{h}}^i \right) \left(X_{\mathrm{out}}^j - X_{\mathrm{h}}^j \right) = \rho_{\mathrm{h}}^2, \\ X_{\mathrm{out}}^i = X_0^i + (\eta_0 - \eta_{\mathrm{out}})\, d^i \end{cases} \qquad (4.4)$$

where X_{h}^i and X_0^i are the respective Cartesian coordinates of the hole and the observer, while d^i is the spatial direction of observation. Although conceptually similar, the determination of $\mathcal{E}_{\mathrm{out}}$ for a FL solution with arbitrary spatial curvature is technically harder.

In general, we deduce from Eq. (4.3) that the wave vector at $\mathcal{E}_{\mathrm{out}}$ is $k_{\mathrm{out}}^\mu = (a_0/a_{\mathrm{out}})^2 k_0^\mu$, where $a_{\mathrm{out}} \equiv a(\eta_{\mathrm{out}})$.

3. Wronski matrix

In the FL region, the Sachs basis (s_1, s_2) is defined with respect to the fundamental observers, comoving with four-velocity $u = \partial_T$. The explicit form of this basis does not need to be specified here.

The Sachs equation can be solved analytically by means of a conformal transformation to the static metric

$$\mathrm{d}\tilde{s}^2 = a_0^2 \left[-\mathrm{d}\eta^2 + \mathrm{d}\chi^2 + f_K^2(\chi)\mathrm{d}\Omega^2 \right] \equiv \tilde{g}_{\mu\nu}\mathrm{d}x^\mu\mathrm{d}x^\nu. \tag{4.5}$$

Because the geometries associated with $g_{\mu\nu}$ and $\tilde{g}_{\mu\nu}$ are conformal, any null geodesic for $g_{\mu\nu}$ affinely parametrized by v is also a null geodesic for $\tilde{g}_{\mu\nu}$ affinely parametrized by $\tilde{v}$, with $a^2\mathrm{d}\tilde{v} = a_0^2\mathrm{d}v$. As $\mathrm{d}v = (a^2/a_0)\mathrm{d}\eta$, it follows that $\tilde{v} = a_0\eta$.

For the static geometry, the optical tidal matrix reads $\widetilde{\mathcal{R}} = -(K/a_0^2)\mathbf{1}$, so that the Sachs equation is simply

$$\frac{\mathrm{d}^2\tilde{\boldsymbol{\xi}}}{\mathrm{d}\eta^2} = -K\,\tilde{\boldsymbol{\xi}}. \tag{4.6}$$

We then easily obtain the Jacobi and scale matrices:

$$\widetilde{\mathcal{D}} = a_0 f_K(\eta - \eta_{\mathrm{init}})\mathbf{1}, \qquad \widetilde{\mathcal{C}} = f_K'(\eta - \eta_{\mathrm{init}})\mathbf{1}. \tag{4.7}$$

To go back to the original FL spacetime, we use that $\mathrm{d}v = a^2\mathrm{d}\eta$ and the fact that the screen projections of the separation vectors for both geometries are related by $a\tilde{\boldsymbol{\xi}} = a_0\boldsymbol{\xi}$. The final result is

$$\mathcal{D}_{\mathrm{FL}} = a_{\mathrm{init}}\,\frac{a}{a_0}f_K(\eta - \eta_{\mathrm{init}})\mathbf{1}, \tag{4.8}$$

$$\mathcal{C}_{\mathrm{FL}} = \frac{a}{a_{\mathrm{init}}}\left[f_K'(\eta - \eta_{\mathrm{init}}) - \mathcal{H}_{\mathrm{init}}f_K(\eta - \eta_{\mathrm{init}}) \right]\mathbf{1}, \tag{4.9}$$

where $\mathcal{H} \equiv a'(\eta)/a(\eta)$ is the conformal Hubble function. This completely determines $\boldsymbol{\mathcal{W}}_{\mathrm{FL}}$.

Note that we can recover the standard expression of the angular distance by taking the initial condition at the observer. The relation (3.14) then implies

$$D_{\mathrm{A}} = \sqrt{\det \mathcal{D}_{\mathrm{FL}}} = \frac{a_0}{(1+z)}\,f_K(\eta_{\mathrm{source}}), \tag{4.10}$$

where $z = a_0/a - 1$ is the redshift of a photon that only travels through a FL region.

B. Kottler region *(from $\mathcal{E}_{\mathrm{out}}$ to $\mathcal{E}_{\mathrm{in}}$)*

1. Initial condition at $\mathcal{E}_{\mathrm{out}}$

In the previous section, we have determined $\mathcal{E}_{\mathrm{out}}$ and k_{out}^μ in terms of the FL coordinate system. However, in order to proceed inside the hole, we need to express them in terms of the Kottler coordinate system (t, r, θ, φ).

A preliminary task consists in expressing $\mathcal{E}_{\mathrm{out}}$ and k_{out}^μ in terms of FL spherical coordinates, with origin at the center of the hole. This operation is straightforward. The event $\mathcal{E}_{\mathrm{out}}$ is then easily converted, since (a) we are free to set $t_{\mathrm{out}} = 0$, (b) Eq. (2.15) implies $r_{\mathrm{out}} = a(\eta_{\mathrm{out}})\rho_{\mathrm{h}}$, and (c) the angular coordinates $\theta_{\mathrm{out}}, \varphi_{\mathrm{out}}$ remain unchanged if the Kottler axes are chosen parallel to the FL ones.

The first junction condition ensures that light is not deflected when it crosses the boundary Σ of the hole. Indeed, the continuity of the metric implies that the connection does not diverge on Σ. Integrating the geodesic equation $\mathrm{d}k^\mu = -\Gamma_{\alpha\beta}^\mu k^\alpha k^\beta \mathrm{d}v$ between v_{out}^- and v_{out}^+ then shows that k^μ is continuous at $\mathcal{E}_{\mathrm{out}}$. Therefore, we just need to convert its components from the FL coordinate system to the Kottler one. The result is

$$k_{\mathrm{out}}^t = \frac{a_{\mathrm{out}}}{A(r_{\mathrm{out}})}\left[k_{\mathrm{out}}^\eta + \sqrt{1 - A(r_{\mathrm{out}})}k_{\mathrm{out}}^\chi \right] \tag{4.11}$$

$$k_{\mathrm{out}}^r = a_{\mathrm{out}}\left[\sqrt{1 - A(r_{\mathrm{out}})}k_{\mathrm{out}}^\eta + k_{\mathrm{out}}^\chi \right] \tag{4.12}$$

$$k_{\mathrm{out}}^\theta = k_{\mathrm{out}}^\theta \tag{4.13}$$

$$k_{\mathrm{out}}^\varphi = k_{\mathrm{out}}^\varphi. \tag{4.14}$$

2. Shifting to the equatorial plane

Since the Kottler spacetime is spherically symmetric, it is easier to integrate the geodesic equation in the equatorial plane $\theta = \pi/2$. In general, however, we must perform rotations to bring both $\mathcal{E}_{\mathrm{out}}$ and k_{out} into this plane.

Starting from arbitrary initial conditions $(\mathcal{E}_{\mathrm{out}}, k_{\mathrm{out}}^\mu)$, we can shift to the equatorial plane in two steps. In the following, $\boldsymbol{R}_i(\vartheta)$ denotes the rotation of angle ϑ about the x^i-axis. The operations are depicted in Fig. 5.

- First, bring $\mathcal{E}_{\mathrm{out}}$ to the point $\mathcal{E}_{\mathrm{out,eq}}$ on the equatorial plane by the action of two successive rotations, $\boldsymbol{R}_z(-\varphi_{\mathrm{out}})$ followed by $\boldsymbol{R}_y(\pi/2 - \theta_{\mathrm{out}})$. The wave vector after the two rotations is denoted $k_{\mathrm{out}}'^\mu$.

- Then, bring $k_{\mathrm{out}}'^\mu$ to the equatorial plane with $\boldsymbol{R}_x(-\psi)$, where ψ is the angle between the projection of $k_{\mathrm{out}}'^\mu$ on the yz-plane and the y-axis. Note that such a rotation leaves $\mathcal{E}_{\mathrm{out,eq}}$ unchanged.

It follows that, after the three rotations

$$\boldsymbol{R} = \boldsymbol{R}_x(-\psi) \circ \boldsymbol{R}_y\left(\frac{\pi}{2} - \theta_{\mathrm{out}}\right) \circ \boldsymbol{R}_z(-\varphi_{\mathrm{out}}), \tag{4.15}$$

$\mathcal{E}_{\mathrm{out}}$ and k_{out}^μ are changed into $\mathcal{E}_{\mathrm{out,eq}}$ and $k_{\mathrm{out,eq}}^\mu$ which lie in the equatorial plane. In the following, we omit subscripts "eq," keeping in mind that we will have to apply $\boldsymbol{R}^{-1}$ to recover the original system of axes.
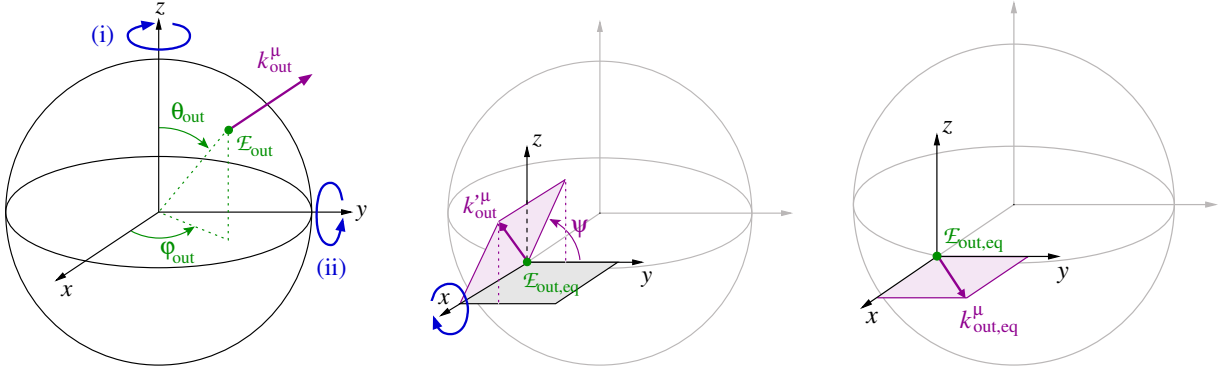
FIG. 5. An arbitrary initial condition is rotated so that the geodesic lies in the equatorial plane $\theta = \pi/2$. Left: $\mathcal{E}_{\text{out}}$ is brought (i) to $\varphi = 0$ by the rotation $\boldsymbol{R}_z(-\varphi_{\text{out}})$, and (ii) to $\theta = \pi/2$ by the rotation $\boldsymbol{R}_y(\pi/2 - \theta_{\text{out}})$. The resulting event and wave vector are denoted $\mathcal{E}_{\text{out,eq}}$ and k'^{μ}_{out}. Middle: k'^{μ}_{out} is brought to the equatorial plane by the rotation $\boldsymbol{R}_x(-\psi)$. Right: Final situation.

3. Null geodesics in Kottler geometry[1]

In the Kottler region, the existence of two Killing vectors associated to statisticity and spherical symmetry implies the existence of two conserved quantities, the energy E and the angular momentum L of the photon. It follows that a null geodesic is a solution of

$$A(r)\frac{\mathrm{d}t}{\mathrm{d}v} = E, \quad \left(\frac{\mathrm{d}r}{\mathrm{d}v}\right)^2 + \left(\frac{L}{r}\right)^2 A(r) = E^2, \quad r^2\frac{\mathrm{d}\varphi}{\mathrm{d}v} = L. \tag{4.16}$$

Introducing the dimensionless variable $u \equiv r_S/r$ and the impact parameter $b = L/E$, Eqs. (4.16) imply

$$r_S^2 \left(\frac{\mathrm{d}u}{\mathrm{d}t}\right)^2 = \frac{u^4}{\varepsilon_1^2} P(u) A^2(u), \tag{4.17}$$

$$\left(\frac{\mathrm{d}u}{\mathrm{d}\varphi}\right)^2 = P(u), \tag{4.18}$$

$$\frac{r_S^2}{E^2}\left(\frac{\mathrm{d}u}{\mathrm{d}v}\right)^2 = \frac{u^4}{\varepsilon_1^2} P(u), \tag{4.19}$$

with

$$A(u) = 1 - u - \varepsilon_2 u^{-2}, \quad P(u) \equiv \varepsilon_1^2 - u^2 A(u), \tag{4.20}$$

and where $\varepsilon_1 \equiv r_S/b$ and $\varepsilon_2 \equiv \Lambda r_S^2/3$.

Our purpose is now to compute the coordinates $(t_{\text{in}}, r_{\text{in}}, \varphi_{\text{in}})$ and the components k^{μ}_{in} of the wave vector at the entrance event $\mathcal{E}_{\text{in}}$, given those at $\mathcal{E}_{\text{out}}$. The situation is summarized in Fig. 6.

The radius r_{in} (or alternatively u_{in}) and time t_{in} at entrance are determined by comparing the radial dynamics of the photon, governed by Eq. (4.17), to the one of the
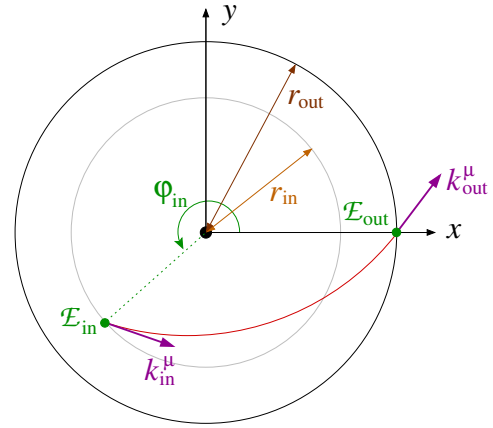

FIG. 6. Null geodesic in the Kottler region. Depicted with the Kottler coordinate system, the hole grows so that the ray enters with r_{in} and exits with $r_{\text{out}} > r_{\text{in}}$.

hole boundary. The latter is obtained from Eqs. (2.14) and (2.18). By introducing $u_{\text{h}} = r_S/r_{\text{h}}$, it reads

$$r_S \frac{\mathrm{d}u_{\text{h}}}{\mathrm{d}t} = -u_{\text{h}}^2 A(u_{\text{h}})\sqrt{1 - A(u_{\text{h}})}. \tag{4.21}$$

Equations (4.17) and (4.21) are then integrated[2] as $t_{\text{photon}}(u)$ and $t_{\text{hole}}(u_{\text{h}})$. The entrance radius then results from solving numerically the equation $t_{\text{photon}}(u_{\text{in}}) = t_{\text{hole}}(u_{\text{in}})$, which also provides t_{in}.

The usual textbook calculation of the deflection angle $\Delta\varphi_{\infty}$ of a light ray in Kottler geometry yields

$$\Delta\varphi_{\infty} = 2\varepsilon_1\sqrt{1 + \frac{\varepsilon_2}{\varepsilon_1^2}} = \frac{4\,GM}{b}\sqrt{1 + \frac{\Lambda b^2}{3}} \tag{4.22}$$

---

[1] See e.g. Refs. [70, 71] for early works on the propagation of light rays in spacetimes with a non-vanishing cosmological constant.

[2] The integration can be performed either numerically, or analytically in the case of Eq. (4.17) and perturbatively for Eq. (4.21).

at lowest order in ε_1 and ε_2. However, we cannot use this expression here—although it gives its typical order of magnitude—because $\Delta\varphi_\infty$ represents the angle between the *asymptotic* incoming and outgoing directions of a ray, whereas we must take into account the *finite* extension of the hole (see Fig. 6).

In general, the deflection angle $\Delta\varphi = \varphi_{\text{out}} - \varphi_{\text{in}}$ is

$$\Delta\varphi = \int_{u_{\text{in}}}^{u_{\text{m}}} \frac{\mathrm{d}u}{\sqrt{P(u)}} + \int_{u_{\text{out}}}^{u_{\text{m}}} \frac{\mathrm{d}u}{\sqrt{P(u)}} - 2\pi \qquad (4.23)$$

where $P(u)$ is the polynomial defined in Eq. (4.20), and u_{m} is the value of u at minimal approach. The integral involved in Eq. (4.23) can be rewritten as

$$\int_u^{u_{\text{m}}} \frac{\mathrm{d}u'}{\sqrt{P(u')}} = \frac{2}{\sqrt{u_3 - u_2}}\, F\left[\arcsin\sqrt{\frac{u_2 - u}{u_2 - u_1}}, \frac{u_2 - u_1}{u_2 - u_3} \right],$$
$$(4.24)$$

where $u_1 < u_2 = u_{\text{m}} < u_3$ are the three (real) roots of $P(u)$, and $F(\psi, e)$ denotes the elliptic function of the first kind [72]

$$F(\psi, e) \equiv \int_0^\psi \frac{\mathrm{d}\theta}{\sqrt{1 - e\sin^2\theta}}. \qquad (4.25)$$

Thus, Eq. (4.24) provides an exact expression of the deflection angle $\Delta\varphi$, and therefore of φ_{in}.

Once $\mathcal{E}_{\text{in}}$ is determined, it is easy to obtain k_{in}^μ by using the constants of motion. The result is

$$k_{\text{in}}^t = \frac{E}{A(r_{\text{in}})} = \frac{A(r_{\text{out}})}{A(r_{\text{in}})}\, k_{\text{out}}^t, \qquad (4.26)$$

$$k_{\text{in}}^\varphi = \frac{L}{r_{\text{in}}^2} = \left(\frac{r_{\text{out}}}{r_{\text{in}}}\right)^2 k_{\text{out}}^\varphi, \qquad (4.27)$$

$$k_{\text{in}}^r = -\sqrt{\left[A(r_{\text{in}})\, k_{\text{in}}^t\right]^2 - A(r_{\text{in}})\left(r_{\text{in}}\, k_{\text{in}}^\varphi\right)^2}. \qquad (4.28)$$

4. Final conditions at $\mathcal{E}_{\text{in}}$

The last step consists in coming back to the original FL coordinate system. That means (a) using $\boldsymbol{R}^{-1}$ to recover the initial system of axes, and (b) converting the components of $\mathcal{E}_{\text{in}}$ and k_{in}^μ in terms of the FL coordinate system. We have already described such operations in § IV B 2 and § IV B 1 respectively, except for the time coordinate (since we set $t_{\text{out}} = 0$).

The easiest way to compute the cosmic time T_{in} at entrance is to use the relation $r_{\text{in}} = a(T_{\text{in}})f_K(\rho_{\text{h}})$. In a spatially Euclidean FL spacetime ($K = 0$), we get

$$T_{\text{in}} = \frac{2}{3H_0\sqrt{\Omega_\Lambda}}\,\mathrm{argsinh}\left[\sqrt{\frac{\Omega_\Lambda}{1 - \Omega_\Lambda}}\left(\frac{r_{\text{in}}}{a_0\rho_{\text{h}}}\right)^{3/2} \right].$$
$$(4.29)$$

With this last result, we have completely determined the entrance event $\mathcal{E}_{\text{in}}$.

5. Sachs basis and optical tidal matrix

Once the geodesic equation is completely solved, we are ready to integrate the Sachs equation in the Kottler region, that is, to determine the Wronski matrix $\boldsymbol{\mathcal{W}}_{\text{K}}$. Such a task requires us first to define the Sachs basis (s_1, s_2) with respect to which $\boldsymbol{\mathcal{W}}_{\text{K}}$ will be calculated.

The four-velocity u is chosen to be the one of a radially free-falling observer,

$$u \equiv \frac{1}{A(r)}\,\partial_t + \sqrt{1 - A(r)}\,\partial_r. \qquad (4.30)$$

This choice ensures the continuity of u through the hole frontier, where $u = \partial_T$. The wave four-vector k is imposed by the null geodesic equations, and reads

$$k = \frac{E}{A(r)}\,\partial_t \pm E\sqrt{1 - \frac{b^2 A(r)}{r^2}}\,\partial_r + \frac{L}{r^2}\,\partial_\varphi \qquad (4.31)$$

where the $\pm$ sign depends on whether the photon approaches $(-)$ or recedes $(+)$ from the center of the hole.

By definition, the screen vectors s_1, s_2 form an orthonormal basis of the plane orthogonal to both u and k. Here, since the trajectory occurs in the equatorial plane, the first one can be trivially chosen as

$$s_1 \equiv \partial_z = -\frac{1}{r}\,\partial_\theta. \qquad (4.32)$$

The second one is obtained from the orthogonality and normalization constraints, and reads

$$s_2 \equiv \frac{1}{N}\left[\frac{\sqrt{1 - A(r)}}{A(r)}\,\partial_t + \partial_r \right.$$
$$\left. + \frac{1}{b\,A(r)}\left(\sqrt{1 - A(r)} \mp \sqrt{1 - \frac{b^2 A(r)}{r^2}} \right)\partial_\varphi \right], \quad (4.33)$$

where the normalization function is

$$N \equiv \frac{r}{b\,A(r)}\left(1 \mp \sqrt{1 - A(r)}\sqrt{1 - \frac{b^2 A(r)}{r^2}} \right). \qquad (4.34)$$

Using the Sachs basis defined by Eqs. (4.30), (4.31), (4.32), and (4.33), we can finally compute the optical tidal matrix, and get

$$\boldsymbol{\mathcal{R}} = \begin{pmatrix} -\mathcal{R}(r) & 0 \\ 0 & \mathcal{R}(r) \end{pmatrix}, \qquad (4.35)$$

where the function $\mathcal{R}(r)$ is

$$\mathcal{R}(r) \equiv \frac{3}{2}\left(\frac{L}{r_{\text{S}}^2}\right)^2\left(\frac{r_{\text{S}}}{r}\right)^5. \qquad (4.36)$$

As expected from the general decomposition (3.8), $\boldsymbol{\mathcal{R}}$ is trace free because only Weyl focusing is at work. Let us finally emphasize that Λ does not appear in the expression (4.36) of $\mathcal{R}(r)$, which is not surprising since a pure cosmological constant does not deflect light.

6. Wronski matrix

The Sachs equations can now be integrated in order to determine the scale matrix $\mathcal{C}_{\mathrm{K}}$ and the Jacobi matrix $\mathcal{D}_{\mathrm{K}}$ that compose the Wronski matrix $\mathcal{W}_{\mathrm{K}}$.

First, since $\mathcal{R}$ is diagonal, the Sachs equations (3.7) only consist of the following two decoupled ordinary differential equations

$$\frac{\mathrm{d}^2\xi_1}{\mathrm{d}v^2} = -\mathcal{R}[r(v)]\,\xi_1(v), \qquad (4.37)$$

$$\frac{\mathrm{d}^2\xi_2}{\mathrm{d}v^2} = +\mathcal{R}[r(v)]\,\xi_2(v). \qquad (4.38)$$

Clearly, the decoupling implies that the off-diagonal terms of $\mathcal{C}_{\mathrm{K}}$ and $\mathcal{D}_{\mathrm{K}}$ vanish,

$$\mathcal{C}_{12}^{\mathrm{K}} = \mathcal{C}_{21}^{\mathrm{K}} = \mathcal{D}_{12}^{\mathrm{K}} = \mathcal{D}_{21}^{\mathrm{K}} = 0. \qquad (4.39)$$

The calculation of the diagonal coefficients requires us to integrate Eqs. (4.37) and (4.38). This cannot be performed analytically because there is no exact expression for r as a function of v along the null geodesic. Indeed, we can write v as a function of r from Eq. (4.19) but this relation is not invertible by hand.

Nevertheless, we are able to perform the integration perturbatively in the regime where $\varepsilon_2/\varepsilon_1 \ll \varepsilon_1 \ll 1$, the relevance of which shall be justified by the orders of magnitude discussed in the next section. Solving Eq. (4.19) at leading order in ε_1, ε_2 leads to

$$u(v) = \frac{\varepsilon_1}{\sqrt{1 + (v - v_{\mathrm{m}})^2/\Delta v^2}} + \mathcal{O}\left(\varepsilon_1^2, \frac{\varepsilon_2}{\varepsilon_1}\right) \qquad (4.40)$$

with $\Delta v \equiv b/E$, and where v_{m} denotes the value of the affine parameter v at the point of minimal approach. Equation (4.37) then becomes, at leading order in $\varepsilon_1, \varepsilon_2$, and using the dimensionless variable $w \equiv (v - v_{\mathrm{m}})/\Delta v$,

$$\frac{\mathrm{d}^2\xi_1}{\mathrm{d}w^2} = -\frac{3\,\varepsilon_1}{2}\left(\frac{1}{1 + w^2}\right)^{5/2}\xi_1. \qquad (4.41)$$

The perturbative resolution of Eq. (4.41) from v_{init} to v finally leads to

$$\mathcal{C}_{11}^{\mathrm{K}} = 1 - \frac{3\,\varepsilon_1}{2}\Big[-B'(w_{\mathrm{init}})(w - w_{\mathrm{init}})$$
$$+ B(w) - B(w_{\mathrm{init}})\Big] + \mathcal{O}\left(\varepsilon_1^2, \frac{\varepsilon_2}{\varepsilon_1}\right), \quad (4.42)$$

and

$$\mathcal{D}_{11}^{\mathrm{K}} = (v - v_{\mathrm{init}}) + \frac{3\,\varepsilon_1}{2}\Delta v\Big\{w_{\mathrm{init}}\big[B(w) - B(w_{\mathrm{init}})$$
$$- B'(w_{\mathrm{init}})(w - w_{\mathrm{init}})\big] - \big[C(w) - C(w_{\mathrm{init}})$$
$$- C'(w_{\mathrm{init}})(w - w_{\mathrm{init}})\big]\Big\} + \mathcal{O}\left(\varepsilon_1^2, \frac{\varepsilon_2}{\varepsilon_1}\right), \quad (4.43)$$

where the functions B and C are given by

$$B(w) \equiv \frac{1 + 2\,w^2}{3\sqrt{1 + w^2}} \quad \text{and} \quad C(w) \equiv \frac{-w}{3\sqrt{1 + w^2}}. \quad (4.44)$$

The expressions of $\mathcal{C}_{22}^{\mathrm{K}}$ and $\mathcal{D}_{22}^{\mathrm{K}}$ are respectively obtained from Eqs. (4.42) and (4.43) by turning ε_1 into $-\varepsilon_1$.

Note that in the limit $\varepsilon_1, \varepsilon_2/\varepsilon_1 \to 0$, i.e. $b \to \infty$ and $\Lambda = 0$, we find $\mathcal{C} = \mathbf{1}$ and $\mathcal{D} = (v - v_{\mathrm{init}})\mathbf{1}$, which are the expected expressions in Minkowski spacetime.

C. Practical implementation

This section has described the complete resolution of the equations for light propagation in a Swiss-cheese universe. All the results are included in a Mathematica program `OneHole` which takes, as input, the observation conditions and the properties of the hole; and returns $\mathcal{E}_{\mathrm{in}}$, k_{in} and $\mathcal{W}(v_{\mathrm{source}}; v_{\mathrm{obs}}) = \mathcal{W}_{\mathrm{K}}(v_{\mathrm{in}}; v_{\mathrm{out}}) \cdot \mathcal{W}_{\mathrm{FL}}(v_{\mathrm{out}}; v_{\mathrm{obs}})$. For simplicity, this program has been written assuming that *the FL region has Euclidean spatial sections* ($K = 0$).

Iterating `OneHole` allows us to propagate a light signal back to an arbitrary emission event. Eventually, the redshift z is obtained by comparing the wave vector at emission and reception; and the luminosity distance is extracted from the block $\mathcal{D}(v_{\mathrm{source}}; v_{\mathrm{obs}})$ of the Wronski matrix $\mathcal{W}(v_{\mathrm{source}}; v_{\mathrm{obs}})$, according to

$$D_{\mathrm{L}} = (1 + z)^2 \sqrt{\det \mathcal{D}(v_{\mathrm{source}}; v_{\mathrm{obs}})}. \qquad (4.45)$$

Note finally that, when iterating `OneHole`, we must also rotate the Sachs basis (s_1, s_2), to take into account that the plane of motion differs for two successive holes.

V. EFFECT OF ONE HOLE

Our method is first applied to a Swiss cheese with a single hole. The purpose is to study the effects on the redshift and luminosity distance—for the light emitted by a standard candle—due to the presence of the hole.

A. Numerical values and "opacity" assumption

The mass M of the clump inside the hole depends on what object it is supposed to model. The choice must be driven by the typical scales probed by the light beams involved in supernova observations. As discussed in the introduction the typical width of such beams is $\sim$ AU; for comparison the typical interstellar distance within a galaxy is $\sim$ pc. Hence, SN beams are sensitive to the very fine structure of the Universe, including the internal content of galaxies. This suggests that the clump inside the hole should represent a star, so that the natural choice should be $M \sim M_\odot$. Unfortunately, we cannot afford to deal with such a fine description, for numerical reasons.

Instead, the clump is chosen to stand for a gravitationally bound system, such as a galaxy ($M \sim 10^{11} M_\odot$), or a cluster of galaxies ($M \sim 10^{15} M_\odot$). By virtue of Eq. (2.19), the corresponding hole radii are respectively $r_\mathrm{h} \sim 1\,\mathrm{Mpc}$ and $r_\mathrm{h} \sim 20\,\mathrm{Mpc}$. It is important to note that this choice keeps entirely relevant as far as the light beam does not enter the clump (so that its internal structure does not matter), that is, as long as

$$b > b_\mathrm{min} \approx r_\mathrm{phys}, \qquad (5.1)$$

where r_phys is the physical size of the clump. For a galaxy $r_\mathrm{phys} \sim 10\,\mathrm{kpc}$, and for a cluster $r_\mathrm{phys} \sim 1\,\mathrm{Mpc}$. We choose to work under the assumption of Eq.(5.1), in other words *we proceed as if the clumps were opaque spheres.*

In the case of galactic clumps this "opacity" assumption can be justified by the three following arguments (in the case of clusters, however, it is highly questionable).

Statistics.: Since $r_\mathrm{phys} \ll r_\mathrm{h}$ the cross section of the clumps is very smal; thus we expect that *most* of the observations satisfy the condition (5.1).

Screening.: A galaxy standing on the line of sight can simply be bright enough to flood a SN located behind it. For comparison, the absolute magnitude of a galaxy ranges from -16 to -24 [73], while for a SN it is typically -19.3 [74].

Strong lensing.: A light beam crossing a galaxy enters the strong lensing regime, because the associated Einstein radius is $r_\mathrm{E} \sim \sqrt{r_\mathrm{S} D_\mathrm{A,SN}} \lesssim 10\,\mathrm{kpc} \sim r_\mathrm{phys}$. In this case, we expect a significant magnification of the SN which could be isolated, or even removed during data processing.

The "opacity" assumption is at the same time a key ingredient and a limitation of our approach.

The various distance scales involved in the model are clearly separated. The resulting hierarchy is depicted in Fig. 7, and the typical orders of magnitude are summarized in Table I. The latter includes the small parameters $\varepsilon_1 = r_\mathrm{S}/b$ and $\varepsilon_2 = \Lambda r_\mathrm{S}^2/3 \sim (r_\mathrm{S}/r_\mathrm{Hubble})^2$. Their values justify *a posteriori* the perturbative expansion performed in § IV B 6, where we assumed that $\varepsilon_2/\varepsilon_1 \ll \varepsilon_1 \ll 1$. In fact, one can show from Eq. (2.19) that $\varepsilon_2 \sim \varepsilon_{1,\mathrm{min}}^3$.

Type	r_S (pc)	r_phys (kpc)	r_h (Mpc)	ε_1	ε_2
Galaxy	10^{-2}	10	1	10^{-8}–10^{-6}	10^{-23}
Cluster	100	1000	20	10^{-6}–10^{-4}	10^{-15}

TABLE I. Typical orders of magnitude for galaxylike ($M \sim 10^{11} M_\odot$) and clusterlike ($M \sim 10^{15} M_\odot$) Swiss-cheese holes.

In this section and the next one, we *temporarily* set for simplicity the cosmological constant to zero. The FL region is therefore characterized by the Einstein–de Sitter (EdS) cosmological parameters

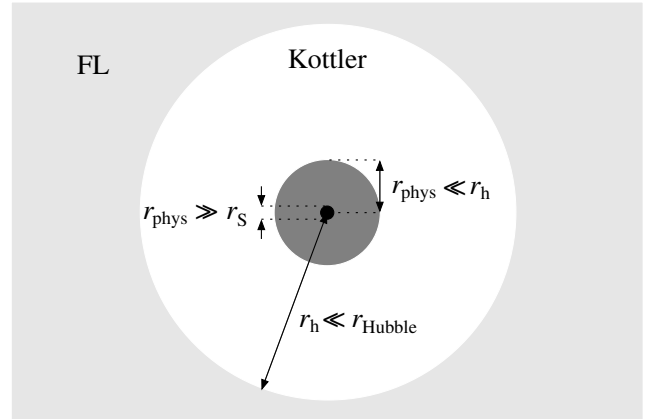$$\Omega_\mathrm{m} = 1, \qquad \Omega_K = 0, \qquad \Omega_\Lambda = 0. \qquad (5.2)$$

FIG. 7. Geometry and hierarchy of distances for a typical Swiss-cheese hole: $r_\mathrm{S} \ll r_\mathrm{phys} \ll r_\mathrm{h} \ll r_\mathrm{Hubble}$.

The effect of the cosmological constant will be studied in detail in Sec. VII. The value of the Hubble parameter is fixed to $H_0 = h \times 100\,\mathrm{km/s/Mpc}$, with $h = 0.72$.

B. Setup

In order to study the corrections to the redshift z and luminosity distance D_L, due to the presence of the hole, we consider the situation depicted in Fig. 8.
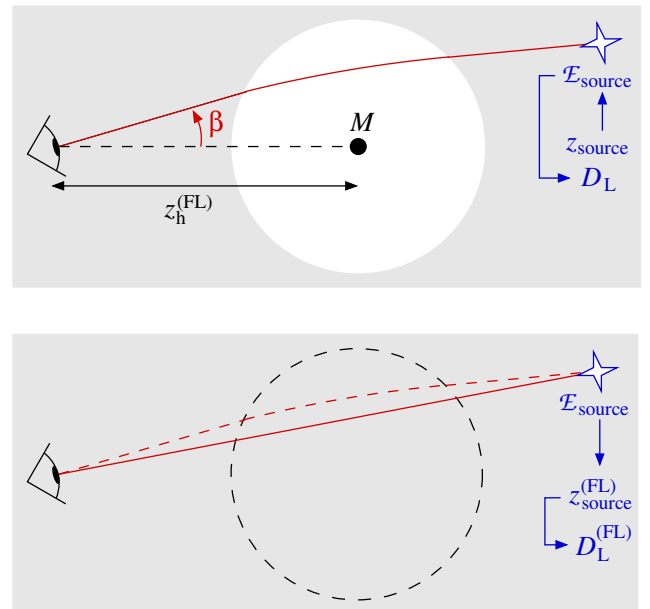

FIG. 8. Setup for evaluating the effect of one hole on the redshift and luminosity distance.

Our method is the following. We first choose the mass M inside the hole and the redshift z_source of the source. We then fix the comoving distance between the

observer and the center of the hole, in terms of the cosmological (FL) redshift $z_h^{(FL)}$ of the latter. To finish, we choose a direction of observation, defined by the angle β between the line of sight and the line connecting the observer to the center of the hole.

Given those parameters, the light beam is propagated (in presence of the hole) until the redshift reaches z_{source}. We obtain the emission event $\mathcal{E}_{source}$ and the luminosity distance D_L. We then compute $z_{source}^{(FL)}$ and $D_L^{(FL)}$ by considering a light beam that propagates from $\mathcal{E}_{source}$ to the observer without the hole (bottom panel of Fig. 8).

C. Corrections to the redshift

1. Numerical results

The effect of the hole on the redshift is quantified by

$$\delta z \equiv \frac{z - z^{(FL)}}{z^{(FL)}}, \qquad (5.3)$$

where we used the short notation z instead of z_{source}. Figure 9 shows the evolution of δz with β, for $z_{source} = 0.05$ and various hole positions and masses. We have chosen $M \sim 10^{15} M_\odot$ because the effect is more significant and displays fewer numerical artifacts than for $M \sim 10^{11} M_\odot$.

We only consider directions of observation such that the light beam crosses the hole. Thus, $\beta_{min} < \beta < \beta_{max}$ where β_{min} and β_{max} depend on the physical cutoff r_{phys}, the radius r_h of the hole, and its distance to the observer $z_h^{(FL)}$. Those dependences can be eliminated by plotting δz as a function of $(\beta - \beta_{min})/(\beta_{max} - \beta_{min})$ instead of β, as displayed in Fig. 10.

As expected, δz tends to zero when β approaches β_{max} (light ray tangent to the hole boundary). We notice that δz does not significantly depend on the distance between the observer and the hole. However, the effect clearly grows with the mass of the hole.

2. Analytical estimation of the effect

The correction in redshift due to hole can be understood as an integrated Sachs-Wolfe effect (see e.g. Chapter 7 of Ref. [1]). As the boundary of the hole grows with time (see Fig. 6), the light signal undergoes a stronger gravitational potential at entrance than at exit. That induces a gravitational redshift δz_{grav} which adds to the cosmological one, and reads

$$1 + \delta z_{grav} = \frac{k_{in}^t}{k_{out}^t} = \frac{A(r_{out})}{A(r_{in})}. \qquad (5.4)$$

The order of magnitude of δz_{grav} can be evaluated as follows. Let $\delta r = r_{out} - r_{in}$ be the increase of the radius of the hole between entrance and exit. The expansion

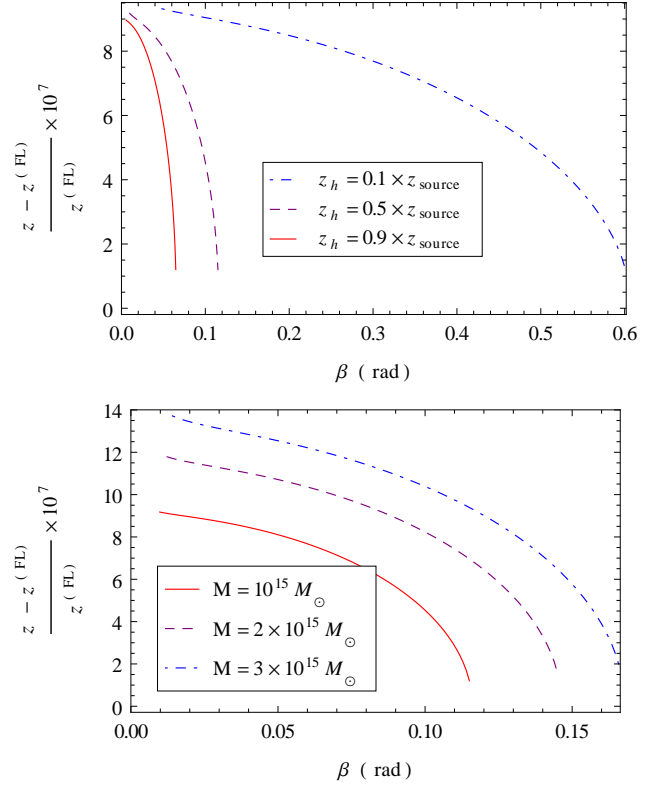FIG. 9. Relative correction to the redshift z, due to the hole in the line of sight, as a function of the direction of observation β, for a source at $z_{source} = 0.05$. Top panel: The mass of the hole is $M = 10^{15} M_\odot$, and three positions between the source and the observer are tested, $z_h^{(FL)}/z_{source} = 0.1$ (blue, dot-dashed), 0.5 (purple, dashed), and 0.9 (red, solid). Bottom panel: The hole is at $z_h^{(FL)} = 0.5\,z_{source}$ and three values for the mass are tested, $M/10^{15} M_\odot = 3$ (blue, dot-dashed), 2 (purple, dashed), and 1 (red, solid).

dynamics implies $\delta r \sim \sqrt{\varepsilon_1}\Delta t$, where $\Delta t = t_{out} - t_{in} \sim r_{in}$, r_{out} is the time spent by the photon inside the hole. Using Eq. (5.4), we conclude that

$$\delta z_{grav} \sim \varepsilon_1^{3/2}. \qquad (5.5)$$

For $M = 10^{15} M_\odot$ (clusterlike hole), the numerical values given in Table I yield $\delta z_{grav,max} \sim 10^{-6}$. This order of magnitude is compatible with the full numerical integration displayed in Figs. 9 and 10.

Such an analytical estimate enables us to understand why δz increases with M, that is, with the size of the hole. Indeed, the bigger the hole, the longer the photon travel time so that the hole has more time to grow, and finally $A(r_{out}) - A(r_{in})$ is larger.
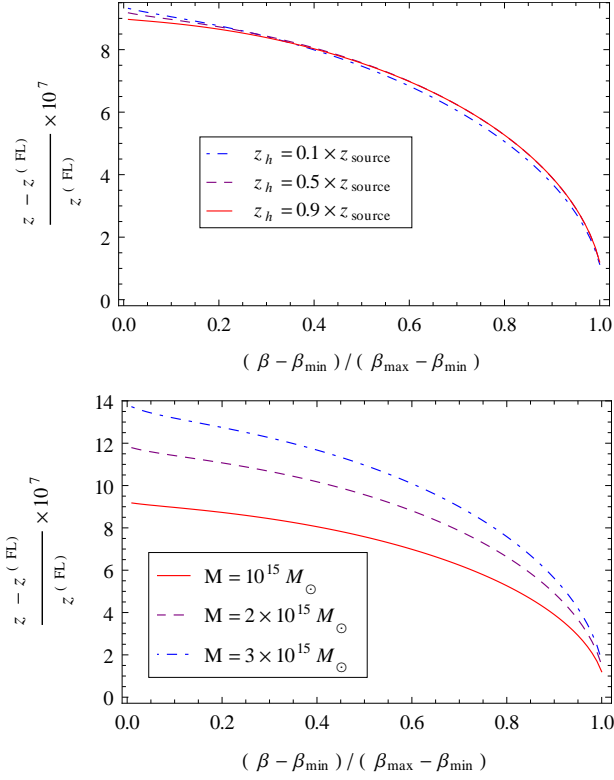
FIG. 10. Same as Fig. 9, but plotted in terms of the centered and normalized observation direction $(\beta - \beta_{\min})/(\beta_{\max} - \beta_{\min})$.
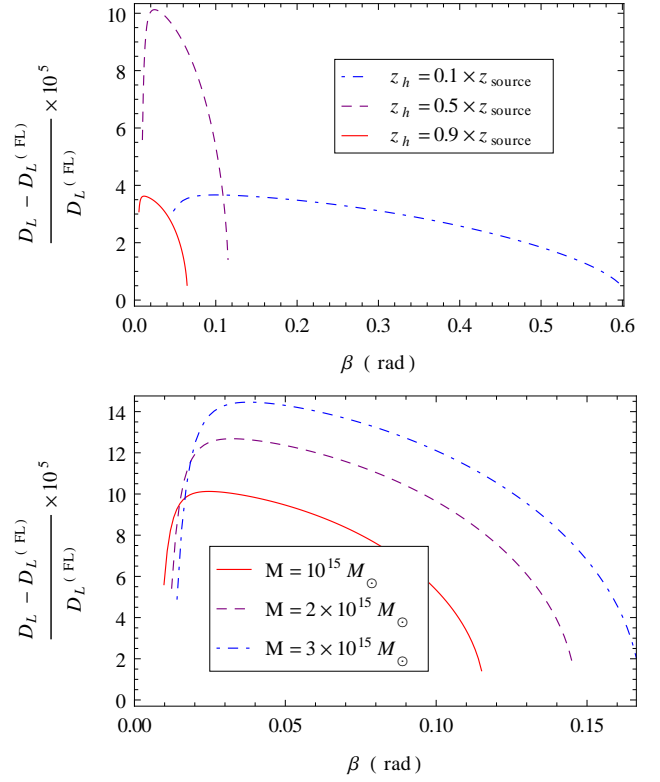
FIG. 11. Relative correction to the luminosity distance D_{L}, due to the hole in the line of sight, as a function of the direction of observation β, for a source at $z_{\mathrm{source}} = 0.05$. Top panel: The mass of the hole is $M = 10^{15} M_{\odot}$, and three positions between the source and the observer are tested, $z_{\mathrm{h}}^{\mathrm{(FL)}}/z_{\mathrm{source}} = 0.1$ (blue, dot-dashed), 0.5 (purple, dashed), and 0.9 (red, solid). Bottom panel: The hole is at $z_{\mathrm{h}}^{\mathrm{(FL)}} = 0.5\,z_{\mathrm{source}}$ and three values for the mass are tested, $M/10^{15}M_{\odot} = 3$ (blue, dot-dashed), 2 (purple, dashed), and 1 (red, solid).

D. Corrections to the luminosity distance

The effect of the hole on the luminosity distance can be characterized in a similar way by

$$\delta D_{\mathrm{L}} \equiv \frac{D_{\mathrm{L}} - D_{\mathrm{L}}^{\mathrm{(FL)}}}{D_{\mathrm{L}}^{\mathrm{(FL)}}}. \qquad (5.6)$$

The associated results, in the same conditions as in the previous paragraph, are displayed in Figs. 11 and 12.

We notice that δD_{L} is maximum if the hole lies halfway between the source and the observer, which is indeed expected since the lensing effects scale as

$$\frac{D_{\mathrm{A}}(\text{observer, lens}) \times D_{\mathrm{A}}(\text{lens, source})}{D_{\mathrm{A}}(\text{observer, source})}, \qquad (5.7)$$

which typically peaks for $z_{\mathrm{lens}} \approx z_{\mathrm{source}}/2$. The maximal amplitude of the correction is of order 10^{-4}, for masses ranging from $10^{15} M_{\odot}$ to $3 \times 10^{15} M_{\odot}$. Just as for the redshift, the effect increases with the size of the hole.

Note that δD_{L} can be related to the relative magnification μ, frequently used in the weak-lensing formalism, and defined by

$$\mu \equiv \left(\frac{D_{\mathrm{A}}^{\mathrm{(FL)}}}{D_{\mathrm{A}}}\right)^2 = \left(\frac{1+z}{1+z^{\mathrm{(FL)}}}\right)^4 \left(\frac{D_{\mathrm{L}}^{\mathrm{(FL)}}}{D_{\mathrm{L}}}\right)^2. \qquad (5.8)$$

Hence, if the correction on z is negligible compared to the one of D_{A}, then the relation between δD_{L} and μ is

$$\delta D_{\mathrm{L}} \approx \frac{1}{\sqrt{\mu}} - 1. \qquad (5.9)$$

E. Summary

The presence of a single hole between the source and the observer induces both a correction in redshift and luminosity distance. For a hole with mass $M \sim 10^{15} M_{\odot}$, the relative amplitudes of those corrections are $\delta z \sim 10^{-7}$–10^{-6} and $\delta D_{\mathrm{L}} \sim 100\,\delta z$. The same study for $M \sim 10^{11} M_{\odot}$ leads to similar results with $\delta z \sim 10^{-10}$–10^{-9}. Therefore, the effects of a single hole seem negligible.
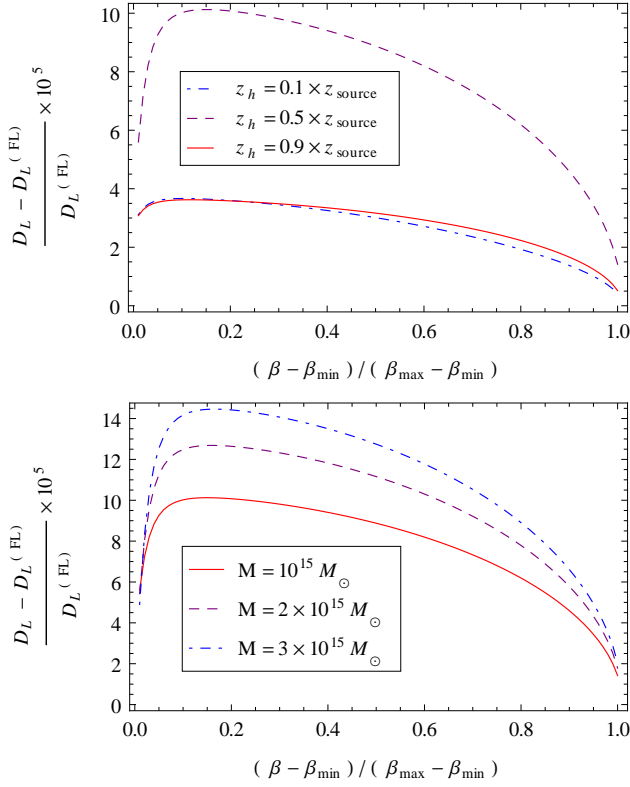
FIG. 12. Same as Fig. 11, but plotted in terms of the centered and normalized observation direction $(\beta - \beta_{\min})/(\beta_{\max} - \beta_{\min})$.

VI.   EFFECT OF SEVERAL HOLES

We now investigate a Swiss-cheese model containing many holes arranged on a regular lattice. Again, in this entire section, the cosmological parameters characterizing the FL region are the EdS ones.

A.   Description of the arrangement of holes

1.   Smoothness parameter

The smoothness of the distribution of matter within a Swiss cheese can be quantified by a parameter f constructed as follows. Choose a region of space with—comoving or physical—volume V, where $V^{1/3}$ is large compared to the typical distance between two holes. Thus, this volume contains many holes, the total volume of which is V_{holes}, while the region left with homogeneous matter occupies a volume $V_{\text{FL}} = V - V_{\text{holes}}$. We define the smoothness parameter by

$$f \equiv \lim_{V \to \infty} \frac{V_{\text{FL}}}{V}. \tag{6.1}$$

In particular, $f = 1$ corresponds to a Swiss cheese with no hole—that is, perfectly smooth—while $f = 0$ corresponds

to the case where matter is under the form of clumps. Of course, f also characterizes the ratio between the energy density of the continuous matter and the mean energy density.

2.   Lattice

We want to construct a Swiss cheese for which the smoothness parameter is as small as possible. If all holes are identical, this close-packing problem can be solved by using, for instance, a hexagonal lattice. The corresponding arrangement is pictured in Fig. 13. The minimal value of the smoothness parameter is in this case

$$f_{\min} = 1 - \frac{\pi}{3\sqrt{2}} \approx 0.26. \tag{6.2}$$

In order to reach a smoothness parameter smaller than $f_{\min}$, one would have to insert a second family of smaller holes. By iterating the process, one can in principle make f as close as one wants to zero.
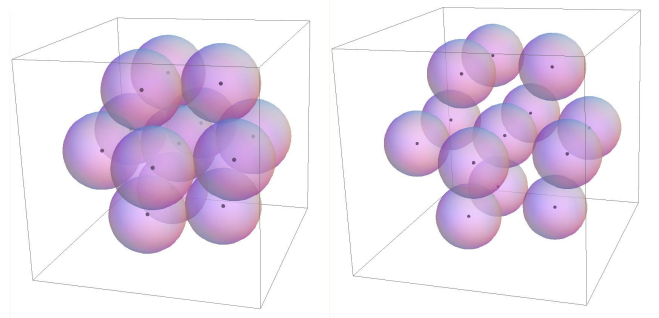

FIG. 13. Hexagonal lattice of identical holes. On the left, the arrangement is close-packed, so that the smoothness parameter is $f = f_{\min} \approx 0.26$. On the right, $f = 0.7$.

B.   Observations in a unique line of sight

We now focus on the corrections to the redshift and luminosity distance of a source whose light travels through the Swiss-cheese universe described previously. We study the influence of (a) the distance between the source and the observer, (b) the smoothness parameter f, and (c) the mass M of the holes.

1.   Setup

After having chosen the parameters (f, M) of the model, we arbitrarily choose the spatial position of the observer in the FL region, and fix its direction of observation. The method is then identical to the one of Sec. V. The light beam is propagated from the observer until the redshift reaches the one of the source, z. The ending

point defines the emission event $\mathcal{E}_{\text{source}}$. We emphasize that only emission events occurring in the FL region are considered in this article.

2.   *Influence of the smoothness parameter*

In this paragraph, the mass of every hole is fixed to $M = 10^{11} M_\odot$ (galactic holes). The relative corrections to the redshift δz and luminosity distance δD_{L}, as functions of the redshift z of the source, have been computed and are displayed in Fig. 14 for different values of the smoothness parameter f.
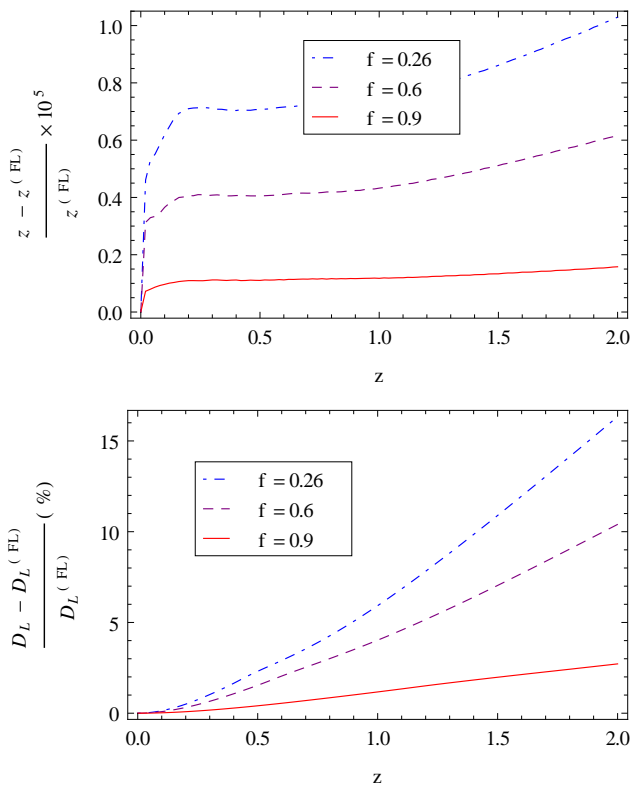
FIG. 14.   Relative corrections to the redshift z (top panel) and luminosity distance D_{L} (bottom panel) as functions of z, for an arbitrary light beam traveling through a Swiss-cheese universe. All holes are identical, their mass is $M = 10^{11} M_\odot$. Three different smoothness parameters are tested: $f = 0.26$ (blue, dot-dashed), 0.6 (purple, dashed), and 0.9 (red, solid).

While the corrections to the redshift remain small— typically $\delta z < 10^{-5}$—the cumulative effect of lensing on the luminosity distance is significant. For instance, a source at $z \sim 1.5$ would appear $10\,\%$ farther in a Swiss cheese with $f = 0.26$, than in a strictly homogeneous universe. Both δz and δD_{L} increase with z and decrease with f, as intuitively expected. Thus, the more holes, the stronger the effect. As examples, the light beam crosses ~ 300 holes for $(f = 0.26, z = 0.1)$ or $(f = 0.9, z = 1)$, but it crosses ~ 2000 holes for $(f = f_{\text{min}}, z = 1)$.

3.   *Influence of the mass of the holes*

We now set the smoothness parameter to its minimal value $f_{\text{min}} \approx 0.26$, and repeat the previous analysis for various hole masses. The results are displayed in Fig. 15.
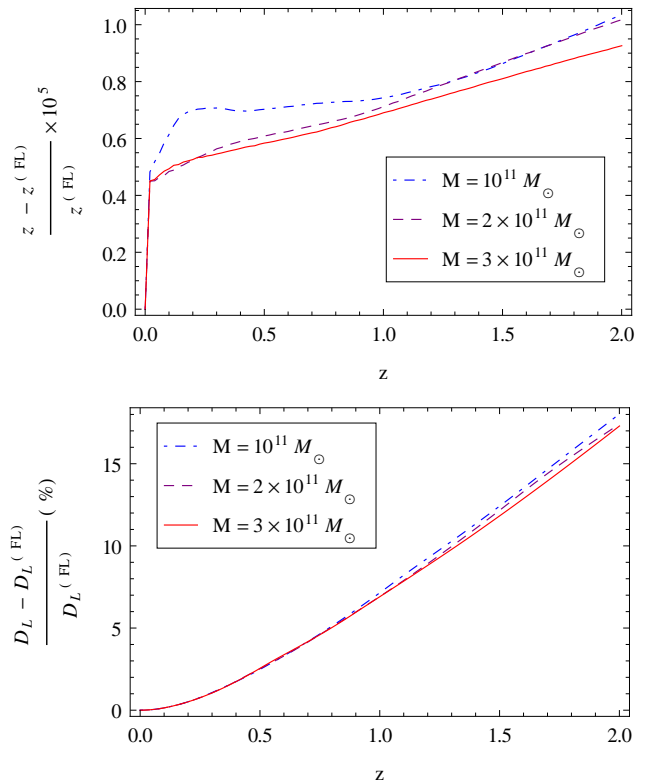

FIG. 15.   Same as Fig. 14 but with $f = 0.26$ and three different values for the masses: $M/10^{11} M_\odot = 1$ (blue, dot-dashed), 2 (purple, dashed), and 3 (red, solid).

We conclude that neither δz nor δD_{L} depends significantly on M, that is, on the size of the holes. Thus, what actually matters is not the number of holes intersected by the beam, but rather the total time spent inside holes.

C.   **Statistical study for random directions of observation**

The previous study was restricted to a single line of sight, but since a Swiss-cheese universe is not strictly homogeneous, the corrections to z and D_{L} are expected to vary from one line of sight to another. As pointed out by e.g. Refs. [57, 61], such a restrictive analysis can lead to overestimate the mean corrections induced by inhomogeneities. Besides, as stressed by Ref. [8], the dispersion of the data is crucial for interpreting SN observations. Hence, the conclusions of the previous subsection need to be completed by a statistical study, with randomized directions of observation.

Since the effect on the redshift is observationally negligible, we focus on the luminosity distance. After having set the parameters (f, M) of the model, we fix the position of the observer in the FL region. Then, for a given redshift z, we consider a statistical sample of N_{obs} randomly distributed directions of observation $\vec{d} \in \mathcal{S}^2$, and compute $\delta D_{\mathrm{L}}(z, \vec{d})$ for each one.

Figure 16 shows the probability distribution of δD_{L} for sources at redshifts $z = 0.1$ (top panel) and $z = 1$ (bottom panel). We compare two Swiss-cheese models with the same smoothness parameter $f = f_{\mathrm{min}}$ but with different values for the masses of their holes ($M = 10^{11} M_{\odot}$ and $10^{15} M_{\odot}$). The histograms of Fig. 16 are generated from statistical samples which contain $N_{\mathrm{obs}} = 200$ directions of observation each.
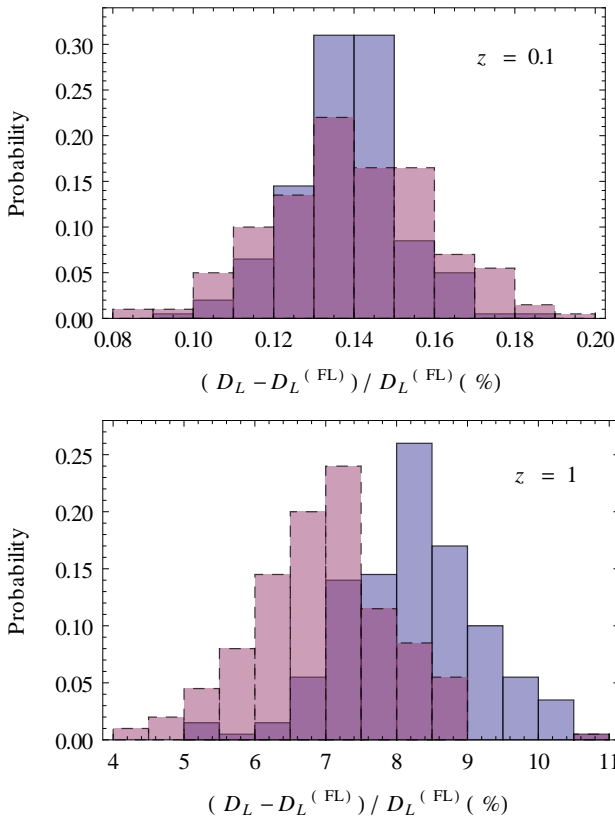

FIG. 16. Probability distribution of the relative correction to the luminosity distance for random directions of observation, at $z = 0.1$ (top panel) and $z = 1$ (bottom panel). The smoothness parameter is $f = f_{\mathrm{min}}$ and two different values for the masses of the holes are tested: $M = 10^{11} M_{\odot}$ (blue, solid) and $M = 10^{15} M_{\odot}$ (purple, dashed).

From the statistical samples, we can compute the mean correction $\langle \delta D_{\mathrm{L}} \rangle(z)$ and its standard deviation $\sigma_{\delta D_{\mathrm{L}}}(z)$, whose evolutions are plotted in Fig. 17.

The results displayed in Fig. 17 confirm the conclusions of Subsec. VI B. The distance-redshift relation in a Swiss cheese is biased with respect to the one of a purely ho-
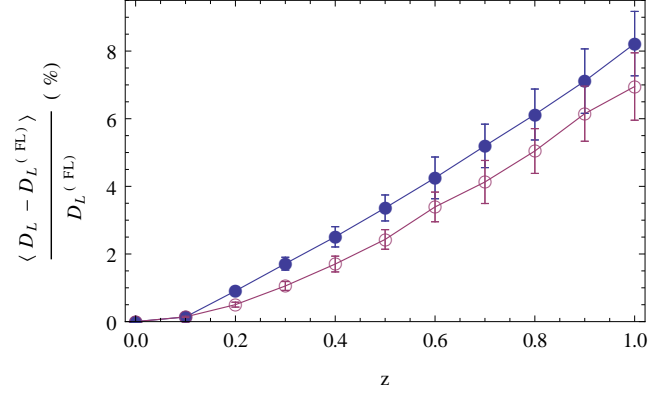

FIG. 17. Evolution, with redshift z, of the relative correction to the luminosity distance averaged over $N_{\mathrm{obs}} = 200$ random directions of observation. Error bars indicate the dispersion $\sigma_{\delta D_{\mathrm{L}}}$ around the mean correction $\langle \delta D_{\mathrm{L}} \rangle$. As in Fig. 16, we compare Swiss-cheese models with $M = 10^{11} M_{\odot}$ (blue, filled markers) and $M = 10^{15} M_{\odot}$ (purple, empty markers).

mogenous universe. This effect is statistically significant, we indeed estimate (empirically) that

$$\langle \delta D_{\mathrm{L}} \rangle(z) \approx 8 \times \sigma_{\delta D_{\mathrm{L}}}(z). \qquad (6.3)$$

The bias slightly decreases with the mass parameter M. However, it can be considered quite robust because a variation of 4 orders of magnitude for M only induces a variation of $\sim 10\%$ for the bias.

The intrinsic dispersion of D_{L}, associated with $\sigma_{\delta D_{\mathrm{L}}}$, can be compared with the typical dispersion of the observation. For instance, at $z = 1$ the former is $\sim 1\%$, while the latter is estimated to be typically $\sim 10\%$ [75]. It follows that the dispersion induced by the inhomogeneity of the distribution of matter remains small compared to the observational dispersion.

D. Summary and discussion

This section has provided a complete study of the effect of inhomogeneities on the Hubble diagram, investigating both the corrections to the redshift and luminosity distance of standard candles. The Swiss-cheese models are made of identical holes, defined by their mass M, and arranged on a regular hexagonal lattice. The fraction of matter remaining in FL regions defines the smoothness parameter f. For the hexagonal lattice, $f_{\mathrm{min}} \approx 0.26$.

The effect on the redshift is negligible ($\delta z < 10^{-5}$), while the correction to the luminosity distance is significant ($\delta D_{\mathrm{L}} > 10\%$ at high redshift). Compared to the homogeneous case, sources are systematically demagnified in a Swiss-cheese universe. The effect increases with z and decreases with f.

Our results differ from those obtained in Swiss-cheese models with Lemaître-Tolman-Bondi (LTB) solutions inside the holes. In the latter case, a source can be either demagnified if light mostly propagates through underdense

regions [54, 55, 59] (and if the observer is far away from a void, see Ref. [76]), or magnified otherwise. It has been proven in Refs. [58, 61, 62] that the global effect averages to zero when many sources are considered. Hence, LTB holes introduce an additional dispersion to the Hubble diagram, but no statistically significant bias. On the contrary, in the present study, light only propagates through underdense regions, because we only consider light beams which remain far from the hole centers. This assumption has been justified in Subsec. V A by an "opacity" argument. The bias displayed by our results is mostly due to the selection of the light beams which can be considered observationally relevant.

Our results also differ qualitatively from those obtained in the framework of the perturbation theory. In Ref. [31], the probability density function $P(\mu)$ of the weak lensing magnification μ, due to the large scale structure, has been analytically calculated by assuming an initial power spectrum with slope $n = -2$. Just as for LTB Swiss-cheese models, the magnification shows no intrinsic bias (i.e. $\langle \mu \rangle = 1$), but it is shown that $P(\mu)$ peaks at a value μ_{peak} slightly smaller than 1. Hence, a bias of order $\mu_{\text{peak}} - \langle \mu \rangle$, which is typically 1% at $z = 1$, can emerge from observations because of insufficient statistics. However, this bias is far smaller than the one obtained in our Swiss-cheese model, of order $2\,\delta D_{\text{L}} \sim 15\%$ at $z = 1$.

Besides, the dispersion around the mean magnification is stronger for perturbation theory ($\sim 10\%$) than for both LTB and Kottler Swiss-cheese models ($\sim 2\%$).

VII.   COSMOLOGICAL CONSEQUENCES

Since the Hubble diagram is modified by the presence of inhomogeneities, the resulting determination of the cosmological parameters must be affected as well.

More precisely, consider a Swiss-cheese universe whose FL regions are characterized by a set of cosmological parameters $(\Omega_{\text{m}}, \Omega_K, \Omega_\Lambda)$, called *background* parameters in the following. If an astronomer observes SNe in this inhomogeneous universe and constructs the resulting Hubble diagram, but fits it with the usual FL luminosity-redshift relation—that is, assuming that he lives in a strictly homogeneous universe—then he will infer *apparent* cosmological parameters $(\bar{\Omega}_{\text{m}}, \bar{\Omega}_K, \bar{\Omega}_\Lambda)$ which shall differ from the background ones. Evaluating this difference is the purpose of Subsecs. VII A, VII B, and VII C.

The natural question which comes after is, assuming that our own Universe is well described by a Swiss-cheese model, what are the *background* cosmological parameters which best reproduce the actual SN observations? This issue is addressed in Subsec. VII D.

A.   Generating mock Hubble diagrams

The Hubble diagram observed in a given Swiss-cheese universe is constructed in the following way. We first choose the parameters of the model: f, M, and the background cosmology $(\Omega_{\text{m}}, \Omega_\Lambda = 1 - \Omega_{\text{m}})$.[3] We then fix arbitrarily the position of the observer in the FL region, and we simulate observations by picking randomly the line of sight $\vec{d}$, the redshift $z \in [0, z_{\text{max}}]$, and we compute the associated luminosity distance $D_{\text{L}}(z, \vec{d})$ as in Sec. VI. In order to make our mock SNe catalog resemble the SNLS 3 data set [77], we choose $z_{\text{max}} = 1.4$ and $N_{\text{obs}} = 472$.

An example of mock Hubble diagram, corresponding to a Swiss-cheese model with $f = f_{\text{min}}$, $M = 10^{11} M_\odot$ and $(\Omega_{\text{m}}, \Omega_K, \Omega_\Lambda) = (1, 0, 0)$ is plotted in Fig. 18. As a comparison, we also displayed $D_{\text{L}}(z)$ for a homogeneous universe with (1) the same cosmological parameters, and (2) with $(\Omega_{\text{m}}, \Omega_K, \Omega_\Lambda) = (0.3, 0, 0.7)$.
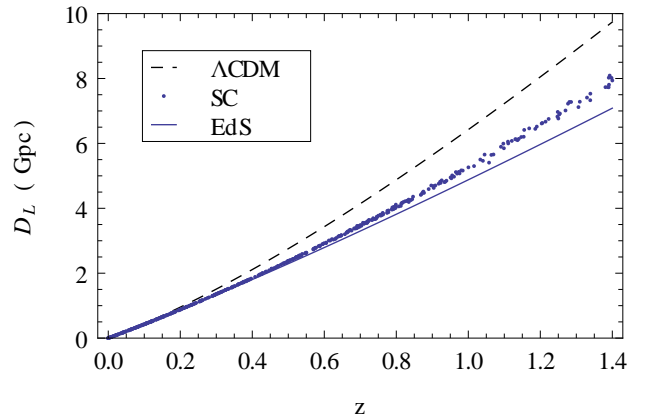

FIG. 18. Hubble diagram of a Swiss-cheese universe (dots) with $f = f_{\text{min}}$, $M = 10^{11} M_\odot$ and EdS background cosmology. For comparison, we also display the distance-redshift relations of purely FL universes, with EdS parameters (blue, solid) and $(\Omega_{\text{m}}, \Omega_K, \Omega_\Lambda) = (0.3, 0, 0.7)$—(black, dashed).

B.   Determining apparent cosmological parameters

The apparent cosmological parameters $\bar{\Omega}_{\text{m}}$, $\bar{\Omega}_\Lambda$ and $\bar{\Omega}_K = 1 - \bar{\Omega}_{\text{m}} - \bar{\Omega}_\Lambda$ are determined from the mock Hubble diagrams by performing a χ^2 fit. The χ^2 is defined by

$$\chi^2(\bar{\Omega}_{\text{m}}, \bar{\Omega}_\Lambda) \equiv \sum_{i=1}^{472} \left[\frac{\mu_i - \mu_{\text{FL}}(z_i \,|\, \bar{\Omega}_{\text{m}}, \bar{\Omega}_\Lambda)}{\Delta \mu_i} \right]^2, \quad (7.1)$$

where μ no longer denotes the magnification, but rather the distance modulus associated with D_{L}, so that

$$\mu \equiv 5 \log_{10} \left(\frac{D_{\text{L}}}{10\,\text{pc}} \right). \quad (7.2)$$

---

[3] Recall that in the practical implementation of the theoretical results (see Subsec. IV C), we assumed that $K = 0$, so that the background cosmology of our Swiss-cheese models is completely determined by Ω_{m} or Ω_Λ. Nevertheless, the *apparent* curvature parameter $\bar{\Omega}_K$ is *a priori* nonzero.

In Eq. (7.1), (z_i, μ_i) is the ith observation of the simulated catalog. In order to make the analysis more realistic, we have attributed to each data point an observational error bar $\Delta \mu_i$ estimated by comparison with the SNLS 3 data set [77]. Besides, $\mu_{\mathrm{FL}}(z \,|\, \bar{\Omega}_{\mathrm{m}}, \bar{\Omega}_{\Lambda})$ is the theoretical distance modulus of a source at redshift z, in a FL universe with cosmological parameters $\bar{\Omega}_{\mathrm{m}}, \bar{\Omega}_{\Lambda}, \bar{\Omega}_K = 1 - \bar{\Omega}_{\mathrm{m}} - \bar{\Omega}_{\Lambda}$.

The results of this analysis for two mock Hubble diagrams are shown in Fig. 19. An EdS background leads to apparent parameters $(\bar{\Omega}_{\mathrm{m}}, \bar{\Omega}_K, \bar{\Omega}_{\Lambda}) = (0.5, 0.8, -0.3)$, which are very different from $(1, 0, 0)$. Thus, the positive shift of $D_{\mathrm{L}}(z)$—clearly displayed in Fig. 18—turns out to be mostly associated to an apparent spatial curvature, rather than to an apparent cosmological constant. In this case the apparent curvature is necessary to obtain a good fit ($\bar{\Omega}_K = 0$ is out of the 2σ confidence contour), because a spatially flat FL model does not allow us to reproduce both the low-z and high-z behaviors of the diagram. The effect is weaker for a background with $(\Omega_{\mathrm{m}}, \Omega_{\Lambda}) = (0.3, 0.7)$, which leads to $(\bar{\Omega}_{\mathrm{m}}, \bar{\Omega}_K, \bar{\Omega}_{\Lambda}) = (0.2, 0.2, 0.6)$.

C. Quantitative results

1. Influence of the smoothness parameter

Consider a Swiss-cheese model with EdS background cosmology. Figure 20 shows the evolution of the apparent cosmological parameters with smoothness f. As expected, we recover $\bar{\Omega}_i = \Omega_i$ when $f = 1$, the discrepancy between background and apparent cosmological parameters being maximal when $f = f_{\min}$. Surprisingly, a Swiss-cheese universe seems progressively dominated by a negative spatial curvature for small values of f.
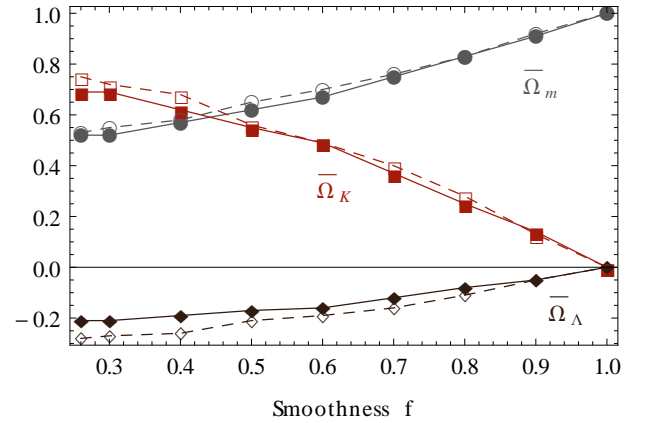
FIG. 20. Apparent cosmic parameters $\bar{\Omega}_{\mathrm{m}}$ (gray disks), $\bar{\Omega}_K$ (red squares) and $\bar{\Omega}_{\mathrm{m}}$ (black diamonds) versus smoothness parameter f, for a Swiss-cheese universe with EdS background $(\Omega_{\mathrm{m}}, \Omega_K, \Omega_{\Lambda}) = (1, 0, 0)$. Solid lines and filled markers correspond to $M = 10^{11} M_{\odot}$, dashed lines and empty markers to $M = 10^{15} M_{\odot}$.

The apparent deceleration parameter $\bar{q} = \bar{\Omega}_{\mathrm{m}}/2 - \bar{\Omega}_{\Lambda}$ is plotted in Fig. 21 as a function of f. Interestingly, even for $f = f_{\min}$, $\bar{q}$ remains almost equal to its background value $q = 1/2$. Therefore, though the apparent cosmological parameters can strongly differ from the background ones, the apparent expansion history is almost the same—at second order—as the background one.

Note that the results displayed in Figs. 20 and 21 are consistent with each other. The apparent cosmological constant $\bar{\Omega}_{\Lambda}$ is slightly smaller for $M = 10^{15} M_{\odot}$ than for $M = 10^{11} M_{\odot}$, so that $\bar{q}$ is slightly larger.
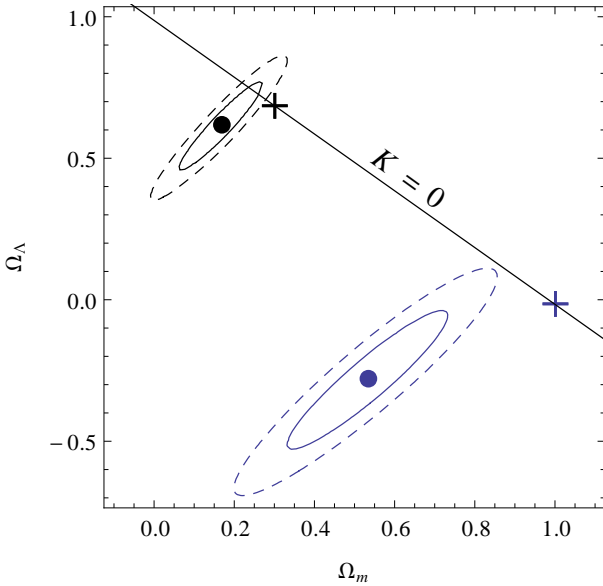
FIG. 19. Comparison between background parameters (crosses) and apparent parameters (disks) for two Swiss-cheese models with $f = f_{\min}$ and $M = 10^{15} M_{\odot}$. In blue, $(\Omega_{\mathrm{m}}, \Omega_{\Lambda}) = (1, 0)$ leads to $(\bar{\Omega}_{\mathrm{m}}, \bar{\Omega}_{\Lambda}) = (0.5, -0.3)$. In black, $(\Omega_{\mathrm{m}}, \Omega_{\Lambda}) = (0.3, 0.7)$ leads to $(\bar{\Omega}_{\mathrm{m}}, \bar{\Omega}_{\Lambda}) = (0.2, 0.6)$. The 1σ and 2σ contours are respectively the solid and dashed ellipses. The solid straight line indicates the configurations with zero spatial curvature.

2. Influence of the background cosmological constant

Now consider a Swiss-cheese model with $f = f_{\min}$ and change its background cosmology. Figure 22 shows the evolution of the apparent cosmological parameters versus the background cosmological constant Ω_{Λ}. As it could have already been suspected from Fig. 19, the difference between apparent and background parameters decreases with Ω_{Λ}, and vanishes in a de Sitter universe.
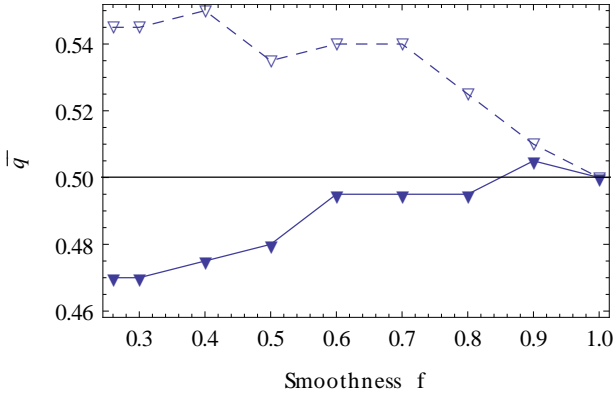
FIG. 21. Apparent deceleration parameter $\bar{q}$ as a function of smoothness parameter f, for Swiss-cheese models with EdS background ($q = 1/2$). Solid lines and filled markers correspond to $M = 10^{11} M_\odot$, dashed lines and empty markers to $M = 10^{15} M_\odot$.

FIG. 23. Difference between apparent and background deceleration parameters $\bar{q} - q$ as a function of q, for Swiss-cheese models with $f = f_{\min}$. Solid lines and filled markers correspond to $M = 10^{11} M_\odot$, dashed lines and empty markers to $M = 10^{15} M_\odot$.

This can be understood as follows. The construction of a Swiss-cheese universe consists in changing the spatial distribution of the pressureless matter, while the cosmological constant remains purely homogeneous. Thus, the geometry of spacetime is less affected by the presence of inhomogeneities if $\Omega_\Lambda/\Omega_{\rm m}$ is greater. In the extreme case $(\Omega_{\rm m}, \Omega_\Lambda) = (0, 1)$, any Swiss cheese is identical to its background, since there is no matter to be reorganized.
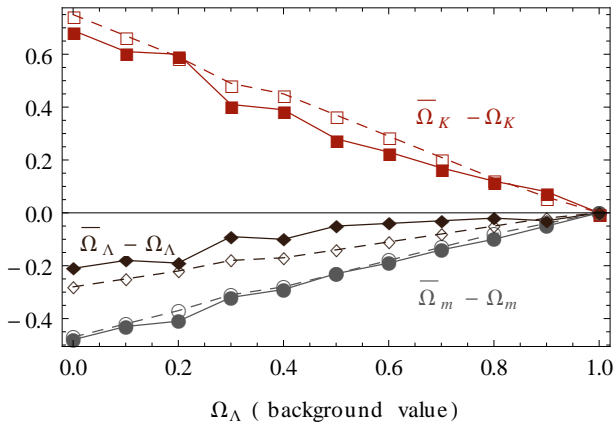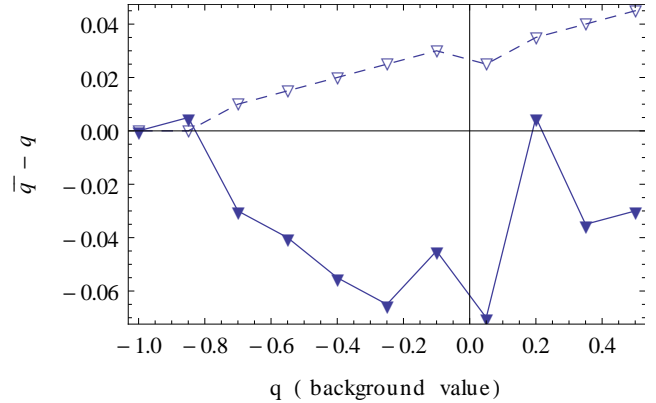

FIG. 22. Difference between apparent and background cosmological parameters $\bar{\Omega}_{\rm m} - \Omega_{\rm m}$ (gray disks), $\bar{\Omega}_K - \Omega_K$ (red squares) and $\bar{\Omega}_\Lambda - \Omega_\Lambda$ (black diamonds) versus background Ω_Λ, for Swiss-cheese models with $f = f_{\min}$. Solid lines and filled markers correspond to $M = 10^{11} M_\odot$, dashed lines and empty markers to $M = 10^{15} M_\odot$.

We also plot in Fig. 23 the difference between the apparent deceleration parameter $\bar{q}$ and the background one $q = \Omega_{\rm m}/2 - \Omega_\Lambda$, as a function of q. Again, $\bar{q}$ does not significantly differ from q. This result must be compared with Fig. 11 of Ref. [53], where $(\bar{q} - q)/q \approx 100\%$.

3.   *Comparison with other recent studies*

The impact of a modified luminosity-redshift relation—due to inhomogeneities—on the cosmological parameters has already been investigated by several authors. In Ref. [55], it has been suggested that a Swiss-cheese model with LTB holes and EdS background displays an apparent cosmological constant $\bar{\Omega}_\Lambda = 0.4$; but as already mentioned in Subsec. VI D, such a claim was proven to be inaccurate in Refs. [57, 58, 62], because it relies on observations along a peculiar line of sight. When many random directions of observation are taken into account, the mean magnification goes back to 1. Hence, contrary to our results, the apparent cosmological parameters of a Swiss-cheese model with LTB holes are identical to the background ones. This conclusion is in agreement with Ref. [78], where similar studies are performed in various cosmological toy models; and also with Ref. [31] in the framework of perturbation theory.

However, it is crucial to distinguish those approaches (LTB Swiss-cheese models and perturbation theory) from the one adopted in this article, because they do not address the same issue. The former share the purpose of evaluating the influence of inhomogeneities smoothed on large scales, while we focused on smaller scales for which matter cannot be considered smoothly distributed. Thus, our results must not be considered different, but rather complementary.

D.   **An alternative way to fit the Hubble diagram**

Let us now address the converse problem, and determine the background cosmological parameters of the Swiss-cheese model that best reproduces the actual observations. For that purpose, the simplest method would be to fit our observed Hubble diagram using the theoretical luminosity-

redshift relation $D_{\mathrm{L}}^{\mathrm{SC}}(z)$ of a Swiss-cheese universe. Hence, we need to derive such a relation in order to proceed.

1. Analytical estimation of the distance-redshift relation of a Swiss-cheese universe

As argued in Sec. V, any observationally relevant light beam which crosses a Kottler region has an impact parameter b much larger than the Schwarzschild radius r_{S} of the central object. Moreover, since the cosmological constant has no effect on light focusing, we conclude that inside a hole, the evolution of the cross-sectional area of a light beam behaves essentially as in Minkowski spacetime. This conclusion is supported by the perturbative calculation of the Wronski matrix $\boldsymbol{\mathcal{W}}_{\mathrm{K}}$ performed in § IV B 6.

If both the observer and the source are located on the surface of a hole, their angular distance is therefore $D_{\mathrm{A}}^{\mathrm{hole}} = \sqrt{\det \boldsymbol{\mathcal{D}}} \approx v_{\mathrm{out}} - v_{\mathrm{in}}$, where v denotes the affine parameter. More generally, for a beam which crosses N contiguous holes, we get

$$D_{\mathrm{A}}^{\mathrm{holes}} \approx \sum_{i=1}^{N} \Delta v_i, \qquad (7.3)$$

where $\Delta v_i \equiv v_{\mathrm{out},i} - v_{\mathrm{in},i}$ is the variation of the affine parameter between entrance into and exit from the ith hole. Let us now evaluate Δv_i. The time part of the geodesic equation in Kottler geometry yields

$$k^t \equiv \frac{\mathrm{d}t}{\mathrm{d}v} = \frac{E}{A(r)} \stackrel{r \gg r_{\mathrm{S}}}{\approx} E = \text{constant}, \qquad (7.4)$$

where E is the usual constant of motion. We conclude that $\Delta v_i \approx k_{\mathrm{out},i}^t \Delta t_i$. Besides, the relations (2.16) and (4.11) between FL and Kottler coordinates on the junction hypersurface, together with $A(r_{\mathrm{h}}) \approx 1$, lead to $\Delta t_i \approx \Delta T_i$ and $k_{\mathrm{out}}^t \approx a_{\mathrm{out}}/a_0$. Finally,

$$D_{\mathrm{A}}^{\mathrm{holes}} \approx \sum_{i=1}^{N} \frac{a_{\mathrm{out},i}}{a_0} \Delta T_i \approx \int_{T}^{T_{\mathrm{obs}}} \frac{a(T')}{a_0} \, \mathrm{d}T', \qquad (7.5)$$

where we approximated the sum over i by an integral. This operation is valid as far as ΔT_i remains small compared to the Hubble time. In terms of redshifts, we have

$$D_{\mathrm{A}}^{\mathrm{holes}}(z) = \int_{0}^{z} \frac{\mathrm{d}z'}{(1+z')^2 H(z')}. \qquad (7.6)$$

By construction, this formula describes the behavior of the angular distance when light only travels through Kottler regions. In order to take the FL regions into account, we write the distance-redshift relation $D_{\mathrm{A}}^{\mathrm{SC}}(z)$ of the Swiss cheese as the following (heuristic) linear combination

$$D_{\mathrm{A}}^{\mathrm{SC}}(z) = (1-f) \, D_{\mathrm{A}}^{\mathrm{holes}}(z) + f \, D_{\mathrm{A}}^{\mathrm{FL}}(z), \qquad (7.7)$$

where f still denotes the smoothness parameter defined in § VI A 1, and $D_{\mathrm{A}}^{\mathrm{FL}}(z)$ is the distance-redshift relation in a FL universe, given by Eq. (4.10).

A comparison between the above analytical estimation and the numerical results is plotted in Fig. 24. The agreement is qualitatively good, especially as it is obtained without any fitting procedure. Moreover, it is straightforward to show that $D_{\mathrm{A}}^{\mathrm{SC}}(z)$ and $D_{\mathrm{A}}^{\mathrm{FL}}(z)$ are identical up to second order in z. This is in agreement with—and somehow explains—the numerical results of § VII C 1 and § VII C 2, where we showed that the apparent deceleration parameter $\bar{q}$ is the same as the background one q.

Note finally that the general tendency of our analytical relation is to overestimate δD_{L} at high redshifts. The main reason is that its derivation uses the behavior of $\boldsymbol{\mathcal{W}}_{\mathrm{K}}$ at zeroth order in r_{S}/b; that is, it neglects the effect of the central mass in the Kottler region. The first-order term in $\boldsymbol{\mathcal{W}}_{\mathrm{K}}$—taken into account in the numerical results—tends to lower the associated luminosity distance.
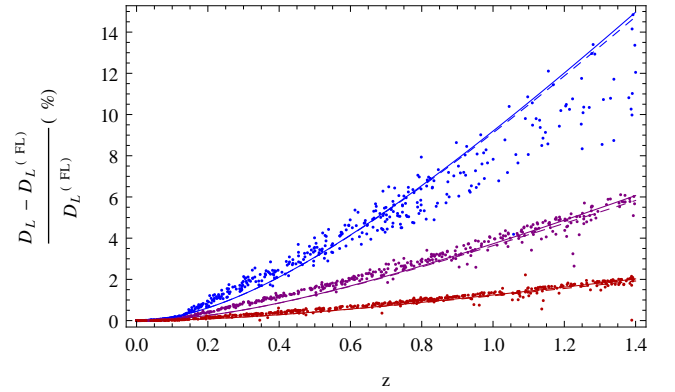
FIG. 24. Comparison between the approximate luminosity-redshift relation $D_{\mathrm{L}}^{\mathrm{SC}}(z) = (1+z)^2 D_{\mathrm{A}}^{\mathrm{SC}}(z)$ in a Swiss-cheese universe (solid lines), simulated observations (dots), and the Dyer-Roeder model $D_{\mathrm{L}}^{\mathrm{DR}}(z)$ with $\alpha(z) = f$ (dashed lines). Three different values of the smoothness parameter are tested, from top to bottom: $f = f_{\min} \approx 0.26$, $f = 0.7$, $f = 0.9$.

2. Comparison with the Dyer-Roeder approach

Another widely used approximation to model the propagation of light in underdense regions was proposed by Dyer and Roeder [10] in 1972. It assumes that (1) the Sachs equation and the relation $v(z)$ are the same as in a FL spacetime—in particular, the null shear vanishes—and (2) the optical parameter Φ_{00} (see § III B 2) is replaced by $\alpha(z)\Phi_{00}$, where $\alpha(z)$ represents the fraction of matter intercepted by the geodesic bundle. In brief, the DR model encodes that light propagates mostly in underdense regions by reducing the Ricci focusing, while still neglecting the Weyl focusing. Under such conditions, the DR ex-

pression of the angular distance $D_A^{DR}(z)$ is determined by

$$
\frac{d^2 D_A^{DR}}{dz^2} + \left(\frac{d \ln H}{dz} + \frac{2}{1+z} \right) \frac{d D_A^{DR}}{dz}
$$
$$
= -\frac{3\,\Omega_m}{2} \left(\frac{H_0}{H} \right)^2 (1+z)\,\alpha(z)\,D_A^{DR}(z). \quad (7.8)
$$

This attempt to model the average effect of inhomogeneities, while assuming that the dynamics of the Universe is the same as an isotropic and homogeneous spacetime, has been widely questioned [79–82] and recently argued to be mathematically inconsistent [8].

Interestingly, our estimation $D_A^{SC}(z)$ of the distance-redshift relation in a Swiss-cheese universe reads

$$
\frac{d^2 D_A^{SC}}{dz^2} + \left(\frac{d \ln H}{dz} + \frac{2}{1+z} \right) \frac{d D_A^{SC}}{dz}
$$
$$
= -\frac{3\,\Omega_m}{2} \left(\frac{H_0}{H} \right)^2 (1+z)\,f\,D_A^{FL}(z). \quad (7.9)
$$

which is similar to Eq. (7.8) with $\alpha(z) = f$, except that the right-hand side is proportional to D_A^{FL} instead of D_A^{SC}. Nevertheless, it turns out that such a difference has only a very weak impact, in the sense that

$$
D_A^{SC}(z) \approx D_A^{DR}(z), \quad \text{i.e.} \quad D_L^{SC}(z) \approx D_L^{DR}(z), \quad (7.10)
$$

if $\alpha(z) = f$. This appears clearly in Fig. 24, where the dashed and solid lines are almost superimposed. In fact, it is not really surprising, since both approaches rely on the same assumptions: no backreaction, no Weyl focusing and an effective reduction of the Ricci focusing.

Note however that this approach models the effect of the inhomogeneities on the mean value of the luminosity distance but does not address the dispersion of the data.

3.   Fitting real data with $D_L^{SC}(z)$

The modified luminosity-redshift relation $D_L^{SC}(z)$ derived in the previous paragraph can be used to fit the observed Hubble diagram. We apply the same χ^2 method as described in Subsec. VII B, except that now (1) the triplets $(z_i, \mu_i, \Delta\mu_i)$ are observations of the SNLS 3 catalog [77], and (2) $\mu_{FL}(z \,|\, \bar{\Omega}_m, \bar{\Omega}_\Lambda)$ is replaced by $\mu_{SC}(z \,|\, \Omega_m, f)$, where the background curvature Ω_K is fixed to 0 (so that $\Omega_\Lambda = 1 - \Omega_m$). Hence, we are looking for the smoothness parameter f, and the background cosmological parameters, of the spatially Euclidean Swiss-cheese model which best fits the actual SN observations.

The results of the χ^2 fit are displayed in Fig. 25. First of all, we note that the confidence areas are very stretched horizontally, so that the smoothness parameter f cannot be reasonably constrained by the Hubble diagram. There are two reasons for this. On the one hand, we know from § VII C 2 that f has only a weak influence on the luminosity-redshift relation in a universe dominated by the cosmological constant, which is the case here ($\Omega_\Lambda \sim$

0.7–0.8). On the other hand, since $D_L^{SC}(z)$ and $D_L^{FL}(z)$ only differ by terms of order z^3 and higher, one would need more high-redshift observations to discriminate them. However, all the current SNe catalogs—including the SNLS 3 data set—contain mostly low-redshift SNe.

Besides, Fig. 25 shows that fixing a given value of f changes the best-fit value of Ω_m. In the extreme case of a Swiss cheese only made of clumps ($f = 0$) we get $\Omega_m = 0.3$, while in the FL case ($f = 1$) the best value is $\Omega_m = 0.24$, in agreement with Ref. [77]. Such a discrepancy, of order $20\,\%$, is significant in the era of precision cosmology, where one aims at determining the cosmological parameters at the percent level.

Let us finally emphasize that such a fit is only indicative, because it relies on an approximation of the luminosity-redshift relation in a Swiss-cheese universe.
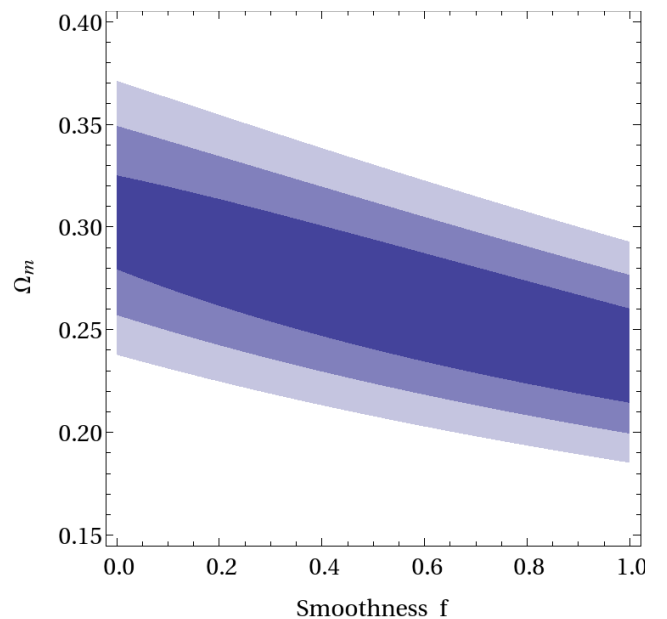

FIG. 25.   Fit of the Hubble diagram constructed from the SNLS 3 data set [77], by using the luminosity-redshift relation $D_L^{SC}(z \,|\, \Omega_m, f)$ of a spatially Euclidean Swiss-cheese model. The colored areas indicate (from the darkest to the lightest) the 1σ, 2σ and 3σ confidence levels.

VIII.   CONCLUSION

In this article, we have investigated the effect of the distribution of matter on the Hubble diagram, and on the resulting inference of the cosmological parameters. For that purpose, we have studied light propagation in Swiss-cheese models. This class of exact solutions of the Einstein field equations is indeed very suitable, because it can describe a strongly inhomogeneous distribution of matter which does not backreact on the global cosmic expansion. The latter is entirely governed by the background cosmological parameters Ω_m, Ω_Λ characterizing the FL

regions of the model. The inhomogeneities are clumps of mass M, while the fraction of remaining fluid matter is f—called smoothness parameter. The Swiss-cheese models are therefore defined by two "dynamical" parameters $(\Omega_\mathrm{m}, \Omega_\Lambda)$, and two "structural" parameters (f, M).

The laws of light propagation in a Swiss-cheese universe have been determined by solving the geodesic equation and the Sachs equation. For the latter, we have introduced a new technique—based on the Wronski matrix—in order to deal more easily with a patchwork of spacetimes. Our results, mostly analytical, have been included in a Mathematica program, and used to compute the impact of the Swiss-cheese holes on the redshift and on the luminosity distance. For a light beam which crosses many holes, we have shown that the effect on the redshift remains negligible, while the luminosity distance increases significantly with respect to the one observed in a FL universe ($\delta D_\mathrm{L} \sim 10\,\%$ for sources at $z \sim 1$), inducing a bias in the Hubble diagram.

The consequences of the bias on the inference of the cosmological parameters have been investigated by simulating Hubble diagrams for various Swiss-cheese models, and by fitting them with the usual FL luminosity-redshift relation. In general, the resulting "apparent" cosmological parameters are very different from the "background" ones which govern the cosmic expansion, but in a way that leaves the deceleration parameter unchanged. Moreover, the discrepancy between apparent and background cosmological parameters turns out to decrease with Λ, and is therefore small for a universe dominated by the cosmological constant. Finally, we have derived an approximate luminosity-redshift relation for Swiss-cheese models, which is similar to the one obtained following the Dyer-Roeder approach. Using this relation to fit the Hubble diagram constructed from the SNLS 3 data set, we have found that the smoothness parameter cannot be constrained by such observations. However, turning arbitrarily $f = 1$ into $f = 0$ has an impact of order $20\,\%$ on the best-fit value of Ω_m, which is significant in the era of precision cosmology (see Ref. [83] for further discussion).

Of course, our model is oversimplifying for various reasons. First, it does not take into account either the complex distribution of the large scale structures, or the presence of diffuse matter on small scales—such as gas and possibly dark matter. Second, it does not take strong lensing effects into account, assuming that clumps are "opaque". We can conjecture that this overestimates the actual effect of the inhomogeneities. Nevertheless, it shows that their imprint on the Hubble diagram cannot be neglected, and should be modeled beyond the perturbation regime. Note finally that several extensions are allowed by our formalism. For instance, we could introduce different kinds of inhomogeneities, in order to construct fractal structures for which the smoothness parameter is arbitrarily close to zero. Additionally to the Hubble diagrams, we could also generate the shear maps of Swiss-cheese models, and determine whether their combination allows for better constraints on the various parameters.

This work explicitly raises the question of the meaning of the cosmological parameters, and of whether the values we measure under the hypothesis of a pure FL background represent their "true" or some "dressed" values. Similar ideas have actually been held in other contexts [84, 85], and in particular regarding the spatial curvature [86, 87]. We claim that the simplest Swiss-cheese models are good models to address such questions—as well as the Ricci-Weyl problem and the fluid approximation—with their own use, between the perturbation theory and N-body simulations.

[1] P. Peter and J.-P. Uzan, *Primordial Cosmology* (Oxford University Press, New York, 2009).

[2] G.F.R. Ellis and T. Buchert, Phys. Lett. A **347**, 38 (2005), `arXiv:gr-qc/0506106`.

[3] G.F.R. Ellis and W. Stoeger, Classical Quantum Gravity **4**, 1697 (1987).

[4] T. Buchert, Gen. Relativ. Gravit. **32**, 105 (2000), `arXiv:gr-qc/9906015`; **33**, 1381 (2001), `arXiv:gr-qc/0102049`; S. Räsänen, J. Cosmol. Astropart. Phys. 02 (2004) 003, `arXiv:astro-ph/0311257`; E.

Barausse, S. Matarrese, and A. Riotto, Phys. Rev. D **71**, 063537 (2005), `arXiv:astro-ph/0501152`; E. W. Kolb, S. Matarrese, and A. Riotto, New J. Phys. **8**, 322 (2006), `arXiv:astro-ph/0506534` S. Räsänen, J. Cosmol. Astropart. Phys. 11 (2006) 003 `arXiv:astro-ph/0607626`; M. Kasai, Prog. Theor. Phys. **117**, 1067 (2007), `arXiv:astro-ph/0703298`.

[5] A. Ishibashi and R. M. Wald, Classical Quantum Gravity **23**, 235 (2006), `arXiv:gr-qc/0509108`; E. E. Flanagan, Phys. Rev. D **71**, 103521 (2005), `arXiv:hep-th/0503202`

C. M. Hirata and U. Seljak, Phys. Rev. D **72**, 083501 (2005), `astro-ph/0503582`; S. R. Green and R. M. Wald, Phys. Rev. D **83**, 084020 (2011),`arXiv:1011.4920`.

[6] E. W. Kolb, S. Matarrese, A. Notari, and A. Riotto, Phys. Rev. D **71**, 023524 (2005), `arXiv:hep-ph/0409038`; N. Li and D. J. Schwarz, Phys. Rev. D **76**, 083011 (2007), `arXiv:gr-qc/0702043`; N. Li and D. J. Schwarz, Phys. Rev. D **78**, 083531 (2008), `arXiv:0710.5073`; C. Clarkson, K. Ananda, and J. Larena, Phys. Rev. D **80**, 083525 (2009); `arXiv:0907.3377`; O. Umeh, J. Larena, and C. Clarkson, J. Cosmol. Astropart. Phys. 03 (2011) 029, `arXiv:1011.3959`; G. Marozzi, J.-P. Uzan, Phys. Rev. D **86**, 063528 (2012), `arXiv:1206.4887`.

[7] C. Clarkson, G. Ellis, J. Larena and O. Umeh, Rep. Prog. Phys. **74**, 112901 (2011), `arXiv:1109.2314`.

[8] C. Clarkson, G.F.R. Ellis, A. Faltenbacher, R. Maartens, O. Umeh, J.-P. Uzan, Month. Not. R. Astron. Soc. **426**, 1121 (2012), `arXiv:1109.2484`.

[9] Ya. B. Zel'dovich, Astron. Zh. **41**, 19 (1964) [Sov. Astron. **8**, 13 (1964)].

[10] C. C. Dyer and R. C. Roeder, Astrophys. J. **174**, L115 (1972); C. C. Dyer and R. C. Roeder, Astrophys. J. **180**, L31 (1973).

[11] V. M. Dashevskii and V. I. Slysh, Astron. Zh. **42**, 863 (1965) [Sov. Astron. **9**, 671 (1966)].

[12] B. Bertotti, Proc. R. Soc. (London) A **294**, 195 (1966).

[13] J. E. Gunn, Astrophys. J. **147**, 61 (1967); J. E. Gunn, Astrophys. J. **150**, 737 (1967).

[14] S. Refsdal, Astrophys. J. **159**, 357 (1970).

[15] S. Weinberg, Astrophys. J. **208**, L1 (1976).

[16] C.C. Dyer and R.C. Roeder, Gen. Relat. Grav. **13**, 1157 (1981).

[17] L. Fang and X. Wu, Chin. Phys. Lett. **6**, 223 (1989); X. Wu, Astron. Astrophys. **239**, 29 (1990).

[18] H. G. Rose, Astrophys. J. **560**, L15 (2001); `arXiv:astro-ph/0106489`.

[19] T. W. B. Kibble and R. Lieu, Astrophys. J. **632**, 718 (2005), `arXiv:astro-ph/0412275`.

[20] V. Kostov, J. Cosmol. Astropart. Phys. 04 (2010) 001, `arXiv:0910.2611`.

[21] E.V. Linder, Astron. Astrophys. **206**, 190 (1988).

[22] K. Tomita, Prog. Theor. Phys. **100**, 79 (1998), `arXiv:astro-ph/9806047`.

[23] E. Mortsell, `arXiv:astro-ph/0109197`.

[24] K. Bolejko, Mon. Not. R. Astron. Soc. **412**, 1937 (2011), `arXiv:1011.3876`.

[25] R. Takahashi, M. Oguri, M. Sato, and T. Hamana, `arXiv:1106.3823`.

[26] U. Seljak and D. E. Holz, Astron. Astrophys. Lett. **351**, L10 (1999), `astro-ph/9910482`.

[27] R. B. Metcalf and J. Silk, Astrophys. J. **519**, L1 (1999), `arXiv:astro-ph/9901358`.

[28] R. B. Metcalf and J. Silk, Phys. Rev. Lett. **98**, 071302 (2007), `arXiv:astro-ph/0612253`.

[29] R. Kantowski, T. Vaughan, and D. Branch, Astrophys. J. **447**, 35 (1995), `arXiv:astro-ph/9511108`; J.A. Frieman, Commun. Astrophys. **18**, 323 (1996), `arXiv:astro-ph/9608068`; Y. Wang, Astrophys. J. **531**, 676 (2000); Y. Wang, Astrophys. J. **536**, 531 (2000); Y. Wang, J. Cosmol. Astropart. Phys. 03 (2005) 5.

[30] C. Bonvin, R. Durrer, and M. A. Gasparini, Phys. Rev. D **73**, 023523 (2006), `arXiv:astro-ph/0511183`.

[31] P. Valageas, Astron. Astrophys. **354**, 767, (2000), `arXiv:astro-ph/9904300v2`.

[32] N. Meures and M. Bruni, Mon. Not. R. Astron. Soc. **419**, 1937 (2012), `arXiv:1107.4433`.

[33] I. Ben-Dayan, M. Gasperini, G. Marozzi, F. Nugier, and G. Veneziano, Phys. Rev. Lett. **110**, 021301 (2013), `arXiv:1207.1286`.

[34] E. Di Dio and R. Durrer, Phys. Rev. D **86**, 023510 (2012), `arXiv:1205.3366`.

[35] I. Ben-Dayan, M. Gasperini, G. Marozzi, F. Nugier, and G. Veneziano, `arXiv:1302.0740`.

[36] D. E. Holz and E. V. Linder, Astrophys. J. **631**, 678 (2005), `arXiv:astro-ph/0412173`.

[37] A. Cooray, D. Holz, and D. Huterer, Astrophys. J. **637**, L77 (2006), `arXiv:astro-ph/0509579`; S. Dodelson and A. Vallinotto, Phys. Rev. D **74**, 063515 (2006), `arXiv:astro-ph/0511086`.

[38] A. Cooray, D. Huterer, and D. Holz, Phys. Rev. Lett. **96**, 021301 (2006), `arXiv:astro-ph/0509581`.

[39] D. Sarkar, A. Amblard, D. E. Holz, and A. Cooray, `arXiv:0710.4143`.

[40] A. R. Cooray, D. E. Holz, and R. Caldwell, J. Cosmol. Astropart. Phys. 11 (2010) 015, `arXiv:0812.0376`.

[41] A. Vallinotto, S. Dodelson, and P. Zhang, `arXiv:1009.5590`.

[42] B. Ménard, T. Hamana, M. Bartelmann, and N. Yoshida, Astron. Astrophys. **403**, 817 (2003), `arXiv:astro-ph/0210112`

[43] N. Dalal, D. E. Holz, X. l. Chen, and J. A. Frieman, Astrophys. J. **585**, L11 (2003), `arXiv:astro-ph/0206339`.

[44] K. P. Rauch, Astrophys. J. **374**, 83 (1991).

[45] D. E. Holz and R. M. Wald, Phys. Rev. D **58**, 063501 (1998), `arXiv:astro-ph/9708036`.

[46] R. W. Lindquist and J. A. Wheeler, Rev. Mod. Phys. **29**, 432 (1957).

[47] E. Gausmann, R. Lehoucq, J.-P. Luminet, J.-P. Uzan, and J. Weeks, Classical Quantum Gravity **18**, 5155 (2001), `arXiv:gr-qc/0106033`; R. Lehoucq, J. Weeks, J.-P. Uzan, E. Gausmann, and J.-P. Luminet, Classical Quantum Gravity **19**, 4683 (2002), `arXiv:gr-qc/0205009`; J. Weeks, R. Lehoucq, and J.-P. Uzan, Classical Quantum Gravity **20**, 1529 (2003), `arXiv:astro-ph/0209389`; J.-P. Uzan, A. Riazuelo, R. Lehoucq, and J. Weeks, Phys. Rev. D **69**, 043003 (2004), `arXiv:astro-ph/0303580`.

[48] T. Clifton and P.G. Ferreira, Phys. Rev. D **80**, 103503 (2009), `arXiv:0907.4109`; T. Clifton and P.G. Ferreira, J. Cosmol. Astropart. Phys. 10 (2009) 26, `arXiv:0908.4488`.

[49] J.-P. Bruneton and J. Larena, Classical Quantum Gravity **29** (2012) 155001, `arXiv:1204.3433`; J.-P. Bruneton and J. Larena, Class. Quantum Grav. **30** (2013) 025002, `arXiv:1208.1411`.

[50] K. Kainulainen and V. Marra, Phys. Rev. D **80**, 127301 (2009), `arXiv:0906.3871`. K. Kainulainen and V. Marra, Phys. Rev. D **83**, 023009 (2011), `arXiv:1011.0732`.

[51] A. Einstein and E.G. Straus, Rev. Mod. Phys. **17**, 120 (1945); **18**, 148 (1946).

[52] R. Kantowski, Astrophys. J. **155**, 89 (1969).

[53] C. C. Dyer and R. C. Roeder, Astrophys. J. **189**, 167 (1974).

[54] N. Brouzakis, N. Tetradis, and E. Tzavara, J. Cosmol. Astropart. Phys. 02 (2007) 013, `arXiv:astro-ph/0612179`.

[55] V. Marra, E. W. Kolb, S. Matarrese, and A. Riotto, Phys. Rev. D **76**, 123004 (2007), `arXiv:0708.3622`.

[56] T. Biswas and A. Notari, J. Cosmol. Astropart. Phys. 06 (2008) 021, `arXiv:astro-ph/0702555`.

[57] R. A. Vanderveld, E. E. Flanagan, and I. Wasserman, Phys. Rev. D **78**, 083511 (2008), `arXiv:0808.1080`.

[58] N. Brouzakis, N. Tetradis, and E. Tzavara, J. Cosmol. Astropart. Phys. 04 (2008) 008, `arXiv:astro-ph/0703586`.

[59] T. Clifton and J. Zuntz, Mon. Not. R. Astron. Soc. **400**, 2185 (2009), `arXiv:0902.0726`.

[60] W. Valkenburg, J. Cosmol. Astropart. Phys. 06 (2009) 010, `arXiv:0902.4698`.

[61] S. J. Szybka, Phys. Rev. D **84**, 044011 (2011), `arXiv:1012.5239`.

[62] E. E. Flanagan, N. Kumar, I. Wasserman, and R. A. Vanderveld; Phys. Rev. D **85**, 023510 (2012), `arXiv:1109.1873`.

[63] F. Kottler, Ann. Phys. (Berlin), **361**, 401 (1918).

[64] H. Weyl, Phys. Z. **20**, 31 (1919).

[65] V. Perlick, Living Rev. in Relativity **7**, 9 (2004), (section 5.2), `http://relativity.livingreviews.org/Articles/lrr-2004-9/`.

[66] W. Israel, Nuovo Cimento B **44**, 1 (1966).

[67] W. Israel, Nuovo Cimento B **48**, 463 (1967).

[68] R. Sachs, Proc. R. Soc. Lond. A **264**, 309 (1961).

[69] P. Schneider, J. Ehlers, and E. E. Falco, *Gravitational Lenses* (Springer, New York, 1992).

[70] Z. Stuchlík, Bull. Astron. Instit. Czechoslovakia, **34**, No. 3, 129 (1983).

[71] Z. Stuchlík, Bull. Astron. Instit. Czechoslovakia **35**, No. 4, 205 (1984).

[72] I. S. Gradshteyn and I. M. Ryzhik, *Table of Integrals, Series, and Products* (Academic Press, New York, 2007).

[73] F. Combes, P. Boissé, A. Mazure, and A. Blanchard, *Galaxies et Cosmologie*, (CNRS, Paris, 2003).

[74] N. Suzuki *et al.*(The Supernova Cosmology Project), Astrophys. J. **746**, 85 (2012), `arXiv:1105.3470`;

[75] S. Perlmutter *et al.*, Astrophys. J. **517**, 565 (1999), `arXiv:astro-ph/9812133`; A.G. Riess *et al.*, Astron. J. **116**, 1009 (1998), `arXiv:astro-ph/9805201`; J.L. Tonry *et al.*, Astrophys. J. **594**, 1 (2003), `arXiv:astro-ph/0305008`; R.A. Knop *et al.*, Astrophys. J. **598**, 102 (2003), `http://arxiv.org/abs/astro-ph/0309368`; A.G. Riess *et al.*, Astrophys. J. **607**, 665 (2004), `http://arxiv.org/abs/astro-ph/0402512`.

[76] K. Bolejko, C. Clarkson, R. Maartens, D. Bacon, N. Meures, and E. Beynon, Phys. Rev. Lett. **110**, 021302 (2013), `arXiv:1209.3142`.

[77] A. Conley *et al.*, Astrophys. J., Suppl. Ser. **192**, 1 (2011), `arXiv:1104.1443`.

[78] K. Bolejko and P. Ferreira, J. Cosmol. Astropart. Phys. 05 (2012) 003, `arXiv:1204.0909`.

[79] J. Ehlers and P. Schneider, Astron. Astrophys. **168**, 57 (1986).

[80] M. Sasaki, Prog. Theor. Phys. **90**, 753 (1993).

[81] K. Tomita, H. Asada, and T. Hamana, Prog. Theor. Phys. Suppl. **133**, 155 (1999), `arXiv:astro-ph/9904351`.

[82] S. Räsänen, J. Cosmol. Astropart. Phys. 02 (2009) 011, `arXiv:0812.2872`.

[83] P. Fleury, H. Dupuy, and J. P. Uzan, `arXiv:1304.7791`.

[84] T. Buchert and M. Carfora, Phys. Rev. Lett. **90**, 031101 (2003); `arXiv:gr-qc/0210045`.

[85] D.L. Wiltshire, New J. Phys. **9**, 377 (2007), `arXiv:gr-qc/0702082`; D.L. Wiltshire, Int. J. Mod. Phys. **D17**, 641(2008), `arXiv:0712.3982`; P.R. Smale and D.L. Wiltshire, Mon. Not. R. Astron. Soc. **413**, 367 (2011), `arXiv:1009.5855`.

[86] C. Clarkson, T. Clifton, A. Coley, and R. Sung, `arXiv:1111.2214`.

[87] A. A. Coley, N. Pelavas, R. M. Zalaletdinov, Phys. Rev. Lett. **95** 151102 (2005), `arXiv:gr-qc/0504115`.

Can all cosmological observations be accurately interpreted with a unique geometry?

Pierre Fleury[1,2],* Hélène Dupuy[1,2,3],† and Jean-Philippe Uzan[1,2‡]

[1] *Institut d'Astrophysique de Paris, UMR-7095 du CNRS,*
Université Pierre et Marie Curie, 98 bis bd Arago, 75014 Paris, France.
[2] *Sorbonne Universités, Institut Lagrange de Paris, 98 bis bd Arago, 75014 Paris, France.*
[3] *Institut de Physique Théorique, CEA, IPhT, URA 2306 CNRS, F-91191 Gif-sur-Yvette, France.*
(Dated: 29 August 2013)

The recent analysis of the Planck results reveals a tension between the best fits for $(\Omega_{\mathrm{m}0}, H_0)$ derived from the cosmic microwave background or baryonic acoustic oscillations on the one hand, and the Hubble diagram on the other hand. These observations probe the universe on very different scales since they involve light beams of very different angular sizes, hence the tension between them may indicate that they should not be interpreted the same way. More precisely, this letter questions the accuracy of using only the (perturbed) Friedmann-Lemaître geometry to interpret all the cosmological observations, regardless of their angular or spatial resolution. We show that using an inhomogeneous "Swiss-cheese" model to interpret the Hubble diagram allows us to reconcile the inferred value of $\Omega_{\mathrm{m}0}$ with the Planck results. Such an approach does not require us to invoke new physics nor to violate the Copernican principle.

PACS numbers: 98.80.-k, 04.20.-q, 42.15.-i.

The standard interpretation of cosmological data relies on the description of the Universe by a spatially homogeneous and isotropic spacetime with a Friedmann-Lemaître (FL) geometry, allowing for perturbations [1]. The emergence of a dark sector, including dark matter and dark energy, emphasizes the need for extra degrees of freedom, either physical (new fundamental fields or interactions) or geometrical (e.g. a cosmological solution with lower symmetry). This has driven a lot of activity to test the hypotheses [2] of the cosmological model, such as general relativity or the Copernican principle.

The recent Planck data were analyzed in such a framework [3] in which the cosmic microwave background (CMB) anisotropies are treated as perturbations around a FL universe, with most of the analysis performed at linear order. Nonlinear effects remain small [4] and below the constraints on non-Gaussianity derived by Planck [5]. The results nicely confirm the standard cosmological model of a spatially Euclidean FL universe with a cosmological constant, dark matter and initial perturbations compatible with the predictions of inflation.

Among the constraints derived from the CMB, the Hubble parameter H_0 and the matter density parameter $\Omega_{\mathrm{m}0}$ are mostly constrained through the combination $\Omega_{\mathrm{m}0}h^3$, where $H_0 = h \times 100$ km/s/Mpc. It is set by the acoustic scale $\theta_* = r_{\mathrm{s}}/D_{\mathrm{A}}$, defined as the ratio between the sound horizon and the angular distance at the time of last scattering. The measurement of seven acoustic peaks enables one to determine θ_* with a precision better than 0.1%. The constraints on the plane $(\Omega_{\mathrm{m}0}, H_0)$ are presented in Fig. 3 of Ref. [3] and clearly show this degeneracy. The marginalized constraints on the two parameters were then derived [3] to be

$$H_0 = (67.3 \pm 1.2) \text{ km/s/Mpc}, \quad \Omega_{\mathrm{m}0} = 0.315 \pm 0.017 \quad (1)$$

at a 68% confidence level. It was pointed out (see Secs. 5.2–5.4 of Ref. [3]) that the values of H_0 and $\Omega_{\mathrm{m}0}$ are, respectively, low and high compared with their values inferred from the Hubble diagram. Such a trend was already indicated by WMAP-9 [6] which concluded $H_0 = (70 \pm 2.2)$ km/s/Mpc.

Regarding the Hubble constant, two astrophysical measurements are in remarkable agreement. First, the estimation based on the distance ladder calibrated by three different techniques (masers, Milky Way cepheids, and Large Magellanic Cloud cepheids) gives [7] $H_0 = (74.3 \pm 1.5 \pm 2.1)$ km/s/Mpc, respectively with statistical and systematic errors. This improves the earlier constraint obtained by the HST Key program [8], $H_0 = (72 \pm 8)$ km/s/Mpc. Second, the Hubble diagram of type Ia supernovae (SNe Ia) calibrated with the Hubble Space Telescope (HST) observations of cepheids leads [9] to $H_0 = (73.8 \pm 2.4)$ km/s/Mpc. Other determinations of the Hubble constant, e.g., from very-long-baseline interferometry observations [10] or from the combination of Sunyaev-Zel'dovich effect and X-ray observations [11], have larger error bars and are compatible with both CMB and distance measurements.

Additionally, the analysis of the Hubble diagram of SNe Ia leads to a lower value of $\Omega_{\mathrm{m}0}$—e.g. 0.222 ± 0.034 with the SNLS 3 data set [12]—compared to the constraint (1) by Planck. As concluded in Ref. [3], there is no direct inconsistency, and it was pointed out that there could be residual systematics not properly accounted for in the SN data. Still, it was stated that "the tension between CMB-based estimates and the astrophysical measurements of H_0 is intriguing and merits further discussion."

Interestingly, the CMB constraints on $(\Omega_{\mathrm{m}0}, H_0)$ are in excellent agreement with baryon acoustic oscillation

(BAO) measurements [13], which allow one to determine the angular distance up to redshifts of order 0.7. The common point between the CMB and BAO measurements is that they involve light beams much larger than those involved in astronomical observations. Indeed, a pixel of Planck's high-resolution CMB maps corresponds to 5 arc min [14], while the typical angular size of a SN is 10^{-7} arc sec. This means that *the two kinds of observations probe the universe at very different scales.* Moreover, for both the CMB and BAO measurements the crucial information is encoded in correlations, while SN observations rely on "1-point measurements" (we are interested in the luminosity/redshift of each SN, not in the correlations between several SNe). Because of such distinctions one can expect from the two classes of cosmological observations to be affected differently by the inhomogeneity of the Universe, through gravitational lensing.

The effect of lensing on CMB measurements is essentially due to the large-scale structure, and it can be taken into account in the framework of cosmological perturbation theory at linear order [15] (see, however, Ref. [16] for a discussion about the impact of strong inhomogeneities). We refer to Ref. [17] for a description of the lensing effects on BAO measurements. Regarding the Hubble diagram, the influence of lensing has also been widely investigated [18]. The propagation of light in an inhomogeneous universe gives rise to both distortion and magnification. Most images are expected to be demagnified because their lines of sight probe underdense regions, while some are amplified due to strong lensing. It shall thus induce a dispersion of the luminosities of the sources, that is, an extra scatter in the Hubble diagram [19]. Its amplitude can be determined from the perturbation theory [20] and subtracted [21]. However, a considerable fraction of the lensing effects arises from sub-arc-min scales, which are not probed by shear maps smoothed on arc min scales [22].

The tension on (Ω_{m0}, H_0) may indicate that, given the accuracy of the observations achieved today, the use of a (perturbed) FL geometry to interpret the astrophysical data is no longer adapted. More precisely, the question that we want to raise is *whether the use of a unique space-time geometry is relevant for interpreting all the cosmological observations, regardless of their angular or spatial resolution and of their location (redshift).* Indeed, each observation is expected to probe the Universe smoothed on a typical scale related to its resolution, and this can lead to fundamentally different geometrical situations. In a universe with a discrete distribution of matter, the Riemann curvature experienced by a beam of test particles or photons is dominated by the Weyl tensor. Conversely, in a (statistically spatially isotropic) universe smoothed on large scales it is dominated by the Ricci tensor. Both situations correspond to distinct optical properties [23].

In the framework of geometric optics, a light beam is described by a bundle of null geodesics. All the information about the size and the shape of a beam can be encoded in a 2×2 matrix $\mathcal{D}^A{}_B$ called the Jacobi map (see Ref. [24] for further details). In particular, the angular and luminosity distances read, respectively,

$$D_{\mathrm{A}} = \sqrt{|\det \mathcal{D}^A{}_B|}, \qquad D_{\mathrm{L}} = (1+z)^2 D_{\mathrm{A}}. \qquad (2)$$

where z denotes the redshift. The evolution of the Jacobi map with light propagation is governed by the Sachs equation [25, 26]

$$\frac{\mathrm{d}^2}{\mathrm{d}v^2} \mathcal{D}^A{}_B = \mathcal{R}^A{}_C \mathcal{D}^C{}_B, \qquad (3)$$

where v is an affine parameter along the geodesic bundle. The term $\mathcal{R}_{AB}$ which controls the evolution of $\mathcal{D}^A{}_B$ is a projection of the Riemann tensor called the optical tidal matrix. It is defined by $\mathcal{R}_{AB} \equiv R_{\mu\nu\alpha\beta} s_A^\mu k^\nu k^\alpha s_B^\beta$, where k^μ is the wave vector of an arbitrary ray, and the Sachs basis $\{s_A^\mu\}_{A=1,2}$ spans a screen on which the observer projects the light beam. Because the Riemann tensor can be split into a Ricci part $R_{\mu\nu}$ and a Weyl part $C_{\mu\nu\alpha\beta}$, the optical tidal matrix can also be decomposed as

$$(\mathcal{R}_{AB}) = \underbrace{\begin{pmatrix} \Phi_{00} & 0 \\ 0 & \Phi_{00} \end{pmatrix}}_{\text{Ricci lensing}} + \underbrace{\begin{pmatrix} -\mathrm{Re}\,\Psi_0 & \mathrm{Im}\,\Psi_0 \\ \mathrm{Im}\,\Psi_0 & \mathrm{Re}\,\Psi_0 \end{pmatrix}}_{\text{Weyl lensing}} \qquad (4)$$

with $\Phi_{00} \equiv -(1/2) R_{\mu\nu} k^\mu k^\nu$ and $\Psi_0 \equiv -(1/2) C_{\mu\nu\alpha\beta}(s_1^\mu - \mathrm{i} s_2^\mu) k^\nu (s_1^\beta - \mathrm{i} s_2^\beta) k^\beta$. It clearly appears in Eq. (4) that the Ricci term tends to isotropically focus the light beam, while the Weyl term tends to shear and rotate it. The behavior of a light beam is thus different whether it experiences Ricci-dominated lensing (large beams, e.g. CMB measurements) or Weyl-dominated lensing (narrow beams, e.g. SN observations).

This Ricci-Weyl problem can be addressed with different methods. One possibility, a representative of which is the Dyer-Roeder approximation [27], is to construct a general distance-redshift relation which would take into account the effect of inhomogeneities in some average way. However, such approaches are in general difficult to control [18] because they rely on approximations whose domain of applicability is unknown. An alternative possibility consists in constructing inhomogeneous cosmological models, with a discrete distribution of matter, and studying the impact on light propagation. Several models exist in the literature: the Schwarzschild-cell method [28] or the lattice universe [29] which are both approximate solutions of the Einstein equations; and the Swiss-cheese models [30] which are constructed by matching together patches of exact solutions of the Einstein equations. This last approach is the one that we shall follow in this Letter.

Consider a Swiss-cheese model in which clumps of matter (modeling e.g. galaxies), each of them lying at the center of a spherical void, are embedded in a FL spacetime. The interior region of a void is described by the

Kottler geometry—i.e., Schwarzschild with a cosmological constant—while the exterior geometry is the FL one. By construction, such inhomogeneities do not modify the expansion dynamics of the embedding FL universe, thus avoiding any discussion regarding backreaction. The resulting spacetime is well defined, because the Darmois-Israel junction conditions are satisfied on the boundary of every void. Compared to a strictly homogeneous universe, a Swiss-cheese model is therefore characterized by two additional parameters: the size of the voids (or equivalently the mass of their central bodies), and the volumic fraction of the remaining FL regions which encodes the smoothness of the distribution of matter. It is naturally quantified by the *smoothness parameter*

$$f \equiv \lim_{V \to \infty} \frac{V_{\mathrm{FL}}}{V}, \tag{5}$$

where V_{FL} is the volume occupied by the FL region within a volume V of the Swiss cheese. With the definition (5), $f = 1$ corresponds to a model with no hole (i.e. a FL universe), while $f = 0$ corresponds to the case where matter is exclusively under the form of clumps inside voids.

Of course such a model cannot be considered realistic, but neither does the exact FL geometry, used to interpret the Hubble diagram. Both spacetimes describe a spatially statistically homogeneous and isotropic universe, and the former permits additionally the investigation of the effect of a discrete distribution of matter. Since the FL universe is a particular Swiss-cheese model, this family of spacetimes therefore allows us to estimate how good the hypothesis of strict spatial homogeneity—with a continuous matter distribution at *all* scales—is.

The propagation of light in a Swiss-cheese model has been comprehensively investigated in Ref. [24], generalizing earlier works [31], with the key assumption that *light never crosses the clumps*. This "opacity assumption" can be observationally justified in the case of SN observations if the clumps represent galaxies (see Ref. [24] for a discussion). Compared to the strictly homogeneous case, any light signal traveling through a Swiss cheese then experiences a reduced Ricci focusing. This leads [see Eqs. (2)-(4)] to an increase of the observed luminosity distance D_{L}. The effect of Weyl lensing—i.e. here shear—is relatively small.

This systematic effect, due to inhomogeneities, tends to bias the Hubble diagram in a way that mimics the contribution of a negative spatial curvature or a positive cosmological constant. In other words, if one interprets the Hubble diagram of a Swiss-cheese universe by wrongly assuming that it is strictly homogeneous, then one underestimates the value of Ω_{m0}. The error reaches a few percent, which is comparable to other estimates in similar contexts [32]. Note, however, that in the case of Swiss-cheese models with Lemaître-Tolman-Bondi patches instead of Kottler voids, the effect of inhomogeneities has a much smaller impact on the Hubble diagram [33]. Thus,

the systematic effect exhibited in Ref. [24] must be attributed to the discreteness of the distribution of matter.

Simulating the mock Hubble diagrams for Swiss-cheese universes with various values of its parameters, we inferred a phenomenological expression for the luminosity distance $D_{\mathrm{L}}(z; \Omega_{\mathrm{m0}}, \Omega_{\Lambda 0}, H_0, f)$ which is very close to the Dyer-Roeder one. This expression was then used to fit the Hubble diagram constructed from the SNLS 3 catalog [12]. Figure 25 of Ref. [24] shows that f influences the result of the best fit on Ω_{m0} that can shift from 0.22 for $f = 1$ (in agreement with the standard FL analysis performed in Ref. [12]) to 0.3 for $f = 0$.

Figure 1 shows the constraints in the plane $(h, \Omega_{\mathrm{m0}})$ imposed by Planck on the one hand, and by the Hubble diagram on the other hand, whether it is interpreted in a spatially flat FL universe ($f = 1$) or in a spatially flat Swiss-cheese model for which matter is entirely clumped ($f = 0$). The agreement between the CMB and the Hubble diagram is clearly improved for small values of f, especially regarding Ω_{m0}, while h is almost unaffected.

Note that SN observations *alone* cannot constrain H_0, because of the degeneracy with the (unknown) absolute magnitude M of the SNe. For the results of Fig. 1 the degeneracy was broken by fixing $M = -19.21$, according to the best-fit value obtained by Ref. [12] with a fiducial Hubble constant $h = 0.7$. Thus the horizontal positions of the SN contours in Fig. 1 are only *indicative*.
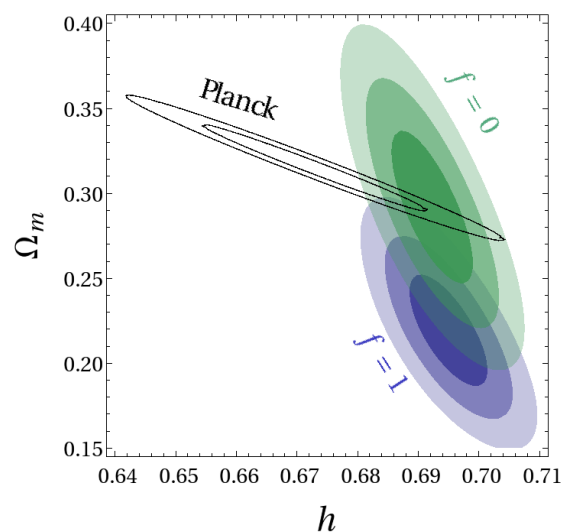
FIG. 1. Comparison of the constraints obtained by Planck on $(\Omega_{\mathrm{m0}}, h)$ [3] and from the analysis of the Hubble diagram constructed from the SNLS 3 catalog [12]. The colored contour plots correspond to two different smoothness parameters. For $f = 1$, the geometry used to fit the data is the FL one.

Alleviating the tension on H_0 remains an open issue. Because inferring its value from SNe is a *local* measurement, a promising approach consists in taking into account the impact of our close environment. It has been

suggested [34] that cosmic variance increases the uncertainty on H_0^{local} and thus reduces the tension with H_0^{CMB}. More speculatively, $H_0^{\text{local}} > H_0^{\text{CMB}}$ may be a hint that our local environment is underdense [35]. Our conclusions on Ω_{m0} remains, however, unaffected by this issue.

Our analysis, though relying on a particular class of models, indicates that the FL geometry is probably too simplistic to describe the Universe for certain types of observations, given the accuracy reached today. In the end, a single metric may not be sufficient to describe all the cosmological observations, just as Lilliputians and Brobdingnag's giants [36] cannot use a map with the same resolution to travel. A better cosmological model probably requires an atlas of maps with various smoothing scales, determined by the observations at hand.

Other observations, such as lensing [37], may help to characterize the distribution and the geometry of voids [38], in order to construct a better geometrical model. For the first time, the standard FL background geometry may be showing its limits to interpret the cosmological data with the accuracy they require.

---

* fleury@iap.fr

† helene.dupuy@cea.fr

‡ uzan@iap.fr

[1] P. Peter and J.-P. Uzan, *Primordial Cosmology*, (Oxford University Press, Oxford, England, 2009).

[2] J.-P. Uzan, Gen. Relativ. Gravit. **39**, 307 (2007); J.-P. Uzan, arXiv:0912.5452; J.-P. Uzan, Living Rev. Relativity **14**, 2 (2011).

[3] P. A. R. Ade *et al.* (Planck Collaboration), arXiv:1303.5076.

[4] C. Pitrou, J.-P. Uzan, and F. Bernardeau, Phys. Rev. D **78**, 063526 (2008); C. Pitrou, J.-P. Uzan, and F. Bernardeau, J. Cosmol. Astropart. Phys. 07 (**2010**) 003; Z. Huang and F. Vernizzi, Phys. Rev. Lett. **110**, 101303 (2013).

[5] P. A. R. Ade *et al.* (Planck Collaboration), arXiv:1303.5084.

[6] G. Hinshaw *et al.*, arXiv:1212.5226

[7] W. L. Freedman, B. F. Madore, V. Scowcroft, C. Burns, A. Monson, S. E. Persson, M. Seibert, and J. Rigby, Astrophys. J. **758**, 24 (2012).

[8] W. L. Freedman *et al.*, Astrophys. J. **553**, 47 (2001).

[9] A. G. Riess, L. Macri, S. Casertano, H. Lampeitl, H. C. Ferguson, A. V. Filippenko, S. W. Jha, W. Li, and R. Chornock, Astrophys. J. **730**, 119 (2011).

[10] M. J. Reid *et al.*, arXiv:1207.7292.

[11] M. Bonamente, M. K. Joy, S. J. LaRoque, J. E. Carlstrom, E. D. Reese, and K. S. Dawson, Astrophys. J. **647** 25 (2006).

[12] J. Guy *et al.*, Astronom. Astrophys. **523**, A7 (2010).

[13] S. Cole *et al.*, Mon. Not. R. Astron. Soc. **362**, 505 (2005); D.J. Eisenstein *et al.*, Astrophys. J. **633**, 560 (2005); W.J. Percival *et al.*, Mon. Not. R. Astron. Soc. **401**, 2148 (2011); N. Padmanabhan *et al.*, Mon. Not. R. Astron. Soc. **427**, 2132 (2012).

[14] P. A. R. Ade *et al.* (Planck Collaboration), arXiv:1303.5062

[15] P. A. R. Ade *et al.* (Planck Collaboration), arXiv:1303.5077

[16] K. Bolejko, J. Cosmol. Astropart. Phys. 02 (**2011**) 025 .

[17] A. Vallinotto, S. Dodelson, C. Schimd and J.-P. Uzan, Phys. Rev. D **75**, 103509 (2007).

[18] C. Clarkson, G. F. R. Ellis, A. Faltenbacher, R. Maartens, O. Umeh, and J.-P. Uzan, Mon. Not. R. Astron. Soc. **426**, 1121 (2012).

[19] R. Kantowski, T. Vaughan and D. Branch, Astrophys. J. **447**, 35 (1995); J.A. Frieman, Commun. Astrophys. **18**, 323 (1998); Y. Wang, Astrophys. J. **531**, 676 (2000).

[20] C. Bonvin, R. Durrer and M. A. Gasparini, Phys. Rev. D **73**, 023523 (2006); N. Meures and M. Bruni, Mon. Not. R. Astron. Soc. **419**, 1937 (2012); P. Valageas, Astron. Astrophys. **354**, 767, (2000).

[21] A. Cooray, D. Holz and D. Huterer, Astrophys. J. **637**, L77 (2006); S. Dodelson and A. Vallinotto, Phys. Rev. D **74**, 063515 (2006); A. Cooray, D. Huterer, and D. E. Holz, Phys. Rev. Lett. **96**, 021301 (2006); D. Sarkar, D. Sarkar, A. Amblard, D. E. Holz, and A. Cooray, Astrophys. J. **678**, 1 (2008); A. R. Cooray, D. E. Holz and R. Caldwell, J. Cosmol. Astropart. Phys. 11 (**2010**) 015; A. Vallinotto, S. Dodelson and P. Zhang, Phys. Rev. D **84**, 103004 (2011); B. Ménard *et al.*, Astron. Astrophys. **403**, 817 (2003).

[22] N. Dalal *et al.*, Astrophys. J. **585**, L11 (2003).

[23] C.C. Dyer and R.C. Roeder, Gen. Relativ. Grav. **13**, 1157 (1981).

[24] P. Fleury, H. Dupuy, and J.-P. Uzan, Phys. Rev. D **87** 123526 (2013).

[25] R. Sachs, Proc. R. Soc. London A **264**, 309 (1961).

[26] P. Schneider, J. Ehlers, and E. E. Falco, *Gravitational Lenses* (Springer, New York, 1992).

[27] C. C. Dyer and R. C. Roeder, Astrophys. J. **174**, L115 (1972); C. C. Dyer and R. C. Roeder, Astrophys. J. **180**, L31 (1973).

[28] R.W. Lindquist and J.A. Wheeler, Rev. Mod. Phys. **29**, 432 (1957); T. Clifton and P.G. Ferreira, Phys. Rev. D **80**, 103503 (2009); T. Clifton and P.G. Ferreira, J. Cosmol. Astropart. Phys. 10 (**2009**) 26,

[29] D. E. Holz and R. M. Wald, Phys. Rev. D **58**, 063501 (1998); J.-P. Bruneton and J. Larena, Classical Quantum Gravity **29**, 155001 (2012); J.-P. Bruneton and J. Larena, Classical Quantum Gravity **30**, 025002 (2013); K. Kainulainen and V. Marra, Phys. Rev. D **80**, 127301 (2009).

[30] A. Einstein and E.G. Straus, Rev. Mod. Phys. **17**, 120 (1945); A. Einstein and E.G. Straus, Rev. Mod. Phys. **18**, 148 (1945).

[31] R. Kantowski, Astrophys. J. **155**, 89 (1969); C. C. Dyer and R. C. Roeder, Astrophys. J. **189**, 167 (1974).

[32] K. Bolejko and P.G. Ferreira, J. Cosmol. Astropart. Phys.

05 (**2012**) 003.

[33] N. Brouzakis, N. Tetradis, and E. Tzavara, J. Cosmol. Astropart. Phys. 02 (**2007**) 013; V. Marra, E. W. Kolb, S. Matarrese, and A. Riotto, Phys. Rev. D **76**, 123004 (2007); T. Biswas and A. Notari, J. Cosmol. Astropart. Phys. 06 (**2008**) 021; R. A. Vanderveld, E. E. Flanagan and I. Wasserman, Phys. Rev. D **78**, 083511 (2008); N. Brouzakis, N. Tetradis and E. Tzavara, J. Cosmol. Astropart. Phys. 04 (**2008**) 008; T. Clifton and J. Zuntz, Mon. Not. R. Astron. Soc. **400**, 2185 (2009); W. Valkenburg, J. Cosmol. Astropart. Phys. 06 (**2009**) 010; S. J. Szybka, Phys. Rev. D **84**, 044011 (2011);

E. E. Flanagan, N. Kumar, I. Wasserman, and R. A. Vanderveld, Phys. Rev. D **85**, 023510 (2012).

[34] V. Marra, L. Amendola, I. Sawicki, and W. Valkenburg, Phys. Rev. Lett. **110**, 241305 (2013).

[35] S. Jha, A. Riess, and R. Kirshner, Astrophys. J. **659**, 122 (2007).

[36] J. Swift, *Travels into Several Remote Nations of the World, in Four Parts*.

[37] K. Bolejko *et al.*, Phys. Rev. Lett. **110**, 021302 (2013).

[38] G. Lavaux and B. D. Wandelt, Mon. Not. R. Astron. Soc. **1392**, 403 (2010).

Swiss-cheese models and the Dyer-Roeder approximation

Pierre Fleury

Institut d'Astrophysique de Paris, UMR-7095 du CNRS, Université Pierre et Marie Curie, 98 bis, boulevard Arago, 75014 Paris, France.
Sorbonne Universités, Institut Lagrange de Paris,
98 bis, boulevard Arago, 75014 Paris, France.

E-mail: fleury@iap.fr

Abstract. In view of interpreting the cosmological observations precisely, especially when they involve narrow light beams, it is crucial to understand how light propagates in our statistically homogeneous, clumpy, Universe. Among the various approaches to tackle this issue, Swiss-cheese models propose an inhomogeneous spacetime geometry which is an exact solution of Einstein's equation, while the Dyer-Roeder approximation deals with inhomogeneity in an effective way. In this article, we demonstrate that the distance-redshift relation of a certain class of Swiss-cheese models is the same as the one predicted by the Dyer-Roeder approach, at a well-controlled level of approximation. Both methods are therefore equivalent when applied to the interpretation of, e.g., supernova obervations. The proof relies on completely analytical arguments, and is illustrated by numerical results.

Contents

Introduction

All cosmological observations involve, today, exclusively photons as the carrier of the information. In order to interpret them correctly, it is thus primordial to understand how light propagates through the Universe. In particular, the relation between the angular diameter distance D_A (or the luminosity distance D_L) and the redshift z of remote sources, is a key ingredient both in the interpretation of the baryon acoustic oscillation (BAO) signal, whether

it is extracted from the correlation function of the matter distribution [1, 2] or from the anisotropies of the cosmic microwave background (CMB) [3]; and, of course, in the analysis of the Hubble diagram, constructed from supernova (SN) observations [4, 5].

Though crucial, the determination of a reliable optical model of our Universe, known as the fitting problem [6], still remains to be done. In practice, observational cosmologists always rely on the somehow least worst model, in which light propagates through a Friedmann-Lemaître (FL) spacetime, describing a perfectly homogeneous and isotropic universe [7]. While such an approximation may be valid for wide light beams (e.g., involved in BAO observations), typically sensitive to the large-scale structure of the Universe, it is much more questionable regarding the very narrow beams involved in astronomical observations, e.g., SNe [8].

Of course, the challenge of establishing a better optical model for the Universe led to many studies based on various methods. Popular ones, in the paradigm of standard cosmology, consist in the analysis of weak lensing in a perturbed FL spacetime [9–17], or in cosmological simulations [18]. Alternative relativistic models for the inhomogeneous Universe can also be considered, such as Swiss-cheese models [19–30], lattice models [31, 32], or plane-symmetric models [33]. Finally, rather than specifying any spacetime model, one can use simplifying assumptions about the impact of the inhomogeneity of matter distribution on light propagation, in order derive an effective model. It is the case of the Dyer-Roeder approach [34], inspired from Zel'dovich's original intuition [35]. We refer the reader to, e.g., Refs. [36, 37] for elements of review and comparison.

Among all those approaches, the Dyer-Roeder (DR) approximation on the one hand, and the "traditional" Swiss-cheese (SC) models generated by the Einstein-Straus method [38, 39] on the other hand, used to be studied in parallel and presented together (see, e.g., Textbook [40]). This is actually not surprising, because, in its origin, the DR approximation was motivated by such SC models. Though very different in their philosophy—the former is an effective theory, based on assumptions, while the latter relies on a well-defined spacetime model—, both approaches seem to generate similar distance-redshift relations [41]

$$D_{\mathrm{A}}^{\mathrm{DR}}(z) \approx D_{\mathrm{A}}^{\mathrm{SC}}(z). \tag{0.1}$$

However, to the knowledge of the author, such a correspondence has never been explained, nor rigorously proved, in the litterature. The purpose of this article is thus to fill the blank, not only by checking the *conjecture* (0.1) numerically, but also by proposing an analytical proof of it, in order to understand the underlying mechanisms, and its domain of validity.

In Sec. 1, we recall theoretical elements about geometric optics, needed for the remainder of the article. In Secs. 2 and 3 we introduce, respectively, the DR approximation and SC models. Section 4 is then dedicated to the analysis of the optical properties of SC models, that we prove to be equivalent to the ones predicted by the DR approach, at a very good level of approximation. Finally, in Sec. 5, we propose numerical illustrations of our results, and we analyse the origin of the small discrepancies between the SC and DR approaches.

1   Geometric optics in curved spacetime

This section reviews some generic elements about the propagation of light in arbitrary spacetimes. We define our notations, and introduce several tools which will be useful in the remainder of the article.

1.1   Description of a light beam

A light beam is a collection of light rays, that is, a bundle of null geodesics $\{x^\mu(v,r)\}$, where r labels the rays and v is the affine parameter along them. The wave four-vector $k^\mu \equiv \partial x^\mu/\partial v$ is a null vector field, tangent to the rays $r = $ cst. It therefore satisfies

$$k^\mu k_\mu = 0, \qquad k^\nu \nabla_\nu k_\mu = 0. \tag{1.1}$$

Besides, the relative behavior of two neighboring rays $x^\mu(\cdot, r)$ and $x^\mu(\cdot, r + \mathrm{d}r)$ is described by their separation vector $\xi^\mu \equiv \partial x^\mu/\partial r$. One can always choose the origin of the affine parametrization of each ray $r = $ cst so that

$$k^\mu \xi_\mu = 0. \tag{1.2}$$

Note that this condition is automatically satisfied if one sets $v = 0$, for each geodesic, at a vertex point of the bundle, that is an event where $\xi^\mu = 0$. When the condition (1.2) is satisfied, the evolution of ξ^μ along the light beam is governed by the geodesic deviation equation

$$k^\alpha k^\beta \nabla_\alpha \nabla_\beta \xi^\mu = R^\mu{}_{\nu\alpha\beta} k^\nu k^\alpha \xi^\beta, \tag{1.3}$$

where $R^\mu{}_{\nu\alpha\beta}$ is the Riemann tensor.

1.2   The Sachs formalism

Consider an observer, with four-velocity u^μ ($u_\mu u^\mu = -1$), who crosses the light beam. With respect to this observer, one defines the spatial direction of light propagation as the opposite of the only direction for which the observer can detect a signal. It is spanned by the purely spatial unit vector d^μ,

$$d^\mu u_\mu = 0, \qquad d^\mu d_\mu = 1, \tag{1.4}$$

which leads to the 3+1 decomposition of the wave four-vector

$$k^\mu = \omega(u^\mu - d^\mu), \tag{1.5}$$

where $\omega = 2\pi\nu \equiv -u_\mu k^\mu$ is the cyclic frequency of the light signal in the observer's rest frame. Note that $\mathrm{d}\ell = \omega \mathrm{d}v$ is the proper distance (measured by the observer) travelled by light for a change $\mathrm{d}v$ of the affine parameter. The redshift z is defined as the relative difference between the emitted frequency ν_s, in the source's frame, and the observed frequency ν_o, in the observer's frame, so that

$$1 + z \equiv \frac{\nu_\mathrm{s}}{\nu_\mathrm{o}} = \frac{u_\mathrm{s}^\mu k_\mu(v_\mathrm{s})}{u_\mathrm{o}^\mu k_\mu(v_\mathrm{o})}. \tag{1.6}$$

Now suppose that the observer wishes to measure the size and the shape of the light beam. For that purpose, he must use a (spatial) screen orthogonal to the line of sight. This screen is spanned by the so-called Sachs basis $(s_A^\mu)_{A \in \{1,2\}}$, defined by

$$s_A^\mu u_\mu = s_A^\mu d_\mu = 0, \qquad g_{\mu\nu} s_A^\mu s_B^\nu = \delta_{AB}, \tag{1.7}$$

and by the transport property (1.8) below. The projections $\xi_A \equiv s_A^\mu \xi_\mu$ indicate the relative position, on the oberver's screen, of the light points corresponding to two neighboring rays separated by ξ^μ. Thus, it encodes all the information about the size and shape of the beam.

Consider a family of observers $u^\mu(v)$, along the beam, who wants to follow the evolution of the shape of the beam (typically for shear measurements). For that purpose, they must all

use the "same" Sachs basis, in order to avoid any spurious rotation of the pattern observed on the screens. This is ensured by a partial parallel transportation

$$S_{\mu\nu}k^\rho \nabla_\rho s_A^\nu = 0, \tag{1.8}$$

where $S^{\mu\nu} = \delta^{AB}s_A^\mu s_B^\nu = g^{\mu\nu} + u^\mu u^\nu - d^\mu d^\nu$ is the screen projector. The reason why s_A^μ cannot be completely parallel-transported is that, in general, u^μ is not[1].

The evolution of ξ_A, with light propagation, is determined by projecting the geodesic deviation equation (1.3) on the Sachs basis. The result is known as the Sachs equation [40, 42],

$$\frac{\mathrm{d}^2\xi_A}{\mathrm{d}v^2} = \mathcal{R}_{AB}\,\xi^B, \tag{1.9}$$

where $\mathcal{R}_{AB} = R_{\mu\nu\alpha\beta}k^\nu k^\alpha s_A^\mu s_B^\beta$ is the screen-projected Riemann tensor, called the optical tidal matrix. The properties of the Riemann tensor imply that this matrix is symmetric, $\mathcal{R}_{AB} = \mathcal{R}_{BA}$. Note that the altitude of the "screen indices" $(A, B, \dots)$ does not matter, since they are raised and lowered by δ_{AB}. In the following, to alleviate the notation, we use bold symbols for quantities with screen indices, and an overdot for derivatives with respect to the affine parameter v. The Sachs equation (1.9) thus becomes $\ddot{\boldsymbol{\xi}} = \boldsymbol{\mathcal{R}}\boldsymbol{\xi}$.

The Riemann tensor can be decomposed into a Ricci part and a Weyl part,

$$R_{\mu\nu\alpha\beta} = g_{\mu[\alpha}R_{\beta]\nu} - g_{\nu[\alpha}R_{\beta]\mu} - \frac{1}{3}R\,g_{\mu[\alpha}g_{\beta]\nu} + C_{\mu\nu\alpha\beta}, \tag{1.10}$$

where the Ricci tensor $R_{\mu\nu}$ is directly related to the local density of energy-momentum via Einstein's equations; and the Weyl tensor $C_{\mu\nu\alpha\beta}$ contains the long-range effects of gravitation. As a consequence, the optical tidal matrix can also be splitted into a pure-trace Ricci-lensing term and a traceless Weyl-lensing term as

$$\boldsymbol{\mathcal{R}} = \underbrace{\begin{pmatrix} \Phi_{00} & 0 \\ 0 & \Phi_{00} \end{pmatrix}}_{\text{Ricci lensing}} + \underbrace{\begin{pmatrix} -\mathrm{Re}\,\Psi_0 & \mathrm{Im}\,\Psi_0 \\ \mathrm{Im}\,\Psi_0 & \mathrm{Re}\,\Psi_0 \end{pmatrix}}_{\text{Weyl lensing}}, \tag{1.11}$$

with

$$\Phi_{00} \equiv -\frac{1}{2}R_{\mu\nu}k^\mu k^\nu, \qquad \text{and} \qquad \Psi_0 \equiv -\frac{1}{2}C_{\mu\nu\alpha\beta}(s_1^\mu - \mathrm{i}s_2^\mu)k^\nu k^\alpha(s_1^\beta - \mathrm{i}s_2^\beta). \tag{1.12}$$

It is then clear, from the Sachs equation (1.9), that the Ricci term tends to isotropically focus the light beam, while the Weyl term tends to shear it. For this reason, Φ_{00} is called "source of convergence" and Ψ_0 "source of shear[2]" [43].

---

[1]In fact, it is also possible to choose a family of observers such that the four-velocity field u^μ is parallel-transported along the beam, without affecting the optical equations [40]. In this case, however, the observers are generally not comoving, and thus have no clear cosmological interpretation.

[2]This name, however, omits a part of the optical effects due to Ψ_0; strictly speaking, we should write "source of shear *and rotation*". Indeed, even though the beam is an irrotational bundle of null geodesics ($\nabla_{[\mu}k_{\nu]} = 0$), a rotation of the image can appear due to cumulative shearing along different directions.

1.3 Wronski matrix, Jacobi matrix

Because the Sachs equation is a second-order homogeneous linear differential equation, any solution is linearly related to its initial conditions ($v = v_0$), so that

$$\boldsymbol{\xi}(v) = \boldsymbol{\mathcal{C}}(v \leftarrow v_0)\boldsymbol{\xi}(v_0) + \boldsymbol{\mathcal{D}}(v \leftarrow v_0)\dot{\boldsymbol{\xi}}(v_0), \tag{1.13}$$

$$\dot{\boldsymbol{\xi}}(v) = \dot{\boldsymbol{\mathcal{C}}}(v \leftarrow v_0)\boldsymbol{\xi}(v_0) + \dot{\boldsymbol{\mathcal{D}}}(v \leftarrow v_0)\dot{\boldsymbol{\xi}}(v_0), \tag{1.14}$$

where $\boldsymbol{\mathcal{C}}(v \leftarrow v_0)$ and $\boldsymbol{\mathcal{D}}(v \leftarrow v_0)$ are 2×2 matrices, respectively called scale matrix and Jacobi matrix, which satisfy the Sachs equation like $\boldsymbol{\xi}(v)$, with initial conditions

$$\begin{cases} \boldsymbol{\mathcal{C}}(v_0 \leftarrow v_0) = \mathbf{1}_2 \\ \dot{\boldsymbol{\mathcal{C}}}(v_0 \leftarrow v_0) = \mathbf{0}_2 \end{cases} \quad \text{and} \quad \begin{cases} \boldsymbol{\mathcal{D}}(v_0 \leftarrow v_0) = \mathbf{0}_2 \\ \dot{\boldsymbol{\mathcal{D}}}(v_0 \leftarrow v_0) = \mathbf{1}_2 \end{cases}, \tag{1.15}$$

where $\mathbf{0}_n$ and $\mathbf{1}_n$ denote respectively the $n \times n$ zero and identity matrices. Equations (1.13), (1.14) can finally be gathered into a single 4×4 matrix relation:

$$\begin{pmatrix} \boldsymbol{\xi} \\ \dot{\boldsymbol{\xi}} \end{pmatrix}(v) = \boldsymbol{\mathcal{W}}(v \leftarrow v_0) \begin{pmatrix} \boldsymbol{\xi} \\ \dot{\boldsymbol{\xi}} \end{pmatrix}(v_0), \qquad \text{where} \qquad \boldsymbol{\mathcal{W}} \equiv \begin{pmatrix} \boldsymbol{\mathcal{C}} & \boldsymbol{\mathcal{D}} \\ \dot{\boldsymbol{\mathcal{C}}} & \dot{\boldsymbol{\mathcal{D}}} \end{pmatrix} \tag{1.16}$$

is the 4×4 Wronski matrix of the Sachs equation. As we will see in Sec. 4, it is particularly convenient for dealing with light propagation through a patchwork of spacetimes, such as Swiss-cheese models, because by construction

$$\boldsymbol{\mathcal{W}}(v_3 \leftarrow v_1) = \boldsymbol{\mathcal{W}}(v_3 \leftarrow v_2)\boldsymbol{\mathcal{W}}(v_2 \leftarrow v_1). \tag{1.17}$$

It is easy to see that the Wronski matrix is the only solution of

$$\dot{\boldsymbol{\mathcal{W}}}(v \leftarrow v_0) = \begin{pmatrix} \mathbf{0}_2 & \mathbf{1}_2 \\ \boldsymbol{\mathcal{R}}(v) & \mathbf{0}_2 \end{pmatrix} \boldsymbol{\mathcal{W}}(v \leftarrow v_0) \qquad \text{with} \qquad \boldsymbol{\mathcal{W}}(v_0 \leftarrow v_0) = \mathbf{1}_4. \tag{1.18}$$

This differential equation is formally solved by

$$\boldsymbol{\mathcal{W}}(v \leftarrow v_0) = \text{Vexp} \int_{v_0}^{v} \begin{pmatrix} \mathbf{0}_2 & \mathbf{1}_2 \\ \boldsymbol{\mathcal{R}}(w) & \mathbf{0}_2 \end{pmatrix} \mathrm{d}w, \tag{1.19}$$

where Vexp is the affine-parameter ordered exponential, analogous to the time-ordered exponential in quantum field theory. It is defined, for any matrix-valued function $\boldsymbol{\mathcal{M}}$, by

$$\text{Vexp} \int_{v_0}^{v} \boldsymbol{\mathcal{M}}(w)\mathrm{d}w \equiv \sum_{n=0}^{\infty} \int_{v_0}^{v} \mathrm{d}w_1 \int_{v_0}^{w_1} \mathrm{d}w_2 \ldots \int_{v_0}^{w_{n-1}} \mathrm{d}w_n\, \boldsymbol{\mathcal{M}}(w_1)\boldsymbol{\mathcal{M}}(w_2)\ldots\boldsymbol{\mathcal{M}}(w_n). \tag{1.20}$$

This expression reduces to a regular exponential if, for all v, v', $\boldsymbol{\mathcal{M}}(v)$ commutes with $\boldsymbol{\mathcal{M}}(v')$. In the case of Eq. (1.19), this apples if, and only if, the optical tidal matrix $\boldsymbol{\mathcal{R}}(v)$ is a constant.

1.4 Angular distance and luminosity distance

The observational notion of angular distance D_{A}, which relates the emission cross-sectional area $\mathrm{d}^2 A_{\mathrm{s}}$ of a source to the observed angular aperture $\mathrm{d}\Omega_{\mathrm{o}}^2$, via

$$\mathrm{d}^2 A_{\mathrm{s}} = D_{\mathrm{A}}^2 \mathrm{d}\Omega_{\mathrm{o}}^2, \tag{1.21}$$

is naturally related to the Jacobi part $\boldsymbol{\mathcal{D}}$ of the Wronski matrix. Indeed, on the one hand $\boldsymbol{\xi}(v_{\mathrm{s}}) = \boldsymbol{\ell}_{\mathrm{s}}$ is the proper separation (in the source's frame) between two emission points within the extended source; on the other hand $\dot{\boldsymbol{\xi}}(v_{\mathrm{o}})/\omega_{\mathrm{o}} = \boldsymbol{\theta}_{\mathrm{o}}$ is the observed angular separation between the light rays emitted by these points. Thus, from Eq. (1.13), we find

$$\omega_{\mathrm{o}} \boldsymbol{\mathcal{D}}(v_{\mathrm{s}} \leftarrow v_{\mathrm{o}}) = \frac{\partial \boldsymbol{\xi}(v_{\mathrm{s}})}{\partial \dot{\boldsymbol{\xi}}(v_{\mathrm{o}})/\omega_{\mathrm{o}}} = \frac{\partial \boldsymbol{\ell}_{\mathrm{s}}}{\partial \boldsymbol{\theta}_{\mathrm{o}}}, \tag{1.22}$$

so that

$$D_{\mathrm{A}} = \sqrt{\det \omega_{\mathrm{o}} \boldsymbol{\mathcal{D}}(\mathrm{s} \leftarrow \mathrm{o})}. \tag{1.23}$$

The observational luminosity distance D_{L}, relating the source's intrinsic luminosity L_{s} and the observed flux F_{o} via $L_{\mathrm{s}} = 4\pi D_{\mathrm{L}}^2 F_{\mathrm{o}}$, can also be expressed in terms of $\boldsymbol{\mathcal{D}}$ [44] according to

$$D_{\mathrm{L}} = (1+z)\sqrt{\det \omega_{\mathrm{s}} \boldsymbol{\mathcal{D}}(\mathrm{o} \leftarrow \mathrm{s})} = (1+z)^2 D_{\mathrm{A}}. \tag{1.24}$$

We stress that, contrary to what it is sometimes wrongly believed, the duality law (1.24) is true for *any* spacetime, as far as the number of photons is conserved during light travel.

Since the Jacobi matrix $\boldsymbol{\mathcal{D}}$ not only encodes information about the size of the beam, but also about its shape, all the weak-lensing observational quantities (convergence, shear, magnification) can be extracted from it; see, e.g., Ref. [43] for more details. Moreover, some genuinely relativistic effects, such as optical rotation, which are usually not taken into account by weak lensing studies, are also encoded in $\boldsymbol{\mathcal{D}}$; Ref. [45] provides an example in the context of anisotropic cosmology. Let us finally indicate that, by a suitable choice of coordinates adapted to the lightcone, called GLC gauge [46] (inspired from the observational coordinates [47]), the expression of the Jacobi matrix can be trivialized [48], so that the whole information is, in this case, contained in the Sachs basis only.

2 The Dyer-Roeder approximation

In this section, we describe in detail the propagation of light in a homogeneous and isotropic universe, and how it must be modified according to the Dyer-Roeder (DR) prescription. The last subsection is dedicated to a discussion about its physical motivations and its limitations.

2.1 Light propagation in a homogeneous and isotropic universe

Let us apply the formalism developed in the previous section to the Friedmann-Lemaître (FL) geometry. The associated metric reads (in three different coordinate systems)

$$\mathrm{d}s^2 = -\mathrm{d}T^2 + a^2(T)\left[\frac{\mathrm{d}R^2}{1 - KR^2} + R^2 \mathrm{d}\Omega^2\right] \tag{2.1}$$

$$= -\mathrm{d}T^2 + a^2(T)\left[\mathrm{d}\chi^2 + f_K(\chi)^2 \mathrm{d}\Omega^2\right] \tag{2.2}$$

$$= a^2(\eta)\left[-\mathrm{d}\eta^2 + \mathrm{d}\chi^2 + f_K(\chi)^2 \mathrm{d}\Omega^2\right], \tag{2.3}$$

where $\mathrm{d}\Omega^2 \equiv \mathrm{d}\theta^2 + \sin^2\theta \mathrm{d}\varphi^2$ is the infinitesimal solid angle; T, η denote respectively the cosmic and conformal times, with $\mathrm{d}T = a\mathrm{d}\eta$; a is the scale factor; χ is the comoving radius, $R = f_K(\chi)$ the comoving areal radius, with

$$f_K(\chi) \equiv \begin{cases} \sin(\sqrt{K}\chi)/\sqrt{K} & \text{if } K > 0 \\ \chi & \text{if } K = 0 \; ; \\ \sinh(\sqrt{-K}\chi)/\sqrt{-K} & \text{if } K < 0 \end{cases} \tag{2.4}$$

and finally $6K/a^2$ is the (intrinsic) scalar curvature of the $T = \text{cst}$ spatial hypersurfaces. The time evolution of the scale factor $a(T)$ is ruled by the Friedmann equation

$$H^2 \equiv \left(\frac{1}{a}\frac{\mathrm{d}a}{\mathrm{d}T}\right)^2 = \frac{8\pi G\rho_0}{3}\left(\frac{a_0}{a}\right)^3 - \frac{K}{a^2} + \frac{\Lambda}{3}, \tag{2.5}$$

where ρ is the homogeneous energy density of matter, modelled by a dust fluid filling space, and Λ is the cosmological constant. As usual, a subscript 0 denotes the present value of a quantity. The Friedmann equation can be also written in terms of the cosmological parameters $\{\Omega\}$,

$$H^2 = H_0^2 \left[\Omega_{\mathrm{m0}}\left(\frac{a_0}{a}\right)^3 + \Omega_{K0}\left(\frac{a_0}{a}\right)^2 + \Omega_{\Lambda 0}\right], \tag{2.6}$$

with

$$\Omega_{\mathrm{m0}} \equiv \frac{8\pi G\rho_0}{3H_0^2}, \qquad \Omega_{K0} \equiv \frac{-K}{a_0^2 H_0^2}, \qquad \Omega_{\Lambda 0} \equiv \frac{\Lambda}{3H_0^2}. \tag{2.7}$$

We now focus on light propagation. Consider a comoving observer, who can be chosen without loss of generality at the origin of the spatial coordinate system. A light ray reaching this central observer today is purely radial, and propagates according to $\chi = \eta_0 - \eta$. Along it, the affine parameter v satisfies $\mathrm{d}\eta/\mathrm{d}v = \omega/a$, and $a\omega$ is a constant (whence the FL expression for the redshift, $1 + z = a_{\mathrm{o}}/a_{\mathrm{s}}$). The evolution of the redshift with the affine parameter is therefore ruled by

$$\frac{1}{\omega_{\mathrm{o}}}\frac{\mathrm{d}}{\mathrm{d}v}\left(\frac{1}{1+z}\right) = H. \tag{2.8}$$

The screen vectors s_1, s_2, forming the Sachs basis, do not need here to be specified explicitely to get the optical tidal matrix $\boldsymbol{\mathcal{R}}$, because of the high degree of symmetry (in particular, spatial isotropy) of the FL spacetime. The result is

$$\boldsymbol{\mathcal{R}}_{\mathrm{FL}} = -4\pi G\rho\omega^2 \mathbf{1}_2. \tag{2.9}$$

As expected, a FL spacetime only focus light via a Ricci term (source of convergence), because conformal flatness imposes that the Weyl tensor (source of shear and rotation) vanishes. The Sachs equation (1.9) can then be solved exactly, e.g., by taking advantage of the conformal flatness [41], in order to obtain the blocks of the Wronski matrix:

$$\boldsymbol{\mathcal{C}}_{\mathrm{FL}}(2 \leftarrow 1) = \frac{a_2}{a_1}\left[f_K'(\eta_2 - \eta_1) - \mathcal{H}_1\, f_K(\eta_2 - \eta_1)\right]\mathbf{1}_2, \tag{2.10}$$

$$\dot{\boldsymbol{\mathcal{C}}}_{\mathrm{FL}}(2 \leftarrow 1) = \frac{\omega_2}{a_2}\left\{\mathcal{H}_2\,\boldsymbol{\mathcal{C}}(2 \leftarrow 1) - \frac{a_2}{a_1}\left[K\, f_K(\eta_2 - \eta_1) + \mathcal{H}_1\, f_K'(\eta_2 - \eta_1)\right]\mathbf{1}_2\right\}, \tag{2.11}$$

$$\omega_1 \boldsymbol{\mathcal{D}}_{\mathrm{FL}}(2 \leftarrow 1) = a_2\, f_K(\eta_2 - \eta_1)\,\mathbf{1}_2, \tag{2.12}$$

$$\omega_1 \dot{\boldsymbol{\mathcal{D}}}_{\mathrm{FL}}(2 \leftarrow 1) = \frac{a_1}{a_2^2}\,\mathcal{H}_2\left[\omega_1 \boldsymbol{\mathcal{D}}(2 \leftarrow 1)\right] + \omega_1 \frac{a_1}{a_2}\, f_K'(\eta_2 - \eta_1)\,\mathbf{1}_2, \tag{2.13}$$

where $\mathcal{H} \equiv a'(\eta)/a = aH$ is the conformal Hubble parameter, and a prime denotes a derivative with respect to conformal time η. Note that (2.12) gives the well-known expression for the angular distance in a FL universe,

$$D_{\mathrm{A}}^{\mathrm{FL}} = \sqrt{\det \omega_{\mathrm{o}}\boldsymbol{\mathcal{D}}_{\mathrm{FL}}(\mathrm{s} \leftarrow \mathrm{o})} = a_{\mathrm{s}} f_K(\chi_{\mathrm{s}}). \tag{2.14}$$

Although it is not obvious when written under this form, *Eq. (2.14) must be considered a relation between the angular distance and the affine parameter*, because it results from solving $\mathrm{d}^2\boldsymbol{\mathcal{D}}/\mathrm{d}v^2 = \boldsymbol{\mathcal{R}}\boldsymbol{\mathcal{D}}$. From this point of view, the usual distance-redshift relation $D_A(z)$—as used, e.g., for interpreting the SN data—arises from *both* Eq. (2.8) and Eq. (2.14). The importance of such a remark will become clearer in the next subsection.

2.2 The Dyer-Roeder approximation

As first pointed out by Zel'dovich [35], at the scale of the typical cross-sectional area of a light beam involved in astronomical observations, such as SNe, our Universe cannot be reasonably considered as homogeneously filled by a fluid, but rather composed of more or less concentrated clumps of matter. Therefore, the light signals involved in these observations must essentially propagate through vacuum, and consequently undergo focusing effects which are different from the FL case, presented in the previous subsection.

Such an intuition led Zel'dovich to propose an "empty-beam" approximation, generalized later into a "partially-filled-beam" approach [34, 49], better known today as the DR approximation. The aim is to provide an *effective* distance-redshift relation $D_A(z)$ which would take the small-scale inhomogeneity (i.e. the clumpiness) of our Universe into account. Such a relation can then be used for interpreting the SN data, instead of the standard FL one.

The DR approximation is based on three hypotheses:

DR1 The relation between the redshift z and the affine parameter v is essentially unaffected by the inhomogeneity of the distribution of matter.

DR2 Weyl focusing is negligible regarding the evolution of the angular distance.

DR3 Ricci focusing is effectively reduced, with respect to the FL case, by a factor $0 \leq \alpha \leq 1$, called smoothness parameter, due to the fact that light mostly propagates through underdense regions of the universe. The physical meaning of α is thus the effective fraction of diffuse matter intercepted by the light beam during its propagation.

Those conditions imply that the DR relation between angular distance and redshift, $D_A^{\mathrm{DR}}(z)$, is generated by solving both

$$\frac{1}{\omega_o}\frac{\mathrm{d}}{\mathrm{d}v}\left(\frac{1}{1+z}\right) = H \qquad \text{(unchanged w.r.t. the FL case),} \tag{2.15}$$

$$\frac{\mathrm{d}^2\boldsymbol{\mathcal{D}}_{\mathrm{DR}}}{\mathrm{d}v^2} = \alpha\boldsymbol{\mathcal{R}}_{\mathrm{FL}}\boldsymbol{\mathcal{D}}_{\mathrm{DR}} \qquad \text{(reduced Ricci focusing, no Weyl focusing).} \tag{2.16}$$

Note that, since $\boldsymbol{\mathcal{R}}_{\mathrm{FL}} \propto \mathbf{1}_2$, the Jacobi matrix $\boldsymbol{\mathcal{D}}_{\mathrm{DR}}$ can be replaced in Eq. (2.16) by the square-root of its determinant, that is D_A^{DR}. Equations (2.15) and (2.16) can also be gathered in order to get a unique, second-order, differential equation

$$\frac{\mathrm{d}^2 D_A^{\mathrm{DR}}}{\mathrm{d}z^2} + \left(\frac{2}{1+z} + \frac{\mathrm{d}\ln H}{\mathrm{d}z}\right)\frac{\mathrm{d}D_A^{\mathrm{DR}}}{\mathrm{d}z} + \frac{3\alpha\Omega_{\mathrm{m}0}}{2}\left[\frac{H_0}{H(z)}\right]^2(1+z)D_A^{\mathrm{DR}}(z) = 0, \tag{2.17}$$

known as the DR equation. In the original formulation of the DR approximation, the smoothness parameter α was assumed to be a constant. However, according to its very definition, one can expect α (i) to depend on the line of sight, and (ii) to vary even along a given line of sight. In particular, it has been shown empirically [50] that, at least in a particular model for matter distribution, the DR equation gives results in good agreement with weak lensing if $\alpha - 1 \propto (1+z)^{-5/4}$. See also Ref. [51] for a discussion about how to measure α and test the DR approximation.

2.3 On the physical relevance of the approximation

The physical relevance and the mathematical consistency of the DR approximation have been both questioned in the litterature [37, 52–55]. One of the criticisms, which lead to a "modified DR approximation" [37, 56], relies on the argument that it is inconsistent to consider the Universe effectively underdense *only* in the focusing term, and not in the $z(v)$ relation. In other words, hypotheses **DR1** and **DR3** would be incompatible.

In reaction to this argument, we stress that the essence of the DR approximation is precisely to notice that $z(v)$ and $D_A(v)$ are ruled by the properties of the Universe considered *at distinct scales*. On the one hand, $z(v)$ essentially[3] depends on how the source and the observer move with respect to each other (adopting a Doppler-like interpretation of the cosmological redshift [57]). he geodesic deviation equation indicates that this relative motion is governed by spacetime curvature on the scale of the distance between the source and the observer. On the other hand, $D_A(v)$ depends on the relative motion of two neighbouring rays within the beam, governed by spacetime curvature on the scale of the beam itself. The ratio between both scales is given by the angular aperture of the beam, which is typically $\sim 10^{-10}$ for SN observations. Therefore, it is not inconsistent to suppose that a typical light beam could "feel" an underdense universe while the source and the observer do not.

Let us close this section by a word on backreaction. It is known since the late 90s that inhomogeneities of the distribution of matter in the Universe potentially affect its expansion averaged on cosmological scales (see, e.g., Refs. [58–60] for reviews). For the purpose of tracking such an effect in cosmological observations, one must wonder which properties of light propagation would be the most affected. Proceeding the rationale of the above paragraph, we expect the $D_A(v)$ relation to be unaffected by any backreaction effect, because it involves too small scales. On the contrary, since the $z(v)$ relation has much more to do with a notion of global expansion, backreaction should have an impact on it. Therefore, one way of reading hypothesis **DR1** of the DR approximation is that it describes a clumpy universe with *no backreaction*. This is, precisely, one of the main properties of the Swiss-cheese models presented in the next section (although this can be discussed, see Sec. 3.4.)

3 Swiss-cheese models

Historically, Swiss-cheese (SC) models were introduced by Einstein and Straus [38, 39], in 1945, as a method to embed a compact object within the expanding universe. It consists in removing a spherical comoving region from a FL spacetime, and replacing it by a point mass at the center of the region (see Fig. 1). This creates a "hole" within the Friedmannian "cheese", and the operation can be repeated anywhere else, as long as the holes do not overlap. The reason why such a construction is possible is that the Schwarzschild (or Kottler) and FL geometries glue perfectly on a spherical frontier. This property can be justified (see, e.g., Refs. [20, 41]) invoking the Darmois-Israel junction conditions [61–63] between two spacetimes. In this section, we propose a slightly more intuitive approach.

3.1 Free-fall coordinates for the Kottler metric

The Kottler geometry [64] is the extension of the Schwarzschild geometry to the case of a non-vanishing cosmological constant. Written with the usual Droste-Schwarzschild coordinates,

---

[3]i.e., neglecting purely gravitational effects such as the (integrated) Sachs-Wolfe or Rees-Sciama effects.
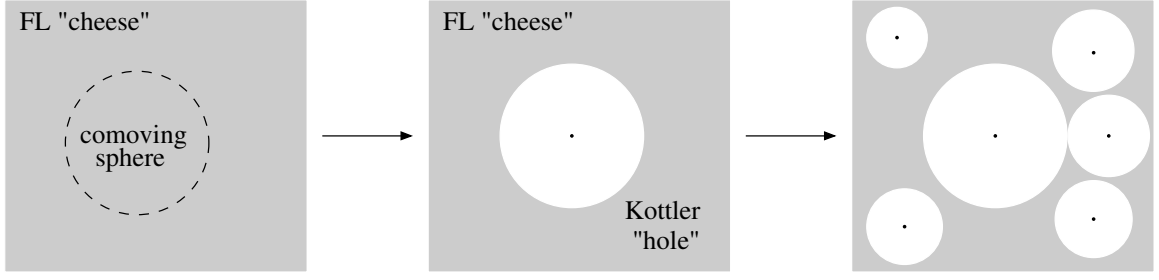
Figure 1. Schematic construction of a Swiss-cheese model.

the associated metric reads

$$ds^2 = -A(r)\,dt^2 + \frac{dr^2}{A(r)} + r^2 d\Omega^2, \tag{3.1}$$

with $A(r) \equiv 1 - r_S/r - \Lambda r^2/3$, $r_S \equiv 2GM$ being the Schwarzschild radius associated with the central mass M. It is possible to make this metric resemble the FL one (2.1), by using comoving and synchronous coordinates adapted to radially free-falling observers, analogous to the ones used to describe the Lemaître-Tolman-Bondi (LTB) geometry [65–67]. The construction is the following. Consider a test particle, which starts (at $t = 0$) a radial free fall from $r = R$. Since R is, here, an initial position, it can play the role of *label* for the particle, like a Lagrangian coordinate. If, from the point of view of a static observer at infinity, the particle has an energy $\gamma(R)$, then its free-fall is characterized by the four-velocity

$$u = \frac{\gamma(R)}{A(r)}\partial_t + \sqrt{\gamma^2(R) - A(r)}\,\partial_r. \tag{3.2}$$

One can indeed check that u satisfies the geodesic equation. Let T be the proper time of the particle ($dT = u_\mu dx^\mu$), with an arbitrary origin $T = T_0(R)$. Since $u^r = dr/dT$, the relation between r, R, and T can be obtained by integrating Eq. (3.2), so that

$$T - T_0(R) = \int_R^r \frac{d\bar{r}}{\sqrt{\gamma^2(R) - A(\bar{r})}}. \tag{3.3}$$

We now consider an infinity of such free-falling particles, filling space, and we rewrite the Kottler metric (3.1) using the coordinates (T, R) instead of (t, r). It is not necessary, for that purpose, to integrate explicitly Eq. (3.3). Using only the free-fall four-velocity u, we get

$$ds^2 = -dT^2 + \frac{1}{\gamma^2(R)}\left(\left.\frac{\partial r}{\partial R}\right|_T\right)^2 dR^2 + r^2(T, R)\,d\Omega^2. \tag{3.4}$$

Furthermore, taking the derivative of Eq. (3.3) with respect to R (with T fixed) leads to

$$\left.\frac{\partial r}{\partial R}\right|_T = \sqrt{\gamma^2(R) - A(r)}\left[\frac{1}{\sqrt{\gamma^2(R) - A(R)}} + \frac{1}{2}\frac{d\gamma^2}{dR}\int_R^r \frac{d\bar{r}}{[\gamma^2(R) - A(\bar{r})]^{3/2}} - \frac{dT_0}{dR}\right]. \tag{3.5}$$

The generic "free-fall form" of the Kottler metric therefore depends on two arbitrary functions, namely $\gamma(R)$ and $T_0(R)$. Note that the above calculations implicitly assume $\gamma(R) \geq 1$, in other words, all the particles have initially a velocity greater than the escape velocity, so that

their Droste radial coordinate r goes from R to infinity. Nevertheless, the same construction is also possible for $\gamma(R) \leq 1$, provided one considers two successive phases of the particles' motion: outgoing first and then ingoing (see Novikov coordinates, at page 826 of Ref. [68]).

Various coordinate systems, which already exist in the litterature, can be recovered from the above construction by specifying particular functions $\gamma(R)$, $T_0(R)$. For example:

- Lemaître coordinates [65, 69] with $\gamma = 1$, $\mathrm{d}T_0/\mathrm{d}R = 1/\sqrt{1 - A(R)} - 1$;

- Robertson coordinates [70] with $\gamma = 1$ and $T_0 = 0$;

- Novikov coordinates [68] with $\gamma^2(R) = A(R)$ and $T_0 = 0$. The actual radial coordinate used by Novikov was, however, $R^* = \sqrt{A(R)/[1 - A(R)]}$ instead of R. Note that one cannot use Eq. (3.5) in this case.

Here, we generalize the Lemaître coordinate system by choosing $\gamma = \mathrm{cst} \neq 1$, and $\mathrm{d}T_0/\mathrm{d}R = 1/\sqrt{\gamma^2 - A(R)} - 1$. We define an inhomogeneous scale factor $\tilde{a}(T, R) = r(T, R)/R$, and the associated expansion rate $\tilde{H}(T, R) = (\partial \tilde{a}/\partial T)/\tilde{a}$. The Kottler metric then reads

$$\mathrm{d}s^2 = -\mathrm{d}T^2 + \tilde{a}^2(T, R) \left[\frac{\tilde{H}^2 R^2}{\gamma^2} \, \mathrm{d}R^2 + R^2 \mathrm{d}\Omega^2 \right], \qquad (3.6)$$

the scale factor $\tilde{a}(T, R)$ satisfying a Friedmann-like equation

$$\tilde{H}^2 = \frac{8\pi G \tilde{\rho}_0(R)}{3} \left(\frac{a_0}{\tilde{a}} \right)^3 - \frac{\tilde{K}(R)}{\tilde{a}^2} + \frac{\Lambda}{3}, \qquad (3.7)$$

where $\tilde{\rho}_0(R) \equiv M/[4\pi(a_0 R)^3/3]$ is the mean density of the sphere of radius $a_0 R$, and $\tilde{K}(R) \equiv (1 - \gamma^2)/R^2$. We conclude that each hypersurface $R = \mathrm{cst}$ behaves exactly as a (layer of a) FL universe, with comoving density $\tilde{\rho}_0(R)$ and spatial curvature parameter $\tilde{K}(R)$. Moreover, $\tilde{K}$ can indeed be related to spatial curvature, because the Ricci scalar of a $T = \mathrm{cst}$ hypersurface can be shown to be

$$^{(3)}R = \frac{2(1 - \gamma^2)}{r^2} = \frac{2\tilde{K}}{\tilde{a}^2}. \qquad (3.8)$$

3.2   Matching the Friedmann-Lemaître and Kottler geometries

Free-fall coordinates provide a natural extension of cosmic time and comoving coordinates inside the Kottler holes of a SC universe. They also allow us to understand more intuitively the junction between the FL and Kottler spacetimes at the boundary of a hole. Indeed, as we have seen above, each layer $R = \mathrm{cst}$ expands as a FL universe with density $\tilde{\rho}_0(R)$ and curvature parameter $\tilde{K}(R)$. Hence, if we choose the boundary of a Kottler hole as a sphere of radius R_h, so that

$$\rho_0 = \tilde{\rho}_0(R_\mathrm{h}) \equiv \frac{3M}{4\pi(a_0 R_\mathrm{h})^3}, \qquad (3.9)$$

and, additionally, set γ so that $\tilde{K}(R_\mathrm{h}) = K$, then such a sphere will have the same expansion dynamics as the one of the FL cheese. In other words,

$$\forall T \qquad \tilde{a}(T, R_\mathrm{h}) = a(T), \qquad (3.10)$$

which matches the Kottler and FL geometries on the layer $R = R_\mathrm{h}$.

For the sake of completeness, let us also check that, under the conditions specified above, the two Darmois-Israel junction conditions are automatically satisfied. First, the intrinsic metric of the junction hypersurface (i.e., the hole boundary) is the same whether one computes it from the inside of from the outside,

$$ds^2_{in}(R = R_h) = -dT^2 + \tilde{a}^2(T, R_h)R_h^2 d\Omega^2 \tag{3.11}$$

$$= -dT^2 + a^2(T)R_h^2 d\Omega^2 \tag{3.12}$$

$$= ds^2_{out}(R = R_h). \tag{3.13}$$

Secondly, the extrinsic curvature of the junction hypersurface $R = R_h$ is identical whether one computes it from the inside or from the outside. Recall that the extrinsic curvature tensor of a hypersurface is

$$\mathcal{K}_{ab} \equiv e_a{}^\mu e_b{}^\nu \nabla_\mu n_\nu, \tag{3.14}$$

where n is a normal unit vector, and the e_a are three tangent vectors to the hypersurface. Here, the latter can be trivially chosen as $(e_a) = (\partial_T, \partial_\theta, \partial_\varphi)$. From the FL (outside) point of view, the unit normal vector reads $n_\mu = a\delta^R_\mu / \sqrt{1 - KR_h^2}$, from which one deduces

$$\mathcal{K}^{out}_{ab} dx^a dx^b = a(T)R_h\sqrt{1 - KR_h^2}\, d\Omega^2. \tag{3.15}$$

From the Kottler (inside) point of view, normal vector reads $n_\mu = \tilde{a}\tilde{H}R_h\delta^R_\mu / \gamma$, from which one computes

$$\mathcal{K}^{in}_{ab} dx^a dx^b = \tilde{a}(T, R_h)R_h\sqrt{1 - \tilde{K}(R_h)R_h^2}\, d\Omega^2. \tag{3.16}$$

Thus, both tensors (3.15) and (3.16) coincide, provided that $\tilde{K}(R_h) = K$ and $\tilde{a}(T, R_h) = a(T)$.

3.3 Orders of magnitude

For a SC model to fit with the general philosophy of the DR approximation, it must aim at representing the clumpy, small-scale structure of the Universe. In principle, to be consistent with the typical cross-sectional scale of a light beam associated with astronomical observations, the holes should represent the local environment of individual stars. However, as already discussed in Ref. [41], we will not consider such an extreme resolution, but rather stop at the scale of individual galaxies. This leads us to choose the mass parameter of the Kottler regions as $M \sim M_{gal} \sim 10^{11}\, M_\odot$, which corresponds, because of the junction condition (3.9), to a typical hole radius

$$R_h \sim 1\,\text{Mpc}. \tag{3.17}$$

A crucial assumption, for the above choice to be meaningful and the calculations of this article to be justifed, is that *the clumps at the center of the holes are considered effectively opaque*. In other terms, when studying light propagation through a Swiss cheese in Sec. 4 below, we will impose a lower cutoff, for the photon's impact parameter in the Kottler regions, corresponding to the physical size of the central galaxy (see Fig. 2)

$$b > r_{gal} \sim 10\,\text{kpc}. \tag{3.18}$$

Albeit an instrinsic limitation to the SC approach, such an assumption can be justified statistically (the cross-section of a galaxy is relatively small) and observationally (a galaxy is bright enough to hide a supernova behind it). See Refs. [41, 71] for further discussions.

Summarizing, Kottler holes are characterized by a hierarchy of length scales

$$r_{\mathrm{S}} \ll r_{\mathrm{gal}} \ll R_{\mathrm{h}} \ll H_0^{-1} \lesssim K^{-1/2}, \Lambda^{-1/2}, \tag{3.19}$$

essentially controlled by the single dimensionless parameter ε, so that

$$\varepsilon \equiv \frac{r_{\mathrm{S}}}{R_{\mathrm{h}}} \sim (H_0 R_{\mathrm{h}})^2 \sim 10^{-8}. \tag{3.20}$$

The second relation is deduced from the junction condition (3.9) and the Friedmann equation (2.5). Parameter ε will be ubiquitous in the perturbative expansions of Sec. 4.
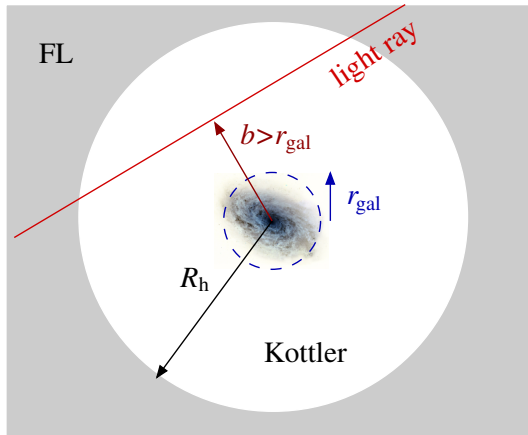
Figure 2. Hierarchy of length scale and opacity radius in a Kottler hole.

3.4   Backreaction and Swiss-cheese models

By construction, the Einstein-Straus method allows one to introduce inhomogeneities in a FL universe *without changing its expansion law*. This implies, in particular, that the physical distance between the point masses at the center of two neighbouring holes increases according the Hubble law. In this sense, SC models can be considered backreaction free. In principle, this reasoning should also remain valid for other classes of SC models, a notable representative of which is the LTB SC model, whose holes are filled with an inhomogeneous, non-static, and spherically symmetric dust fluid. While such models differ from the Einstein-Straus one by the choice of the interior metric, the general philosophy is still the same: pick a comoving ball within a FL universe, and reorganize the matter inside it. Again, by construction, this does not change the exterior expansion law (i.e., the expansion law of the FL regions of the SC).

Nevertheless, it might be naive to directly conclude that SC models are backreaction free. Indeed, the *spatially averaged* expansion rate of, e.g., a LTB SC model, can differ from the exterior one [59, 72, 73]. Thus, in this sense, SC models are in general *not* backreaction free. We emphasize that this interpretation tacitly considers the averaged expansion rate as the relevant physical quantity to decribe the dynamics of the Universe, which is a highly non-trivial, and widely debated assumption. Notable contributions to this debate [55, 73–75] concluded that, in a fluid-filled and shell-crossing-free universe, the spatially averaged expansion rate really governs the angular distance-redshift relation, and therefore has a powerful physical and observational meaning. However, there is a priori not reason why this result should hold

for a more realistic description of the Universe, with shell crossings, formation of virialized structures decoupled from the expansion, etc.

In particular, the class of Swiss-cheese models that we study in the present article, where holes are composed of vaccum and structures in equilibrium, seems precisely to be a counterexample. Indeed, in vacuum there is no unique and natural way to define a 3+1 foliation, and a fortiori a spatially averaged expansion rate. Hence such a notion automatically loses its relevance and its observational meaning—in particular, it cannot drive the distance-redshift relation—when Kottler holes are present. The very meaning of backreaction also becomes unclear, since it usually refers to the influence of inhomogeneities on the average expansion rate. Here, we choose to avoid this issue and identify the expansion rate of our SC model to the one of its FL regions, because it is the only unambiguous choice that we can make. Thus, *from this naive point of view* and according to the discussion of the first paragraph above, the model is backreaction free.

4   Geometric optics in Swiss-cheese models

Swiss-cheese models have been used since the late 60s [19–21, 41] to investigate the impact of a clumpy distribution of matter on light propagation, and its consequences on cosmological observables. More recently, they were revisited by replacing Kottler holes by LTB holes, in order to model the large-scale structure of the Universe (voids and walls) rather than its small-scale clumpiness. See Refs. [22–30] for detailed studies about their optical properties.

In this section, we prove analytically that the DR approximation captures the essential physics of light propagation in SC models with Kottler holes, provided the conditions described in Sec. 3.3 are fulfilled.

4.1   Relation between affine parameter and redshift

The presence of Kottler holes, in a SC universe, modifies the $z(v)$ relation. In this subsection, we show that such a correction is of order $N\varepsilon$, where N is the number of holes crossed by the light beam, and ε the small parameter defined in Sec. 3.3.

Let us start by investigating the effect of a single hole. Consider a source and an observer comoving with the boundary of the hole (both have a four-velocity $u = \partial_T$); denote respectively "in" and "out" the emission and the reception events. The redshift of a photon which has travelled through the hole is

$$(1 + z)_{\text{in}\to\text{out}} \equiv \frac{\nu_{\text{in}}}{\nu_{\text{out}}} = \frac{(u_\mu k^\mu)_{\text{in}}}{(u_\mu k^\mu)_{\text{out}}} = \frac{k^T_{\text{in}}}{k^T_{\text{out}}}. \tag{4.1}$$

Without any loss of generality, we assume that the photon travels in the plane $\theta = \pi/2$. The symmetries (Killing vectors) of the Kottler geometry imply the existence of two conserved quantities: the "energy" E and the "orbital momentum" L of the photon, so that, in terms of Droste coordinates,

$$A(r)k^t = E, \qquad r^2 k^\varphi = L. \tag{4.2}$$

Besides, the coordinate transformation $(t, r) \mapsto (T, R)$ implies

$$k^T = \gamma\, k^t - \frac{\sqrt{\gamma^2 - A}}{A}\, k^r = \left[\gamma \pm \sqrt{\gamma^2 - A}\sqrt{1 - A\left(\frac{b}{r}\right)^2}\right]\frac{E}{A}, \tag{4.3}$$

where $b \equiv L/E$ is the impact parameter, and $\pm \equiv \text{sign}(k^r)$ depends on whether the photon is approaching $(-)$ or receding $(+)$ from the center of the hole. In Eq. (4.3), we have used the constants of motion, and the fact that k is null-like. The redshift is therefore

$$(1+z)_{\text{in}\to\text{out}} = \frac{A_{\text{out}}}{A_{\text{in}}} \frac{1 + \sqrt{1 - A_{\text{in}}/\gamma^2}\sqrt{1 - A_{\text{in}}\left(b/r_{\text{in}}\right)^2}}{1 - \sqrt{1 - A_{\text{out}}/\gamma^2}\sqrt{1 - A_{\text{out}}\left(b/r_{\text{out}}\right)^2}}, \tag{4.4}$$

where $A_{\text{in}} \equiv A(r_{\text{in}}) = A(a_{\text{in}}R_{\text{h}})$, and the same for A_{out}. This relation is exact. Using the equations which rule the dynamics of the photon and of the hole boundary, it is possible to show that the right-hand side of Eq. (4.4) is essentially the cosmological redshift $a_{\text{out}}/a_{\text{in}}$, modulo corrections of order ε (see Appendix A for a proof),

$$(1+z)_{\text{in}\to\text{out}} = \frac{a_{\text{out}}}{a_{\text{in}}} \left[1 + \mathcal{O}(\varepsilon)\right]. \tag{4.5}$$

The corrections hidden in the $\mathcal{O}(\varepsilon)$ term contain both the effect of light deflection in the Kottler hole, and the integrated Sachs-Wolfe (or Rees-Sciama) effect.

If, during its travel through the SC, the photon crosses N holes, then the total redshift is

$$(1+z)_{\text{s}\to\text{o}} = \frac{a_{\text{o}}}{a_{\text{s}}} \prod_{i=1}^{N} \left[1 + \mathcal{O}(\varepsilon)\right] = \frac{a(T_{\text{o}})}{a(T_{\text{s}})} \left[1 + \mathcal{O}(N\varepsilon)\right]. \tag{4.6}$$

Equation (4.6) indicates that if a photon is emitted at cosmic time T_{s} and observed at T_{o}, then the redshift z_{SC} measured in a SC universe is $z_{\text{FL}} + \mathcal{O}(N\varepsilon)$, where z_{FL} is the redshift that would be measured in a FL universe. Interestingly, this *also* implies that the corresponding affine parameters read $v_{\text{SC}} = [1 + \mathcal{O}(N\varepsilon)]v_{\text{FL}}$. Let us justify this subtle point. By definition, the $T(v)$ relation is governed by

$$\frac{\mathrm{d}T}{\mathrm{d}v} = k^T = \omega = \omega_{\text{o}}(1+z), \tag{4.7}$$

thus, because of Eq. (4.6),

$$\frac{\mathrm{d}v_{\text{SC}}}{\mathrm{d}T} = [1 + \mathcal{O}(N\varepsilon)]\frac{\mathrm{d}v_{\text{FL}}}{\mathrm{d}T} \qquad \text{whence} \qquad v_{\text{SC}} = [1 + \mathcal{O}(N\varepsilon)]v_{\text{FL}}. \tag{4.8}$$

We conclude that the affine parameter-redshift relation of a SC only differs by terms of order $N\varepsilon$ from the FL one. This corresponds to the hypothesis **DR1** of the DR approximation. A numerical illustration, performed by ray tracing in a SC model, is proposed in Sec. 5.

We emphasize that, in the above proof, both the source and the observer were assumed to be *comoving within FL regions*. Hence, two effects which affect the $z(v)$ relation were neglected. First, a source and an observer lying inside Kottler holes would in general undergo a different gravitational potential, depending on their distance to the hole center. The actual redshift must therefore be corrected by a factor $A(r_{\text{o}})/A(r_{\text{s}})$, which is at most $\sim 1 + r_{\text{S}}/r_{\text{gal}} = 1 + \mathcal{O}(100\varepsilon)$. This effect is therefore subdominant when many holes are crossed $(N > 100)$. The second neglected effect is the one of peculiar velocities (Doppler shift), and is potentially much more significant. Note that it would not only affect the redshift, but also the angular/luminosity distance [15, 76–78].

For a more general point of view, as already mentioned in Sec. 2.3, we suspect that the deep underlying reason why, here, there is no strong modification of the $v(z)$ relation, is the *absence of backreaction* in SC models. Proving this intuition may however require a dedicated study, whose starting point can be elements proposed in Refs. [37, 55].

4.2 Ricci and Weyl focusing in holes

The focusing properties of a Kottler hole are ruled by its optical tidal matrix $\boldsymbol{\mathcal{R}}_{\mathrm{K}}$. In order to compute it, we first need to specify a Sachs basis. The reference observers' family is chosen as "generalized comoving observers", that is, observers with constant Lemaître radial coordinate R. As already seen in Sec. 3, such observers have the four-velocity $u = \partial_T$ defined by Eq. (3.2). The screen vectors s_1, s_2 form an orthonormal basis of the plane orthogonal to both u and k. As before, we can, without loss of generality, assume that the light's trajectory occurs in the equatorial plane $\theta = \pi/2$, so that a first screen vector can be trivially chosen as

$$s_1 \equiv \partial_z = -\frac{1}{r}\,\partial_\theta. \tag{4.9}$$

It is straightforward to check that s_1 fulfills the transport condition (1.8). The second screen vector, s_2, can then be obtained from the orthogonality and normalization constraints defining the Sachs basis, but it turns out that its explicit expression is not required here.

We now compute the optical tidal matrix $\boldsymbol{\mathcal{R}}_{\mathrm{K}}$. It is convenient, here, to use the Ricci-Weyl decomposition (1.12). Indeed, since the Kottler geometry describes vacuum, the only contribution to its Ricci tensor is the cosmological constant, $R_{\mu\nu} \propto \Lambda g_{\mu\nu}$, so that

$$\Phi_{00} \equiv -\frac{1}{2}R_{\mu\nu}k^\mu k^\nu = 0 \tag{4.10}$$

Thus, there is no source of convergence in a Kottler hole, and $\boldsymbol{\mathcal{R}}_{\mathrm{K}}$ is trace free. The calculation of the source of shear Ψ_0 is detailed in Appendix B, and the result leads to

$$\boldsymbol{\mathcal{R}}_{\mathrm{K}} = \begin{pmatrix} -\Psi_0 & 0 \\ 0 & \Psi_0 \end{pmatrix}, \qquad \text{with} \qquad \Psi_0 = \frac{3}{2}\left(\frac{L}{r_{\mathrm{S}}^2}\right)^2\left(\frac{r_{\mathrm{S}}}{r}\right)^5. \tag{4.11}$$

As one could expect, the effect of the central mass is to vertically squeeze and horizontally stretch the light beam via tidal forces. The effect is stronger as M increases, and as b decreases. Besides, it is remarkable that the cosmological constant Λ, though having an impact on light *deflection*, does not *focus* light. From an observational point of view, it means that for a given value of the affine parameter v, the position on the sky of a light source can be affected by Λ, but not its magnitude.

The Sachs equation $\ddot{\boldsymbol{\xi}} = \boldsymbol{\mathcal{R}}_{\mathrm{K}}\boldsymbol{\xi}$ can be solved perturbatively [41] in order to get the expression of the Wronski matrix $\boldsymbol{\mathcal{W}}_{\mathrm{K}}$. However, at the order of interest for the discussion of this article, the result is simply

$$\boldsymbol{\mathcal{W}}_{\mathrm{K}}(\text{out} \leftarrow \text{in}) = \begin{pmatrix} \mathbf{1}_2 & (v_{\text{out}} - v_{\text{in}})\mathbf{1}_2 \\ \mathbf{0}_2 & \mathbf{1}_2 \end{pmatrix} + \mathcal{O}(\varepsilon). \tag{4.12}$$

In other words, light behaves in the Kottler geometry as in Minkowski spacetime, modulo small tidal terms contained in the $\mathcal{O}(\varepsilon)$ term, that we neglect here. Note that neglecting tidal effects, i.e., the source of shear, in the Kottler holes, corresponds to hypothesis **DR2** of the DR approximation.

4.3 Effective Ricci focusing in a Swiss cheese

As already mentioned in Sec. 1.3, the Wronski matrix is a particularly convenient tool for dealing with a patchwork of spacetimes, such as a SC model, thanks to its "Chasles

relation" (1.17). Indeed, consider a light beam which travels, in a SC universe, from a source, s, to an observer, o, both located in FL regions. If this beam crosses N Kottler holes, then the Wronski matrix describing its evolution can be decomposed as

$$\boldsymbol{\mathcal{W}}_{\mathrm{SC}}(\mathrm{o} \leftarrow \mathrm{s}) = \boldsymbol{\mathcal{W}}_{\mathrm{FL}}(\mathrm{o} \leftarrow \mathrm{out}_N) \ldots \underbrace{\boldsymbol{\mathcal{W}}_{\mathrm{FL}}(\mathrm{in}_{n+1} \leftarrow \mathrm{out}_n) \boldsymbol{\mathcal{W}}_{\mathrm{K}}(\mathrm{out}_n \leftarrow \mathrm{in}_n)}_{\boldsymbol{\mathcal{W}}_{\mathrm{SC}}(\mathrm{in}_{n+1} \leftarrow \mathrm{in}_n) \equiv \boldsymbol{\mathcal{W}}_{\mathrm{SC}}^{(n)}} \ldots \boldsymbol{\mathcal{W}}_{\mathrm{FL}}(\mathrm{in}_1 \leftarrow \mathrm{s})$$

(4.13)

where in_n, out_n respectively denote the entrance and exit of the nth hole (see Fig. 3).
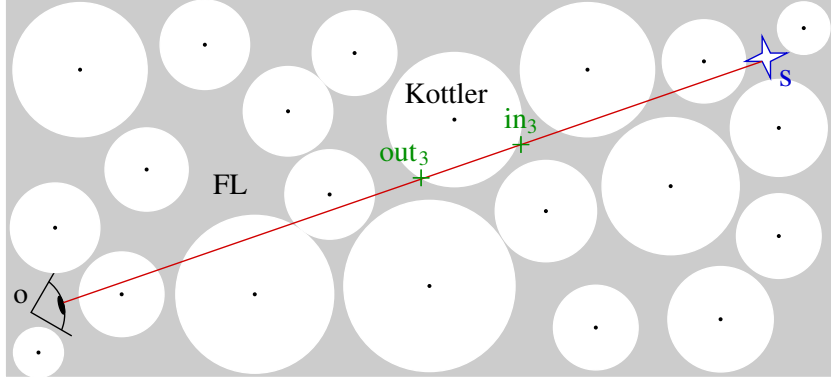

Figure 3. A light beam travels, through the Swiss-cheese universe, from a source s to an observer o. The entrance and exit event for the nth Kottler hole are respectively denoted in_n and out_n.

The matrices $\boldsymbol{\mathcal{W}}_n \equiv \boldsymbol{\mathcal{W}}_{\mathrm{SC}}(\mathrm{in}_{n+1} \leftarrow \mathrm{in}_n)$ represent the elementary bricks of the complete evolution. As we will see below, they merge the FL and Kottler optical properties into an effective behavior, which coincides with the one proposed by the Dyer-Roeder approximation. First consider the FL part. Since the path between the holes n and $n+1$ is small compared to the cosmological scale H^{-1}, one can expand the exact results (2.10), (2.11), (2.12), and (2.13) to obtain

$$\boldsymbol{\mathcal{W}}_{\mathrm{FL}}(\mathrm{in}_{n+1} \leftarrow \mathrm{out}_n) = \begin{pmatrix} \mathbf{1}_2 & \left[v_{\mathrm{in}}^{(n+1)} - v_{\mathrm{out}}^{(n)} \right] \mathbf{1}_2 \\ -4\pi G \rho_n \omega_n^2 \left[v_{\mathrm{in}}^{(n+1)} - v_{\mathrm{out}}^{(n)} \right] \mathbf{1}_2 & \mathbf{1}_2 \end{pmatrix} + \mathcal{O}\left[(H \Delta T)^2 \right],$$

(4.14)

where $\Delta T \equiv T_{\mathrm{in}}^{(n+1)} - T_{\mathrm{out}}^{(n)}$. The matrix product between Eqs. (4.12) and (4.14) then yields

$$\boldsymbol{\mathcal{W}}_{\mathrm{SC}}^{(n)} = \mathbf{1}_4 + \begin{pmatrix} \mathbf{0}_2 & \left[v_{\mathrm{in}}^{(n+1)} - v_{\mathrm{in}}^{(n)} \right] \mathbf{1}_2 \\ -4\pi G \rho_n \omega_n^2 \left[v_{\mathrm{in}}^{(n+1)} - v_{\mathrm{out}}^{(n)} \right] \mathbf{1}_2 & \mathbf{0}_2 \end{pmatrix} + \mathcal{O}\left[\varepsilon, (H \Delta T)^2 \right] \quad (4.15)$$

$$= \mathbf{1}_4 + \begin{pmatrix} \mathbf{0}_2 & \mathbf{1}_2 \\ \alpha_n \boldsymbol{\mathcal{R}}_{\mathrm{FL}}(v_n) & \mathbf{0}_2 \end{pmatrix} \left[v_{\mathrm{in}}^{(n+1)} - v_{\mathrm{in}}^{(n)} \right] + \mathcal{O}\left[\varepsilon, (H \Delta T)^2 \right],$$

(4.16)

where we have recognized the FL optical tidal matrix $\boldsymbol{\mathcal{R}}_{\mathrm{FL}}$, given in Eq. (2.9), while

$$\alpha_n \equiv \frac{v_{\mathrm{in}}^{(n+1)} - v_{\mathrm{out}}^{(n)}}{v_{\mathrm{in}}^{(n+1)} - v_{\mathrm{in}}^{(n)}}$$

(4.17)

represents the portion of the path ($\text{in}_n \to \text{in}_{n+1}$) that light spent in the FL region. Interpolating the sequence (α_n) allows one to define a function $\alpha(v)$, which, in principle, depends on the path of light through the Swiss cheese. Note that the way we deal with the expansion (4.16) is licit; it is indeed reasonable to consider that the separation between successive holes has the same order of magnitude as the radius of a hole, thus $(H\Delta T)^2 \sim (HR_{\text{h}})^2 \sim \varepsilon$ (see Sec. 3.3).

We now show that $\alpha \mathcal{R}_{\text{FL}}$ plays the role of an effective optical tidal matrix. First note that Eq. (4.16) can be seen as a first-order Taylor expansion of $\mathcal{W}_{\text{SC}}(v)$, so that, at leading order in the small parameters of the problem,

$$\begin{pmatrix} \mathbf{0}_2 & \mathbf{1}_2 \\ \alpha(v)\mathcal{R}_{\text{FL}}(v) & \mathbf{0}_2 \end{pmatrix} = \lim_{v' \to v} \frac{\partial \mathcal{W}_{\text{SC}}}{\partial v}(v \leftarrow v') \equiv \frac{\partial \mathcal{W}_{\text{SC}}}{\partial v}(v \leftarrow v), \tag{4.18}$$

Besides, taking the derivative of the "Chasles relation" (1.17) with respect to v_3, and evaluating the result for $v_2 = v_3$, yields

$$\frac{\partial \mathcal{W}_{\text{SC}}}{\partial v_3}(v_3 \leftarrow v_1) = \frac{\partial \mathcal{W}_{\text{SC}}}{\partial v_3}(v_3 \leftarrow v_3)\mathcal{W}_{\text{SC}}(v_3 \leftarrow v_1) \tag{4.19}$$

$$\overset{(4.18)}{=} \begin{pmatrix} \mathbf{0}_2 & \mathbf{1}_2 \\ \alpha(v_3)\mathcal{R}_{\text{FL}}(v_3) & \mathbf{0}_2 \end{pmatrix} \mathcal{W}_{\text{SC}}(v_3 \leftarrow v_1). \tag{4.20}$$

Therefore, comparing the above relation with Eq. (1.18) shows that $\alpha \mathcal{R}_{\text{FL}}$ is the effective optical tidal matrix $\mathcal{R}_{\text{SC}}(v)$ for the Swiss cheese. In particular, the Jacobi matrix equation inherited from Eq. (4.20) is

$$\ddot{\mathcal{D}}_{\text{SC}} = \alpha \mathcal{R}_{\text{FL}} \mathcal{D}_{\text{SC}}. \tag{4.21}$$

This is exactly the hypothesis **DR3** of the Dyer-Roeder approximation. It also provides a precise definition of the smoothness parameter α in the context of SC models, namely, the *fraction of light path* spent in the FL regions.

5 Numerical results

This last section aims at illustrating the results of the previous one, using numerical ray tracing in a SC universe.

5.1 Details of the numerical model and ray-tracing technique

We consider SC models with a *random* distribution of Kottler holes. As mentioned in Sec. 3.3, each hole is supposed to model the local environment of a galaxy, the central mass being the galaxy itself. Since we do not want all galaxies to have the same mass, we use, in our model, the (stellar) mass function proposed in Ref. [79], to which we add artificially a factor 10 to take dark matter into account. The result is

$$p(M)\text{d}M = \frac{1}{\mathcal{N}} \left(\frac{M}{10M^*} \right)^{\alpha} \exp\left(-\frac{M}{10M^*} \right) \text{d}M, \tag{5.1}$$

with $\alpha = -1.16$, $M^* = 7.5 \times 10^{10}\, h^{-2} M_{\odot}$. This expression is considered valid in the interval $M_{\text{min}} < M < M_{\text{max}}$, with [79] $M_{\text{min}} = 10^{8.5} M_{\odot}$, $M_{\text{max}} = 10^{13} M_{\odot}$, and set to zero elsewhere. Thus, the normalization factor N is

$$\mathcal{N} = \int_{M_{\text{min}}}^{M_{\text{max}}} \left(\frac{M}{10M^*} \right)^{\alpha} \exp\left(-\frac{M}{10M^*} \right) \text{d}M. \tag{5.2}$$

Regarding ray tracing, the random character of the spatial distribution of holes is modelled using a simple technique where each ray "creates its own universe". This method was first proposed by Ref. [80], and it has already been used in many studies involving SC models, see, e.g., Refs. [24, 29, 30, 81]. It consists in putting holes on the light's trajectory, with random (comoving areal[4]) impact parameter B, random impact angle θ, and with a random comoving length $\Delta\chi_{\mathrm{FL}}$ between the exit of the nth hole and the entrance of the $(n+1)$th one. The situation is depicted in Fig. 4.
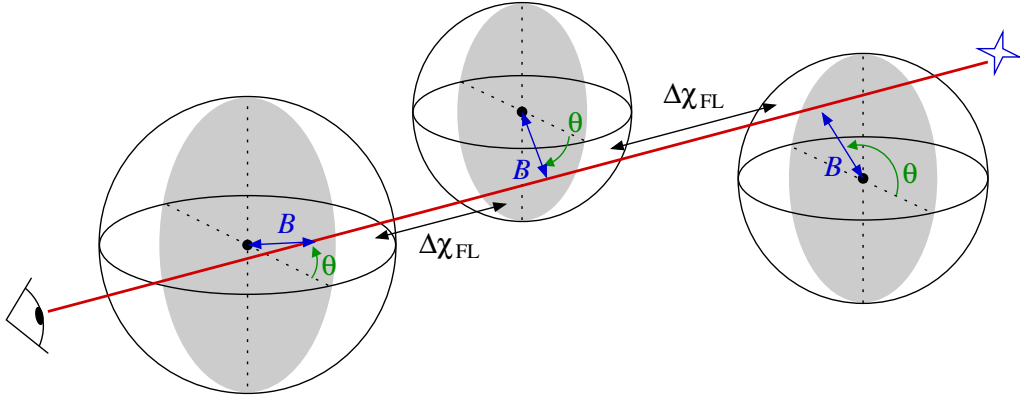

Figure 4. Ray tracing in a random SC universe. For each hole, the impact angle θ, the impact parameter B, and the separation $\Delta\chi_{\mathrm{FL}}$ until the next hole, are random numbers.

We consider that all the impacts positions, within the authorized cross section of a given hole, are equiprobable. Thus, the random impact angle θ is uniformly distributed; and the probability density function (PDF) of the impact parameter B reads

$$p(B)\,\mathrm{d}B = \frac{2B\,\mathrm{d}B}{R_{\mathrm{h}}^2 - R_{\mathrm{gal}}^2}, \qquad R_{\mathrm{gal}} < B < R_{\mathrm{h}}, \tag{5.3}$$

where R_{h} is the comoving areal radius of the hole—related to its central mass via Eq. (3.9)—and R_{gal} is the opacity radius mentioned in Sec. 3.3. We choose to link it to the mass M of the galaxy via a constant density $\rho_{\mathrm{gal}} = 5 \times 10^6\,M_\odot\,\mathrm{kpc}^{-3}$, so that

$$R_{\mathrm{gal}}(M) \equiv \left(\frac{3M}{4\pi\rho_{\mathrm{gal}}}\right)^{1/3} = \left(\frac{\rho_0}{\rho_{\mathrm{gal}}}\right)^{1/3} R_{\mathrm{h}}(M). \tag{5.4}$$

As a last simplifying assumption, the FL separation $\Delta\chi_{\mathrm{FL}}$ between two successive holes is also chosen to be uniformly distributed[5] between 0 and $\max(\Delta\chi_{\mathrm{FL}}) = 2\langle\Delta\chi_{\mathrm{FL}}\rangle$. We parametrize the mean value with an effective constant smoothness parameter $\bar{\alpha}$, so that

$$\langle\Delta\chi_{\mathrm{FL}}\rangle = \frac{\bar{\alpha}}{1-\bar{\alpha}}\,\langle\Delta\chi_{\mathrm{K}}\rangle, \tag{5.5}$$

---

[4]The usual impact parameter $b = L/E$ is defined with respect to the Droste coordinate system. Its comoving counterparts are $\beta = b/a_{\mathrm{in}}$ and $B = f_K(\beta)$. Note that, in practice, $B \approx \beta$ since $\sqrt{|K|}\beta \sim bH_0 \ll 1$.

[5]Note that this *does not* correspond to a Swiss-cheese model with randomly distributed, non-overlapping, holes. Strictly speaking, in the latter situation, there would be a correlation between the impact parameter B and $\Delta\chi_{\mathrm{FL}}$, because, e.g., $\Delta\chi_{\mathrm{FL}} = 0$ is only possible between two holes with the same impact parameter. We do not take this correlation into account for simplicity.

where $\langle \Delta\chi_{\mathrm{K}} \rangle$ is the comoving distance spent inside a Kottler hole. The calculation of this quantity is given in Appendix C, and the result is

$$\langle \Delta\chi_{\mathrm{K}} \rangle \approx \frac{4}{3} \left(\frac{3}{4\pi\rho_0} \right)^{1/3} \int_{M_{\mathrm{min}}}^{M_{\mathrm{max}}} p(M) M^{1/3} \, \mathrm{d}M. \tag{5.6}$$

In practice, the author wrote a Mathematica program to perform ray tracing in the conditions decribed previously. Calculations start at the observation event and go backward in time. The code consists in iterating the following steps. (i) Pick a FL comoving distance $\Delta\chi_{\mathrm{FL},n}$ and propagate the beam across it; (ii) pick a mass M_n, an impact parameter B_n, and an impact angle θ_n defining light propagation through the nth Kottler hole; (iii) compute the redshift and Wronski matrix across this hole. We stress that, for those numerical calculations, we did not use the lowest-order expression (4.12) for the Wronski matrix $\mathcal{W}_{\mathrm{K}}$, but rather the one of Ref. [41], which takes into account tidal effects at order one.

5.2 Relation between affine parameter and redshift

In this paragraph, we illustrate the results of Sec. 4.1, regarding the affine parameter-redshift relation. Figure 5 shows the relative difference, for the $v(z)$ relation, between a FL model and three different SC models, from very clumpy ($\bar{\alpha} = 0$) to very smooth ($\bar{\alpha} = 0.9$). All the models are characterized by the cosmological parameters obtained by the Planck experiment [3], namely $\Omega_{\mathrm{m}0} = 0.315$, $\Omega_{\Lambda 0} = 0.685$. For each SC model, 500 observations are simulated within the range $0 < z < 1.5$, according to the method presented in Sec. 5.1.
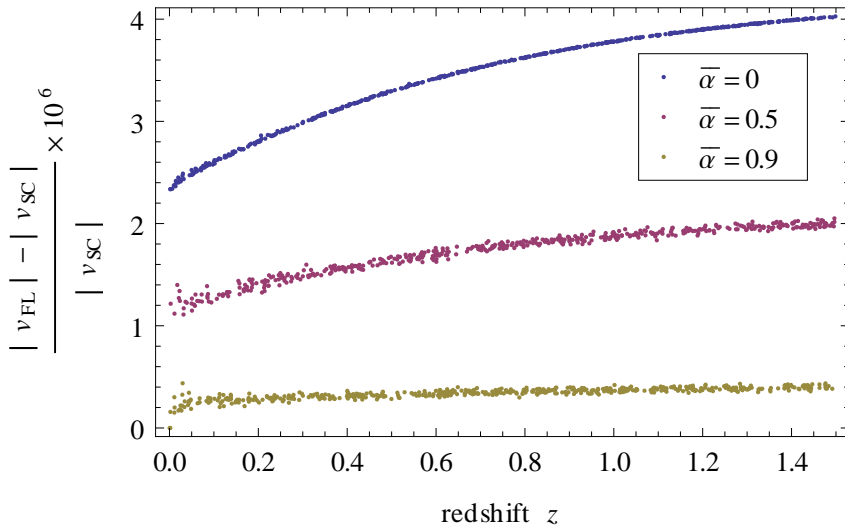
Figure 5. Relative difference between the affine parameter-redshift relation $|v_{\mathrm{FL}}(z)|$ of a FL model and of a SC model $|v_{\mathrm{SC}}(z)|$, with different values for the mean smoothness parameter $\bar{\alpha}$. From top to bottom, $\bar{\alpha} = 0$ (blue), $\bar{\alpha} = 0.5$ (magenta), and $\bar{\alpha} = 0.9$ (yellow). Absolute values are used in order to avoid any conventional discussions about whether v increases or decreases towards the past.

Even for a model entirely filled by Kottler holes ($\bar{\alpha} = 0$), we see that the relative correction to the $v(z)$ relation is very small, less than 10^{-5}. This order of magnitude is compatible with the results of Sec. 4.1.

5.3   Relation between distance and redshift

In this paragraph, we illustrate the results of Sec. 4.3, regarding effective Ricci focusing in a SC model, and its comparison with the DR approximation. Figure 6 shows the relative correction to the $D_A(z)$ relation, for three different SC and DR models, with respect to the corresponding FL models. As before, the cosmological parameters are Planck's best-fit ones, and for each SC model, 500 observations are simulated within the range $0 < z < 1.5$.
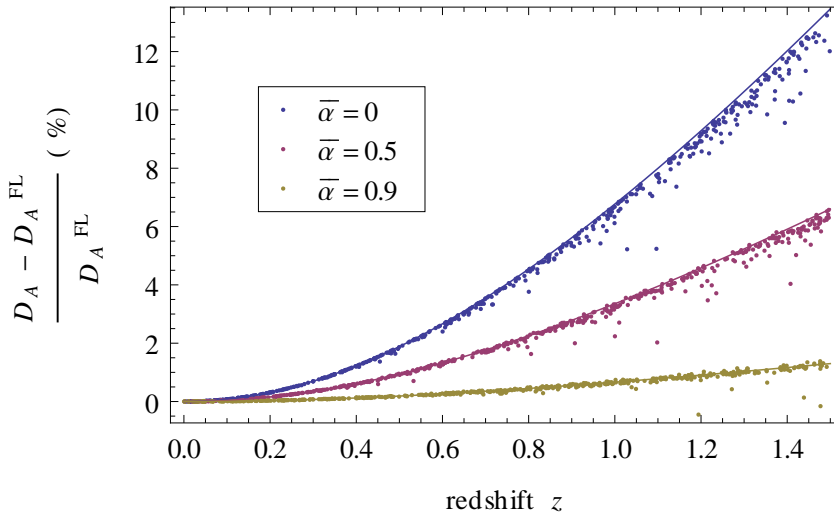
Figure 6. Correction, with respect to FL, of the angular distance-redshift relation $D_A(z)$ of several models. Dots are simulated observations in SC models with three different mean smoothness parameters $\bar{\alpha}$. From top to bottom, $\bar{\alpha} = 0$ (blue), $\bar{\alpha} = 0.5$ (magenta), and $\bar{\alpha} = 0.9$ (yellow). Solid lines indicate the corresponding DR relations $D_A^{DR}(z)$ with constant smoothness parameter $\alpha = \bar{\alpha}$.

First note that the difference between D_A^{SC} and D_A^{FL} is of the percent order, and reaches more than 12% at $z = 1.5$ for a very clumpy SC model (the cosmological implications of this difference are discussed in Refs. [8, 41]). It confirms that, in SC models, the correction to the $v(z)$ relation (Fig. 5) is negligible compared to the $D_A(v)$ one.

In Fig. 6, the good agreement between dots and solid lines numerically confirms the main point of this article, namely, that the Dyer-Roeder approximation provides a good effective description of light propagation in SC models. However, this agreement is not perfect, especially for $\bar{\alpha} = 0$, where the mean behavior of $D_A^{SC}(z)$ is slightly overestimated by $D_A^{DR}(z)$, with some rare events in strong disagreement. As we shall see in the next subsection, this is due to the neglected Weyl lensing effects, i.e., departures from hypothesis **DR2**.

5.4   Lensing beyond the Dyer-Roeder approximation

This last subsection is dedicated to some lensing effects which are present in a SC model, but not taken into account by the DR approximation. In order to compare the focusing properties of a given spacetime with those of FL model, it is convenient to introduce the amplification (or magnification) matrix

$$\mathcal{A} \equiv \mathcal{D} \cdot \mathcal{D}_{FL}^{-1} = \frac{\mathcal{D}}{\omega_o D_A^{FL}}. \tag{5.7}$$

This matrix describes the geometrical transformations of an image (magnification, deformation, rotation) which add to the global FL focusing effect. For instance, the relative magnification μ,

defined as the ratio between observed angular size of an object, and the one that would be observed in a FL universe, is related to $\boldsymbol{\mathcal{A}}$ via[6]

$$\mu \equiv \frac{\mathrm{d}\Omega_\mathrm{o}^2}{\mathrm{d}\Omega_\mathrm{o,FL}^2} = \left(\frac{D_\mathrm{A}^\mathrm{FL}}{D_\mathrm{A}}\right)^2 = \frac{1}{\det \boldsymbol{\mathcal{A}}}. \tag{5.8}$$

In general, as any 2×2 matrix, $\boldsymbol{\mathcal{A}}$ can be decomposed as the product between an SO(2) matrix, encoding the image rotation; and a symmetric matrix, encoding its distortion:

$$\boldsymbol{\mathcal{A}} = \begin{pmatrix} \cos\psi & \sin\psi \\ -\sin\psi & \cos\psi \end{pmatrix} \begin{pmatrix} 1-\kappa-\gamma_1 & -\gamma_2 \\ -\gamma_2 & 1-\kappa+\gamma_1 \end{pmatrix}, \tag{5.9}$$

where

$$\psi = \arctan\left(\frac{\mathcal{A}_{12} - \mathcal{A}_{21}}{\mathcal{A}_{11} + \mathcal{A}_{22}}\right) \tag{5.10}$$

is the rotation angle, κ is the convergence, and $\gamma = \gamma_1 + \mathrm{i}\gamma_2$ the shear, of the image. It is straighforward to check that the magnification is related to those quantities according to

$$\mu = \frac{1}{(1-\kappa)^2 - |\gamma|^2}. \tag{5.11}$$

In the DR approximation, shear and rotation are neglected. But since we are able to compute them numerically for SC models, it is interesting to see how they can induce a departure from the DR behavior. Figure 7 shows, as examples, the PDFs of the optical quantities, generated by simulating 10^4 observations at redshift $z = 1$ in three different SC models with $\bar{\alpha} = 0$, 0.5, 0.9. The values predicted by the DR approximation, with $\alpha = \bar{\alpha}$, are indicated for comparison. The evolution of the first two moments of the PDFs (mean and standard deviation) with the mean smoothness parameter $\bar{\alpha}$ of the SC model are depicted in Fig. 8. In this figure, the mean magnification $\langle\mu\rangle$ and convergence $\langle\kappa\rangle$ are also compared with the DR values.

We see that the DR approximation predicts a value for the convergence in excellent agreement with the mean convergence $\langle\kappa\rangle$ in SC models, but slightly underestimates the mean magnification $\langle\mu\rangle$, as already suspected in Fig. 6. The difference increases as the mean smoothness parameter $\bar{\alpha}$ decreases, and reaches $\langle\mu\rangle - \mu_\mathrm{DR} = 0.4\%$ for $\bar{\alpha} = 0$. More precisely, we see from the top panel of Fig. 7 that μ_DR gives essentially the *most probable* magnification, which is different from the *mean* magnification because the PDF is clearly skewed. Besides, since the PDF of the convergence seems much more symmetric, such a skewness can only come from the shear. Thus, we conclude that, in SC models, departures from the DR behavior are due to neglecting Weyl lensing, i.e. hypothesis **DR2**.

However, such departures remain small, since in the worst case $\langle\mu\rangle - \mu_\mathrm{DR} = 0.4\%$, while $\langle\mu\rangle - \mu_\mathrm{FL} = \langle\mu\rangle - 1 = -12\%$. This could be surprising, because *the shear is not intrinscally negligible* compared to the convergence, we indeed see from Fig. 8 that $\langle\kappa\rangle \sim \langle|\gamma|\rangle \sim \%$. The difference between those optical quantities is that, fortunately, the magnification μ involves κ at order one, but γ only at order two [see Eq. (5.11)]. This justifies a posteriori the expression (4.12) of $\boldsymbol{\mathcal{W}}_\mathrm{K}$, used in the proof of Sec. 4.3, where we completely dropped the Weyl focusing effects. Such an approximation would not have been consistent if we were interested in anything else than the angular distance, i.e. the determinant of the Jacobi matrix.

---

[6]Note by the way that the usual names "amplification" or "magnification" matrix for $\boldsymbol{\mathcal{A}}$ are particularly misleading, and would be much more adapted to $\boldsymbol{\mathcal{A}}^{-1}$.
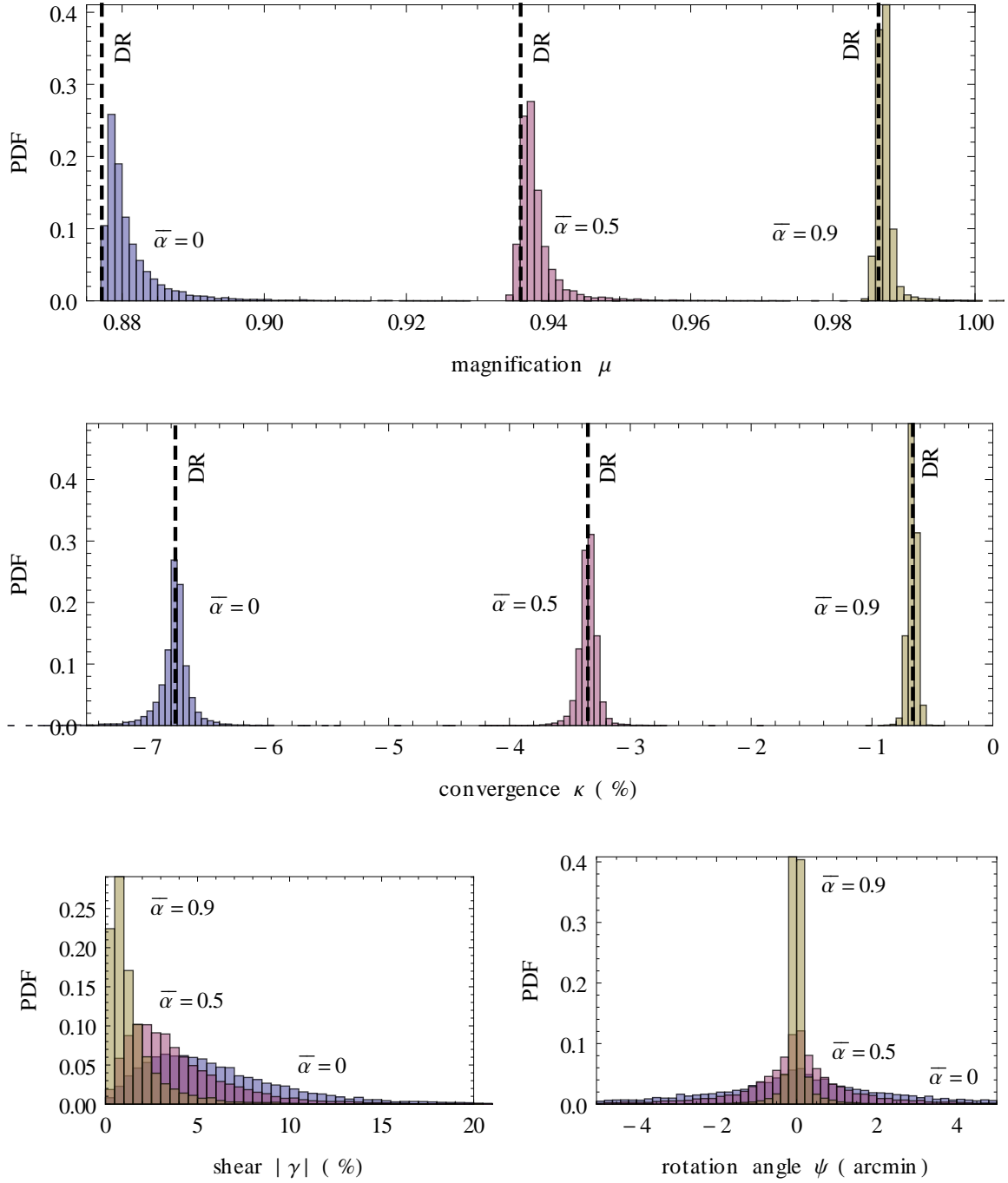
Figure 7. Probability density functions (PDFs) of the magnification μ (top panel), convergence κ (middle panel), shear $|\gamma|$ (bottom-left panel), and rotation angle ψ (bottom-right panel), in three different SC models with respective mean smoothness parameter $\bar{\alpha} = 0$ (blue), $\bar{\alpha} = 0.5$ (magenta), and $\bar{\alpha} = 0.9$ (yellow). The magnification and convergence predicted by the DR approximation are also indicated, for comparison, by vertical dashed lines.

Conclusion

In this article, we analysed the suspected correspondence between light propagation in Einstein-Straus Swiss-cheese (SC) models and the Dyer-Roeder (DR) approximation. Invoking both
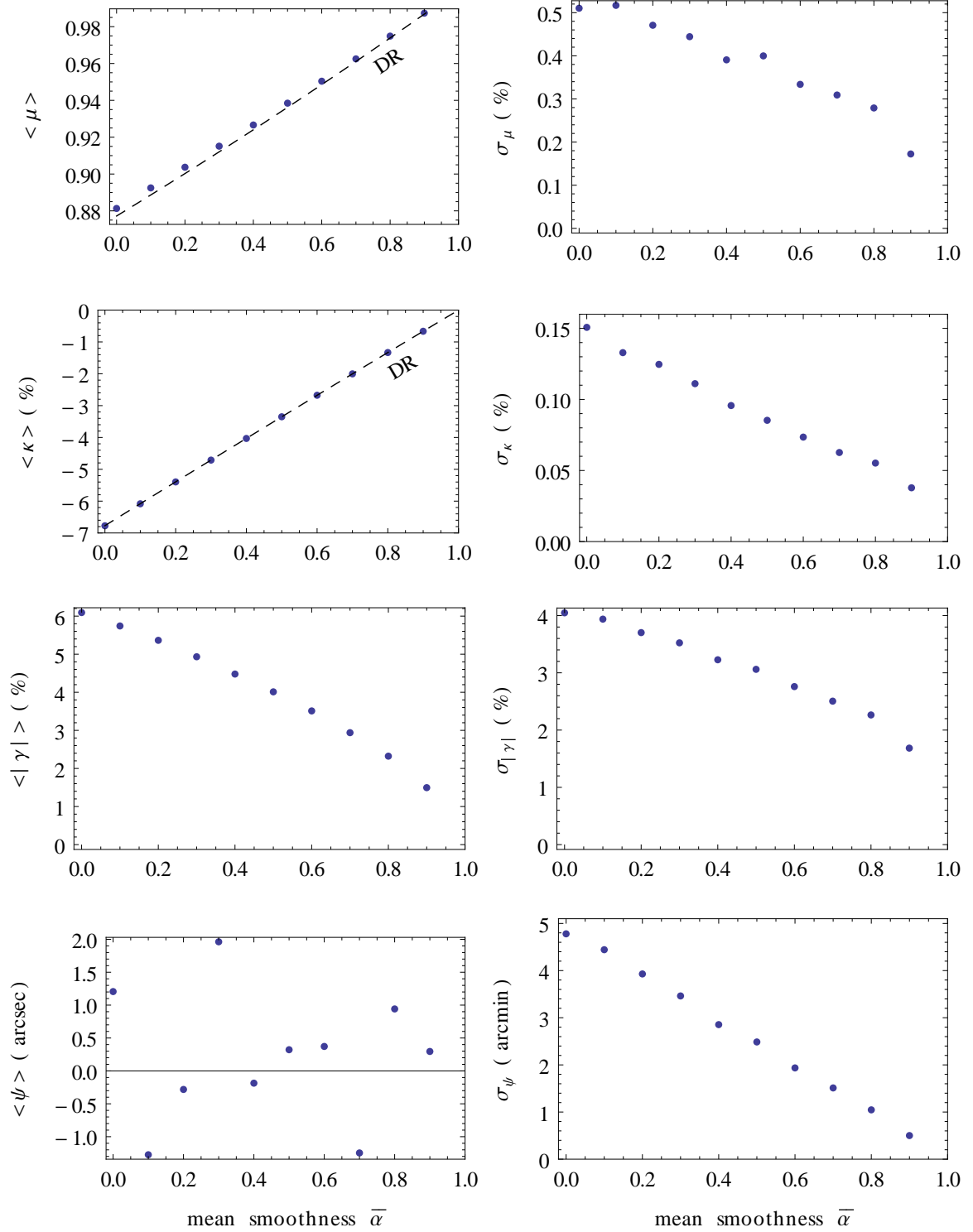
Figure 8. First two moments—mean (left column) and standard deviation (right column)—of the PDFs of, from top to bottom, the magnification μ, convergence κ, shear $|\gamma|$, and rotation angle ψ, in SC models, as a function of their mean smoothness parameter $\bar{\alpha}$. The magnifications and convergences obtained from the DR approach are indicated by dashed lines, for comparison.

analytical proofs and numerical illustrations, we proved that such an approximation is indeed excellent for predicting the distance-redshift relation of SC models, provided that (1) the matter clumps at the center of SC holes are effectively opaque, and (2) reasonable orders of magnitude are taken for the mass and compacity of the clumps.

Rather than just checking the good agreement between the results of both approaches, our main purpose was to understand why the various hypotheses of the DR approximation are satisfied in SC models. It appeared that:

- The affine parameter-redshift relation $v(z)$ is essentially the same in SC and FL models because the deflection and ISW effects are negligible. Independently of such effects, we also suspect that the absence of backreaction in our SC model (the holes do not affect the expansion law of the FL regions) is the deep reason why the FL $v(z)$ relation holds.

- In SC models, Weyl lensing (source of shear and rotation) and Ricci lensing (source of convergence) are intrinsically comparable. However, compared to the latter, the former have a negligible impact on the angular distance-affine parameter relation $D_{\mathrm{A}}(v)$, because shear only appears at order two in the expression of the magnification.

- The way the DR approximation deals with Ricci lensing, i.e., making heuristically the replacement $\rho \to \alpha\rho$ in the Sachs equation, works in SC models because (i) the clumps inside the holes are considered opaque; and (ii) FL regions and Kottler regions alternate many times over cosmological scales. This, indeed, allows the SC Wronski matrix to get an effective behavior which fits the DR one.

In the case of extremely clumpy SC models (entirely filled by Kottler holes), small departures from the DR predictions are observed, regarding the mean magnification. We saw that they were due to the effect of the neglected Weyl lensing. However, such departures remain small, since at worst $\langle\mu\rangle - \mu_{\mathrm{DR}} = 0.4\%$, to be compared with $\langle\mu\rangle - \mu_{\mathrm{FL}} = -12\%$. Moreover, the PDF of the magnification in SC models being skewed, the most probable magnification is smaller than the mean one, and thus in even better agreement with μ_{DR}. We conclude that, regarding the distance redshift relation, one can safely consider the DR and SC approaches as *equivalent*.

The question of whether those approaches are relevant alternatives to the standard interpretation cosmological data is beyond the scope of this article. It regroups at least two crucial issues of modern cosmology. The first one is the amplitude of backreaction, neglected in both the DR and SC approaches. The second one concerns the actual clumpiness of our Universe, which is closely related to the problem of structure formation, and even to the question of the nature of dark matter.

Acknowledgements

A   Redshift through a Kottler hole

Let us show that the redshift of a photon crossing a Kottler hole is essentially $a_{\text{out}}/a_{\text{in}}$,

$$(1 + z)_{\text{in}\to\text{out}} = \frac{a_{\text{out}}}{a_{\text{in}}} \times \underbrace{\frac{A_{\text{out}}}{A_{\text{in}}} \frac{r_{\text{in}} + \sqrt{1 - A_{\text{in}}/\gamma^2}\sqrt{r_{\text{in}}^2 - b^2 A_{\text{in}}}}{r_{\text{out}} - \sqrt{1 - A_{\text{out}}/\gamma^2}\sqrt{r_{\text{out}}^2 - b^2 A_{\text{out}}}}}_{1 + \mathcal{O}(\varepsilon)}, \tag{A.1}$$

where $\varepsilon \equiv r_{\text{S}}/R_{\text{h}}$. To do so, we must use both the dynamics of the photon $r_{\text{p}}(t)$ and of the hole boundary $r_{\text{h}}(t)$, in terms of Droste coordinates:

$$\frac{\mathrm{d}r_{\text{p}}}{\mathrm{d}t} = \pm A(r_{\text{p}})\sqrt{1 - A(r_{\text{p}})\left(\frac{b}{r_{\text{p}}}\right)^2}, \tag{A.2}$$

$$\frac{\mathrm{d}r_{\text{h}}}{\mathrm{d}t} = A(r_{\text{h}})\sqrt{1 - \frac{A(r_{\text{h}})}{\gamma^2}}, \tag{A.3}$$

where the $\pm$ sign depends on whether the photon is approaching $(-)$ or receding $(+)$ from the hole center. The order of magnitude of the time spent by the photon inside a hole is the radius of the latter, $\Delta t \sim r_{\text{h}}$. From Eq. (A.3), we deduce that, during this amount of time, the hole radius increases by $\delta r_{\text{h}}/r_{\text{h}} \sim \sqrt{\varepsilon}$. The corresponding variation of $A(r_{\text{h}})$ is then $A_{\text{out}}/A_{\text{in}} - 1 \sim \varepsilon^{3/2}$. Hence, since we aim at studying the expression of $(1 + z)_{\text{in}\to\text{out}}$ up to order one in ε, we can already neglect the ratio $A_{\text{out}}/A_{\text{in}}$ which appears in Eq. (A.1).

Let t_{m} be the instant when the coordinate distance between the photon and the center of the hole is minimal, $r_{\text{p}}(t_{\text{m}}) = r_{\text{m}}$. Taylor-expanding the function $r_{\text{h}}(t)$ from t_{in} to t_{m} leads to

$$r_{\text{h}}(t_{\text{m}}) = r_{\text{in}} + (t_{\text{m}} - t_{\text{in}})A_{\text{in}}\sqrt{1 - \frac{A_{\text{in}}}{\gamma^2}} + r_{\text{in}}\mathcal{O}(\varepsilon), \tag{A.4}$$

where we replaced $(\mathrm{d}r_{\text{h}}/\mathrm{d}t)_{\text{in}}$ by its expression (A.3). Besides, from Eq. (A.2), we get

$$t_{\text{m}} - t_{\text{in}} = \int_{r_{\text{m}}}^{r_{\text{in}}} \frac{\mathrm{d}r}{A\sqrt{1 - (b/r)^2 A}} = \frac{\sqrt{r_{\text{in}}^2 - b^2 A_{\text{in}}}}{A_{\text{in}}} + \underbrace{\int_{r_{\text{m}}}^{r_{\text{in}}} \frac{r^2 - b^2 A/2}{\sqrt{r^2 - b^2 A}} \frac{A'\mathrm{d}r}{2A^2}}_{\delta_{\text{in}}}, \tag{A.5}$$

where the second equality is an integration by parts. A rough analysis shows that $\delta_{\text{in}} = (r_{\text{in}}^3/b^2)\mathcal{O}(\varepsilon)$, that is, using the orders of magnitude of Sec. 3.3, $\delta_{\text{in}} = r_{\text{in}}\mathcal{O}(\varepsilon^{1/2})$. Hence, we conclude that Eq. (A.4) can be rewritten as

$$r_{\text{h}}(t_{\text{m}}) = r_{\text{in}} + \sqrt{r_{\text{in}}^2 - b^2 A_{\text{in}}}\sqrt{1 - \frac{A_{\text{in}}}{\gamma^2}} + r_{\text{in}}\mathcal{O}(\varepsilon). \tag{A.6}$$

The same calculations, but starting from an expansion of $r_{\text{h}}(t)$ from t_{in} to t_{m}, give

$$r_{\text{h}}(t_{\text{m}}) = r_{\text{out}} - \sqrt{r_{\text{out}}^2 - b^2 A_{\text{out}}}\sqrt{1 - \frac{A_{\text{out}}}{\gamma^2}} + r_{\text{out}}\mathcal{O}(\varepsilon), \tag{A.7}$$

so that, finally,

$$\frac{r_{\text{in}} + \sqrt{1 - A_{\text{in}}/\gamma^2}\sqrt{r_{\text{in}}^2 - b^2 A_{\text{in}}}}{r_{\text{out}} - \sqrt{1 - A_{\text{out}}/\gamma^2}\sqrt{r_{\text{out}}^2 - b^2 A_{\text{out}}}} = \frac{r_{\text{h}}(t_{\text{m}}) + r_{\text{in}}\mathcal{O}(\varepsilon)}{r_{\text{h}}(t_{\text{m}}) + r_{\text{out}}\mathcal{O}(\varepsilon)} = 1 + \mathcal{O}(\varepsilon). \tag{A.8}$$

B Source of shear in Kottler geometry

We compute the Weyl part (source of shear) of the optical tidal matrix $\mathcal{R}_{\mathrm{K}}$ for the Kottler geometry, using the regular Droste coordinates (t, r, θ, φ). The non-zero components of the Riemann tensor are

$$R_{trtr} = \frac{A'}{2}, \qquad R_{t\theta t\theta} = \frac{rA'A}{2}, \qquad R_{t\varphi t\varphi} = \sin^2\theta R_{t\theta t\theta}, \tag{B.1}$$

$$R_{r\theta r\theta} = -\frac{rA'}{2A}, \qquad R_{r\varphi r\varphi} = \sin^2\theta R_{r\theta r\theta}, \qquad R_{\theta\varphi\theta\varphi} = r^2(1-A)\sin^2\theta. \tag{B.2}$$

Without loss of generality, we assume that the axes have been chosen so that the light path lies in the plane $\theta = \pi/2$, which implies $k^\theta = 0$. The four-velocity of the reference observers is given by Eq. (3.2), in particular $u^\theta = 0$.

$$\mathcal{R}_{11}^{\mathrm{K}} = R_{\mu\nu\alpha\beta} s_1^\mu k^\nu k^\alpha s_1^\beta \tag{B.3}$$

$$= -r^{-2} R_{\mu\theta\nu\theta} k^\mu k^\nu \tag{B.4}$$

$$= -r^{-2} \left[\frac{rA'A}{2}(k^t)^2 - \frac{rA'}{2A}(k^r)^2 + r^2(1-A)(k^\varphi)^2 \right]. \tag{B.5}$$

but

$$\frac{rA'A}{2}(k^t)^2 - \frac{rA'}{2A}(k^r)^2 = -\frac{rA'}{2}\left[g_{tt}(k^t)^2 + g_{rr}(k^r)^2 \right] = \frac{rA'}{2} g_{\varphi\varphi}(k^\varphi)^2 = \frac{r^3 A'}{2}(k^\varphi)^2 \tag{B.6}$$

therefore,

$$\mathcal{R}_{11}^{\mathrm{K}} = \left[-\frac{rA'}{2} - (1-A) \right] (k^\varphi)^2 = -\frac{3r_{\mathrm{S}}}{2}\frac{L^2}{r^5}. \tag{B.7}$$

Since the Ricci-focusing term is zero, the optical tidal matrix is trace-free, so that $\mathcal{R}_{11}^{\mathrm{K}} = -\mathcal{R}_{22}^{\mathrm{K}}$. Besides, the off-diagonal terms $\mathcal{R}_{12}^{\mathrm{K}} = \mathcal{R}_{21}^{\mathrm{K}}$ are zero, indeed

$$\mathcal{R}_{12}^{\mathrm{K}} \propto R_{\theta\nu\alpha\beta} k^\nu k^\alpha s_2^\beta, \tag{B.8}$$

and the vectors k, s_2 have no components along ∂_θ (so that $\nu, \alpha, \beta \neq \theta$), while all the components of the Riemann tensor involving a single index θ vanish.

C Mean Kottler path

Let us compute the mean comoving distance $\langle \Delta\chi_{\mathrm{K}} \rangle$ spent inside a Kottler hole. First note that, as already mentioned in Footnote 4, since the size of the holes is small compared to cosmological scales, we can reasonably consider

$$\Delta\chi_{\mathrm{K}} \approx f_K(\Delta\chi_{\mathrm{K}}). \tag{C.1}$$

Moreover, if a hole is crossed with (comoving areal) impact parameter B, and neglecting light deflection, we have

$$f_K(\Delta\chi_{\mathrm{K}}) \approx 2\sqrt{R_{\mathrm{h}}^2 - B^2}, \tag{C.2}$$

thus

$$\langle \Delta\chi_{\mathrm{K}} \rangle \approx 2\left\langle \sqrt{R_{\mathrm{h}}^2 - B^2} \right\rangle = 2\int_{R_{\min}}^{R_{\max}} \mathrm{d}R_{\mathrm{h}}\, p(R_{\mathrm{h}}) \int_{R_{\mathrm{gal}}}^{R_{\mathrm{h}}} \mathrm{d}B\, p(B)\sqrt{R_{\mathrm{h}}^2 - B^2}, \tag{C.3}$$

where $R_{\min} \equiv R_{\mathrm{h}}(M_{\min}) = (3M_{\min}/4\pi\rho_0)^{1/3}$, idem for $R_{\max}$. The integral over B is easily calculated, and we finally obtain

$$\langle \Delta\chi_{\mathrm{K}} \rangle \approx \frac{4}{3} \int_{R_{\min}}^{R_{\max}} \mathrm{d}R_{\mathrm{h}}\, p(R_{\mathrm{h}}) \sqrt{R_{\mathrm{h}}^2 - R_{\mathrm{gal}}^2} \tag{C.4}$$

$$= \frac{4}{3} \int_{M_{\min}}^{M_{\max}} \mathrm{d}M p(M) \sqrt{R_{\mathrm{h}}^2(M) - R_{\mathrm{gal}}^2(M)} \tag{C.5}$$

$$= \frac{4}{3} \left(\frac{3}{4\pi\rho_0} \right)^{1/3} \sqrt{1 - \left(\frac{\rho_0}{\rho_{\mathrm{gal}}} \right)^{2/3}} \int_{M_{\min}}^{M_{\max}} \mathrm{d}M\, p(M)\, M^{1/3} \tag{C.6}$$

$$\approx \frac{4}{3} \left(\frac{3}{4\pi\rho_0} \right)^{1/3} \int_{M_{\min}}^{M_{\max}} \mathrm{d}M\, p(M)\, M^{1/3}. \tag{C.7}$$

References

[1] L. Anderson, E. Aubourg, S. Bailey, F. Beutler, V. Bhardwaj, M. Blanton, A. S. Bolton, J. Brinkmann, J. R. Brownstein, A. Burden, C.-H. Chuang, A. J. Cuesta, K. S. Dawson, D. J. Eisenstein, S. Escoffier, J. E. Gunn, H. Guo, S. Ho, K. Honscheid, C. Howlett, D. Kirkby, R. H. Lupton, M. Manera, C. Maraston, C. K. McBride, O. Mena, F. Montesano, R. C. Nichol, S. E. Nuza, M. D. Olmstead, N. Padmanabhan, N. Palanque-Delabrouille, J. Parejko, W. J. Percival, P. Petitjean, F. Prada, A. M. Price-Whelan, B. Reid, N. A. Roe, A. J. Ross, N. P. Ross, C. G. Sabiu, S. Saito, L. Samushia, A. G. Sanchez, D. J. Schlegel, D. P. Schneider, C. G. Scoccola, H.-J. Seo, R. A. Skibba, M. A. Strauss, M. E. C. Swanson, D. Thomas, J. L. Tinker, R. Tojeiro, M. Vargas Magana, L. Verde, D. A. Wake, B. A. Weaver, D. H. Weinberg, M. White, X. Xu, C. Yeche, I. Zehavi, and G.-B. Zhao, *The clustering of galaxies in the SDSS-III Baryon Oscillation Spectroscopic Survey: Baryon Acoustic Oscillations in the Data Release 10 and 11 galaxy samples*, ArXiv e-prints (Dec., 2013) [`arXiv:1312.4877`].

[2] T. Delubac, J. E. Bautista, N. G. Busca, J. Rich, D. Kirkby, S. Bailey, A. Font-Ribera, A. Slosar, K.-G. Lee, M. M. Pieri, J.-C. Hamilton, É. Aubourg, M. Blomqvist, J. Bovy, J. Brinkmann, W. Carithers, K. S. Dawson, D. J. Eisenstein, J.-P. Kneib, J.-M. Le Goff, D. Margala, J. Miralda-Escudé, A. D. Myers, R. C. Nichol, P. Noterdaeme, R. O'Connell, M. D. Olmstead, N. Palanque-Delabrouille, I. Pâris, P. Petitjean, N. P. Ross, G. Rossi, D. J. Schlegel, D. P. Schneider, D. H. Weinberg, C. Yèche, and D. G. York, *Baryon Acoustic Oscillations in the Lyα forest of BOSS DR11 quasars*, ArXiv e-prints (Apr., 2014) [`arXiv:1404.1801`].

[3] Planck Collaboration, P. A. R. Ade, N. Aghanim, C. Armitage-Caplan, M. Arnaud, M. Ashdown, F. Atrio-Barandela, J. Aumont, C. Baccigalupi, A. J. Banday, and et al., *Planck 2013 results. XVI. Cosmological parameters*, ArXiv e-prints (Mar., 2013) [`arXiv:1303.5076`].

[4] A. Conley, J. Guy, M. Sullivan, N. Regnault, P. Astier, C. Balland, S. Basa, R. G. Carlberg, D. Fouchez, D. Hardin, I. M. Hook, D. A. Howell, R. Pain, N. Palanque-Delabrouille, K. M. Perrett, C. J. Pritchet, J. Rich, V. Ruhlmann-Kleider, D. Balam, S. Baumont, R. S. Ellis, S. Fabbro, H. K. Fakhouri, N. Fourmanoit, S. González-Gaitán, M. L. Graham, M. J. Hudson, E. Hsiao, T. Kronborg, C. Lidman, A. M. Mourao, J. D. Neill, S. Perlmutter, P. Ripoche, N. Suzuki, and E. S. Walker, *Supernova Constraints and Systematic Uncertainties from the First Three Years of the Supernova Legacy Survey*, ApJS **192** (Jan., 2011) 1, [`arXiv:1104.1443`].

[5] N. Suzuki, D. Rubin, C. Lidman, G. Aldering, R. Amanullah, K. Barbary, L. F. Barrientos, J. Botyanszki, M. Brodwin, N. Connolly, K. S. Dawson, A. Dey, M. Doi, M. Donahue, S. Deustua, P. Eisenhardt, E. Ellingson, L. Faccioli, V. Fadeyev, H. K. Fakhouri, A. S. Fruchter, D. G. Gilbank, M. D. Gladders, G. Goldhaber, A. H. Gonzalez, A. Goobar, A. Gude, T. Hattori, H. Hoekstra, E. Hsiao, X. Huang, Y. Ihara, M. J. Jee, D. Johnston, N. Kashikawa, B. Koester,

K. Konishi, M. Kowalski, E. V. Linder, L. Lubin, J. Melbourne, J. Meyers, T. Morokuma, F. Munshi, C. Mullis, T. Oda, N. Panagia, S. Perlmutter, M. Postman, T. Pritchard, J. Rhodes, P. Ripoche, P. Rosati, D. J. Schlegel, A. Spadafora, S. A. Stanford, V. Stanishev, D. Stern, M. Strovink, N. Takanashi, K. Tokita, M. Wagner, L. Wang, N. Yasuda, H. K. C. Yee, and T. Supernova Cosmology Project, *The Hubble Space Telescope Cluster Supernova Survey. V. Improving the Dark-energy Constraints above z>1 and Building an Early-type-hosted Supernova Sample*, ApJ **746** (Feb., 2012) 85, [`arXiv:1105.3470`].

[6] G. F. R. Ellis and W. Stoeger, *The 'fitting problem' in cosmology*, Classical and Quantum Gravity **4** (Nov., 1987) 1697–1729.

[7] P. Peter and J.-P. Uzan, *Primorial Cosmology*. Oxford University, New York, 2009.

[8] P. Fleury, H. Dupuy, and J.-P. Uzan, *Can All Cosmological Observations Be Accurately Interpreted with a Unique Geometry?*, Physical Review Letters **111** (Aug., 2013) 091302, [`arXiv:1304.7791`].

[9] P. Valageas, *Weak gravitational lensing effects on the determination of Ω_{m} and Ω_{Λ} from SNeIa*, A&A **354** (Feb., 2000) 767–786, [`astro-ph/9904300`].

[10] C. Bonvin, R. Durrer, and M. A. Gasparini, *Fluctuations of the luminosity distance*, Phys. Rev. D **73** (Jan., 2006) 023523, [`astro-ph/0511183`].

[11] K. Kainulainen and V. Marra, *Accurate modeling of weak lensing with the stochastic gravitational lensing method*, Phys. Rev. D **83** (Jan., 2011) 023009, [`arXiv:1011.0732`].

[12] E. Di Dio and R. Durrer, *Vector and tensor contributions to the luminosity distance*, Phys. Rev. D **86** (July, 2012) 023510, [`arXiv:1205.3366`].

[13] O. Umeh, C. Clarkson, and R. Maartens, *Nonlinear relativistic corrections to cosmological distances, redshift and gravitational lensing magnification. I - Key results*, ArXiv e-prints (July, 2012) [`arXiv:1207.2109`].

[14] I. Ben-Dayan, G. Marozzi, F. Nugier, and G. Veneziano, *The second-order luminosity-redshift relation in a generic inhomogeneous cosmology*, JCAP **11** (Nov., 2012) 45, [`arXiv:1209.4326`].

[15] I. Ben-Dayan, M. Gasperini, G. Marozzi, F. Nugier, and G. Veneziano, *Average and dispersion of the luminosity-redshift relation in the concordance model*, JCAP **6** (June, 2013) 2, [`arXiv:1302.0740`].

[16] F. Nugier, *Lightcone Averaging and Precision Cosmology*, ArXiv e-prints (Sept., 2013) [`arXiv:1309.6542`].

[17] O. Umeh, C. Clarkson, and R. Maartens, *Nonlinear relativistic corrections to cosmological distances, redshift and gravitational lensing magnification. II - Derivation*, ArXiv e-prints (Feb., 2014) [`arXiv:1402.1933`].

[18] R. Teyssier, S. Pires, S. Prunet, D. Aubert, C. Pichon, A. Amara, K. Benabed, S. Colombi, A. Refregier, and J.-L. Starck, *Full-sky weak-lensing simulation with 70 billion particles*, A&A **497** (Apr., 2009) 335–341, [`arXiv:0807.3651`].

[19] J. E. Gunn, *On the Propagation of Light in Inhomogeneous Cosmologies. I. Mean Effects*, ApJ **150** (Dec., 1967) 737.

[20] R. Kantowski, *Corrections in the Luminosity-Redshift Relations of the Homogeneous Fried-Mann Models*, ApJ **155** (Jan., 1969) 89.

[21] C. C. Dyer and R. C. Roeder, *Observations in Locally Inhomogeneous Cosmological Models*, ApJ **189** (Apr., 1974) 167–176.

[22] N. Brouzakis, N. Tetradis, and E. Tzavara, *The effect of large scale inhomogeneities on the luminosity distance*, JCAP **2** (Feb., 2007) 13, [`astro-ph/0612179`].

[23] V. Marra, E. W. Kolb, S. Matarrese, and A. Riotto, *Cosmological observables in a Swiss-cheese universe*, Phys. Rev. D **76** (Dec., 2007) 123004, [arXiv:0708.3622].

[24] N. Brouzakis, N. Tetradis, and E. Tzavara, *Light propagation and large-scale inhomogeneities*, JCAP **4** (Apr., 2008) 8, [astro-ph/0703586].

[25] T. Biswas and A. Notari, *'Swiss-cheese' inhomogeneous cosmology and the dark energy problem*, JCAP **6** (June, 2008) 21, [astro-ph/0702555].

[26] R. A. Vanderveld, É. É. Flanagan, and I. Wasserman, *Luminosity distance in "Swiss cheese" cosmology with randomized voids. I. Single void size*, Phys. Rev. D **78** (Oct., 2008) 083511, [arXiv:0808.1080].

[27] W. Valkenburg, *Swiss cheese and a cheesy CMB*, JCAP **6** (June, 2009) 10, [arXiv:0902.4698].

[28] T. Clifton and J. Zuntz, *Hubble diagram dispersion from large-scale structure*, MNRAS **400** (Dec., 2009) 2185–2199, [arXiv:0902.0726].

[29] S. J. Szybka, *Light propagation in Swiss-cheese cosmologies*, Phys. Rev. D **84** (Aug., 2011) 044011, [arXiv:1012.5239].

[30] É. É. Flanagan, N. Kumar, I. Wasserman, and R. A. Vanderveld, *Luminosity distance in "Swiss cheese" cosmology with randomized voids. II. Magnification probability distributions*, Phys. Rev. D **85** (Jan., 2012) 023510, [arXiv:1109.1873].

[31] R. W. Lindquist and J. A. Wheeler, *Dynamics of a Lattice Universe by the Schwarzschild-Cell Method*, Reviews of Modern Physics **29** (July, 1957) 432–443.

[32] J.-P. Bruneton and J. Larena, *Observables in a lattice Universe: the cosmological fitting problem*, Classical and Quantum Gravity **30** (Jan., 2013) 025002, [arXiv:1208.1411].

[33] J. Adamek, E. Di Dio, R. Durrer, and M. Kunz, *The distance-redshift relation in plane symmetric universes*, ArXiv e-prints (Jan., 2014) [arXiv:1401.3634].

[34] C. C. Dyer and R. C. Roeder, *The Distance-Redshift Relation for Universes with no Intergalactic Medium*, ApJL **174** (June, 1972) L115.

[35] Y. B. Zel'dovich, *Observations in a Universe Homogeneous in the Mean*, Astron. Zh. **41** (1964) 19.

[36] K. Bolejko and P. G. Ferreira, *Ricci focusing, shearing, and the expansion rate in an almost homogeneous Universe*, JCAP **5** (May, 2012) 3, [arXiv:1204.0909].

[37] C. Clarkson, G. F. R. Ellis, A. Faltenbacher, R. Maartens, O. Umeh, and J.-P. Uzan, *(Mis)interpreting supernovae observations in a lumpy universe*, MNRAS **426** (Oct., 2012) 1121–1136, [arXiv:1109.2484].

[38] A. Einstein and E. G. Straus, *The Influence of the Expansion of Space on the Gravitation Fields Surrounding the Individual Stars*, Reviews of Modern Physics **17** (Apr., 1945) 120–124.

[39] A. Einstein and E. G. Straus, *Corrections and Additional Remarks to our Paper: The Influence of the Expansion of Space on the Gravitation Fields Surrounding the Individual Stars*, Reviews of Modern Physics **18** (Jan., 1946) 148–149.

[40] P. Schneider, J. Ehlers, and E. E. Falco, *Gravitational Lenses.* 1992.

[41] P. Fleury, H. Dupuy, and J.-P. Uzan, *Interpretation of the Hubble diagram in a nonhomogeneous universe*, Phys. Rev. D **87** (June, 2013) 123526, [arXiv:1302.5308].

[42] R. Sachs, *Gravitational Waves in General Relativity. VI. The Outgoing Radiation Condition*, Royal Society of London Proceedings Series A **264** (Nov., 1961) 309–338.

[43] M. Bartelmann and P. Schneider, *Weak gravitational lensing*, Phys. Rep. **340** (Jan., 2001) 291–472, [astro-ph/9912508].

[44] V. Perlick, *Gravitational Lensing from a Spacetime Perspective*, *Living Reviews in Relativity* **7** (Sept., 2004) 9.

[45] C. Pitrou, J.-P. Uzan, and T. S. Pereira, *Weak lensing B modes on all scales as a probe of local isotropy*, *Phys. Rev. D* **87** (Feb., 2013) 043003, [arXiv:1203.6029].

[46] M. Gasperini, G. Marozzi, F. Nugier, and G. Veneziano, *Light-cone averaging in cosmology: formalism and applications*, *JCAP* **7** (July, 2011) 8, [arXiv:1104.1167].

[47] G. F. R. Ellis, S. D. Nel, R. Maartens, W. R. Stoeger, and A. P. Whitman, *Ideal observational cosmology.*, *Phys. Rep.* **124** (1985) 315–417.

[48] G. Fanizza, M. Gasperini, G. Marozzi, and G. Veneziano, *An exact Jacobi map in the geodesic light-cone gauge*, *JCAP* **11** (Nov., 2013) 19, [arXiv:1308.4935].

[49] V. M. Dashevskii and V. I. Slysh, *On the Propagation of Light in a Nonhomogeneous Universe*, *Astron. Zh.* **42** (1965) 863.

[50] K. Bolejko, *Weak lensing and the Dyer-Roeder approximation*, *MNRAS* **412** (Apr., 2011) 1937–1942, [arXiv:1011.3876].

[51] V. C. Busti and J. A. S. Lima, *Influence of small-scale inhomogeneities on the cosmological consistency tests*, *MNRAS* **426** (Oct., 2012) L41–L45, [arXiv:1204.1083].

[52] J. Ehlers and P. Schneider, *Self-consistent probabilities for gravitational lensing in inhomogeneous universes*, *A&A* **168** (Nov., 1986) 57–61.

[53] T. Futamase and M. Sasaki, *Light propagation and the distance-redshift relation in a realistic inhomogeneous universe*, *Phys. Rev. D* **40** (Oct., 1989) 2502–2510.

[54] M. Sasaki, *Cosmological Gravitational Lens Equation — Its Validity and Limitation —*, *Progress of Theoretical Physics* **90** (Oct., 1993) 753–781.

[55] S. Räsänen, *Light propagation in statistically homogeneous and isotropic dust universes*, *JCAP* **2** (Feb., 2009) 11, [arXiv:0812.2872].

[56] V. C. Busti, R. F. L. Holanda, and C. Clarkson, *Supernovae as probes of cosmic parameters: estimating the bias from under-dense lines of sight*, *JCAP* **11** (Nov., 2013) 20, [arXiv:1309.6540].

[57] E. F. Bunn and D. W. Hogg, *The kinematic origin of the cosmological redshift*, *American Journal of Physics* **77** (Aug., 2009) 688–694, [arXiv:0808.1081].

[58] C. Clarkson, G. Ellis, J. Larena, and O. Umeh, *Does the growth of structure affect our dynamical models of the universe? The averaging, backreaction and fitting problems in cosmology*, *ArXiv e-prints* (Sept., 2011) [arXiv:1109.2314].

[59] T. Buchert, *Toward physical cosmology: focus on inhomogeneous geometry and its non-perturbative effects*, *Classical and Quantum Gravity* **28** (Aug., 2011) 164007, [arXiv:1103.2016].

[60] D. L. Wiltshire, *Cosmic structure, averaging and dark energy*, *ArXiv e-prints* (Nov., 2013) [arXiv:1311.3787].

[61] G. Darmois, *Les équations de la gravitation einsteinienne*. Mémorial des sciences mathématiques, 1927.

[62] W. Israel, *Singular hypersurfaces and thin shells in general relativity*, *Nuovo Cimento B Serie* **44** (July, 1966) 1–14.

[63] W. Israel, *Singular hypersurfaces and thin shells in general relativity*, *Nuovo Cimento B Serie* **48** (Apr., 1967) 463–463.

[64] F. Kottler, *Über die physikalischen Grundlagen der Einsteinschen Gravitationstheorie*, *Annalen der Physik* **361** (1918) 401–462.

[65] G. Lemaître, *L'Univers en expansion*, Annales de la Societe Scietifique de Bruxelles **53** (1933) 51.

[66] R. C. Tolman, *Effect of Inhomogeneity on Cosmological Models*, Proceedings of the National Academy of Science **20** (Mar., 1934) 169–176.

[67] H. Bondi, *Spherically symmetrical models in general relativity*, MNRAS **107** (1947) 410.

[68] C. W. Misner, K. S. Thorne, and J. A. Wheeler, *Gravitation.* 1973.

[69] J. Eisenstaedt, *Lemaître and the Schwarzschild Solution*, p. 353. 1993.

[70] H. P. Robertson and T. W. Noonan, *Relativity and cosmology.* 1968.

[71] T. Okamura and T. Futamase, *Distance-Redshift Relation in a Realistic Inhomogeneous Universe*, Progress of Theoretical Physics **122** (Aug., 2009) 511–520, [`arXiv:0905.1160`].

[72] R. A. Sussman, *Back-reaction and effective acceleration in generic LTB dust models*, Classical and Quantum Gravity **28** (Dec., 2011) 235002, [`arXiv:1102.2663`].

[73] M. Lavinto, S. Räsänen, and S. J. Szybka, *Average expansion rate and light propagation in a cosmological Tardis spacetime*, JCAP **12** (Dec., 2013) 51, [`arXiv:1308.6731`].

[74] S. Räsänen, *Light propagation in statistically homogeneous and isotropic universes with general matter content*, JCAP **3** (Mar., 2010) 18, [`arXiv:0912.3370`].

[75] S. Räsänen, *Light propagation and the average expansion rate in near-FRW universes*, Phys. Rev. D **85** (Apr., 2012) 083528, [`arXiv:1107.1176`].

[76] L. Hui and P. B. Greene, *Correlated fluctuations in luminosity distance and the importance of peculiar motion in supernova surveys*, Phys. Rev. D **73** (June, 2006) 123526, [`astro-ph/0512159`].

[77] K. Bolejko, C. Clarkson, R. Maartens, D. Bacon, N. Meures, and E. Beynon, *Antilensing: The Bright Side of Voids*, Physical Review Letters **110** (Jan., 2013) 021302, [`arXiv:1209.3142`].

[78] D. J. Bacon, S. Andrianomena, C. Clarkson, K. Bolejko, and R. Maartens, *Cosmology with Doppler Lensing*, ArXiv e-prints (Jan., 2014) [`arXiv:1401.3694`].

[79] B. Panter, A. F. Heavens, and R. Jimenez, *The mass function of the stellar component of galaxies in the Sloan Digital Sky Survey*, MNRAS **355** (Dec., 2004) 764–768, [`astro-ph/0406299`].

[80] D. E. Holz and R. M. Wald, *New method for determining cumulative gravitational lensing effects in inhomogeneous universes*, Phys. Rev. D **58** (Sept., 1998) 063501, [`astro-ph/9708036`].

[81] K. Kainulainen and V. Marra, *New stochastic approach to cumulative weak lensing*, Phys. Rev. D **80** (Dec., 2009) 123020, [`arXiv:0909.0822`].

Stochastic cosmological lensing

ALTHOUGH Swiss-cheese models seem to capture some essential features of the small-scale inhomogeneity of the Universe, they remain toy models which suffer from a number of intrinsic limitations. First, they are unable to model at the same time small-scale and large-scale inhomogeneities, such as a cluster or a filament, *with* their substructure. One has to choose between a large-scale description—using for instance LTB or Szekeres holes—or a small-scale description—using Schwarzschild holes—where clumps are then homogeneously distributed, the junction conditions preventing from any over- or underdensity (a larger hole implies a more massive clump inside). Second, even though the distance-redshift relation in a SC model is well approximated by the Kantowski-Dyer-Roeder approximation, the latter only characterizes its mean behaviour, so it tells us nothing about the dispersion, or any higher-order moment of the statistics of gravitational lensing. Determining such statistical quantities in a SC model requires to perform computationally expensive and time-consuming ray-tracing simulations.

Yet extracting this information could be very useful for constraining the cosmological parameters from SN lensing, as emphasized by Marra, Quartin, and Amendola [263–265]. Those works exploited an efficient weak-lensing code by Kainulainen & Marra [266–268], where inhomogeneities such as dark matter halos of filaments are randomly placed on the line of sight, according to a statistic dictated by the cosmological parameters. This chapter presents a complementary approach, which (i) focuses on smaller scales; (ii) is purely analytical; and (iii) does not rely on the weak-lensing approximation. It consists of an article written in collaboration with Julien Larena and Jean-Philippe Uzan. Our goal was to design an efficient framework for investigating small-scale lensing, which would be at the same time more practical and flexible than model-based approaches. In particular, it is aimed at eventually being combined with large-scale cosmic lensing.

Small-scale structures are expected to manifest in the lensing equations as a very rapidly fluctuating contribution to the source terms $\mathscr{R}, \mathscr{W}$. This is reminiscent of the problem of Brownian motion, e.g., for a dust particle suspended in water due to the myriad of collisions with the molecules forming the liquid. This phenomenon cannot be explained by relying on a purely fluid description of water; one usually adopts a semi-microscopic approach in which collisions are encoded in a stochastic force, mathematically modelled by a white noise. We here apply the same idea to lensing, splitting its sources into an average, slowly varying contribution and a stochastic contribution as

$$\mathscr{R} = \langle \mathscr{R} \rangle + \delta\mathscr{R}, \tag{7.1}$$

$$\mathscr{W} = \langle \mathscr{W} \rangle + \delta\mathscr{W}, \tag{7.2}$$

where the $\langle X \rangle$ terms stand for the lensing sources due to the mean universe and the large-scale structure, while the δX terms encode the effect of small scales. The present chapter

only deals with the latter, i.e. to the *diffusive* behaviour of lensing, its combination with the large-scale behaviour being left for future studies. Summarising the results obtained so far, we derived the Fokker-Planck-Kolmogorov equations governing the evolution of the probability density functions of the lensing observables, and used them to deduce general results on the mean and standard deviation of the angular distance. We then tested the validity of our formalism by applying it to Swiss-cheese models. This allowed us in particular to derive a post-Kantowski-Dyer-Roeder approximation, which turns out to be in excellent agreement with ray-tracing simulations. Regarding the dispersion of the angular distance, however, there can appear discrepancies between the predictions of our stochastic lensing formalism and the output of ray tracing. We found out that those discrepancies stemmed from the non-Gaussianity of the lensing sources, which therefore seem to constitute the main limitation of the present approach. Despite this weakness, the stochastic lensing framework opens a new window towards a precise and consistent treatment of very small scales.

The theory of stochastic cosmological lensing

Pierre Fleury,[a,b] **Julien Larena,**[c] **Jean-Philippe Uzan**[a,b]

[a]Institut d'Astrophysique de Paris, UMR 7095 du CNRS, 98 bis Bd Arago, 75014 Paris, France.
[b]Sorbonne Universités, Institut Lagrange de Paris, 98 bis, Bd Arago, 75014 Paris, France.
[c]Department of Mathematics, Rhodes University, Grahamstown 6140, South Africa

E-mail: fleury@iap.fr, j.larena@ru.ac.za, uzan@iap.fr

Abstract. On the scale of the light beams subtended by small sources, e.g. supernovae, matter cannot be accurately described as a fluid, which questions the applicability of standard cosmic lensing to those cases. In this article, we propose a new formalism to deal with small-scale lensing as a diffusion process: the Sachs and Jacobi equations governing the propagation of narrow light beams are treated as Langevin equations. We derive the associated Fokker-Planck-Kolmogorov equations, and use them to deduce general analytical results on the mean and dispersion of the angular distance. This formalism is applied to random Einstein-Straus Swiss-cheese models, allowing us to: (1) show an explicit example of the involved calculations; (2) check the validity of the method against both ray-tracing simulations and direct numerical integration of the Langevin equation. As a byproduct, we obtain a post-Kantowski-Dyer-Roeder approximation, accounting for the effect of tidal distortions on the angular distance, in excellent agreement with numerical results. Besides, the dispersion of the angular distance is correctly reproduced in some regimes.

Contents

1   Introduction

The understanding of light propagation in the Universe, in particular through the relation between distances and redshifts, is central for the interpretation of almost all cosmological observations. The standard approach consists in assuming that light propagates through a strictly homogeneous and isotropic Friedmann-Lemaître (FL) spacetime [1], assumed to be a good model on cosmological scales.[1] Such a crude—but surprisingly efficient—approximation can be refined by taking into account: (i) the actual non-comobility of both the light sources and the observer; (ii) the gravitational lensing caused by the large-scale structure. This more realistic description generally relies on the cosmological perturbation theory [5–7]. At first order, it essentially introduces a dispersion of the distance-redshift relation with respect to the background FL prediction [8–12], which can be partially corrected if a lensing map is known. There was recently an interesting debate on the bias potentially introduced by second-order corrections: based on the calculations of Refs. [13, 14] (see also Refs. [15–17] for earlier results), Ref. [18] suggested that second-order lensing could significantly affect the standard interpretation of the cosmic microwave background (CMB) observations. Nevertheless, this statement turned out to be inaccurate, due to confusions between several averaging schemes for the observable quantities at stake [19–22].

This problem of determining the effect of inhomogeneities on light propagation can also been tackled in a nonperturbative way, e.g. by relying on toy models. The most common examples are Swiss-cheese models [23, 24], where inhomogeneities are introduced within a background FL spacetime by inserting spherical patches of another exact solution of Einstein's equation. Recent analyses generally exploit the Lemaître-Tolman-Bondi (LTB) [25–39] or Szekeres [40–43] geometries as interior solutions, which aim at describing large-scale inhomogeneities such as superclusters or cosmic voids (see also Refs. [44, 45]). Observations have also been connected to the cosmic coarse-graining and backreaction issues in the series of works [46–54].

---

[1]See however Refs. [2–4] for a recent debate on this specific issue.

All the above-mentioned approaches have in common that they describe matter in the Universe as a fluid. However, when it comes to narrow beams, such as those involved in supernova (SN) observations, this approximation should no longer hold.[2] The applicability of the perturbation theory in this regime, in particular, has been questioned in Ref. [55]. This specific issue of how the *clumpiness* of the Universe affects the interpretation of cosmological observables was first raised by Zel'dovich [56] and Feynman [57]. The basic underlying idea is that in a clumpy medium, light mostly propagates through vacuum, and therefore experiences an underdense Universe. This stimulated a corpus of seminal articles [58–64], including the first analyses based on a Swiss-cheese model with Schwarzschild vacuoles [65–70]. Contrary to LTB or Szekeres holes, the latter aim at modelling relatively small gravitationally bound structures, such as individual galaxies or stars. The analysis of light propagation in such models resulted in the so-called Dyer-Roeder approximation—that we shall rather call the Kantowski-Dyer-Roeder (KDR) approximation in this article, the name of Kantowski being unfairly omitted in the literature. Its correspondence with Swiss-cheese models has been carefully rederived and numerically checked in Ref. [71], although its mathematical consistency was questioned in Refs. [49, 55]. Analyses based on other models than Swiss cheeses, albeit physically similar in the sense that they also describe universes made of point masses, have been proposed in Refs. [72–77]. When applied to the interpretation of SN data, these various approaches generically do find a bias in the measurement of the cosmological parameters, on the order of a few to more than ten percent [78–82]. It has been shown in Ref. [81] that such an effect improves the agreement between SN and CMB observations regarding the measurement of Ω_{m0}.

While the KDR approximation may capture the main effects of the Universe's clumpiness on the average distance-redshift relation, it does not tell anything about its dispersion, and a fortiori about its higher-order moments. Model-based approaches do not in principle suffer from this weakness, but in all the works cited above, extracting e.g. the probability density function (PDF) of the observed angular distance at a fixed redshift requires numerical simulations which, because of their computational cost, lack of flexibility. A practical solution was proposed with the sGL method of Kainulainen and Marra [83–85], in which weak-lensing simulations have been maximally optimised so that generating 10^5 mock observations only takes a few seconds. This method has been applied to forecast to which extent future SN observation campaigns, e.g. with the Large Synoptic Survey Telescope (LSST), would be able to constrain cosmological parameters from the moments of the distribution of SN magnitudes [86–89].

The goal of the present work is to propose an analytical and a priori non-perturbative framework for determining the statistical impact of small-scale structures on light propagation. Possible applications are the analysis of the bias and dispersion induced by these structures on cosmological observables, non only for distances measurements but also, e.g., cosmic shear. The main idea is that, on very small scales, the matter density field (i.e. the source of lensing) can be treated a *white noise*, giving to lensing a diffusive behaviour. The equations of geometric optics in curved spacetime then take the form of generalised Langevin equations, which come with the whole machinery of statistical physics. Indeed, similar approaches have been exploited in other domains of physics [90, 91], e.g., for describing the secular evolution of the Solar system. This systematic treatment of lensing as a stochastic process allows us to

---

[2]The typical physical size of a supernova explosion is on the order of a hundred astronomical units, which fixes the typical maximum cross-sectional diameter of the associated light beam. On such scales, the distribution of matter in the Universe cannot be considered smooth.

derive Fokker-Planck-Kolmogorov (FPK) equations for the PDF of the lensing observables, such as the angular distance, on which we will particularly focus in this article.

The benefits of this new approach are multiple. Its analytical character potentially provides a better physical understanding of small-scale lensing, together with avoiding to rely on heavy ray-tracing simulations. It must be considered complementary to cosmic lensing due to the large-scale structure, with which it is planned to be merged in the future, in order to design a consistent multiscale description of lensing. Similarly to Refs. [86–89], we have in mind applications to a better characterisation of the matter distribution within the Universe. These various applications lie beyond the scope of the present article, which however proposes, as starters: (i) an extension of the KDR approximation, and (ii) an analytical calculation of the variance of the angular distance in an Einstein-Straus Swiss-cheese model.

The article is organised as follows. Section 2 provides a theoretical lensing toolkit, which contains all the necessary material exploited in the remainder of the article, in particular the Jacobi matrix and the optical scalars. Sections 3 and 4 are the heart of our approach: the former presents our fundamental hypotheses; the latter derives the FPK equations governing the PDF of the Jacobi matrix and of the optical scalars. Section 5 deduces general analytical results from the FPK equations, in particular regarding the first two moments of the PDF of the angular distance. In order to test our formalism, we apply it to a Swiss-cheese model, and confront the associated predictions to numerical ray-tracing results in Section 6. Section 7 is finally devoted to a second check of our calculations, based on the numerical integration of the Langevin equation using the stochastic Euler method. It sheds some light of the connection between the accuracy of our predictions and the Gaussianity of the sources of lensing.

2 Propagation of narrow light beams: two complementary formalisms

Consider a narrow light beam, that is an infinitesimal bundle of null geodesics, converging at an observation event O. Among the geodesics of the bundle, we arbitrarily pick a reference ray $\bar{x}^\mu(v)$, where v is an affine parameter along the ray. The associated tangent vector $k^\mu \equiv \mathrm{d}x^\mu/\mathrm{d}v$ represents the wave four-vector of the light beam. If we choose $\boldsymbol{k}$ as *past oriented* (so v increases from O to the source), then the (cyclic) frequency measured by an observer crossing the beam with four-velocity $\boldsymbol{u}$ is $\omega \equiv u^\mu k_\mu$. In this article, we set by convention $v = 0$ at O, and normalise all frequencies with respect to the observed one $\omega_\mathrm{o} \equiv (u^\mu k_\mu)|_O = 1$.

The behaviour of any ray $x^\mu(v)$ of the beam, relative to $\bar{x}^\mu(v)$, is characterised by its connecting vector $\xi^\mu \equiv x^\mu - \bar{x}^\mu$. If an observer at $\bar{x}^\mu(v)$ projects the beam on a screen, spanned by the Sachs basis (see Appendix A), then the relative position of the two light spots associated with $\bar{x}^\mu$ and x^μ is a Euclidean two-dimensional vector $(\xi^A)_{A=1,2}$.

2.1 Jacobi matrix

The first standard tool for describing the effects of gravitational lensing is the Jacobi matrix, whose evolution with light propagation is a *second-order linear differential equation*.

2.1.1 Definition

The Jacobi matrix is a 2×2 matrix $\boldsymbol{\mathcal{D}} = [\mathcal{D}_{AB}]$ which relates the physical separation ξ^A (in screen space) between two rays with their angular separation $\dot{\xi}^B(0)$—a dot denotes a derivative with respect to v—on the observer's celestial sphere, according to

$$\xi^A(v) = \mathcal{D}^A{}_B(v)\, \dot{\xi}^B(0). \tag{2.1}$$

The determinant of $\mathcal{D}$ thus represents the ratio between the beam's cross-sectional area $A(v) = \mathrm{d}^2\xi(v)$ at v with its observed angular aperture $\Omega_\mathrm{o} = \mathrm{d}^2\dot{\xi}$. When evaluated at the source event $(v = v_\mathrm{s})$, we recognise the definition of the (squared) angular diameter distance between the source and the observer

$$\det \mathcal{D}(v_\mathrm{s}) = \frac{A_\mathrm{s}}{\Omega_\mathrm{o}} \equiv D_\mathrm{A}^2. \tag{2.2}$$

We recall that, if the number of photons is conserved during their travel from the source to the observer, then the angular diameter distance D_A is related to the luminosity distance—used e.g. in the Hubble diagram of SNe—by the distance duality relation

$$D_\mathrm{L} = (1 + z)^2 D_\mathrm{A}, \tag{2.3}$$

which involves the redshift $z = (\omega_\mathrm{s} - \omega_\mathrm{o})/\omega_\mathrm{o}$ between the emitted and observed frequencies.

The other three degrees of freedom of $\mathcal{D}$ encode the deformations of the light beam, i.e. the deformations between the intrinsic source's shape and the observed image. This information is conveniently extracted from $\mathcal{D}$ by the decomposition given in Appendix A.

2.1.2   Evolution: the Jacobi matrix equation

Because $\mathcal{D}$ describes the relative behaviour of two neighbouring light rays, its evolution with light propagation (i.e. with v) is inherited from the geodesic deviation equation; it results into the following second-order linear Jacobi matrix equation [92]

$$\ddot{\mathcal{D}} = \mathcal{R}(v)\mathcal{D}(v) \tag{2.4}$$

where $\mathcal{R}_{AB} \equiv R_{\mu\nu\rho\sigma} s_A^\mu k^\nu k^\rho s_B^\sigma$ is called the optical tidal matrix, and $(s_A^\mu)_{A=1,2}$ denotes the Sachs basis. The optical tidal matrix is symmetric due to the symmetries of the Riemann tensor $R_{\mu\nu\rho\sigma}$. The decomposition of the latter into a Ricci (trace) part and a Weyl (trace-free) part implies, for the optical tidal matrix,

$$\mathcal{R} = \mathscr{R}\,\mathbf{1}_2 + \mathcal{W}, \tag{2.5}$$

$\mathbf{1}_2$ standing for the 2×2 unity matrix, while

$$\mathscr{R} \equiv -\frac{1}{2}R_{\mu\nu}k^\mu k^\nu \tag{2.6}$$

$$\mathcal{W}_{AB} \equiv C_{\mu\nu\rho\sigma} s_A^\mu k^\nu k^\rho s_B^\sigma, \tag{2.7}$$

where $R_{\mu\nu}$ and $C_{\mu\nu\rho\sigma}$ denote respectively the Ricci and Weyl tensors. It is straightforward to check that $\mathcal{W}$ is trace free, and can thus be written as

$$\mathcal{W} = \begin{pmatrix} -\mathscr{W}_1 & \mathscr{W}_2 \\ \mathscr{W}_2 & \mathscr{W}_1 \end{pmatrix}, \qquad \text{with} \quad \mathscr{W}_1 + \mathrm{i}\mathscr{W}_2 \equiv \mathscr{W} \equiv -\frac{1}{2}C_{\mu\nu\rho\sigma}(s_1^\mu - \mathrm{i}s_2^\mu)k^\nu k^\rho(s_1^\sigma - \mathrm{i}s_2^\sigma) \tag{2.8}$$

The Ricci term, on the one hand, is directly related to the local energy-momentum density via the Einstein equation, $\mathscr{R} = -4\pi G T_{\mu\nu}k^\mu k^\nu \leq 0$ (under the null energy condition); it translates the isotropic focusing effect caused by smooth matter enclosed by the light beam. The Weyl term, on the other hand, essentially encodes tidal distortion effects, due to matter outside the beam, which tends to shear and rotate it.

The initial conditions ($v = 0$) for Eq. (2.4) are by definition [see Eq. (2.1)]

$$\boldsymbol{\mathcal{D}}(0) = \boldsymbol{0}_2 \qquad (2.9)$$

$$\dot{\boldsymbol{\mathcal{D}}}(0) = \boldsymbol{1}_2, \qquad (2.10)$$

so that, near the observer ($v \to 0$), the Jacobi matrix admits the expansion

$$\boldsymbol{\mathcal{D}}(v) = v\,\boldsymbol{1}_2 + \frac{v^3}{3!}\,\boldsymbol{\mathcal{R}}_{\mathrm{o}} + \mathcal{O}(v^4). \qquad (2.11)$$

It also implies, using that for any matrix $\boldsymbol{M}$, $\det(1 + \varepsilon\boldsymbol{M}) = 1 + \varepsilon\,\mathrm{tr}\boldsymbol{M} + \mathcal{O}(\varepsilon^2)$,

$$D_{\mathrm{A}}(v) = v + \frac{v^3}{3!}\,\mathscr{R}_{\mathrm{o}} + \mathcal{O}(v^4). \qquad (2.12)$$

2.2   Optical scalars

A standard alternative to the Jacobi matrix consists in a set of optical scalars, describing the deformation rate of the beam rather than net transformations. The resulting light propagation equations (Sachs equations) are a set of *first-order nonlinear equations.*

2.2.1   Definition

The deformation rate of the light beam is naturally defined by a logarithmic derivative of the Jacobi matrix, namely through

$$\boldsymbol{\mathcal{S}} \equiv \dot{\boldsymbol{\mathcal{D}}}\boldsymbol{\mathcal{D}}^{-1}. \qquad (2.13)$$

This deformation rate matrix can be shown to be symmetric, because of the symmetry of $\boldsymbol{\mathcal{R}}$, and is thus decomposed as

$$\boldsymbol{\mathcal{S}} = \begin{pmatrix} \theta & 0 \\ 0 & \theta \end{pmatrix} + \begin{pmatrix} -\sigma_1 & \sigma_2 \\ \sigma_2 & \sigma_1 \end{pmatrix}, \qquad (2.14)$$

where θ and $\sigma = \sigma_1 + i\sigma_2$ are the optical scalars, respectively called the expansion rate and the shear rate. The first one is directly related to the increase rate of the angular diameter distance, since $\mathrm{d}(\ln \det \boldsymbol{\mathcal{D}})/\mathrm{d}v = \mathrm{tr}\boldsymbol{\mathcal{S}}$, i.e.

$$\theta = \frac{\dot{D}_{\mathrm{A}}}{D_{\mathrm{A}}}. \qquad (2.15)$$

2.2.2   Evolution: the Sachs scalar equations

Inserting the definition (2.13) into Eq. (2.4) yields the evolution equation for $\boldsymbol{\mathcal{S}}$,

$$\dot{\boldsymbol{\mathcal{S}}} + \boldsymbol{\mathcal{S}}^2 = \boldsymbol{\mathcal{R}}, \qquad (2.16)$$

from which the Sachs scalar equations follow:

$$\dot{\theta} + \theta^2 + |\sigma|^2 = \mathscr{R} \qquad (2.17)$$

$$\dot{\sigma} + 2\theta\sigma = \mathscr{W}. \qquad (2.18)$$

Using that $\theta = \dot{D}_{\mathrm{A}}/D_{\mathrm{A}}$, the above equation yields the so-called *focusing theorem*

$$\ddot{D}_{\mathrm{A}} = (\mathscr{R} - |\sigma|^2)D_{\mathrm{A}}, \qquad (2.19)$$

where we see that, while Ricci lensing has a direct focusing effect which tends to reduce D_{A}, Weyl lensing has a similar but indirect effect, via the shear rate.

The initial conditions for the optical scalars are nontrivial, because $\boldsymbol{\mathcal{D}}$ vanishes for $v = 0$, which implies that $\boldsymbol{\mathcal{S}}$ must have a pole at the observation event. Precisely, the initial behaviour (2.11) of the Jacobi matrix yields

$$\boldsymbol{\mathcal{S}}(v) = \left[\mathbf{1}_2 + \mathcal{O}(v^2)\right]\left[v\,\mathbf{1}_2 + \mathcal{O}(v^3)\right]^{-1} = v^{-1}\mathbf{1}_2 + \mathcal{O}(v), \tag{2.20}$$

and we conclude that the initial conditions $(v \to 0)$ for the optical scalars are

$$\theta(v) = \frac{1}{v} + \mathcal{O}(v), \tag{2.21}$$

$$\sigma(v) = \mathcal{O}(v). \tag{2.22}$$

Hence only the expansion rate has a pole at $v = 0$, while the shear rate is regular.

3   Small-scale lensing as a diffusion process

We now focus on the specific issue of lensing caused by the small-scale inhomogeneity of the Universe, i.e, down to scales where the matter distribution experienced by the light beam cannot be considered a continuous medium, but rather by a multitude of mass clumps that all slightly distort it. This situation is analogous to the Brownian motion of a particle suspended in water, where a macroscopic—continuous-medium—description of the liquid is no longer sufficient, and must be replaced by a semi-microscopic approach in order to account for the collisions between the particle and water molecules.

The approach developed in the present article is based on this analogy. Just like in the standard treatment of the Brownian motion, where particle-molecule collisions are modelled by a stochastic force, we propose to introduce stochastic terms in the lensing scalars $\mathscr{R}, \mathscr{W}$. The equations governing light propagation will thus take the form of Langevin equations.

3.1   Fundamental hypotheses

We split the Ricci and Weyl lensing scalars experienced by the light beam into a deterministic part representing their average, slowly varying behaviour, and a stochastic part modelling their rapid fluctuations:

$$\mathscr{R} = \langle\mathscr{R}\rangle + \delta\mathscr{R}, \tag{3.1}$$

$$\mathscr{W} = \langle\mathscr{W}\rangle + \delta\mathscr{W}, \tag{3.2}$$

where $\langle\ldots\rangle$ is an ensemble average, and $\langle\delta\mathscr{R}\rangle = \langle\delta\mathscr{W}\rangle = 0$. All these quantities are in principle functions of the affine parameter. Note that, despite the notation, $\delta\mathscr{R}$ *and* $\delta\mathscr{W}$ *are not necessarily small with respect to* $\langle\mathscr{R}\rangle$ *and* $\langle\mathscr{W}\rangle$, they are not dealt with as perturbations. The deterministic components can be thought of as the optical properties of an average universe, in the sense e.g. of Ref. [54]—a notion which may not coincide with a spatial average, or with a FL model.

We now make the following hypotheses:

Azimuthal symmetry about the beam. We suppose that the Universe is statistically homogeneous and isotropic, which implies statistical symmetry with respect to rotations about any light beam. This motivates us to assume that the direction along which a

beam is sheared is *independent* from the shear amplitude. It is also independent from Ricci focusing. In other words, decomposing the Weyl lensing scalar as $\mathscr{W} = |\mathscr{W}|e^{-2i\beta}$, we assume that β is statistically independent from $|\mathscr{W}|$ and $\mathscr{R}$. However, we emphasize that $|\mathscr{W}|$ is *not* independent from $\mathscr{R}$.

Statistical isotropy. We suppose that the Universe has no preferred (spatial) direction, which implies that β must be uniformly distributed in $[0, \pi]$. As a consequence,

$$\langle \mathscr{W} \rangle = \langle |\mathscr{W}| \rangle \left\langle e^{-2i\beta} \right\rangle = 0, \tag{3.3}$$

where we have also used our first hypothesis. We can thus omit the δ in the stochastic part of $\mathscr{W}$. Furthermore, for any v, w

$$\langle \delta\mathscr{R}(v)\mathscr{W}(w) \rangle = \langle \delta\mathscr{R}(v)|\mathscr{W}(w)| \rangle \left\langle e^{-2i\beta(w)} \right\rangle = 0, \tag{3.4}$$

$$\langle \mathscr{W}_1(v)\mathscr{W}_2(v) \rangle = \frac{1}{2} \left\langle |\mathscr{W}(v)|^2 \right\rangle \langle \sin 4\beta(v) \rangle = 0. \tag{3.5}$$

White noises. Because they model rapidly fluctuating functions, the coherence scale of $\delta\mathscr{R}$ and $\mathscr{W}$ is much smaller than the typical evolution scale of the Jacobi matrix, of the optical scalars, and than the typical distance between the source and the observer. Therefore, they can be considered *white noises*, i.e. *δ-correlated Gaussian random processes*[3], with

$$\langle \delta\mathscr{R}(v)\delta\mathscr{R}(w) \rangle = C_{\mathscr{R}}(v)\delta(v - w) \tag{3.7}$$

$$\langle \mathscr{W}_A(v)\mathscr{W}_B(w) \rangle = C_{\mathscr{W}}(v)\delta_{AB}\delta(v - w), \tag{3.8}$$

where the δ_{AB} in Eq. (3.8) comes from statistical isotropy. The functions $C_{\mathscr{R}}, C_{\mathscr{W}}$ shall be called the *covariance amplitudes* of Ricci and Weyl lensing. Gaussianity, which is motivated by the central limit theorem, ensures that $\delta\mathscr{R}(v)$ [resp. $\mathscr{W}(v)$] and $\delta\mathscr{R}(w \neq v)$ [resp. $\mathscr{W}(w \neq v)$] are not only uncorrelated, but also independent.

Physically speaking, the covariance amplitude C_X of the white noise $X(t)$ modelling a physical process $X_{\text{phys}}(t)$ must be understood as $C_X \sim (\delta X_{\text{phys}})^2 \Delta t_{\text{coh}}$, where δX_{phys} is the typical fluctuation amplitude of X_{phys}, while Δt_{coh} is the scale on which it remains coherent. For classical Brownian motion, this scale corresponds to the duration of a typical particle-molecule collision; in gravitational lensing, it will represent the typical extension of a gas cloud/dark matter halo (Ricci lensing), or the affine-parameter length over which the beam undergoes the tidal influence of a given deflector (Weyl lensing).

In principle, the deterministic components $\langle \mathscr{R} \rangle$ and $\langle \mathscr{W} \rangle$ could also allow for the large-scale structure of the Universe (cosmic voids, walls, and filaments). For simplicity, we do not consider this possibility in the present paper, and focus our attention on the rapidly

---

[3] A random process $t \mapsto X(t)$ is Gaussian if any of its finite-dimensional probability distributions is a multivariate Gaussian,

$$p_{t_1,\ldots t_n}(x_1, \ldots x_n) \propto \exp\left(-\frac{1}{2}\sum_{i,j=1}^{n} x_i C_{ij}^{-1} x_j\right), \tag{3.6}$$

where $C_{ij} = C(t_i, t_j) \equiv \langle X(t_i)X(t_j) \rangle$ is the covariance of the process, and C^{-1} denotes its inverse. A white noise corresponds to the limit where $C(t_i, t_j) \propto \delta(t_i, t_j)$. Hence, for a white noise, $X(t_1)$ and $X(t_2 \neq t_1)$ are independent.

fluctuating terms. It will be convenient, in the following, to gather them into a 3-dimensional *noise vector* $\boldsymbol{N}$ such that

$$\boldsymbol{N}^{\mathrm{T}} \equiv (\delta\mathscr{R}, \mathscr{W}_1, \mathscr{W}_2). \tag{3.9}$$

We also introduce the *diffusion matrix* $\boldsymbol{Q}$ of $\boldsymbol{N}$, defined by[4] $\left\langle \boldsymbol{N}(v)\boldsymbol{N}^{\mathrm{T}}(w) \right\rangle = \boldsymbol{Q}(v)\delta(v-w)$, which here reads

$$\boldsymbol{Q} = \mathrm{diag}(C_{\mathscr{R}}, C_{\mathscr{W}}, C_{\mathscr{W}}). \tag{3.10}$$

3.2 Langevin equation for the Jacobi matrix

The Jacobi matrix equation (2.4) reads

$$\ddot{\boldsymbol{D}} = \langle\mathscr{R}\rangle \, \boldsymbol{D} + (\delta\mathscr{R} + \boldsymbol{W}) \, \boldsymbol{D}, \tag{3.11}$$

where we have separated the deterministic and stochastic terms on the right-hand side. It is analogous to a system of coupled harmonic oscillators with fluctuating stiffness. Some further insights on this dynamical system can be obtained thanks to a Hamiltonian formulation

$$\begin{cases} \dot{\mathcal{D}}_{AB} = \mathcal{P}_{AB} = \dfrac{\partial H}{\partial \mathcal{P}_{AB}} \\[2mm] \dot{\mathcal{P}}_{AB} = -\dfrac{\partial V_{\mathrm{Jac}}}{\mathcal{D}_{AB}} = -\dfrac{\partial H}{\partial \mathcal{D}_{AB}} + \mathcal{N}_{AB}(v) \end{cases}, \tag{3.12}$$

with

$$H \equiv \frac{1}{2}\mathrm{tr}\left(\boldsymbol{\mathcal{P}}^{\mathrm{T}}\boldsymbol{\mathcal{P}} - \langle\mathscr{R}\rangle\,\boldsymbol{\mathcal{D}}^{\mathrm{T}}\boldsymbol{\mathcal{D}}\right), \qquad \boldsymbol{\mathcal{N}} \equiv (\delta\mathscr{R}\mathbf{1}_2 + \boldsymbol{W})\,\boldsymbol{\mathcal{D}}, \tag{3.13}$$

and where the Hamiltonian H encodes only the non-stochastic part of the process. Such a dynamics is very similar to the integrable systems with stochastic perturbations discussed e.g. in Ref. [90], except that (i) due to the explicit v-dependence of H, through $\langle\mathscr{R}\rangle$, the unperturbed system is not fully integrable; and (ii) the stochastic term $\boldsymbol{\mathcal{N}}$ contains the variable $\boldsymbol{\mathcal{D}}$: the noise is *multiplicative*. This analogy with dynamical systems in statistical mechanics also provides a nice interpretation of the deformation rate matrix $\boldsymbol{S}$: as a Ricatti variable associated with $\boldsymbol{\mathcal{D}}$, it defines the so-called Kolmogorov-Sinai entropy of the random process, $h_{\mathrm{KS}} = \mathrm{tr}(\boldsymbol{S})$.

Let us now put the Jacobi matrix equation in the form of a first-order *Langevin* equation, which will be useful for deriving the associated Fokker-Planck-Kolmogorov equations in Sec. 4. For that purpose, we first need to vectorise the Jacobi matrix as

$$\boldsymbol{D} \equiv (D_\alpha)_{\alpha\in\{1...4\}} \qquad \text{with} \qquad \mathcal{D}_{AB} = D_{2(A-1)+B}; \tag{3.14}$$

in other words, we represent the couples of matrix indices (AB) by one single index α, so that $1 = (11)$, $2 = (12)$, $3 = (21)$, $4 = (22)$. We then construct an 8-dimensional vector $\boldsymbol{J}^{\mathrm{T}} \equiv (\boldsymbol{D}, \dot{\boldsymbol{D}})$, whose dynamics is described by the Langevin equation

$$\frac{\mathrm{d}\boldsymbol{J}}{\mathrm{d}v} = \boldsymbol{M}(v)\boldsymbol{J}(v) + \boldsymbol{L}_{\mathrm{Jac}}(\boldsymbol{J})\boldsymbol{N}(v). \tag{3.15}$$

where the *drift* matrix is

$$\boldsymbol{M} \equiv \begin{bmatrix} \mathbf{0}_4 & \mathbf{1}_4 \\ \langle\mathscr{R}\rangle\,\mathbf{1}_4 & \mathbf{0}_4 \end{bmatrix}, \tag{3.16}$$

---

[4]Equivalently, the diffusion matrix can be defined from the increments of the Brownian motion $\boldsymbol{B}$ associated with $\boldsymbol{N}$, i.e. such that $\mathrm{d}\boldsymbol{B} = \boldsymbol{N}\mathrm{d}v$. Between v_1 and v_2, the increment of $\boldsymbol{B}$ is $\Delta\boldsymbol{B} \equiv \boldsymbol{B}(v_2) - \boldsymbol{B}(v_1)$, and its variance reads $\left\langle \Delta\boldsymbol{B}\Delta\boldsymbol{B}^{\mathrm{T}} \right\rangle = \boldsymbol{Q}\Delta v$, with $\Delta v \equiv v_2 - v_1$.

and the *noise-mixing* matrix reads

$$\boldsymbol{L}_{\mathrm{Jac}} \equiv \begin{bmatrix} \boldsymbol{0}_{4\times3} \\ D_1 & -D_1 & D_3 \\ D_2 & -D_2 & D_4 \\ D_3 & D_3 & D_1 \\ D_4 & D_4 & D_2 \end{bmatrix} = \begin{bmatrix} \boldsymbol{0}_{4\times3} \\ \mathcal{D}_{11} & -\mathcal{D}_{11} & \mathcal{D}_{21} \\ \mathcal{D}_{12} & -\mathcal{D}_{12} & \mathcal{D}_{22} \\ \mathcal{D}_{21} & \mathcal{D}_{21} & \mathcal{D}_{11} \\ \mathcal{D}_{22} & \mathcal{D}_{22} & \mathcal{D}_{12} \end{bmatrix}. \tag{3.17}$$

Equation (3.15) is linear, with a multiplicative noise.

3.3 Langevin equation for the optical scalars

A similar procedure can be achieved for the optical scalars. The Sachs equations (2.17-2.18), together with the relation (2.15) between the angular distance and the beam's expansion rate, form the system

$$\dot{D}_{\mathrm{A}} = \theta D_{\mathrm{A}}, \tag{3.18}$$

$$\dot{\theta} = -\theta^2 - |\sigma|^2 + \langle\mathscr{R}\rangle + \delta\mathscr{R}, \tag{3.19}$$

$$\dot{\sigma} = -2\theta\sigma + \mathscr{W}, \tag{3.20}$$

which, defining the 4-dimensional vector $\boldsymbol{S}^{\mathrm{T}} \equiv (D_{\mathrm{A}}, \theta, \sigma_1, \sigma_2)$, becomes the *Sachs-Langevin* equation

$$\frac{\mathrm{d}\boldsymbol{S}}{\mathrm{d}v} = \boldsymbol{F}(v, \boldsymbol{S}) + \boldsymbol{L}_{\mathrm{scal}}\boldsymbol{N}(v), \tag{3.21}$$

where the drift term reads $\boldsymbol{F}^{\mathrm{T}} \equiv (\theta D_{\mathrm{A}}, -\theta^2 - |\sigma|^2 + \langle\mathscr{R}\rangle, -2\theta\sigma_1, -2\theta\sigma_2)$, while the noise mixing matrix is

$$\boldsymbol{L}_{\mathrm{scal}} \equiv \begin{bmatrix} 0 & 0 & 0 \\ 1 & 0 & 0 \\ 0 & 1 & 0 \\ 0 & 0 & 1 \end{bmatrix}. \tag{3.22}$$

Contrary to Eq. (3.15), Eq. (3.21) has a nonlinear drift term (which reflects the nonlinearity of the Sachs scalar equations), but its noise is additive, in the sense that the stochastic term $\boldsymbol{L}_{\mathrm{scal}}\boldsymbol{N}$ is independent of the variable $\boldsymbol{S}$.

4 The lensing Fokker-Planck-Kolmogorov equations

The presence of stochastic terms in the optical equations gives a diffusive behaviour to the lensing observables, which can be quantified by their PDFs. When a dynamical system is ruled by a Langevin equation, its PDF in phase space satisfies a partial differential equation called the Fokker-Planck-Kolmogorov (FPK) equation. In § 4.1, we recall the general procedure to derive the FPK equation associated with a Langevin equation; we then apply it to the Jacobi matrix (§ 4.2) and to the optical scalars (§ 4.3).

4.1 From Langevin to Fokker-Planck-Kolmogorov

Consider the following general Langevin equation governing the evolution of a n-dimensional random process $t \mapsto \boldsymbol{X}(t)$,

$$\frac{\mathrm{d}\boldsymbol{X}}{\mathrm{d}t} = \boldsymbol{f}(\boldsymbol{X}, t) + \boldsymbol{L}(\boldsymbol{X}, t)\boldsymbol{N}(t), \tag{4.1}$$

where the n-dimensional vector $\boldsymbol{f}$ and the $n \times n$ matrix $\boldsymbol{L}$ are deterministic, while $\boldsymbol{N}$ is a white noise. One can easily see that both our Langevin equations (3.15) and (3.21) have this form, the affine parameter playing the role of time t, and the random process being either $\boldsymbol{J}$ or $\boldsymbol{S}$. The mathematical difficulty of Eq. (4.1) is that it cannot be treated with the ordinary theory of differential equations, because $\boldsymbol{N}(t)$ is discontinuous everywhere. In general, the solution of Eq. (4.1) is not unique, even for a given realization of $\boldsymbol{N}$.

A standard approach [94–99] consists in introducing the Itō calculus, the main properties of which we summarise below. One can formally integrate Eq. (4.1) as

$$\boldsymbol{X}(t) - \boldsymbol{X}(t_0) = \int_{t_0}^t \boldsymbol{f}(\boldsymbol{X}, t) \, \mathrm{d}t + \int_{t_0}^t \boldsymbol{L}(\boldsymbol{X}, t) \, \boldsymbol{N}(t) \mathrm{d}t, \qquad (4.2)$$

where the second integral requires particular attention, because the Riemann or Lebesgue definitions cannot apply, due to the unboundedness and discontinuity of $\boldsymbol{N}$. First, it must be reformulated as a Stieltjes integral

$$\int_{t_0}^t \boldsymbol{L}(\boldsymbol{X}, t) \, \mathrm{d}\boldsymbol{B} \qquad (4.3)$$

where $\boldsymbol{B}$ is a *Brownian motion*, i.e. a stochastic process whose any increment $\Delta \boldsymbol{B}_k \equiv \boldsymbol{B}(t_{k+1}) - \boldsymbol{B}(t_k)$ is a zero mean Gaussian random variable with variance $\left\langle \Delta \boldsymbol{B}_k \Delta \boldsymbol{B}_k^{\mathrm{T}} \right\rangle = \boldsymbol{\mathcal{Q}}(t_k, t_{k+1}) \Delta t_k$. $\boldsymbol{\mathcal{Q}}$ is called the *diffusion matrix* of $\boldsymbol{B}$. The white noise $\boldsymbol{N}$ is thus considered a formal derivative of the Brownian motion $\boldsymbol{B}$, i.e. $\mathrm{d}\boldsymbol{B} = \boldsymbol{N}\mathrm{d}t$. One possible definition for the integral (4.3) follows the so-called Itō stochastic prescription [100],

$$\int_{t_0}^t \boldsymbol{L}(\boldsymbol{X}, t) \, \mathrm{d}\boldsymbol{B} \equiv \lim_{n \to \infty} \sum_{k=0}^{n-1} \boldsymbol{L}[\boldsymbol{X}(t_k), t_k] \left[\boldsymbol{B}(t_{k+1}) - \boldsymbol{B}(t_k) \right]. \qquad (4.4)$$

This definition leads to some modifications with respect to ordinary differential calculus when $\boldsymbol{B}$ is involved. For example, it can be shown by calculating explicitly the Itō integral of $B_i \mathrm{d}B_j$ that $\mathrm{d}(B_i B_j) = B_i \mathrm{d}B_j + B_j \mathrm{d}B_i + \mathcal{Q}_{ij} \mathrm{d}t$, which implies

$$\mathrm{d}\boldsymbol{B} \, \mathrm{d}\boldsymbol{B}^{\mathrm{T}} = \boldsymbol{\mathcal{Q}} \, \mathrm{d}t. \qquad (4.5)$$

The above quantity is thus of order 1 in $\mathrm{d}t$, contrary to what we would naively expect by replacing $\mathrm{d}\boldsymbol{B}$ by $\boldsymbol{N}\mathrm{d}t$. Equation (4.5) is the most important rule of the Itō calculus. As a consequence, the first-order Taylor expansion of any function $\phi(t, \boldsymbol{X})$ must actually include second-order terms $\propto \mathrm{d}X_i \, \mathrm{d}X_j$, since

$$\mathrm{d}\boldsymbol{X} = \boldsymbol{f}(\boldsymbol{X}, t)\mathrm{d}t + \boldsymbol{L}(\boldsymbol{X}, t) \, \mathrm{d}\boldsymbol{B}, \qquad (4.6)$$

contains $\mathrm{d}\boldsymbol{B}$. More precisely,

$$\mathrm{d}\phi = \frac{\partial \phi}{\partial t}\mathrm{d}t + \frac{\partial \phi}{\partial X_i}\mathrm{d}X_i + \frac{1}{2}\frac{\partial^2 \phi}{\partial X_i \partial X_j}\mathrm{d}X_i \mathrm{d}X_j \qquad (4.7)$$

$$= \left(\frac{\partial \phi}{\partial t} + \frac{1}{2}\frac{\partial^2 \phi}{\partial X_i \partial X_j}L_{ik}\mathcal{Q}_{kl}L_{jl} \right) \mathrm{d}t + \frac{\partial \phi}{\partial X_i}\mathrm{d}X_i, \qquad (4.8)$$

which is known as the Itō formula [94–100] .

From the Itō formula, one can deduce the Fokker-Planck-Kolmogorov (FPK) equation governing the PDF $p(t; \boldsymbol{X})$ of the stochastic process $\boldsymbol{X}(t)$. The derivation [95, 97] relies on a trick which consists in inserting Eq. (4.8) in the time derivative of the expectation value of an arbitrary function $\phi(t, \boldsymbol{X})$,

$$\langle \phi \rangle (t) \equiv \int \phi(t, \boldsymbol{X}) \, p(t; \boldsymbol{X}) \, \mathrm{d}^n \boldsymbol{X}, \tag{4.9}$$

which, after a few integration by parts, yields

$$\frac{\partial p(t; \boldsymbol{X})}{\partial t} = -\frac{\partial}{\partial X_i}[f_i(\boldsymbol{X}, t)p(t; \boldsymbol{X})] + \frac{1}{2}\frac{\partial^2}{\partial X_i \partial X_j} \left\{ \left[\boldsymbol{L}(t; \boldsymbol{X})\boldsymbol{Q}(t)\boldsymbol{L}^{\mathrm{T}}(\boldsymbol{X}, t) \right]_{ij} p(t; \boldsymbol{X}) \right\}. \tag{4.10}$$

The first term on the right-hand side is a drift term, it drives the global displacement of the probability packet, while the second is a diffusion term, which tends to spread it. With this summary of textbook results [94–100] we wish to emphasize that the derivation of the FPK equation requires the noise to be white, i.e. $\boldsymbol{N} = \mathrm{d}\boldsymbol{B}/\mathrm{d}t$ where $\boldsymbol{B}$ is a Brownian motion, so that the Itō calculus can be applied. The hypotheses formulated in § 3.1 are therefore crucial for this formalism to be applicable.

4.2 FPK equation for the Jacobi matrix

Let us now derive the FPK equation governing the PDF of the Jacobi matrix. Applying the general formula (4.10) to the Langevin equation (3.15) leads to the following equation for the PDF $p(v; \boldsymbol{J})$,

$$\frac{\partial p}{\partial v} = -\frac{\partial}{\partial J_a} \left(M_{ab} J_b \, p \right) + \frac{1}{2}\frac{\partial}{\partial J_a \partial J_b} \left[\left(\boldsymbol{L}_{\mathrm{Jac}} \boldsymbol{Q} \boldsymbol{L}_{\mathrm{Jac}}^{\mathrm{T}} \right)_{ab} p \right], \tag{4.11}$$

where the indices a, b run from 1 to 8. Using the explicit expression (3.17) of $\boldsymbol{L}_{\mathrm{Jac}}$, we can write the matrix involved in the diffusion term as

$$\boldsymbol{L}_{\mathrm{Jac}} \boldsymbol{Q} \boldsymbol{L}_{\mathrm{Jac}}^{\mathrm{T}} = \begin{bmatrix} \boldsymbol{0}_4 & \boldsymbol{0}_4 \\ \boldsymbol{0}_4 & \boldsymbol{\Gamma} \end{bmatrix}, \tag{4.12}$$

where the components of the 4×4 symmetric matrix $\boldsymbol{\Gamma}$ are

$$\begin{aligned}
\Gamma_{11} &= (C_{\mathscr{R}} + C_{\mathscr{W}})\mathcal{D}_{11}^2 + C_{\mathscr{W}}\mathcal{D}_{21}^2 \\
\Gamma_{12} &= (C_{\mathscr{R}} + C_{\mathscr{W}})\mathcal{D}_{11}\mathcal{D}_{12} + C_{\mathscr{W}}\mathcal{D}_{21}\mathcal{D}_{22} = \Gamma_{21} \\
\Gamma_{13} &= C_{\mathscr{R}}\mathcal{D}_{21}\mathcal{D}_{11} = \Gamma_{31} \\
\Gamma_{14} &= (C_{\mathscr{R}} - C_{\mathscr{W}})\mathcal{D}_{11}\mathcal{D}_{22} + C_{\mathscr{W}}\mathcal{D}_{21}\mathcal{D}_{12} = \Gamma_{41} \\
\Gamma_{22} &= (C_{\mathscr{R}} + C_{\mathscr{W}})\mathcal{D}_{12}^2 + C_{\mathscr{W}}\mathcal{D}_{22}^2 \\
\Gamma_{23} &= (C_{\mathscr{R}} - C_{\mathscr{W}})\mathcal{D}_{12}\mathcal{D}_{21} + C_{\mathscr{W}}\mathcal{D}_{11}\mathcal{D}_{22} = \Gamma_{32} \\
\Gamma_{24} &= C_{\mathscr{R}}\mathcal{D}_{12}\mathcal{D}_{22} = \Gamma_{42} \\
\Gamma_{33} &= (C_{\mathscr{R}} + C_{\mathscr{W}})\mathcal{D}_{21}^2 + C_{\mathscr{W}}\mathcal{D}_{11}^2 \\
\Gamma_{34} &= (C_{\mathscr{R}} + C_{\mathscr{W}})\mathcal{D}_{21}\mathcal{D}_{22} + C_{\mathscr{W}}\mathcal{D}_{11}\mathcal{D}_{12} = \Gamma_{43} \\
\Gamma_{44} &= (C_{\mathscr{R}} + C_{\mathscr{W}})\mathcal{D}_{22}^2 + C_{\mathscr{W}}\mathcal{D}_{12}^2.
\end{aligned} \tag{4.13}$$

A few calculations and reorganizations yield the following explicit form of the FPK equation of $p(v; \boldsymbol{J}) = p(v; \boldsymbol{\mathcal{D}}, \dot{\boldsymbol{\mathcal{D}}})$,

$$
\boxed{
\begin{aligned}
\frac{\partial p}{\partial v} = &-\dot{\mathcal{D}}_{AB}\frac{\partial p}{\partial \mathcal{D}_{AB}} - \langle \mathscr{R} \rangle \, \mathcal{D}_{AB}\frac{\partial p}{\partial \dot{\mathcal{D}}_{AB}} \\
&+ \frac{1}{2}\left[C_{\mathscr{R}}\,\delta_{AE}\delta_{CF} + C_{\mathscr{W}}(\delta_{AC}\delta_{EF} - \varepsilon_{AC}\varepsilon_{EF}) \right]\mathcal{D}_{EB}\mathcal{D}_{FD}\frac{\partial^2 p}{\partial \dot{\mathcal{D}}_{AB}\partial \dot{\mathcal{D}}_{CD}}
\end{aligned}
}
\tag{4.14}
$$

where ε_{AB} is the two-dimensional antisymmetric matrix with $\varepsilon_{12} = 1$. Equation (4.14) can also be rewritten in an elegant formal way as

$$
\begin{aligned}
\frac{\partial p}{\partial v} = \Bigg\{ &- \operatorname{tr}\left(\dot{\boldsymbol{\mathcal{D}}}^{T}\frac{\partial}{\partial \boldsymbol{\mathcal{D}}} \right) - \langle \mathscr{R} \rangle \operatorname{tr}\left(\boldsymbol{\mathcal{D}}^{T}\frac{\partial}{\partial \dot{\boldsymbol{\mathcal{D}}}} \right) + \frac{C_{\mathscr{R}}}{2}\operatorname{tr}\left[\left(\boldsymbol{\mathcal{D}}^{T}\frac{\partial}{\partial \dot{\boldsymbol{\mathcal{D}}}} \right)^{2} \right] \\
&+ \frac{C_{\mathscr{W}}}{2}\left[\operatorname{tr}\left(\boldsymbol{\mathcal{D}}^{T}\frac{\partial}{\partial \dot{\boldsymbol{\mathcal{D}}}} \right) \right]^{2} - C_{\mathscr{W}}\det\left(\boldsymbol{\mathcal{D}}^{T}\frac{\partial}{\partial \dot{\boldsymbol{\mathcal{D}}}} \right) \Bigg\} p
\end{aligned}
\tag{4.15}
$$

which involves in particular the 2×2 matrix differential operator

$$
\left(\boldsymbol{\mathcal{D}}^{T}\frac{\partial}{\partial \dot{\boldsymbol{\mathcal{D}}}} \right)_{AB} \equiv \mathcal{D}_{CA}\frac{\partial}{\partial \dot{\mathcal{D}}_{CB}}.
\tag{4.16}
$$

Finally, the boundary condition for Eq. (4.14) is deduced from the initial conditions (2.9), (2.10), and reads

$$
p(0; \boldsymbol{\mathcal{D}}, \dot{\boldsymbol{\mathcal{D}}}) = \delta(\boldsymbol{\mathcal{D}})\delta(\dot{\boldsymbol{\mathcal{D}}} - \mathbf{1}_2).
\tag{4.17}
$$

4.3 FPK for the optical scalars

Regarding optical scalars, starting from the Langevin equation (3.21), one can derive the following FPK equation for $p(v; \boldsymbol{S}) = p(v; D_{\mathrm{A}}, \theta, \sigma_1, \sigma_2)$,

$$
\frac{\partial p}{\partial v} = -\frac{\partial F_\alpha p}{\partial S_\alpha} + \frac{1}{2}\frac{\partial^2}{\partial S_\alpha \partial S_\beta}\left[\left(\boldsymbol{L}_{\mathrm{scal}}\boldsymbol{\mathcal{Q}}\boldsymbol{L}_{\mathrm{scal}}^{\mathrm{T}} \right)_{\alpha\beta} p \right],
\tag{4.18}
$$

where α, β run from 1 to 4, and where the diffusion term reads

$$
\boldsymbol{L}_{\mathrm{scal}}\boldsymbol{\mathcal{Q}}\boldsymbol{L}_{\mathrm{scal}}^{\mathrm{T}} = \begin{bmatrix} 0 & 0 & 0 & 0 \\ 0 & C_{\mathscr{R}} & 0 & 0 \\ 0 & 0 & C_{\mathscr{W}} & 0 \\ 0 & 0 & 0 & C_{\mathscr{W}} \end{bmatrix}.
\tag{4.19}
$$

It follows that Eq. (4.18) takes the explicit form

$$
\boxed{
\begin{aligned}
\frac{\partial p}{\partial v} = &-\theta\frac{\partial D_{\mathrm{A}} p}{\partial D_{\mathrm{A}}} + \frac{\partial}{\partial \theta}\left[\left(\theta^2 + |\sigma|^2 - \langle \mathscr{R} \rangle \right)p \right] + 2\theta\left(\frac{\partial \sigma_1 p}{\partial \sigma_1} + \frac{\partial \sigma_2 p}{\partial \sigma_2} \right) \\
&+ \frac{C_{\mathscr{R}}}{2}\frac{\partial^2 p}{\partial \theta^2} + \frac{C_{\mathscr{W}}}{2}\left(\frac{\partial^2 p}{\partial \sigma_1{}^2} + \frac{\partial^2 p}{\partial \sigma_2{}^2} \right).
\end{aligned}
}
\tag{4.20}
$$

The initial condition for θ being singular, it is not possible to write a boundary condition for Eq. (4.20) as we did for Eq. (4.14).

5   General analytical results

Because it is a partial differential equation, the FPK equation is generally impossible to solve analytically, except in a few known special cases [99]. Nevertheless, it can be used to derive evolution equations for the moments of the PDF, some of which are solvable. In this section, we derive some general analytical formulae on the moments of lensing observables. The results for the Jacobi matrix (§ 5.1) and for the optical scalars (§ 5.2) will turn out to be complementary, and used for deriving an evolution equation for the variance of the angular diameter distance in § 5.3.

5.1   Moments of the Jacobi matrix distribution

The Jacobi matrix formalism has this considerable advantage on the optical scalar formalism that it enjoys a *linear* Langevin equation. Despite the fact that its noise is multiplicative, this implies that all the moments of order-n of the PDF of $\boldsymbol{\mathcal{D}}$ satisfy a *closed* system of differential equations. It is not the case when nonlinearities are present, in which case emerges a hierarchy of equations, where the evolution of the lower-order moments depends on moments of higher-order.

5.1.1   Order-one moments

Let us start by deriving the evolution equations for the expectation values $\langle \boldsymbol{\mathcal{D}} \rangle$ and $\langle \dot{\boldsymbol{\mathcal{D}}} \rangle$. We proceed by multiplying the FPK equation (4.14) by $\mathcal{D}_{IJ}$ (or $\dot{\mathcal{D}}_{IJ}$) and then integrating it with respect to $\boldsymbol{\mathcal{D}}$ and $\dot{\boldsymbol{\mathcal{D}}}$. For $\mathcal{D}_{IJ}$, this procedure yields

$$
\frac{\mathrm{d}}{\mathrm{d}v} \int \mathcal{D}_{IJ}\, p\, \mathrm{d}^4\boldsymbol{\mathcal{D}}\, \mathrm{d}^4\dot{\boldsymbol{\mathcal{D}}} = - \int \mathcal{D}_{IJ} \frac{\partial \dot{\mathcal{D}}_{AB}\, p}{\partial \mathcal{D}_{AB}}\, \mathrm{d}^4\boldsymbol{\mathcal{D}}\, \mathrm{d}^4\dot{\boldsymbol{\mathcal{D}}} - \langle \mathscr{R} \rangle \int \mathcal{D}_{IJ} \frac{\partial \mathcal{D}_{AB}\, p}{\partial \dot{\mathcal{D}}_{AB}}\, \mathrm{d}^4\boldsymbol{\mathcal{D}}\, \mathrm{d}^4\dot{\boldsymbol{\mathcal{D}}}
$$

$$
+ \frac{1}{2} \int \mathcal{D}_{IJ} \frac{\partial^2}{\partial \dot{\mathcal{D}}_{AB} \partial \dot{\mathcal{D}}_{CD}} \left\{ \left[C_{\mathscr{R}}\, \delta_{AE}\delta_{CF} + C_{\mathscr{W}} \left(\delta_{AC}\delta_{EF} - \varepsilon_{AC}\varepsilon_{EF} \right) \right] \mathcal{D}_{EB}\mathcal{D}_{FD}\, p \right\}\, \mathrm{d}^4\boldsymbol{\mathcal{D}}\, \mathrm{d}^4\dot{\boldsymbol{\mathcal{D}}}.
$$

$$(5.1)$$

The left-hand side is clearly $\mathrm{d}\langle \mathcal{D}_{IJ} \rangle / \mathrm{d}v$. On the right-hand side, the first term can be integrated by parts to give $\langle \dot{\mathcal{D}}_{IJ} \rangle$; the other two vanish since they can both be written as the integral of a derivative with respect to $\dot{\mathcal{D}}_{AB}$. Equation (5.1) is thus simply

$$
\frac{\mathrm{d}\langle \boldsymbol{\mathcal{D}} \rangle}{\mathrm{d}v} = \langle \dot{\boldsymbol{\mathcal{D}}} \rangle \tag{5.2}
$$

as one can intuitively expect.

The same method applied to $\dot{\mathcal{D}}_{IJ}$ leads to

$$
\frac{\mathrm{d}\langle \dot{\boldsymbol{\mathcal{D}}} \rangle}{\mathrm{d}v} = \langle \mathscr{R} \rangle \langle \boldsymbol{\mathcal{D}} \rangle , \tag{5.3}
$$

so that the expectation value of the Jacobi matrix reads

$$
\frac{\mathrm{d}^2 \langle \boldsymbol{\mathcal{D}} \rangle}{\mathrm{d}v^2} = \langle \mathscr{R} \rangle \langle \boldsymbol{\mathcal{D}} \rangle . \tag{5.4}
$$

Note that this result could also have been obtained by directly averaging the Sachs-Langevin equation. However, this naive method would not work for higher-order moments, which is

why we preferred to directly use a rigorous technique for deriving the evolution equation for the expectation value of $\boldsymbol{\mathcal{D}}$.

It is tempting to conclude that the average angular diameter distance $\langle D_A \rangle$ satisfies Eq. (5.4) as well, but such an assertion would be wrong, because $D_A = \sqrt{\det \boldsymbol{\mathcal{D}}}$ is a nonlinear function of the components of the Jacobi matrix.

5.1.2   Order-two moments

We apply the same method to get evolution equations for the order-two moments of $\boldsymbol{\mathcal{D}}$. This leads to the following closed system of equations

$$\frac{\mathrm{d}}{\mathrm{d}v} \langle \mathcal{D}_{AB} \mathcal{D}_{CD} \rangle = \langle \dot{\mathcal{D}}_{AB} \mathcal{D}_{CD} \rangle + \langle \mathcal{D}_{AB} \dot{\mathcal{D}}_{CD} \rangle \tag{5.5}$$

$$\frac{\mathrm{d}}{\mathrm{d}v} \langle \dot{\mathcal{D}}_{AB} \mathcal{D}_{CD} \rangle = \langle \dot{\mathcal{D}}_{AB} \dot{\mathcal{D}}_{CD} \rangle + \langle \mathscr{R} \rangle \langle \mathcal{D}_{AB} \mathcal{D}_{CD} \rangle \tag{5.6}$$

$$\frac{\mathrm{d}}{\mathrm{d}v} \langle \dot{\mathcal{D}}_{AB} \dot{\mathcal{D}}_{CD} \rangle = \langle \mathscr{R} \rangle \left(\langle \dot{\mathcal{D}}_{AB} \mathcal{D}_{CD} \rangle + \langle \mathcal{D}_{AB} \dot{\mathcal{D}}_{CD} \rangle \right) + C_{\mathscr{R}} \langle \mathcal{D}_{AB} \mathcal{D}_{CD} \rangle$$
$$+ C_{\mathscr{W}} \left(\delta_{AC} \delta_{EF} - \varepsilon_{AC} \varepsilon_{EF} \right) \langle \mathcal{D}_{EB} \mathcal{D}_{FD} \rangle \tag{5.7}$$

which consists of $10 + 16 + 10 = 36$ independent equations for the quantities $\langle \mathcal{D}_{AB} \mathcal{D}_{CD} \rangle$, $\langle \dot{\mathcal{D}}_{AB} \mathcal{D}_{CD} \rangle$ and $\langle \dot{\mathcal{D}}_{AB} \dot{\mathcal{D}}_{CD} \rangle$. By combining the second derivative of Eq. (5.5) with the derivative of Eq. (5.6) and Eq. (5.7), we can eliminate the moments $\langle \dot{\mathcal{D}}_{AB} \mathcal{D}_{CD} \rangle$ and $\langle \dot{\mathcal{D}}_{AB} \dot{\mathcal{D}}_{CD} \rangle$, in order to end up with a closed system for $\langle \mathcal{D}_{AB} \mathcal{D}_{CD} \rangle$,

$$\frac{\mathrm{d}^3}{\mathrm{d}v^3} \langle \mathcal{D}_{AB} \mathcal{D}_{CD} \rangle = 4 \langle \mathscr{R} \rangle \frac{\mathrm{d}}{\mathrm{d}v} \langle \mathcal{D}_{AB} \mathcal{D}_{CD} \rangle + 2 \left(\frac{\mathrm{d} \langle \mathscr{R} \rangle}{\mathrm{d}v} + C_{\mathscr{R}} \right) \langle \mathcal{D}_{AB} \mathcal{D}_{CD} \rangle$$
$$+ 2 C_{\mathscr{W}} \left(\delta_{AC} \delta_{EF} - \varepsilon_{AC} \varepsilon_{EF} \right) \langle \mathcal{D}_{EB} \mathcal{D}_{FD} \rangle, \quad (5.8)$$

which consists of 10 independent third-order differential equations. We shall not try to solve this system, but rather extract from it information on the angular distance.

5.1.3   Application to the squared angular distance

The square of the angular distance is the determinant of $\boldsymbol{\mathcal{D}}$, hence quadratic in its components. Its expectation value,

$$\langle D_A^2 \rangle \equiv \langle \det \boldsymbol{\mathcal{D}} \rangle = \langle \mathcal{D}_{11} \mathcal{D}_{22} \rangle - \langle \mathcal{D}_{12} \mathcal{D}_{21} \rangle, \tag{5.9}$$

is therefore ruled by Eq. (5.8). Applying it for $ABCD = 1122$ and $ABCD = 1221$, we have

$$\frac{\mathrm{d}^3}{\mathrm{d}v^3} \langle \mathcal{D}_{11} \mathcal{D}_{22} \rangle = 4 \langle \mathscr{R} \rangle \frac{\mathrm{d}}{\mathrm{d}v} \langle \mathcal{D}_{11} \mathcal{D}_{22} \rangle + 2 \left(\frac{\mathrm{d} \langle \mathscr{R} \rangle}{\mathrm{d}v} + C_{\mathscr{R}} \right) \langle \mathcal{D}_{11} \mathcal{D}_{22} \rangle - 2 C_{\mathscr{W}} \langle D_A^2 \rangle, \tag{5.10}$$

$$\frac{\mathrm{d}^3}{\mathrm{d}v^3} \langle \mathcal{D}_{12} \mathcal{D}_{21} \rangle = 4 \langle \mathscr{R} \rangle \frac{\mathrm{d}}{\mathrm{d}v} \langle \mathcal{D}_{12} \mathcal{D}_{21} \rangle + 2 \left(\frac{\mathrm{d} \langle \mathscr{R} \rangle}{\mathrm{d}v} + C_{\mathscr{R}} \right) \langle \mathcal{D}_{12} \mathcal{D}_{21} \rangle + 2 C_{\mathscr{W}} \langle D_A^2 \rangle, \tag{5.11}$$

which, by subtraction, yields the following equation for $\langle D_A^2 \rangle$ *only*,

$$\boxed{\frac{\mathrm{d}^3 \langle D_A^2 \rangle}{\mathrm{d}v^3} = 4 \langle \mathscr{R} \rangle \frac{\mathrm{d} \langle D_A^2 \rangle}{\mathrm{d}v} + 2 \left(\frac{\mathrm{d} \langle \mathscr{R} \rangle}{\mathrm{d}v} + C_{\mathscr{R}} - 2 C_{\mathscr{W}} \right) \langle D_A^2 \rangle.} \tag{5.12}$$

To our knowledge, it is the first time that such a general exact equation for the evolution of the dispersion of the angular distance in an inhomogeneous universe is derived.

Solving this differential equation requires initial conditions for $\langle D_{\mathrm{A}}^2 \rangle$ and its first and second derivatives. They are easily obtained from the Taylor expansion (2.12) of D_{A} for $v \to 0$,

$$\langle D_{\mathrm{A}}^2 \rangle (0) = 0, \qquad \frac{\mathrm{d} \langle D_{\mathrm{A}}^2 \rangle}{\mathrm{d}v}(0) = 0, \qquad \frac{\mathrm{d}^2 \langle D_{\mathrm{A}}^2 \rangle}{\mathrm{d}v^2}(0) = 2. \tag{5.13}$$

Equation (5.12) can also be elegantly rewritten in terms of a variable x defined by

$$\mathrm{d}x \equiv \frac{\mathrm{d}v}{D_0^2(v)}, \tag{5.14}$$

where $D_0(v)$ is the background angular distance, i.e. satisfying $\ddot{D}_0 = \langle \mathscr{R} \rangle D_0$. It is indeed straightforward to show that the differential operator involved in Eq. (5.12) reads

$$\frac{\mathrm{d}^3}{\mathrm{d}v^3} - 4 \langle \mathscr{R} \rangle \frac{\mathrm{d}}{\mathrm{d}v} + 2 \frac{\mathrm{d} \langle \mathscr{R} \rangle}{\mathrm{d}v} = D_0^{-4} \frac{\mathrm{d}^3}{\mathrm{d}x^3} D_0^{-2} \tag{5.15}$$

so that

$$\frac{\mathrm{d}^3}{\mathrm{d}x^3} \left(\frac{\langle D_{\mathrm{A}}^2 \rangle}{D_0^2} \right) = 2 D_0^4 \left(C_{\mathscr{R}} - 2 C_{\mathscr{W}} \right) \langle D_{\mathrm{A}}^2 \rangle . \tag{5.16}$$

Though formally simpler, this alternative form of Eq. (5.12) cannot be used for numerical integration, because x is singular at the observation event—$D_0(v_{\mathrm{o}}) = 0$—usually chosen as initial condition.

5.1.4 Expectation value of a general function

More generally, by multiplying the FPK equation with an arbitrary function $F(\mathcal{D}, \dot{\mathcal{D}})$ and integrating the right-hand side by parts, we obtain

$$\frac{\mathrm{d} \langle F \rangle}{\mathrm{d}v} = \left\langle \dot{\mathcal{D}}_{AB} \frac{\partial F}{\partial \mathcal{D}_{AB}} \right\rangle + \langle \mathscr{R} \rangle \left\langle \mathcal{D}_{AB} \frac{\partial F}{\partial \dot{\mathcal{D}}_{AB}} \right\rangle$$
$$+ \frac{1}{2} \left\langle \left[C_{\mathscr{R}} \, \delta_{AE} \delta_{CF} + C_{\mathscr{W}} \left(\delta_{AC} \delta_{EF} - \varepsilon_{AC} \varepsilon_{EF} \right) \right] \mathcal{D}_{EB} \mathcal{D}_{FD} \frac{\partial^2 F}{\partial \dot{\mathcal{D}}_{AB} \partial \dot{\mathcal{D}}_{CD}} \right\rangle . \tag{5.17}$$

If F is an order-n monomial of the form $F = \mathcal{D}^p \dot{\mathcal{D}}^q$, with $p + q = n$, and where $\mathcal{D}^p$ stands for any product of p components of the Jacobi matrix, then the left-hand side of Eq. (5.17) is $\mathrm{d}\langle \mathcal{D}^p \dot{\mathcal{D}}^q \rangle / \mathrm{d}v$, while the three terms on the right-hand side are respectively of the form $\langle \mathcal{D}^{p-1} \dot{\mathcal{D}}^{q+1} \rangle$, $\langle \mathcal{D}^{p+1} \dot{\mathcal{D}}^{q-1} \rangle$, and $\langle \mathcal{D}^{p+2} \dot{\mathcal{D}}^{q-2} \rangle$, so they are all order-$n$ moments. This confirms what we claimed in the introduction of this section, namely that order-n moments form a closed system of differential equations.

5.2 Moments of the optical-scalar distribution

Contrary to the Jacobi matrix, the optical scalars satisfy a nonlinear Langevin equation. An important consequence on the associated FPK equation (4.20) is that it generates an infinite hierarchy of evolution equations for the moments of the distribution $p(v; \boldsymbol{S})$. For instance, if

one is interested in computing the average angular distance $\langle D_A \rangle$, then Eq. (4.20) generates (using the same technique as in § 5.1)

$$\frac{\mathrm{d}}{\mathrm{d}v} \langle D_A \rangle = \langle \theta D_A \rangle \tag{5.18}$$

$$\frac{\mathrm{d}}{\mathrm{d}v} \langle \theta D_A \rangle = -\langle |\sigma|^2 D_A \rangle + \langle \mathscr{R} \rangle \langle D_A \rangle \tag{5.19}$$

$$\frac{\mathrm{d}}{\mathrm{d}v} \langle |\sigma|^2 D_A \rangle = -3 \langle |\sigma|^2 \theta D_A \rangle + 2C_{\mathscr{W}} \langle D_A \rangle, \tag{5.20}$$

$$\cdots$$

where the evolution of an order-n moment systematically involves order-$(n+1)$ moments. Clearly, such a system cannot be solved analytically, and requires a perturbative approach to be dealt with. A first possibility consists postulating a closure relation for the hierarchy at a given order, but such a method does not seem particularly adapted to the present situation, because the physical meaning of the underlying approximation is unclear, and therefore poorly controlled.

We choose instead to perform a perturbative expansion with respect to the shear rate σ, that we assume to be a small quantity. In the following, we focus on the average angular diameter distance $\langle D_A \rangle$, and determine its evolution at first and second order in $|\sigma|^2$.

5.2.1 First-order perturbative expansion

We decompose the angular distance and the expansion scalar as

$$D_A = D_0 + D_1, \tag{5.21}$$

$$\theta = \theta_0 + \theta_1, \tag{5.22}$$

where D_0, already introduced in § 5.1.3, is the solution of $\ddot{D}_0 = \langle \mathscr{R} \rangle D_0$, and $\theta_0 \equiv \dot{D}_0 / D_0$ is the corresponding expansion rate; both are deterministic quantities. We assume that the stochastic quantities D_1, θ_1 are small, in the sense that their probability distributions are concentrated on values much smaller than D_0, θ_0 respectively.

We then expand Eq. (5.18) and the following two equations, generated by FPK,

$$\frac{\mathrm{d}}{\mathrm{d}v} \langle \theta \rangle = -\langle \theta^2 \rangle - \langle |\sigma|^2 \rangle + \langle \mathscr{R} \rangle, \tag{5.23}$$

$$\frac{\mathrm{d}}{\mathrm{d}v} \langle |\sigma|^2 \rangle = -4 \langle \theta |\sigma|^2 \rangle + 2C_{\mathscr{W}}, \tag{5.24}$$

at first order in $D_1, \theta_1, |\sigma|^2$, which gives

$$\frac{\mathrm{d} \langle D_1 \rangle}{\mathrm{d}v} = \theta_0 \langle D_1 \rangle + \langle \theta_1 \rangle D_0 \tag{5.25}$$

$$\frac{\mathrm{d} \langle \theta_1 \rangle}{\mathrm{d}v} = -2\theta_0 \langle \theta_1 \rangle - \langle |\sigma|^2 \rangle \tag{5.26}$$

$$\frac{\mathrm{d} \langle |\sigma|^2 \rangle}{\mathrm{d}v} = -4\theta_0 \langle |\sigma|^2 \rangle + 2C_{\mathscr{W}}, \tag{5.27}$$

whence

$$\boxed{\delta_{D_A}^{(1)} \equiv \frac{\langle D_1 \rangle}{D_0} = -2 \int_0^v \frac{\mathrm{d}v_1}{D_0^2(v_1)} \int_0^{v_1} \frac{\mathrm{d}v_2}{D_0^2(v_2)} \int_0^{v_2} \mathrm{d}v_3 \, D_0^4(v_3) C_{\mathscr{W}}(v_3) < 0,} \tag{5.28}$$

which represents the relative correction between $\langle D_{\mathrm{A}} \rangle$ and D_0 at first order in Weyl lensing. Note that, again, the above result naturally exhibits the integration measure $D_0^{-2}\mathrm{d}v = \mathrm{d}x$, it can therefore be rewritten as

$$\frac{\mathrm{d}^3 \delta_{D_{\mathrm{A}}}^{(1)}}{\mathrm{d}x^3} = -2D_0^6 C_{\mathscr{W}}. \tag{5.29}$$

5.2.2 The shear rate at first order

From Eq. (5.27) we have deduced the following expression for the variance of the shear rate,

$$\langle |\sigma|^2 \rangle = 2 \int_0^v \mathrm{d}w \left[\frac{D_0(w)}{D_0(v)} \right]^4 C_{\mathscr{W}}(w), \tag{5.30}$$

at first order. Let us simply mention that, to this order of approximation, we can easily obtain the full PDF of σ. Linearizing the second scalar Sachs equation (2.18), we indeed get

$$\dot{\sigma} = -2\theta_0 \sigma + \mathscr{W} + \mathcal{O}(\sigma^2). \tag{5.31}$$

which is identical to the historical Langevin equation for diffusion. The associated FPK equation for the PDF $p_\sigma(v; \sigma)$ is easily shown to be

$$\frac{\partial p_\sigma}{\partial v} = 2\theta_0 \left(\frac{\partial \sigma_1 p_\sigma}{\partial \sigma_1} + \frac{\partial \sigma_2 p_\sigma}{\partial \sigma_2} \right) + \frac{C_{\mathscr{W}}}{2} \left(\frac{\partial^2 p_\sigma}{\partial \sigma_1^2} + \frac{\partial^2 p_\sigma}{\partial \sigma_2^2} \right). \tag{5.32}$$

It can be solved by (i) using a polar description for $\sigma = \sigma_1 + \mathrm{i}\sigma_2 = |\sigma|\mathrm{e}^{\mathrm{i}\phi}$, then (ii) using the statistical isotropy assumption that implies $p_\sigma(v; \sigma_1; \sigma_2) = f(v, |\sigma|)$, and (iii) performing simple changes of variable to recover a standard diffusion equation. The result is a Gaussian distribution, describing a 2-dimensional random walk with nonconstant diffusion coefficient,

$$p_\sigma(v; \sigma) = \frac{1}{\pi \langle |\sigma|^2 \rangle(v)} \exp \left(-\frac{|\sigma|^2}{\langle |\sigma|^2 \rangle(v)} \right) \tag{5.33}$$

where $\langle |\sigma|^2 \rangle$ is given by Eq. (5.30).

5.2.3 Second-order perturbative expansion

In § 5.1.3 we derived an evolution equation for $\langle D_{\mathrm{A}}^2 \rangle$, while § 5.2.1 provided an expression for $\langle D_{\mathrm{A}} \rangle$. Subtracting the results should therefore lead to the variance of the angular diameter distance. However, the first-order expansion performed in the previous paragraphs is not sufficient for that purpose. This can be understood the following way: if $D_{\mathrm{A}} = D_0 + \delta D$, then

$$\mathrm{var}(D_{\mathrm{A}}) \equiv \langle D_{\mathrm{A}}^2 \rangle - \langle D_{\mathrm{A}} \rangle^2 = \langle \delta D^2 \rangle - \langle \delta D \rangle^2 \tag{5.34}$$

involves second-order quantities, neglected in § 5.2.1. In this paragraph, we therefore expand the equations governing the evolution of $\langle D_{\mathrm{A}} \rangle$ up to second order in $\langle |\sigma|^2 \rangle$, i.e. formally up to second order in $C_{\mathscr{W}}$.

We start back from Eqs. (5.18), (5.19), (5.20), which can be gathered as

$$\frac{\mathrm{d}^3}{\mathrm{d}x^3} \left(\frac{\langle D_{\mathrm{A}} \rangle}{D_0} \right) = -2C_{\mathscr{W}} D_0^5 \langle D_{\mathrm{A}} \rangle + 3D_0^5 \langle |\sigma|^2 D_{\mathrm{A}}(\theta - \theta_0) \rangle. \tag{5.35}$$

The difficulty now consists in evaluating the last term. First note that, since it is already a second-order quantity,

$$\left\langle\, |\sigma|^2\, D_{\mathrm{A}}(\theta-\theta_0)\right\rangle = D_0\left\langle\, |\sigma|^2\,\theta_1\right\rangle + \mathcal{O}(C_{\mathscr{W}}^3). \tag{5.36}$$

Let us then write

$$\left\langle\, |\sigma|^2\,\theta_1\right\rangle = \left\langle\, |\sigma|^2\,\right\rangle\langle\theta_1\rangle + \underbrace{\left\langle\, |\sigma|^2\,\theta\right\rangle - \left\langle\, |\sigma|^2\,\right\rangle\langle\theta\rangle}_{\equiv\Gamma_{\theta\sigma}}. \tag{5.37}$$

The first term on the right-hand side can be expressed using the first-order results of § 5.2.1, which, using the x variable, take the simple form

$$\left\langle\, |\sigma|^2\,\right\rangle = -D_0^{-4}\frac{\mathrm{d}^2\delta_{D_{\mathrm{A}}}^{(1)}}{\mathrm{d}x^2} + \mathcal{O}(C_{\mathscr{W}}^2), \tag{5.38}$$

$$\langle\theta_1\rangle = D_0^{-2}\frac{\mathrm{d}\delta_{D_{\mathrm{A}}}^{(1)}}{\mathrm{d}x} + \mathcal{O}(C_{\mathscr{W}}^2). \tag{5.39}$$

Evaluating the cross-correlation term $\Gamma_{\theta\sigma}$ can be achieved by using again the hierarchy of moments generated by the FPK equation. Combining Eqs. (5.23), (5.24) with

$$\frac{\mathrm{d}}{\mathrm{d}v}\left\langle\theta\,|\sigma|^2\,\right\rangle = -5\left\langle\theta^2\,|\sigma|^2\,\right\rangle - \left\langle\, |\sigma|^4\,\right\rangle + \left\langle\mathscr{R}\right\rangle\left\langle\, |\sigma|^2\,\right\rangle + 2C_{\mathscr{W}}\langle\theta\rangle, \tag{5.40}$$

we get

$$\dot{\Gamma}_{\theta\sigma} + 6\theta_0\Gamma_{\theta\sigma} = \left\langle\, |\sigma|^2\,\right\rangle^2 - \left\langle\, |\sigma|^4\,\right\rangle + \mathcal{O}(C_{\mathscr{W}}^3), \tag{5.41}$$

where we have expanded the higher-order correlator $\langle\theta^2\,|\sigma|^2\rangle$ as $\theta_0^2\langle|\sigma|^2\rangle + 2\theta_0\langle\theta_1\,|\sigma|^2\rangle + \mathcal{O}(C_{\mathscr{W}})$. Now, by comparing the evolution equations for $\langle|\sigma|^2\rangle^2$ and $\langle|\sigma|^4\rangle$, which are

$$\frac{\mathrm{d}}{\mathrm{d}v}\left\langle\, |\sigma|^2\,\right\rangle^2 = -8\left\langle\theta\,|\sigma|^2\,\right\rangle\left\langle\, |\sigma|^2\,\right\rangle + 4C_{\mathscr{W}}\left\langle\, |\sigma|^2\,\right\rangle, \tag{5.42}$$

$$\frac{\mathrm{d}}{\mathrm{d}v}\left\langle\, |\sigma|^4\,\right\rangle = -8\left\langle\theta\,|\sigma|^4\,\right\rangle + 8C_{\mathscr{W}}\left\langle\, |\sigma|^2\,\right\rangle, \tag{5.43}$$

we conclude that $\langle|\sigma|^4\rangle = 2\langle|\sigma|^2\rangle^2$ at leading order. Note that this result coincides with the predictions of the Gaussian distribution (5.33) obtained for σ in the previous paragraph. Hence Eq. (5.41) is solved as

$$\Gamma_{\theta\sigma} = -D_0^{-6}\int_0^v\mathrm{d}w\, D_0^6\left\langle\, |\sigma|^2\,\right\rangle^2 + \mathcal{O}(C_{\mathscr{W}}^3) \tag{5.44}$$

$$= -D_0^{-6}\int_{\mathrm{o}}^x\mathrm{d}x'\,\left(\frac{\mathrm{d}^2\delta_{D_{\mathrm{A}}}^{(1)}}{\mathrm{d}x^2}\right)^2 + \mathcal{O}(C_{\mathscr{W}}^3), \tag{5.45}$$

where we used Eq. (5.38). The lower bound "o" of the latter integral is formal, because variable x is singular for $v=0$. This was the last missing piece to the differential equation governing the evolution of $\langle D_{\mathrm{A}}\rangle$ at second order in $C_{\mathscr{W}}$,

$$\frac{\mathrm{d}^3}{\mathrm{d}x^3}\left(\frac{\langle D_{\mathrm{A}}\rangle}{D_0}\right) + 2C_{\mathscr{W}}D_0^6\frac{\langle D_{\mathrm{A}}\rangle}{D_0} = -3\frac{\mathrm{d}\delta_{D_{\mathrm{A}}}^{(1)}}{\mathrm{d}x}\frac{\mathrm{d}^2\delta_{D_{\mathrm{A}}}^{(1)}}{\mathrm{d}x^2} - 3\int_{\mathrm{o}}^x\mathrm{d}x'\,\left(\frac{\mathrm{d}^2\delta_{D_{\mathrm{A}}}^{(1)}}{\mathrm{d}x^2}\right)^2 + \mathcal{O}(C_{\mathscr{W}}^3). \tag{5.46}$$

In terms of an expansion of the form $D_{\mathrm{A}} = D_0 + D_1 + D_2$, and defining the second-order mean correction $\delta^{(2)}_{D_{\mathrm{A}}} \equiv \langle D_2 \rangle / D_0$ to the angular distance, the above result reads

$$
\frac{\mathrm{d}^3 \delta^{(2)}_{D_{\mathrm{A}}}}{\mathrm{d}x^3} = -3 \frac{\mathrm{d}\delta^{(1)}_{D_{\mathrm{A}}}}{\mathrm{d}x} \frac{\mathrm{d}^2 \delta^{(1)}_{D_{\mathrm{A}}}}{\mathrm{d}x^2} - 3 \int_{\mathrm{o}}^{x} \mathrm{d}x' \left(\frac{\mathrm{d}^2 \delta^{(1)}_{D_{\mathrm{A}}}}{\mathrm{d}x^2} \right)^2 < 0.
\tag{5.47}
$$

5.3 Variance of the angular distance

We now have enough material to propose an approximate evolution equation for the variance of the angular distance. On the one hand, we have obtained in § 5.1 the following exact equation for $\langle D_{\mathrm{A}}^2 \rangle$,

$$
\frac{\mathrm{d}^3}{\mathrm{d}x^3} \left(\frac{\langle D_{\mathrm{A}}^2 \rangle}{D_0^2} \right) + 2 D_0^6 \left(2 C_{\mathscr{W}} - C_{\mathscr{R}} \right) \frac{\langle D_{\mathrm{A}}^2 \rangle}{D_0^2} = 0.
\tag{5.48}
$$

On the other hand, the second-order Eq. (5.46) is easily turned into an equation for $\langle D_{\mathrm{A}} \rangle^2$,

$$
\frac{\mathrm{d}^3}{\mathrm{d}x^3} \left(\frac{\langle D_{\mathrm{A}} \rangle}{D_0} \right)^2 + 4 C_{\mathscr{W}} D_0^6 \left(\frac{\langle D_{\mathrm{A}} \rangle}{D_0} \right)^2 = -6 \int_{\mathrm{o}}^{x} \mathrm{d}x' \left(\frac{\mathrm{d}^2 \delta^{(1)}_{D_{\mathrm{A}}}}{\mathrm{d}x^2} \right)^2 + \mathcal{O}(C_{\mathscr{W}}^3).
\tag{5.49}
$$

By subtraction, we finally obtain

$$
\boxed{\frac{\mathrm{d}^3}{\mathrm{d}x^3} \left[\frac{\mathrm{var}(D_{\mathrm{A}})}{D_0^2} \right] + 2 D_0^6 (2 C_{\mathscr{W}} - C_{\mathscr{R}}) \frac{\mathrm{var}(D_{\mathrm{A}})}{D_0^2} = 2 C_{\mathscr{R}} D_0^6 + 6 \int_{\mathrm{o}}^{x} \mathrm{d}x' \left[\frac{\mathrm{d}^2 \delta^{(1)}_{D_{\mathrm{A}}}}{\mathrm{d}x^2} \right]^2 + \mathcal{O}(C_{\mathscr{W}}^3),}
$$

$$
\tag{5.50}
$$

where we recall that $\mathrm{d}x = D_0^{-2} \mathrm{d}v$, and that the third derivative $\mathrm{d}^3/\mathrm{d}x^3$ is given by Eq. (5.15). We see that both Ricci lensing and Weyl lensing drive the variance of D_{A}. This can be easily understood from the focusing theorem (2.19), where $\mathscr{R}$ is the main driving term, which explains why $C_{\mathscr{R}}$ appears directly on the right-hand side of (5.50); $\mathscr{W}$, on the other hand, affects D_{A} only indirectly, via $|\sigma|^2$. It is the reason why $\mathrm{d}^2 \delta^{(1)}_{D_{\mathrm{A}}}/\mathrm{d}x^2 \propto \langle |\sigma|^2 \rangle$ is also present on the right-hand side of Eq. (5.50).

It is remarkable that this result on the variance of D_{A} required the use of both the Jacobi matrix and the optical scalars. Although they are completely equivalent formulations, it would have been much more painful to derive Eq. (5.50) by using exclusively one of them.

6 Application to a Swiss-cheese model

The stochastic lensing formalism developed throughout Secs. 3, 4, and 5 depends on three free functions: the average Ricci focusing $\langle \mathscr{R} \rangle (v)$, and the two covariances amplitudes $C_{\mathscr{R}}(v)$, $C_{\mathscr{W}}(v)$ which need to be specified, or deduced from a spacetime model, in order to draw any physical conclusion. In this section, we propose an application of this formalism to Swiss-cheese (SC) cosmological models. Our goal is twofold: on the one hand, it provides an explicit example about how stochastic lensing can be applied, and of the involved calculations; on the other hand, it allows us to test its validity, by comparing its analytical predictions with the numerical results of a ray-tracing code for SC models, which was developed by one of the authors and used in Refs. [71, 101]. As a byproduct, we also obtain an improvement of the Kantowski-Dyer-Roeder approximation, which allows for shear.

6.1   The Einstein-Straus Swiss-cheese model

We consider here an Einstein-Straus [23, 24, 102–104] SC model, where individual masses, whose vicinity is characterised by the Schwarzschild solution (or the Kottler solution, for a nonvanishing cosmological constant), are embedded in an expanding homogeneous and isotropic Universe, forming spherical holes within the Friedmannian cheese. This model aims at describing static, gravitationally bound objects, such as stars, galaxies, or clusters of galaxies, and is therefore more adapted to the problematic of small-scale inhomogeneities tackled here than LTB [105, 106] or Szekeres [106, 107] Swiss-cheese models.

6.1.1   Spacetime geometry

Let us briefly summarise the main geometrical properties of the Einstein-Straus model—more detailed explanations can be found, e.g., in our previous works [71, 101]. Consider one hole of the SC, whose centre is taken to be the origin of the coordinate system, without loss of generality. On the one hand, the metric of the exterior region is

$$\mathrm{d}s^2 = -\mathrm{d}T^2 + a^2(T)\left[\frac{\mathrm{d}R^2}{1-KR^2} + R^2\,\mathrm{d}\Omega^2\right], \tag{6.1}$$

with $\mathrm{d}\Omega^2 \equiv \mathrm{d}\theta^2 + \sin^2\theta\mathrm{d}\varphi^2$, $K = \mathrm{cst}$, and where the evolution of the scale factor a with cosmic time T is ruled by the Friedmann equations, in particular

$$H^2 \equiv \left(\frac{1}{a}\frac{\mathrm{d}a}{\mathrm{d}T}\right)^2 = \frac{8\pi G\rho_0}{3}\left(\frac{a_0}{a}\right)^3 - \frac{K}{a^2} + \frac{\Lambda}{3}, \tag{6.2}$$

where ρ_0 is today's mean density of matter, modelled by a pressureless fluid. The cosmological parameters quantifying the relative importance of matter, spatial curvature, and cosmological constant in the expansion dynamics are respectively $\Omega_\mathrm{m} \equiv 8\pi G\rho_0/(3H^2)$, $\Omega_K \equiv -K/(aH)^2$, and $\Omega_\Lambda \equiv \Lambda/(3H^2)$. The interior geometry is, on the other hand, given by the Kottler (or Schwarzschild-de Sitter) metric

$$\mathrm{d}s^2 = -A(r)\,\mathrm{d}t^2 + A^{-1}(r)\,\mathrm{d}r^2 + r^2\mathrm{d}\Omega^2 \qquad \text{with} \quad A(r) \equiv 1 - \frac{r_\mathrm{S}}{r} - \frac{\Lambda\,r^2}{3}, \tag{6.3}$$

and where $r_\mathrm{S} \equiv 2\,GM$ is the Schwarzschild radius associated with the mass M at the centre of the hole.

The metrics (6.1) and (6.3) are glued together on a spacelike hypersurface corresponding a comoving sphere (the boundary of the hole), hence defined by $R = R_\mathrm{h} = \mathrm{cst}$ in terms of exterior coordinates, and $r = r_\mathrm{h}(t)$ in terms of interior coordinates. The Darmois-Israel junction conditions [108–110] then impose

$$r_\mathrm{h}(t) = a(T)R_\mathrm{h}, \tag{6.4}$$

$$M = \frac{4\pi}{3}\rho_0 R_\mathrm{h}^3. \tag{6.5}$$

Equation (6.5) must be understood as follows: the mass M at the centre of the hole is identical to the one that should be contained in the sphere of comoving radius R_h, if the latter were homogeneously filled with the same comoving density ρ_0 as the exterior.

6.1.2 Optical properties of each region

Within the cheese, since the FL metric is conformally flat, light rays follow straight lines in terms of a suitable coordinate system. The cyclic frequency of the associated wave, as measured by a comoving observer (with four-velocity ∂_T), and normalised by the observed frequency at O, reads

$$1 + z = \omega = k^T = \frac{\mathrm{d}T}{\mathrm{d}v} = \frac{a_0}{a(T)} \tag{6.6}$$

from which follows the relation between redshift z and affine parameter v for a light ray propagating through the cheese only,

$$\frac{\mathrm{d}v}{\mathrm{d}z} = \frac{1}{H(z)(1+z)^2}. \tag{6.7}$$

Besides, the Ricci and Weyl lensing scalars are shown to be

$$\mathscr{R}_{\mathrm{FL}} = -4\pi G \omega^2 \rho(T) \tag{6.8}$$

$$\mathscr{W}_{\mathrm{FL}} = 0. \tag{6.9}$$

Inside the hole, a light ray propagating in the $\theta = \pi/2$-plane admits two constants of motion, $E = A(r)k^t$ and $L = r^2 k^\varphi$, respectively associated with the stationarity and spherical symmetry of the metric. Their ratio defines the impact parameter $b = L/E$, roughly equal to the closest approach radius $r_{\mathrm{min}} \approx b$ of the photon trajectory if $b \gg r_{\mathrm{S}}$. The Ricci and Weyl lensing scalars read, in this case,

$$\mathscr{R}_{\mathrm{K}} = 0 \tag{6.10}$$

$$\mathscr{W}_{\mathrm{K}} = \frac{3GML^2}{r^5}\,\mathrm{e}^{-2\mathrm{i}\beta}, \tag{6.11}$$

where β is the impact angle, corresponding to the angle between the plane of the trajectory and the first vector of the Sachs basis, as represented on Fig. 1.

6.2 Effective optical properties

Because of the intrinsically discrete nature of the SC model, we need to design an effective approach to be able to use the formalism developed in this paper.

6.2.1 The Kantowski-Dyer-Roeder approximation

The first set of effective optical properties for SC models was proposed by Kantowski [65] in 1969, assuming that the mass clumps modelled by the central mass of the holes are extended and opaque, i.e., imposing a cutoff for the impact parameter $b > b_{\mathrm{min}}$, which corresponds to the physical radius r_{phys} of the clump. This work was generalised in 1974 by Dyer and Roeder [69] in order to include the cosmological constant. The resulting behaviour at lowest order, that we shall call the Kantowski-Dyer-Roeder (KDR) approximation, can be summarised as follows:

KDR1 The relation between affine parameter v and redshift z is not significantly affected by the holes, so that Eq. (6.7) can still be applied in a SC model.

KDR2 The effect of the shear, due to Weyl lensing in the holes, on the angular distance is negligible. In other words, $\mathscr{W}_{\mathrm{KDR}} = 0$.
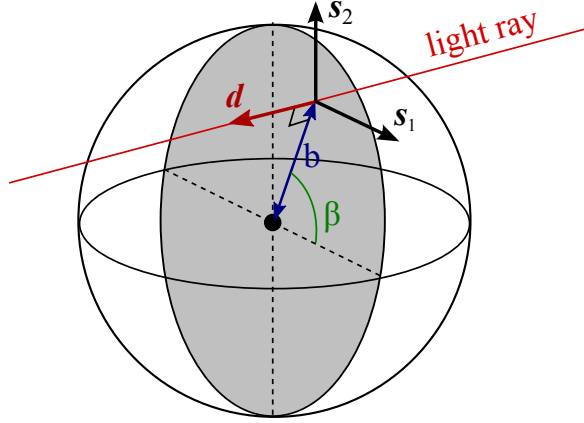
Figure 1: Impact parameters in a Kottler hole. The grey disk is the intersection between the hole and the plane orthogonal to the wave-vector $\boldsymbol{k}$ at minimal approach, also spanned by the Sachs basis $(\boldsymbol{s}_1, \boldsymbol{s}_2)$ there. The impact parameter $b \equiv L/E$ is approximately the minimal approach radial coordinate of the photon, and β is the angle between the plane of the trajectory and the plane spanned by $\boldsymbol{k}$, $\boldsymbol{s}_1$ at minimal approach. It is also the angle corresponding the basis change which diagonalises the optical tidal matrix $\boldsymbol{\mathcal{R}}_{\mathrm{K}}$ in the hole.

KDR3 Ricci lensing is the same as in the cheese but reduced by a factor $\bar{\alpha} \in [0, 1]$, called smoothness parameter, so that $\mathscr{R}_{\mathrm{KDR}} = \bar{\alpha}\mathscr{R}_{\mathrm{FL}} = -4\pi G\omega^2\bar{\alpha}\rho(T)$.

A detailed analysis of this approximation was presented recently in Ref. [71]. Hypothesis **KDR1** turns out to be valid up to terms on the order of the ratio $r_{\mathrm{S}}/r_{\mathrm{h}}$ between the Schwarzschild radius of the central mass and the radius of the hole, which is very small in practice. Therefore, *we will adopt **KDR1** for the remainder of this article*. The relevance of **KDR3** can be understood as follows: consider an interval $[v_n, v_{n+1}]$ of the light path, where v_n corresponds to the entrance into the hole number n, and $v_{n+1} = v_n + \Delta v_n$ to the entrance into the next one; the effective Ricci focusing over this interval can be defined as

$$\mathscr{R}_{\mathrm{eff}} \equiv \frac{1}{\Delta v_n} \int_{v_n}^{v_{n+1}} \mathscr{R} \, \mathrm{d}v \approx \frac{\Delta v_n^{\mathrm{FL}}}{\Delta v_n} \mathscr{R}_{\mathrm{FL}}, \tag{6.12}$$

where Δv_n^{FL} is the fraction of light path spent into the FL region (between the exit from the hole n and the entrance into the hole $n + 1$) over which $\mathscr{R}_{\mathrm{FL}}$ can be considered constant. This defines a local smoothness parameter $\alpha_n \equiv \Delta v_n^{\mathrm{FL}}/\Delta v_n$. Interpolating the sequence (α_n) on the whole light path yields a function $\alpha(v)$ which, after averaging over many lines of sights, defines $\bar{\alpha}(v)$.

In terms of the stochastic lensing formalism, we can thus identify

$$\langle\mathscr{R}\rangle = \mathscr{R}_{\mathrm{KDR}}. \tag{6.13}$$

As a consequence, the angular diameter distance predicted by the KDR approximation corresponds to D_0 introduced in § 5.1.3, i.e. satisfying $\ddot{D}_0 = \langle\mathscr{R}\rangle D_0$.

6.2.2 Effective Weyl lensing in a hole

Numerical ray-tracing simulations in SC models [71] show that, while the KDR approximation satisfactorily reproduces the true $D_{\mathrm{A}}(v)$ relation for most lines of sights, some exhibit significant

deviations. Such discrepancies are due to Weyl lensing, neglected in the KDR approach (**KDR2**), but which we would like to include in the stochastic approach. It will be convenient, for that purpose, to first derive an effective expression for the Weyl lensing scalar $\mathscr{W}$ in a single hole, defined as

$$\mathscr{W}_{\mathrm{eff}} \equiv \frac{1}{v_{\mathrm{out}} - v_{\mathrm{in}}} \int_{v_{\mathrm{in}}}^{v_{\mathrm{out}}} \mathscr{W}_{\mathrm{K}}(v) \, \mathrm{d}v, \tag{6.14}$$

where v_{in}, v_{out} respectively denote the affine parameter at entrance and exit.

Like in the KDR approach, we assume from now on that the central mass is an extended opaque object, whose physical radius $r_{\mathrm{phys}} \gg r_{\mathrm{S}}$ is thus a lower cutoff of impact parameters. As shown in Ref. [101], the radial coordinate $r(v)$ of a photon propagating through the hole with an impact parameter b reads, at lowest order in r_{S}/b,

$$r(v) \approx \sqrt{b^2 + E^2(v - v_{\mathrm{m}})^2}, \tag{6.15}$$

where v_{m} denotes the affine parameter at minimal approach, and $E \approx \omega_{\mathrm{in}} \approx \omega_{\mathrm{out}}$. Moreover, if we neglect the growth of the hole between the photon entrance and exit, then

$$v_{\mathrm{out}} - v_{\mathrm{m}} \approx v_{\mathrm{m}} - v_{\mathrm{in}} \approx E^{-1}\sqrt{r_{\mathrm{h}}^2 - b^2}. \tag{6.16}$$

Calculating the integral of Eq. (6.14) thus yields

$$\mathscr{W}_{\mathrm{eff}} = GME^2 \left[\frac{1}{r_{\mathrm{h}}^3} + \frac{2}{b^2 r_{\mathrm{h}}} \right] \mathrm{e}^{-2\mathrm{i}\beta} \tag{6.17}$$

$$= 4\pi G\rho\omega^2 \left[\frac{1}{3} + \frac{2}{3}\left(\frac{r_{\mathrm{h}}}{b}\right)^2 \right] \mathrm{e}^{-2\mathrm{i}\beta}. \tag{6.18}$$

We see that, for $b \ll r_{\mathrm{h}}$, the ratio between Weyl and Ricci lensing can actually be very large, $|\mathscr{W}_{\mathrm{eff}}|/\mathscr{R}_{\mathrm{eff}} \propto (r_{\mathrm{h}}/b)^2$. It is the randomization of β which, in practice, drastically reduces the net impact of Weyl lensing on the angular distance.

6.3 Calculation of the covariance amplitudes

We now turn to the calculation of the statistical quantities $C_{\mathscr{R}}$, $C_{\mathscr{W}}$ of the white noises which best reproduce lensing in a Swiss-cheese model.

6.3.1 Statistical setup

The randomness of our SC model is constructed in a way that—as originally formulated by Ref. [72]—"each ray creates its own Universe". One realization of the various stochastic processes at stake thus corresponds to the disposition of successive holes on a photon's trajectory, with random sizes, impact parameters, and separations. Expectation values $\langle \ldots \rangle$ will be considered with respect to such realizations. As in Ref. [71], we make the following assumptions:

- The properties (mass, size, impact parameters) of two different holes are independent, as well as the separation between different successive holes.

- All the impact positions, within a given hole cross-section, are equiprobable. In other words, the impact angle β is uniformly distributed in $[0, 2\pi]$, and the PDF of the comoving areal impact parameter B is

$$p(B) \, \mathrm{d}B = [R_{\mathrm{c}} \leq B \leq R_{\mathrm{h}}] \frac{B \, \mathrm{d}B}{R_{\mathrm{h}}^2 - R_{\mathrm{c}}^2}, \tag{6.19}$$

where the squared bracket is 1 if the assertion inside is true, 0 if not; R_c denotes the comoving areal radius of the central matter clump, and R_h the comoving areal radius of the hole. We assume that the matter clump is static, i.e., its physical radius $r_c \equiv a R_c$ is constant, hence $R_c \propto a^{-1}$ is not, contrary to R_h.

- The distributions of both R_h and r_c are governed by the specific matter clumps that one wishes to model. For most of our theoretical results, they do not need to be explicitly specified. For numerical illustrations, we consider galaxylike clumps which all have the same physical density $\rho_c = 3M/(4\pi r_c^3) = 3.47 \times 10^{-22}\,\mathrm{kg/m^3}$—this fixes the relation between r_c and M (hence R_h)—, and whose mass function is inspired from Ref. [111],

$$ p(M)\mathrm{d}M \propto M^{-1.16} \exp\left(-\frac{M}{7.5 \times 10^{11} h^{-2} M_\odot} \right) \mathrm{d}M. \qquad (6.20) $$

- The PDF of the comoving separation $\Delta\chi_{\mathrm{FL}}$ between two successive holes is taken to be uniform, between 0 and $2\langle\Delta\chi_{\mathrm{FL}}\rangle$, with

$$ \langle\Delta\chi_{\mathrm{FL}}\rangle = \frac{4}{3}\frac{\bar{\alpha}}{1-\bar{\alpha}}\langle R_h\rangle. \qquad (6.21) $$

This choice ensures that the mean smoothness parameter $\langle\alpha\rangle = \langle\Delta v_{\mathrm{FL}}/\Delta v\rangle$ is indeed $\bar{\alpha}$.

6.3.2 Ricci-lensing covariance

In reality, the Ricci and Weyl lensing scalars in a random Swiss-cheese model are not white noises: they have a self-correlation length on the order of the hole sizes. We here aim at determining the properties of the white noises which best reproduce the actual behaviour of $\mathscr{R}$ and $\mathscr{W}$. In the case of the Ricci covariance amplitude, this can be achieved by integrating Eq. (3.7) with respect to w,

$$ C_{\mathscr{R}}(v) = \int \mathrm{d}w \, \langle\delta\mathscr{R}(v)\delta\mathscr{R}(w)\rangle \approx \int \mathrm{d}w \, \langle\delta\mathscr{R}_{\mathrm{eff}}(v)\delta\mathscr{R}_{\mathrm{eff}}(w)\rangle, \qquad (6.22) $$

with

$$ \delta\mathscr{R}_{\mathrm{eff}} \equiv \mathscr{R}_{\mathrm{eff}} - \langle\mathscr{R}_{\mathrm{eff}}\rangle = -4\pi G\rho_0\,\omega^5\delta\alpha, \qquad (6.23) $$

and $\delta\alpha(v) \equiv \alpha(v) - \bar{\alpha}$. As mentioned above, the expectation value $\langle\ldots\rangle$ is identified with an average over all possible realizations (r) of the SC, that is over the position, size, and impact parameter of each hole that is crossed by the light beam,

$$ \langle\delta\mathscr{R}_{\mathrm{eff}}(v)\delta\mathscr{R}_{\mathrm{eff}}(w)\rangle = \lim_{N\to\infty} \frac{1}{N} \sum_{r=1}^{N} \delta\mathscr{R}_{\mathrm{eff}}^{(r)}(v)\delta\mathscr{R}_{\mathrm{eff}}^{(r)}(w). \qquad (6.24) $$

For each realization (r), the complete light path through the SC can be split into elementary intervals $I_n \equiv [v_n, v_{n+1}]$, of affine parameter length Δv_n where, as before, v_n corresponds to the entrance into the nth hole. Within each interval, $\delta\mathscr{R}_{\mathrm{eff}} = \delta\mathscr{R}_n$ is considered constant, and $\delta\mathscr{R}_n$ is independent of $\delta\mathscr{R}_m$ if $n \neq m$. Hence, if we call $I_{(r)}(v)$ the elementary interval of (r) such that $v \in I_{(r)}(v)$, then there are two categories of realizations: those where $w \in I_{(r)}(v)$ as well; and those where $w \notin I_{(r)}(v)$. The net contribution of the second category to the sum of Eq. (6.24) vanishes.

In order to calculate this sum, it is convenient to sort the realizations (r) in terms of the properties of $I_{(r)}(v)$. The affine-parameter length Δv of any elementary interval I can be decomposed into its FL and hole contributions as

$$\Delta v = \Delta v_{\mathrm{FL}} + \Delta v_{\mathrm{h}} = \frac{1}{\omega^2}\left(\Delta\chi_{\mathrm{h}} + 2\sqrt{R_{\mathrm{h}}^2 - B^2}\right), \tag{6.25}$$

where we neglected the global beam deflection in the hole part, and used the FL relation between affine parameter and comoving distance, even in the hole[5]. Δv thus depends on the random parameters $\Delta\chi_{\mathrm{FL}}$, R_{h}, and B, which we regroup in a triple $\mathbf{\Pi} = (\Delta\chi_{\mathrm{FL}}, r_{\mathrm{h}}, B)$. We now organise the sum of Eq. (6.24) in terms of the parameters $\mathbf{\Pi}$ characterizing the interval containing v, which yields

$$\langle\delta\mathscr{R}_{\mathrm{eff}}(v)\delta\mathscr{R}_{\mathrm{eff}}(w)\rangle = \int \mathrm{d}\mathbf{\Pi}\, p(\mathbf{\Pi}|v \in I_{\mathbf{\Pi}})\,\mathrm{Prob}(w \in I_{\mathbf{\Pi}}|v \in I_{\mathbf{\Pi}}, \mathbf{\Pi})\,\delta\mathscr{R}_{\mathrm{eff}}^2(\mathbf{\Pi}). \tag{6.26}$$

In the above equation, $p(\mathbf{\Pi}|v \in I_{\mathbf{\Pi}})\,\mathrm{d}\mathbf{\Pi}$ represents the (conditional) probability that the interval $I_{\mathbf{\Pi}}$ containing v has its parameters within $\mathrm{d}\mathbf{\Pi}$ around $\mathbf{\Pi}$. It can be rewritten thanks to the Bayes formula as

$$p(\mathbf{\Pi}|v \in I_{\mathbf{\Pi}}) = \frac{\mathrm{Prob}(v \in I_{\mathbf{\Pi}}|\mathbf{\Pi})}{\mathrm{Prob}(v \in I)} \times p(\mathbf{\Pi}), \tag{6.27}$$

where $p(\mathbf{\Pi})$ is the unconstrained PDF of $\mathbf{\Pi}$, i.e. as provided by the assumptions of § 6.3.1. Simple geometric arguments show that the probability that v belongs to a given interval $I_{\mathbf{\Pi}}$, with affine-parameter length $\Delta v(\mathbf{\Pi})$, is

$$\mathrm{Prob}(v \in I_{\mathbf{\Pi}}|\mathbf{\Pi}) \propto \Delta v, \tag{6.28}$$

so that the normalization factor in the denominator of Eq. (6.27) is simply $\mathrm{Prob}(v \in I) \propto \langle\Delta v\rangle_{\mathbf{\Pi}}$, where the average is performed with respect to $p(\mathbf{\Pi})$.

The second term in the integral of Eq. (6.26) represents the probability that w belongs to the interval $I_{\mathbf{\Pi}}$, given its parameters $\mathbf{\Pi}$ and the fact that v already belongs to it. Again, simple geometry yields

$$\mathrm{Prob}(w \in I_{\mathbf{\Pi}}|v \in I_{\mathbf{\Pi}}, \mathbf{\Pi}) = \left(1 - \frac{|v - w|}{\Delta v}\right)\Theta(\Delta v - |v - w|), \tag{6.29}$$

where Θ denotes the Heaviside function. Gathering all the results, and using the expression of $\delta\mathscr{R}_{\mathrm{eff}}$, we obtain

$$\langle\delta\mathscr{R}_{\mathrm{eff}}(v)\delta\mathscr{R}_{\mathrm{eff}}(w)\rangle = (4\pi G\rho_0\omega^5)^2 \int \mathrm{d}\mathbf{\Pi}\, p(\mathbf{\Pi})\,\frac{\Delta v - |v - w|}{\langle\Delta v\rangle_{\mathbf{\Pi}}}\,\Theta(\Delta v - |v - w|)\left(\frac{\Delta v_{\mathrm{FL}}}{\Delta v} - \bar{\alpha}\right)^2. \tag{6.30}$$

Performing the integration, plus the one with respect to w, finally yields

$$\boxed{C_{\mathscr{R}} = \bar{\alpha}^2(1 - \bar{\alpha})H_0^4\Omega_{\mathrm{m}0}^2(1 + z)^8\left(\frac{11}{8}\langle R_{\mathrm{h}}\rangle + \frac{27}{8}\frac{\langle R_{\mathrm{h}}^2\rangle - \langle R_{\mathrm{h}}\rangle^2}{\langle R_{\mathrm{h}}\rangle}\right)} \tag{6.31}$$

---

[5]This operation is justified by **KDR1**, which is very accurately satisfied in a SC model

in terms of the usual cosmological quantities. In the above equations, angle brackets denote averaging with respect to the mass function of the matter clumps, which rules the size of the hole they belong to via Eq. (6.5). Note that we get $C_{\mathscr{R}} = 0$ in both limits $\bar{\alpha} = 0, 1$. This was indeed expected: for $\bar{\alpha} = 0$ the Swiss cheese is completely filled by holes, so that $\mathscr{R} = 0$ everywhere; for $\bar{\alpha} = 1$, we recover the strictly homogeneous FL spacetime, in which $\mathscr{R} = \langle\mathscr{R}\rangle$ everywhere. In both cases the fluctuation $\delta\mathscr{R}$ vanishes.

6.3.3 Weyl-lensing covariance

Just like in the Ricci case, the covariance amplitude $C_{\mathscr{W}}$ of the white noise which best reproduces Weyl lensing in a SC model is

$$C_{\mathscr{W}}(v) = \frac{1}{2} \int \mathrm{d}w \, \langle \mathscr{W}(v)\mathscr{W}^*(w)\rangle \approx \frac{1}{2} \int \mathrm{d}w \, \left\langle |\mathscr{W}_{\mathrm{eff}}(v)\mathscr{W}_{\mathrm{eff}}(w)| \, \mathrm{e}^{2\mathrm{i}\beta(w)-2\mathrm{i}\beta(v)} \right\rangle, \qquad (6.32)$$

where a star denotes the complex conjugate, and the $1/2$ prefactor comes from the fact that in Eq. (3.8) we defined $C_{\mathscr{W}}$ as the covariance amplitude of each independent component $\mathscr{W}_A$.

We then proceed as before, decomposing the expectation value $\langle \mathscr{W}_{\mathrm{eff}}(v)\mathscr{W}_{\mathrm{eff}}^*(w)\rangle$ as a sum over all possible realizations of the SC. Since $\mathscr{W}_{\mathrm{eff}}$ is nonzero only in holes, we fully decompose each realization into FL and hole elementary paths (rather that {FL+hole} sets as before). In the average, only the realizations such that v and w belong to the same hole H contribute to the net result. Hence the analogue of Eq. (6.26) is

$$\langle |\mathscr{W}_{\mathrm{eff}}(v)\mathscr{W}_{\mathrm{eff}}(w)|\rangle = (1-\bar{\alpha}) \int \mathrm{d}\mathbf{\Pi} \, p(\mathbf{\Pi}|v \in H_{\mathbf{\Pi}}) \, \mathrm{Prob}(w \in H_{\mathbf{\Pi}}|v \in H_{\mathbf{\Pi}}, \mathbf{\Pi}) \, |\mathscr{W}_{\mathrm{eff}}(\mathbf{\Pi})|^2, \qquad (6.33)$$

where $\mathbf{\Pi}$ is now the couple (B, R_{h}) characterising a hole H. The $(1-\bar{\alpha})$ prefactor corresponds to the probability that the elementary interval to which belong v is a hole. The involved probabilities are formally identical to the Ricci case, except that the interval length is now Δv_{h} instead of $\Delta v = \Delta v_{\mathrm{h}} + \Delta v_{\mathrm{FL}}$. The integral to calculate is therefore

$$\langle |\mathscr{W}_{\mathrm{eff}}(v)\mathscr{W}_{\mathrm{eff}}(w)|\rangle = (1-\bar{\alpha})(4\pi G\rho_0\omega^5)^2 \int \mathrm{d}\mathbf{\Pi} \, p(\mathbf{\Pi}) \frac{\Delta v_{\mathrm{h}} - |v-w|}{\langle \Delta v_{\mathrm{h}}\rangle_{\mathbf{\Pi}}} \, \Theta(\Delta v_{\mathrm{h}} - |v-w|)$$

$$\times \left[\frac{1}{3} + \frac{2}{3}\left(\frac{R_{\mathrm{h}}}{B}\right)^2\right]^2. \qquad (6.34)$$

The final result, after integration over $\mathbf{\Pi}$ and w, is

$$\boxed{C_{\mathscr{W}} = \frac{3}{2}(1-\bar{\alpha})H_0^2\Omega_{\mathrm{m0}}(1+z)^6 \frac{\left\langle r_{\mathrm{S}}^{4/3} r_{\mathrm{c}}^{-2}\right\rangle}{\left\langle r_{\mathrm{S}}^{1/3}\right\rangle}}, \qquad (6.35)$$

Like in Eq. (6.31), angle brackets denote here averages with respect to the statistical properties of the matter clumps.

A comparison of the covariance amplitudes $C_{\mathscr{R}}$ and $C_{\mathscr{W}}$, calculated with the setup and numerical values listed in § 6.3.1, is depicted in Fig. 2. It is clear here that Weyl covariance dominates over Ricci covariance. This result is characteristic of the Einstein-Straus SC model, where the local matter density experienced by light oscillates between ρ (cheese) and 0 (holes); this *highly underestimates* the fluctuations of Ricci focusing compared to reality.
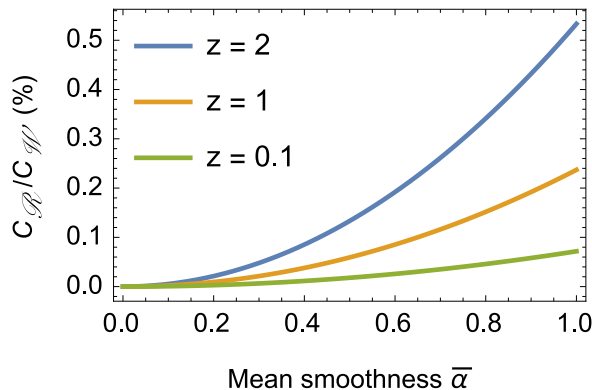
Figure 2: Ratio $C_{\mathscr{R}}/C_{\mathscr{W}}$ between the covariance amplitudes of the Ricci lensing and Weyl lensing in a Swiss-cheese model, as a function of the mean smoothness parameter $\bar{\alpha}$, for three different values of the redshift $z = 2$ (blue), $z = 1$ (orange), and $z = 0.1$ (green).

6.4 Results and comparison with ray tracing

We now apply the general results derived in Sec. 5 with the expressions (6.31) and (6.35) for $C_{\mathscr{R}}$ and $C_{\mathscr{W}}$. After having discussed our expression of the average shear rate with respect to earlier works, we compare the predictions of our formalism for $\langle D_A \rangle$ and $\mathrm{var}(D_A)$ with the output of numerical ray-tracing simulations in a SC model.

6.4.1 Shear rate and astrophysical parameter

Introducing the expression (6.35) of $C_{\mathscr{W}}$ in Eq. (5.30) yields the following formula for the average shear rate

$$\left\langle |\sigma|^2 \right\rangle = \mathcal{A} \, H_0^3 \Omega_{\mathrm{m0}} \int_0^v \mathrm{d}w \left[\frac{D_0(w)}{D_0(v)} \right]^4 (1 + z)^6, \tag{6.36}$$

where we introduced a dimensionless *astrophysical parameter*

$$\mathcal{A} \equiv \frac{3}{H_0}(1 - \bar{\alpha}) \frac{\left\langle r_{\mathrm{S}}^{4/3} r_{\mathrm{c}}^{-2} \right\rangle}{\left\langle r_{\mathrm{S}}^{1/3} \right\rangle}, \tag{6.37}$$

which encodes the statistical assumptions about the mass and compacity of the matter clumps. It also contains the main dependence with respect to the smoothness parameter $\bar{\alpha}$, since the integral of Eq. (6.36) is almost independent from it, as shown in Fig. 3. In terms of orders of magnitude, for $\bar{\alpha} = 0$, $\mathcal{A}_0 \sim g/H_0$, where $g \equiv GM/r_{\mathrm{c}}^2$ is the surface gravity of the central matter clumps. If they represent galaxies, then $\mathcal{A}_0$ is typically of order unity, but it is potentially much larger for more compact objects (see table 1).

Equation (6.36) is very similar to the ones obtained, e.g., by Gunn [62] or Kantowski [65] by different methods. Both get the same integral term, but their estimations of the astrophysical parameter differ with ours. In particular, Kantowski obtains[6] (Eq. (42) of Ref. [65])

$$\mathcal{A}_{\mathrm{K}} = \frac{3}{H_0}(1 - \bar{\alpha}) \frac{\left\langle r_{\mathrm{S}}^2 r_{\mathrm{c}}^{-2} \right\rangle}{\left\langle r_{\mathrm{S}} \right\rangle}, \tag{6.38}$$

---

[6]Dyer and Roeder also obtained the same result, given in Eq. (25) of Ref. [69] with no derivation, but referring to Dyer's PhD thesis [68].

Nature of the clumps	M	r_S	r_c	$\mathcal{A}_0$
galaxy clusters	$10^{15} M_\odot$	$100\,\text{pc}$	$10\,\text{Mpc}$	10^{-3}
galaxies	$10^{11} M_\odot$	$10^{-2}\,\text{pc}$	$10\,\text{kpc}$	1
stars	$M_\odot$	km	$10^6\,\text{km}$	10^{10}

Table 1: Typical orders of magnitude for the mass M, Schwazschild radius r_S, and physical size r_c of three possible types of matter clumps modelled in a SC model, with the associated astrophysical parameter $\mathcal{A}_0 \sim r_S/(H_0 r_c^2)$ for $\bar{\alpha} = 0$.

which only differs from Eq. (6.37) by the powers of r_S in the averages. In a SC model where all the holes are identical, we thus have $\mathcal{A}_K = \mathcal{A}$, but if their masses are distributed according to the same distribution as in Ref. [71], then $\mathcal{A}_K/\mathcal{A} = 1.9$. Although the calculation leading to Eq. (6.38) is not fully detailed in Ref. [65], its discrepancy with our result (6.37) may be due to different statistical assumptions. In particular, we suspect that Kantowski took into account that bigger SC holes have a larger probability to be encountered by a light beam, whereas we did not—in our approach, holes are randomly placed on the line of sight, irrespective of their sizes. While the former is relevant in an exact SC model, the latter may better correspond to the actual small-scale structure of the Universe.
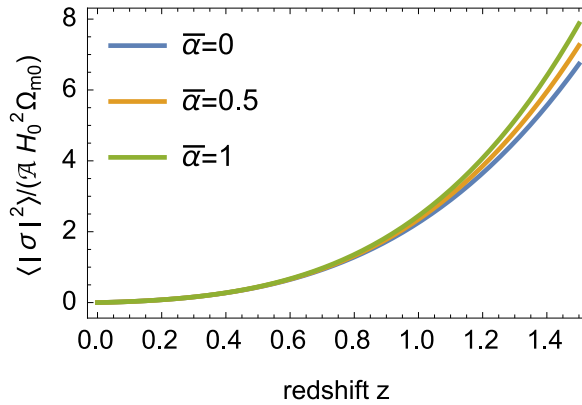

Figure 3: Evolution of the integral of Eq. (6.36), as a function of the redshift, for three different smoothness parameters $\bar{\alpha} = 0, 0.5, 1$.

6.4.2   A post-Kantowski-Dyer-Roeder approximation

In § 5.2.1 we have derived the general expression (5.28) of the correction $\delta_{D_A}^{(1)} = (\langle D_A \rangle - D_0)/D_0$ to the mean angular distance with respect to the zero-shear distance D_0—here given by the KDR approximation. With the formula (6.35) for $C_{\mathscr{W}}$ in a SC model, this *post-Kantowski-Dyer-Roeder* (pKDR) term reads

$$\delta_{D_A}^{(1)} = -\mathcal{A}\,\Omega_{m0} \int_0^z \frac{dz_1}{E(z_1)} \int_0^{z_1} \frac{dz_2}{E(z_2)} \int_0^{z_2} \frac{dz_3}{E(z_3)} \left[\frac{\hat{D}_0^2(z_3)}{\hat{D}_0(z_1)\hat{D}_0(z_2)} \right]^2. \tag{6.39}$$

with $E(z) \equiv H(z)/H_0 = \sqrt{\Omega_{m0}(1+z)^3 + \Omega_{\Lambda 0}}$, and where $\hat{D}_0(z) \equiv (1+z)D_0(z)$ is sometimes called the corrected luminosity distance, here associated with the KDR distance D_0.

Figure 4 represents $\delta_{D_\mathrm{A}}^{(1)}$ as a function of the smoothness parameter $\bar{\alpha}$ (4a) and of the redshift z (4b), comparing our calculation with the earlier result of Kantowski [65]. On Fig. 4a are also plotted the results of ray-tracing simulations in SC model, as described in Ref. [71]. Each square represents the average of $(D_\mathrm{A} - D_0)/D_0$ over 1000 runs. These numerical results are thus in excellent agreement with the predictions of the stochastic lensing calculations, which proves its efficiency.
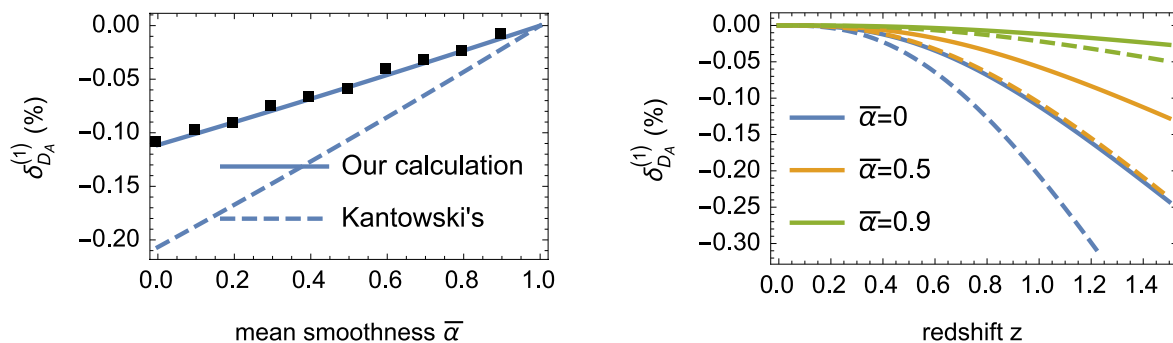
(a) Post-KDR correction $\delta_{D_\mathrm{A}}^{(1)}$ as a function of the smoothness parameter $\bar{\alpha}$, at redshift $z = 1$. Black squares are results from simulations.

(b) Post-KDR correction $\delta_{D_\mathrm{A}}^{(1)}$ as a function of redshift z for three different smoothness parameters $\bar{\alpha} = 0, 0.5, 0.9$.

Figure 4: pKDR correction on the angular diameter distance $\delta_{D_\mathrm{A}}^{(1)} \equiv (\langle D_\mathrm{A} \rangle - D_0)/D_0$, at linear order in Weyl lensing, in SC models made of galaxylike clumps, with $\mathcal{A}_0 = 0.5$. Solid lines correspond to our calculations and dashed lines to Kantowski's.

The results depicted on Fig. 4, namely $\delta_{D_\mathrm{A}}^{(1)} \sim 10^{-3}$, confirm that the KDR approximation provides a very good effective description of the angular distance-redshift relation in SC models [71], at least when galaxy-like clumps are at stake. Nevertheless, since $\delta_{D_\mathrm{A}}^{(1)} \propto \mathcal{A}$, this pKDR correction can become very large as the clumps are more compacts; the orders of magnitude given in table 1 suggests that for a SC model made of stars, $\delta_{D_\mathrm{A}}^{(1)} \sim 10^7$. This unreasonably large number is a hint that our calculations may break down if too small deflectors are involved. In particular, the infinitesimal light beam approximation—on which both the Jacobi matrix and optical scalar formalisms are based—is not valid for describing the lensing of a star at cosmological distances, which rather requires a microlensing description. See also a discussion by Gunn in Ref. [63] on this issue.

### 6.4.3 Dispersion of the angular distance

The general equation governing the variance of the angular distance, $\mathrm{var}(D_\mathrm{A})$, based on second-order calculations in Weyl lensing, has been derived in § 5.3. In terms of the redshift,

using both Eqs. (5.14), (6.7), it reads

$$
\left\{\frac{\mathrm{d}^3}{\mathrm{d}z^3} + \left(\frac{H'}{H} + \frac{6}{1+z}\right)\frac{\mathrm{d}^2}{\mathrm{d}z^2} + \left[\frac{H''}{H} + \left(\frac{H'}{H}\right)^2 + \frac{8}{1+z}\frac{H'}{H} + \frac{6}{(1+z)^2}\right.\right.
$$
$$
\left.\left. - \frac{4\langle\mathscr{R}\rangle}{(1+z)^4 H^2}\right]\frac{\mathrm{d}}{\mathrm{d}z} + \frac{2\langle\mathscr{R}\rangle'}{(1+z)^4 H^2} + \frac{4C_{\mathscr{W}} - 2C_{\mathscr{R}}}{(1+z)^6 H^3}\right\}\mathrm{var}(D_\mathrm{A})
$$
$$
= \frac{2D_0^2 C_{\mathscr{R}}}{(1+z)^6 H^3} + \frac{6}{(1+z)^6 H^3 D_0^4}\int_0^z \frac{\mathrm{d}z_1}{(1+z_1)^2 H D_0^2}\left[\int_0^{z_1}\mathrm{d}z_2\,\frac{2D_0^4 C_{\mathscr{W}}}{(1+z_2)^2 H}\right]^2, \quad (6.40)
$$

where a prime denotes here a derivative with respect to z. To our knowledge, it is the first time that such a theoretical prediction of the dispersion of the angular distance though a SC model is proposed. This equation is solved numerically, using $\langle\mathscr{R}\rangle = -(3/2)H_0^2\bar{\alpha}\Omega_{\mathrm{m}0}(1+z)^5$ and the expressions for $C_{\mathscr{R}}$ and $C_{\mathscr{W}}$ derived previously; the output is shown in Fig. 5 with, on Fig. 5a, a comparison with simulated data.
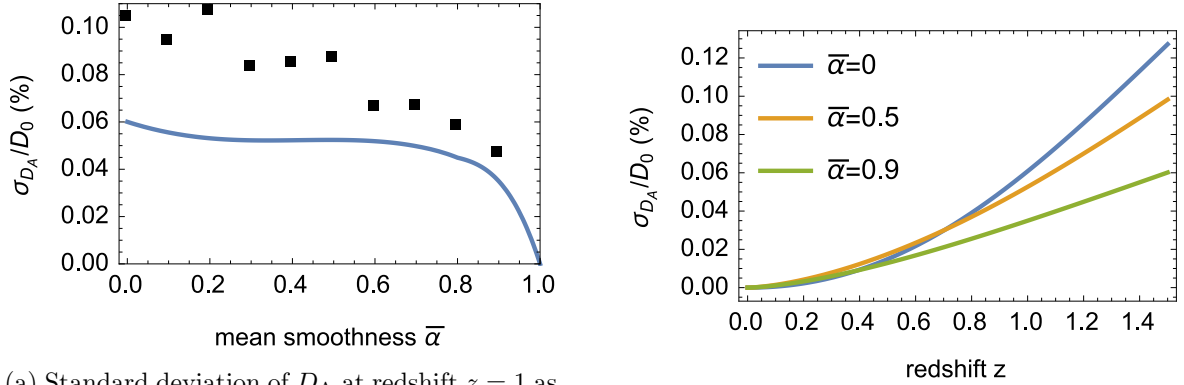
(a) Standard deviation of D_A at redshift $z = 1$ as a function of smoothness $\bar{\alpha}$. Black squares result from ray-tracing simulations and lines from the numerical integration of Eq. (6.40).

(b) Standard deviation of D_A as a function of redshift z, for three different smoothness parameters, $\bar{\alpha} = 0, 0.5, 0.9$.

Figure 5: Standard deviation $\sigma_{D_\mathrm{A}} \equiv \sqrt{\mathrm{var}(D_\mathrm{A})}$ of the angular distance D_A in SC models, normalised by the KDR distance D_0, as a function of the smoothness parameter $\bar{\alpha}$ and redshift z.

We see that, contrary to its average $\langle D_\mathrm{A}\rangle$, the standard deviation σ_{D_A} of the angular distance predicted by the stochastic lensing formalism does not fit with the results of ray-tracing simulations. They differ here by a factor 1.7 for $\bar{\alpha} = 0$. We performed a number of consistency checks on both the analytical and numerical sides, and found no errors. It turns out that such a discrepancy between theoretical and numerical results is actually a genuine limitation of our formalism, due to the fact that we modelled Weyl fluctuation by a *Gaussian* noise.

Let us first show that the problem indeed comes from Weyl lensing. Formally, Eq. (6.40) reads

$$
\mathrm{D}_z^3\,\mathrm{var}(D_\mathrm{A}) = S_{\mathscr{R}} + S_{\mathscr{W}}, \quad (6.41)
$$

where D_z is a linear differential operator, and $S_{\mathscr{R}}, S_{\mathscr{W}}$ are source functions respectively due to Ricci and Weyl lensing. Contrary to $C_{\mathscr{R}}/C_{\mathscr{W}}$, the ratio $S_{\mathscr{W}}/S_{\mathscr{R}}$ is not necessarily small here;

in fact, it is of order unity in the SC model used to generate the results of Fig. 5. A way to tune this ratio—and thus to decide which among Ricci and Weyl fluctuations dominates the dispersion of D_A—consists in changing the lower cutoff $b_{\min} = r_c$ of impact parameters in the holes. By virtue of Eq. (6.35), decreasing r_c, i.e. enhancing the compacity of the central clumps, increases $C_{\mathscr{W}}$.

In Fig. 6, we compare again the predictions of the stochastic lensing formalism with ray-tracing results, but for two different classes of SC models: with less compact clumps (twice larger for the same mass, left panel); or more compact clumps (twice smaller for the same mass, right panel) than before. We see that the agreement between theory and numerics is now excellent in the first case, where $S_{\mathscr{R}} \gg S_{\mathscr{W}}$, while it is slightly worse than in Fig. 5a in the second case, where on the contrary $S_{\mathscr{R}} \ll S_{\mathscr{W}}$. The very good agreement regarding $\delta_{D_A}^{(1)}$ in both cases confirms that there are no mistakes in the evaluation of $C_{\mathscr{W}}$

Such results suggest that our modelling of Ricci lensing fluctuations is more accurate than the one of Weyl lensing fluctuations. The weakness does not seem to be related with the δ-correlation hypothesis, because (i) the numerical SC model is constructed so that the properties of two different holes are indeed independent; (ii) the size of the holes is much smaller than the typical evolution scale of D_A; and (iii) this hypothesis equally applies to both Ricci and Weyl fluctuations, any deviation from it would therefore be manifest for any value of $S_{\mathscr{R}}/S_{\mathscr{W}}$, which is not what we observe.

The Gaussian hypothesis is more questionable. In the standard Langevin description of Brownian motion, the Gaussianity of the random force is justified by the central-limit theorem: during a mesoscopic time interval Δt, the Brownian particle is hit by many molecules, and the associated microscopic momentum transfers $\delta \boldsymbol{p}_{\mathrm{micro}}$ *sum* into an effective transfer $\Delta \boldsymbol{p}$, whose PDF is therefore well approximated by a Gaussian, whatever the PDF of each $\delta \boldsymbol{p}_{\mathrm{micro}}$.

However, while a microscopic Brownian particle undergoes $\sim 10^{20}$ collisions per second, a typical light beam in a SC models encounters only $\sim 10^3$ holes from the source to the observer. The convergence towards central limit must therefore be very efficient for the Gaussian model to be adapted. In the case of Ricci lensing, $\mathscr{R}$ simply oscillates between 0 and $\mathscr{R}_{\mathrm{FL}}$; the sum of such a random variable converges quite quickly towards the Gaussian limit, in particular because its support is compact. The case of Weyl lensing is different. One can easily check from the statistical assumptions of § 6.3.1 and the expression (6.18) of $\mathscr{W}_{\mathrm{eff}}$ that its PDF reads

$$p(|\mathscr{W}_{\mathrm{eff}}|) = \frac{2}{3\mathscr{W}_{\min}} \left(\frac{|\mathscr{W}_{\mathrm{eff}}|}{\mathscr{W}_{\min}} - \frac{1}{3} \right)^{-2} [\mathscr{W}_{\min} \leq |\mathscr{W}_{\mathrm{eff}}| \leq \mathscr{W}_{\max}], \qquad (6.42)$$

with $\mathscr{W}_{\min} = 4\pi G \rho_0 (1+z)^5$ and $\mathscr{W}_{\max} = \mathscr{W}_{\min}[1 + 2(r_h/r_c)^2]/3 \gg \mathscr{W}_{\min}$. This PDF thus has a very long algebraic tail, which drastically slows down the convergence towards central limit. This argument is, in our opinion, the most probable explanation of the discrepancy between theory and numerics observed in Fig. 5a, and of its disappearance in the left panel of Fig. 6, where Ricci lensing dominates. This argument shall be reinforced by the results of the next section.

7   Numerical integration of the Langevin equation

The FPK equation, Eq. (4.14) for the Jacobi matrix or Eq. (4.20) for the optical scalars, contains all the information necessary to characterise the statistical properties of stochastic lensing, provided this part of lensing can be well approximated by a Gaussian, uncorrelated noise (white noise). However, as mentioned before, it is in general impossible to solve explicitly
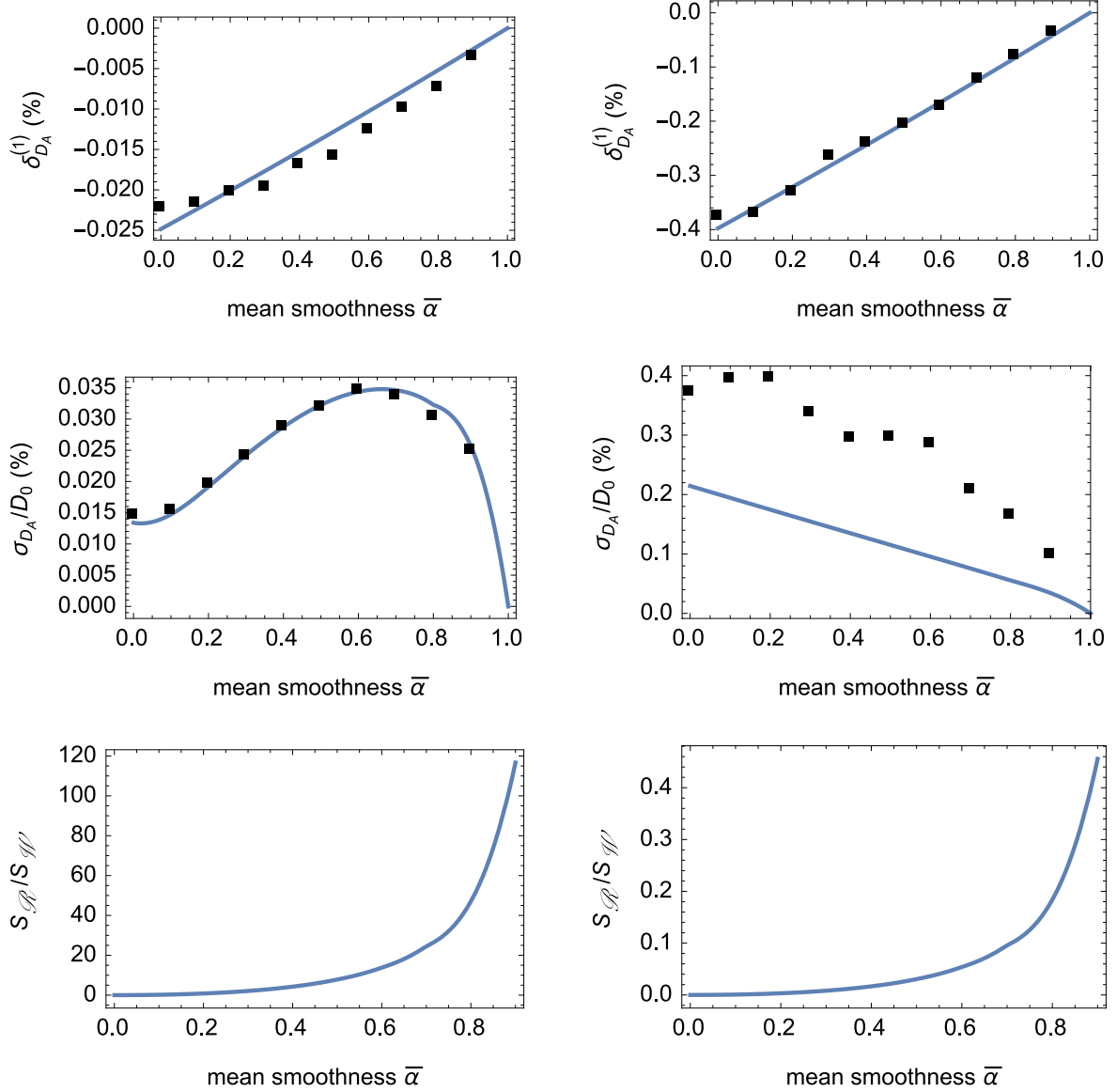
Figure 6: pKDR correction to the mean angular distance $\delta_{D_A}^{(1)}$ (top); normalised standard deviation σ_{D_A}/D_0 (middle); and ratio $S_{\mathscr{R}}/S_{\mathscr{W}}$ between the Ricci and Weyl sources of variance (bottom), as a function of the mean smoothness parameter $\bar{\alpha}$ at redshift $z = 1$, for SC models with two different clump densities: $\rho_c/8 \Leftrightarrow 2r_c$ (left panel) and $8\rho_c \Leftrightarrow r_c/2$ (right panel), where $\rho_c = 3.5 \times 10^{-22} \, \mathrm{kg/m^3}$ is the density used for the previous plots 4a, 5a. For a given SC hole, the minimal impact parameter $b_{\min} = r_c$ is thus respectively increased or reduced by a factor 2 with respect to the previous calculations. As before, squares correspond to the output of ray-tracing simulations, while lines are the predictions of the stochastic lensing formalism.

the FPK equation, and one ought to rely on numerical methods to extract the statistical information available. From the numerical point of view, solving a partial differential equation is harder than tackling an ordinary differential equation and therefore, it is certainly better to concentrate on the Langevin equation rather than on the FPK equation. In this section, we

aim at solving the Langevin equation for the Jacobi matrix, Eq. (3.15) for a double purpose. First, we wish to show that, in the approximation of a white noise for the Ricci and Weyl lensing, the ray-tracing and analytical results of the previous section are well re-produced by directly solving the Langevin equation. Second, we would like to probe the effect of relaxing the Gaussian approximation: we will show that in the SC model, if the 'true' PDF of $\mathscr{W}_{\text{eff}}$, Eq. (6.42), is used, the discrepancy in the fluctuations of D_A between the ray-tracing results and the analytical estimates coming from the FPK equation can clearly be attributed to the non-Gaussianity of the noise and the lack of convergence towards the central limit when the number of holes encountered is too small.

7.1 The stochastic Euler method

We begin by a short exposition of the numerical discretisation of the general Langevin equation (4.1). For an infinitesimal time step $\mathrm{d}t$, we can rewrite this equation as

$$\boldsymbol{X}(t + \mathrm{d}t) = \boldsymbol{X}(t) + \boldsymbol{f}(\boldsymbol{X}, t)\,\mathrm{d}t + \boldsymbol{L}(\boldsymbol{X}, t)\boldsymbol{N}(t)\,\mathrm{d}t. \tag{7.1}$$

Noting $\mathrm{d}\boldsymbol{B}(t) = \boldsymbol{N}(t)\mathrm{d}t$, this becomes simply

$$\boldsymbol{X}(t + \mathrm{d}t) = \boldsymbol{X}(t) + \boldsymbol{f}(\boldsymbol{X}, t)\mathrm{d}t + \boldsymbol{L}(\boldsymbol{X}, t)\,\mathrm{d}\boldsymbol{B}(t), \tag{7.2}$$

which, after discretisation, gives the Euler approximation to the Langevin equation

$$\boldsymbol{X}(t_{i+1}) = \boldsymbol{X}(t_i) + \boldsymbol{f}[\boldsymbol{X}(t_i), t_i]\,\Delta t + \boldsymbol{L}[\boldsymbol{X}(t_i), t_i]\,\Delta \boldsymbol{B}(t_i), \tag{7.3}$$

where we have assumed, for simplicity, a constant time step Δt. As discussed in Sec. 4.1, if the noise $\boldsymbol{N}$ is a white noise, then $\boldsymbol{B}$ is a Brownian motion, i.e. its increment $\Delta \boldsymbol{B}$ is a zero-mean Gaussian process with covariance matrix

$$\left\langle \Delta \boldsymbol{B}(t_i)\Delta \boldsymbol{B}^{\mathrm{T}}(t_j) \right\rangle = \boldsymbol{\mathcal{Q}}(t_i)\delta_{ij}\,\Delta t \qquad \text{(no summation over } i\text{)}. \tag{7.4}$$

In practice, simulating one realisation of the process $\boldsymbol{X}(t)$ is thus identical to numerically solving an ordinary differential equation, except that at each time step t_i the quantity $\Delta \boldsymbol{B}(t_i)$ is randomly picked, according to a Gaussian PDF with variance $\boldsymbol{\mathcal{Q}}(t_i)\Delta t$, and independently of the other steps. This means that the components of the stochastic term $\Delta \boldsymbol{B}$ have fluctuations on the order of $\sqrt{\Delta t}$: the stochastic Euler method only converges as $\sqrt{\Delta t}$, instead of Δt for its deterministic counterpart. This limitation will not be a problem in what follows.

Note also that we can still apply this discretisation if the noise is not Gaussian, but the term $\boldsymbol{N}(t)\Delta t$ must then be evaluated from the true PDF of $\boldsymbol{N}$. The main caveat, in this case, lies on the fact that the simulation is no longer resolution independent (see § 7.3).

7.2 Application to the Swiss-cheese model – Gaussian case

Let us now turn to our specific Langevin equation for the Jacobi matrix (4.14), in the SC model. Using the relationship between affine parameter and redshift, we can rewrite it as

$$\frac{\mathrm{d}\boldsymbol{J}}{\mathrm{d}z} = \frac{1}{H(z)(1 + z)^2}\left[\boldsymbol{M}(z)\boldsymbol{J}(z) + \boldsymbol{L}_{\text{Jac}}(\boldsymbol{J})\boldsymbol{N}(z)\right]. \tag{7.5}$$

Discretising this equation with a constant redshift step Δz (for simplicity), one gets

$$\boldsymbol{J}_{k+1} = \boldsymbol{J}_k + \frac{1}{H(z_k)(1 + z_k)^2}\left[\boldsymbol{M}(z_k)\boldsymbol{J}_k\Delta z + \boldsymbol{L}_{\text{Jac}}(\boldsymbol{J}_k)\Delta \boldsymbol{B}(z_k)\right], \tag{7.6}$$

with $\boldsymbol{J}_k \equiv \boldsymbol{J}(z_k)$, and where the covariance matrix of $\Delta\boldsymbol{B}$ involves the diffusion matrix of Eq. (3.10) according to

$$\left\langle \Delta\boldsymbol{B}(z_k)\Delta\boldsymbol{B}^{\mathrm{T}}(z_k) \right\rangle = \boldsymbol{\mathcal{Q}}(z_k)\Delta z \tag{7.7}$$

$$= \mathrm{diag}(C_{\mathscr{R}}, C_{\mathscr{W}}, C_{\mathscr{W}})\Delta z. \tag{7.8}$$

At each time step, the quantity $\Delta\boldsymbol{B}^{\mathrm{T}} = (\Delta B_{\mathscr{R}}, \Delta B_{\mathscr{W}_1}, \Delta B_{\mathscr{W}_2})$ is obtained by randomly picking $\Delta B_{\mathscr{R}}$ and $\Delta B_{\mathscr{W}_A}$ according to a zero-mean Gaussian distribution with variance $C_{\mathscr{R}}\Delta z$ and $C_{\mathscr{W}}\Delta z$, respectively.

Using the expressions for $C_{\mathscr{R}}(z)$ and $C_{\mathscr{W}}(z)$ found in the case of the SC model, Eqs. (6.31) and (6.35) respectively, we can now integrate numerically the Langevin equation. Results are presented in Fig. 7, for the same set of parameters as those used in the previous section, i.e. with a standard distribution of galaxy-type holes. Statistical averages are performed over 1000 realisations of $\boldsymbol{J}(z)$, for each possible value of $\bar{\alpha}$, each realisation being simulated according to the stochastic Euler method with a redshift step $\Delta z = 10^{-4}$. The agreement with the results from the FPK approach is striking, and provides strong support for the analytical expressions found previously. Compared to ray-tracing simulations, the pKDR corrections to $\langle D_{\mathrm{A}} \rangle$ are very accurately reproduced, but the dispersion of D_{A} suffers from the same systematic underestimation as in the previous section. If one could resolve this tension, because the numerical integration of the Langevin equation is much faster than ray-tracing simulations, it would provide an efficient way to estimate statistical quantities.
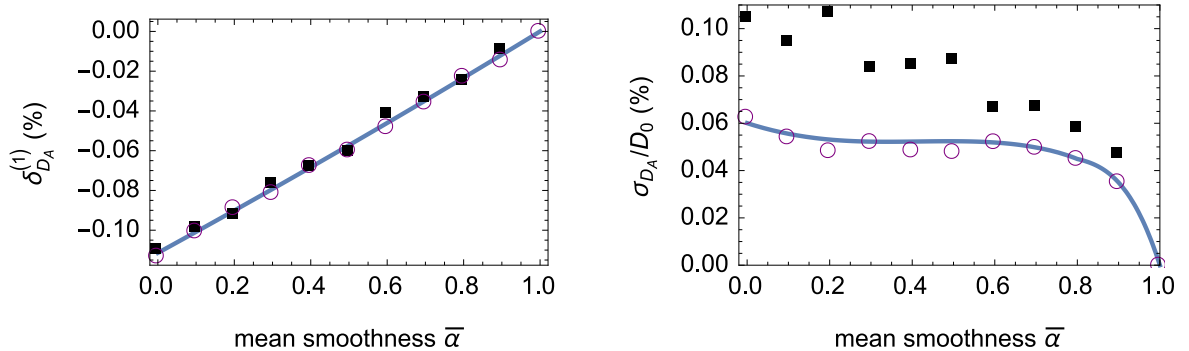

Figure 7: Results of the numerical integration of the Langevin equation with a Gaussian noise (empty purple circles), compared with analytical calculations (blue lines) and ray-tracing simulations (black squares) in the SC model. Left panel (same as Fig. 4a): pKDR correction, in percent, to the angular distance at $z = 1$, as a function of $\bar{\alpha}$. Right panel (same as Fig. 5a): fractional dispersion, in percent, of D_{A} at $z = 1$ as a function of $\bar{\alpha}$.

7.3 Beyond the Gaussian approximation

Now that we have shown that numerically integrating the Langevin equation leads to the same results as the use of the FPK equation in the Gaussian noise limit, we would like to show that the discrepancy between these results and the ray-tracing results stems from non-Gaussianity. Indeed, as discussed in the previous section, the Weyl lensing is very poorly described by a Gaussian noise, since its actual PDF in a SC model presents a long non-Gaussian tail, corresponding to not so rare events during which light rays pass very close to masses and experience significant tidal distortions. In order to probe this effect, in this subsection, we

limit ourselves to the case $\bar{\alpha} = 0$ in which the Ricci lensing is zero, thus isolating effects due to a pure Weyl lensing. We also use an SC model with one size of holes for simplicity.

We come back to Eq. (7.5) but we no longer treat the noise term as the increments $\Delta\boldsymbol{B}$ of a Brownian motion $\boldsymbol{B}$, and replace it by $\Delta\tilde{\boldsymbol{B}}$ such that

$$\Delta\tilde{B}_{\mathscr{W}_1} = \sqrt{\frac{3R_{\mathrm{h}}\Delta z}{(1+z)^4 H(z)}}\, |\mathscr{W}_{\mathrm{eff}}| \cos 2\beta, \tag{7.9}$$

$$\Delta\tilde{B}_{\mathscr{W}_2} = -\sqrt{\frac{3R_{\mathrm{h}}\Delta z}{(1+z)^4 H(z)}}\, |\mathscr{W}_{\mathrm{eff}}| \sin 2\beta, \tag{7.10}$$

where β is uniformly distributed within $[0, 2\pi]$, while the PDF of $|\mathscr{W}_{\mathrm{eff}}|$ is given by Eq. (6.42). One can check that the above choice ensures that $\left\langle \Delta\tilde{\boldsymbol{B}}\Delta\tilde{\boldsymbol{B}}^{\mathrm{T}} \right\rangle = \mathrm{diag}(C_{\mathscr{R}}, C_{\mathscr{W}}, C_{\mathscr{W}})\Delta z$ as before. In other words, the resulting $\Delta\tilde{\boldsymbol{B}}$ is a non-Gaussian process whose first two moments match the ones of the Gaussian model. Note that this is somehow artificial, because the noise modelled by $\Delta\tilde{\boldsymbol{B}}$ now depends on the resolution Δz used for integrating the Langevin equation. This can be understood as follows. Suppose one solves the Langevin equation with two different resolutions: a low resolution (LR) Δz_{LR}, and a high resolution (HR) $\Delta z_{\mathrm{HR}} = \Delta z_{\mathrm{LR}}/n$. During a given interval $[z, z + \Delta z_{\mathrm{LR}}]$, the HR simulation performs n steps, and the effective noise associated with the set of these n steps reads

$$\Delta\tilde{\boldsymbol{B}}_{\mathrm{HR}}(z \to z + \Delta z_{\mathrm{LR}}) = \sum_{k=0}^{n-1} \Delta\tilde{\boldsymbol{B}}_{\mathrm{HR}}(z_k \to z_{k+1}), \tag{7.11}$$

with $z_k = z + k\Delta z_{\mathrm{HR}}$. Contrary to the Gaussian case, the above sum is *not* equal to $\Delta\tilde{\boldsymbol{B}}_{\mathrm{LR}}$, because any random variable does not enjoy the invariance under addition; in particular, for $n \to \infty$ it becomes Gaussian itself, by virtue of the central limit theorem.

We therefore expect the output of numerical integration of the Langevin equation with $\Delta\tilde{\boldsymbol{B}}$ (i) to depend on the resolution Δz, and (ii) to converge towards the Gaussian case for $\Delta z \to 0$. This is illustrated in Fig. 8, where the mean and dispersion of the angular distance at $z = 1$, obtained by integrating Langevin equation in the Gaussian and non-Gaussian cases, are plotted as a function of Δz. We also indicate, for comparison, the analytical and ray-tracing results. A number of comments shall be formulated about those figures. First, all the results on the mean angular distance $\langle D_{\mathrm{A}} \rangle$—more precisely, its pKDR correction $\delta_{D_{\mathrm{A}}}^{(1)}$—are in excellent agreement. It is not the case concerning the dispersion $\sigma_{D_{\mathrm{A}}}$ of D_{A}. Then, as expected, the Gaussian numerical results coincide with the analytical calculations, as well as the non-Gaussian result for $\Delta z \to 0$. The latter however depart from the formers as Δz increases, and coincides with the ray-tracing results for $\Delta z \approx 2.5 \times 10^{-4}$. This particular value can be understood as follows: physically speaking, a non-Gaussian Langevin simulation with redshift step Δz corresponds to a SC model where successive holes are typically separated by Δz, that is z/N where z is the redshift of the source and N the typical number of holes between the source and the observer. As a matter of fact, with the parameters used for generating Fig. 8, the average number of holes encountered by a photon is on the order of 3000, corresponding to a $\Delta z \sim 3 \times 10^{-4}$, which is very close to the value 2.5×10^{-4} where the ray-tracing and the stochastic non-Gaussian results match.

This confirms our point that, in the SC models investigated here, the typical number of collisions is marginally too small to warrant a treatment of the lensing in terms of a pure

white noise, i.e. with a FPK equation. This understanding of the problem provides two ways of escaping from it: (1) dealing with smaller-scale structures; (2) increasing the redshift z of the source. In both situation, the number N of deflectors, that is the physical resolution of the problem, is increased, which should thus improve the agreement between exact ray-tracing results and the analytical FPK calculations. A quantitative criterion, allowing us to estimate the precision of the FPK approach, remains nevertheless to be determined.
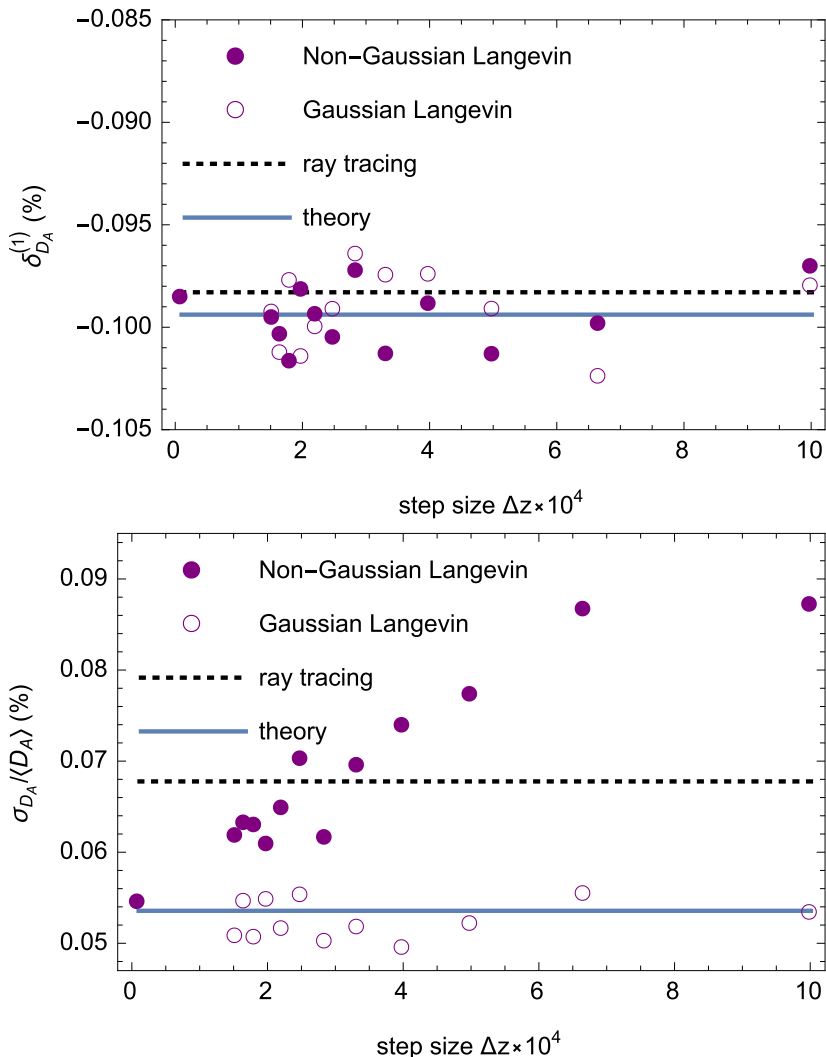

Figure 8: pKDR correction to $\langle D_{\mathrm{A}} \rangle$ (top panel) and dispersion of D_{A} (bottom panel) at $z = 1$, computed from numerical integration of the Langevin equation (7.5) with a Gaussian noise $\Delta \boldsymbol{B}$ (empty circles) or a non-Gaussian noise $\Delta \tilde{\boldsymbol{B}}$ (filled circles), as functions of the redshift step Δz used in the Euler method. Each circle is obtained from the statistical properties of a sample of 1000 realisations of $\boldsymbol{J}$. For comparison, dotted lines indicate the output of ray-tracing simulations, while the solid lines are the analytical predictions of the stochastic lensing formalism, i.e. given by Eqs. (6.39), (6.40). The smoothness parameter of the underlying SC model is $\bar{\alpha} = 0$; all holes have the same mass $M = 10^{11} M_{\odot}$ and density ρ_{c}.

8   Conclusion

In this article, we proposed a new theoretical framework in which the gravitational lensing caused by the small-scale structure of the Universe is treated as a diffusion process. The Sachs equations governing the propagation of narrow light beams were provided with stochastic components modelled as white noises. We derived the associated Fokker-Planck-Kolmogorov equations for the PDF of the Jacobi matrix and the optical scalars. We used them to deduce (1) the corrections to the mean angular distance due to Weyl lensing, and (2) a differential equation for the dispersion of the angular distance. These results depend on three free functions, namely the mean Ricci lensing $\langle \mathscr{R} \rangle$ and the covariance amplitudes of Ricci and Weyl lensing $C_{\mathscr{R}}, C_{\mathscr{W}}$, which need to be specified from a model. As both an illustration and a test of this new formalism, we applied it to Einstein-Straus Swiss-cheese models. The results on $\langle D_{\mathrm{A}} \rangle$ offer an extension to the Kantowski-Dyer-Roeder approximation, in excellent agreement with numerical simulations. The theoretical predictions for the variance of D_{A} are however systematically lower than their numerical counterpart. We located the origin of this discrepancy in the actual non-Gaussianity of Weyl lensing, which cannot be captured by the FPK approach. This was confirmed by direct simulations of the Langevin equation with Gaussian and non-Gaussian source terms.

This new approach has the advantage of dealing with small-scale lensing in a mathematically consistent and efficient way, without the need for computationally expensive ray-tracing simulations. It complements the standard description of weak lensing caused by the large-scale structure, allowing for the effect of smaller scales. It is also very flexible, in the sense that it can be applied, in principle, to any model for the distribution of matter on those scales.

The main limitation of our formalism, under its present form, lies in the assumption of Gaussianity. This hypothesis is indeed central in the general derivation of the Fokker-Planck-Kolmogorov equation, on which our main results are based, but it may not hold in the actual Universe, as illustrated on the particular example of Swiss-cheese models. There is, on the mathematics side, active ongoing research on stochastic processes with non-Gaussian noises. Unfortunately no definite standard prescription about how to modify the FPK equation has been established so far, which is the reason why we did not enter into such discussions in the present article. Nevertheless, from a practical point of view, we empirically checked that the Gaussian limit provides good estimations of the lensing quantities, as far as only their mean and variance are concerned: the largest discrepancies are expected to appear for higher-order moments.

In the future, we plan to apply the stochastic lensing framework to more realistic models than the Swiss cheese, in particular for comparing its output with the numerical results of Refs. [86, 87]. We also intend to include the effect of peculiar velocities, which is not expected to contain major difficulties. On longer terms, we aim at explicitly combining our formalism with the standard perturbation theory, which would ideally provide a consistent multiscale treatment of cosmological lensing. This will however require to establish a quantitative criterion about the transition scale from one behaviour to the other. Finally, we emphasize the very general character of the approach presented here, which may also be applied to spacetimes with very different symmetries, to treat e.g. the microlensing due to stars in a galaxy, or the effect of a stochastic background of gravitational waves.

A   Geometric optics in curved spacetime

This appendix summarises textbook elements about the propagation of light in arbitrary spacetimes, which aims at supplementing the relatively sharp presentation of Sec. 2. For more general introductions, see Refs. [92, 93, 112–114].

A.1   Description of a light beam

A light beam is a collection of light rays, that is, a bundle of null geodesics $\{v \mapsto x^\mu(v, y^a)\}$ converging at a given event (here taken to be the observation event O), where the two coordinates $(y^a)_{a=1,2}$ label the rays, while v is the affine parameter along them. There is no need for a fourth coordinate because the beam entirely belongs to the lightcone of O, which is an isophase hypersurface.

The wave four-vector $k^\mu \equiv \partial x^\mu / \partial v$ is a null vector field, tangent to the rays $y^a = \text{cst}$. It satisfies the null geodesic equations

$$k^\mu k_\mu = 0, \qquad \text{and} \qquad k^\nu \nabla_\nu k_\mu = 0. \tag{A.1}$$

Besides, the relative behaviour of two neighbouring geodesics of the bundle, $x^\mu(\cdot, y^a)$ and $x^\mu(\cdot, y^a + \delta y^a)$, is described by their connecting vector $\xi^\mu \equiv (\partial x^\mu / \partial y^a) \delta y^a$. If the origin $v = 0$ of the affine parametrisation of all rays is taken at O, then

$$k^\mu \xi_\mu = 0. \tag{A.2}$$

As soon as the condition (A.2) is satisfied, the evolution of ξ^μ along the beam is governed by the geodesic deviation equation

$$k^\alpha k^\beta \nabla_\alpha \nabla_\beta \xi^\mu = R^\mu{}_{\nu\alpha\beta} k^\nu k^\alpha \xi^\beta, \tag{A.3}$$

where $R^\mu{}_{\nu\alpha\beta}$ is the Riemann tensor.

A.2   The Sachs formalism

Consider an observer, with four-velocity u^μ ($u_\mu u^\mu = -1$), who crosses the light beam. The spatial direction of propagation of the beam, relative to this observer, is defined as the opposite of the direction in which the observer must look to detect a signal. It is spanned by a purely spatial unit vector d^μ,

$$d^\mu u_\mu = 0, \qquad d^\mu d_\mu = 1, \tag{A.4}$$

such that (remember that we took k^μ future oriented in this article)

$$k^\mu = -\omega(u^\mu + d^\mu), \tag{A.5}$$

where

$$\omega = 2\pi\nu \equiv u_\mu k^\mu \tag{A.6}$$

is the cyclic frequency of the light signal in the observer's rest frame. Note that $d\ell = \omega dv$ is the proper distance (measured by the observer) travelled by light for a change dv of the affine parameter. The redshift z is defined as the relative change between the emitted frequency ν_s, in the source's frame, and the observed frequency ν_o, in the observer's frame, that is

$$1 + z \equiv \frac{\nu_s}{\nu_o} = \frac{u_s^\mu k_\mu(v_s)}{u_o^\mu k_\mu(v_o)}. \tag{A.7}$$

Suppose that the observer measures the size and the shape of the light beam. For that purpose, he must use (and thus define) a (spatial) screen orthogonal to the line of sight. This screen is spanned by the so-called Sachs basis $(s_A^\mu)_{A \in \{1,2\}}$, defined by

$$s_A^\mu u_\mu = s_A^\mu d_\mu = 0, \qquad g_{\mu\nu} s_A^\mu s_B^\nu = \delta_{AB}, \tag{A.8}$$

and by the transport property (A.9) below. The projections $\xi_A \equiv s_A^\mu \xi_\mu$ indicate the relative position, on the observer's screen, of the light points corresponding to two neighbouring rays separated by ξ^μ. Thus, it encodes all the information about the size and shape of the beam.

Consider a family of observers $u^\mu(v)$, along the beam, who wants to follow the evolution of the shape of the beam (typically for shear measurements). For that purpose, they must all use the "same" Sachs basis, in order to avoid any spurious rotation of the pattern observed on the screens. This is ensured by imposing that the Sachs basis is a parallel transported as

$$S_{\mu\nu} k^\rho \nabla_\rho s_A^\nu = 0, \tag{A.9}$$

where

$$S^{\mu\nu} = \delta^{AB} s_A^\mu s_B^\nu = g^{\mu\nu} + u^\mu u^\nu - d^\mu d^\nu \tag{A.10}$$

is the screen projector. The reason why s_A^μ cannot be completely parallel-transported is that, in general, u^μ is not[7].

The evolution of ξ_A, with light propagation, is determined by projecting the geodesic deviation equation (A.3) on the Sachs basis. The result is known as the *Sachs equation* [93, 115, 116],

$$\frac{d^2 \xi_A}{dv^2} = \mathcal{R}_{AB} \xi^B, \tag{A.11}$$

where

$$\mathcal{R}_{AB} = R_{\mu\nu\alpha\beta} k^\nu k^\alpha s_A^\mu s_B^\beta \tag{A.12}$$

is the screen-projected Riemann tensor, usually called the *optical tidal matrix*. The properties of the Riemann tensor imply that this matrix is symmetric, $\mathcal{R}_{AB} = \mathcal{R}_{BA}$. Note that the position of the screen indices $(A, B, \ldots)$ does not matter, since they are raised and lowered by δ_{AB}. In this article, to alleviate the notation, we use bold symbols for quantities with screen indices, and an overdot for derivatives with respect to the affine parameter v. The Sachs equation (A.11) thus becomes

$$\ddot{\boldsymbol{\xi}} = \mathcal{R} \boldsymbol{\xi}. \tag{A.13}$$

---

[7]In fact, it is also possible to choose a family of observers such that the four-velocity field u^μ is parallel-transported along the beam, without affecting the optical equations [93]. In this case, however, the observers are generally not comoving, and thus have no clear cosmological interpretation.

A.3 Evolution in terms of potentials

It is interesting to note that the Sachs equation can be reformulated in terms of a potential, as

$$\ddot{\xi}_A = \frac{\partial V}{\partial \dot{\xi}^A}, \tag{A.14}$$

with

$$V(\boldsymbol{\mathcal{D}}) \equiv -\frac{1}{2}\xi_A \mathcal{R}_{AB}\xi_B = -\frac{1}{2}\boldsymbol{\xi}^{\mathrm{T}}\boldsymbol{\mathcal{R}}\boldsymbol{\xi}. \tag{A.15}$$

This equally applies to the Jacobi matrix equation $\ddot{\mathcal{D}}_{AB} = -\partial V_{\mathrm{Jac}}/\partial \mathcal{D}_{AB}$, with $V_{\mathrm{Jac}}(\boldsymbol{\mathcal{D}}) \equiv -(1/2)\mathcal{D}_{AB}\mathcal{R}_{AC}\mathcal{D}_{CB} = -(1/2)\mathrm{tr}\left(\boldsymbol{\mathcal{D}}^{\mathrm{T}}\boldsymbol{\mathcal{R}}\boldsymbol{\mathcal{D}}\right)$.

Regarding the optical scalars, the Sachs equations can be rewritten as[8]

$$\frac{\mathrm{d}}{\mathrm{d}v}\begin{pmatrix}\theta \\ \sigma\end{pmatrix} = -\begin{pmatrix}\partial_\theta \\ \partial_\sigma\end{pmatrix}V_{\mathrm{scal}} + \begin{pmatrix}\mathcal{R} \\ \mathcal{W}\end{pmatrix}, \tag{A.17}$$

where

$$V_{\mathrm{scal}} \equiv \frac{\theta^3}{3} + |\sigma|^2\theta, \tag{A.18}$$

and the focusing scalars $\mathcal{R}$ and $\mathcal{W}$ are here treated as an external force; they could also have been included in the potential according to

$$\tilde{V}_{\mathrm{scal}} \equiv V_{\mathrm{scal}} - \mathcal{R}\theta - \mathcal{W}\sigma. \tag{A.19}$$

Note however that V_{scal} does not depend explicitly on v, while $\tilde{V}_{\mathrm{scal}}$ and V_{Jac} generally do, because of the presence of $\mathcal{R}$ and $\mathcal{W}$.

A.4 Decompositions of the Jacobi matrix

As defined in Sec. 2, the Jacobi matrix relates the physical separation $\xi^A(v)$ of two neighbouring rays of a beam at v to their observed separation $\dot{\xi}^A(0)$, as

$$\xi^A(v) = \mathcal{D}^A{}_B(v)\dot{\xi}^B(0). \tag{A.20}$$

When applied to an observed image, $\boldsymbol{\mathcal{D}}(v_{\mathrm{s}})$ thus returns the intrinsic physical properties of the source.

A.4.1 General decomposition

As any 2×2 (nonsymmetric) matrix, the Jacobi matrix has 4 degrees of freedom. It can be decomposed in a way that highlights the geometrical transformations between the source and the image. First of all, up to frequency factor ω_{o} fixed to 1 in this article, the determinant of the Jacobi matrix is related to the angular diameter distance as

$$D_{\mathrm{A}}^2(v) \equiv \frac{\text{area of the source at } v}{\text{observed angular size}} = \det \boldsymbol{\mathcal{D}}(v). \tag{A.21}$$

---

[8]As usual, we define the complex derivative as

$$\frac{\partial f}{\partial \sigma} = \frac{1}{2}\left(\frac{\partial f}{\partial \sigma_1} - \mathrm{i}\frac{\partial f}{\partial \sigma_2}\right), \tag{A.16}$$

for $\sigma = \sigma_1 + \mathrm{i}\sigma_2$.

Factorising the determinant, we are left with a 2×2 matrix of determinant 1, which can be decomposed as the product between a symmetric matrix and the exponential of a symmetric traceless matrix:

$$\boldsymbol{\mathcal{D}} = D_\mathrm{A} \begin{pmatrix} \cos\psi & \sin\psi \\ -\sin\psi & \cos\psi \end{pmatrix} \exp \begin{pmatrix} -\gamma_1 & \gamma_2 \\ \gamma_2 & \gamma_1 \end{pmatrix}. \tag{A.22}$$

The exponential matrix can also be diagonalised by defining $\gamma \geq 0$ and ϑ as

$$(\gamma_1, \gamma_2) = \gamma(\cos 2\vartheta, -\sin 2\vartheta), \tag{A.23}$$

so that

$$\boldsymbol{\mathcal{D}} = D_\mathrm{A} \begin{pmatrix} \cos\psi & -\sin\psi \\ \sin\psi & \cos\psi \end{pmatrix} \begin{pmatrix} \cos\vartheta & -\sin\vartheta \\ \sin\vartheta & \cos\vartheta \end{pmatrix} \begin{pmatrix} \mathrm{e}^{-\gamma} & 0 \\ 0 & \mathrm{e}^{\gamma} \end{pmatrix} \begin{pmatrix} \cos\vartheta & \sin\vartheta \\ -\sin\vartheta & \cos\vartheta \end{pmatrix}. \tag{A.24}$$

This decomposition shows that, in order to reconstruct the physical properties of a light source from its observed image, one must:

1. Contract it by a factor $\mathrm{e}^{-\gamma}$ along a direction inclined of ϑ with respect to the Sachs basis, and stretch it by a factor e^{γ} along the orthogonal direction. This represent the *net shear*, which preserves the area of the image.

2. Rotate anticlockwise the result by an angle ψ.

3. Scale it with D_A to turn angles into lengths.

Note that, by virtue of Etherington's reciprocity relation [92, 118], which stipulates that the Jacobi matrix obtained by integrating the Sachs equation (A.11) from the observer O to the source S or from the source to the observer are opposite and transposed with respect to each other,[9]

$$\boldsymbol{\mathcal{D}}(S \leftarrow O) = -\boldsymbol{\mathcal{D}}^\mathrm{T}(O \leftarrow S), \tag{A.26}$$

the net shear γ is independent of the sense in which this integration is made. This is the general nonperturbative generalization of the shear reciprocity relation mentioned in appendix A of Ref. [39].

A.4.2 Perturbative case

Usually, when dealing with weak lensing as caused by perturbations with respect to Minkowski or Friedmann-Lemaître spacetimes, one uses that at background level both shear and rotation vanish so that $\bar{\boldsymbol{\mathcal{D}}} = \bar{D}_\mathrm{A}\, \boldsymbol{1}$. The decomposition (A.24) can then be expanded at first order in γ_1, γ_2 and ψ to get the definition of the *amplification matrix* as

$$\boldsymbol{\mathcal{D}} = \boldsymbol{\mathcal{A}}\bar{\boldsymbol{\mathcal{D}}} + \mathcal{O}(2) \tag{A.27}$$

with

$$\boldsymbol{\mathcal{A}} = \begin{pmatrix} 1 - \kappa - \gamma_1 & \gamma_2 + \psi \\ \gamma_2 - \psi & 1 - \kappa + \gamma_1 \end{pmatrix}, \tag{A.28}$$

---

[9] This can directly be shown from the fact that $\boldsymbol{\mathcal{R}}^\mathrm{T} = \boldsymbol{\mathcal{R}}$, which implies that, for any two v_1, v_2 the function $\boldsymbol{C}(v)$ defined by $\boldsymbol{C}(v) \equiv \dot{\boldsymbol{\mathcal{D}}}^\mathrm{T}(v \leftarrow v_1)\boldsymbol{\mathcal{D}}(v \leftarrow v_2) - \boldsymbol{\mathcal{D}}^\mathrm{T}(v \leftarrow v_1)\dot{\boldsymbol{\mathcal{D}}}(v \leftarrow v_2)$ is a constant. Writing $\boldsymbol{C}(v_1) = \boldsymbol{C}(v_2)$, we conclude that

$$\boldsymbol{\mathcal{D}}(v_1 \leftarrow v_2) = -\boldsymbol{\mathcal{D}}^\mathrm{T}(v_2 \leftarrow v_1). \tag{A.25}$$

This relation is central to the derivation of the distance duality relation $D_\mathrm{L} = (1+z)^2 D_\mathrm{A}$. The latter is however more easily achieved by abandoning the convention $\omega_\mathrm{o} = 1$. See e.g. Ref. [119] for further details.

where the *convergence* is defined as

$$\kappa \equiv 1 - \frac{1}{2}\text{tr}\boldsymbol{\mathcal{A}} = \frac{D_{\text{A}} - \bar{D}_{\text{A}}}{\bar{D}_{\text{A}}} + \mathcal{O}(2). \tag{A.29}$$

The rotation angle ψ can be proved to be on the order of γ^2, and can thus be omitted at linear order, which yields the standard form of the amplification matrix. The decomposition (A.24) is however much more relevant in nonperturbative cases, or when either the shear or the rotation does not vanish at background level; see e.g. Ref [120].

References

[1] P. Peter and J.-P. Uzan, *Primordial Cosmology.* Oxford University Press, 2009.

[2] S. R. Green and R. M. Wald, *How well is our Universe described by an FLRW model?*, *Classical and Quantum Gravity* **31** (Dec., 2014) 234003, [arXiv:1407.8084].

[3] T. Buchert, M. Carfora, G. F. R. Ellis, E. W. Kolb, M. A. H. MacCallum, J. J. Ostrowski, S. Räsänen, B. F. Roukema, L. Andersson, A. A. Coley, and D. L. Wiltshire, *Is there proof that backreaction of inhomogeneities is irrelevant in cosmology?*, *ArXiv e-prints* (May, 2015) [arXiv:1505.0780].

[4] S. R. Green and R. M. Wald, *Comments on Backreaction*, *ArXiv e-prints* (June, 2015) [arXiv:1506.0645].

[5] T. Futamase and M. Sasaki, *Light Propagation and the Distance Redshift Relation in a Realistic Inhomogeneous Universe*, *Phys. Rev.* **D40** (1989) 2502.

[6] A. Cooray, D. Holz, and D. Huterer, *Cosmology from supernova magnification maps*, *Astrophys. J.* **637** (2006) L77–L80, [astro-ph/0509579].

[7] S. Dodelson and A. Vallinotto, *Learning from the scatter in type ia supernovae*, *Phys. Rev.* **D74** (2006) 063515, [astro-ph/0511086].

[8] P. Valageas, *Weak gravitational lensing effects on the determination of omega_0 and lambda from sneia*, *Astron. Astrophys.* **354** (2000) 767, [astro-ph/9904300].

[9] C. Bonvin, R. Durrer, and M. A. Gasparini, *Fluctuations of the luminosity distance*, *Phys. Rev.* **D73** (2006) 023523, [astro-ph/0511183]. [Erratum: Phys. Rev.D85,029901(2012)].

[10] N. Meures and M. Bruni, *Redshift and distances in a Lambda-CDM cosmology with non-linear inhomogeneities*, *Mon. Not. Roy. Astron. Soc.* **419** (2012) 1937, [arXiv:1107.4433].

[11] I. Ben-Dayan, M. Gasperini, G. Marozzi, F. Nugier, and G. Veneziano, *Average and dispersion of the luminosity-redshift relation in the concordance model*, *JCAP* **6** (June, 2013) 2, [arXiv:1302.0740].

[12] I. Ben-Dayan, M. Gasperini, G. Marozzi, F. Nugier, and G. Veneziano, *Do Stochastic Inhomogeneities Affect Dark-Energy Precision Measurements?*, *Physical Review Letters* **110** (Jan., 2013) 021301, [arXiv:1207.1286].

[13] O. Umeh, C. Clarkson, and R. Maartens, *Nonlinear relativistic corrections to cosmological distances, redshift and gravitational lensing magnification: I. Key results*, *Classical and Quantum Gravity* **31** (Oct., 2014) 202001, [arXiv:1207.2109].

[14] O. Umeh, C. Clarkson, and R. Maartens, *Nonlinear relativistic corrections to cosmological distances, redshift and gravitational lensing magnification: II. Derivation*, *Classical and Quantum Gravity* **31** (Oct., 2014) 205001, [arXiv:1402.1933].

[15] E. Barausse, S. Matarrese, and A. Riotto, *Effect of inhomogeneities on the luminosity distance-redshift relation: Is dark energy necessary in a perturbed universe?*, *Phys. Rev. D* **71** (Mar., 2005) 063537, [astro-ph/0501152].

[16] I. Ben-Dayan, G. Marozzi, F. Nugier, and G. Veneziano, *The second-order luminosity-redshift relation in a generic inhomogeneous cosmology*, *JCAP* **11** (Nov., 2012) 45, [`arXiv:1209.4326`].

[17] S. Andrianomena, C. Clarkson, P. Patel, O. Umeh, and J.-P. Uzan, *Non-linear relativistic contributions to the cosmological weak-lensing convergence*, *JCAP* **1406** (2014) 023, [`arXiv:1402.4350`].

[18] C. Clarkson, O. Umeh, R. Maartens, and R. Durrer, *What is the distance to the CMB?*, *JCAP* **11** (Nov., 2014) 36, [`arXiv:1405.7860`].

[19] T. W. B. Kibble and R. Lieu, *Average Magnification Effect of Clumping of Matter*, *ApJ* **632** (Oct., 2005) 718–726, [`astro-ph/0412275`].

[20] N. Kaiser and J. A. Peacock, *On the Bias of the Distance-Redshift Relation from Gravitational Lensing*, *ArXiv e-prints* (Mar., 2015) [`arXiv:1503.0850`].

[21] C. Bonvin, C. Clarkson, R. Durrer, R. Maartens, and O. Umeh, *Cosmological ensemble and directional averages of observables*, *JCAP* **7** (July, 2015) 40, [`arXiv:1504.0167`].

[22] C. Bonvin, C. Clarkson, R. Durrer, R. Maartens, and O. Umeh, *Do we care about the distance to the CMB? Clarifying the impact of second-order lensing*, *JCAP* **6** (June, 2015) 50, [`arXiv:1503.0783`].

[23] A. Einstein and E. Straus, *The influence of the expansion of space on the gravitation fields surrounding the individual stars*, *Rev. Mod. Phys.* **17** (1945) 120.

[24] A. Einstein and E. Straus, *Corrections and additional remarks to our paper: The influence of the expansion of space on the gravitation fields surrounding the individual stars*, *Rev. Mod. Phys.* **18** (1945) 148.

[25] V. Marra, E. W. Kolb, S. Matarrese, and A. Riotto, *On cosmological observables in a swiss-cheese universe*, *Phys. Rev.* **D76** (2007) 123004, [`arXiv:0708.3622`].

[26] N. Brouzakis, N. Tetradis, and E. Tzavara, *Light Propagation and Large-Scale Inhomogeneities*, *JCAP* **0804** (2008) 008, [`astro-ph/0703586`].

[27] N. Brouzakis, N. Tetradis, and E. Tzavara, *The effect of large scale inhomogeneities on the luminosity distance*, *JCAP* **2** (Feb., 2007) 13, [`astro-ph/0612179`].

[28] T. Biswas and A. Notari, *Swiss-Cheese Inhomogeneous Cosmology and the Dark Energy Problem*, *JCAP* **0806** (2008) 021, [`astro-ph/0702555`].

[29] V. Marra, E. W. Kolb, and S. Matarrese, *Light-cone averages in a Swiss-cheese universe*, *Phys. Rev. D* **77** (Jan., 2008) 023003, [`arXiv:0710.5505`].

[30] T. Clifton and J. Zuntz, *Hubble Diagram Dispersion From Large-Scale Structure*, *Mon. Not. Roy. Astron. Soc.* **400** (2009) 2185, [`arXiv:0902.0726`].

[31] S. J. Szybka, *On light propagation in Swiss-Cheese cosmologies*, *Phys. Rev.* **D84** (2011) 044011, [`arXiv:1012.5239`].

[32] R. A. Vanderveld, E. E. Flanagan, and I. Wasserman, *Luminosity distance in 'Swiss cheese' cosmology with randomized voids: I. Single void size*, *Phys. Rev.* **D78** (2008) 083511, [`arXiv:0808.1080`].

[33] W. Valkenburg, *Swiss Cheese and a Cheesy CMB*, *JCAP* **0906** (2009) 010, [`arXiv:0902.4698`].

[34] K. Bolejko, *The effect of inhomogeneities on the distance to the last scattering surface and the accuracy of the CMB analysis*, *JCAP* **2** (Feb., 2011) 25, [`arXiv:1101.3338`].

[35] E. E. Flanagan, N. Kumar, I. Wasserman, and R. A. Vanderveld, *Luminosity distance in Swiss cheese cosmology with randomized voids. II. Magnification probability distributions*, *Phys. Rev.* **D85** (2012) 023510, [`arXiv:1109.1873`].

[36] E. E. Flanagan, N. Kumar, and I. Wasserman, *Luminosity distance in Swiss cheese cosmology with randomized voids and galaxy halos*, Phys. Rev. **D88** (2013), no. 4 043004, [`arXiv:1207.3711`].

[37] K. Bolejko, C. Clarkson, R. Maartens, D. Bacon, N. Meures, and E. Beynon, *Antilensing: The Bright Side of Voids*, Physical Review Letters **110** (Jan., 2013) 021302, [`arXiv:1209.3142`].

[38] M. Lavinto, S. Räsänen, and S. J. Szybka, *Average expansion rate and light propagation in a cosmological Tardis spacetime*, JCAP **12** (Dec., 2013) 51, [`arXiv:1308.6731`].

[39] M. Lavinto and S. Räsänen, *CMB seen through random Swiss Cheese*, ArXiv e-prints (July, 2015) [`arXiv:1507.0659`].

[40] K. Bolejko, *The Szekeres Swiss Cheese model and the CMB observations*, General Relativity and Gravitation **41** (Aug., 2009) 1737–1755, [`arXiv:0804.1846`].

[41] K. Bolejko and M.-N. Célérier, *Szekeres Swiss-cheese model and supernova observations*, Phys. Rev. D **82** (Nov., 2010) 103510, [`arXiv:1005.2584`].

[42] A. Peel, M. A. Troxel, and M. Ishak, *Effect of inhomogeneities on high precision measurements of cosmological distances*, Phys. Rev. D **90** (Dec., 2014) 123536, [`arXiv:1408.4390`].

[43] M. A. Troxel, M. Ishak, and A. Peel, *The effects of structure anisotropy on lensing observables in an exact general relativistic setting for precision cosmology*, JCAP **3** (Mar., 2014) 40, [`arXiv:1311.5936`].

[44] J. Adamek, E. Di Dio, R. Durrer, and M. Kunz, *Distance-redshift relation in plane symmetric universes*, Phys. Rev. **D89** (2014), no. 6 063543, [`arXiv:1401.3634`].

[45] K. Bolejko and P. G. Ferreira, *Ricci focusing, shearing, and the expansion rate in an almost homogeneous Universe*, JCAP **1205** (2012) 003, [`arXiv:1204.0909`].

[46] E. V. Linder, *Light propagation in generalized Friedmann universes*, A&A **206** (Nov., 1988) 190–198.

[47] E. V. Linder, *Transition from Clumpy to Smooth Angular Diameter Distances*, ApJ **497** (Apr., 1998) 28–31, [`astro-ph/9707349`].

[48] E. V. Linder, *Averaging Inhomogeneous Universes: Volume, Angle, Line of Sight*, ArXiv Astrophysics e-prints (Jan., 1998) [`astro-ph/9801122`].

[49] S. Räsänen, *Light propagation in statistically homogeneous and isotropic dust universes*, JCAP **0902** (2009) 011, [`arXiv:0812.2872`].

[50] S. Räsänen, *Light propagation in statistically homogeneous and isotropic universes with general matter content*, JCAP **1003** (2010) 018, [`arXiv:0912.3370`].

[51] S. Räsänen, *Light propagation and the average expansion rate in near-FRW universes*, Phys. Rev. **D85** (2012) 083528, [`arXiv:1107.1176`].

[52] M. Gasperini, G. Marozzi, F. Nugier, and G. Veneziano, *Light-cone averaging in cosmology: formalism and applications*, JCAP **7** (July, 2011) 8, [`arXiv:1104.1167`].

[53] I. Ben-Dayan, M. Gasperini, G. Marozzi, F. Nugier, and G. Veneziano, *Backreaction on the luminosity-redshift relation from gauge invariant light-cone averaging*, JCAP **4** (Apr., 2012) 36, [`arXiv:1202.1247`].

[54] S. Bagheri and D. J. Schwarz, *Light propagation in the averaged universe*, JCAP **10** (Oct., 2014) 73, [`arXiv:1404.2185`].

[55] C. Clarkson, G. F. R. Ellis, A. Faltenbacher, R. Maartens, O. Umeh, and J.-P. Uzan, *(Mis-)Interpreting supernovae observations in a lumpy universe*, Mon. Not. Roy. Astron. Soc. **426** (2012) 1121–1136, [`arXiv:1109.2484`].

[56] Y. Zel'dovich, , *Sov. Astron. Lett.* **8** (1964) 13.

[57] R. P. Feynman, 1964. Unpublished colloquium given at the California Institute of Technology.

[58] V. M. Dashevskii and Y. B. Zel'dovich, *Propagation of light in a nonhomogeneous nonflat universe ii*, *Sov. Astronom.* **8** (1965) 854.

[59] V. M. Dashevskii and V. I. Slysh, *On the Propagation of Light in a Nonhomogeneous Universe*, *Astron. Zh.* **42** (1965) 863.

[60] V. M. Dashevskii and V. I. Slysh, *On the Propagation of Light in a Nonhomogeneous Universe*, *Sov. Astronom.* **9** (Feb., 1966) 671.

[61] B. Bertotti, *The Luminosity of Distant Galaxies*, *Royal Society of London Proceedings Series A* **294** (Sept., 1966) 195–207.

[62] J. E. Gunn, *On the Propagation of Light in Inhomogeneous Cosmologies. I. Mean Effects*, *ApJ* **150** (Dec., 1967) 737.

[63] J. E. Gunn, *A Fundamental Limitation on the Accuracy of Angular Measurements in Observational Cosmology*, *ApJ* **147** (Jan., 1967) 61.

[64] S. Weinberg, *Apparent luminosities in a locally inhomogeneous universe*, *ApJL* **208** (Aug., 1976) L1–L3.

[65] R. Kantowski, *Corrections in the Luminosity-Redshift Relations of the Homogeneous Friedmann Models*, *ApJ* **155** (Jan., 1969) 89.

[66] C. Dyer and R. Roeder, *The Distance-Redshift Relation for Universes with no Intergalactic Medium*, *Astrophys. J.* **174** (1972) L115.

[67] C. C. Dyer and R. C. Roeder, *Distance-Redshift Relations for Universes with Some Intergalactic Medium*, *ApJL* **180** (Feb., 1973) L31.

[68] C. C. Dyer, *Observational Aspects of Locally Inhomogeneous Cosmological Models.* PhD thesis, University of Toronto (Canada), 1973.

[69] C. C. Dyer and R. C. Roeder, *Observations in Locally Inhomogeneous Cosmological Models*, *ApJ* **189** (Apr., 1974) 167–176.

[70] R. C. Roeder, *Apparent magnitudes, redshifts, and inhomogeneities in the universe*, *ApJ* **196** (Mar., 1975) 671–673.

[71] P. Fleury, *Swiss-cheese models and the Dyer-Roeder approximation*, *JCAP* **1406** (2014) 054, [arXiv:1402.3123].

[72] D. E. Holz and R. M. Wald, *A New method for determining cumulative gravitational lensing effects in inhomogeneous universes*, *Phys. Rev.* **D58** (1998) 063501, [astro-ph/9708036].

[73] T. Okamura and T. Futamase, *Distance-Redshift Relation in a Realistic Inhomogeneous Universe*, *Prog. Theor. Phys.* **122** (2009) 511–520, [arXiv:0905.1160].

[74] J.-P. Bruneton and J. Larena, *Observables in a lattice Universe*, *Class. Quant. Grav.* **30** (2013) 025002, [arXiv:1208.1411].

[75] T. Clifton and P. G. Ferreira, *Archipelagian Cosmology: Dynamics and Observables in a Universe with Discretized Matter Content*, *Phys. Rev.* **D80** (2009) 103503, [arXiv:0907.4109]. [Erratum: Phys. Rev.D84,109902(2011)].

[76] T. Clifton and P. G. Ferreira, *Errors in estimating $\Omega_?$ due to the fluid approximation*, *JCAP* **10** (Oct., 2009) 26, [arXiv:0908.4488].

[77] T. Clifton, P. G. Ferreira, and K. O'Donnell, *Improved treatment of optics in the Lindquist-Wheeler models*, *Phys. Rev. D* **85** (Jan., 2012) 023502, [arXiv:1110.3191].

[78] R. Kantowski, *The Effects of Inhomogeneities on Evaluating the Mass Parameter Ω_m and the Cosmological Constant Λ*, *ApJ* **507** (Nov., 1998) 483–496, [astro-ph/9802208].

[79] A. Cooray, D. Huterer, and D. Holz, *Problems with pencils: lensing covariance of supernova distance measurements*, Phys. Rev. Lett. **96** (2006) 021301, [`astro-ph/0509581`].

[80] D. Sarkar, A. Amblard, D. E. Holz, and A. Cooray, *Lensing and Supernovae: Quantifying The Bias on the Dark Energy Equation of State*, Astrophys. J. **678** (2008) 1, [`arXiv:0710.4143`].

[81] P. Fleury, H. Dupuy, and J.-P. Uzan, *Can all cosmological observations be accurately interpreted with a unique geometry?*, Phys.Rev.Lett. **111** (2013) 091302, [`arXiv:1304.7791`].

[82] V. C. Busti, R. F. L. Holanda, and C. Clarkson, *Supernovae as probes of cosmic parameters: estimating the bias from under-dense lines of sight*, JCAP **1311** (2013) 020, [`arXiv:1309.6540`].

[83] K. Kainulainen and V. Marra, *A new stochastic approach to cumulative weak lensing*, Phys. Rev. **D80** (2009) 123020, [`arXiv:0909.0822`].

[84] K. Kainulainen and V. Marra, *Accurate Modeling of Weak Lensing with the sGL Method*, Phys. Rev. **D83** (2011) 023009, [`arXiv:1011.0732`].

[85] K. Kainulainen and V. Marra, *Weak lensing observables in the halo model*, Phys. Rev. D **84** (Sept., 2011) 063004, [`arXiv:1101.4143`].

[86] V. Marra, M. Quartin, and L. Amendola, *Accurate weak lensing of standard candles. I. Flexible cosmological fits*, Phys. Rev. D **88** (Sept., 2013) 063004, [`arXiv:1304.7689`].

[87] M. Quartin, V. Marra, and L. Amendola, *Accurate weak lensing of standard candles. II. Measuring σ_8 with supernovae*, Phys. Rev. D **89** (Jan., 2014) 023009, [`arXiv:1307.1155`].

[88] L. Amendola, T. Castro, V. Marra, and M. Quartin, *Constraining the growth of perturbations with lensing of supernovae*, MNRAS **449** (May, 2015) 2845–2852, [`arXiv:1412.3703`].

[89] L. Amendola, K. Kainulainen, V. Marra, and M. Quartin, *Large-scale inhomogeneities may improve the cosmic concordance of supernovae*, Phys. Rev. Lett. **105** (2010) 121302, [`arXiv:1002.1232`].

[90] K.-D. Nguyen Thu Lam and J. Kurchan, *Stochastic perturbation of integrable systems: a window to weakly chaotic systems*, ArXiv e-prints (May, 2013) [`arXiv:1305.4503`].

[91] B. I. Halperin, *Green's Functions for a Particle in a One-Dimensional Random Potential*, Physical Review **139** (July, 1965) 104–117.

[92] V. Perlick, *Gravitational Lensing from a Spacetime Perspective*, Living Reviews in Relativity **7** (Sept., 2004) 9.

[93] P. Schneider, J. Ehlers, and E. E. Falco, *Gravitational Lenses.* Springer-Verlag Berlin/Heidelberg/New York, 1992.

[94] W. Feller, *An introduction to probability theory and its applications.* Wiley Series in Probability and Mathematical Statistics. New York etc.: John Wiley and Sons, 1971.

[95] L. Arnold, *Stochastic Differential Equations: Theory and Applications.* Wiley, 1974.

[96] I. Karatzas and S. E. Shreve, *Brownian Motion and Stochastic Calculus.* Springer-Verlag Berlin/Heidelberg/New York, 1991.

[97] R. S. Liptser and A. Shiryaev, *Statistics of random processes. 1: General theory.* Springer-Verlag Berlin/Heidelberg/New York, 2001.

[98] B. Oksendal, *Stochastic Differential Equations: An Introduction with Applications.* Springer-Verlag Berlin/Heidelberg/New York, 2003.

[99] H. Risken, *The Fokker-Planck equation. Methods of solution and applications.* Springer Series in Synergetics, Berlin, New York: Springer, |c1989, 2nd ed., 1989.

[100] H. McKean, *Stochastic Integrals.* Academic Press, 1969.

[101] P. Fleury, H. Dupuy, and J.-P. Uzan, *Interpretation of the Hubble diagram in a nonhomogeneous universe*, Phys.Rev. **D87** (2013), no. 12 123526, [arXiv:1302.5308].

[102] Z. Stuchlik, *An Einstein-Strauss-de Sitter model of the universe*, Bul. Astronom. Inst. Czechoslovakia **35** (1984) 205.

[103] J.-P. Uzan, G. F. R. Ellis, and J. Larena, *A two-mass expanding exact space-time solution*, Gen. Rel. Grav. **43** (2011) 191–205, [arXiv:1005.1809].

[104] M. Mars, F. C. Mena, and R. Vera, *Review on exact and perturbative deformations of the Einstein-Straus model: uniqueness and rigidity results*, General Relativity and Gravitation **45** (Nov., 2013) 2143–2173, [arXiv:1307.4371].

[105] G. Lemaître, *L'Univers en expansion*, Ann. Soc. Sci. Bruxelles, A **53** (1933) 51.

[106] A. Krasinski, *Inhomogeneous Cosmological Models*. Cambridge University Press, 1997.

[107] P. Szekeres, *Quasispherical gravitational collapse*, Phys. Rev. D **12** (1975) 2941.

[108] G. Darmois, *Les équations de la gravitation einsteinienne*. Mémorial des sciences mathématiques, 1927.

[109] W. Israel, *Singular hypersurfaces and thin shells in general relativity*, Nuovo Cimento B Serie **44** (July, 1966) 1–14.

[110] W. Israel, *Singular hypersurfaces and thin shells in general relativity*, Nuovo Cimento B Serie **48** (Apr., 1967) 463–463.

[111] B. Panter, A. F. Heavens, and R. Jimenez, *The mass function of the stellar component of galaxies in the Sloan Digital Sky Survey*, MNRAS **355** (Dec., 2004) 764–768, [astro-ph/0406299].

[112] M. Bartelmann and P. Schneider, *Weak gravitational lensing*, Phys. Rept. **340** (2001) 291–472, [astro-ph/9912508].

[113] N. Deruelle and J.-P. Uzan, *Théories de la relativité*. Belin, Paris, 2014.

[114] M. Sasaki, *Cosmological gravitational lens equation: Its validity and limitation*, Prog. Theor. Phys. **90** (1993) 753–781.

[115] R. K. Sachs, *Gravitational waves in general relativity. 6. The outgoing radiation condition*, Proc. Roy. Soc. Lond. **A264** (1961) 309–338.

[116] S. Seitz, P. Schneider, and J. Ehlers, *Light propagation in arbitrary space-times and the gravitational lens approximation*, Class. Quant. Grav. **11** (1994) 2345–2374, [astro-ph/9403056].

[117] M. Bartelmann and P. Schneider, *Weak gravitational lensing*, Phys. Rept. **340** (2001) 291–472, [astro-ph/9912508].

[118] J. Etherington, *On the definition of distance in general relativity*, Phil. Mag. **15** (1933) 761.

[119] P. Fleury, *Light propagation in inhomogeneous and anisotropic cosmologies*. PhD thesis, Université Pierre et Marie Curie, Paris 6, Nov., 2015. (in prep.).

[120] P. Fleury, C. Pitrou, and J.-P. Uzan, *Light propagation in a homogeneous and anisotropic universe*, Phys. Rev. **D91** (2015), no. 4 043511, [arXiv:1410.8473].

PART IV

ANISOTROPIC COSMOLOGIES

A PART from homogeneity, the cosmological principle stipulates that the Universe is *isotropic.* Both hypotheses are not redundant, in particular homogeneity does not imply isotropy; for example, the Universe can be the same everywhere while having an expansion faster in some directions than in others. Just like cosmic homogeneity, cosmic isotropy is therefore an assumption to be tested in order to validate or falsify the standard model. For that purpose, it is natural to start by investigating cosmological models where isotropy only is relaxed. The corresponding spacetimes follow Bianchi's classification of three-dimensional homogeneous spaces [269], and were therefore baptised the *Bianchi spacetimes.* For details about their construction and classification, see Ref. [270]. In these models, anisotropy can show up in both the intrinsic and extrinsic curvatures of the homogeneity hypersurfaces. The simplest case is Bianchi I, whose metric reads

$$\mathrm{d}s^2 = -\mathrm{d}t^2 + a_x^2(t)\mathrm{d}x^2 + a_y^2(t)\mathrm{d}y^2 + a_z^2(t)\mathrm{d}z^2,$$

where t is a cosmic time with the same meaning as in the FL case: it is the proper time measured by fundamental observers following $x^i = \mathrm{cst}$ worldlines. In this particular example, the homogeneity hypersurfaces ($t = \mathrm{cst}$) are intrinsically Euclidean, hence anisotropy is only present in their extrinsic curvature, i.e. in the difference between the time evolution of the three scale factors a_x, a_y, a_z. As a total, there are nine types of Bianchi models, two of which have two subcases (VI_0, VI_h, VII_0, VII_h). Only types I, V, VII, and IX enjoy an isotropic (FL) limit [271].

Of course, since we observe a very isotropic CMB, less attention was dedicated to testing cosmic isotropy than homogeneity. However, since an anisotropy of cosmic expansion—such as in the Bianchi I case—only sources the low multipoles of the CMB temperature map, the precision of any constraint is strongly affected by cosmic variance, which limits the ever achievable level of precision of these constraints. Subtler signatures of anisotropy can also be found in the CMB polarisation, as shown by Ref. [272] in the case of a type-VII_h Bianchi model. To date no evidence of such signatures have been found [176], but the CMB is not the only possible probe of cosmic anisotropy. In particular, it is not particularly adapted to investigating any *late-time anisotropy*, which could be sourced by anisotropic dark energy [273], or emerge from backreaction mechanisms [274] or if gravity actually follows bimetric theories [275]. Late-time anisotropy is usually tested from SN data by dividing the sky in two and fitting the Hubble diagram independently in each hemisphere. This allows to look for both local anisotropy (the "bulk flow") [276–278] and global anisotropy [273, 279–287]. The very sparse sky coverage of current SN data is however a strong limitation to this approach, so that no definite conclusion could be drawn so far [288]. A very different method has been proposed recently in Refs. [28, 289, 290], where anisotropy is traced from weak-lensing B-modes, i.e. curl patterns in the distribution of galaxy ellipticities across the sky.

This last part of the present dissertation is a contribution to the cosmic anisotropy issue. Chapter 8 analyses in great details how light propagates in Bianchi I spacetimes. Chapter 9 is devoted to scalar-vector field theories, which are potential candidates as sources of anisotropy, and puts fundamental constraints on their action on the basis of stability and causality requirements.

Observing an anisotropic universe

BESIDES the quest for detecting any large-scale anisotropy in the Universe arises the question of how such a discovery would affect the way we interpret cosmological observations. In other words: how does light propagate through an anisotropic universe? Elements of answer have been provided in a seminal article by Ellis and MacCallum [291], for general Bianchi models. More specifically, a remarkably simple expression for the angular distance has been derived by Saunders [292,293] in the Bianchi I case. The present chapter is a complement to those earlier studies. It consists of an article, written in collaboration with Cyril Pitrou and Jean-Philippe Uzan, which proposes a comprehensive analysis of geometric optics in the Bianchi I spacetime. In particular, in addition to Saunders' result, I solved explicitly the Jacobi matrix equation, and therefore determined the impact of Weyl curvature—caused by the anisotropy of the expansion flow—not only on the angular distance, but also on the shear and rotation of images.

Light propagation in a homogeneous and anisotropic universe

Pierre Fleury,* Cyril Pitrou,† and Jean-Philippe Uzan‡

Institut d'Astrophysique de Paris, UMR-7095 du CNRS,
Université Pierre et Marie Curie,
98 bis bd Arago, 75014 Paris, France, and
Sorbonne Universités, Institut Lagrange de Paris,
98 bis bd Arago, 75014 Paris, France.

(Dated: 10 February 2015)

This article proposes a comprehensive analysis of light propagation in an anisotropic and spatially homogeneous Bianchi I universe. After recalling that null geodesics are easily determined in such a spacetime, we derive the expressions of the redshift and direction drifts of light sources; by solving analytically the Sachs equation, we then obtain an explicit expression of the Jacobi matrix describing the propagation of narrow light beams. As a by-product, we recover the old formula by Saunders for the angular diameter distance in a Bianchi I spacetime, but our derivation goes further since it also provides the optical shear and rotation. These results pave the way to the analysis of both supernovae data and weak lensing by the large-scale structure in Bianchi universes.

PACS numbers: 98.80.-k, 04.20.-q, 42.15.-i

I. INTRODUCTION

The standard cosmological model relies heavily on the assumption that on the large scale it is well described by a spacetime with homogeneous and isotropic spatial sections. All cosmological observations tend to agree with this geometrical assumption, and to back up the predictions of the ΛCDM model with a primordial inflationary phase.

A lot of efforts are invested in order to determine whether the source of the acceleration of the expansion of the Universe is due to a cosmological constant or has a dynamical origin (new matter fields dubbed dark energy or gravity beyond general relativity); see e.g. Refs. [1, 2]. It has also revived the importance of testing the validity of the Copernican principle.

While a primordial shear decays if it is not sourced, late-time anisotropy appears in many phenomenological models of dark energy [3–7] and is a generic prediction of bigravity models [8] and backreaction [9]. Contrary to the former [10–14], the latter remains weakly constrained by the observation of the cosmic microwave background temperature field; this naturally stimulated analyses based, e.g., on the observation of supernovae [15–27], or using low-redshift galaxies [28, 29]. Besides the strict detection of anisotropy, drawing quantitative conclusions from such analyses requires one to understand how light propagates through an anisotropic universe. This issue has been addressed since the late sixties [30–33], in particular, a remarkably simple expression of the angular diameter distance in Bianchi I models was found by Saunders [30, 31] using observational coordinates [34], and recently derived in Ref. [16].

The purpose of this article is to provide a complete analytical study of light propagation in Bianchi I spacetimes. On the one hand, the integration of the null geodesic equation (though already well known) allows us to derive the expressions of the redshift, redshift drift and position drift of an arbitrary light source. More importantly, on the other hand, we solve the Sachs equation governing the geometry of geodesic bundles. From the resulting Jacobi matrix, we not only recover Saunders' formula for the angular diameter distance, but also characterize the whole lensing properties generated by anisotropy. These results pave the way to the computation of the lensing B-mode signal induced in an anisotropic universe—as predicted in Ref. [35]—since it provides the background result for the general computation in perturbed Bianchi models.

The article is organized as follows. After summarizing the main geometrical properties of a Bianchi I universe in Sec. II, and the laws of geometric optics in curved spacetime in Sec. III, we solve the null geodesic equation and derive the expressions of the redshift and direction drifts in Sec. IV. One technical key point of our construction is the use of a conformal transformation, whose dictionary is detailed in Sec. V. The heart of our derivation is then exposed in Secs. VI and VII, in which, respectively, we construct the Sachs basis and obtain the expression of the Jacobi matrix—see in particular Eq. (7.8). An algorithmic way of using our results is proposed in Sec. VIII. Finally, in the Appendix we give a proof of the result of Ref. [31].

II. THE BIANCHI I SPACETIME

The classification of spatially anisotropic and homogeneous spacetimes [36] is based on the Bianchi's classification of homogeneous but not necessarily isotropic

———————
* fleury@iap.fr
† pitrou@iap.fr
‡ uzan@iap.fr

three-dimensional spaces [37]. The spatial sections of these spacetimes are Bianchi spaces characterized by their Riemann tensor (more precisely the Riemann tensor of the induced metric on the spatial sections), and the full geometry is then determined from the extrinsic curvature of the spatial sections. The simplest of these spacetimes is Bianchi I, which enjoys Euclidean spatial sections, that is with a vanishing Riemann tensor of the induced 3-metric. Its metric reads simply

$$\mathrm{d}s^2 = g_{\mu\nu}\mathrm{d}x^\mu\mathrm{d}x^\nu = -\mathrm{d}t^2 + a^2(t)\gamma_{ij}\mathrm{d}x^i\mathrm{d}x^j, \qquad (2.1)$$

where the spatial metric is given by

$$\gamma_{ij} = \mathrm{e}^{2\beta_i(t)}\delta_{ij} \qquad (2.2)$$

with the constraint

$$\sum_{i=1}^{3}\beta_i = 0. \qquad (2.3)$$

The inverse spatial metric is $\gamma^{ij} = \mathrm{e}^{-2\beta_i(t)}\delta_{ij}$, such that $\gamma_{ik}\gamma^{kj} = \delta_i^j$. With this choice of the metric parametrization, the volume expansion is encoded in the scale factor $a(t)$, while the evolution of γ_{ij} is volume preserving, thanks to the condition (2.3). The conformal time η is defined from cosmic time t by the usual relation $\mathrm{d}t = a\mathrm{d}\eta$.

The *conformal* shear (rate) tensor σ_{ij} is defined by

$$\sigma_{ij} \equiv \frac{1}{2}(\gamma_{ij})' = \beta_i'\gamma_{ij} \qquad (2.4)$$

where a prime denotes a derivative with respect to conformal time η. Its geometrical interpretation is simple as it is directly related to the traceless part of the extrinsic curvature of space sections, whose components are just $a^2\sigma_{ij}$. The indices of σ_{ij} are respectively raised and lowered by γ^{ij} and γ_{ij}. Note that $\gamma_{ik}\gamma^{kj} = \delta_i^j$ implies

$$\sigma^{ij} = \beta_i'\gamma^{ij} = -\frac{1}{2}(\gamma^{ij})', \qquad \sigma_i^j = \beta_i'\delta_i^j. \qquad (2.5)$$

Since the spatial sections are homogeneous, there exists a class of preferred observers—called *fundamental observers*—for which space indeed looks homogeneous. They are comoving with respect to the Cartesian coordinate system introduced in Eq. (2.1), and cosmic time t represents their proper time, so that the four-velocity of fundamental observers reads $u^\mu = (\partial_t)^\mu$.

For a universe filled by a homogeneous fluid, the stress-energy tensor is

$$T_{\mu\nu} = \rho u_\mu u_\nu + P(g_{\mu\nu} + u_\mu u_\nu) + \Pi_{\mu\nu}, \qquad (2.6)$$

with ρ and P being the energy density and the isotropic pressure, and where $\Pi_{\mu\nu}$ the anisotropic stress. This latter symmetric tensor is traceless and spatial, in the sense that $u^\mu\Pi_{\mu\nu} = 0 = \Pi_\mu^\mu$. We further define the *conformal* anisotropic pressure by $\pi_{ij} \equiv \Pi_{ij}/a^2$ and $\pi^{ij} \equiv \Pi^{ij}a^2$

such that the indices of π_{ij} are respectively raised and lowered by γ_{ij} and γ^{ij}, as is the case for σ_{ij}.

The Einstein field equations then read

$$\mathcal{H}^2 = \frac{8\pi G}{3}a^2\rho + \frac{\sigma^2}{6}, \qquad (2.7)$$

$$\mathcal{H}' = -\frac{4\pi G}{3}a^2(\rho + 3P) - \frac{\sigma^2}{3}, \qquad (2.8)$$

$$(\sigma_j^i)' = -2\mathcal{H}\sigma_j^i + 8\pi Ga^2\pi_j^i, \qquad (2.9)$$

where $\mathcal{H} \equiv a'/a$ is the conformal expansion rate, and

$$\sigma^2 \equiv \sigma^{ij}\sigma_{ij} = \sum_{i=1}^{3}(\beta_i')^2. \qquad (2.10)$$

III. GEOMETRIC OPTICS IN A GENERAL CURVED SPACETIME

This section briefly reviews the essential equations governing light propagation in curved spacetime, its main purpose being to fix the notations. For further details, we refer the reader e.g., to the textbook [38] or the review [39] and our previous papers [40–42].

A. Light rays

Electromagnetic waves, described by Maxwell electrodynamics and identified to light rays in the eikonal approximation, are shown to follow null geodesics [43]. If v denotes an affine parameter along such a geodesic, its tangent vector $k^\mu = \mathrm{d}x^\mu/\mathrm{d}v$—which is also the wave four-vector of the electromagnetic signal—is a null vector ($k^\mu k_\mu = 0$) that satisfies the geodesic equation

$$\frac{\mathrm{D}k^\mu}{\mathrm{d}v} \equiv k^\nu\nabla_\nu k^\mu = 0, \qquad (3.1)$$

where ∇_μ denotes the covariant derivative associated to the metric $g_{\mu\nu}$.

An observer whose worldline intersects the ray can naturally define the notions of pulsation (or energy) ω, and spatial direction of observation d^μ, by performing a $3 + 1$ decomposition of k^μ with respect to his own four-velocity u^μ, as

$$k^\mu = \omega(u^\mu - d^\mu), \qquad (3.2)$$

where $\omega \equiv -u_\mu k^\mu$, and d^μ is a unit spatial vector, i.e. $u^\mu d_\mu = 0$ and $d^\mu d_\mu = 1$.

B. Light beams

A (narrow) light beam is a collection of neighboring light rays, i.e. an infinitesimal bundle of null geodesics. The behavior of any such geodesic, with respect to an

arbitrary reference one, is described by the separation (or connecting) vector ξ^μ. If all the rays converge at a given event O—the observation event "here and now" denoted with the index "o" in the following—then $\xi^\mu(v_{\rm o}) = 0$. The evolution of $\xi^\mu(v)$ along the beam is governed by the geodesic deviation equation [43]

$$\frac{{\rm D}^2\xi^\mu}{{\rm d}v^2} = R^\mu_{\ \nu\rho\sigma}k^\nu k^\rho \xi^\sigma, \qquad (3.3)$$

where $R_{\mu\nu\rho\sigma}$ denotes the Riemann tensor.

C. Sachs basis

For any observer whose worldline intersects the light beam at an event different from O, the beam has a nonzero extension since *a priori* $\xi^\mu \neq 0$. The observer can thus project it on a *screen* to characterize its size and shape. This screen is by essence a two-dimensional spacelike plane chosen to be orthogonal to the local line-of-sight d^μ. Thus, if $(s^\mu_A)_{A=1,2}$ is an orthonormal basis of the screen, then

$$s^\mu_A u_\mu = s^\mu_A d_\mu = 0, \qquad s^\mu_A s_{B\mu} = \delta_{AB}. \qquad (3.4)$$

Note that, by virtue of Eq. (3.2), we also have $s^\mu_A k_\mu = 0$.

Now, consider a flow of observers lying all along the beam [defining a four-velocity field $u^\mu(v)$] who want to compare the size, shape, and orientation of the pattern they observe on their respective screen. To avoid any spurious rotation of this pattern, one has to further impose that the basis vectors $(s^\mu_A)_{A=1,2}$ are Fermi-Walker transported along the beam,

$$S^\mu_\nu \frac{{\rm D}s^\nu_A}{{\rm d}v} = 0, \qquad (3.5)$$

where

$$S^{\mu\nu} \equiv \delta^{AB} s^\mu_A s^\nu_B = g^{\mu\nu} + u^\mu u^\nu - d^\mu d^\nu \qquad (3.6)$$

is the screen projector. The transport rule (3.5) must be understood as: s^μ_A is parallel transported as much as possible while keeping it orthogonal to u^μ and d^μ.

The set of vectors $(s^\mu_A)_{A=1,2}$ satisfying Eqs. (3.4) and (3.5) is known as the *Sachs basis*.

D. Jacobi matrix

The screen projection of the connecting vector, $\xi_A \equiv s^\mu_A \xi_\mu$, represents the relative position on the screen of the two light spots associated with two rays separated by ξ^μ. Similarly, and if we set by convention $\omega_{\rm o} = 1$, $\theta_A \equiv -({\rm d}\xi_A/{\rm d}v)_{\rm o}$ represents the angular separation of those rays, as observed from O. The matrix relating $\xi_A(v)$ to θ_A via

$$\xi_A(v) = \mathcal{D}_{AB}(v \leftarrow v_{\rm o})\theta_B, \qquad (3.7)$$

is known as the *Jacobi matrix*. The equation governing its evolution along the beam derives from the geodesic deviation equation (3.3), and reads

$$\frac{{\rm d}^2\mathcal{D}_{AB}}{{\rm d}v^2} = \mathcal{R}_{AC}\mathcal{D}_{CB}, \qquad (3.8)$$

where $\mathcal{R}_{AB} = -R_{\mu\nu\rho\sigma}s^\mu_A k^\nu s^\rho_B k^\sigma$ is called the *optical tidal matrix*. Note that the position of the screen indices $A, B, C, \dots$ does not matter, since they are raised and lowered by δ_{AB}. The initial conditions for Eq. (3.8) are

$$\mathcal{D}_{AB}(v_{\rm o} \leftarrow v_{\rm o}) = 0, \qquad (3.9)$$

$$\frac{{\rm d}\mathcal{D}_{AB}}{{\rm d}v}(v_{\rm o} \leftarrow v_{\rm o}) = -\delta_{AB}. \qquad (3.10)$$

By definition (3.7), the Jacobi matrix relates the size and shape of the beam to its observed angular aperture. It is thus naturally related to the angular diameter distance $D_{\rm A}$, linked to the ratio of the area ${\rm d}^2A_{\rm s}$ of a (small) light source to its observed angular size ${\rm d}^2\Omega_{\rm o}$,

$$D_{\rm A} \equiv \sqrt{\frac{{\rm d}^2 A_{\rm s}}{{\rm d}^2 \Omega_{\rm o}}} = \sqrt{\det \boldsymbol{\mathcal{D}}(v_{\rm s} \leftarrow v_{\rm o})}. \qquad (3.11)$$

More generally, the Jacobi matrix encodes all the information about the deformation of a light beam with its propagation through a curved spacetime, i.e., gravitational lensing. A canonical decomposition[1] of $\boldsymbol{\mathcal{D}}$ that makes such effects explicit is

$$\boldsymbol{\mathcal{D}} = D_{\rm A} \underbrace{\begin{bmatrix} \cos\psi & \sin\psi \\ -\sin\psi & \cos\psi \end{bmatrix}}_{\text{rotation}} \underbrace{\exp\begin{bmatrix} -\Gamma_1 & \Gamma_2 \\ \Gamma_2 & \Gamma_1 \end{bmatrix}}_{\text{shear}}. \qquad (3.13)$$

According to this decomposition, the real size and shape of a light source is obtained from its image by performing the following transformations: (i) an area-preserving shear, (ii) a global rotation, (iii) a global scaling.

IV. GEODESIC MOTION IN BIANCHI I

There is a simple and elegant way to determine geodesics in a spacetime with spatial homogeneity, without explicitly solving the geodesic equation (3.1). It relies

---

[1] Although the authors have never seen this decomposition used in the literature so far, they advocate that it is more meaningful than the standard one

$$\boldsymbol{\mathcal{D}} = D_{\rm A}^{\rm FL} \begin{bmatrix} 1 - \kappa - \gamma_1 & \gamma_2 - \omega \\ \gamma_2 + \omega & 1 - \kappa + \gamma_1 \end{bmatrix}, \qquad (3.12)$$

which explicitly makes use of the angular distance in a Friedmann-Lemaître (FL) spacetime, $D_{\rm A}^{\rm FL}$, and the "convergence" κ, "shear" $\gamma_{1,2}$, and "rotation" ω with respect to it. Additionally to the fact that such a decomposition relies on the choice of a specific background (namely FL), the quantities κ, $\gamma_{1,2}$, and ω lose their geometrical meaning for *finite* (noninfinitesimal) lensing effects. This is why, for instance, γ appears in the expression of the magnification. It is not the case for the decomposition proposed in Eq. (3.13).

on the basic fact [44] that for any Killing vector ζ^μ of the metric, the scalar $k^\mu \zeta_\mu$ is constant along the geodesic whose tangent vector is k^μ (whether it is null or not).

A. Light rays

Since ∂_i is a Killing vector of the Bianchi I spacetime, the quantity $g(\partial_i, k) = k_i$ is a constant of geodesic motion. Moreover, since k is a null vector, $\omega^2 \equiv (k^t)^2 = g^{ij} k_i k_j$ and the wave four-vector thus reads

$$k_i = \text{cst}, \qquad k^i = a^{-2} \gamma^{ij} k_j \neq \text{cst}, \qquad (4.1)$$

$$\omega = \frac{\tilde{\omega}}{a}, \qquad (4.2)$$

where

$$\tilde{\omega} \equiv \sqrt{\sum_{i=1}^{3} (e^{-\beta_i} k_i)^2}. \qquad (4.3)$$

The components of the direction of observation vector d^μ are, by definition,

$$d_i = -k_i/\omega, \qquad d^i = -k^i/\omega. \qquad (4.4)$$

From now on, we set by convention $a(t_o) = 1$ and $\beta_i(t_o) = 0$ at O ($t = t_o$), hence the redshift is given by

$$1 + z \equiv \frac{\omega_s}{\omega_o} = \frac{1}{a(t_s)} \sqrt{\sum_{i=1}^{3} \left[e^{-\beta_i(t_s)} k_i \right]^2}. \qquad (4.5)$$

The constants of motion k_i are directly related to the direction in which the observer at O needs to look to detect the light signal. Indeed, with the conventions specified above, at the observation event $(g_{ij})_o = \delta_{ij}$, moreover we have used the remaining freedom to set $\omega_o = 1$, so that $-k_i = (d_i)_o$ is a unitary Euclidean three-vector.

B. Parentheses: On timelike geodesics

The previous reasonings also apply to timelike geodesics. Consider a general observer, whose four-velocity v^μ can be decomposed with respect to the four-velocity u^μ of the fundamental (comoving) observers as

$$v^\mu = E u^\mu + p^\mu \qquad (4.6)$$

with $u^\mu p_\mu = 0$ and $u^\mu u_\mu = -1$. Since $v^\mu v_\mu = -1$, we have $p^\mu p_\mu = -1 + E^2$. Now the constancy of p_i implies that $E^2 = 1 + a^{-2} \gamma^{ij} p_i p_j \to 1$ as t increases (in an expanding universe), so that the worldline of the observer tends to align with the worldline of the fundamental observers, i.e. the Hubble flow, exactly as in Friedmann-Lemaître spacetimes [45].

C. Redshift and direction drifts

1. Redshift drift

As originally pointed out by Sandage and McVittie [46, 47] a consequence of the expansion of the Universe is the existence of a drift of the cosmological redshifts. This effect is thought to be observationally accessible [48, 49] in the standard cosmological framework [50–53].

Consider a photon received at $t_o + \delta t_o$, corresponding to the emission time $t_s + \delta t_s$; by definition of the redshift,

$$1 + z + \delta z \equiv \frac{\omega(t_s + \delta t_s)}{\omega(t_o + \delta t_o)} = \sqrt{\frac{g^{ij}(t_s + \delta t_s) k_i k_j}{g^{ij}(t_o + \delta t_o) k_i k_j}}. \quad (4.7)$$

We can expand the above formula at first order in δt_o and δt_s using $g^{ij} = \gamma^{ij}/a^2$, which leads to

$$\frac{\delta z}{1+z} = \frac{\delta t_o}{a_o} \left(\mathcal{H} + \sigma_j^i d_i d^j \right)_o - \frac{\delta t_s}{a_s} \left(\mathcal{H} + \sigma_j^i d_i d^j \right)_s. \quad (4.8)$$

Since moreover $\delta t_s / \delta t_o = 1/(1 + z)$, we finally get the redshift drift $\dot{z}_o \equiv \delta z / \delta t_o$ observed by O:

$$\dot{z}_o = (1 + z) H_o^\parallel - H_s^\parallel, \qquad (4.9)$$

where

$$H^\parallel(z, d^i) \equiv \frac{1}{a} \left(\mathcal{H} + \sigma_j^i d_i d^j \right). \qquad (4.10)$$

It is interesting to notice that Eq. (4.9) is identical to the one obtained in a Lemaître-Tolman-Bondi universe [51], and indeed reduces to the Sandage formula [46, 47] in the isotropic case.

2. Direction drift

A consequence of anisotropic expansion is that, besides redshift drift, the position of a comoving light source on the observer's celestial sphere also changes with time. Let us compute the velocity of this direction drift. The position x_s^i of the source is obtained by integrating the wave vector k^i with respect to the affine parameter,

$$x_s^i = \int_{v_o}^{v_s} k^i \, dv = \left(\int_{v_o}^{v_s} a^{-2} e^{-2\beta_i} \, dv \right) d_o^i, \qquad (4.11)$$

where we used $k_i = \text{cst} = d_o^i$. Like for redshift drift, we can evaluate the above relation at a later observation time $t_o + \delta t_o$ corresponding to an emission time $t_s + \delta t_s$. If the source is comoving, then x_s^i remains unchanged, so that

$$\left(\int_{v(t_o)}^{v(t_s)} a^{-2} e^{-2\beta_i} \, dv \right) d_o^i$$

$$= \left(\int_{v(t_o + \delta t_o)}^{v(t_s + \delta t_s)} a^{-2} e^{-2\beta_i} \, dv \right) (d_o^i + \delta d_o^i). \quad (4.12)$$

The direction drift velocity $\dot{d}_o^i \equiv \delta d_o^i/\delta t_o$ is finally obtained by performing a first-order expansion of Eq. (4.12), using in particular $v(t + \delta t) = v(t) + \delta t/\omega$, and the result is

$$\dot{d}_o^i = \left(\int_{v_o}^{v_s} a^{-2} e^{-2\beta_i} \, dv \right)^{-1} \left(d_o^i - \frac{d_s^i}{1+z} \right). \quad (4.13)$$

V. THE CONFORMAL DICTIONARY

The determination of the Jacobi matrix in a Bianchi I spacetime is greatly simplified by using the fact that two conformal spacetimes have the same light cone.[2] Let the conformal metric $\tilde{g}_{\mu\nu}$ be defined by

$$g_{\mu\nu} = a^2 \tilde{g}_{\mu\nu}. \quad (5.1)$$

Property.—Any null geodesic for $g_{\mu\nu}$, affinely parametrized by v, is also a null geodesic for $\tilde{g}_{\mu\nu}$, affinely parametrized by $\tilde{v}$ with $dv = a^2 d\tilde{v}$. The associated wave four-vectors then read $\tilde{k}^\mu = a^2 k^\mu$.

As a consequence, the *covariant* components of k are unchanged by the conformal transformation, indeed

$$\tilde{k}_\mu = \tilde{g}_{\mu\nu} \tilde{k}^\nu = a^{-2} g_{\mu\nu} a^2 k^\mu = k_\mu. \quad (5.2)$$

The four-velocities of comoving observers for both geometries are respectively $u = \partial_t$ and $\tilde{u} = \partial_\eta$, so that $\tilde{u}^\mu = a\, u^\mu$, thus

$$\omega \equiv g_{\mu\nu} u^\mu k^\nu = a^{-1} \tilde{g}_{\mu\nu} \tilde{u}^\mu \tilde{k}^\nu = \tilde{\omega}/a. \quad (5.3)$$

The 3+1 decomposition of $\tilde{k}^\mu$ is therefore

$$\tilde{k}^\mu = \tilde{\omega}(\tilde{u}^\mu - \tilde{d}^\mu) \quad (5.4)$$

with $\tilde{d}^\mu \equiv a\, d^\mu$ implying $\tilde{d}_\mu = d_\mu/a$.

The Sachs basis $(\tilde{s}_A^\mu)_{A=1,2}$ for the conformal geometry is related to the original one by

$$\tilde{s}_A^\mu = a\, s_A^\mu. \quad (5.5)$$

One can indeed check that, with Eq. (5.5), the usual orthonormality and Fermi-Walker transport conditions are preserved by the conformal transformation,[3] i.e.

$$\begin{cases} s_A^\mu u_\mu = 0, \\ s_A^\mu d_\mu = 0, \\ s_A^\mu s_{B\mu} = \delta_{AB}, \\ S_\mu^\nu k^\rho \nabla_\rho s_A^\nu = 0. \end{cases} \Longleftrightarrow \begin{cases} \tilde{s}_A^\mu \tilde{u}_\mu = 0, \\ \tilde{s}_A^\mu \tilde{d}_\mu = 0, \\ \tilde{s}_A^\mu \tilde{s}_{B\mu} = \delta_{AB}, \\ \tilde{S}_\mu^\nu \tilde{k}^\rho \tilde{\nabla}_\rho \tilde{s}_A^\nu = 0. \end{cases} \quad (5.7)$$

─────────

[2] In four dimensions, this result can be related to the conformal invariance of Maxwell theory. However, this property of the null geodesics holds even in higher dimensions whilst Maxwell theory is no more conformal invariant. From the physical point of view, this is due to the fact that *in the eikonal approximation* all the terms which are not conformally invariant are subdominant. It follows that geometric optics enjoys more symmetries that the microscopic theory it derives from.

[3] The connections $\tilde{\nabla}$ and ∇ are related by

$$\tilde{\nabla}_\mu V_\nu = \nabla_\mu V_\nu - V_\alpha \left[2\delta_{(\mu}^\alpha \nabla_{\nu)} \ln a - g_{\mu\nu} g^{\alpha\beta} \nabla_\beta \ln a \right]. \quad (5.6)$$

In these relations, $S_{\mu\nu}$ is the screen projector defined in Eq. (3.6) and we have an analogous definition for the conformal geometry, which implies $S_{\mu\nu} = a^2 \tilde{S}_{\mu\nu}$.

The separation four-vector ξ^μ between two neighboring geodesics is defined by comparing events only, independently from any metric. It is therefore invariant under conformal transformations. However, its projection over the Sachs basis changes (since the Sachs basis itself changes), indeed

$$\xi_A \equiv s_A^\mu \xi_\mu = a^{-1} \tilde{s}_A^\mu a^2 \tilde{\xi}_\mu = a\, \tilde{\xi}_A. \quad (5.8)$$

The above relation allows us to relate the Jacobi matrices calculated in both geometries, and the result is

$$\mathcal{D}_{AB}(s \leftarrow o) = a_s \tilde{\mathcal{D}}_{AB}(s \leftarrow o), \quad (5.9)$$

which, by virtue of Eq. (3.11), implies

$$D_A = a_s \tilde{D}_A. \quad (5.10)$$

VI. SACHS BASIS IN A CONFORMAL BIANCHI I GEOMETRY

Important remark.—In this section, all the calculations are performed in the conformal geometry $\tilde{g}_{\mu\nu}$. Since only intermediary results are at stake, *we temporarily drop all the tildes on the vectors $\tilde{d}^\mu$, $\tilde{s}_A^\mu$ to alleviate notation.* However, we do not drop the tilde on $\tilde{\omega}$ because it could lead to ambiguities.

By definition, the Sachs basis is purely spatial, so

$$u_\mu s_A^\mu = 0. \quad (6.1)$$

The evolution of the nonzero spatial part of s_A^μ follows from the Fermi-Walker transport (3.5), which takes the form

$$(s_A^i)' + S_j^i \sigma_k^j s_A^k = 0, \quad (6.2)$$

where $S_j^i = \delta_j^i - d^i d_j$ (since $u^i = 0$) and we used that the only nonvanishing Christoffel coefficients are

$$\tilde{\Gamma}_{0j}^i = \sigma_j^i, \qquad \tilde{\Gamma}_{ij}^0 = \sigma_{ij}. \quad (6.3)$$

A. General solution of the transport equation

Let $(n_A^\mu)_{A=1,2}$ be an arbitrary orthonormal basis of the screen space (i.e. orthogonal to both u^μ and d^μ), not necessarily Fermi-Walker transported along the light beam. Explicit examples of such a basis will be given in Sec. VI C. The Sachs basis $(s_A^\mu)_{A=1,2}$ being also an orthonormal basis of the same space, the two basis are related by a rotation

$$\begin{cases} s_1^\mu = \cos\vartheta\, n_1^\mu + \sin\vartheta\, n_2^\mu, \\ s_2^\mu = -\sin\vartheta\, n_1^\mu + \cos\vartheta\, n_2^\mu. \end{cases} \quad (6.4)$$

Hence, provided the basis $(n^\mu_A)_{A=1,2}$ is known, the Sachs basis is entirely determined by the angle ϑ.

In order to determine the evolution of this angle, it is convenient to rewrite Eq. (6.2) in terms of the components of s_A over a tetrad basis $(e_a)_{a=1\ldots3}$ rather than over the coordinate basis $(\partial_i)_{i=1\ldots3}$. The choice $e^i_a = \exp(-\beta_i)\delta^i_a$ and $e^a_i = \exp(\beta_i)\delta^a_i$ implies that the components $s^a_A \equiv g(s_A, e_a)$ read

$$(s^a_A)' + d^a(d_b)'s^b_A = 0, \qquad (6.5)$$

thus

$$(\cos\vartheta)' = (n_{1a}s^a_1)' = (n_{1a})'s^a_1 - \underbrace{n_{1a}d^a}_{=0}(d_b)'s^b_1. \qquad (6.6)$$

Since n_1 is normalized, $(n_{1a})'n^a_1 = 0$, so $(n_{1a})' = (n_{1b})'n^b_2 n_{2a} + (n_{1b})'d^b d_a$, therefore

$$(\cos\vartheta)' = (n_{1b})'n^b_2 n_{2a}s^a_1 = (n_{1b})'n^b_2 \sin\vartheta, \qquad (6.7)$$

which finally reduces to

$$\vartheta' = -(n_{1a})'n^a_2 = (n_{2a})'n^a_1. \qquad (6.8)$$

Summarizing, if a basis (n^μ_1, n^μ_2) can be found, then the Sachs basis is completely determined by Eq. (6.4) with ϑ given by the integral of $(n_{2a})'n^a_1$.

B.   Evolution matrix

Let $\boldsymbol{\mathcal{E}}$ be the 2×2 matrix that relates the components s^i_A of the Sachs basis to their values at O, $(s^i_A)_\mathrm{o} \equiv s^i_A(\eta_\mathrm{o})$,

$$s^i_A(\eta) = \mathcal{E}_{AB}(\eta \leftarrow \eta_\mathrm{o})(s^i_B)_\mathrm{o}. \qquad (6.9)$$

It is straightforward to show that this *evolution matrix* is the solution of

$$\mathcal{E}'_{AB} + \sigma_{AC}\mathcal{E}_{CB} = 0, \qquad (6.10)$$
$$\mathcal{E}_{AB}(\eta_\mathrm{o} \leftarrow \eta_\mathrm{o}) = \delta_{AB}, \qquad (6.11)$$

where $\sigma_{AB} \equiv s^i_A s^j_B \sigma_{ij}$. Note that, by definition (6.9),

$$\mathcal{E}_{AB}(\eta \leftarrow \eta_\mathrm{o}) = s^i_A(\eta)s_{Bi}(\eta_\mathrm{o}). \qquad (6.12)$$

Note also that the position of i *does matter* in the above relation, because the vectors $s_A(\eta)$ and $s_A(\eta_\mathrm{o})$ do not live in the same tangent spaces of the spacetime manifold $\mathcal{M}$. The former live in $\mathrm{T}_\eta(\mathcal{M})$, their indices are raised and lowered by $\gamma_{ij}(\eta)$, while the latter live in $\mathrm{T}_{\eta_\mathrm{o}}(\mathcal{M})$, their indices are raised and lowered by $\gamma_{ij}(\eta_\mathrm{o}) = \delta_{ij}$.

In fact, inverting the position of the i indices in Eq. (6.12) leads to the *transposed inverse* $(\boldsymbol{\mathcal{E}}^{-1})^T$ of the evolution matrix, because

$$\begin{aligned} s_{Ai}(\eta)s^i_B(\eta_\mathrm{o}) &= s_{Ai}(\eta)\mathcal{E}_{BC}(\eta_\mathrm{o} \leftarrow \eta)s^i_C(\eta) \\ &= \mathcal{E}_{BA}(\eta_\mathrm{o} \leftarrow \eta) \\ &= \mathcal{E}^{-1}_{BA}(\eta \leftarrow \eta_\mathrm{o}). \end{aligned} \qquad (6.13)$$

It is straightforward to check that $(\boldsymbol{\mathcal{E}}^{-1})^T$ satisfies a differential equation almost identical to Eq. (6.10), *except for a minus sign* before σ_{AC},

$$(\mathcal{E}^{-1}_{BA})' - \sigma_{AC}\mathcal{E}^{-1}_{BC} = 0. \qquad (6.14)$$

Using the general solution for the Sachs basis constructed in Sec. VI A, the evolution matrix and its transposed inverse take the form

$$\boldsymbol{\mathcal{E}} = \begin{bmatrix} \cos\vartheta & \sin\vartheta \\ -\sin\vartheta & \cos\vartheta \end{bmatrix} \begin{bmatrix} n^i_1(s_{1i})_\mathrm{o} & n^i_1(s_{2i})_\mathrm{o} \\ n^i_2(s_{1i})_\mathrm{o} & n^i_2(s_{2i})_\mathrm{o} \end{bmatrix}, \quad (6.15)$$

$$(\boldsymbol{\mathcal{E}}^{-1})^T = \begin{bmatrix} \cos\vartheta & \sin\vartheta \\ -\sin\vartheta & \cos\vartheta \end{bmatrix} \begin{bmatrix} n_{1i}(s^i_1)_\mathrm{o} & n_{1i}(s^i_2)_\mathrm{o} \\ n_{2i}(s^i_1)_\mathrm{o} & n_{2i}(s^i_2)_\mathrm{o} \end{bmatrix}, \quad (6.16)$$

with the angle ϑ given by Eq. (6.26).

Let us close this subsection by showing that the determinant of $\boldsymbol{\mathcal{E}}$ has a remarkably simple expression. Indeed

$$\begin{aligned} (\det\boldsymbol{\mathcal{E}})' &= \mathrm{Tr}(\boldsymbol{\mathcal{E}}^{-1}\boldsymbol{\mathcal{E}}')\det\boldsymbol{\mathcal{E}} \\ &= -\mathrm{Tr}(\boldsymbol{\mathcal{E}}^{-1}\boldsymbol{\sigma}\boldsymbol{\mathcal{E}})\det\boldsymbol{\mathcal{E}} \\ &= -\mathrm{Tr}\boldsymbol{\sigma}\det\boldsymbol{\mathcal{E}}, \end{aligned} \qquad (6.17)$$

where $\boldsymbol{\sigma} \equiv (\sigma_{AB})$ is the projection of σ_{ij} on the Sachs basis, as defined below Eq. (6.11); its trace reads

$$\mathrm{Tr}\boldsymbol{\sigma} = \sigma^A_A = \sigma_{ij}S^{ij} = \sigma^i_i - \sigma_{ij}d^i d^j, \qquad (6.18)$$

but, on the one hand, remember that Eq. (2.3) implies

$$\sigma^i_i = \sum_{i=1}^{3}\beta'_i = 0, \qquad (6.19)$$

and, on the other hand,

$$\sigma_{ij}d^i d^j = \frac{\sigma^{ij}k_i k_j}{\tilde\omega^2} = \frac{(-\gamma^{ij}k_i k_j)'}{2\tilde\omega^2} = -\frac{\tilde\omega'}{\tilde\omega}, \qquad (6.20)$$

so that finally

$$(\det\boldsymbol{\mathcal{E}})' = -\frac{\tilde\omega'}{\tilde\omega}\det\boldsymbol{\mathcal{E}} \qquad \text{whence} \qquad \det\boldsymbol{\mathcal{E}} = \frac{1}{\tilde\omega}. \qquad (6.21)$$

We shall see in Sec. VII that the evolution matrix is a key ingredient in the expression of the Jacobi matrix.

C.   Explicit examples

This subsection provides three explicit examples of orthonormal basis (n_1, n_2) which can be used for the construction described in Sec. VI A, and the associated rotation angle ϑ. For the last example, we also give the expression of the evolution matrix.

1.   Frenet basis

Since d^μ is a unit vector, it is easy to construct a vector orthogonal to it from its own derivative. Here again,

calculations are easier if one works with the components over the tetrad basis $(e_a)_{a=1\ldots3}$. We thus define

$$n_1^a \equiv \frac{(d^a)'}{\sqrt{(d_b)'(d^b)'}}, \qquad (6.22)$$

and complete it by $n_2^a \equiv \varepsilon^a{}_{bc}d^b n_1^c$. In terms of components over the coordinate basis (∂_i), we have

$$n_1^i = \left(\sigma_j^i d^j + \frac{\tilde{\omega}'}{\tilde{\omega}}d^i\right)\left(d^i \sigma_{ij} S_k^j \sigma_\ell^k d^\ell\right)^{-1/2}, \qquad (6.23)$$

$$n_2^i = \varepsilon^i{}_{jk}d^j n_1^k. \qquad (6.24)$$

The equation (6.8) for the evolution angle ϑ then reads

$$\vartheta' = (n_{2a})' n_1^a = \frac{\varepsilon_{abc}d^a(d^b)'(d^c)''}{(d^a)'(d_a)'}, \qquad (6.25)$$

which, in terms of components over the coordinate basis, becomes

$$\vartheta' = \frac{\varepsilon^{ijk}d_i \beta_j' d_j \left[(\beta_k')^2 d_k - \beta_k'' d_k\right]}{d^i \sigma_{ij} S_k^j \sigma_\ell^k d^\ell}. \qquad (6.26)$$

Interestingly, the two terms in the numerator of Eq. (6.26) are sourced by distinct geometrical properties of the Bianchi I spacetime. On the one hand, the term in $(\beta_k')^2$ is essentially a Vandermonde determinant,

$$\varepsilon^{ijk}d_i \beta_j' d_j(\beta_k')^2 d_k = d_1 d_2 d_3 \prod_{i>j}(\beta_i' - \beta_j'). \qquad (6.27)$$

It depends on the *triaxiality* of the Bianchi spacetime, and vanishes for an axisymmetric Bianchi I since two β_i' are equal. On the other hand, the term in β_k'' in Eq. (6.26) can be rewritten in terms of matter's anisotropic stress. Indeed, using Eq. (2.9) and $\sigma_i^j = \beta_i' \delta_i^j$ (without summation), we get

$$\varepsilon^{ijk}d_i \beta_j' d_j \beta_k'' d_k = 8\pi G a^2 \varepsilon^{ijk}d_i \sigma_j^\ell d_\ell \pi_k^m d_m. \qquad (6.28)$$

Thus, with the choice of Eqs. (6.23–6.24) for (n_1, n_2), the angle ϑ is ruled by an equation of the form

$$\vartheta' = \vartheta'_{\text{tri}} + \vartheta'_{\text{stress}}, \qquad (6.29)$$

where ϑ'_{tri} and $\vartheta'_{\text{stress}}$ vanish in, respectively, an axisymmetric and anisotropic-stress-free Bianchi I model.

Though having interesting properties, the Frenet basis presented in this paragraph suffers from singularities: for a beam propagating along a principal axis of the Bianchi spacetime, $d^a = \text{cst}$, so that n_1 cannot be defined. The next two examples will be free from such problems.

2. Initial basis

Another way of constructing vectors which keep orthogonal to d^μ is to use that k_i are constants of motion

[see Eq. (4.1)], which implies that the covariant vector $d_i = \tilde{\omega}^{-1}k_i$ always points towards the same direction. Thus, the Sachs basis $(s_A^i)_{\text{o}}$ at O remains orthogonal to $d_i(\eta)$ at any time:

$$\forall \eta \qquad d_i(\eta)(s_A^i)_{\text{o}} = 0. \qquad (6.30)$$

This motivates the following definitions,

$$\begin{cases} n_1^i \equiv \dfrac{(s_1^i)_{\text{o}}}{\sqrt{\mathring{\gamma}_{11}}} \\[2mm] n_2^i \equiv \varepsilon^i{}_{jk}d^j n_1^k, \end{cases} \qquad (6.31)$$

with $\mathring{\gamma}_{11}(\eta) \equiv \gamma_{ij}(\eta)(s_1^i s_1^j)_{\text{o}}$. Note that n_2^i cannot be constructed from $(s_2^i)_{\text{o}}$ in the same way as n_1^i is from $(s_1^i)_{\text{o}}$, because then n_1 and n_2 would not be orthogonal to each other.

In this example, the angle ϑ reads

$$\vartheta' = (n_{2a})' n_1^a = -\sigma_{ij}n_1^i n_2^j = \frac{-\varepsilon_{ijk}d^i \sigma_\ell^k (s_1^j s_1^\ell)_{\text{o}}}{\gamma_{ij}(s_1^i s_1^j)_{\text{o}}}. \qquad (6.32)$$

All these quantities are well behaved, as long as $\mathring{\gamma}_{11} \neq 0$.

3. Symmetrized initial basis

The construction of the previous example can be slightly improved in order to be more symmetric. As mentioned above, if we define

$$v_1^i \equiv \frac{(s_1^i)_{\text{o}}}{\sqrt{\mathring{\gamma}_{11}}}, \qquad v_2^i \equiv \frac{(s_2^i)_{\text{o}}}{\sqrt{\mathring{\gamma}_{22}}}, \qquad (6.33)$$

with

$$\mathring{\gamma}_{AB}(\eta) \equiv \gamma_{ij}(\eta)(s_A^i s_B^j)_{\text{o}} \qquad (6.34)$$

as in Eq. (6.31), then v_A^i is normalized and $d_i v_A^i = 0$, but v_1 and v_2 are not orthogonal to each other. Let us call $\delta(\eta)$ the angle expressing their departure from orthogonality,

$$\cos\left(\frac{\pi}{2} + \delta\right) = -\sin\delta \equiv \gamma_{ij}v_1^i v_2^j = \frac{\mathring{\gamma}_{12}}{\sqrt{\mathring{\gamma}_{11}\mathring{\gamma}_{22}}}. \qquad (6.35)$$

Albeit not orthogonal itself, (v_1, v_2) can easily be used to obtain an orthonormal basis. Like for any couple of unit vectors, $v_1 + v_2$ is orthogonal to $v_1 - v_2$, which encourages us to define

$$n_\pm^i \equiv \frac{v_1^i \pm v_2^i}{\sqrt{2 \mp 2\sin\delta}}. \qquad (6.36)$$

This could be used as the orthonormal basis of this last example, however we will prefer its rotation by $\pi/4$,

$$n_1^i \equiv \frac{1}{\sqrt{2}}\left(n_+^i + n_-^i\right), \qquad n_2^i \equiv \frac{1}{\sqrt{2}}\left(n_+^i - n_-^i\right), \qquad (6.37)$$

so that $(n_A^i)_\mathrm{o} = (s_A^i)_\mathrm{o}$, i.e. $\vartheta_\mathrm{o} = 0$. In this case, and after a few calculations, we obtain that the angle ϑ reads

$$\vartheta' = (n_{2a})'n_1^a = (n_{+a})'n_-^a \qquad (6.38)$$

$$= \frac{1}{4}\tan\delta\left[\ln\left(\frac{\mathring{\tilde{\gamma}}_{22}}{\mathring{\tilde{\gamma}}_{11}}\right)\right]', \qquad (6.39)$$

that can also be written $(\tan\delta)\sigma_{ij}(v_2^i v_2^j - v_1^i v_1^j)/2$.

Finally, let us also give the (transposed inverse) evolution matrix which, in the present example, enjoys the relatively simple expression

$$(\boldsymbol{\mathcal{E}}^{-1})^T = \begin{bmatrix} \cos\vartheta & \sin\vartheta \\ -\sin\vartheta & \cos\vartheta \end{bmatrix}\begin{bmatrix} \cos(\delta/2) & \sin(\delta/2) \\ \sin(\delta/2) & \cos(\delta/2) \end{bmatrix}$$
$$\cdot \begin{bmatrix} \sqrt{\mathring{\tilde{\gamma}}_{11}} & 0 \\ 0 & \sqrt{\mathring{\tilde{\gamma}}_{22}} \end{bmatrix}. \quad (6.40)$$

Note that the second matrix of Eq. (6.40) is *not* a rotation matrix. From this result one can deduce the interesting relation

$$\tilde{\omega} = \det\boldsymbol{\mathcal{E}}^{-1} = \sqrt{\mathring{\tilde{\gamma}}_{11}\mathring{\tilde{\gamma}}_{22}}\cos\delta = \sqrt{\mathring{\tilde{\gamma}}_{11}\mathring{\tilde{\gamma}}_{22} - \mathring{\tilde{\gamma}}_{12}^2}, \quad (6.41)$$

which can also be checked by brute-force calculation.

VII.   JACOBI MATRIX IN A CONFORMAL BIANCHI I GEOMETRY

As in the previous one, all the calculations of this section are performed in the conformal geometry $\tilde{g}_{\mu\nu}$. However, all the tildes will here be carefully written, because nonintermediary results are derived.

A.   General solution for the Jacobi matrix

Let us now solve the Jacobi matrix equation

$$\frac{\mathrm{d}^2\tilde{\mathcal{D}}_{AB}}{\mathrm{d}\tilde{v}^2} = \tilde{\mathcal{R}}_{AC}\tilde{\mathcal{D}}_{CB}, \qquad (7.1)$$

where we recall that the optical tidal matrix is defined by

$$\tilde{\mathcal{R}}_{AB} \equiv -\tilde{R}_{\mu\nu\rho\sigma}\tilde{k}^\mu\tilde{s}_A^\nu\tilde{k}^\rho\tilde{s}_B^\sigma. \qquad (7.2)$$

The nonzero components of the Riemann tensor for the conformal Bianchi I geometry being

$$\tilde{R}_{0i0j} = \sigma_i^k\sigma_{kj} - \sigma_{ij}', \qquad \tilde{R}_{ijk\ell} = 2\sigma_{k[i}\sigma_{j]\ell}. \qquad (7.3)$$

A straightforward calculation, using in particular Eqs. (6.2) and (6.20), then leads to

$$\tilde{\mathcal{R}}_{AB} = \tilde{\omega}^2\left[(\sigma_{AB})' + \sigma_{AC}\sigma_{CB} + \frac{\tilde{\omega}'}{\tilde{\omega}}\sigma_{AB}\right]. \qquad (7.4)$$

Therefore, since $\mathrm{d}/\mathrm{d}\tilde{v} = \tilde{\omega}\mathrm{d}/\mathrm{d}\eta$, Eq. (7.1) reads

$$\tilde{\mathcal{D}}_{AB}'' + \frac{\tilde{\omega}'}{\tilde{\omega}}\tilde{\mathcal{D}}_{AB}' = \left[(\sigma_{AC})' + \sigma_{AD}\sigma_{DC} + \frac{\tilde{\omega}'}{\tilde{\omega}}\sigma_{AC}\right]\tilde{\mathcal{D}}_{CB}. \qquad (7.5)$$

Now notice that if a matrix M_{AB} is solution of $M_{AB}' = \sigma_{AC}M_{CB}$, then it is also solution of Eq. (7.5). Comparing with Eq. (6.14), we deduce that the transposed inverse $(\boldsymbol{\mathcal{E}}^{-1})^T$ of the evolution matrix is such a solution. However, it is *not* the Jacobi matrix, because it does not satisfy the right initial conditions (3.9) and (3.10), but rather

$$(\mathcal{E}^{-1})_{BA}(\eta_\mathrm{o} \leftarrow \eta_\mathrm{o}) = \delta_{AB}, \qquad (7.6)$$

$$\frac{\mathrm{d}(\mathcal{E}^{-1})_{AB}^T}{\mathrm{d}v}(\eta_\mathrm{o} \leftarrow \eta_\mathrm{o}) = (\sigma_{AB})_\mathrm{o}. \qquad (7.7)$$

From this particular solution, one can obtain the Jacobi matrix by use, for instance, of the method of the "variation of the constant" to get

$$\tilde{\boldsymbol{\mathcal{D}}}(\eta_\mathrm{s} \leftarrow \eta_\mathrm{o}) = (\boldsymbol{\mathcal{E}}^{-1})^T\int_{\eta_\mathrm{s}}^{\eta_\mathrm{o}}\tilde{\omega}^{-1}\boldsymbol{\mathcal{E}}^T\boldsymbol{\mathcal{E}}\,\mathrm{d}\eta. \qquad (7.8)$$

This formula is the main result of our article. Since

$$\mathcal{E}_{AB}(\eta_\mathrm{s} \leftarrow \eta_\mathrm{o}) = \tilde{s}_A^i(\eta_\mathrm{s})\tilde{s}_{Bi}(\eta_\mathrm{o}), \qquad (7.9)$$

$$(\mathcal{E}^{-1})_{AB}^T(\eta_\mathrm{s} \leftarrow \eta_\mathrm{o}) = \tilde{s}_{Ai}(\eta_\mathrm{s})\tilde{s}_B^i(\eta_\mathrm{o}), \qquad (7.10)$$

it can also be rewritten in terms of the components of the Sachs basis as

$$\tilde{\mathcal{D}}_{AB}(\eta_\mathrm{s} \leftarrow \eta_\mathrm{o}) = (\tilde{s}_{Ai})_\mathrm{s}(\tilde{s}_C^i\tilde{s}_{Cj})_\mathrm{o}$$
$$\times\left(\int_{\eta_\mathrm{s}}^{\eta_\mathrm{o}}\tilde{\omega}^{-1}\tilde{S}^{jk}\,\mathrm{d}\eta\right)(\tilde{s}_{Bk})_\mathrm{o}. \quad (7.11)$$

This form of the Jacobi matrix, entirely determined by the Sachs basis, reminds us about the recent results of Refs. [54, 55], based on the geodesic-light-cone coordinates [56]. The connection between the two formalisms is left for further studies.

B.   An explicit expression

Of course, Eq. (7.8) cannot be considered explicit as long as one does not have an expression for $\boldsymbol{\mathcal{E}}$, which was precisely the purpose of Sec. VI. Here, we choose to use the results of our third example (Sec. VI C 3): plugging the expression (6.40) of $\boldsymbol{\mathcal{E}}$ into Eq. (7.8), we obtain

$$\tilde{\boldsymbol{\mathcal{D}}}(\eta_\mathrm{s} \leftarrow \eta_\mathrm{o}) = \begin{bmatrix} \cos\vartheta_\mathrm{s} & \sin\vartheta_\mathrm{s} \\ -\sin\vartheta_\mathrm{s} & \cos\vartheta_\mathrm{s} \end{bmatrix}\begin{bmatrix} \cos(\delta_\mathrm{s}/2) & \sin(\delta_\mathrm{s}/2) \\ \sin(\delta_\mathrm{s}/2) & \cos(\delta_\mathrm{s}/2) \end{bmatrix}$$
$$\cdot\begin{bmatrix} \sqrt{\mathring{\tilde{\gamma}}_{11}(\eta_\mathrm{s})} & 0 \\ 0 & \sqrt{\mathring{\tilde{\gamma}}_{22}(\eta_\mathrm{s})} \end{bmatrix}\int_{\eta_\mathrm{s}}^{\eta_\mathrm{o}}\frac{\mathrm{d}\eta}{\tilde{\omega}^3}\begin{bmatrix} \mathring{\tilde{\gamma}}_{22} & \mathring{\tilde{\gamma}}_{12} \\ \mathring{\tilde{\gamma}}_{12} & \mathring{\tilde{\gamma}}_{11} \end{bmatrix} \quad (7.12)$$

where the various quantities are defined in Sec. VI C 3, and thing$_\mathrm{s} \equiv$ thing(η_s). In particular,

$$\vartheta_\mathrm{s} = \frac{1}{4}\int_{\eta_\mathrm{s}}^{\eta_\mathrm{o}}\frac{\mathring{\tilde{\gamma}}_{12}}{\tilde{\omega}}\left[\ln\left(\frac{\mathring{\tilde{\gamma}}_{22}}{\mathring{\tilde{\gamma}}_{11}}\right)\right]'\,\mathrm{d}\eta. \qquad (7.13)$$

C. Angular diameter distance

The angular diameter distance is related to the Jacobi matrix via Eq. (3.11), that is here

$$\tilde{D}_{\mathrm{A}} = \sqrt{\det \boldsymbol{\mathcal{E}}^{-1}} \sqrt{\det \int_{\eta_{\mathrm{s}}}^{\eta_{\mathrm{o}}} \tilde{\omega}^{-1} \boldsymbol{\mathcal{E}}^T \boldsymbol{\mathcal{E}} \, \mathrm{d}\eta}. \qquad (7.14)$$

We have already seen at the end of Sec. VI B that the determinant of $\boldsymbol{\mathcal{E}}^{-1}$ is $\tilde{\omega}$, see Eq. (6.21), so that

$$\tilde{D}_{\mathrm{A}} = \sqrt{\tilde{\omega}\Delta}, \qquad (7.15)$$

where Δ denotes the second determinant involved in Eq. (7.14). As originally found by Saunders in Ref. [31], this determinant admits the remarkably simple expression

$$\Delta = \sum_{i \neq j \neq \ell} I_i I_j k_\ell^2 \qquad (7.16)$$

with

$$I_i \equiv \int_{\eta_{\mathrm{s}}}^{\eta_{\mathrm{o}}} \tilde{\omega}^{-3} \mathrm{e}^{2\beta_i} \, \mathrm{d}\eta. \qquad (7.17)$$

It is however surprising that the author of Ref. [31] gives this nontrivial expression of Δ with no derivation. Since we did not find any elsewhere in the literature, we propose one in the Appendix. Note that, by computing directly the determinant of the explicit expression (7.12), one can obtain an alternative form—though mathematically equivalent—of Saunders' determinant

$$\Delta = \mathcal{I}_{11}\mathcal{I}_{22} - \mathcal{I}_{12}^2, \qquad (7.18)$$

with

$$\mathcal{I}_{AB} \equiv \int_{\eta_{\mathrm{s}}}^{\eta_{\mathrm{o}}} \tilde{\omega}^{-3} \mathring{\gamma}_{AB} \, \mathrm{d}\eta. \qquad (7.19)$$

D. The weak shear regime

Our solution for the Jacobi matrix is completely general, which means that it remains valid even for very anisotropic Bianchi I spacetimes [with $\beta_i = \mathcal{O}(1)$]. However, because cosmological observations suggest that our Universe is extremely close to isotropic, it can be interesting in practice to study the weak-shear behavior of our solution. We now perform such an expansion of the Jacobi matrix—and the related quantities—at first order in $\beta_i \ll 1$, in the conformal Bianchi I geometry.

In this regime, the cyclic frequency of the photons and the evolution matrix of the Sachs basis respectively read

$$\tilde{\omega} = 1 - \mathcal{B} + \mathcal{O}(\beta_i^2), \qquad (7.20)$$

$$\mathcal{E}_{AB} = \delta_{AB} + \mathcal{B}_{AB} + \mathcal{O}(\beta_i^2), \qquad (7.21)$$

where we have defined the first order quantities

$$\mathcal{B}_{AB}(\eta) \equiv \sum_{i=1}^{3} \beta_i(\eta)(s_A^i s_B^i)_{\mathrm{o}}, \qquad (7.22)$$

$$\mathcal{B}(\eta) \equiv \sum_{i=1}^{3} \beta_i(\eta) k_i^2 = -\mathrm{Tr}(\mathcal{B}_{AB}). \qquad (7.23)$$

Note that, in terms of the notations of Sec. VI C, $\mathring{\gamma}_{AB} = \delta_{AB} + 2\mathcal{B}_{AB} + \mathcal{O}(\beta_i^2)$. The expression of the Jacobi matrix is then easily found to be

$$\tilde{\mathcal{D}}_{AB}(\eta_{\mathrm{s}} \leftarrow \eta_{\mathrm{o}}) = \delta_{AB}\left[(\eta_{\mathrm{s}} - \eta_{\mathrm{o}}) + \int_{\eta_{\mathrm{s}}}^{\eta_{\mathrm{o}}} \mathcal{B} \, \mathrm{d}\eta\right]$$
$$+ (\eta_{\mathrm{s}} - \eta_{\mathrm{o}})\mathcal{B}_{AB}(\eta_{\mathrm{s}}) - 2\int_{\eta_{\mathrm{s}}}^{\eta_{\mathrm{o}}} \mathcal{B}_{AB} \, \mathrm{d}\eta + \mathcal{O}(\beta_i^2). \quad (7.24)$$

Note that, at this order, the Jacobi matrix remains *symmetric*. In terms of the decomposition of Eq. (3.13), it means that the rotation angle vanishes $\psi = \mathcal{O}(\beta_i^2)$. The angular diameter distance is obtained by computing the (square root of the) determinant of (7.24), which leads to

$$\tilde{D}_{\mathrm{A}} = \left(1 - \frac{\mathcal{B}_{\mathrm{s}}}{2}\right)(\eta_{\mathrm{o}} - \eta_{\mathrm{s}}) + 2\int_{\eta_{\mathrm{s}}}^{\eta_{\mathrm{o}}} \mathcal{B} \, \mathrm{d}\eta + \mathcal{O}(\beta_i^2). \quad (7.25)$$

Finally, the optical shear, encoded into the exponential matrix of Eq. (3.13) is at this order equal to the traceless part of the Jacobi matrix $\tilde{\mathcal{D}}_{\langle AB \rangle}$,

$$\begin{bmatrix} -\Gamma_1 & \Gamma_2 \\ \Gamma_2 & \Gamma_1 \end{bmatrix} = (\eta_{\mathrm{s}} - \eta_{\mathrm{o}})\mathcal{B}_{\langle AB \rangle}(\eta_{\mathrm{s}})$$
$$- 2\int_{\eta_{\mathrm{s}}}^{\eta_{\mathrm{o}}} \mathcal{B}_{\langle AB \rangle} \, \mathrm{d}\eta + \mathcal{O}(\beta_i^2), \quad (7.26)$$

where $\langle AB \rangle$ means the traceless part with respect to δ_{AB}; in particular $\mathcal{B}_{\langle AB \rangle} = \mathcal{B}_{AB} - \mathcal{B}\,\delta_{AB}/2$. Note that the above shear does not need to be tilded, because $\tilde{\boldsymbol{\mathcal{D}}} \propto \boldsymbol{\mathcal{D}}$ so that $(\tilde{\Gamma}_1, \tilde{\Gamma}_2) = (\Gamma_1, \Gamma_2)$.

VIII. SUMMARY

Before concluding, let us summarize the main results of this paper, under the form of a recipe for the reader who would like to use them in practice. It is also the occasion to recover the untilded quantities from the tilded ones using the dictionary of Sec. V.

1. Solve for the cosmology (Sec. II) to determine the scale factor $a(\eta)$, and the functions $\beta_i(\eta)$ characterizing the spatial conformal metric γ_{ij}. Set by convention $a(\eta_{\mathrm{o}}) = 1$ and $\beta_i(\eta_{\mathrm{o}})$ so that $(g_{\mu\nu})_{\mathrm{o}} = \eta_{\mu\nu}$. Note that, by virtue of the dictionary of Sec. V, all conformal (tilded) quantities are equal to their untilded counterpart at $\eta = \eta_{\mathrm{o}}$. An example of such dynamics can be found in Ref. [11].

2. Pick a direction of observation $d_{\rm o}^i$ on the sky and an initial Sachs basis $(s_A^i)_{\rm o}$ orthogonal to it. A possible choice using spherical coordinates $(\theta_{\rm o}, \varphi_{\rm o})$ is

$$(d^i)_{\rm o} = (\sin\theta_{\rm o}\cos\varphi_{\rm o}, \sin\theta_{\rm o}\sin\varphi_{\rm o}, \cos\theta_{\rm o}) \qquad (8.1)$$

$$(s_1^i)_{\rm o} = (\cos\theta_{\rm o}\cos\varphi_{\rm o}, \cos\theta_{\rm o}\sin\varphi_{\rm o}, -\sin\theta_{\rm o}) \qquad (8.2)$$

$$(s_2^i)_{\rm o} = (-\sin\varphi_{\rm o}, \cos\varphi_{\rm o}, 0) \qquad (8.3)$$

3. Set by convention $\omega_{\rm o} = 1$. The wave four-vector of the photon is then characterized at any time by $k_i = {\rm cst} = d_{\rm o}^i$ and $k^t = \omega = \tilde\omega/a$ where $\tilde\omega$ is given by Eq. (4.3). This is enough to compute the redshift $z \equiv 1/\omega - 1$, the redshift drift (4.9), the direction drift (4.13), and the angular diameter distance $D_{\rm A} = a\tilde{D}_{\rm A} = \sqrt{a^3\omega\Delta}$, where Δ is given by Eqs. (7.16) and (7.17)). In the weak shear regime, use the expression (7.25) for $\tilde{D}_{\rm A}$.

4. In order to get the full Jacobi matrix $\boldsymbol{\mathcal{D}}$, first determine the evolution matrix $\boldsymbol{\mathcal{E}}$ using the method described in Sec. VI, then plug it into Eq. (7.8) to obtain $\tilde{\boldsymbol{\mathcal{D}}}$. An example of this procedure had been given in Sec. VII B. Apply finally the conformal dictionary relation $\boldsymbol{\mathcal{D}} = a\tilde{\boldsymbol{\mathcal{D}}}$.

5. Quantities such as optical shear and optical rotation are obtained by performing the canonical decomposition (3.13) of the obtained Jacobi matrix. Their weak-shear expressions are the ones obtained in Sec. VII D.

IX. CONCLUSION

This article detailed an analytic integration of all the equations governing light propagation in a Bianchi I space-time. From a technical point of view, the symmetries of the problem were central in our derivations. First, in Sec. IV, the invariance of the metric under spatial translation allowed us to solve the null geodesic equation without any calculation. Second, the invariance of the equations governing light propagation under conformal transformations allowed us to greatly simplify the calculation of the Jacobi matrix in Sec. VII.

As a first output, we obtained formulas for the redshift and direction drift in a Bianchi I universe, which are comparable to former papers generally restricted to Lemaître-Tolman-Bondi spacetimes [51, 53]. As a second output and sanity check, we recovered the already known [16, 30, 31] expression of the angular diameter distance. However, we emphasize that our results are more powerful, because they also give access to the complete lensing behavior of Bianchi I, including optical shear and rotation. This new step will be the starting point of a deeper analysis of light propagation in a *perturbed* Bianchi I spacetime, which would allow us to evaluate the amplitude of the comic shear B-mode signal associated with a violation of local isotropy, as predicted by Ref. [35].

Our study can therefore be used to set constraints on the spatial isotropy of the Hubble flow from the analysis of the Hubble diagram, but also from possible future observation such as the redshift drift [48, 49] (see e.g. Ref. [52] for a review of the observational possibilities concerning both the time and direction drifts). Together with weak lensing [35], this offers a set of tools to constrain any late-time anisotropy of cosmic expansion.

APPENDIX: DERIVATION OF SAUNDERS' FORMULA

Let us calculate Saunders' determinant [31], defined as

$$\Delta \equiv \det \int_{\eta_{\rm s}}^{\eta_{\rm o}} \tilde\omega^{-1} \boldsymbol{\mathcal{E}}^T \boldsymbol{\mathcal{E}} \, {\rm d}\eta \qquad (1)$$

$$= \det\left[(s_{Ai})_{\rm o} \mathcal{I}^{ij} (s_{Bj})_{\rm o}\right] \qquad (2)$$

where we have denoted

$$\mathcal{I}^{ij} \equiv \int_{\eta_{\rm s}}^{\eta_{\rm o}} \tilde\omega^{-1} \tilde{S}^{ij} \, {\rm d}\eta, \qquad (3)$$

so that the quantity Δ is the determinant of the restriction of $\boldsymbol{\mathcal{I}} \equiv (\mathcal{I}^{ij})$ on the 2-plane spanned by $[(s_{Ai})_{\rm o}]_{A=1,2}$. It turns out that this restriction actually encodes the whole matrix $\boldsymbol{\mathcal{I}}$. Indeed, since $\mathcal{I}^{ij}k_i = 0$ (k_i being a constant, it can safely enter into the integral), it is easy to check that

$$\mathcal{I}^{ij} = \left[(s_{Ak})_{\rm o}\mathcal{I}^{k\ell}(s_{B\ell})_{\rm o}\right](s_A^i s_B^j)_{\rm o}; \qquad (4)$$

in other words, written in the basis $[k^i, (s_1^i)_{\rm o}, (s_2^i)_{\rm o}]$, the matrix $\boldsymbol{\mathcal{I}}$ reads

$$\boldsymbol{\mathcal{I}} = \begin{bmatrix} 0 & 0 & 0 \\ 0 & (s_{1i})_{\rm o}\mathcal{I}^{ij}(s_{1j})_{\rm o} & (s_{1i})_{\rm o}\mathcal{I}^{ij}(s_{2j})_{\rm o} \\ 0 & (s_{2i})_{\rm o}\mathcal{I}^{ij}(s_{1j})_{\rm o} & (s_{2i})_{\rm o}\mathcal{I}^{ij}(s_{2j})_{\rm o} \end{bmatrix}. \qquad (5)$$

We conclude that if $(0, \mathcal{I}_+, \mathcal{I}_-)$ denote the three eigenvalues of $\boldsymbol{\mathcal{I}}$, then $\Delta = \mathcal{I}_+\mathcal{I}_-$ is the product of the last two. Let us now calculate this product.

The characteristic polynomial of $\boldsymbol{\mathcal{I}}$ reads

$$\chi_{\boldsymbol{\mathcal{I}}}(X) \equiv \det(\boldsymbol{\mathcal{I}} - X\boldsymbol{1}_3) \qquad (6)$$

$$= -\frac{X}{2}\left[({\rm Tr}\boldsymbol{\mathcal{I}})^2 - {\rm Tr}(\boldsymbol{\mathcal{I}}^2)\right] + X^2{\rm Tr}\boldsymbol{\mathcal{I}} - X^3 \qquad (7)$$

$$= -X\mathcal{I}_+\mathcal{I}_- + X^2(\mathcal{I}_+ + \mathcal{I}_-) - X^3, \qquad (8)$$

where we have used that $\det \boldsymbol{\mathcal{I}} = 0$, and the fact that the roots of $\chi_{\boldsymbol{\mathcal{I}}}$ are $(0, \mathcal{I}_+, \mathcal{I}_-)$; thus

$$\Delta = \mathcal{I}_+ \mathcal{I}_- = \frac{1}{2} \left[(\mathrm{Tr}\boldsymbol{\mathcal{I}})^2 - \mathrm{Tr}(\boldsymbol{\mathcal{I}}^2) \right]. \qquad (9)$$

Written explicitly, the expression above is

$$\begin{aligned} \Delta = &\mathcal{I}^{11}\mathcal{I}^{22} + \mathcal{I}^{11}\mathcal{I}^{33} + \mathcal{I}^{22}\mathcal{I}^{33} \\ &- (\mathcal{I}^{13})^2 - (\mathcal{I}^{12})^2 - (\mathcal{I}^{23})^2, \end{aligned} \qquad (10)$$

but it can be further simplified using again that $\mathcal{I}^{ij}k_i = 0$, which implies

$$\mathcal{I}^{11} = -\frac{k_2}{k_1}\mathcal{I}^{12} - \frac{k_3}{k_1}\mathcal{I}^{13}, \qquad (11)$$

$$\mathcal{I}^{22} = -\frac{k_1}{k_2}\mathcal{I}^{12} - \frac{k_3}{k_2}\mathcal{I}^{23}, \qquad (12)$$

$$\mathcal{I}^{33} = -\frac{k_2}{k_3}\mathcal{I}^{23} - \frac{k_1}{k_3}\mathcal{I}^{13}. \qquad (13)$$

Plugging these relations in Eq. (10) indeed leads to

$$\Delta = \frac{k_1\mathcal{I}^{12}\mathcal{I}^{13} + k_2\mathcal{I}^{12}\mathcal{I}^{23} + k_3\mathcal{I}^{13}\mathcal{I}^{23}}{k_1 k_2 k_3}. \qquad (14)$$

Finally, with the definitions

$$I_1 \equiv -\frac{\mathcal{I}^{23}}{k_2 k_3}, \quad I_2 \equiv -\frac{\mathcal{I}^{13}}{k_1 k_3}, \quad I_3 \equiv -\frac{\mathcal{I}^{12}}{k_1 k_2}, \qquad (15)$$

we recover Saunders' formula

$$\Delta = k_1^2 I_2 I_3 + k_2^2 I_1 I_3 + k_3^2 I_1 I_2. \qquad (16)$$

Of course, we also have to check that the I_is defined in Eq. (15) agree with the expressions given in Eq. (7.17). Consider for instance I_1, starting from

$$I_1 \equiv -\frac{\mathcal{I}^{23}}{k_2 k_3} = -\frac{1}{k_2 k_3} \int_{\eta_s}^{\eta_o} \tilde{\omega}^{-1} \tilde{S}^{23} \, \mathrm{d}\eta. \qquad (17)$$

Because $\tilde{S}^{23} = \gamma^{23} - \tilde{d}^2\tilde{d}^3$, and (γ^{ij}) is diagonal, we have

$$\begin{aligned} -\tilde{S}^{23} &= \tilde{d}^2\tilde{d}^3 \\ &= \mathrm{e}^{-2\beta_2}\mathrm{e}^{-2\beta_3}\tilde{d}_2\tilde{d}_3 \\ &= \mathrm{e}^{2\beta_1}(\tilde{\omega}^{-1}\tilde{k}_2)(\tilde{\omega}^{-1}\tilde{k}_3) \qquad (18) \\ &= \mathrm{e}^{2\beta_1}\tilde{\omega}^{-2}k_2 k_3. \qquad (19) \end{aligned}$$

whence

$$I_1 = \int_{\eta_s}^{\eta_o} \tilde{\omega}^{-3}\mathrm{e}^{2\beta_1} \, \mathrm{d}\eta. \qquad (20)$$

In Eq. (18) we have used that $\sum_{i=1}^{3} \beta_i = 0$, and in Eq. (19) the relation $\tilde{k}_i = k_i$ established in Sec. V. Equation (20) agrees with Eq. (7.17), and it is clear that the same calculation can be done for I_2, I_3.

---

[1] J.-P. Uzan, Gen. Rel. Grav. **39**, 307 (2007), [astro-ph/0605313].

[2] J.-P. Uzan (2009), [arXiv:0912.5452].

[3] M. Bucher and D. N. Spergel, Phys. Rev. D **60**, 043505 (1999), [astro-ph/9812022].

[4] D. Mota, J. Kristiansen, T. Koivisto, and N. Groeneboom, Mon. Not. R. Astron. Soc. **382**, 793 (2007), [arXiv:0708.0830].

[5] T. Koivisto and D. F. Mota, Astrophys. J. **679**, 1 (2008), 0707.0279.

[6] S. A. Appleby and E. V. Linder, Phys. Rev. D **87**, 023532 (2013), [arXiv:1210.8221].

[7] S. Appleby, R. Battye, and A. Moss, Phys. Rev. D **81**, 081301 (2010), [arXiv;0912.0397].

[8] T. Damour, I. I. Kogan, and A. Papazoglou, Phys. Rev. D **66**, 104025 (2002), [hep-th/0206044].

[9] G. Marozzi and J.-P. Uzan, Phys. Rev. D **86**, 063528 (2012), [arXiv:1206.4887].

[10] T. S. Pereira, C. Pitrou, and J.-P. Uzan, JCAP **0709**, 006 (2007), [arXiv:0707.0736].

[11] C. Pitrou, T. S. Pereira, and J.-P. Uzan, JCAP **0804**, 004 (2008), [arXiv:0801.3596].

[12] R. Maartens, G. F. Ellis, and W. R. Stoeger, Phys.Rev. **D51**, 5942 (1995).

[13] R. Battye and A. Moss, Phys. Rev. D **80**, 023531 (2009), [arXiv:0905.3403].

[14] R. A. Battye and A. Moss, JCAP **0506**, 001 (2005), [astro-ph/0503033].

[15] T. Koivisto and D. F. Mota, JCAP **0806**, 018 (2008), [arXiv:0801.3676].

[16] T. Schucker, A. Tilquin, and G. Valent, Month. Not. R. Astron. Soc. **444**, 2820 (2014), [arXiv:1405.6523].

[17] J. B. Jimenez, V. Salzano, and R. Lazkoz (2014), 1402.1760.

[18] T. S. Kolatt and O. Lahav, Month. Not. R. Astron. **323**, 859 (2001), astro-ph/0008041.

[19] J. Colin, R. Mohayaee, S. Sarkar, and A. Shafieloo, Month. Not. R. Astron. **414**, 264 (2011), 1011.6292.

[20] B. Kalus, D. J. Schwarz, M. Seikel, and A. Wiegand, Astron. Astrophys. **553**, A56 (2013), 1212.3691.

[21] M. Blomqvist, J. Enander, and E. Mörtsell, JCAP **10**, 018 (2010), 1006.4638.

[22] R.-G. Cai, Y.-Z. Ma, B. Tang, and Z.-L. Tuo, Phys. Rev. D **87**, 123522 (2013), 1303.0961.

[23] D. J. Schwarz and B. Weinhorst, Astron. Astrophys. **474**, 717 (2007), 0706.0165.

[24] I. Antoniou and L. Perivolaropoulos, JCAP **12**, 012 (2010), 1007.4347.

[25] U. Feindt, M. Kerschhaggl, M. Kowalski, G. Aldering, P. Antilogus, C. Aragon, S. Bailey, C. Baltay, S. Bongard, C. Buton, et al., Astron. Astrophys. **560**, A90 (2013), 1310.4184.

[26] S. Appleby and A. Shafieloo, JCAP **3**, 007 (2014), 1312.3415.

[27] S. Appleby, A. Shafieloo, and A. Johnson, ArXiv e-prints (2014), 1410.5562.

[28] S. Appleby and A. Shafieloo, JCAP **10**, 070 (2014), 1405.4595.

[29] M. Yoon, D. Huterer, C. Gibelyou, A. Kovács, and I. Szapudi, Month. Not. R. Astron. **445**, L60 (2014), 1406.1187.

[30] P. T. Saunders, Month. Not. R. Astron. Soc. **141**, 427 (1968).

[31] P. T. Saunders, Month. Not. R. Astron. Soc. **142**, 213 (1969).

[32] K. Tomita, Progress of Theoretical Physics **40**, 264 (1968).

[33] M. A. H. MacCallum and G. F. R. Ellis, Communications in Mathematical Physics **19**, 31 (1970).

[34] G. Ellis, S. Nel, R. Maartens, W. R. Stoeger, and A. P. Whitman, Phys. Rep. **124**, 315 (1985).

[35] C. Pitrou, J.-P. Uzan, and T. S. Pereira, Phys. Rev. D **87**, 043003 (2013), [arXiv:1203.6029].

[36] G. Ellis and M. A. MacCallum, Comm. Math. Phys. **12**, 108 (1969).

[37] L. Bianchi, Soc. Ital. Sci. Mem. Mat. **11**, 267 (1898).

[38] P. Schneider, J. Ehlers, and E. E. Falco, *Gravitational Lenses* (Springer-Verlag Berlin/Heidelberg/New York, 1992).

[39] V. Perlick, Living Reviews in Relativity **7**, 9 (2004).

[40] P. Fleury, H. Dupuy, and J.-P. Uzan, Phys. Rev. D **87**, 123526 (2013), [arXiv:1302.5308].

[41] P. Fleury, H. Dupuy, and J.-P. Uzan, Phys. Rev. Lett. **111**, 091302 (2013), [arXiv:1304.7791].

[42] P. Fleury, JCAP **1406**, 054 (2014), 1402.3123.

[43] C. W. Misner, K. S. Thorne, and J. A. Wheeler, *Gravitation* (San Francisco: W.H. Freeman and Co., 1973).

[44] N. Deruelle and J.-P. Uzan, *Théories de la relativité* (Belin, Paris, 2009).

[45] P. Peter and J.-P. Uzan, *Primordial Cosmology* (Oxford University Press, 2009).

[46] A. Sandage, Astrophys. J. **136**, 319 (1962).

[47] G. C. McVittie, Astrophys. J. **136**, 334 (1962).

[48] L. Pasquini, S. Cristiani, H. Dekker, M. Haehnelt, P. Molaro, F. Pepe, G. Avila, B. Delabre, S. D'Odorico, J. Liske, et al., The Messenger **122**, 10 (2005).

[49] J. Liske, A. Grazian, E. Vanzella, M. Dessauges, M. Viel, et al., Mon. Not. R. Astron. Soc. **386**, 1192 (2008), [arXiv:0802.1532].

[50] J.-P. Uzan, F. Bernardeau, and Y. Mellier, Phys. Rev. D **D77**, 021301 (2008), [arXiv:0711.1950].

[51] J.-P. Uzan, C. Clarkson, and G. F. Ellis, Phys. Rev. Lett. **100**, 191303 (2008), [arXiv:0801.0068].

[52] C. Quercellini, L. Amendola, A. Balbi, P. Cabella, and M. Quartin, Phys. Rep. **521**, 95 (2012), [aXiv:1011.2646].

[53] L. Amendola, O. E. Baelde, W. Valkenburg, and Y. Y. Y. Wong, JCAP **1312**, 042 (2013), [arXiv:1307.2377].

[54] G. Fanizza and F. Nugier (2014), [arXiv:1408.1604].

[55] G. Fanizza, M. Gasperini, G. Marozzi, and G. Veneziano, JCAP **1311**, 019 (2013), [arXiv:1308.4935].

[56] M. Gasperini, G. Marozzi, F. Nugier, and G. Veneziano, JCAP **7**, 008 (2011), 1104.1167.

Sources of anisotropy

A NY anisotropy tends to decay if it is not sourced by matter or anisotropic spatial curvature. In the previous chapter, we have seen in the Bianchi I case that the shear rate tensor σ^i_j of the Hubble flow reads

$$(\sigma^i_j)' + 2\mathcal{H}\sigma^i_j = 8\pi G a^2 \pi^i_j. \tag{9.1}$$

If matter has vanishing anisotropic stress ($\pi^i_j = 0$), then $\sigma^i_j \propto a^{-2}$ rapidly decreases as the Universe expands; such a component is therefore necessary for anisotropy to persist. The simplest possible sources of anisotropy are vector fields, because they naturally possess a preferred direction. Let us illustrate their effect with the example of a single cosmic electromagnetic field $\boldsymbol{A}$, described by Maxwell's theory, in a Bianchi I universe. For homogeneity to be respected, the field must have vanishing Lie derivatives along any vector $\boldsymbol{V}$ tangent to the homogeneity hypersurfaces, $\mathcal{L}_{\boldsymbol{V}}\boldsymbol{A} = \boldsymbol{0}$. In comoving coordinates, it implies simply $\partial_i A_\mu = 0$, so that the field strength of $\boldsymbol{A}$ has no magnetic component (with respect to this coordinate system). Using the expression (1.23) of the stress-energy tensor of the electromagnetic field, we conclude that its conformal anisotropic stress reads

$$\pi^i_j = \frac{1}{4\pi a^2}\left(\frac{E^2}{3}\,\delta^i_j - E^i E_j\right) \tag{9.2}$$

with $E_i = -\partial_t A_i$, and $E^i \equiv \gamma^{ij}E_j$. The gravitational effect of a homogeneous electric field thus consists in decelerating cosmic expansion in the direction of $\boldsymbol{E}$, and accelerating it in the orthogonal directions.

Research on potential sources of anisotropy was recently stimulated by low-multipole anomalies in the CMB temperature map, first reported by WMAP [294–296] and confirmed by *Planck* [297,298]. The independence of both experiments suggests that those anomalies are not due to systematics, but rather are genuine physical features of the CMB. Some of them were interpreted as hints of statistical anisotropy, which could arise either from an anisotropic inflation era [299], or from anisotropic dark energy [273]. Such properties can be obtained (among many other possibilities) by modifying the usual scalar-field paradigm with the addition of a vector field, forming the class of *scalar-vector theories*. The most emblematic example couples the scalar ϕ with the kinetic term of Maxwell's Lagrangian as $g(\phi)F^{\mu\nu}F_{\mu\nu}$, where g is a positive function. It was highlighted in Ref. [300] as a counterexample to the so-called cosmic no-hair theorem. In a quite different context, similar models have been proposed as mechanisms for generating magnetic fields during inflation, giving a primordial origin to the large-scale intergalactic magnetic fields that we observe today [301]. There is however an infinity of ways to couple a scalar with a vector, leading to a huge variety of models which cannot be investigated one by one. The

aim of the article presented in this chapter was to reduce this variety, by excluding the models which do not fulfil the fundamental physical requirements of *stability* (Hamiltonian bounded by below) and *causality* (hyperbolic equations of motion). The work reported here has been performed in collaboration with Juan Pablo Beltrán Almeida, Cyril Pitrou, and Jean-Philippe Uzan.

Its conclusion can be summarised under the form of the following **theorem**. Consider a field theory with one scalar ϕ and one vector $\boldsymbol{A}$. If (a) the fields are minimally coupled to spacetime geometry, and if the associated action (b) contains at most order-one derivatives of $\phi, \boldsymbol{A}$, (c) is gauge invariant, and (d) is at most quadratic in $\boldsymbol{A}$, then the most general form of the action leading to a stable and causal theory is

$$S[\phi, \boldsymbol{A}; \boldsymbol{g}] = \int \mathrm{d}^4 x \sqrt{-g} \left[-\frac{1}{2} f_0(\phi, K) - \frac{1}{4} f_1(\phi) F^{\mu\nu} F_{\mu\nu} - \frac{1}{4} f_2(\phi) F^{\mu\nu} \tilde{F}_{\mu\nu} \right], \qquad (9.3)$$

with $K \equiv (\partial \phi)^2$, $\tilde{F}_{\mu\nu} \equiv \varepsilon_{\mu\nu\rho\sigma} F^{\rho\sigma}/2$, and where the coupling functions $f_{0,1,2}$ obey:

- $\partial f_0 / \partial K \geq 0$;

- $\phi \mapsto f_0(\phi, K \geq 0)$ is bounded by below;

- $f_1 \geq 0$;

- $\partial f_0 / \partial K + 2K \partial^2 f_0 / \partial K^2 \geq 0$.

On the stability and causality of scalar-vector theories

Pierre Fleury,[a,b] **Juan P. Beltrán Almeida,**[c] **Cyril Pitrou,**[a,b]
Jean-Philippe Uzan.[a,b]

[a]Institut d'Astrophysique de Paris, CNRS UMR 7095, Université Pierre & Marie Curie - Paris VI, 98 bis Bd Arago, 75014 Paris, France.
[b]Sorbonne Universités, Institut Lagrange de Paris, 98 bis, Bd Arago, 75014 Paris, France.
[c]Departamento de Física, Universidad Antonio Nariño, Cra 3 Este # 47A-15, Bogotá DC, Colombia.

E-mail: fleury@iap.fr, juanpbeltran@uan.edu.co, pitrou@iap.fr, uzan@iap.fr

Abstract. Various extensions of standard inflationary models have been proposed recently by adding vector fields. Because they are generally motivated by large-scale anomalies, and the possibility of statistical anisotropy of primordial fluctuations, such models require to introduce non-standard couplings between vector fields on the one hand, and either gravity or scalar fields on the other hand. In this article, we study models involving a vector field coupled to a scalar field. We derive restrictive necessary conditions for these models to be both stable (Hamiltonian bounded by below) and causal (hyperbolic equations of motion).

Contents

1 Introduction

Inflationary models including a vector-field sector have been studied following diverse approaches over the past few years. Among the most recent models, a sizable fraction was motivated mainly by the appearance of certain "anomalies" pointed out by observations [1–6], later confirmed by *Planck*'s results [7], which suggested the presence of statistical anisotropies and maybe signals of parity violation in the cosmic microwave background (CMB). Although the statistical significance of these anomalies is still a matter of debate [8, 9] (possible systematic errors, contamination by foregrounds, asymmetric beams, etc.), it is not excluded that they are actually seeded by a source, different than an inflaton scalar field, during the early stages of the Universe. In this context, vector fields arise as suitable, simple and natural candidates to explain the origin of such anomalies as they possess intrinsically a preferred

direction. With these motivations and the requirement to generate both the inflationary dynamics and the presence of a detectable level of statistical anisotropy in the CMB within an unified framework, several models involving vector fields have recently been proposed. Their classical dynamics and statistical properties have thus been explored in great details [10–46] (for reviews see Refs. [47–49]). The determination of cosmological parameters related to the presence of a statistical anisotropy in the CMB can provide valuable information about the mechanisms governing the dynamics of the inflationary Universe, and their possible deviations from the reference single-field model.

In the recent literature, popular models propose to couple scalar and vector fields by modifying the standard kinetic term of the vector as $f(\phi)F^{\mu\nu}F_{\mu\nu}$ [14, 22]; or adding a term of the form $\phi F_{\mu\nu}\tilde{F}^{\mu\nu}$ ($\tilde{F}$ being the Hodge dual of F) which couples vectors and "pseudo scalars" or axions [50–54] (see the review [55] for further references); or variants and generalizations of the above ideas including non-Abelian gauge fields [23, 24, 41, 46, 47]. These models have been proved to be free from instabilities, in particular they do not possess any longitudinal propagating mode; they also have the virtue of generating a non-diluting amount of statistical anisotropy [22, 35] which could leave measurable imprints in the CMB. Note also that such scalar-vector models have been proposed recently [56] to give an inflationary origin to extragalactic magnetic fields [57–59].

Of course, scalar-vector theories offer a very broad set of possibilities, among which the examples mentioned above are somehow the simplest representatives. Apart from Occam's razor, there is a priori no reason to focus on these models specifically, hence one could wonder which subset of all possibilities are worth investigating. This motivates the present article, whose purpose is to identify a class of fundamentally healthy scalar-vector theories, which could then be safely considered candidates for inflationary or dark energy models. More precisely, we focus on theories involving one scalar field and one (gauge-invariant) vector field, both minimally coupled to spacetime geometry, and we study the necessary conditions for such theories to be stable—their Hamiltonian must be bounded by below—and causal—their dynamics must be governed by hyperbolic equations of motion. This method has the advantage of being nonperturbative, and thus more general than only studying the behavior of small perturbations about a given background. The application of the healthy models to cosmology, together with the tests of their compatibility with current observations, are beyond the scope of our analysis and left as future projects.

The article is organized as follows. In Sec. 2, we derive the most general form of a theory involving a scalar field and a gauge-invariant vector field, both minimally coupled to gravity, and propose a reasonable restriction motivated by previous works. The Hamiltonian stability of this theory is analyzed in Sec. 3, and then its causality in Sec. 4. Finally, Sec. 5 is dedicated to a summary of the results, followed by a discussion about possible extensions.

2 Building general scalar-vector models

2.1 General assumptions

Consider, as a starting point, the most conservative theory in which matter is described by the standard model of particle physics, while being minimally coupled to spacetime geometry governed by general relativity. To this theory, we add two new fields, namely a scalar ϕ and a vector A^μ, which for convenience will be referred to as "dark sector", though it can stand for inflationary models as well as for dark energy models (see, e.g., Ref. [60] for a discussion of the different classes of universality of extensions).

The presence of such new fields potentially offers a huge amount of possibilities, depending on how they couple to standard matter, to spacetime geometry, or simply to each other. Among them, many shall lead to unhealthy theories, typically due to instabilities (e.g., ghosts), or violations of causality. Since obviously we cannot analyse all possible theories, we choose to focus on those satisfying the following three conditions.

1. *The fields ϕ, A^μ are uncoupled to standard matter, and minimally coupled to gravity.* In other words, the action of the theory takes the form

$$S = S_{\rm EH}[g_{\mu\nu}] + S_{\rm SM}[\psi_{\rm m}; g_{\mu\nu}] + S_{\rm DS}[\phi, A^\mu; g_{\mu\nu}], \tag{2.1}$$

   where $S_{\rm EH}$ is the Einstein-Hilbert action, $S_{\rm SM}$ the action of the standard model of particle physics, and $S_{\rm DS}$ the action of the dark sector. This assumption ensures (a) the non-violation of the equivalence principle, and (b) the constancy of fundamental constants [61, 62]. Note that for a scalar field alone, non-minimal couplings to spacetime geometry have been actively studied, e.g. in the context of scalar-tensor theories, and now well understood [63, 64]. For a vector field alone, it has been proved that non-minimal coupling generically leads to instabilities [17, 21]. See also Refs. [65, 66] for stability analyses of Horndeski's vector-tensor theory [67] in a cosmological context.

2. *The action only contains at most order-one derivatives of ϕ, A^μ.* This is a sufficient condition to have second-order equations of motion, though not necessary—see for instance Horndeski and Galileon models [68–73].

3. *The action is gauge invariant*[1]. This restriction is essentially chosen for simplicity. The variety of models breaking gauge invariance is indeed extremely broad, even in the absence of scalar fields (see, e.g., Refs. [73, 74]), which would make the analysis performed in the present article much more involved.

The last two asumptions imply that the action of the dark sector reads

$$S_{\rm DS} = \int {\rm d}^4 x \sqrt{-g}\, \mathcal{L}_{\rm DS}(\phi, \partial_\mu \phi, F_{\mu\nu}; g_{\mu\nu}), \tag{2.2}$$

where g is the determinant of spacetime's metric, and $F \equiv {\rm d}A = (F_{\mu\nu}/2)\,{\rm d}x^\mu \wedge {\rm d}x^\nu$, with $F_{\mu\nu} = \partial_\mu A_\nu - \partial_\nu A_\mu$, is the field-strength two-form associated with the vector field. The latter can only appear through F in $\mathcal{L}_{\rm DS}$, since any other type of term (e.g., $A^\mu A_\mu$ or $\partial_\mu A^\mu$) would be gauge dependent, which is excluded by assumption 3.

2.2 A general class of Lagrangians

Let us construct the most general Lagrangian density for the dark sector, under the assumptions formulated above. As a scalar, $\mathcal{L}_{\rm DS}$ can only depend on the scalars that can be constructed from $\phi, \partial_\mu \phi, F_{\mu\nu}$; in principle, their free indices could be contracted with arbitary tensors—standing for parameters of the theory—and lead to terms of the form

$$T^{\alpha_1 \dots \alpha_n \mu_1 \dots \mu_p \nu_1 \dots \nu_p}(\phi)\, \partial_{\alpha_1}\phi \dots \partial_{\alpha_n}\phi F_{\mu_1\nu_1} \dots F_{\mu_p\nu_p}. \tag{2.3}$$

---

[1]In the sense of gauge transformations of the vector field, i.e. $A_\mu \to A_\mu + \partial_\mu \Lambda$, where Λ is an arbitrary scalar function.

However, from a tensorial parameter there generally emerges fundamentally preferred directions in spacetime[2], that we do not wish in the theories considered here. The only nondynamical tensor escaping from this rule is the Levi-Civita tensor $\varepsilon_{\mu\nu\rho\sigma} \equiv -\sqrt{-g}[\mu\nu\rho\sigma]$, where $[\mu\nu\rho\sigma]$ stands for the permutation symbol, with the convention $[0123] = 1$. It turns out that any scalar constructed from ϕ, $\partial_\mu\phi$, $F_{\mu\nu}$, $g_{\mu\nu}$, and $\varepsilon_{\mu\nu\rho\sigma}$ can be written as a function of ϕ,

$$K \equiv \partial_\mu\phi\partial^\mu\phi, \tag{2.4}$$

$$X \equiv F^{\mu\nu}F_{\mu\nu}, \tag{2.5}$$

$$Y \equiv F^{\mu\nu}\tilde{F}_{\mu\nu}, \tag{2.6}$$

$$Z \equiv (\partial_\mu\phi\tilde{F}^{\mu\alpha})(\partial_\nu\phi\tilde{F}^\nu{}_\alpha), \tag{2.7}$$

where $\tilde{F}_{\mu\nu} \equiv \varepsilon_{\mu\nu\rho\sigma}F^{\rho\sigma}/2$ are the components of the Hodge dual $\star F$ of F; so that

$$\mathcal{L}_{\mathrm{DS}}(\phi, K, X, Y, Z). \tag{2.8}$$

Let us prove this assertion. First, it is clear that the Levi-Civita tensor cannot be involved without being contracted with $F_{\mu\nu}$; if both indices of the latter are contracted with the former, then it leads to $\tilde{F}_{\mu\nu}$; if only one index is contracted, then we get

$$\varepsilon_{\mu\nu\rho\sigma}F^{\lambda\sigma} = -\frac{1}{2}\varepsilon_{\mu\nu\rho\sigma}\varepsilon^{\alpha\beta\lambda\sigma}\tilde{F}_{\alpha\beta} \tag{2.9}$$

$$= \frac{1}{2}\delta_\mu^{[\alpha}\delta_\nu^\beta\delta_\rho^{\lambda]}\tilde{F}_{\alpha\beta} \tag{2.10}$$

$$= \tilde{F}_{\mu\nu}\delta_\rho^\lambda + \tilde{F}_{\rho\mu}\delta_\nu^\lambda + \tilde{F}_{\nu\rho}\delta_\mu^\lambda. \tag{2.11}$$

So when the Levi-Civita tensor appears, the associated expression can be rewritten in terms of $\star F$, whence $\mathcal{L}_{\mathrm{DS}}(\phi, \partial_\mu\phi, F_{\mu\nu}, \tilde{F}_{\mu\nu})$. There are two elementary classes of scalars that can be constructed from contractions of $\partial_\mu\phi, F_{\mu\nu}, \tilde{F}_{\mu\nu}$, namely

$$\widehat{F}^\mu{}_{\alpha_1}\widehat{F}^{\alpha_1}{}_{\alpha_2}\ldots\widehat{F}^{\alpha_n}{}_\mu, \qquad \text{or} \qquad \partial_\mu\phi\left(\widehat{F}^\mu{}_{\alpha_1}\widehat{F}^{\alpha_1}{}_{\alpha_2}\ldots\widehat{F}^{\alpha_n}{}_\nu\right)\partial^\nu\phi, \tag{2.12}$$

where $\widehat{F}$ stands either for F or for $\tilde{F}$. Indeed, since $\partial_\mu\phi$ has only one index, it always ends a contraction branch, hence if more than two $\partial_\mu\phi$ are involved in a scalar term, then it can be factorized into chains of the form (2.12). Finally, such $\widehat{F}$-chains can in general be reduced thanks to the identities[3]

$$F^{\mu\alpha}F_{\nu\alpha} - \tilde{F}^{\mu\alpha}\tilde{F}_{\nu\alpha} = \frac{1}{2}X\delta_\nu^\mu, \tag{2.14}$$

$$F^{\mu\alpha}\tilde{F}_{\nu\alpha} = \frac{1}{4}Y\delta_\nu^\mu. \tag{2.15}$$

---

[2]An example can be found in Refs. [75, 76], where the arrow of time emerges from the gradient of a nondynamical scalar within a Riemannian manifold.

[3]These identities can be considered a special case of the following *lemma*: in a four-dimensional manifold, for any two 2-forms $A = (A_{\mu\nu}/2)\mathrm{d}x^\mu \wedge \mathrm{d}x^\nu$ and $B = (B_{\mu\nu}/2)\mathrm{d}x^\mu \wedge \mathrm{d}x^\nu$,

$$A^{\mu\alpha}\tilde{B}_{\nu\alpha} + B^{\mu\alpha}\tilde{A}_{\nu\alpha} = \frac{1}{2}\left(B^{\alpha\beta}\tilde{A}_{\alpha\beta}\right)\delta_\nu^\mu. \tag{2.13}$$

This can be easily derived by using the contraction of two Levi-Civita tensors $\varepsilon_{\mu\nu\rho\sigma}\varepsilon^{\alpha\beta\lambda\sigma} = -\delta_\mu^{[\alpha}\delta_\nu^\beta\delta_\rho^{\lambda]}$.

Indeed, if in a $\widehat{F}$-chain, an F and an $\tilde{F}$ are contiguous, then we can use Eq. (2.15) to factorize the couple. If there are only Fs (or only $\tilde{F}$s) in a chain with strictly more than two $\widehat{F}$s, then we use Eq. (2.14) to create $F\tilde{F}$ pairs, and so on. The only irreducible chain[4] is therefore $F^{\mu\alpha}F_{\nu\alpha}$ (or alternatively $\tilde{F}^{\mu\alpha}\tilde{F}_{\nu\alpha}$), that is, if contracted with the gradient of the scalar field, $\partial_\mu\phi F^{\mu\alpha}F_{\nu\alpha}\partial^\nu\phi$ (or alternatively $\partial_\mu\phi\tilde{F}^{\mu\alpha}\tilde{F}_{\nu\alpha}\partial^\nu\phi = -Z$). In this article, we consider Z instead of the untilded contraction, because it will turn out to be more convenient for presenting the results of Sec. 3.

2.3   A reasonable restriction

In Ref. [21], the authors have analyzed the stability and causality conditions for vector theories whose Lagrangian density is an arbitrary function of F^2 and $F\tilde{F}$, i.e. $\mathcal{L}_{\mathrm{vec}}(X, Y)$. Although general conclusions could not be drawn, it appeared that nonlinear functions of only X, or only Y, are excluded. This motivates our fourth restrictive assumption: *we only consider models which are at most linear in X, Y, and Z, i.e., at most quadratic in the vector field.* Thus, in the remainder of this article, we consider a dark-sector Lagrangian density of the form

$$\mathcal{L}_{\mathrm{DS}} = -\frac{1}{2}f_0(\phi, K) - \frac{1}{4}f_1(\phi, K)X - \frac{1}{4}f_2(\phi, K)Y + \frac{1}{2}f_3(\phi, K)Z, \qquad (2.16)$$

and investigate under which conditions on the four functions $f_{0,1,2,3}$ a model is both stable—Hamiltonian bounded by below—and causal—hyperbolic equations of motion.

Our analysis can also be considered a starting point for more ambitious ones, where some of our four restrictive assumptions would be dropped (see, e.g., appendix B for elements about Lagrangian densities $\mathcal{L}_{\mathrm{DS}}$ which are nonlinear in X, Y, Z).

3   Stability of the models

In this section, we turn to the study of the stability of a dark sector defined by the Lagrangian density (2.16). After having computed the associated Hamiltonian density (Subsec. 3.1), we investigate in details the conditions under which it is bounded by below (Subsec. 3.2), that is necessary for the stability of the quantum theory, and we summarize the results in Subsec. 3.3. In this last subsection, we also discuss why all the results, though derived in Minkowski spacetime, are also completely valid in the presence of gravity.

3.1   Hamiltonian formulation

3.1.1   Canonical momenta

The canonical momentum conjugate to the scalar field ϕ is

$$\pi^\phi \equiv \frac{\partial\mathcal{L}}{\partial\dot{\phi}} = \dot{\phi}\left(\frac{\partial f_0}{\partial K} + \frac{1}{2}\frac{\partial f_1}{\partial K}X + \frac{1}{2}\frac{\partial f_2}{\partial K}Y - \frac{\partial f_3}{\partial K}Z\right) + f_3(\phi, K)\partial_\mu\phi\tilde{F}^{\mu i}\tilde{F}^0{}_i, \qquad (3.1)$$

where an overdot stands for a time derivative $\dot{\phi} \equiv \partial_t\phi$; as usual, greek indices run from 0 to 3, while latin indices run from 1 to 3. The canonical momentum π^ϕ can be expressed in terms of the electric and magnetic parts $\boldsymbol{E}$, $\boldsymbol{B}$ of the field strength tensor, defined by

$$E^i \equiv F^{0i}, \qquad B^i \equiv \tilde{F}^{0i} = \frac{1}{2}\varepsilon^{ijk}F_{jk}, \qquad (3.2)$$

---

[4]The situation changes, however, in the case of non-Abelian gauge fields, since there appear non-zero terms of the form FFF, $FF\tilde{F}$, etc. This will be briefly discussed in Sec. 5.

(we use bold fonts for spatial vectors) as

$$\pi^\phi = \dot{\phi} \left\{ \frac{\partial f_0}{\partial K} + \frac{\partial f_1}{\partial K}(\boldsymbol{B}^2 - \boldsymbol{E}^2) - 2\frac{\partial f_2}{\partial K}\boldsymbol{E} \cdot \boldsymbol{B} + \frac{\partial f_3}{\partial K}\left[(\boldsymbol{B} \cdot \boldsymbol{\nabla}\phi)^2 - (\dot{\phi}\boldsymbol{B} - \boldsymbol{E} \times \boldsymbol{\nabla}\phi)^2\right] \right\}$$
$$+ f_3(\phi, K)\left[\dot{\phi}\boldsymbol{B}^2 + \det(\boldsymbol{\nabla}\phi, \boldsymbol{E}, \boldsymbol{B})\right], \quad (3.3)$$

where $\boldsymbol{\nabla} \equiv (\partial_i)$ is the spatial gradient, an in-line dot and a cross respectively denote the Euclidean scalar product $\boldsymbol{U} \cdot \boldsymbol{V} \equiv \delta_{ij}U^i V^j$ and vector product $(\boldsymbol{U} \times \boldsymbol{V})^k \equiv [ijk]U^i V^j$, and $\det(\boldsymbol{U}, \boldsymbol{V}, \boldsymbol{W}) \equiv (\boldsymbol{U} \times \boldsymbol{V}) \cdot \boldsymbol{W} = [ijk]U^i V^j W^k$ is the 3-dimensional determinant.

The canonical momenta conjugate to the vector field A^μ are

$$\pi^0 \equiv \frac{\partial \mathcal{L}}{\partial \dot{A}_0} = 0 \tag{3.4}$$

$$\pi^i \equiv \frac{\partial \mathcal{L}}{\partial \dot{A}_i} = f_1(\phi, K)F^{i0} + f_2(\phi, K)\tilde{F}^{i0} - f_3(\phi, K)\varepsilon^{ijk}\partial_k\phi\partial_\mu\phi\tilde{F}^\mu{}_j. \tag{3.5}$$

When expressed in terms of the electric and magnetic fields, the latter reads

$$\boldsymbol{\pi} = -f_1(\phi, K)\boldsymbol{E} - f_2(\phi, K)\boldsymbol{B} - f_3(\phi, K)\left[\dot{\phi}\boldsymbol{B} \times \boldsymbol{\nabla}\phi - (\boldsymbol{E} \times \boldsymbol{\nabla}\phi) \times \boldsymbol{\nabla}\phi\right]. \tag{3.6}$$

3.1.2 Constraint on the nondynamical field component

Since the total Lagrangian density $\mathcal{L}$ does not involve any $\dot{A}_0$ term, A_0 is a nondynamical degree of freedom. The associated (Euler-Lagrange) equation of motion,

$$\frac{\partial}{\partial x^\mu}\left[\frac{\partial \mathcal{L}}{\partial(\partial_\mu A_0)}\right] - \frac{\partial \mathcal{L}}{\partial A_0} = 0, \tag{3.7}$$

is therefore a *constraint*. Equation (3.7) can be rewritten using $\partial\mathcal{L}/\partial\dot{A}_0 = 0$ and that $\partial_i A_0$ only appears within terms of the form F_{i0}, thus it always comes with $-\dot{A}_i$. As a consequence

$$\frac{\partial \mathcal{L}}{\partial(\partial_i A_0)} = \frac{\partial \mathcal{L}}{\partial F_{i0}} = -\frac{\partial \mathcal{L}}{\partial \dot{A}_i} = -\pi^i, \tag{3.8}$$

and the constraint reads

$$\boldsymbol{\nabla} \cdot \boldsymbol{\pi} = 0. \tag{3.9}$$

Had we considered terms breaking the gauge invariance in the action, then this constraint would have been altered on its right hand side.

3.1.3 Hamiltonian density

Since the dark sector is decoupled from the other fields, its contribution to the Hamiltonian density is obtained by

$$\mathcal{H}_{\mathrm{DS}} \equiv \pi^\phi \dot{\phi} + \pi^i \dot{A}_i - \mathcal{L}_{\mathrm{DS}}. \tag{3.10}$$

The canonical term $\pi^i \dot{A}_i$ can be rewritten in the following way:

$$\pi^i \dot{A}_i = \pi^i\left(F_{0i} + \partial_i A_0\right) = \pi^i F_{0i} - A_0\partial_i\pi^i + \partial_i\left(A_0\pi^i\right), \tag{3.11}$$

and the spatial divergence $\partial_i\left(A_0\pi^i\right)$ can be dropped, since it would disappear in a boundary term while integrating $\mathcal{H}_{\mathrm{DS}}$ to build the Hamiltonian. Using the constraint (3.9) then yields

$$\pi^i \dot{A}_i = \pi^i F_{0i} = -\boldsymbol{\pi} \cdot \boldsymbol{E}. \tag{3.12}$$

Finally, we inject the expression of the canonical momenta and of the Lagrangian density, and reorganize the various terms to obtain

$$\mathcal{H}_{\mathrm{DS}} = \sum_{a=0}^{3} \mathcal{H}_a \tag{3.13}$$

with

$$\mathcal{H}_0 = \frac{1}{2} f_0(\phi, K) + \frac{\partial f_0}{\partial K} \dot{\phi}^2, \tag{3.14}$$

$$\mathcal{H}_1 = \frac{1}{2} f_1(\phi, K)(\boldsymbol{E}^2 + \boldsymbol{B}^2) + \frac{\partial f_1}{\partial K} \dot{\phi}^2 (\boldsymbol{B}^2 - \boldsymbol{E}^2), \tag{3.15}$$

$$\mathcal{H}_2 = -2 \frac{\partial f_2}{\partial K} \dot{\phi}^2 \boldsymbol{E} \cdot \boldsymbol{B}, \tag{3.16}$$

$$\mathcal{H}_3 = \frac{1}{2} f_3(\phi, K) \left[(\boldsymbol{B} \cdot \boldsymbol{\nabla}\phi)^2 + (\dot{\phi}\boldsymbol{B} - \boldsymbol{E} \times \boldsymbol{\nabla}\phi)^2 \right] + \frac{\partial f_3}{\partial K} \dot{\phi}^2 \left[(\boldsymbol{B} \cdot \boldsymbol{\nabla}\phi)^2 - (\dot{\phi}\boldsymbol{B} - \boldsymbol{E} \times \boldsymbol{\nabla}\phi)^2 \right]. \tag{3.17}$$

In Eq. (3.13), the Hamiltonian density is not expressed in terms of its natural variables, which are π^ϕ, $\boldsymbol{\nabla}\phi$, $\boldsymbol{\pi}$, and $\boldsymbol{\nabla}A^\mu$. Here, we actually *choose* to describe a physical state of the theory using the time derivatives of the fields instead of the canonical momenta. This is perfectly licit, since there exists a one-to-one and onto relation between both descriptions, and this choice will turn out to make the discussions of the following sections easier.

3.2   Hamiltonian stability of the theory

In this subsection, we study the necessary conditions on the functions $f_{0,1,2,3}$ for the Hamiltonian density (3.13) to be bounded by below. Our method relies on proofs by contradiction: given some properties of $f_{0,1,2,3}$, we look for configurations of the fields ϕ, A^μ, such that $\mathcal{H}_{\mathrm{DS}}$ can be made arbitrarily negative. If at least one such state can be exhibited, then the theory is unstable, thus forbidden.

3.2.1   Conditions on f_0

For this paragraph only, and without loss of generality, we consider states for which $\boldsymbol{E} = \boldsymbol{B} = \boldsymbol{0}$, so that the contributions $\mathcal{H}_{1,2,3}$ of the Hamiltonian density do not enter into the discussion. There are two necessary conditions on f_0 for $\mathcal{H}_{\mathrm{DS}}$ to be bounded by below, namely:

$\partial f_0/\partial K \geq 0$. *If there existed a state (ϕ, K) of the scalar field so that $\partial f_0/\partial K < 0$*, then we could take $\dot{\phi}, |\boldsymbol{\nabla}\phi| \to \infty$ while keeping K constant, which would make the Hamiltonian density diverge towards $-\infty$. Such a situation is therefore excluded.

$f_0(\phi, K \geq 0)$ **must be bounded by below.** *If there existed a positive value of K so that $\phi \mapsto f_0(\phi, K)$ was not bounded by below*, then we could set the derivatives of ϕ so that $\dot{\phi} = 0$, hence $\mathcal{H}_{\mathrm{DS}} = f_0/2$, which would not be bounded by below.

Note that the above reasoning does not apply for negative values of K, since the term $\dot{\phi}^2 \partial f_0/\partial K$ can possibly compensate the divergence of f_0. As an example, $f_0(\phi, K) = \phi^2 K$ is clearly not bounded by below for $K < 0$, but its contribution in the Hamiltonian density is

$$\mathcal{H}_0 = \frac{f_0}{2} + \frac{\partial f_0}{\partial K} \dot{\phi}^2 = \frac{\phi^2}{2} \left[\dot{\phi}^2 + (\boldsymbol{\nabla}\phi)^2 \right] \geq 0, \tag{3.18}$$

hence completely admissible.

3.2.2 Conditions on f_3

There are two conditions on f_3 for the Hamiltonian density to be bounded by below:

$\partial f_3 / \partial K = 0$. *If there existed a configuration (ϕ, K) so that this derivative was not zero, then we could always tune $\boldsymbol{E}$, $\boldsymbol{B}$ so that $\partial_K f_3[(\boldsymbol{B} \cdot \boldsymbol{\nabla}\phi)^2 - (\dot{\phi}\boldsymbol{B} - \boldsymbol{E} \times \boldsymbol{\nabla}\phi)^2] < 0$, and take $\dot{\phi}, |\boldsymbol{\nabla}\phi| \to \infty$ (while keeping K constant) which would imply $\mathcal{H}_{\mathrm{DS}} \to -\infty$. This divergence would have no chance to be compensated by the terms $\mathcal{H}_{0,1,2}$, since they are quadratic in the derivatives of ϕ, whereas $\mathcal{H}_3$ is quartic.*

$f_3 \geq 0$. Consider a state for which $\boldsymbol{E} \perp \boldsymbol{B}$ and $\boldsymbol{E}^2 = \boldsymbol{B}^2$, so that both $\mathcal{H}_2$ and the term associated with $\partial f_1 / \partial K$ vanish. Also set, for instance, $\boldsymbol{\nabla}\phi$ parallel to $\boldsymbol{B}$, so that all the terms of $\mathcal{H}_{\mathrm{DS}}$ involving the electric and magnetic fields gather into

$$\left[f_1 + \frac{f_3}{2}(\dot{\phi}^2 + |\boldsymbol{\nabla}\phi|^2) \right] \boldsymbol{B}^2. \tag{3.19}$$

Thus, *if there existed a configuration (ϕ, K) so that $f_3(\phi, K) < 0$, then the prefactor of $\boldsymbol{B}^2$ in Eq. (3.19) could be made strictly negative by taking $\dot{\phi}, |\boldsymbol{\nabla}\phi|$ large enough (while keeping K constant). Finally, $\boldsymbol{B}^2 \to \infty$ would imply $\mathcal{H}_{\mathrm{DS}} \to -\infty$.*

Therefore, we consider $f_3(\phi, K) = f_3(\phi) \geq 0$ from now on.

3.2.3 Conditions on f_1

The conditions on f_1 turn out to be the same as those on f_3, although their proofs are slightly subtler due to the difficulty of controlling the possible compensations between terms.

$\partial f_1 / \partial K = 0$. *If there existed a configuration (ϕ, K) so that $\partial f_1 / \partial K > 0$, then a state with, for example, $\boldsymbol{B} = \boldsymbol{0}$, $\boldsymbol{E}$ parallel to $\boldsymbol{\nabla}\phi$, and $\dot{\phi}, |\boldsymbol{\nabla}\phi| \to \infty$ (while keeping K constant) would make $\mathcal{H}_{\mathrm{DS}} \to -\infty$.*

If there existed a configuration (ϕ, K) so that $\partial f_1 / \partial K < 0$, then we could choose a state where $\boldsymbol{E}$, $\boldsymbol{B}$, $\boldsymbol{\nabla}\phi$ are all orthogonal to each other, and

$$\frac{E}{B} = \frac{f_3\sqrt{1 + K/\dot{\phi}^2}}{f_3(1 + K/\dot{\phi}^2) - 2\partial_K f_1}, \tag{3.20}$$

so that

$$\mathcal{H}_{\mathrm{DS}} = \mathcal{H}_0 + \frac{f_1}{2}(\boldsymbol{E}^2 + \boldsymbol{B}^2) + \underbrace{\frac{f_3 K/(2\dot{\phi}^2) - (\partial_K f_1)^2}{f_3(1 + K/\dot{\phi}^2)/2 - \partial_K f_1}}_{< 0 \text{ for } \dot{\phi} \text{ large enough}} \dot{\phi}^2 \boldsymbol{B}^2; \tag{3.21}$$

in this situation, $\dot{\phi}^2, \boldsymbol{B}^2 \to \infty$ (keeping K constant) would imply $\mathcal{H}_{\mathrm{DS}} \to -\infty$.

$f_1 \geq 0$. Consider a state for which $\dot{\phi}\boldsymbol{B} = \boldsymbol{E} \times \boldsymbol{\nabla}\phi$, so that $\mathcal{H}_2 = \mathcal{H}_3 = 0$. *If there existed a configuration (ϕ, K) so that $f_1(\phi, K) < 0$, then taking $\boldsymbol{E}^2 \to \infty$ or $\boldsymbol{B}^2 \to \infty$ would make $\mathcal{H}_{\mathrm{DS}} \to -\infty$.*

Therefore, we consider $f_1(\phi, K) = f_1(\phi) \geq 0$ from now on.

3.2.4 Condition on f_2

Just as $f_{1,3}$, f_2 cannot depend on K for the theory to be stable. Indeed, *if there existed a configuration (ϕ, K) so that $\partial f_2/\partial K \neq 0$*, then we could consider a state for which $\boldsymbol{E}$, $\boldsymbol{B}$, $\boldsymbol{\nabla}\phi$ are aligned, with $\mathrm{sgn}(\boldsymbol{E}\cdot\boldsymbol{B}) = \mathrm{sgn}(\partial_K f_2)$, and set for instance

$$\frac{E}{B} = \frac{1 + f_3}{2|\partial_K f_2|}. \tag{3.22}$$

In this situation, the Hamiltonian density would become

$$\mathcal{H}_{\mathrm{DS}} = \mathcal{H}_0 + \mathcal{H}_1 - \dot{\phi}^2 \boldsymbol{B}^2 + \frac{f_3 K \boldsymbol{B}^2}{2}, \tag{3.23}$$

so that $\dot{\phi}^2, \boldsymbol{B}^2 \to \infty$, while keeping K constant, would imply $\mathcal{H}_{\mathrm{DS}} \to -\infty$. Hence, we can consider $f_2(\phi, K) = f_2(\phi)$ from now on. Note that, contrary to $f_{1,3}$, there is no restriction on the sign of f_2, since the function itself does not appear in the Hamiltonian.

3.3 Summary and discussion

We have proved that, among the various couplings between the scalar field and the vector fields, many bring uncompensated instabilities in the theory, by making the Hamiltonian unbounded by below. In the framework chosen in this article, the most general Lagrangian density for the dark sector leading to a *stable* theory is

$$\mathcal{L}_{\mathrm{DS}} = -\frac{1}{2}f_0(\phi, K) - \frac{1}{4}f_1(\phi)X - \frac{1}{4}f_2(\phi)Y + \frac{1}{2}f_3(\phi)Z, \tag{3.24}$$

where f_1, f_3 are positive functions, $\phi \mapsto f_0(\phi, K \geq 0)$ is bounded by below, and $\partial f_0/\partial K \geq 0$.

So far, our analysis has been performed on a Minkowski spacetime. Nevertheless, *our conclusions remain valid in the presence of gravity, thanks to the equivalence principle.* Indeed, the divergences underlined in the previous paragraphs are local properties, namely, they regard the Hamiltonian *density* rather than the Hamiltonian itself. Suppose one wishes to perform the same study in an arbitrary spacetime. Then, in the vicinity of any event E, one is free to work in a free-falling frame, where spacetime is locally Minkowskian, and thus where the above calculations are valid (modulo negligible gravitational tidal effects). In other words, in the vicinity of E, one could construct a configuration of the fields so that the Hamiltonian density is arbitrarily negative. Note that this reasoning would not be true if the fields were non-minimally coupled to gravity, or more generally in any scenario where the equivalence principle is not respected.

4 Causality of the models

A field theory is considered causal if it admits an unambiguous notion of time evolution; any initial condition of the fields— i.e., their state on a spacelike hypersurface—must generate a unique final state through the equations of motion. In other words, time evolution must be a well-posed Cauchy problem. This is equivalent to the mathematical statement that the equations of motion must be hyperbolic, that is, whose second-order part involve a differential operator $G^{\mu\nu}\partial_\mu\partial_\nu$ with signature $(-, +, +, +)$, where the $(-)$-direction is timelike with respect to spacetime's metric.

4.1 Equations of motion

Let us first determine the equations of motion induced by the action (3.24). On the one hand, stationarity with respect to variations of the scalar field implies

$$0 = \frac{\delta S}{\delta \phi} = \partial_\mu \left(\frac{\partial f_0}{\partial K} \partial^\mu \phi \right) - f_3 \partial_\mu \left(\tilde{F}^{\mu\rho} \tilde{F}^\nu{}_\rho \partial_\nu \phi \right) - \frac{1}{2} \frac{\partial f_0}{\partial \phi} - \frac{1}{4} f_1' X - \frac{1}{4} f_2' Y + \frac{1}{2} f_3' Z, \quad (4.1)$$

where primes in $f'_{1,2,3}$ denote derivatives with respect to ϕ. On the other hand, stationarity of the action with respect to variations of the vector field implies

$$0 = \frac{\delta S}{\delta A_\sigma} = \partial_\mu \left[f_1 F^{\mu\sigma} + f_2 \tilde{F}^{\mu\sigma} - f_3 \varepsilon^{\alpha\rho\mu\sigma} \partial_\alpha \phi \partial_\beta \phi \tilde{F}^\beta{}_\rho \right]. \quad (4.2)$$

Equations (4.1) and (4.2) form a coupled system of second-order differential equations for ϕ and A^μ, which can be formally written as

$$\underbrace{\begin{bmatrix} \mathcal{D}^\phi_\phi & \mathcal{D}^\phi_{\sigma'} \\ \mathcal{D}^\sigma_\phi & \mathcal{D}^\sigma_{\sigma'} \end{bmatrix}}_{\mathcal{D}} \begin{bmatrix} \phi \\ A^{\sigma'} \end{bmatrix} = \begin{bmatrix} H^\phi(\phi, \partial\phi, \partial A) \\ H^\sigma(\phi, \partial\phi, \partial A) \end{bmatrix}, \quad (4.3)$$

where the first line corresponds to Eq. (4.1) and the second line to Eq. (4.2). The matrix of operators denoted $\mathcal{D}$ contains the second-order part of the equations of motion, while $[H^\phi, H^\sigma]$ contains the remaining part. Explicitly, we have

$$\mathcal{D}^\phi_\phi = \frac{\partial f_0}{\partial K} \Box + \left[2 \frac{\partial^2 f_0}{\partial K^2} \partial^\mu \phi \partial^\nu \phi - f_3(\phi) \tilde{F}^{\mu\rho} \tilde{F}^\nu{}_\rho \right] \partial_\mu \partial_\nu, \quad (4.4)$$

$$\mathcal{D}^\sigma_\phi = \eta^{\sigma\sigma'} \mathcal{D}^\phi_{\sigma'} = -f_3(\phi) \varepsilon^{\alpha\rho\mu\sigma} \partial_\alpha \phi \tilde{F}^\nu{}_\rho \partial_\mu \partial_\nu, \quad (4.5)$$

$$\mathcal{D}^\sigma_{\sigma'} = f_1(\phi) \left(\delta^\sigma_{\sigma'} \Box - \partial^\sigma \partial_{\sigma'} \right) - f_3(\phi) \varepsilon^{\alpha\rho\mu\sigma} \varepsilon^\beta{}_{\rho}{}^\nu{}_{\sigma'} \partial_\alpha \phi \partial_\beta \phi \partial_\mu \partial_\nu. \quad (4.6)$$

where $\Box \equiv \partial^\mu \partial_\mu$ denotes the d'Alembertian.

4.2 Diagonalizing the system of equations of motion

As it appears clearly in the expression (4.5) of $\mathcal{D}$, the presence of f_3 couples the equations of motion of the scalar and vector fields even in their second-order part. As a consequence, we cannot investigate their hyperbolicity independently from each other; instead, we must consider the whole system (4.3), diagonalize[5] it, and study the hyperbolicity of each "eigenequation". In practice, we proceed by diagonalizing the *principal symbol* $\boldsymbol{\sigma}_\mathcal{D}(p_\mu)$ of the system, defined as the matrix-valued polynomial obtained from the principal differential operator $\mathcal{D}$ by replacing ∂_μ with an abstract variable p_μ.

In the expression of $\boldsymbol{\sigma}_\mathcal{D}$, there naturally appear three vectors, namely p^μ, $\partial^\mu \phi$, and $\mathcal{B}^\mu \equiv p_\alpha \tilde{F}^{\alpha\mu}$, from which we can construct an orthonormal tetrad $(e_a)_{a=1...4}$; assuming that p^μ is not null-like, we define indeed

$$e_1^\mu \equiv p^\mu / \sqrt{|p^2|}, \quad (4.7)$$

$$e_2^\mu \equiv \partial^\mu_\perp \phi / \sqrt{|(\partial_\perp \phi)^2|} \qquad \text{with} \qquad \partial^\mu_\perp \phi \equiv \partial^\mu \phi - \frac{(p^\nu \partial_\nu \phi) p^\mu}{p^2}, \quad (4.8)$$

$$e_3^\mu \equiv \mathcal{B}^\mu_\perp / \sqrt{|\mathcal{B}^2_\perp|} \qquad \text{with} \qquad \mathcal{B}^\mu_\perp \equiv \mathcal{B}^\mu - \frac{(\mathcal{B}_\nu \partial^\nu_\perp \phi) \partial^\mu_\perp \phi}{(\partial_\perp \phi)^2}, \quad (4.9)$$

$$e_4^\mu \equiv \varepsilon^{\alpha\beta\gamma\mu} e_{1\alpha} e_{2\beta} e_{3\gamma}. \quad (4.10)$$

---

[5] Concretely, this diagonalization procedure is equivalent to finding new fields, combinations of ϕ and A^μ, whose second-order part of the equations of motion are decoupled.

the orthogonality between e_1^μ and e_3^μ being ensured by the antisymmetry of $\tilde{F}^{\mu\nu}$. Let us use these notations to rewrite the various contractions involved in the symbol $\boldsymbol{\sigma}_\mathcal{D}$,

$$\tilde{F}^{\mu\rho}\tilde{F}^\nu{}_\rho p_\mu p_\nu = \mathcal{B}^2, \tag{4.11}$$

$$\varepsilon^{\alpha\rho\nu}{}_{\sigma'}\partial_\alpha\phi\tilde{F}^\mu{}_\rho p_\mu p_\nu = \sqrt{|p^2(\partial_\perp\phi)^2\mathcal{B}_\perp^2|}\, e_{4\sigma'}, \tag{4.12}$$

$$p^\sigma p_{\sigma'} = \left|p^2\right| e_1^\sigma e_{1\sigma'}, \tag{4.13}$$

$$\varepsilon^{\alpha\rho\mu\sigma}\varepsilon^\beta{}_\rho{}^\nu{}_{\sigma'}\partial_\alpha\phi\partial_\beta\phi p_\mu p_\nu = \left|p^2(\partial_\perp\phi)^2\right|\left(e_4^2 e_3^\sigma e_{3\sigma'} + e_3^2 e_4^\sigma e_{4\sigma'}\right). \tag{4.14}$$

Since the above expressions exhibit projections over the tetrad vectors (such as $e_{1\sigma'}e_1^\sigma$), we expect the symbol to be much simpler if it is written in the tetrad basis[6] (e_4, e_1, e_2, e_3) instead of the coordinate basis $(\partial_\mu)_{\mu=0\ldots3}$; and indeed the result is

$$\boldsymbol{\sigma}_\mathcal{D} = \begin{bmatrix} \sigma_\phi^\phi & \sigma_4^\phi & 0 & 0 & 0 \\ \sigma_\phi^4 & \sigma_4^4 & 0 & 0 & 0 \\ 0 & 0 & 0 & 0 & 0 \\ 0 & 0 & 0 & f_1 p^2 & 0 \\ 0 & 0 & 0 & 0 & f_1 p^2 + f_3(\partial_\perp\phi)^2 p^2 \end{bmatrix}. \tag{4.15}$$

with

$$\sigma_\phi^\phi = \frac{\partial f_0}{\partial K}p^2 + 2\frac{\partial^2 f_0}{\partial K^2}(p^\mu\partial_\mu\phi)^2 - f_3(\phi)\mathcal{B}^2, \tag{4.16}$$

$$\sigma_4^\phi = (e_4)^2\sigma_\phi^4 = -(e_4)^2 f_3(\phi)\sqrt{|p^2(\partial_\perp\phi)^2\mathcal{B}_\perp^2|}, \tag{4.17}$$

$$\sigma_4^4 = f_1(\phi)p^2 + f_3(\phi)(\partial_\perp\phi)^2 p^2. \tag{4.18}$$

The five eigenvalues of $\boldsymbol{\sigma}_\mathcal{D}$ are therefore $\lambda_1 = 0$, $\lambda_2 = f_1 p^2$, $\lambda_3 = f_1 p^2 + f_3(\partial_\perp\phi)^2 p^2$, and the two solutions (λ_0, λ_4) of the second-degree equation $(\sigma_\phi^\phi - \lambda)(\sigma_4^4 - \lambda) = \sigma_4^\phi\sigma_\phi^4$, that is

$$\left[\frac{\partial f_0}{\partial K}p^2 + 2\frac{\partial^2 f_0}{\partial K^2}(p\cdot\partial\phi)^2 - f_3\mathcal{B}^2 - \lambda\right]\left[f_1 p^2 + f_3(\partial_\perp\phi)^2 p^2 - \lambda\right] + f_3^2 p^2(\partial_\perp\phi)^2\mathcal{B}_\perp^2 = 0, \tag{4.19}$$

where we used that $e_1^2 e_2^2 e_3^2 e_4^2 = -1$, since an orthonormal tetrad has only one timelike vector.

If p^μ is null, the construction of the tetrad is slightly different. One can set, e.g., $e_1^\mu = p^\mu$, and $e_2^\mu = \partial^\mu\phi/(p^\nu\partial_\nu\phi) - (\partial\phi)^2 p^\mu/2(p^\nu\partial_\nu\phi)^2$, so that both e_1^μ and e_2^μ are null vectors, and $e_1^\mu e_{2\mu} = 1$. The other two ones, e_3^μ and e_4^μ are defined similarly as before, except that $\mathcal{B}_\perp^\mu$ must be $\mathcal{B}^\mu - (e_2^\nu\mathcal{B}_\nu)p^\mu$. One can check that the expression of the symbol in the basis (e_4, e_1, e_2, e_3) is then the same as in Eq. (4.15) with $p^2 = 0$.

In principle, the second-order differential operators involved in the eigenequations of motion are obtained from the eigenvalues of the principal symbol $\boldsymbol{\sigma}_\mathcal{D}$ by using the correspondance $p_\mu \leftrightarrow \partial_\mu$. This can be directly achieved for $\lambda_{1,2,3}$, yielding the eigenoperators

$$\mathcal{D}_1 = 0, \tag{4.20}$$

$$\mathcal{D}_2 = f_1(\phi)\Box, \tag{4.21}$$

$$\mathcal{D}_3 = [f_1(\phi) + f_3(\phi)K]\Box - f_3(\phi)\partial^\mu\phi\partial^\nu\phi\partial_\mu\partial_\nu. \tag{4.22}$$

---

[6]The odd ordering of the vectors is chosen for the blocks of the matrix (4.15) to appear more clearly.

The fact that one operator is zero is not suprising, because it translates that one of the degrees of freedom of the vector field is non-dynamical. As solutions of Eq. (4.19), the last two eigenvalues of the principal symbol generally involve square roots, and it is unclear how one should interpret them in terms of differential operators. In the case $f_3 = 0$, however, $\boldsymbol{\sigma}_{\mathcal{D}}$ as written in Eq. (4.15) is already diagonal, and the remaining differential operators read

$$\mathcal{D}_0^{[f_3=0]} = \frac{\partial f_0}{\partial K} \Box + 2 \frac{\partial^2 f_0}{\partial K^2} \partial^\mu \phi \partial^\nu \phi \partial_\mu \partial_\nu, \tag{4.23}$$

$$\mathcal{D}_4^{[f_3=0]} = \mathcal{D}_2 = f_1(\phi)\Box. \tag{4.24}$$

4.3 Hyperbolicity of the eigenequations

It turns out that the third eigenoperator $\mathcal{D}_3$ is actually sufficient to rule out the f_3-term. Indeed, consider for instance a state with a purely homogeneous scalar field[7], then

$$\mathcal{D}_3 = f_1(\phi)\Box - f_3(\phi)\dot{\phi}^2\Delta, \tag{4.25}$$

where $\Delta \equiv \partial^i \partial_i$ is the Laplacian. We know from the stability analysis that $f_3 \geq 0$, but if there exists a value of ϕ so that $f_3(\phi) > 0$, then for $\dot{\phi}$ large enough, $\mathcal{D}_3$ becomes elliptical. Therefore, it is *necessary* to have $f_3 = 0$ for the theory to be both stable and causal.

For $f_3 = 0$, the eigenoperators $\mathcal{D}_{1\ldots4}$ are all proportional to $\Box$, which is hyperbolic with a timelike $(-)$-direction, thus the causality requirement does not impose further constraints on f_1. Concerning f_0, additionnally to the condition $\partial f_0/\partial K \geq 0$ imposed by the Hamiltonian stability requirement, we must also have

$$\frac{\partial f_0}{\partial K} + 2K\frac{\partial^2 f_0}{\partial K^2} \geq 0. \tag{4.26}$$

for the eigenoperator $\mathcal{D}_0$ of Eq. (4.23) to be hyperbolic. We propose, in Appendix A, a simple proof of the above condition, which is well known[8] in the context of k-essence [77–81].

5 Conclusion and further remarks

We have derived necessary conditions for the stability and causality of models built from one scalar field and one vector field coupled to each other. Under the restrictions stated in Sec. 2, we showed that the most general action describing a stable vector-scalar dark sector, whose dynamics is ruled by hyperbolic equations of motion, reads

$$S_{\text{DS}} = \int \mathrm{d}^4 x \sqrt{-g}\left[-\frac{1}{2}f_0(\phi, K) - \frac{1}{4}f_1(\phi)F^{\mu\nu}F_{\mu\nu} - \frac{1}{4}f_2(\phi)F^{\mu\nu}\tilde{F}_{\mu\nu}\right], \tag{5.1}$$

with $K \equiv \partial^\mu \phi \partial_\mu \phi$, and where the coupling functions obey:

---

[7]This does not restrict the generality of our discussion. Indeed, just as for the stability analysis, it is sufficient to find one counterexample (here a particular state for which the equations of motion are not hyperbolic) to exclude a theory, provided it is considered fundamental.

[8]Note, by the way, that the discussion about hyperbolicity in one of the first reference article [77] is partially wrong. Indeed, the authors claim that the hyperbolicity conditions are (a) $\partial f_0/\partial K > 0$, and (b) $\partial^2 f_0/\partial K^2 \geq 0$, which is not really the case: (a) is rather imposed by the stability condition, and (b) does not exist at all. They also mention Ineq. (4.26), but as a condition which "assures the stability of the Cauchy problem—that is, small changes in the Cauchy data cannot produce large changes in the solution arbitrarily close to the initial surface".

- $\partial f_0/\partial K \geq 0$, and $f_0(\phi, K \geq 0)$ bounded by below (stability);

- $f_1(\phi) \geq 0$ (stability);

- $\partial f_0/\partial K + 2K\partial^2 f_0/\partial K^2 \geq 0$ (hyperbolicity).

There are no further restrictions over the coupling function f_2. It is remarkable that the class of models satisfying the assumptions of Sec. 2 are so constrained by the basic principles of stability and causality. However, it is worth noting that the theories excluded by our analysis are really ruled out only if one considers them as *fundamental*. If, on the contrary, they represent the effective behavior of a more fundamental but healthy theory, then the only requirement is a reasonable domain of stability and causality. By essence, the present work cannot draw any definite conclusion within the world of such effective theories.

Gauge invariance was a central assumption in our analysis. We shall mention that an important issue with this property in vector-field models was pointed out in Ref. [82], where the authors considered a possible generalization of electromagnetism in Minkowski spacetime, inspired from scalar Galileon theories. Their conclusion came in the form of a "no-go theorem" for generalized vector field Galileons, which states that it is impossible to construct more general theories than standard electromagnetism, because all possible extensions following the Galileon construction procedure lead to topological or boundary terms, and are thus nondynamical. In order to escape this theorem, one can however build models with multicomponent gauge-invariant vector fields, or couple the vector field with another field, e.g., a scalar field as done in this article. The coupling of different types of fields with non-trivial dynamics was addressed earlier in Refs. [71, 83], while Ref. [84] proposed a complete study of scalar Galileons with gauge symmetries.

One may then wonder what models can be built once the condition of gauge invariance is removed. References [73, 74] have recently addressed the problem of gauge-invariance breaking for single-vector-field models, in the spirit of Galileon theories. These analyses conclude that, for some particular combinations of the non-gauge invariant terms, ghost-like instabilities disappear and it is possible to obtain a well-behaved Galileon-type generalization of the Proca theory with three physical propagating degrees of freedom. In general, dropping gauge invariance in a vector-scalar theory leads to a system with more physical degrees of freedom, the dynamics of which can be governed by a huge variety of terms in the action, corresponding to all the possible contractions formed out of $A_\mu, \partial_\mu\phi, \partial_\mu A_\nu$, such as $A^\mu A_\mu$, $A^\mu\partial_\mu\phi$, $\partial^\mu A_\mu$, $A_\mu A_\nu F^{\mu\alpha}F^\nu{}_\alpha$, $A_\mu\partial_\nu\phi F^{\mu\alpha}F^\nu{}_\alpha$, $\partial_\mu A_\nu F^{\mu\alpha}F^\nu{}_\alpha$, etc. Given that the structure of each of these terms is very different, there is a priori no general procedure to deal with all of them together, so that one should probably perform a dedicated analysis of the stability and causality for each model. Nevertheless, we can point out that some particularly interesting terms are often studied, and admit a simple analysis; for instance, vector potentials of the form $V(A^2)$, or couplings of the form $A^\mu\partial_\mu\phi$, $\partial^\mu A_\mu$. A very specific class of models of the form $f(F^2) + V(A^2)$ was recently studied in Ref. [85], and where shown to have hyperbolic equations of motion for some special regions of phase space.

Finally, we should mention that our analysis admits a straightforward generalization to multiple vector fields which are gauge invariant under a non-Abelian gauge group. However, in the non-Abelian case we have an important difference with respect to the U(1) Abelian case. As shown in Subsec. 2.2, in the U(1) case any term of the action involving the vector can always be reduced to even powers of the Faraday tensor or its dual, possibly contracted with the derivatives of the scalar field, which can be further reduced to products of X, Y

and Z. All the odd products of the Faraday tensor and its dual are identically zero. In presence of a non-Abelian gauge group, this is no longer the case, and there appear other combinations which add non-trivial dynamics to the system. Among the lowest order terms, there appear for instance cubic combinations of the form FFF and $FF\tilde{F}$:

$$S_{\text{cubic}} = -\int \mathrm{d}^4 x \sqrt{-g} \left[f(\phi^I) C_{abc} F^{a\mu\rho} F^b_{\ \rho\nu} F^{c\nu}_{\ \ \mu} + g(\phi^I) C_{abc} F^{a\mu\rho} F^b_{\ \rho\nu} \tilde{F}^{c\rho}_{\ \ \nu} \right], \tag{5.2}$$

where C_a^{bc} are the structure constants of the group and a, b, c are Lie algebra indices. These terms are consistent with gauge symmetries and are dynamical. The term FFF appears generically in non-Abelian gauge theories and terms like $FF\tilde{F}$ appear for instance in QCD when discussing CP-violations originated by gluonic operators of dimension six [86]. Recently, the dynamics of such terms was also studied in the context of leptogenesis in non-Abelian gauge fields populated models [87]. Despite of the numerous ways in which the fields can interact when gauge invariance is broken or when non-Abelian gauge groups are considered, it is expected that the stability and the causality analysis would impose constraints over all those possible interactions and it would be interesting and valuable to extend the methods followed here to those cases.

Acknowledgments

A   Hyperbolicity of the scalar sector

Consider the differential operator

$$\left(\frac{\partial f_0}{\partial K} \eta^{\mu\nu} + 2 \frac{\partial^2 f_0}{\partial K^2} \partial^\mu \phi \partial^\nu \phi \right) \partial_\mu \partial_\nu \equiv G^{\mu\nu} \partial_\mu \partial_\nu. \tag{A.1}$$

Its hyperbolicity can be investigated by distiguishing two cases, depending on the sign of K.

1. $K < 0$. Define $n^\mu \equiv -\partial^\mu \phi / \sqrt{-K}$. Since n^μ is a unit timelike vector, we can always find a Lorentz tranformation Λ such that $n^\alpha = \Lambda^\alpha_{\ \mu} n^\mu = \delta^\alpha_0$. Thus, in this new frame ($G^{\alpha\beta} \equiv \Lambda^\alpha_{\ \mu} \Lambda^\beta_{\ \nu} G^{\mu\nu}$), the differential operator reads

$$G^{\alpha\beta} \partial_\alpha \partial_\beta = -\left(\frac{\partial f_0}{\partial K} + 2K \frac{\partial^2 f_0}{\partial K^2} \right) \partial_0^2 + \frac{\partial f_0}{\partial K} \Delta, \tag{A.2}$$

and is therefore hyperbolic if and only if $\partial f_0/\partial K + 2K \partial^2 f_0/\partial K^2 \geq 0$ (additionally to the stability condition $\partial f_0/\partial K \geq 0$).

2. $K > 0$. Define $n^\mu \equiv \partial^\mu \phi / \sqrt{K}$, which is now a unit spacelike vector, thus there exists a Lorentz transformation Λ such that, e.g., $n^\alpha = \Lambda^\alpha{}_\mu n^\mu = \delta_1^\alpha$. In this new frame, the differential operator becomes

$$G^{\alpha\beta}\partial_\alpha\partial_\beta = -\frac{\partial f_0}{\partial K}\partial_0^2 + \left(\frac{\partial f_0}{\partial K} + 2K\frac{\partial^2 f_0}{\partial K^2}\right)\partial_1^2 + \frac{\partial f_0}{\partial K}\Delta_{\mathrm{2D}}, \tag{A.3}$$

and is hyperbolic under the same condition as in the case $K < 0$ above.

3. $K = 0$. This case is slightly less trivial than the previous two ones. Up to a spatial rotation, we can write $\partial^\mu\phi = \dot\phi(-\delta_t^\mu + \delta_1^\mu)$. The differential operator $G^{\mu\nu}\partial_\mu\partial_\nu$ can then be diagonalized using the two vectors

$$\partial_\pm \equiv \frac{f_0''\dot\phi^2\partial_0 - \left[f_0' \pm \sqrt{(f_0')^2 + (f_0''\dot\phi^2)^2}\right]\partial_1}{\sqrt{(f_0''\dot\phi^2)^2 + \left[f_0' \pm \sqrt{(f_0')^2 + (f_0''\dot\phi^2)^2}\right]^2}}, \tag{A.4}$$

where we denoted $f_0' \equiv \partial f_0/\partial K$ for short. Using the basis $(\partial_-, \partial_+, \partial_2, \partial_3)$, the differential operator indeed becomes

$$G^{\alpha\beta}\partial_\alpha\partial_\beta = G^-\partial_-^2 + G^+\partial_+^2 + \Delta_{\mathrm{2D}}, \tag{A.5}$$

with

$$G^- \equiv -f_0''\dot\phi^2 - \sqrt{(f_0')^2 + (f_0''\dot\phi^2)^2} \le 0, \tag{A.6}$$

$$G^+ \equiv -f_0''\dot\phi^2 + \sqrt{(f_0')^2 + (f_0''\dot\phi^2)^2} \ge 0. \tag{A.7}$$

Thus, the differential operator is always hyperbolic. The question is now whether the $(-)$-direction is timelike or spacelike; it is immediate to check that

$$g(\partial_\pm, \partial_\pm) = \frac{\pm 2f_0'\sqrt{(f_0')^2 + (f_0''\dot\phi^2)^2}}{(f_0''\dot\phi^2)^2 + \left[f_0' \pm \sqrt{(f_0')^2 + (f_0''\dot\phi^2)^2}\right]^2}, \tag{A.8}$$

so that ∂_- is timelike (and ∂_+ is spacelike) if and only if $f_0' = \partial f_0/\partial K \ge 0$, which is consistent with the condition found in the previous two cases, for $K = 0$.

B Beyond linearity in X, Y, Z

In this appendix, we provide some results that can be a starting point for the analysis of more general models than the ones described by action (2.16). Namely, consider a dark-sector Lagrangian density $\mathcal{L}_{\mathrm{DS}}(\phi, K, X, Y, Z)$ which is not necessarily linear in $X = F^2$, $Y = F\tilde{F}$, and $Z = (F\partial\phi)^2$. In the following, we drop the 'DS' label to alleviate notation.

B.1 Hamiltonian density

The canonical momenta conjugate to the scalar and vector fields are respectively

$$\pi^\phi = -2\mathcal{L}_{,K}\dot\phi + 2\mathcal{L}_{,Z}\left[\dot\phi\boldsymbol{B}^2 + \det(\boldsymbol{\nabla}\phi, \boldsymbol{E}, \boldsymbol{B})\right], \tag{B.1}$$

$$\boldsymbol{\pi} = 4\mathcal{L}_{,X}\boldsymbol{E} + 4\mathcal{L}_{,Y}\boldsymbol{B} - 2\mathcal{L}_{,Z}\left[\dot\phi\boldsymbol{B}\times\boldsymbol{\nabla}\phi - (\boldsymbol{E}\times\boldsymbol{\nabla}\phi)\times\boldsymbol{\nabla}\phi\right], \tag{B.2}$$

where a coma denotes a derivative. The constraint is unchanged compared to the case where $\mathcal{L}$ is linear in X, Y, Z, namely $\boldsymbol{\nabla} \cdot \boldsymbol{\pi} = 0$. The Hamiltonian density then reads

$$\mathcal{H}_{\mathrm{DS}} = -2\mathcal{L}_{,K}\dot{\phi}^2 - 4\mathcal{L}_{,X}\boldsymbol{E}^2 + Y\mathcal{L}_{,Y} + 2\mathcal{L}_{,Z}(\dot{\phi}\boldsymbol{B} - \boldsymbol{E} \times \boldsymbol{\nabla}\phi)^2 - \mathcal{L}(K, X, Y, Z), \qquad \text{(B.3)}$$

and K, X, Y, and Z are expressed in terms of the fields as

$$K = (\boldsymbol{\nabla}\phi)^2 - \dot{\phi}^2, \qquad \text{(B.4)}$$

$$X = 2(\boldsymbol{B}^2 - \boldsymbol{E}^2), \qquad \text{(B.5)}$$

$$Y = -4\boldsymbol{E} \cdot \boldsymbol{B}, \qquad \text{(B.6)}$$

$$Z = (\dot{\phi}\boldsymbol{B} - \boldsymbol{E} \times \boldsymbol{\nabla}\phi)^2 - (\boldsymbol{B} \cdot \boldsymbol{\nabla}\phi)^2. \qquad \text{(B.7)}$$

It would be tempting to conclude that $\mathcal{L}_{,K}\,\mathcal{L}_{,X} \leq 0$, and $\mathcal{L}_{,Z} \geq 0$ are necessary conditions for $\mathcal{H}_{\mathrm{DS}}$ to be bounded by below, but unfortunately $\dot{\phi}^2$, $\boldsymbol{E}^2$, $(\dot{\phi}\boldsymbol{B} - \boldsymbol{E} \times \boldsymbol{\nabla}\phi)^2$, K, X, Y, Z are not independent variables, so that one cannot take, e.g., $\dot{\phi}^2 \to \infty$ while keeping the others finite. The actual stability conditions could be much subtler, for instance they could involve combinations of the derivatives of $\mathcal{L}$, and thus require a dedicated study.

B.2 Equations of motion

The equations of motion induced by the general Lagrangian (2.8) read

$$0 = \frac{\delta S}{\delta\phi} = \mathcal{L}_{,\phi} - \partial_\mu \left(2\mathcal{L}_{,K}\partial^\mu\phi + 2\mathcal{L}_{,Z}\tilde{F}^{\mu\alpha}\tilde{F}^\nu{}_\alpha\,\partial_\nu\phi\right), \qquad \text{(B.8)}$$

$$0 = \frac{\delta S}{\delta A_\sigma} = -\partial_\mu \left(4\mathcal{L}_{,X}F^{\mu\sigma} + 4\mathcal{L}_{,Y}\tilde{F}^{\mu\sigma} + 2\mathcal{L}_{,Z}\varepsilon^{\beta\gamma\mu\sigma}\partial_\alpha\phi\partial_\beta\phi\tilde{F}^\alpha{}_\gamma\right). \qquad \text{(B.9)}$$

As in Eq. (4.3), we can isolate the second order part of the above system, and write it as the matrix-valued differential operator

$$\boldsymbol{\mathcal{D}} \equiv \begin{bmatrix} \mathcal{D}^\phi_\phi & \mathcal{D}^\phi_{\sigma'} \\ \mathcal{D}^\sigma_\phi & \mathcal{D}^\sigma_{\sigma'} \end{bmatrix}, \qquad \text{(B.10)}$$

where

$$\mathcal{D}^\phi_\phi = \Big(\mathcal{L}_{,K}\eta^{\mu\nu} + \mathcal{L}_{,Z}\tilde{F}^{\mu\rho}\tilde{F}^\nu{}_\rho + 2\mathcal{L}_{,KK}\phi^{,\mu}\phi^{,\nu} + 4\mathcal{L}_{,KZ}\phi^{,\mu}\phi_{,\alpha}\tilde{F}^{\alpha\rho}\tilde{F}^\nu{}_\rho$$
$$+ 2\mathcal{L}_{,ZZ}\phi_{,\alpha}\phi_{,\beta}\tilde{F}^{\mu\rho}\tilde{F}^\alpha{}_\rho\tilde{F}^{\nu\sigma}\tilde{F}^\beta{}_\sigma\Big)\partial_\mu\partial_\nu, \quad \text{(B.11)}$$

$$\mathcal{D}^\sigma_\phi = \eta^{\sigma\sigma'}\mathcal{D}^\phi_{\sigma'} = \Big[\mathcal{L}_{,Z}\varepsilon^{\alpha\rho\mu\sigma}\phi_{,\alpha}\tilde{F}^\nu{}_\rho + 4\phi^{,\mu}\left(\mathcal{L}_{,KX}F^{\nu\sigma} + \mathcal{L}_{,KY}\tilde{F}^{\nu\sigma}\right) + 2\mathcal{L}_{,KZ}\varepsilon^{\alpha\rho\mu\sigma}\phi^{,\nu}\phi_{,\alpha}\phi_{,\beta}\tilde{F}^\beta{}_\rho$$
$$+ 4\phi_{,\alpha}\tilde{F}^{\mu\rho}\tilde{F}^\alpha{}_\rho\left(\mathcal{L}_{,ZX}F^{\nu\sigma} + \mathcal{L}_{,ZY}\tilde{F}^{\nu\sigma}\right) + 2\mathcal{L}_{,ZZ}\varepsilon^{\alpha\rho\mu\sigma}\phi_{,\alpha}\phi_{,\beta}\phi_{,\gamma}\tilde{F}^\beta{}_\rho\tilde{F}^{\nu\lambda}\tilde{F}^\gamma{}_\lambda\Big]\partial_\mu\partial_\nu, \quad \text{(B.12)}$$

$$\mathcal{D}^{\sigma\sigma'} = \Big\{2\mathcal{L}_{,X}\left(\eta^{\mu\nu}\eta^{\sigma\sigma'} - \eta^{\mu\sigma}\eta^{\mu\sigma'}\right) + \mathcal{L}_{,Z}\varepsilon^{\alpha\rho\mu\sigma}\varepsilon^\beta{}_\rho{}^{\nu\sigma'}\phi_{,\alpha}\phi_{,\beta} + 8\mathcal{L}_{,XX}F^{\mu\sigma}F^{\nu\sigma'}$$
$$+ 16\mathcal{L}_{,XY}F^{\mu(\sigma}\tilde{F}^{\nu\sigma')} + 8\mathcal{L}_{,YY}\tilde{F}^{\mu\sigma}\tilde{F}^{\nu\sigma'} + 8\varepsilon^{\alpha\rho\mu(\sigma}\phi_{,\alpha}\phi_{,\beta}\left[\mathcal{L}_{,XZ}F^{\nu\sigma')}F^\beta{}_\rho + \mathcal{L}_{,YZ}F^{\nu\sigma')}\tilde{F}^\beta{}_\rho\right]$$
$$+ 2\mathcal{L}_{,ZZ}\varepsilon^{\alpha\rho\mu\sigma}\varepsilon^{\beta\lambda\nu\sigma'}\phi_{,\alpha}\phi_{,\beta}\phi_{,\gamma}\phi_{,\delta}\tilde{F}^\gamma{}_\rho\tilde{F}^\delta{}_\lambda\Big\}\partial_\mu\partial_\nu, \quad \text{(B.13)}$$

with the symmetrization convention $T^{(\mu\nu)} \equiv (T^{\mu\nu} + T^{\nu\mu})/2$. The above formulae can be used for investigating the hyperbolicity of the equations of motion.

References

[1] N. E. Groeneboom and H. K. Eriksen, *Bayesian analysis of sparse anisotropic universe models and application to the 5-yr WMAP data*, Astrophys.J. **690** (2009) 1807–1819, [`arXiv:0807.2242`].

[2] N. E. Groeneboom, L. Ackerman, I. K. Wehus, and H. K. Eriksen, *Bayesian analysis of an anisotropic universe model: systematics and polarization*, Astrophys.J. **722** (2010) 452–459, [`arXiv:0911.0150`].

[3] D. Hanson and A. Lewis, *Estimators for CMB Statistical Anisotropy*, Phys.Rev. **D80** (2009) 063004, [`arXiv:0908.0963`].

[4] D. Hanson, A. Lewis, and A. Challinor, *Asymmetric Beams and CMB Statistical Anisotropy*, Phys.Rev. **D81** (2010) 103003, [`arXiv:1003.0198`].

[5] **WMAP** Collaboration, C. Bennett et al., *Nine-Year Wilkinson Microwave Anisotropy Probe (WMAP) Observations: Final Maps and Results*, Astrophys.J.Suppl. **208** (2013) 20, [`arXiv:1212.5225`].

[6] **WMAP** Collaboration, G. Hinshaw et al., *Nine-Year Wilkinson Microwave Anisotropy Probe (WMAP) Observations: Cosmological Parameter Results*, Astrophys.J.Suppl. **208** (2013) 19, [`arXiv:1212.5226`].

[7] **Planck** Collaboration, P. Ade et al., *Planck 2013 results. XXIII. Isotropy and statistics of the CMB*, `arXiv:1303.5083`.

[8] J. Kim and E. Komatsu, *Limits on anisotropic inflation from the Planck data*, Phys.Rev. **D88** (2013) 101301, [`arXiv:1310.1605`].

[9] S. R. Ramazanov and G. Rubtsov, *Constraining anisotropic models of the early Universe with WMAP9 data*, Phys.Rev. **D89** (2014) 043517, [`arXiv:1311.3272`].

[10] K. Dimopoulos, *Can a vector field be responsible for the curvature perturbation in the Universe?*, Phys.Rev. **D74** (2006) 083502, [`hep-ph/0607229`].

[11] L. Ackerman, S. M. Carroll, and M. B. Wise, *Imprints of a Primordial Preferred Direction on the Microwave Background*, Phys.Rev. **D75** (2007) 083502, [`astro-ph/0701357`].

[12] A. Golovnev, V. Mukhanov, and V. Vanchurin, *Vector Inflation*, JCAP **0806** (2008) 009, [`arXiv:0802.2068`].

[13] K. Dimopoulos, M. Karciauskas, D. H. Lyth, and Y. Rodriguez, *Statistical anisotropy of the curvature perturbation from vector field perturbations*, JCAP **0905** (2009) 013, [`arXiv:0809.1055`].

[14] S. Yokoyama and J. Soda, *Primordial statistical anisotropy generated at the end of inflation*, JCAP **0808** (2008) 005, [`arXiv:0805.4265`].

[15] B. Himmetoglu, C. R. Contaldi, and M. Peloso, *Instability of anisotropic cosmological solutions supported by vector fields*, Phys.Rev.Lett. **102** (2009) 111301, [`arXiv:0809.2779`].

[16] B. Himmetoglu, C. R. Contaldi, and M. Peloso, *Instability of the ACW model, and problems with massive vectors during inflation*, Phys.Rev. **D79** (2009) 063517, [`arXiv:0812.1231`].

[17] B. Himmetoglu, C. R. Contaldi, and M. Peloso, *Ghost instabilities of cosmological models with vector fields nonminimally coupled to the curvature*, Phys.Rev. **D80** (2009) 123530, [`arXiv:0909.3524`].

[18] M. Karciauskas, K. Dimopoulos, and D. H. Lyth, *Anisotropic non-Gaussianity from vector field perturbations*, Phys.Rev. **D80** (2009) 023509, [`arXiv:0812.0264`].

[19] K. Dimopoulos, M. Karciauskas, and J. M. Wagstaff, *Vector Curvaton with varying Kinetic Function*, Phys.Rev. **D81** (2010) 023522, [`arXiv:0907.1838`].

[20] K. Dimopoulos, M. Karciauskas, and J. M. Wagstaff, *Vector Curvaton without Instabilities*, *Phys.Lett.* **B683** (2010) 298–301, [arXiv:0909.0475].

[21] G. Esposito-Farese, C. Pitrou, and J.-P. Uzan, *Vector theories in cosmology*, *Phys.Rev.* **D81** (2010) 063519, [arXiv:0912.0481].

[22] M.-a. Watanabe, S. Kanno, and J. Soda, *Inflationary Universe with Anisotropic Hair*, *Phys.Rev.Lett.* **102** (2009) 191302, [arXiv:0902.2833].

[23] N. Bartolo, E. Dimastrogiovanni, S. Matarrese, and A. Riotto, *Anisotropic bispectrum of curvature perturbations from primordial non-Abelian vector fields*, *JCAP* **0910** (2009) 015, [arXiv:0906.4944].

[24] N. Bartolo, E. Dimastrogiovanni, S. Matarrese, and A. Riotto, *Anisotropic Trispectrum of Curvature Perturbations Induced by Primordial Non-Abelian Vector Fields*, *JCAP* **0911** (2009) 028, [arXiv:0909.5621].

[25] C. A. Valenzuela-Toledo, Y. Rodriguez, and D. H. Lyth, *Non-gaussianity at tree- and one-loop levels from vector field perturbations*, *Phys.Rev.* **D80** (2009) 103519, [arXiv:0909.4064].

[26] C. A. Valenzuela-Toledo and Y. Rodriguez, *Non-gaussianity from the trispectrum and vector field perturbations*, *Phys.Lett.* **B685** (2010) 120–127, [arXiv:0910.4208].

[27] T. R. Dulaney and M. I. Gresham, *Primordial Power Spectra from Anisotropic Inflation*, *Phys.Rev.* **D81** (2010) 103532, [arXiv:1001.2301].

[28] A. Gumrukcuoglu, B. Himmetoglu, and M. Peloso, *Scalar-Scalar, Scalar-Tensor, and Tensor-Tensor Correlators from Anisotropic Inflation*, *Phys.Rev.* **D81** (2010) 063528, [arXiv:1001.4088].

[29] M.-a. Watanabe, S. Kanno, and J. Soda, *The Nature of Primordial Fluctuations from Anisotropic Inflation*, *Prog.Theor.Phys.* **123** (2010) 1041–1068, [arXiv:1003.0056].

[30] A. Maleknejad and M. Sheikh-Jabbari, *Non-Abelian Gauge Field Inflation*, *Phys.Rev.* **D84** (2011) 043515, [arXiv:1102.1932].

[31] A. Maleknejad, M. Sheikh-Jabbari, and J. Soda, *Gauge-flation and Cosmic No-Hair Conjecture*, *JCAP* **1201** (2012) 016, [arXiv:1109.5573].

[32] A. Maleknejad and M. Sheikh-Jabbari, *Gauge-flation: Inflation From Non-Abelian Gauge Fields*, *Phys.Lett.* **B723** (2013) 224–228, [arXiv:1102.1513].

[33] K. Dimopoulos, *Statistical Anisotropy and the Vector Curvaton Paradigm*, *Int.J.Mod.Phys.* **D21** (2012) 1250023, [arXiv:1107.2779].

[34] C. A. Valenzuela-Toledo, Y. Rodriguez, and J. P. Beltran Almeida, *Feynman-like Rules for Calculating n-Point Correlators of the Primordial Curvature Perturbation*, *JCAP* **1110** (2011) 020, [arXiv:1107.3186].

[35] N. Bartolo, S. Matarrese, M. Peloso, and A. Ricciardone, *The anisotropic power spectrum and bispectrum in the $f(\phi)F^2$ mechanism*, *Phys.Rev.* **D87** (2013) 023504, [arXiv:1210.3257].

[36] Y. Rodriguez, J. P. Beltran Almeida, and C. A. Valenzuela-Toledo, *The different varieties of the Suyama-Yamaguchi consistency relation and its violation as a signal of statistical inhomogeneity*, *JCAP* **1304** (2013) 039, [arXiv:1301.5843].

[37] A. A. Abolhasani, R. Emami, J. T. Firouzjaee, and H. Firouzjahi, *δN formalism in anisotropic inflation and large anisotropic bispectrum and trispectrum* , *JCAP* **1308** (2013) 016, [arXiv:1302.6986].

[38] D. H. Lyth and M. Karciauskas, *The statistically anisotropic curvature perturbation generated by $f(\phi)^2F^2$*, *JCAP* **1305** (2013) 011, [arXiv:1302.7304].

[39] M. Shiraishi, E. Komatsu, M. Peloso, and N. Barnaby, *Signatures of anisotropic sources in the squeezed-limit bispectrum of the cosmic microwave background*, *JCAP* **1305** (2013) 002, [`arXiv:1302.3056`].

[40] R. Namba, E. Dimastrogiovanni, and M. Peloso, *Gauge-flation confronted with Planck*, *JCAP* **1311** (2013) 045, [`arXiv:1308.1366`].

[41] P. Adshead and M. Wyman, *Chromo-Natural Inflation: Natural inflation on a steep potential with classical non-Abelian gauge fields*, *Phys.Rev.Lett.* **108** (2012) 261302, [`arXiv:1202.2366`].

[42] P. Adshead, E. Martinec, and M. Wyman, *Perturbations in Chromo-Natural Inflation*, *JHEP* **1309** (2013) 087, [`arXiv:1305.2930`].

[43] J. Ohashi, J. Soda, and S. Tsujikawa, *Observational signatures of anisotropic inflationary models*, *JCAP* **1312** (2013) 009, [`arXiv:1308.4488`].

[44] R. Namba, *Curvature Perturbations from a Massive Vector Curvaton*, *Phys.Rev.* **D86** (2012) 083518, [`arXiv:1207.5547`].

[45] T. Fujita and S. Yokoyama, *Higher order statistics of curvature perturbations in IFF model and its Planck constraints*, *JCAP* **1309** (2013) 009, [`arXiv:1306.2992`].

[46] K.-i. Maeda and K. Yamamoto, *Stability analysis of inflation with an SU(2) gauge field*, *JCAP* **1312** (2013) 018, [`arXiv:1310.6916`].

[47] E. Dimastrogiovanni, N. Bartolo, S. Matarrese, and A. Riotto, *Non-Gaussianity and Statistical Anisotropy from Vector Field Populated Inflationary Models*, *Adv.Astron.* **2010** (2010) 752670, [`arXiv:1001.4049`].

[48] J. Soda, *Statistical Anisotropy from Anisotropic Inflation*, *Class.Quant.Grav.* **29** (2012) 083001, [`arXiv:1201.6434`].

[49] A. Maleknejad, M. Sheikh-Jabbari, and J. Soda, *Gauge Fields and Inflation*, *Phys.Rept.* **528** (2013) 161–261, [`arXiv:1212.2921`].

[50] M. M. Anber and L. Sorbo, *N-flationary magnetic fields*, *JCAP* **0610** (2006) 018, [`astro-ph/0606534`].

[51] L. Sorbo, *Parity violation in the Cosmic Microwave Background from a pseudoscalar inflaton*, *JCAP* **1106** (2011) 003, [`arXiv:1101.1525`].

[52] F. R. Urban, *Pseudoscalar N-flation and axial coupling revisited*, *Phys.Rev.* **D88** (2013) 063525, [`arXiv:1307.5215`].

[53] K. Dimopoulos and M. Karciauskas, *Parity Violating Statistical Anisotropy*, *JHEP* **1206** (2012) 040, [`arXiv:1203.0230`].

[54] M. Shiraishi, A. Ricciardone, and S. Saga, *Parity violation in the CMB bispectrum by a rolling pseudoscalar*, *JCAP* **1311** (2013) 051, [`arXiv:1308.6769`].

[55] E. Pajer and M. Peloso, *A review of Axion Inflation in the era of Planck*, *Class.Quant.Grav.* **30** (2013) 214002, [`arXiv:1305.3557`].

[56] C. Caprini and L. Sorbo, *Adding helicity to inflationary magnetogenesis*, `arXiv:1407.2809`.

[57] A. Neronov and I. Vovk, *Evidence for Strong Extragalactic Magnetic Fields from Fermi Observations of TeV Blazars*, *Science* **328** (Apr., 2010) 73–, [`arXiv:1006.3504`].

[58] A. M. Taylor, I. Vovk, and A. Neronov, *Extragalactic magnetic fields constraints from simultaneous GeV-TeV observations of blazars*, *A&A* **529** (May, 2011) A144, [`arXiv:1101.0932`].

[59] I. Vovk, A. M. Taylor, D. Semikoz, and A. Neronov, *Fermi/LAT Observations of 1ES 0229+200: Implications for Extragalactic Magnetic Fields and Background Light*, *APJ* **747** (Mar., 2012) L14, [`arXiv:1112.2534`].

[60] J.-P. Uzan, *The acceleration of the universe and the physics behind it*, *Gen.Rel.Grav.* **39** (2007) 307–342, [`astro-ph/0605313`].

[61] J.-P. Uzan, *The Fundamental constants and their variation: Observational status and theoretical motivations*, *Rev.Mod.Phys.* **75** (2003) 403, [`hep-ph/0205340`].

[62] J.-P. Uzan, *Varying Constants, Gravitation and Cosmology*, *Living Rev.Rel.* **14** (2011) 2, [`arXiv:1009.5514`].

[63] T. Damour and G. Esposito-Farese, *Tensor multiscalar theories of gravitation*, *Class.Quant.Grav.* **9** (1992) 2093–2176.

[64] J.-P. Bruneton and G. Esposito-Farese, *Field-theoretical formulations of MOND-like gravity*, *Phys.Rev.* **D76** (2007) 124012, [`arXiv:0705.4043`].

[65] J. D. Barrow, M. Thorsrud, and K. Yamamoto, *Cosmologies in Horndeski's second-order vector-tensor theory*, *JHEP* **1302** (2013) 146, [`arXiv:1211.5403`].

[66] J. B. Jimenez, R. Durrer, L. Heisenberg, and M. Thorsrud, *Stability of Horndeski vector-tensor interactions*, *JCAP* **1310** (2013) 064, [`arXiv:1308.1867`].

[67] G. Horndeski, *Conservation of Charge and the Einstein-Maxwell Field Equations*, *J.Math.Phys.* **17** (1976) 1980–1987.

[68] G. W. Horndeski, *Second-order scalar-tensor field equations in a four-dimensional space*, *Int.J.Theor.Phys.* **10** (1974) 363–384.

[69] A. Nicolis, R. Rattazzi, and E. Trincherini, *The Galileon as a local modification of gravity*, *Phys.Rev.* **D79** (2009) 064036, [`arXiv:0811.2197`].

[70] C. Deffayet, S. Deser, and G. Esposito-Farese, *Generalized Galileons: All scalar models whose curved background extensions maintain second-order field equations and stress-tensors*, *Phys.Rev.* **D80** (2009) 064015, [`arXiv:0906.1967`].

[71] C. Deffayet and D. A. Steer, *A formal introduction to Horndeski and Galileon theories and their generalizations*, *Class.Quant.Grav.* **30** (2013) 214006, [`arXiv:1307.2450`].

[72] J. Khoury, *Les Houches Lectures on Physics Beyond the Standard Model of Cosmology*, `arXiv:1312.2006`.

[73] L. Heisenberg, *Generalization of the Proca Action*, *JCAP* **1405** (2014) 015, [`arXiv:1402.7026`].

[74] G. Tasinato, *Cosmic Acceleration from Abelian Symmetry Breaking*, *JHEP* **1404** (2014) 067, [`arXiv:1402.6450`].

[75] S. Mukohyama and J.-P. Uzan, *From configuration to dynamics: Emergence of Lorentz signature in classical field theory*, *Phys.Rev.* **D87** (2013), no. 6 065020, [`arXiv:1301.1361`].

[76] J. Kehayias, S. Mukohyama, and J.-P. Uzan, *Emergent Lorentz Signature, Fermions, and the Standard Model*, *Phys.Rev.* **D89** (2014) 105017, [`arXiv:1403.0580`].

[77] Y. Aharonov, A. Komar, and L. Susskind, *Superluminal Behavior, Causality, and Instability*, *Physical Review* **182** (June, 1969) 1400–1403.

[78] C. Armendariz-Picon, V. F. Mukhanov, and P. J. Steinhardt, *Essentials of k essence*, *Phys.Rev.* **D63** (2001) 103510, [`astro-ph/0006373`].

[79] A. D. Rendall, *Dynamics of k-essence*, *Class.Quant.Grav.* **23** (2006) 1557–1570, [`gr-qc/0511158`].

[80] J.-P. Bruneton, *Causality and Superluminal Fields*, `hep-th/0612113`.

[81] E. Babichev, V. Mukhanov, and A. Vikman, *k-Essence, superluminal propagation, causality and emergent geometry*, *JHEP* **0802** (2008) 101, [`arXiv:0708.0561`].

[82] C. Deffayet, A. E. Gumrukcuoglu, S. Mukohyama, and Y. Wang, *A no-go theorem for generalized vector Galileons on flat spacetime*, *JHEP* **1404** (2014) 082, [`arXiv:1312.6690`].

[83] C. Deffayet, S. Deser, and G. Esposito-Farese, *Arbitrary p-form Galileons*, *Phys.Rev.* **D82** (2010) 061501, [`arXiv:1007.5278`].

[84] S.-Y. Zhou and E. J. Copeland, *Galileons with Gauge Symmetries*, *Phys.Rev.* **D85** (2012) 065002, [`arXiv:1112.0968`].

[85] A. Golovnev and A. Klementev, *On hyperbolicity violations in cosmological models with vector fields*, *JCAP* **1402** (2014) 033, [`arXiv:1311.0601`].

[86] S. Weinberg, *Larger Higgs Exchange Terms in the Neutron Electric Dipole Moment*, *Phys.Rev.Lett.* **63** (1989) 2333.

[87] A. Maleknejad, *Chiral Gravity Waves and Leptogenesis in Inflationary Models with non-Abelian Gauge Fields*, `arXiv:1401.7628`.

Conclusion

T HIS thesis aimed at providing an extensive picture of light propagation in cosmology, focusing on the potential effects of the small-scale inhomogeneity and large-scale anisotropy. The first issue was motivated by general arguments, such as the Ricci-Weyl paradox, according to which observations involving very narrow beams—such as SNe—are affected by the inhomogeneity of the Universe in a very different way than observations involving much wider beams. Albeit adapted to the latter, the Friedmann-Lemaître geometry should be unable, in principle, to provide an accurate description of the former. In fact, we have deduced from the analysis of Swiss-cheese models in Chap. 6 that the expected effect of small-scale lensing on the interpretation of the Hubble diagram drastically reduces as the cosmological constant increases. In other words, the surprising efficiency of the standard ΛCDM model at consistently fitting all the cosmological data may be due to Λ. If this conclusion turns out to be correct, then it would represent a strong argument in favour of the cosmological constant (or any form of homogeneous dark energy) as driving the recent acceleration of cosmic expansion, and against alternative mechanisms such as backreaction. In the era of precision cosmology, however, Λ shall no longer suffice to ensure the agreement between, e.g., SN and CMB observations. Hints of such a discrepancy are already present in current data, and we have seen that taking the clumpiness of the Universe into account is capable of reducing the resulting tension. In this context, the stochastic lensing approach developed in Chap. 7 arises as a promising framework for dealing with small-scale lensing, in order to interpret SN observations with the accuracy that future surveys will require.

The possibility of a large-scale anisotropy in the Universe has motivations both from the theoretical and observational points of view. May such a scenario be confirmed, the questions of its physical origin and its consequences on light propagation would naturally follow. The present thesis contributed to both sides. In Chap. 8, I solved all the equations of geometric optics in the Bianchi I spacetime, which provides a set of theoretical tools to contrain any late time anisotropy, from the analysis of the Hubble diagram of SNe, or from weak gravitational lensing. Besides, by studying in Chap. 9 the properties of stability and causality of a large class of scalar-vector models, I reduced the landscape of physically viable theories for anisotropic dark energy or inflation.

As always in scientific research, this dissertation raises more questions than it provided answers. Most of the work reported here indeed calls for follow-ups, especially Part. III. Let me mention two of them. First, in Chap. 6, when fitting the Hubble diagram using Swiss-cheese models (or the Kantowski-Dyer-Roeder approximation), all our ignorance about the actual distribution of matter on small scales was hidden in the smoothness parameter f (or α). This parameter is unconstrained by SN data, and was therefore arbitrarily fixed for practical uses. A more satisfactory approach would be to measure it, either directly from numerical simulations, or indirectly via independent observations.

Second, although Chap. 7 established the fundamentals of stochastic lensing, a lot remains to be done: addressing the issue of non-Gaussianity, applying it to the perturbation theory, including the effect of the large-scale structure, etc.

Finally, a few other projects marginally related to the above have called my attention during the last three years. Concerning the fundamentals of gravitational lensing, it seems to me that the range of validity of the infinitesimal beam approximation is not fully understood yet: in which situations the propagation of a light beam can really be described by the geodesic deviation equation? The answer to this question may lead to a better understanding of the transition between the weak and strong lensing regimes, which are currently dealt with using slightly different formalisms. Besides, I am intrigued by the issue of cosmic backreaction. In particular, I am surprised that most of the research activity on this subject has been, so far, dedicated to averaging inhomogeneous cosmologies, while much less was done about the physical consequence of having matter clumps decoupled from cosmic expansion. I intend to address these questions in a near future.

APPENDICES

The equations of Einsteinian gravitation

THIS dissertation extensively exploited the general theory of relativity and the language of differential geometry. The present appendix aims at gathering the main associated definitions and equations. Its title was chosen in the honour of the French mathematician Georges Darmois,[1] referring to his treatise on GR [258].

Contents

---

[1]who turns out to be my great great great grandfather, in the academic sense [302]

A.1   Differential geometry

The general theory of relativity is naturally formulated in the language of differential geometry. Mathematically speaking, spacetime is described by a four-dimensional differential manifold $\mathcal{M}$, i.e. a topological space which is locally homeomorphic to $\mathbb{R}^4$. A homeomorphism $\mathcal{M} \to \mathbb{R}^4$ is called a map, or coordinate system; it associates to each event $E \in \mathcal{M}$ a set of four coordinates $\{x^\mu\}_{\mu=0\ldots3}$.

A.1.1   Vectors, forms, and tensors

Vector fields

Consider a function $f : \mathcal{M} \to \mathbb{R}$. The limit of $[f(x^\mu + \varepsilon u^\mu) - f(x^\mu)]/\varepsilon$ when ε goes to zero defines the derivative of f, at x^μ, in the direction fixed by the four numbers $\{u^\mu\}$. The linear map that associates to any function f such a derivative defines the vector $\boldsymbol{u} : f \mapsto \boldsymbol{u}(f)$. The action of a vector on a product of function satisfies the *Leibnitz rule*

$$\boldsymbol{u}(fg) = \boldsymbol{u}(f)g + f\boldsymbol{u}(g). \tag{A.1}$$

The set of all vectors, i.e. all derivatives, at an event E of $\mathcal{M}$ is called the *tangent space* of $\mathcal{M}$ at E; it is denoted $\mathrm{T}_E\mathcal{M}$. The set of all tangent spaces, $\mathrm{T}\mathcal{M} \equiv \cup_{E\in\mathcal{M}}\mathrm{T}_E\mathcal{M}$, form the *tangent bundle* of $\mathcal{M}$. A section of $\mathrm{T}\mathcal{M}$, i.e. a map $E \in \mathcal{M} \mapsto \boldsymbol{u} \in \mathrm{T}_E\mathcal{M}$, defines a *vector field*. The set of all vector fields along $\mathcal{M}$ is a vector space itself, denoted $\Gamma(\mathcal{M})$.

Any coordinate system $\{x^\mu\}$ naturally defines a basis for $\Gamma(\mathcal{M})$, namely the four partial derivatives $\{\partial/\partial x^\mu\}$, usually denoted $\{\boldsymbol{\partial}_\mu\}$ for short. Any vector field $\boldsymbol{u}$ is then decomposed over this basis as

$$\boldsymbol{u} = u^\mu\boldsymbol{\partial}_\mu. \tag{A.2}$$

Of course, the functions $\{u^\mu\}$ depend on the basis at hand. In particular, if another coordinate system $\{y^\alpha\}$ is chosen, then the components of $\boldsymbol{u}$ over $\{\boldsymbol{\partial}_\alpha\}$ are easily shown to be $u^\alpha = (\partial y^\alpha/\partial x^\mu)u^\mu$.

Lie brackets

Any tangent space $\mathrm{T}_E\mathcal{M}$ enjoys the structure of a Lie algebra, the Lie bracket being simply the commutator between two derivatives. It can indeed be shown that $[\boldsymbol{u}, \boldsymbol{v}] \equiv \boldsymbol{u}\boldsymbol{v} - \boldsymbol{v}\boldsymbol{u}$ is a derivative on $\mathcal{M}$, in the sense that it satisfies the Leibnitz rule. By definition, the Lie bracket also satisfies the Jacobi identity

$$\forall \boldsymbol{u}, \boldsymbol{v}, \boldsymbol{w} \in \Gamma(\mathcal{M}) \qquad [\boldsymbol{u}, [\boldsymbol{v}, \boldsymbol{w}]] + [\boldsymbol{v}, [\boldsymbol{w}, \boldsymbol{u}]] + [\boldsymbol{w}, [\boldsymbol{u}, \boldsymbol{v}]] = \boldsymbol{0}. \tag{A.3}$$

Because of the Schwartz theorem, the commutator of two partial derivatives vanishes $[\boldsymbol{\partial}_\mu, \boldsymbol{\partial}_\nu] = \boldsymbol{0}$. The Lie bracket of any two vector fields $\boldsymbol{u}, \boldsymbol{v}$ thus reads

$$[\boldsymbol{u}, \boldsymbol{v}] = [u^\mu\boldsymbol{\partial}_\mu, v^\nu\boldsymbol{\partial}_\nu] = (u^\mu\partial_\mu v^\nu - v^\mu\partial_\mu u^\nu)\,\boldsymbol{\partial}_\nu. \tag{A.4}$$

Now consider an arbitrary basis $\{\boldsymbol{e}_\mu\}$ of $\Gamma(\mathcal{M})$. Because they are not necessarily associated with a coordinate system, the elements of this basis do not commute with each other in general. Their noncommutativity is quantified by *structure functions* $C^\rho{}_{\mu\nu}$, according to

$$[\boldsymbol{e}_\mu, \boldsymbol{e}_\nu] = C^\rho{}_{\mu\nu}\boldsymbol{e}_\rho. \tag{A.5}$$

If all the structure functions of a basis vanish, the basis is called *holonomous*, and there exists a coordinate system $\{x^\mu\}$ such that $\boldsymbol{e}_\mu = \boldsymbol{\partial}_\mu$. In the opposite case, the basis is said to be anholonomous. For this reason, the structure functions are also called *anholonomies.*

Differential forms

Consider a tangent space $\mathrm{T}_E\mathcal{M}$ of the spacetime manifold. As in any vector space, one can define linear forms, i.e. linear maps $\mathrm{T}_E\mathcal{M} \to \mathcal{R}$. The set of all such linear forms defines the *cotangent space* $\mathrm{T}_E^*\mathcal{M}$ of $\mathcal{M}$ at E, and the set of all cotangent space along $\mathcal{M}$ form its *cotangent bundle* $\mathrm{T}^*\mathcal{M} \equiv \cup_{E\in\mathcal{M}}\mathrm{T}_E\mathcal{M}$. Just like a vector field is a section of $\mathrm{T}\mathcal{M}$, a differential (one-)form is a section of $\mathrm{T}^*\mathcal{M}$, i.e. a map which associate to any event $E \in \mathcal{M}$ a linear form $\boldsymbol{\omega} \in \mathrm{T}_E\mathcal{M}$. The set of all differential one-forms over $\mathcal{M}$, denoted $\Omega^1(\mathcal{M})$, is a vector space.

To a given coordinate system $\{x^\mu\}$ is naturally associated a basis $\{\mathbf{d}x^\mu\}$ of $\Omega^1(\mathcal{M})$. It is defined by the following duality relation

$$\mathbf{d}x^\mu(\boldsymbol{\partial}_\nu) = \delta_\nu^\mu. \tag{A.6}$$

Any one-form $\boldsymbol{\omega}$ is then decomposed as

$$\boldsymbol{\omega} = \omega_\mu \mathbf{d}x^\mu, \qquad \text{with} \qquad \omega_\mu \equiv \boldsymbol{\omega}(\boldsymbol{\partial}_\mu). \tag{A.7}$$

Similarly to the vector case, the functions ω_μ depend on the coordinate system that subtends the basis. If one picks another coordinate system $\{y^\alpha\}$, then the components of $\boldsymbol{\omega}$ over $\{\mathbf{d}y^\alpha\}$ are $\omega_\alpha = (\partial x^\mu/\partial y^\alpha)\omega_\mu$.

Tensors

A means to put together vectors and forms is provided by the *tensor product* $\otimes$. It is a bilinear and associative combination law, such as, for instance

$$\otimes : \begin{array}{l} \Gamma(\mathcal{M}) \times \Gamma(\mathcal{M}) \to \Gamma(\mathcal{M}) \otimes \Gamma(\mathcal{M}) \\ (\boldsymbol{u}, \boldsymbol{v}) \mapsto \boldsymbol{u} \otimes \boldsymbol{v} \end{array} \tag{A.8}$$

where $\Gamma(\mathcal{M})\otimes\Gamma(\mathcal{M})$ is a vector space. The above example defines a particular $(2,0)$-tensor. More generally, a (m,n)-tensor is an element of

$$\mathcal{T}_{m,n}(\mathcal{M}) = \underbrace{\Gamma(\mathcal{M}) \otimes \ldots \otimes \Gamma(\mathcal{M})}_{m \text{ times}} \otimes \underbrace{\Omega^1(\mathcal{M}) \otimes \ldots \otimes \Omega^1(\mathcal{M})}_{n \text{ times}}, \tag{A.9}$$

which is the set of all linear combinations of objects of the form $\boldsymbol{u}_1\otimes\ldots\otimes\boldsymbol{u}_m\otimes\boldsymbol{\omega}_1\otimes\ldots\otimes\boldsymbol{\omega}_n$, where each $\boldsymbol{u}_i$ is a vector field and each $\boldsymbol{\omega}_i$ is a differential one-form on $\mathcal{M}$. The resulting vector space is therefore of dimension 4^{m+n}.

A natural basis for $\mathcal{T}_{m,n}(\mathcal{M})$ is obtained by combining the coordinate bases of $\Gamma(\mathcal{M})$ and $\Omega^1(\mathcal{M})$. Any (m,n)-tensor $\boldsymbol{X}$ is then decomposed as

$$\boldsymbol{X} = X^{\mu_1\ldots\mu_m}{}_{\nu_1\ldots\nu_n} \boldsymbol{\partial}_{\mu_1} \otimes \ldots \otimes \boldsymbol{\partial}_{\mu_m} \otimes \mathbf{d}x^{\nu_1} \otimes \ldots \otimes \mathbf{d}x^{\nu_n}. \tag{A.10}$$

If one decides to change the coordinate system into $\{y^\alpha\}$, then the components of $\boldsymbol{X}$ over the associated basis change as

$$X^{\alpha_1\ldots\alpha_m}{}_{\beta_1\ldots\beta_n} = \frac{\partial y^{\alpha_1}}{\partial x^{\mu_1}} \cdots \frac{\partial y^{\alpha_m}}{\partial x^{\mu_m}} X^{\mu_1\ldots\mu_m}{}_{\nu_1\ldots\nu_n} \frac{\partial x^{\nu_1}}{\partial y^{\beta_1}} \cdots \frac{\partial x^{\nu_n}}{\partial y^{\beta_n}}. \tag{A.11}$$

Lie derivative

We have seen that vector fields can be considered directional derivatives of functions $\mathcal{M} \to \mathbb{R}$. The Lie derivative is an extension of this construction, allowing one to define directional derivatives of vectors, forms, and tensors. Let $\boldsymbol{u}$ be a vector field, the Lie derivative along $\boldsymbol{u}$ is denoted $\mathcal{L}_{\boldsymbol{u}}$. Its action on a function f coincides with the action of $\boldsymbol{u}$, $\mathcal{L}_{\boldsymbol{u}} f \equiv \boldsymbol{u}(f)$. On a vector $\boldsymbol{v} \in \Gamma(\mathcal{M})$, $\mathcal{L}_{\boldsymbol{u}}$ acts as

$$\mathcal{L}_{\boldsymbol{u}} \boldsymbol{v} \equiv [\boldsymbol{u}, \boldsymbol{v}], \tag{A.12}$$

it is thus linear with respect to $\boldsymbol{u}$, and satisfies the Leibnitz rule

$$\mathcal{L}_{\boldsymbol{u}}(f\boldsymbol{v}) = (\mathcal{L}_{\boldsymbol{u}} f)\boldsymbol{v} + f(\mathcal{L}_{\boldsymbol{u}} \boldsymbol{v}). \tag{A.13}$$

The Lie derivative of a one-form $\boldsymbol{\omega} \in \Omega^1(\mathcal{M})$ is another one-form $\mathcal{L}_{\boldsymbol{u}} \boldsymbol{\omega}$ such that

$$\forall \boldsymbol{v} \in \Gamma(\mathcal{M}) \qquad \mathcal{L}_{\boldsymbol{u}}[\boldsymbol{\omega}(\boldsymbol{v})] = (\mathcal{L}_{\boldsymbol{u}} \boldsymbol{\omega})\boldsymbol{v} + \boldsymbol{\omega}[\mathcal{L}_{\boldsymbol{u}}(\boldsymbol{v})], \tag{A.14}$$

which is a kind of Leibnitz rule applied to the contraction of forms and vectors. Its generalisation to tensors is then achieved using the following Leibnitz rule for the tensor product,

$$\mathcal{L}_{\boldsymbol{u}}(\boldsymbol{X} \otimes \boldsymbol{Y}) \equiv (\mathcal{L}_{\boldsymbol{u}} \boldsymbol{X}) \otimes \boldsymbol{Y} + \boldsymbol{X} \otimes (\mathcal{L}_{\boldsymbol{u}} \boldsymbol{Y}), \tag{A.15}$$

for any two tensors $\boldsymbol{X}, \boldsymbol{Y}$. The above relation implies that the Lie derivative of a (m,n)-tensor is a (m,n) tensor.

In terms of components over an arbitrary coordinate basis, we therefore have, for any vector fields $\boldsymbol{u}, \boldsymbol{v}$, one-form $\boldsymbol{\omega}$, and (n,m)-tensor $\boldsymbol{X}$,

$$(\mathcal{L}_{\boldsymbol{u}} \boldsymbol{v})^\mu = u^\nu \partial_\nu v^\mu - v^\nu \partial_\nu u^\mu \tag{A.16}$$

$$(\mathcal{L}_{\boldsymbol{u}} \boldsymbol{\omega})_\mu = u^\nu \partial_\nu \omega_\mu + \omega_\nu \partial_\mu u^\nu \tag{A.17}$$

$$(\mathcal{L}_{\boldsymbol{u}} \boldsymbol{X})^{\mu_1 \ldots \mu_m}{}_{\nu_1 \ldots \nu_n} = u^\rho \partial_\rho X^{\mu_1 \ldots \mu_m}{}_{\nu_1 \ldots \nu_n} - X^{\rho \ldots \mu_m}{}_{\nu_1 \ldots \nu_n} \partial_\rho u^{\mu_1} - \ldots - X^{\mu_1 \ldots \rho}{}_{\nu_1 \ldots \nu_n} \partial_\rho u^{\mu_n}$$
$$+ X^{\mu_1 \ldots \mu_m}{}_{\rho \ldots \nu_n} \partial_{\nu_1} u^\rho + \ldots + X^{\mu_1 \ldots \mu_m}{}_{\nu_1 \ldots \rho} \partial_{\nu_n} u^\rho. \tag{A.18}$$

Note that the parentheses on the left-hand sides of the above relations are often omitted in the literature, so that the components of e.g. $\mathcal{L}_{\boldsymbol{u}} \boldsymbol{v}$ are denoted $\mathcal{L}_{\boldsymbol{u}} v^\mu$.

A.1.2   Linear connections

Covariant derivative

As any vector fibre bundle, $\mathrm{T}\mathcal{M}$ can be equipped with a *linear connection* ∇, which allows vectors of the fibres to be transported and derived along the manifold. Here, since the fibres of $\mathrm{T}\mathcal{M}$ are nothing but the tangent spaces of $\mathcal{M}$, a connection provides a way to take directional derivatives of vectors, forms, and tensors, which differs from the Lie derivative in general.

Let $\boldsymbol{u}$ be a vector field, $\nabla_{\boldsymbol{u}}$ is called the *covariant derivative* along $\boldsymbol{u}$ associated with the connection ∇. Its action on any function f is the same as the Lie derivative, i.e. $\nabla_{\boldsymbol{u}} f \equiv \boldsymbol{u}(f)$, while its effect on vectors is defined by the algebraic properties:

$$\nabla_{\boldsymbol{u}+f\boldsymbol{v}} \boldsymbol{w} = \nabla_{\boldsymbol{u}} \boldsymbol{w} + f \nabla_{\boldsymbol{v}} \boldsymbol{w}, \tag{A.19}$$

$$\nabla_{\boldsymbol{u}}(\boldsymbol{v} + \boldsymbol{w}) = \nabla_{\boldsymbol{u}} \boldsymbol{v} + \nabla_{\boldsymbol{u}} \boldsymbol{w}, \tag{A.20}$$

$$\nabla_{\boldsymbol{u}}(f\boldsymbol{v}) = \boldsymbol{u}(f) + \nabla_{\boldsymbol{u}} \boldsymbol{v}. \tag{A.21}$$

Note that, so far, $\nabla_{\boldsymbol{u}}$ has the same properties as $\mathcal{L}_{\boldsymbol{u}}$, but while the Lie derivative of $\boldsymbol{\partial}_\nu$ along $\boldsymbol{\partial}_\nu$ vanishes by definition, since $\mathcal{L}_{\boldsymbol{\partial}_\mu}\boldsymbol{\partial}_\nu \equiv [\boldsymbol{\partial}_\mu, \boldsymbol{\partial}_\nu] = 0$, its covariant counterpart does not in general. In fact, a linear connection is characterised by its specific action on a basis of $\Gamma(\mathcal{M})$, as

$$\nabla_{\boldsymbol{\partial}_\mu}\boldsymbol{\partial}_\nu \equiv \nabla_\mu \boldsymbol{\partial}_\nu = \Gamma^\rho{}_{\nu\mu}\boldsymbol{\partial}_\rho, \tag{A.22}$$

where $\Gamma^\rho{}_{\nu\mu}$ are called the *connection coefficients*. There exist as many different connections as there are such coefficients. Hence the Lie derivative can be considered a special case of covariant derivative, associated with the trivial connection whose coefficients vanish. Note also that ∇, if considered a map $\Gamma(\mathcal{M})^2 \to \Gamma(\mathcal{M})$, is not a tensor, because is is not perfectly linear with respect to its second argument, as shown by Eq. (A.21). As a consequence, the $\Gamma^\rho{}_{\nu\mu}$ do not change according to Eq. (A.11) under coordinate transformations.

The covariant derivative of any vector $\boldsymbol{u}$ along a basis vector $\boldsymbol{\partial}_\mu$ can be written in terms of the connection coefficients as

$$\nabla_\mu \boldsymbol{u} = \nabla_\mu(u^\nu \boldsymbol{\partial}_\nu) = (\partial_\mu u^\nu)\boldsymbol{\partial}_\nu + \Gamma^\rho{}_{\nu\mu}u^\nu \boldsymbol{\partial}_\rho \tag{A.23}$$

whose components, with the short-hand notation $\nabla_\mu u^\nu \equiv (\nabla_\mu \boldsymbol{u})^\nu$ thus read

$$\nabla_\mu u^\nu = \partial_\mu u^\nu + \Gamma^\nu{}_{\rho\mu}u^\rho. \tag{A.24}$$

Extension to forms and tensors

Covariant derivatives can be extended to act on forms an tensors according to the same rules as the Lie derivatives, that is, assuming a Leibnitz-like rule with respect to both the contraction of forms with vectors, and the tensor product: for any vectors $\boldsymbol{u}, \boldsymbol{v}$, one-form $\boldsymbol{\omega}$, and tensors $\boldsymbol{X}, \boldsymbol{Y}$, we consider

$$\nabla_{\boldsymbol{u}}[\boldsymbol{\omega}(\boldsymbol{v})] = (\nabla_{\boldsymbol{u}}\boldsymbol{\omega})(\boldsymbol{v}) + \boldsymbol{\omega}(\nabla_{\boldsymbol{u}}\boldsymbol{v}), \tag{A.25}$$

$$\nabla_{\boldsymbol{u}}(\boldsymbol{X} \otimes \boldsymbol{Y}) = (\nabla_{\boldsymbol{u}}\boldsymbol{X}) \otimes \boldsymbol{Y} + \boldsymbol{X} \otimes (\nabla_{\boldsymbol{u}}\boldsymbol{Y}). \tag{A.26}$$

The covariant derivative of a (m, n)-tensor is thus also (m, n)-tensor. In terms of components, Eq. (A.25) implies

$$\nabla_\mu \omega_\nu \equiv (\nabla_\mu \boldsymbol{\omega})_\nu = \partial_\mu \omega_\nu - \Gamma^\rho{}_{\nu\mu}\omega_\rho, \tag{A.27}$$

and Eq. (A.26) leads to

$$\nabla_\rho X^{\mu_1...\mu_n}{}_{\nu_1...\nu_m} \equiv (\nabla_\rho \boldsymbol{X})^{\mu_1...\mu_n}{}_{\nu_1...\nu_m} \tag{A.28}$$

$$= \partial_\rho X^{\mu_1...\mu_n}{}_{\nu_1...\nu_m} + \Gamma^{\mu_1}{}_{\sigma\rho}X^{\sigma...\mu_n}{}_{\nu_1...\nu_m} + \ldots + \Gamma^{\mu_n}{}_{\sigma\rho}X^{\mu_1...\sigma}{}_{\nu_1...\nu_m}$$

$$- \Gamma^\sigma{}_{\nu_1\rho}X^{\mu_1...\mu_n}{}_{\sigma...\nu_m} - \ldots - \Gamma^\sigma{}_{\nu_m\rho}X^{\mu_1...\mu_n}{}_{\nu_1...\sigma}. \tag{A.29}$$

Parallel transport and geodesics

Let γ be a curve traced on $\mathcal{M}$. We parametrise γ with $\lambda \in [0, 1]$, so that $\boldsymbol{t} \equiv \mathrm{d}/\mathrm{d}\lambda = (\mathrm{d}x^\mu/\mathrm{d}\lambda)\boldsymbol{\partial}_\mu$ is a *tangent vector* of γ. A tensor $\boldsymbol{X}$ is said to be *parallely transported* along γ iff its covariant derivative with respect to $\boldsymbol{t}$ vanishes all along γ,

$$\nabla_{\boldsymbol{t}}\boldsymbol{X} = \boldsymbol{0}. \tag{A.30}$$

The curve γ is a *geodesic* iff its tangent vector is parallely transported along itself, $\nabla_{\boldsymbol{t}}\boldsymbol{t} = \boldsymbol{0}$. In terms of components, this requirement is equivalent to

$$\frac{\mathrm{d}^2 x^\rho}{\mathrm{d}\lambda^2} + \Gamma^\rho{}_{\mu\nu}\frac{\mathrm{d}x^\mu}{\mathrm{d}\lambda}\frac{\mathrm{d}x^\nu}{\mathrm{d}\lambda} = 0, \tag{A.31}$$

which is called the geodesic equation.

Torsion

Any linear connection ∇ defines two fundamental tensors which characterise its geometrical properties. The first one, called *torsion* $\boldsymbol{T}$, encodes the tendency of parallelograms constructed by parallely transporting vectors not to close (see Ref. [303] for more details). It is an antisymmetric $(1,2)$-tensor defined as

$$\boldsymbol{T}(\boldsymbol{u}, \boldsymbol{v}) \equiv \nabla_{\boldsymbol{u}}\boldsymbol{v} - \nabla_{\boldsymbol{v}}\boldsymbol{u} - [\boldsymbol{u}, \boldsymbol{v}]. \tag{A.32}$$

Its components over a coordinate basis are defined as $\boldsymbol{T}(\boldsymbol{\partial}_\mu, \boldsymbol{\partial}_\nu) = T^\rho{}_{\mu\nu}\boldsymbol{\partial}_\rho$ and read

$$T^\rho{}_{\mu\nu} = 2\Gamma^\rho{}_{[\mu\nu]}. \tag{A.33}$$

Hence the torsion of a connection represents the antisymmetric part of its coefficients. Note that, as a consequence, torsion has no effect on geodesics.

Curvature

The second fundamental tensor associated with a connection is its *curvature* $\boldsymbol{R}$, which quantifies the tendency of vectors to rotate after being parallely transported along a loop. It is a $(1,3)$-tensor defined as

$$\boldsymbol{R}(\boldsymbol{u}, \boldsymbol{v})\boldsymbol{w} \equiv \nabla_{\boldsymbol{u}}\nabla_{\boldsymbol{v}}\boldsymbol{w} - \nabla_{\boldsymbol{v}}\nabla_{\boldsymbol{u}}\boldsymbol{w} - \nabla_{[\boldsymbol{u},\boldsymbol{v}]}\boldsymbol{w}. \tag{A.34}$$

Its components over a coordinate basis are defined as $\boldsymbol{R}(\boldsymbol{\partial}_\mu, \boldsymbol{\partial}_\nu)\boldsymbol{\partial}_\rho = R^\sigma{}_{\rho\mu\nu}\boldsymbol{\partial}_\sigma$ and read

$$R^\sigma{}_{\rho\mu\nu} = \partial_\mu\Gamma^\sigma{}_{\rho\nu} - \partial_\nu\Gamma^\sigma{}_{\rho\mu} + \Gamma^\sigma{}_{\tau\mu}\Gamma^\tau{}_{\rho\nu} - \Gamma^\sigma{}_{\tau\nu}\Gamma^\tau{}_{\rho\mu} \tag{A.35}$$

Bianchi identity

The Jacobi identity for the commutator has been given in Eq. (A.3) for three vector fields, but it is actually valid for any three objects which can be 'multiplied' together, including when the underlying product is noncommutative. In particular, it can be applied to the covariant derivatives along three arbitrary vector fields:

$$[\nabla_{\boldsymbol{u}}, [\nabla_{\boldsymbol{v}}, \nabla_{\boldsymbol{w}}]] + [\nabla_{\boldsymbol{v}}, [\nabla_{\boldsymbol{w}}, \nabla_{\boldsymbol{u}}]] + [\nabla_{\boldsymbol{w}}, [\nabla_{\boldsymbol{u}}, \nabla_{\boldsymbol{v}}]] = \boldsymbol{0}. \tag{A.36}$$

When applied to a coordinate basis, the above equation yields

$$[\nabla_\mu, \boldsymbol{R}(\boldsymbol{\partial}_\nu, \boldsymbol{\partial}_\rho)] + [\nabla_\nu, \boldsymbol{R}(\boldsymbol{\partial}_\rho, \boldsymbol{\partial}_\sigma)] + [\nabla_\rho, \boldsymbol{R}(\boldsymbol{\partial}_\mu, \boldsymbol{\partial}_\nu)] = \boldsymbol{0}, \tag{A.37}$$

which will turn out to be useful in general relativity.

A.1.3   Pseudo-Riemannian geometry

Metric

Let us now introduce an additional structure on $\mathcal{M}$, namely the *metric* $\boldsymbol{g}$. It is defined as a $(0,2)$-tensor which provides a notion of scalar product between two vectors,

$$\boldsymbol{g} : \begin{array}{l} \Gamma(\mathcal{M})^2 \to \mathbb{R} \\ (\boldsymbol{u}, \boldsymbol{v}) \mapsto \boldsymbol{g}(\boldsymbol{u}, \boldsymbol{v}) = \boldsymbol{u} \cdot \boldsymbol{v} \end{array}' \tag{A.38}$$

which is clearly symmetric. In Riemannian geometry, $\boldsymbol{g}$ is positive-definite; in pseudo-Riemannian geometry, this latter assumption is relaxed: there exist nonzero vectors $\boldsymbol{u}$ whose scalar square $\boldsymbol{g}(\boldsymbol{u}, \boldsymbol{u})$ can be zero or even negative. The *signature* of the metric is defined as the signs of the eigenvalues of $[g_{\mu\nu}]$ seen as a matrix.

In GR, there is one eigendirection in spacetime whose associated eigenvalue has a sign opposite to the others, defining the direction of time. In this thesis, we have adopted the conventional signature $(-+++)$, which means that time is associated with a negative eigenvalue of the metric. A nonzero vector $\boldsymbol{u}$ so that $\boldsymbol{g}(\boldsymbol{u}, \boldsymbol{u}) < 0, = 0, > 0$ is then said to be respectively timelike, null, or spacelike.

Dualities and inverse metric

The metric provides a natural duality between vector fields and one-forms. Indeed, given a vector field $\boldsymbol{u}$ there exists a unique one-form $\boldsymbol{\eta_u} \equiv \boldsymbol{g}(\boldsymbol{u}, \cdot)$, which is simply "do the scalar product with $\boldsymbol{u}$". Because this relation is one-to-one and onto between $\Gamma(\mathcal{M})$ and $\Gamma^*(\mathcal{M})$, to any form $\boldsymbol{\omega}$ is conversely associated a vector field $\boldsymbol{e^\omega}$, according to $\boldsymbol{\omega} = \boldsymbol{g}(\boldsymbol{e^\omega}, \cdot)$.

The component of $\boldsymbol{\eta_u}$ over $\mathrm{d}x^\mu$ is by definition $\boldsymbol{\eta_u}(\boldsymbol{\partial}_\mu) = g_{\mu\nu}u^\nu$. This quantity is usually denoted u_μ, in order to emphasize the duality, so that $\boldsymbol{\eta_u} = u_\mu \mathrm{d}x^\mu$. In terms of such notations, the metric tensor can be seen as a machine to lower indices. Now, because the duality procedure also allows us to turn forms into vectors, there should be a quantity which on the contrary raises indices, i.e. such that $(\boldsymbol{e^\omega})^\mu \equiv \omega^\mu = g^{\mu\nu}\omega_\nu$. The coefficients $g^{\mu\nu}$ can be expressed as functions of $g_{\mu\nu}$ by imposing that the 'vectorisation' of a one-form is the inverse of the 'one-formisation' of a vector; in other words
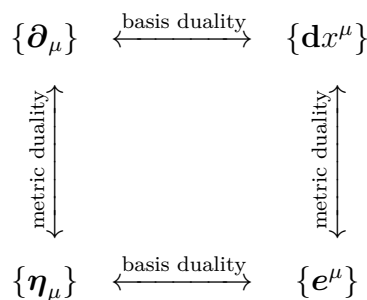
$$\forall \boldsymbol{u} \in \Gamma(\mathcal{M}) \quad \boldsymbol{e^{\eta_u}} = \boldsymbol{u}, \qquad \text{which implies} \qquad g_{\mu\rho}\, g^{\rho\nu} = \delta_\mu^\nu. \tag{A.39}$$

If $g_{\mu\nu}$ and $g^{\mu\nu}$ are seen as the coefficients of two matrices, then the above means that those matrices are inverse to each other. For that reason, the $(2,0)$-tensor $g^{\mu\nu}\boldsymbol{\partial}_\mu \otimes \boldsymbol{\partial}_\nu$ is known as the *inverse metric*.

It is interesting to note that this notion of duality provided by the metric is different from the duality between bases $\{\boldsymbol{\partial}_\mu\}$ and $\{\mathrm{d}x^\mu\}$ mentioned previously. One can indeed define four one-forms $\boldsymbol{\eta}_\mu \equiv \boldsymbol{\eta}_{\boldsymbol{\partial}_\mu} = g_{\mu\nu}\mathrm{d}x^\nu \neq \mathrm{d}x^\mu$. The set $\{\boldsymbol{\eta}^\mu\}$ is called metric-dual to $\{\boldsymbol{\partial}_\mu\}$, while $\{\mathrm{d}x^\mu\}$ is basis-dual to $\{\boldsymbol{\partial}_\mu\}$. Similarly, from the inverse metric we can generate the vector fields $\boldsymbol{e}^\mu \equiv \boldsymbol{e}^{\mathrm{d}x^\mu} = g^{\mu\nu}\boldsymbol{\partial}_\nu \neq \boldsymbol{\partial}_\mu$ which are metric-dual to $\{\mathrm{d}x^\mu\}$. The definition of the inverse metric implies that the sets $\{\boldsymbol{\eta}_\mu\}$ and $\{\boldsymbol{e}^\mu\}$ are basis-dual to each other,

$$\boldsymbol{\eta}_\mu(\boldsymbol{e}^\nu) = g_{\mu\rho}\mathrm{d}x^\rho\left(g^{\nu\sigma}\boldsymbol{\partial}_\sigma\right) = g_{\mu\rho}g^{\nu\sigma}\mathrm{d}x^\rho(\boldsymbol{\partial}_\sigma) = g_{\mu\rho}g^{\nu\rho} = \delta_\mu^\nu. \tag{A.40}$$

This duality scheme can be summarised on the following diagram:

$$
\begin{array}{ccc}
\{\boldsymbol{\partial}_\mu\} & \xleftrightarrow{\text{basis duality}} & \{\mathrm{d}x^\mu\} \\[2pt]
\updownarrow{\scriptstyle\text{metric duality}} & & \updownarrow{\scriptstyle\text{metric duality}} \\[2pt]
\{\boldsymbol{\eta}_\mu\} & \xleftrightarrow{\text{basis duality}} & \{\boldsymbol{e}^\mu\}
\end{array}
$$

Levi-Civita connection

Once a manifold is equipped with both a metric and a connection, one can impose a condition of compatibility between those two structures, that is, roughly speaking, a Leibnitz rule for covariant derivatives with respect to scalar products,

$$\nabla_{\boldsymbol{w}}\left[\boldsymbol{g}(\boldsymbol{u},\boldsymbol{v})\right] = \boldsymbol{g}(\nabla_{\boldsymbol{w}}\boldsymbol{u},\boldsymbol{v}) + \boldsymbol{g}(\boldsymbol{u},\nabla_{\boldsymbol{w}}\boldsymbol{v}) \tag{A.41}$$

for any three vector fields $\boldsymbol{u}, \boldsymbol{v}, \boldsymbol{w}$. Note that the above condition is equivalent to

$$\nabla_{\boldsymbol{u}}\boldsymbol{g} = \boldsymbol{0}. \tag{A.42}$$

Thus, a connection which is compatible with the metric is also said to be *metric preserving.*

Metric-preserving connections have the interesting property that they are entirely and uniquely determined by their torsion [304]. A particular case is the one of zero torsion, which defines the *Levi-Civita connection.* It is the connection of GR. Its coefficients are known as the *Christoffel symbols*, and can be expressed as functions of the metric as

$$\Gamma^{\rho}{}_{\mu\nu} \equiv g^{\rho\sigma}\Gamma_{\sigma\mu\nu}, \qquad \text{with} \qquad \Gamma_{\sigma\mu\nu} \equiv \frac{1}{2}\left(\partial_{\mu}g_{\nu\sigma} + \partial_{\nu}g_{\mu\sigma} - \partial_{\sigma}g_{\mu\nu}\right). \tag{A.43}$$

Riemann tensor

The curvature of the Levi-Civita connection is called the *Riemann tensor.* Its components can be expressed in terms of the metric as

$$R_{\sigma\rho\mu\nu} \equiv \boldsymbol{g}\left[\boldsymbol{\partial}_{\sigma}, \boldsymbol{R}(\boldsymbol{\partial}_{\mu},\boldsymbol{\partial}_{\nu})\boldsymbol{\partial}_{\rho}\right] \tag{A.44}$$

$$= \boldsymbol{g}\left[\boldsymbol{\partial}_{\sigma}, 2\nabla_{[\mu}\nabla_{\nu]}\boldsymbol{\partial}_{\rho}\right] \qquad \text{by definition (A.34) of } \boldsymbol{R} \tag{A.45}$$

$$= 2\boldsymbol{\partial}_{[\mu}\boldsymbol{g}(\boldsymbol{\partial}_{\sigma},\nabla_{\nu]}\boldsymbol{\partial}_{\rho}) - 2\boldsymbol{g}(\nabla_{[\mu}\boldsymbol{\partial}_{\sigma},\nabla_{\nu]}\boldsymbol{\partial}_{\rho}) \qquad \text{by metric preservation} \tag{A.46}$$

$$= 2\Gamma_{\sigma\rho[\nu,\mu]} - 2\Gamma_{\tau\sigma[\mu}\Gamma^{\tau}{}_{\nu]\rho} \qquad \text{with } \Gamma_{\sigma\rho\nu,\mu} \equiv \partial_{\mu}\Gamma_{\sigma\rho\nu} \tag{A.47}$$

$$= \frac{1}{2}\left(g_{\sigma\nu,\mu\rho} - g_{\rho\nu,\mu\sigma}\right) - \frac{1}{4}g^{\tau\omega}\left(g_{\tau\sigma,\mu} + g_{\tau\mu,\sigma} - g_{\sigma\mu,\tau}\right)\left(g_{\omega\nu,\rho} + g_{\omega\rho,\nu} - g_{\nu\rho,\omega}\right)$$
$$- (\mu \leftrightarrow \nu) \qquad \text{from Eq. (A.43).} \tag{A.48}$$

The components of the Riemann tensor enjoy a number of symmetries summarised below:

$$R_{\mu\nu\rho\sigma} = -R_{\mu\nu\sigma\rho} \tag{A.49}$$

$$R_{\mu\nu\rho\sigma} = -R_{\nu\mu\rho\sigma}, \tag{A.50}$$

$$R_{\mu[\nu\rho\sigma]} = 0, \tag{A.51}$$

$$R_{\mu\nu\rho\sigma} = R_{\rho\sigma\mu\nu}, \tag{A.52}$$

$$R_{\mu\nu[\rho\sigma;\tau]} = 0, \tag{A.53}$$

where $R_{\mu\nu\rho\sigma;\tau} \equiv \nabla_{\tau}R_{\mu\nu\rho\sigma}$. While the antisymmetry of the second pair of indices (A.49) is a direct consequence of the definition of curvature, the antisymmetry the first pair of indices (A.50) is due to the fact that the underlying connection ∇ is both metric compatible and torsion free. Equation (A.51), sometimes called first Bianchi identity, is also due to the fact that ∇ is torsion free. The symmetry (A.52) under exchange of the two pairs of indices is a consequence of Eqs. (A.50), (A.51). Those symmetries imply that only 20 among the 256 components of the Riemann tensor are independent. Finally, Eq. (A.53), sometimes called second Bianchi identity, is a consequence of (A.37) and, again, of the fact that ∇ is torsion free.

Ricci and Einstein tensors

The *Ricci tensor* is obtained by contracting the first and third indices of the components of the Riemann tensor,

$$\mathbf{Ric}(\boldsymbol{\partial}_\mu, \boldsymbol{\partial}_\nu) \equiv R_{\mu\nu} \equiv R^\rho{}_{\mu\rho\nu}. \tag{A.54}$$

Note that the Ricci tensor does not require the metric structure to be defined, it therefore exists also in non-Riemannian geometry. In (pseudo-)Riemannian geometry the Ricci tensor is symmetric, due to Eq. (A.52). Moreover, the second Bianchi identity (A.53) implies the interesting relation

$$\nabla_\mu R^\mu{}_{\nu\rho\sigma} = 2\nabla_{[\rho} R_{\sigma]\nu}. \tag{A.55}$$

By contracting indices ν and σ in the above, we obtain

$$\nabla_\nu R^\nu_\mu = \frac{1}{2} \nabla_\mu R, \tag{A.56}$$

where $R \equiv R^\mu_\mu$ is called the *Ricci scalar*.

If we define the *Einstein tensor $\boldsymbol{E}$* as

$$\boldsymbol{E}(\boldsymbol{\partial}_\mu, \boldsymbol{\partial}_\nu) \equiv E_{\mu\nu} \equiv R_{\mu\nu} - \frac{1}{2} R\, g_{\mu\nu}, \tag{A.57}$$

then, by virtue of Eq. (A.56) this tensor is divergence free, $\nabla_\nu E^\nu_\mu = 0$.

A.2 Gravitation

In the general theory of relativity, gravitation is encoded in the pseudo-Riemannian geometry of spacetime, equipped with the Levi-Civita connection. As a field theory, the fundamental quantity is therefore the metric $\boldsymbol{g}$ of the spacetime manifold[2].

A.2.1 Geometrodynamics

Einstein field equations

The metric of spacetime is affected by the presence of matter via its stress-energy tensor $\boldsymbol{T}$, according to the *Einstein field equation*

$$\boxed{\boldsymbol{E} + \Lambda \boldsymbol{g} = 8\pi G \boldsymbol{T},} \tag{A.58}$$

where Λ is the cosmological constant and G is Newton's constant. In other words, any form of energy or momentum locally generates Ricci curvature. Because the Einstein tensor $\boldsymbol{E}$ is divergence free, the Einstein equation imposes the conservation of energy-momentum

$$\nabla_\nu T^\nu_\mu = 0, \tag{A.59}$$

just like the Maxwell equation imposes the conservation of electric charge.

---

[2]In the Palatini formulation of general relativity, the metric and the connection are considered independent dynamical quantities: ∇ is not taken to be the Levi-Civita connection right from the beginning. However, this property emerges from the action of general relativity without the need of any modification [3].

Action formulation

The Einstein field equation (A.58) can be derived from an action principle, with $S = S_{\mathrm{m}} + S_{\mathrm{EH}} + S_{\Lambda}$. The first term S_{m} denotes the action of matter fields, from which derives their stress-energy tensor as

$$T^{\mu\nu} \equiv \frac{2}{\sqrt{-g}} \frac{\delta S_{\mathrm{m}}}{\delta g_{\mu\nu}}, \tag{A.60}$$

where $\delta/\delta g_{\mu\nu}$ denotes the standard functional derivative, here with respect to $g_{\mu\nu}$, while g is the metric determinant defined in Eq. (1.6). In other words, $\boldsymbol{T}$ is such that, for a small variation $\delta\boldsymbol{g}$ of the metric,

$$S_{\mathrm{m}}[\boldsymbol{g} + \delta\boldsymbol{g}] - S_{\mathrm{m}}[\boldsymbol{g}] = \frac{1}{2} \int \mathrm{d}^4 x \sqrt{-g}\, \delta g_{\mu\nu} T^{\mu\nu} + \mathcal{O}(|\delta\boldsymbol{g}|^2). \tag{A.61}$$

Example of such matter actions will be given in § A.2.2. Note that, since $g^{\mu\rho} g_{\rho\nu} = \delta^\mu_\nu$, the variations of the metric and its inverse are related by $\delta g^{\mu\nu} = -g^{\mu\rho} g^{\nu\sigma} \delta g_{\rho\sigma}$, so that the lowered components $T_{\mu\nu}$ are given by

$$T_{\mu\nu} = \frac{-2}{\sqrt{-g}} \frac{\delta S_{\mathrm{m}}}{\delta g^{\mu\nu}}, \tag{A.62}$$

which is very similar to Eq. (A.61), *except for the minus sign.*

The other two terms of S are respectively the Einstein-Hilbert action S_{EH} and a cosmological constant term, they read

$$S_{\mathrm{EH}} \equiv \frac{1}{16\pi G} \int \mathrm{d}^4 x \sqrt{-g}\, R + \text{boundary term}, \tag{A.63}$$

$$S_{\Lambda} \equiv \frac{-1}{8\pi G} \int \mathrm{d}^4 x \sqrt{-g}\, \Lambda, \tag{A.64}$$

where the expression and origin of the boundary term can be found in Ref. [9]. It can indeed be shown that

$$\frac{1}{\sqrt{-g}} \frac{\delta S_{\mathrm{EH}}}{\delta g^{\mu\nu}} = \frac{1}{16\pi G} E_{\mu\nu}, \tag{A.65}$$

$$\frac{1}{\sqrt{-g}} \frac{\delta S_{\Lambda}}{\delta g^{\mu\nu}} = \frac{\Lambda}{16\pi G} g_{\mu\nu}. \tag{A.66}$$

The variation of the cosmological constant term is easily performed: thanks to the formula relating the derivative of the determinant of a matrix to its trace we obtain

$$\delta\sqrt{-g} = \frac{1}{2} \sqrt{-g}\, g^{\mu\nu} \delta g_{\mu\nu} = -\frac{1}{2} \sqrt{-g}\, g_{\mu\nu} \delta g^{\mu\nu}. \tag{A.67}$$

The variation of the Einstein-Hilbert term is more involved, see e.g. Ref. [9] for a clear and detailed derivation. In the end, the extremalisation of the complete action S leads to

$$0 = \frac{\delta S}{\delta g^{\mu\nu}} = \frac{\sqrt{-g}}{16\pi G} \left(E_{\mu\nu} + \Lambda\, g_{\mu\nu} - 8\pi G\, T_{\mu\nu} \right), \tag{A.68}$$

which is the Einstein field equation.

A.2.2 Matter

Point particle

Consider a spinless point particle with rest mass m. Its movement within the spacetime manifold is a curve $x_p^\mu(\lambda)$, where λ is an arbitrary parameter. The proper time τ of this particle is defined as the time measured in its rest frame, i.e. such that $\boldsymbol{u}_p = d/d\tau$, where $\boldsymbol{u}_p$ is the four-velocity of the particle, or $d\tau^2 = -g_{\mu\nu}dx_p^\mu dx_p^\nu$. In absence of any external force, the action of this particle is

$$S_p \equiv -m \int d\tau = -m \int d\lambda \sqrt{-g_{\mu\nu}\frac{dx_p^\mu}{d\lambda}\frac{dx_p^\nu}{d\lambda}}. \tag{A.69}$$

If S_p is considered a functional of the trajectory $x_p^\mu(\lambda)$, then it is straightforward to check that the stationarity of S_p is equivalent to the geodesic equation,

$$\frac{\delta S_p}{\delta x_p^\mu} = 0 \iff \frac{d^2 x_p^\rho}{d\tau^2} + \Gamma^\rho{}_{\mu\nu}\frac{dx_p^\mu}{d\tau}\frac{dx_p^\nu}{d\tau} = 0. \tag{A.70}$$

Free-falling particles therefore follow geodesics of the spacetime manifold.

When written as in Eq. (A.69), S_p cannot be used to derive the expression of the stress-energy tensor associated with the point particle, because it is not an integral over a four-dimensional region of spacetime. This issue can be fixed by introducing a Dirac distribution δ_D as

$$S_p = -m \int d^4x \int d\lambda\, \delta^{(4)}[x^\rho - x_p^\rho(\lambda)]\sqrt{-g_{\mu\nu}\frac{dx_p^\mu}{d\lambda}\frac{dx_p^\nu}{d\lambda}}. \tag{A.71}$$

Applying the definition (A.61) of the stress-energy tensor then yields

$$T_p^{\mu\nu} = m \int d\tau\, \frac{\delta_D[x^\rho - x_p^\rho(\tau)]}{\sqrt{-g}}\frac{dx_p^\mu}{d\tau}\frac{dx_p^\nu}{d\tau} \tag{A.72}$$

$$= \frac{\delta_D[x^i - x_p^i(t)]}{\sqrt{-g}}\gamma m \frac{dx_p^\mu}{dt}\frac{dx_p^\nu}{dt}, \tag{A.73}$$

where, in the second expression, we have used the (arbitrary) time coordinate $t = x^0$ as parameter λ of the particle's trajectory, and introduced the Lorentz factor $\gamma \equiv dt/d\tau$.

Perfect fluid

Consider now an ensemble of noninteracting point particles. Because they do not interact, the action of the system is just the sum of the actions of the individual particles, so the resulting stress-energy tensor is

$$\boldsymbol{T} \equiv \sum_p \boldsymbol{T}_p. \tag{A.74}$$

Let $\mathcal{D}$ be a domain of $\mathcal{M}$ centred around an event E, and whose dimensions are small compared to the typical spacetime curvature radius. Within $\mathcal{D}$, all vectors can be considered to approximately belong to the same tangent space $T_E\mathcal{M}$, in particular the four-momenta $\boldsymbol{p}_p \equiv m_p\boldsymbol{u}_p$ of the particles in $\mathcal{D}$, which implies that they can be summed. Let $\bar{\boldsymbol{p}} = M\bar{\boldsymbol{u}}$ be their ensemble average, where M is such that $\bar{u}^\mu\bar{u}_\mu = -1$. The four-velocity $\bar{\boldsymbol{u}}$ defines a preferred frame, the particles' barycentric frame, with respect to which

we can pick Fermi normal coordinates. In this coordinate system, the total stress-energy tensor reads

$$T^{00} \overset{*}{=} \sum_{p \in \mathcal{D}} \delta_{\mathrm{D}}[x^k - x_{\mathrm{p}}^k(t)] \, \gamma_{\mathrm{p}} m_{\mathrm{p}}, \tag{A.75}$$

$$T^{0i} \overset{*}{=} \sum_{p \in \mathcal{D}} \delta_{\mathrm{D}}[x^k - x_{\mathrm{p}}^k(t)] \, \gamma_{\mathrm{p}} m_{\mathrm{p}} v_{\mathrm{p}}^i, \tag{A.76}$$

$$T^{ij} \overset{*}{=} \sum_{p \in \mathcal{D}} \delta_{\mathrm{D}}[x^k - x_{\mathrm{p}}^k(t)] \, \gamma_{\mathrm{p}} m_{\mathrm{p}} v_{\mathrm{p}}^i v_{\mathrm{p}}^j, \tag{A.77}$$

where $v_{\mathrm{p}}^i \equiv \mathrm{d}x_{\mathrm{p}}^i/\mathrm{d}\bar{\tau}$ is the velocity of particle p in the barycentric frame.

Now if the domain $\mathcal{D}$ contains a large number of particles, and if we coarse-grain $\boldsymbol{T}$ on the scale of $\mathcal{D}$, then

$$T^{00} \overset{*}{=} \rho, \qquad T^{0i} \overset{*}{=} 0, \qquad T^{ij} \overset{*}{=} p \, \delta^{ij}, \tag{A.78}$$

where ρ and p respectively define the energy density and the kinetic pressure of the fluid,

$$\rho \equiv \frac{1}{V_{\mathcal{D}}} \sum_{\mathrm{p}} \gamma_{\mathrm{p}} m_{\mathrm{p}}, \qquad p \equiv \frac{1}{V_{\mathcal{D}}} \sum_{\mathrm{p}} \frac{1}{3} \gamma_{\mathrm{p}} m_{\mathrm{p}} \, \delta_{ij} v_{\mathrm{p}}^i v_{\mathrm{p}}^j. \tag{A.79}$$

When written in a fully covariant form, the stress-energy tensor of the system of particles therefore reads

$$T^{\mu\nu} = (\rho + p) \, \bar{u}^\mu \bar{u}^\nu + p \, g^{\mu\nu}. \tag{A.80}$$

Scalar field

The case of matter fields is more easily handled, because their action directly takes the form of the integral of a Lagrangian density over spacetime. In the case of a scalar field ϕ, minimally coupled to spacetime geometry, the standard action is

$$S = \int \mathrm{d}^4 x \, \sqrt{-g} \left[-\frac{1}{2} \partial_\mu \phi \, \partial^\mu \phi - V(\phi) \right], \tag{A.81}$$

composed of a kinetic term $(\partial\phi)^2$ and a potential term $V(\phi)$. The associated stress-energy tensor is then easily shown to be

$$T_{\mu\nu} = \partial_\mu \phi \, \partial_\nu \phi - \frac{1}{2} (\partial^\rho \phi \, \partial_\rho \phi) \, g_{\mu\nu} - V(\phi) \, g_{\mu\nu}. \tag{A.82}$$

Vector field

The standard action of a minimally coupled vector field $\boldsymbol{A}$ reads

$$S = \int_{\mathcal{M}} \mathrm{d}^4 x \sqrt{-g} \left[-\frac{1}{4} F^{\mu\nu} F_{\mu\nu} - V(A^2) \right], \tag{A.83}$$

where $F_{\mu\nu} \equiv \partial_\mu A_\nu - \partial_\nu A_\mu$ is the field strength of $\boldsymbol{A}$, and $A^2 \equiv A^\mu A_\mu$. The associated stress-energy tensor is

$$T_{\mu\nu} = F_{\mu\rho} F_\nu{}^\rho - \frac{1}{4} (F^{\rho\sigma} F_{\rho\sigma}) \, g_{\mu\nu} - V(A^2) \, g_{\mu\nu}. \tag{A.84}$$

Compte-rendu en français

Sommaire

Introduction

Depuis sa naissance, il y a près d'un siècle, à aujourd'hui, le domaine de la cosmologie physique a levé le voile sur un grand nombre de questions fondamentales quant à la nature et l'origine de l'Univers. La fin du vingtième siècle, en particulier, a vu cette discipline muer en une science de haute précision, grâce à des expériences d'une remarquable qualité, qu'il s'agisse de l'observation du fond diffus cosmologique, des supernovæ, des grands relevés de galaxies, ou encore du lentillage gravitationnel.

La précision atteinte en cosmologie observationnelle contraste toutefois avec la remarquable simplicité du cadre théorique au sein duquel les observations sont interprétées. En particulier, dans le modèle cosmologique standard, la relation entre le décalage spectral z de sources lumineuses lointaines, dû à leur récession, et leur distance angulaire D_{A}, relation indispensable à l'analyse de quasiment toutes les observations cosmologiques, est systématiquement calculée *en supposant que la lumière se propage à travers un univers parfaitement homogène et isotrope*. Quoique plausible pour de très larges faisceaux lumineux, cette hypothèse paraît néanmoins très grossière à petite échelle. Or les échelles mises en jeu dans les observations cosmologiques actuelles sont d'une extrême variété (voir table B.1), s'étalant sur 12 ordres de grandeur. Malgré cela, toutes les observations s'avèrent être cohérentes les unes avec les autres lorsqu'interprétées dans le cadre du modèle standard. L'objectif principal de cette thèse a été de comprendre les raisons d'un succès si surprenant.

observation	échelle angulaire pertinente	valeur typique (rad)
OAB	échelle OAB à $z \sim 0.5, 2$	$10^{-1}, 10^{-2}$
FDC	échelle OAB à $z \sim 1000$	10^{-2}
f_{gaz}	taille apparente d'un amas $z \sim 0.5$	10^{-3}
LF	rayon d'Einstein à des distances cosmologiques	10^{-4}
Lf	taille apparente d'une galaxie à $z \sim 0.5$	10^{-5}
SNeIa	taille apparente d'une supernova à $z \sim 0.5$	10^{-13}

Table B.1   Ouvertures angulaires typiques des faisceaux lumineux impliqués dans différentes observations cosmologiques : oscillation acoustique de baryons (OAB) observée dans les grands relevés de galaxies, ou dans les anisotropies du fond diffus cosmologique (FDC) ; fraction de gaz dans les amas de galaxies (f_{gaz}) ; lentillage gravitationnel fort (LF) ou faible (Lf) ; et enfin supernovæ de type Ia (SNeIa).

B.1   Optique géométrique en espace-temps courbe

Modéliser la propagation de la lumière à travers le cosmos requiert une compréhension profonde des lois de l'optique géométrique en présence de gravitation, c'est-à-dire en espace-temps courbe.

B.1.1   Rayons lumineux

Les lois de l'électrodynamique classique montrent que, dans le régime eikonal, les ondes électromagnétiques constituant la lumière se propagent en suivant des géodésiques de genre lumière à travers l'espace-temps. Le vecteur tangent à une telle courbe, $k^{\mu} \equiv \mathrm{d}x^{\mu}/\mathrm{d}v$, où v

est un paramètre affine, n'est autre que le quadrivecteur d'onde ; par définition, il satisfait aux équations

$$k^\mu \nabla_\mu k^\nu = 0, \qquad k^\mu k_\mu = 0. \tag{B.1}$$

Le décalage spectral z d'une source lumineuse est défini comme étant la différence relative entre la fréquence ω_S émise par la source et celle reçue par l'observateur, ω_O, selon

$$z \equiv \frac{\omega_S - \omega_O}{\omega_O}. \tag{B.2}$$

Cette quantité constitue une mesure de la vitesse de récession de la source (effet Doppler) ainsi que des effets gravitationnels de dilatation du temps (effet Einstein). Soit un référentiel matérialisé par la quadrivitesse $\boldsymbol{u}$, la fréquence d'un signal de quadrivecteur d'onde $\boldsymbol{k}$ est la composante temporelle de celui-ci, c'est-à-dire $\omega = u^\mu k_\mu$. Par conséquent $1 + z = (u^\mu k_\mu)_S/(u^\mu k_\mu)_O$. Le décalage spectral d'une source est donc obtenu en résolvant (B.1).

B.1.2 Distances en cosmologie

En cosmologie, la distance d'une source lumineuse peut être mesurée de deux façons différentes : la première consiste en la comparaison de l'aire de cette source A_S avec sa taille angulaire apparente Ω_O. La quantité

$$D_{\mathrm{A}} \equiv \sqrt{\frac{A_S}{\Omega_S}} \tag{B.3}$$

définit alors une notion de distance, connue sous le nom de distance angulaire. Il s'agit de la notion de distance naturellement exploitée dans l'interprétation du FDC, de l'OAB, ou encore en lentillage gravitationnel.

La seconde possibilité revient à comparer la luminosité intrinsèque L_S de la source à l'intensité lumineuse I_O observée,

$$D_{\mathrm{L}} \equiv \sqrt{\frac{L_S}{4\pi I_O}} \tag{B.4}$$

définit alors la notion de distance de luminosité. Il s'agit de la notion de distance la plus commune en astronomie, son rôle en cosmologie étant incarné par l'observation des SNe. Pour une même source, les deux distances $D_{\mathrm{A}}, D_{\mathrm{L}}$ sont a priori différentes, mais elles ne sont pas indépendantes ; en fait, il est possible de montrer que si le nombre de photon est conservé entre la source et l'observateur, alors $D_{\mathrm{L}} = (1 + z)^2 D_{\mathrm{A}}$.

B.1.3 Faisceaux lumineux

Puisqu'elles font intervenir les notions d'aire et d'intensité lumineuse, les distances définies ci-dessus ne peuvent pas être calculées à partir de la trajectoire d'un simple rayon lumineux : elles nécessitent de considérer un ensemble de rayons, i.e. un faisceau, connectant l'ensemble des points de la source à l'observateur. En optique gravitationnelle, la géométrie d'un faisceau lumineux est commodément décrite par la matrice 2×2 de Jacobi $\boldsymbol{\mathcal{D}}$, reliant la séparation angulaire $\boldsymbol{\theta}_O$ observée entre deux rayons à leur séparation physique $\boldsymbol{\xi}(v)$ en tout autre point du faisceau,

$$\boldsymbol{\xi}(v) = \boldsymbol{\mathcal{D}}(v)\,\boldsymbol{\theta}_O. \tag{B.5}$$

Il est alors clair que la distance angulaire d'une petite source lumineuse est reliée au déterminant de la matrice de Jacobi, selon

$$D_{\mathrm{A}} = \frac{\mathrm{d}^2 \boldsymbol{\xi}_S}{\mathrm{d}^2 \boldsymbol{\theta}_O} = \sqrt{\det \boldsymbol{\mathcal{D}}(v_S)}. \tag{B.6}$$

Si les deux rayons considérés sont très proches l'un de l'autre, alors l'évolution de leur séparation $\boldsymbol{\xi}(v)$ au cours de la propagation est régie par l'équation de déviation géodésique. Il s'ensuit que l'évolution de la matrice de Jacobi avec v satisfait à l'équation de Sachs,

$$\frac{\mathrm{d}^2 \boldsymbol{\mathcal{D}}}{\mathrm{d}v^2} = \boldsymbol{\mathcal{R}} \boldsymbol{\mathcal{D}}, \tag{B.7}$$

où $\boldsymbol{\mathcal{R}}$ est une certaine projection du tenseur de courbure de Riemann, appelée matrice optique de marée. Celle-ci peut être décomposée en une composante associée au tenseur de Ricci $R_{\mu\nu}$ et une composante associée au tenseur de Weyl $C_{\mu\nu\rho\sigma}$, selon

$$\boldsymbol{\mathcal{R}} = \underbrace{\begin{pmatrix} \mathscr{R} & 0 \\ 0 & \mathscr{R} \end{pmatrix}}_{\text{focalisation de Ricci}} + \underbrace{\begin{pmatrix} -\operatorname{Re}\mathscr{W} & \operatorname{Im}\mathscr{W} \\ \operatorname{Im}\mathscr{W} & \operatorname{Re}\mathscr{W} \end{pmatrix}}_{\text{distortions de Weyl}}, \qquad \text{avec} \qquad \begin{cases} \mathscr{R} \propto R_{\mu\nu}, \\ \mathscr{W} \propto C_{\mu\nu\rho\sigma}. \end{cases} \tag{B.8}$$

Cette séparation est à la fois géométriquement et physiquement très sensée. La contribution de Ricci, d'une part, provoque une évolution homothétique de $\boldsymbol{\mathcal{D}}$: elle modifie ses valeurs propres en préservant leur rapport et la direction des axes associés. Il s'agit donc d'une focalisation isotrope du faisceau. La contribution de Weyl, d'autre part, tend au contraire à modifier le rapport des valeurs propres de $\boldsymbol{\mathcal{D}}$ et à faire tourner leurs axes, elle provoque donc un cisaillement et une rotation du faisceau. Il est intéressant de remarquer que ces deux contributions à $\boldsymbol{\mathcal{R}}$ sont liées à des propriétés différentes de la distribution de matière rencontrée par la lumière au cours de sa propagation. En vertu des équations d'Einstein, le tenseur de Ricci est directement lié à la densité locale d'énergie-impulsion, $\mathscr{R}$ est ainsi généré par la présence de matière diffuse (gaz, matière noire) traversée par le faisceau. Au contraire, la courbure de Weyl est générée de façon non-locale, à l'extérieur de corps massifs ; $\mathscr{W}$ est donc due à la matière située à l'extérieur du faisceau.

B.2   Cosmologie au-delà de l'hypothèse d'homogénéité

La discussion ci-dessus est la raison principale du questionnement quant à l'efficacité du modèle cosmologique standard à interpréter toutes les observations cosmologiques avec précision. En effet, la lumière provenant d'une très petite source, par exemple une supernova, se propage essentiellement à travers le vide intergalactique, où la courbure de l'espace-temps est dominée par sa composante de Weyl. Or l'espace-temps du modèle standard, décrit par la géométrie de Friedmann-Lemaître (FL), possède au contraire une courbure de nature purement Ricci. Cette incompatibilité apparente entre réalité et modèle a été soulevée simultanément par Y. Zel'dovich et R. Feynman en 1964.

B.2.1   Observations dans un « grunivers »

Une première façon d'évaluer l'impact de l'inhomogénéité à petite échelle de l'Univers sur la propagation de la lumière consiste en l'utilisation de modèles alternatifs. À ce titre, les

modèles « en gruyère » (Swiss-cheese models en anglais), que l'on baptisera « grunivers » dans la suite, sont des candidats naturels. Leur construction est la suivante (voir Fig. B.1) : à partir d'un univers homogène, choisir une sphère comobile, puis concentrer la matière qu'elle contient en son centre. Ceci forme un « trou » au sein du « fromage » homogène initial. À l'intérieur du trou, la géométrie spatio-temporelle est décrite par la métrique de Schwarzschild (ou Kottler si $\Lambda \neq 0$), tandis qu'à l'extérieur la métrique de FL reste valable. La procédure décrite ci-dessus assure que ces deux géométries se raccordent parfaitement à la frontière du trou, formant un espace-temps bien défini. Physiquement parlant, l'intérieur du trou peut être vu comme représentant le voisinage d'un objet gravitationnellement lié, tel qu'une galaxie ou un amas de galaxie. La masse centrale est donc choisie de l'ordre de $M \sim 10^{11} M_\odot$ (galaxie) ou $M \sim 10^{15} M_\odot$ (amas). Le rayon comobile du trou correspondant, $R_{\rm h} = (3M/4\pi\rho_0)^{1/3}$, où ρ_0 est la masse volumique moyenne de l'Univers aujourd'hui, vaut alors $R_{\rm h} \sim 1\,{\rm Mpc}$ pour une galaxie, $R_{\rm h} \sim 20\,{\rm Mpc}$ pour un amas.
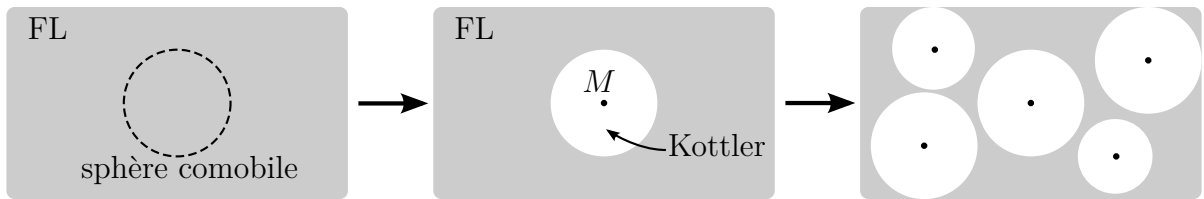
Figure B.1 Construction d'un grunivers à partir d'un modèle homogène et isotrope (FL).

L'opération peut ensuite être répétée pour d'autres sphères, toutes disjointes les unes des autres, d'où l'aspect « en gruyère » du résultat. La quantité de trous introduits dans le modèle est quantifié par le paramètre d'homogénéité

$$f \equiv \lim_{V \to \infty} \frac{V_{\rm FL}}{V}, \tag{B.9}$$

où V représente le volume d'une région du modèle, et $V_{\rm FL}$ la portion de ce volume occupé par des régions homogènes. Les cas $f = 0$ ou $f = 1$ représentent donc respectivement un univers rempli de masses ponctuelles ou un univers parfaitement homogène. L'avantage principal de cette construction est qu'elle génère un modèle potentiellement très inhomogène, sans toutefois affecter sa dynamique d'expansion ; elle est par conséquent très adaptée à l'étude de la question qui nous intéresse ici.

L'analyse de la propagation de la lumière à travers un grunivers, décrite en détails dans les § 6.2 et § 6.4, peut être résumée comme suit :

1. La relation entre paramètre affine v et décalage spectral z est très peu affectée par la présence des inhomogénéités. La correction relative due à un trou est ainsi $(z - z_{\rm FL})/z_{\rm FL} = \mathcal{O}(r_{\rm S}/R_{\rm h})$, où $r_{\rm S} \equiv 2GM$ est le rayon de Schwarzschild de la masse centrale. Cette correction est donc de l'ordre de 10^{-8} pour un trou galactique et 10^{-6} pour un trou contenant un amas.

2. Les effets de distorsions de Weyl à l'intérieur des trous sont négligeables en première approximation.

3. La focalisation de Ricci est, de manière effective, réduite par le facteur f. Tout se passe donc, pour le calcul de la matrice de Jacobi et donc des distances, comme si la lumière se propageait dans un univers homogène de densité réduite $\rho \to f\rho$.

Les propriétés décrite ci-dessus correspondent à l'approche effective de Kantowski-Dyer-Roeder (KDR). Je les ai démontrées analytiquement, puis vérifiées numériquement à l'aide de deux simulations de propagation de lumière réalisées au cours de cette thèse, l'une présentant une distribution régulière de trous, la seconde une distribution aléatoire.

Du point de vue de la cosmologie, j'ai dans un premier temps évalué l'erreur potentielle sur les mesures de paramètres cosmologiques que nous commettons en supposant que l'Univers est parfaitement homogène. Pour ce faire, j'ai simulé des catalogues d'observations de SNe, c'est-à-dire un ensemble de doublets (z, D_L), dans un grunivers dont la dynamique d'expansion est régie par des paramètres « vrais » $\{\Omega\}$. J'ai ensuite déterminé les paramètres cosmologiques « apparents » $\{\bar{\Omega}\}$ obtenus en ajustant ces observations simulées par la courbe théorique $D_L^{FL}(z|\{\bar{\Omega}\})$, autrement dit, en supposant de façon erronée que la lumière provenant de ces SNe s'est propagée à travers un univers homogène. La différence entre les jeux de paramètres $\{\Omega\}$ et $\{\bar{\Omega}\}$ est représentées sur la Fig. B.2a, pour un grunivers dont les régions FL présentent des sections spatiales plates ($\Omega_K = 0$), avec un paramètre d'homogénéité $f = 0.26$. La différence est significative en général, mais diminue fortement avec Ω_Λ, ce qui est somme toute très naturel : la constante cosmologique générant une forme de courbure strictement homogène, si celle-ci domine alors la géométrie spatio-temporelle du grunivers ne diffère que très peu du modèle FL dont il est issu.
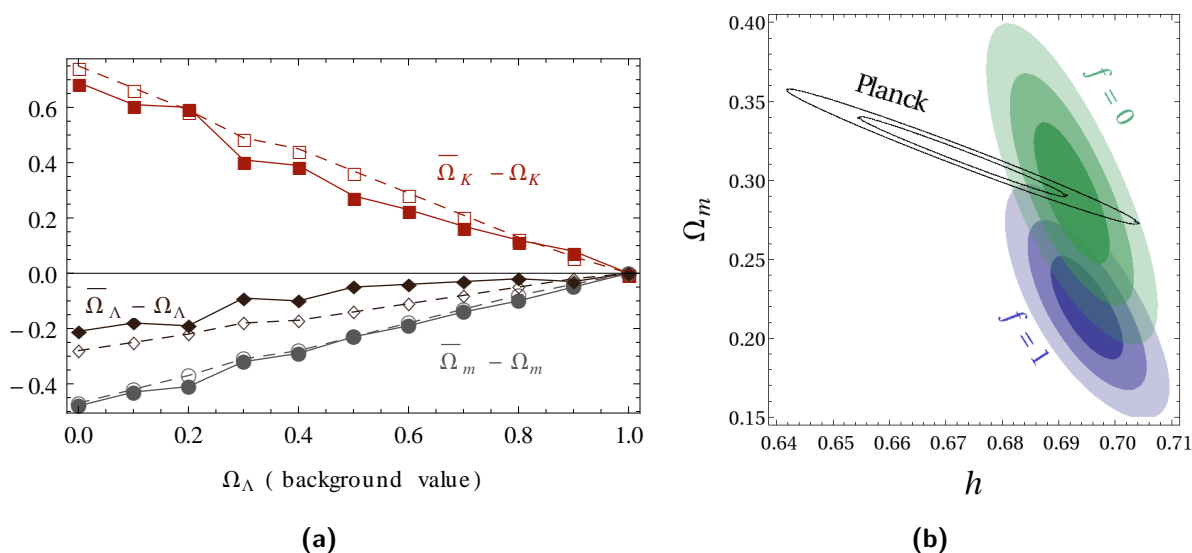

(a)   **(b)**

Figure B.2 *À gauche* : différence entre les paramètres cosmologiques apparents $\{\bar{\Omega}\}$ et réels $\{\Omega\}$ dans des grunivers tels que $\Omega_K = 0$, $f = 0.26$ et $M = 10^{11} M_\odot$ (traits et symboles pleins) ou $M = 10^{15} M_\odot$ (traits pointillés et symboles vides) dans les trous. *À droite* : contraintes observationnelles sur (h, Ω_m) issues de l'analyse du FDC (*Planck*) d'une part, et du diagramme de Hubble (SNLS) d'autre part, en supposant l'Univers soit homogène ($f = 1$) soit très inhomogène ($f = 0$).

Dans un second temps, j'ai comparé deux analyses différentes de données réelles de SNe (issues des trois premières années de la campagne SNLS) : d'abord en supposant que leur lumière s'est propagée à travers un univers homogène (approche standard, $f = 1$) ; puis en remplaçant le modèle FL sous-jacent par un grunivers très inhomogène ($f = 0$), c'est-à-dire en exploitant la relation $D_L(z|\{\Omega\})$ dictée par l'approche de KDR qui, on l'a dit, constitue une bonne approximation des propriété optiques de tels modèles. Les contraintes observationnelles associées, dans le plan (h, Ω_m) où $h \equiv H_0/(100 \, \text{km/s/Mpc})$, sont représentées sur la Fig. B.2b, ainsi que les contraintes indépendantes établies par

l'observation du FDC par la mission *Planck*. Il résulte que la prise en compte de l'inhomogénéité à petite échelle de l'Univers, même à travers un modèle très grossier comme le grunivers, semble améliorer l'accord entre ces différentes observations cosmologiques.

L'analyse résumée ici répond en partie à la problématique principale de cette thèse. Il semble ainsi que la prépondérance de la constante cosmologique dans l'Univers tardif soit un ingrédient crucial du succès du modèle cosmologique standard. En effet, si nous vivions dans un Univers tel que $\Omega_\Lambda \ll \Omega_\mathrm{m}$ aujourd'hui, alors les observations impliquant de très fins faisceaux lumineux (par exemple les SNe) seraient bien davantage affectées par l'inhomogénéité de l'Univers, et paraîtraient alors en profond désaccord avec les observations impliquant de plus larges faisceaux (comme pour le FDC). Néanmoins, même dans notre propre Univers, pourtant dominé par Λ, la Fig. B.2b indique que la précision atteinte par les observations actuelle est désormais suffisante pour que de tels effets soient révélés, et nécessitent par conséquent d'être pris en compte précisément.

B.2.2 Lentillage gravitationnel stochastique

La section précédente a mis en évidence la nécessité de modéliser avec précision l'effet de l'inhomogénéité à petite échelle de l'Univers sur ses propriétés optiques. Bien que révélé par l'étude du grunivers, ce modèle s'avère être trop peu flexible pour permettre une étude réaliste du problème. Une approche effective, qui pourrait prendre en compte les propriétés complexes de l'Univers de façon efficace, serait préférable.

On notera que la situation physique abordée ici, à savoir l'effet d'une multitude de faibles interactions entre un corps (en l'occurrence la lumière) et son environnement, n'est pas sans rappeler le mouvement Brownien. Ce processus désordonné que l'on peut observer, par exemple, pour une poussière micrométrique en suspension sur l'eau, résulte des chocs entre cette poussière et les molécules formant le liquide. Un tel phénomène ne peut donc pas être expliqué en modélisant l'eau comme un fluide, car il n'est pas dû à des courants macroscopiques en son sein. Il n'est cependant pas nécessaire de suivre la dynamique de chaque molécule indépendamment pour décrire le mouvement Brownien : en pratique, leur effet donne lieu à une force stochastique, modélisée par un bruit blanc.

Cette analogie m'a amené à modéliser le lentillage gravitationnel dû aux petites structures de l'Univers par un terme stochastique dans la matrice de marée optique, de sorte que l'équation de Sachs (B.7) prend la forme d'une équation de Langevin,

$$\frac{\mathrm{d}^2\boldsymbol{\mathcal{D}}}{\mathrm{d}v^2} = (\langle\boldsymbol{\mathcal{R}}\rangle + \delta\boldsymbol{\mathcal{R}})\,\boldsymbol{\mathcal{D}}, \tag{B.10}$$

avec $\langle\delta\boldsymbol{\mathcal{R}}\rangle = \mathbf{0}$. On notera que, malgré une notation suggestive, le terme de fluctuation $\delta\boldsymbol{\mathcal{R}}$ n'est pas nécessairement petit par rapport au terme déterministe $\langle\boldsymbol{\mathcal{R}}\rangle$. Les hypothèses d'homogénéité et d'isotropie statistiques de l'Univers impliquent les propriétés suivantes : $\langle\mathscr{W}\rangle = 0$; $\langle\delta\mathscr{R}(v)\mathscr{W}(w)\rangle = 0$; $\langle\mathrm{Re}\,\mathscr{W}(v)\,\mathrm{Im}\,\mathscr{W}(w)\rangle = 0$. Par ailleurs, le fait que l'on cherche à modéliser de très petites échelles permet de traiter le terme de fluctuation comme un bruit blanc, donc δ-corrélé :

$$\langle\delta\mathscr{R}(v)\delta\mathscr{R}(w)\rangle = C_{\mathscr{R}}(v)\delta(v-w), \qquad \langle\mathscr{W}^\star(v)\mathscr{W}(w)\rangle = 2C_{\mathscr{W}}(v)\delta(v-w), \tag{B.11}$$

où l'étoile indique une conjugaison complexe. Les fonctions C_X sont analogues à des coefficients de diffusion, et sont de l'ordre de $\delta X^2 \times \Delta v_\mathrm{coh}$, où δX indique l'amplitude typique des fluctuations de X, et Δv_coh l'échelle typique de paramètre affine pendant lequel X reste cohérent.

De l'équation de Sachs-Langevin (B.10) peut être déduite l'équation de Fokker-Planck-Kolmogorov régissant l'évolution, avec v, de la densité de probabilité $p(v; \boldsymbol{\mathcal{D}}, \dot{\boldsymbol{\mathcal{D}}})$ de la matrice de Jacobi. Cette équation prend ici la forme

$$\frac{\partial p}{\partial v} = -\dot{\mathcal{D}}_{AB} \frac{\partial p}{\partial \mathcal{D}_{AB}} - \langle \mathscr{R} \rangle \, \mathcal{D}_{AB} \frac{\partial p}{\partial \dot{\mathcal{D}}_{AB}}$$

$$+ \frac{1}{2} \left[C_{\mathscr{R}} \, \delta_{AE} \delta_{CF} + C_{\mathscr{W}} (\delta_{AC} \delta_{EF} - \varepsilon_{AC} \varepsilon_{EF}) \right] \mathcal{D}_{EB} \mathcal{D}_{FD} \frac{\partial^2 p}{\partial \dot{\mathcal{D}}_{AB} \partial \dot{\mathcal{D}}_{CD}} \quad \text{(B.12)}$$

où les indices $A, B, \dots$ défilent entre 1 et 2, et ε_{AB} est antisymétrique, avec $\varepsilon_{12} = 1$. Bien que difficilement soluble, cette équation aux dérivées partielles permet toutefois de déterminer les équations différentielles ordinaires régissant les moments de p, desquelles on peut ensuite déduire les moments de la distribution de la distance angulaire D_A. Pour les deux premiers, c'est-à-dire la moyenne $\langle D_\text{A} \rangle$ et la variance σ_{D_A}, on trouve en particulier

$$\delta_{D_\text{A}} \equiv \frac{\langle D_\text{A} \rangle - D_0}{D_0} = -2 \int_0^v \frac{\mathrm{d}v_1}{D_0^2(v_1)} \int_0^{v_1} \frac{\mathrm{d}v_2}{D_0^2(v_2)} \int_0^{v_2} \mathrm{d}v_3 \, D_0^4(v_3) C_{\mathscr{W}}(v_3) + \mathcal{O}(C_{\mathscr{W}}^2), \quad \text{(B.13)}$$

$$\frac{\mathrm{d}^3}{\mathrm{d}x^3} \left[\frac{\sigma_{D_\text{A}}^2}{D_0^2} \right] + 2D_0^6 (2C_{\mathscr{W}} - C_{\mathscr{R}}) \frac{\sigma_{D_\text{A}}^2}{D_0^2} = 2C_{\mathscr{R}} D_0^6 + 6 \int_O^x \mathrm{d}x' \left[\frac{\mathrm{d}^2 \delta_{D_\text{A}}}{\mathrm{d}x^2} \right]^2 + \mathcal{O}(C_{\mathscr{W}}^3), \quad \text{(B.14)}$$

D_0 étant la distance angulaire en l'absence de fluctuations, c'est-à-dire telle que $\mathrm{d}^2 D_0 / \mathrm{d}v^2 = \langle \mathscr{R} \rangle D_0$, et x est une variable abstraite telle que $\mathrm{d}x = \mathrm{d}v / D_0^2(v)$.

Dans le but de tester ce formalisme, je l'ai appliqué au grunivers étudié dans la section précédente, en comparant les prédictions théoriques aux résultats numériques (voir Fig. B.3). On voit que la moyenne de D_A est extrêmement bien prédite par le formalisme de lentillage stochastique ; ce n'est pas le cas pour son écart-type. Une étude approfondie a révélé que l'origine du problème réside dans l'hypothèse de gaussianité des fluctuations de $\mathscr{W}$, sous-entendue dès lors que l'équation de Fokker-Planck-Kolmogorov (B.12) est invoquée.
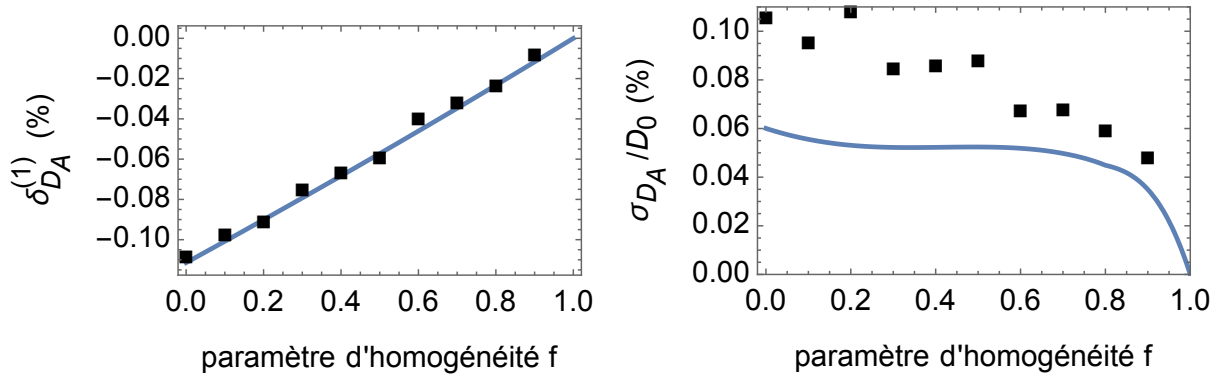

Figure B.3 Moyenne (à gauche) et écart-type (à droite) de la distance angulaire D_A de sources de décalage spectral $z = 1$ à travers un grunivers. La ligne bleue représente les prédictions du formalisme de lentillage stochastique, tandis que les carrés noir indiquent les résultats de simulations numériques.

Malgré cette faiblesse, une telle approche stochastique du lentillage gravitationnel aux petites échelle reste autant prometteuse que novatrice. Elle ouvre la voie vers des méthodes efficaces et flexibles pour estimer, par exemple, le biais et la dispersion du diagramme de Hubble des SNe dus aux petites structures de notre Univers.

B.3   Cosmologie au-delà de l'hypothèse d'isotropie

Le modèle cosmologique standard est fondé sur les hypothèses d'homogénéité et d'isotropie de l'Univers à grande échelle. Il est important de noter que ces deux hypothèses ne sont pas redondantes : l'Univers peut être homogène (identique en tout point) mais anisotrope ; par exemple, son expansion pourrait être plus rapide dans certaines directions que dans d'autres. Comme toute hypothèse fondamentale, l'isotropie cosmique se doit donc d'être testée. Deux aspects de la question peuvent alors être distingués. Du point de vue observationnel, d'abord : comment l'anisotropie modifie-t-elle nos observations et leur interprétation ? Du point de vue théorique ensuite : quelles pourraient être les sources d'une telle anisotropie ?

B.3.1   Optique dans un univers anisotrope

Notre capacité à détecter toute forme d'anisotropie cosmique requiert de comprendre la propagation de la lumière à travers un univers anisotrope. Pour ce faire, il est commode de ne relaxer que l'hypothèse d'isotropie, tout en conservant l'homogénéité. Les modèles correspondants suivent alors la classification de Bianchi des espace tridimensionnels homogènes, et ont donc été baptisés espace-temps de Bianchi. Le plus simple d'entre eux, dit Bianchi I, présente des sections spatiales euclidiennes, et sa métrique s'écrit

$$\mathrm{d}s^2 = -\mathrm{d}t^2 + a^2(t) \sum_{i=1}^{3} \left[\mathrm{e}^{\beta_i(t)} \mathrm{d}x^i \right]^2, \tag{B.15}$$

où la somme des β_i est nulle. Ce modèle peut être vu comme une extension du modèle isotrope de FL admettant trois facteurs d'échelle $a\mathrm{e}^{\beta_i}$ au lieu d'un seul, et présentant donc une expansion différente le long de chaque direction.

   Les propriétés optiques d'un tel modèle peuvent être résumées ainsi :

- La dérive temporelle du décalage spectral n'est pas isotrope. Si l'on observe un ensemble de sources comobiles ayant toutes le même décalage spectral z à un instant donné, à un instant ultérieur ces sources n'auront plus le même décalage spectral les unes par rapport aux autres.

- Les objets dérivent sur la sphère céleste. Si, à un instant donné, l'on pointe un télescope dans une certaine direction pour observer une source lumineuse comobile, alors, à un instant ultérieur la source n'apparaîtra plus dans la ligne de mire. Il s'agit ici d'un effet purement cosmologique, indépendant de l'effet de la rotation de la Terre que l'on suppose avoir corrigé.

- La relation entre distance angulaire et décalage spectral $D_{\mathrm{A}}(z)$ dépend de la direction dans laquelle elle est évaluée.

- Les images sont déformées par rapport à leurs propriétés intrinsèques. L'anisotropie de l'expansion, à cause du lentillage de Weyl qu'elle engendre, tend à cisailler et faire tourner les faisceaux lumineux. Cet effet évolue avec le temps, en général.

J'ai volontairement choisi d'exprimer ces propriétés avec des mots plutôt qu'avec des formules mathématiques. Celles-ci sont exposées en détail au Chap. 8. Je précise toutefois que chacun des effets mentionné ci-dessus a été démontré analytiquement. En particulier, j'ai établi une solution exacte de l'équation de Sachs, obtenant ainsi pour la première fois l'expression de la matrice de Jacobi dans un univers anisotrope.

L'étude rapportée ici ouvre la voie vers de nouvelles stratégies observationnelles visant à contraindre l'anisotropie de l'expansion cosmique, en particulier à l'aide du diagramme de Hubble, ou via l'analyse du lentillage gravitationnel faible des galaxies.

B.3.2   Modèles scalaire-vecteur

L'intérêt pour les modèles cosmologiques anisotropes a récemment été ravivé par l'observation d'anomalies dans le spectre de puissance du FDC aux faibles multipôles, attribuables à une anisotropie cosmique. Le cas échéant, la question de son origine physique devrait alors être abordée. À ce titre, le candidat le plus naturel serait un champ vectoriel de matière, tel qu'un champ électromagnétique à l'échelle cosmologique. Il est également envisageable qu'un tel champ ait été responsable de la phase primordiale d'inflation (inflaton vectoriel), ou encore de l'accélération actuelle de l'expansion cosmique (quintessence vectorielle). Il s'avère toutefois difficile de générer de tels phénomènes à l'aide d'un champ vectoriel seul (en particulier si celui-ci n'a pas de masse ainsi qu'imposé par l'invariance de jauge) sans provoquer une trop grande anisotropie. Une manière de contourner ce problème consiste à coupler le champ vectoriel avec un champ scalaire qui serait, lui, responsable de la majeure partie de l'inflation ou de l'accélération tardive de l'expansion de l'Univers.

C'est dans ce contexte général que s'inscrit la dernière partie de cette thèse. On y analyse les propriétés de stabilité et de causalité d'une large classe de modèles scalaire-vecteur, afin de déterminer s'ils sont fondamentalement viables, sans avoir besoin de recourir à une confrontation fastidieuse avec les observations. La condition de stabilité se traduit mathématiquement par le fait que le hamiltonien de la théorie est minoré par une certaine valeur. En outre, la causalité d'une théorie est assurée si ses équations du mouvement sont des équations aux dérivées partielles du second ordre, de genre hyperbolique. Cette condition implique en effet que le problème de Cauchy associé à la donnée de conditions initiales, c'est-à-dire de l'état des champs et de leur dérivée temporelle le long d'une hypersurface de genre espace, admet une unique solution.

Les résultats de cette étude peuvent être résumés de la façon suivante. Soit une théorie des champs contenant un scalaire ϕ et un vecteur $\boldsymbol{A}$. Si cette théorie dérive d'un principe de moindre action tel que (i) ϕ et $\boldsymbol{A}$ sont minimalement couplés à la gravitation ; (ii) l'action ne contient que des dérivées d'ordre inférieur à 1 en ces champs ; et (iii) est invariante sous les transformations de jauge de $\boldsymbol{A}$; alors la forme la plus générale de cette action est

$$S[\phi, \boldsymbol{A}; \boldsymbol{g}] = \int \mathrm{d}^4 x \sqrt{-g}\, \mathcal{L}(\phi, K, X, Y, Z), \tag{B.16}$$

où les scalaires K, X, Y, Z sont définis par

$$K \equiv \partial_\mu \phi \partial^\mu \phi, \quad X \equiv F^{\mu\nu} F_{\mu\nu}, \quad Y \equiv F^{\mu\nu} \tilde{F}_{\mu\nu}, \quad Z \equiv (\partial_\mu \phi \tilde{F}^{\mu\rho})(\partial_\nu \phi \tilde{F}^\nu{}_\rho), \tag{B.17}$$

avec $\tilde{F}_{\mu\nu} \equiv \varepsilon_{\mu\nu\rho\sigma} F^{\rho\sigma}/2$ le dual de Hodge de la deux-forme de courbure associée à $\boldsymbol{A}$, elle-même définie par $F_{\mu\nu} \equiv \partial_\mu A_\nu - \partial_\nu A_\mu$. Si l'on ajoute à cela l'hypothèse que (iv) $\mathcal{L}$ est, au plus, quadratique en $\boldsymbol{A}$, alors les seuls théories physiquement viables vérifient

$$\mathcal{L} = \frac{1}{2} f_0(\phi, K) - \frac{1}{4} f_1(\phi)\, X - \frac{1}{4} f_2(\phi)\, Y, \tag{B.18}$$

la fonction f_1 étant positive, et la fonction f_0 devant vérifier les conditions suivantes : $f_0(\phi, K \geq 0)$ est minorée ; $\partial f_0 / \partial K \geq 0$; et $\partial f_0 / \partial K + 2K \partial^2 f_0 / \partial K^2 \geq 0$. Cela réduit de façon drastique l'espace des possibilités pour cette classe de théories.

Conclusion

Cette thèse avait pour objectif l'étude approfondie de la propagation de la lumière à travers l'Univers, en particulier lorsque les hypothèses d'homogénéité et d'isotropie sont relaxées. Son premier volet a permis de comprendre que la domination de la constante cosmologique dans la dynamique de l'expansion cosmique aujourd'hui n'est pas étrangère au succès du modèle standard. Il semble néanmoins que la précision croissante des observations cosmologiques ne permettra bientôt plus de négliger l'impact de l'inhomogénéité à petite échelle de notre Univers. Le formalisme de lentillage gravitationnel stochastique proposé dans cette thèse constitue alors une méthode prometteuse pour modéliser ces effets de façon précise et efficace. Le second volet de cette thèse, consacré à la possibilité d'une anisotropie à grande échelle de l'Univers, a contribué à la fois à une meilleure compréhension des propriétés optiques de modèles cosmologiques anisotropes, et aux causes potentielles d'une telle anisotropie. Le travail qui vient d'être résumé appelle naturellement de nombreux compléments, tant du point de vue fondamental qu'observationnel, que je souhaite aborder dans un futur proche.

Bibliography

[1] C. W. Misner, K. S. Thorne, and J. A. Wheeler, *Gravitation*. 1973.

[2] J. D. Jackson, *Classical electrodynamics*. 1975.

[3] J. Baez and J. Muniain, *Gauge fields, knots and gravity*. 1995.

[4] C. Itzykson and J.-B. Zuber, *Quantum Field Theory*. McGraw-Hill, 1980.

[5] N. Deruelle and J.-P. Uzan, *Théories de la Relativité*. Belin, 2014.

[6] G. Esposito-Farèse, C. Pitrou, and J.-P. Uzan, *Vector theories in cosmology*, *Phys. Rev. D* **81** (Mar., 2010) 063519, [`arXiv:0912.0481`].

[7] G. Horndeski, *Conservation of Charge and the Einstein-Maxwell Field Equations*, *J.Math.Phys.* **17** (1976) 1980–1987.

[8] J. Beltrán Jiménez, R. Durrer, L. Heisenberg, and M. Thorsrud, *Stability of Horndeski vector-tensor interactions*, *JCAP* **1310** (2013) 064, [`arXiv:1308.1867`].

[9] E. Poisson, *A relativist's toolkit : the mathematics of black-hole mechanics*. 2004.

[10] N. Deruelle and M. Sasaki, *Conformal Equivalence in Classical Gravity: the Example of "Veiled" General Relativity*, p. 247. 2011.

[11] N. Deruelle, *Nordström's scalar theory of gravity and the equivalence principle*, *General Relativity and Gravitation* **43** (Dec., 2011) 3337–3354, [`arXiv:1104.4608`].

[12] R. M. Wald, *General relativity*. The University of Chicago Press, 1984.

[13] M. Born and E. Wolf, *Principles of Optics*. Oct., 1999.

[14] J.-P. Pérez, *Optique : Fondements et applications*. Dunod, 2004.

[15] I. Kovner, *Fermat principle in arbitrary gravitational fields*, *ApJ* **351** (Mar., 1990) 114–120.

[16] V. Perlick, *On Fermat's principle in general relativity. I. The general case*, *Classical and Quantum Gravity* **7** (Aug., 1990) 1319–1331.

[17] P. Schneider, J. Ehlers, and E. E. Falco, *Gravitational Lenses*. 1992.

[18] N. Kaiser, *Astronomical redshifts and the expansion of space*, *MNRAS* **438** (Mar., 2014) 2456–2465, [`arXiv:1312.1190`].

[19] E. F. Bunn and D. W. Hogg, *The kinematic origin of the cosmological redshift*, *American Journal of Physics* **77** (Aug., 2009) 688–694, [`arXiv:0808.1081`].

[20] M. A. Abramowicz, S. Bajtlik, J.-P. Lasota, and A. Moudens, *Eppur si Espande*, *Acta Astronomica* **57** (June, 2007) 139–148, [`astro-ph/0612155`].

[21] J. L. Synge, *Relativity: the General Theory*. North-Holland Publishing Company, 1960.

[22] G. F. R. Ellis, S. D. Nel, R. Maartens, W. R. Stoeger, and A. P. Whitman, *Ideal observational cosmology.*, *Phys. Rep.* **124** (1985) 315–417.

[23] V. Perlick, *Gravitational Lensing from a Spacetime Perspective*, *Living Reviews in Relativity* **7** (Sept., 2004) 9.

[24] É. É. Flanagan, N. Kumar, I. Wasserman, and R. A. Vanderveld, *Luminosity distance in "Swiss cheese" cosmology with randomized voids. II. Magnification probability distributions*, *Phys. Rev. D* **85** (Jan., 2012) 023510, [`arXiv:1109.1873`].

[25] P. Fleury, H. Dupuy, and J.-P. Uzan, *Interpretation of the Hubble diagram in a nonhomogeneous universe*, *Phys. Rev. D* **87** (June, 2013) 123526, [`arXiv:1302.5308`].

[26] M. Bartelmann and P. Schneider, *Weak gravitational lensing*, *Phys. Rep.* **340** (Jan., 2001) 291–472, [`astro-ph/9912508`].

[27] C. Pitrou, T. S. Pereira, and J.-P. Uzan, *Weak-lensing by the large scale structure in a spatially anisotropic universe: theory and predictions*, *ArXiv e-prints* (Mar., 2015) [`arXiv:1503.01125`].

[28] T. S. Pereira, C. Pitrou, and J.-P. Uzan, *Weak-lensing B-modes as a probe of the isotropy of the universe*, *ArXiv e-prints* (Mar., 2015) [`arXiv:1503.01127`].

[29] I. M. H. Etherington, *On the Definition of Distance in General Relativity.*, *Philosophical Magazine* **15** (1933) 761.

[30] G. F. R. Ellis, *relativistic cosmology.*, in *General Relativity and Cosmology* (R. K. Sachs, ed.), pp. 104–182, 1971.

[31] A. A. Robb, *Optical Geometry of Motion: A New View of the Theory of Relativity*. W. Heffer (Cambridge), 1911.

[32] E. Gourgoulhon, *Relativité restreinte: des particules à l'astrophysique*. EDP Sciences/CNRS Éditions, 2010.

[33] A. Einstein, *Zur Elektrodynamik bewegter Körper*, *Annalen der Physik* **322** (1905) 891–921.

[34] H. Poincaré, *Œuvres*. Gauthier-Villars (Paris), 1924.

[35] E. Poisson, *The Motion of Point Particles in Curved Spacetime*, *Living Reviews in Relativity* **7** (May, 2004) 6, [`gr-qc/0306052`].

[36] T. Buchert, *Toward physical cosmology: focus on inhomogeneous geometry and its non-perturbative effects*, *Classical and Quantum Gravity* **28** (Aug., 2011) 164007, [`arXiv:1103.2016`].

[37] R. D. Reasenberg, I. I. Shapiro, P. E. MacNeil, R. B. Goldstein, J. C. Breidenthal, J. P. Brenkle, D. L. Cain, T. M. Kaufman, T. A. Komarek, and A. I. Zygielbaum, *Viking relativity experiment - Verification of signal retardation by solar gravity*, *ApJL* **234** (Dec., 1979) L219–L221.

[38] Gaia collaboration (ESA). `http://sci.esa.int/gaia/`.

[39] M. Bonamente, M. K. Joy, S. J. LaRoque, J. E. Carlstrom, E. D. Reese, and K. S. Dawson, *Determination of the Cosmic Distance Scale from Sunyaev-Zel'dovich Effect and Chandra X-Ray Measurements of High-Redshift Galaxy Clusters*, *ApJ* **647** (Aug., 2006) 25–54, [`astro-ph/0512349`].

[40] T. Delubac, J. E. Bautista, N. G. Busca, J. Rich, D. Kirkby, S. Bailey, A. Font-Ribera, A. Slosar, K.-G. Lee, M. M. Pieri, J.-C. Hamilton, É. Aubourg, M. Blomqvist, J. Bovy, J. Brinkmann, W. Carithers, K. S. Dawson, D. J. Eisenstein, S. G. A. Gontcho, J.-P. Kneib, J.-M. Le Goff, D. Margala, J. Miralda-Escudé, A. D. Myers, R. C. Nichol, P. Noterdaeme, R. O'Connell, M. D. Olmstead, N. Palanque-Delabrouille, I. Pâris, P. Petitjean, N. P. Ross, G. Rossi, D. J. Schlegel, D. P. Schneider, D. H. Weinberg, C. Yèche, and D. G. York, *Baryon acoustic oscillations in the Lyα forest of BOSS DR11 quasars*, *A&A* **574** (Feb., 2015) A59, [`arXiv:1404.1801`].

[41] A. G. Riess, W. Li, P. B. Stetson, A. V. Filippenko, S. Jha, R. P. Kirshner, P. M. Challis, P. M. Garnavich, and R. Chornock, *Cepheid Calibrations from the Hubble Space Telescope of the Luminosity of Two Recent Type Ia Supernovae and a Redetermination of the Hubble Constant*, *ApJ* **627** (July, 2005) 579–607, [`astro-ph/0503159`].

[42] M. Betoule, R. Kessler, J. Guy, J. Mosher, D. Hardin, R. Biswas, P. Astier, P. El-Hage, M. Konig, S. Kuhlmann, J. Marriner, R. Pain, N. Regnault, C. Balland, B. A. Bassett, P. J. Brown, H. Campbell, R. G. Carlberg, F. Cellier-Holzem, D. Cinabro, A. Conley, C. B. D'Andrea, D. L. DePoy, M. Doi, R. S. Ellis, S. Fabbro, A. V. Filippenko, R. J. Foley, J. A. Frieman, D. Fouchez, L. Galbany, A. Goobar, R. R. Gupta, G. J. Hill, R. Hlozek, C. J. Hogan, I. M. Hook, D. A. Howell, S. W. Jha, L. Le Guillou, G. Leloudas, C. Lidman, J. L. Marshall, A. Möller, A. M. Mourão, J. Neveu, R. Nichol, M. D. Olmstead, N. Palanque-Delabrouille, S. Perlmutter, J. L. Prieto, C. J. Pritchet, M. Richmond, A. G. Riess, V. Ruhlmann-Kleider, M. Sako, K. Schahmaneche, D. P. Schneider, M. Smith, J. Sollerman, M. Sullivan, N. A. Walton, and C. J. Wheeler, *Improved cosmological constraints from a joint analysis of the SDSS-II and SNLS supernova samples*, *A&A* **568** (Aug., 2014) A22, [`arXiv:1401.4064`].

[43] C. M. Will, *The Confrontation between General Relativity and Experiment*, *Living Reviews in Relativity* **9** (Mar., 2006) 3, [`gr-qc/0510072`].

[44] J. G. Williams, X. X. Newhall, and J. O. Dickey, *Relativity parameters determined from lunar laser ranging*, *Phys. Rev. D* **53** (1996) 6730–6739.

[45] J. G. Williams, S. G. Turyshev, and D. H. Boggs, *Progress in lunar laser ranging tests of relativistic gravity*, *Phys. Rev. Lett.* **93** (2004) [`gr-qc/0411113`].

[46] J. G. Williams, R. H. Dicke, P. L. Bender, C. O. Alley, W. E. Carter, D. G. Currie, D. H. Eckhardt, J. E. Faller, W. M. Kaula, J. D. Mulholland, H. H. Plotkin, S. K. Poultney, P. J. Shelus, E. C. Silverberg, W. S. Sinclair, M. A. Slade, and D. T. Wilkinson, *New test of the equivalence principle from lunar laser ranging*, *Phys. Rev. Lett.* **36** (1976) 551–554.

[47] LIGO collaboration. `http://www.ligo.caltech.edu`.

[48] VIRGO collaboration. `http://wwwcascina.virgo.infn.it`.

[49] eLISA collaboration. `https://www.elisascience.org`.

[50] Hipparcos collaboration (ESA). `http://sci.esa.int/hipparcos/`.

[51] P. Jordan, J. Ehlers, and R. K. Sachs, *Republication of: Contributions to the theory of pure gravitational radiation. Exact solutions of the field equations of the general theory of relativity II*, *General Relativity and Gravitation* **45** (Dec., 2013) 2691–2753.

[52] K. Rosquist, *Trigonometric parallaxes of distant objects - What they could tell about the universe*, *ApJ* **331** (Aug., 1988) 648–652.

[53] H. S. Leavitt and E. C. Pickering, *Periods of 25 Variable Stars in the Small Magellanic Cloud.*, *Harvard College Observatory Circular* **173** (Mar., 1912) 1–3.

[54] A. S. Eddington, *The pulsation theory of Cepheid variables*, *The Observatory* **40** (Aug., 1917) 290–293.

[55] B. Wang and Z. Han, *Progenitors of type Ia supernovae*, *New Astronomy Reviews* **56** (June, 2012) 122–141, [`arXiv:1204.1155`].

[56] C. T. Kowal, *Absolute magnitudes of supernovae.*, *AJ* **73** (Dec., 1968) 1021–1024.

[57] G. Risaliti and E. Lusso, *A Hubble Diagram for Quasars*, *ArXiv e-prints* (May, 2015) [`arXiv:1505.07118`].

[58] B. F. Schutz, *Determining the Hubble constant from gravitational wave observations*, *Nature* **323** (Sept., 1986) 310.

[59] D. E. Holz and S. A. Hughes, *Using Gravitational-Wave Standard Sirens*, *ApJ* **629** (Aug., 2005) 15–22, [`astro-ph/0504616`].

[60] J.-P. Uzan, N. Aghanim, and Y. Mellier, *Distance duality relation from x-ray and Sunyaev-Zel'dovich observations of clusters*, *Phys. Rev. D* **70** (Oct., 2004) 083533, [`astro-ph/0405620`].

[61] G. F. R. Ellis, R. Poltis, J.-P. Uzan, and A. Weltman, *Blackness of the cosmic microwave background spectrum as a probe of the distance-duality relation*, *Phys. Rev. D* **87** (May, 2013) 103530, [`arXiv:1301.1312`].

[62] A. Einstein, *Kosmologische Betrachtungen zur allgemeinen Relativitätstheorie*, *Sitzungsberichte der Königlich Preußischen Akademie der Wissenschaften (Berlin), Seite 142-152.* (1917) 142–152.

[63] A. Friedmann, *Über die Krümmung des Raumes*, *Zeitschrift fur Physik* **10** (1922) 377–386.

[64] G. Lemaître, *Un Univers homogène de masse constante et de rayon croissant rendant compte de la vitesse radiale des nébuleuses extra-galactiques*, *Annales de la Société Scientifique de Bruxelles* **47** (1927) 49–59.

[65] E. Hubble, *A Relation between Distance and Radial Velocity among Extra-Galactic Nebulae*, *Proceedings of the National Academy of Science* **15** (Mar., 1929) 168–173.

[66] H. P. Robertson, *On the Foundations of Relativistic Cosmology*, *Proceedings of the National Academy of Science* **15** (Nov., 1929) 822–829.

[67] H. P. Robertson, *Kinematics and World-Structure*, *ApJ* **82** (Nov., 1935) 284.

[68] H. P. Robertson, *Kinematics and World-Structure II.*, *ApJ* **83** (Apr., 1936) 187.

[69] H. P. Robertson, *Kinematics and World-Structure III.*, *ApJ* **83** (May, 1936) 257.

[70] A. G. Walker, *On Milne's Theory of World-Structure*, *Proceedings of the London Mathematical Society* (1937).

[71] S. W. Hawking and G. F. R. Ellis, *The large-scale structure of space-time.* Cambridge University Press, 1973.

[72] S. Tsujikawa, *Quintessence: a review*, *Classical and Quantum Gravity* **30** (Nov., 2013) 214003, [`arXiv:1304.1961`].

[73] P. Ruiz-Lapuente, ed., *Dark Energy: Observational and Theoretical Approaches.* Cambridge University Press, 2010.

[74] V. Gorini, A. Kamenshchik, U. Moschella, and V. Pasquier, *The Chaplygin Gas as a Model for Dark Energy*, in *The Tenth Marcel Grossmann Meeting. Proceedings of the MG10 Meeting held at Brazilian Center for Research in Physics (CBPF), Rio de Janeiro, Brazil, 20-26 July 2003, Eds.: Mário Novello; Santiago Perez Bergliaffa; Remo Ruffini. Singapore: World Scientific Publishing, in 3 volumes, ISBN 981-256-667-8 (set), ISBN 981-256-980-4 (Part A), ISBN 981-256-979-0 (Part B), ISBN 981-256-978-2 (Part C), 2006, XLVIII + 2492 pp.: 2006, p.840* (M. Novello, S. Perez Bergliaffa, and R. Ruffini, eds.), p. 840, Feb., 2006. `gr-qc/0403062`.

[75] J. Khoury, *Les Houches Lectures on Physics Beyond the Standard Model of Cosmology*, *ArXiv e-prints* (Dec., 2013) [`arXiv:1312.2006`].

[76] C. Deffayet and D. A. Steer, *A formal introduction to Horndeski and Galileon theories and their generalizations*, *Classical and Quantum Gravity* **30** (Nov., 2013) 214006, [`arXiv:1307.2450`].

[77] M. Zumalacárregui and J. García-Bellido, *Transforming gravity: From derivative couplings to matter to second-order scalar-tensor theories beyond the Horndeski Lagrangian*, *Phys. Rev. D* **89** (Mar., 2014) 064046, [`arXiv:1308.4685`].

[78] J. Gleyzes, D. Langlois, F. Piazza, and F. Vernizzi, *Exploring gravitational theories beyond Horndeski*, *JCAP* **2** (Feb., 2015) 18, [`arXiv:1408.1952`].

[79] T. Clifton, P. G. Ferreira, A. Padilla, and C. Skordis, *Modified gravity and cosmology*, *Phys. Rep.* **513** (Mar., 2012) 1–189, [`arXiv:1106.2476`].

[80] A. de Felice and S. Tsujikawa, *f(R) Theories*, *Living Reviews in Relativity* **13** (June, 2010) 3, [`arXiv:1002.4928`].

[81] C. de Rham, *Massive Gravity*, *Living Reviews in Relativity* **17** (Aug., 2014) 7, [`arXiv:1401.4173`].

[82] T. Jacobson, *Einstein-aether gravity: a status report*, *ArXiv e-prints* (Jan., 2008) [`arXiv:0801.1547`].

[83] C. Clarkson, G. Ellis, J. Larena, and O. Umeh, *Does the growth of structure affect our dynamical models of the universe? The averaging, backreaction and fitting problems in cosmology*, *ArXiv e-prints* (Sept., 2011) [`arXiv:1109.2314`].

[84] T. Buchert and S. Räsänen, *Backreaction in Late-Time Cosmology*, *Annual Review of Nuclear and Particle Science* **62** (Nov., 2012) 57–79, [`arXiv:1112.5335`].

[85] D. L. Wiltshire, *Cosmic structure, averaging and dark energy*, *ArXiv e-prints* (Nov., 2013) [`arXiv:1311.3787`].

[86] C. Csáki, N. Kaloper, and J. Terning, *Dimming Supernovae without Cosmic Acceleration*, *Physical Review Letters* **88** (Apr., 2002) 161302, [`hep-ph/0111311`].

[87] C. Deffayet, D. Harari, J.-P. Uzan, and M. Zaldarriaga, *Dimming of supernovae by photon-pseudoscalar conversion and the intergalactic plasma*, *Phys. Rev. D* **66** (Aug., 2002) 043517, [`hep-ph/0112118`].

[88] T. Clifton, P. G. Ferreira, and K. Land, *Living in a Void: Testing the Copernican Principle with Distant Supernovae*, *Physical Review Letters* **101** (Sept., 2008) 131302, [`arXiv:0807.1443`].

[89] C. Clarkson, *Establishing homogeneity of the universe in the shadow of dark energy*, *Comptes Rendus Physique* **13** (July, 2012) 682–718, [`arXiv:1204.5505`].

[90] G. Efstathiou, H_0 *revisited*, *MNRAS* **440** (May, 2014) 1138–1152, [`arXiv:1311.3461`].

[91] Planck Collaboration, P. A. R. Ade, N. Aghanim, M. Arnaud, M. Ashdown, J. Aumont, C. Baccigalupi, A. J. Banday, R. B. Barreiro, J. G. Bartlett, and et al., *Planck 2015 results. XIII. Cosmological parameters*, *ArXiv e-prints* (Feb., 2015) [`arXiv:1502.01589`].

[92] G. Bertone, D. Hooper, and J. Silk, *Particle dark matter: evidence, candidates and constraints*, *Phys. Rep.* **405** (Jan., 2005) 279–390, [`hep-ph/0404175`].

[93] R. Brout, F. Englert, and E. Gunzig, *The creation of the Universe as a quantum phenomenon.*, *Annals of Physics* **115** (1978) 78–106.

[94] A. A. Starobinskiǐ, *Spectrum of relict gravitational radiation and the early state of the universe*, *Soviet Journal of Experimental and Theoretical Physics Letters* **30** (Dec., 1979) 682.

[95] A. H. Guth, *Inflationary universe: A possible solution to the horizon and flatness problems*, *Phys. Rev. D* **23** (Jan., 1981) 347–356.

[96] J. Khoury, B. A. Ovrut, P. J. Steinhardt, and N. Turok, *Ekpyrotic universe: Colliding branes and the origin of the hot big bang*, *Phys. Rev. D* **64** (Dec., 2001) 123522, [`hep-th/0103239`].

[97] D. Battefeld and P. Peter, *A critical review of classical bouncing cosmologies*, *Phys. Rep.* **571** (Apr., 2015) 1–66, [`arXiv:1406.2790`].

[98] J. Martin, C. Ringeval, and V. Vennin, *Encyclopædia Inflationaris*, *Physics of the Dark Universe* **5** (Dec., 2014) 75–235, [`arXiv:1303.3787`].

[99] J. Martin, C. Ringeval, and V. Vennin, *Observing Inflationary Reheating*, *Physical Review Letters* **114** (Feb., 2015) 081303, [`arXiv:1410.7958`].

[100] V. de Lapparent, M. J. Geller, and J. P. Huchra, *A slice of the universe*, *ApJL* **302** (Mar., 1986) L1–L5.

[101] P. Peter and J.-P. Uzan, *Primordial Cosmology*. Oxford Graduate Texts, 2009.

[102] R. P. Kerr, *Gravitational Field of a Spinning Mass as an Example of Algebraically Special Metrics*, *Physical Review Letters* **11** (Sept., 1963) 237–238.

[103] F. Bernardeau, *Cosmologie : Des fondements théoriques aux observations*. EDP Sciences/CNRS Éditions, 2010.

[104] F. Bernardeau, S. Colombi, E. Gaztañaga, and R. Scoccimarro, *Large-scale structure of the Universe and cosmological perturbation theory*, *Phys. Rep.* **367** (Sept., 2002) 1–248, [`astro-ph/0112551`].

[105] GADGET code. `http://www.mpa-garching.mpg.de/gadget/`.

[106] M. Tegmark, D. J. Eisenstein, M. A. Strauss, D. H. Weinberg, M. R. Blanton, J. A. Frieman, M. Fukugita, J. E. Gunn, A. J. S. Hamilton, G. R. Knapp, R. C. Nichol, J. P. Ostriker, N. Padmanabhan, W. J. Percival, D. J. Schlegel, D. P. Schneider, R. Scoccimarro, U. Seljak, H.-J. Seo, M. Swanson, A. S. Szalay, M. S. Vogeley, J. Yoo, I. Zehavi, K. Abazajian, S. F. Anderson, J. Annis, N. A. Bahcall, B. Bassett, A. Berlind, J. Brinkmann, T. Budavari, F. Castander, A. Connolly, I. Csabai, M. Doi, D. P. Finkbeiner, B. Gillespie, K. Glazebrook, G. S. Hennessy, D. W. Hogg, Ž. Ivezić, B. Jain, D. Johnston, S. Kent, D. Q. Lamb, B. C. Lee, H. Lin, J. Loveday, R. H. Lupton, J. A. Munn, K. Pan, C. Park, J. Peoples, J. R. Pier, A. Pope, M. Richmond, C. Rockosi, R. Scranton, R. K. Sheth, A. Stebbins, C. Stoughton, I. Szapudi, D. L. Tucker, D. E. vanden Berk, B. Yanny, and D. G. York, *Cosmological constraints from the SDSS luminous red galaxies*, *Phys. Rev. D* **74** (Dec., 2006) 123507, [`astro-ph/0608632`].

[107] C. Pitrou, *Dynamique non-linéaire et anisotropie primordiale en cosmologie*. PhD thesis, Université Pierre et Marie Curie Paris 6, 2008.

[108] J. Lesgourgues, S. Matarrese, M. Pietroni, and A. Riotto, *Non-linear power spectrum including massive neutrinos: the time-RG flow approach*, *JCAP* **6** (June, 2009) 17, [`arXiv:0901.4550`].

[109] D. Blas, M. Garny, T. Konstandin, and J. Lesgourgues, *Structure formation with massive neutrinos: going beyond linear theory*, JCAP **11** (Nov., 2014) 39, [`arXiv:1408.2995`].

[110] H. Dupuy and F. Bernardeau, *Cosmological Perturbation Theory for streams of relativistic particles*, JCAP **3** (Mar., 2015) 30, [`arXiv:1411.0428`].

[111] S. R. Green and R. M. Wald, *How well is our Universe described by an FLRW model?*, Classical and Quantum Gravity **31** (Dec., 2014) 234003, [`arXiv:1407.8084`].

[112] T. Buchert, M. Carfora, G. F. R. Ellis, E. W. Kolb, M. A. H. MacCallum, J. J. Ostrowski, S. Räsänen, B. F. Roukema, L. Andersson, A. A. Coley, and D. L. Wiltshire, *Is there proof that backreaction of inhomogeneities is irrelevant in cosmology?*, ArXiv e-prints (May, 2015) [`arXiv:1505.07800`].

[113] S. R. Green and R. M. Wald, *Comments on Backreaction*, ArXiv e-prints (June, 2015) [`arXiv:1506.06452`].

[114] T. Buchert, *On Average Properties of Inhomogeneous Fluids in General Relativity: Dust Cosmologies*, General Relativity and Gravitation **32** (Jan., 2000) 105–126, [`gr-qc/9906015`].

[115] R. M. Zalaletdinov, *Towards a theory of macroscopic gravity*, General Relativity and Gravitation **25** (July, 1993) 673–695.

[116] A. Paranjape, *The Averaging Problem in Cosmology*. PhD thesis, PhD Thesis, 2009, june, 2009.

[117] J. Adamek, R. Durrer, and M. Kunz, *N-body methods for relativistic cosmology*, Classical and Quantum Gravity **31** (Dec., 2014) 234006, [`arXiv:1408.3352`].

[118] J. Adamek, C. Clarkson, R. Durrer, and M. Kunz, *Does Small Scale Structure Significantly Affect Cosmological Dynamics?*, Physical Review Letters **114** (Feb., 2015) 051302, [`arXiv:1408.2741`].

[119] S. R. Green and R. M. Wald, *New framework for analyzing the effects of small scale inhomogeneities in cosmology*, Phys. Rev. D **83** (Apr., 2011) 084020, [`arXiv:1011.4920`].

[120] T. Buchert and M. Ostermann, *Lagrangian theory of structure formation in relativistic cosmology: Lagrangian framework and definition of a nonperturbative approximation*, Phys. Rev. D **86** (July, 2012) 023520, [`arXiv:1203.6263`].

[121] T. Buchert, C. Nayet, and A. Wiegand, *Lagrangian theory of structure formation in relativistic cosmology. II. Average properties of a generic evolution model*, Phys. Rev. D **87** (June, 2013) 123503, [`arXiv:1303.6193`].

[122] A. Alles, T. Buchert, F. Al Roumi, and A. Wiegand, *Lagrangian theory of structure formation in relativistic cosmology. III. Gravitoelectric perturbation and solution schemes at any order*, Phys. Rev. D **92** (July, 2015) 023512, [`arXiv:1503.02566`].

[123] D. Baumann, A. Nicolis, L. Senatore, and M. Zaldarriaga, *Cosmological non-linearities as an effective fluid*, *JCAP* **7** (July, 2012) 51, [`arXiv:1004.2488`].

[124] P. Fleury, C. Pitrou, and J.-P. Uzan, *Light propagation in a homogeneous and anisotropic universe*, *Phys. Rev. D* **91** (Feb., 2015) 043511, [`arXiv:1410.8473`].

[125] A. Sandage, *The Change of Redshift and Apparent Luminosity of Galaxies due to the Deceleration of Selected Expanding Universes.*, *ApJ* **136** (Sept., 1962) 319.

[126] G. C. McVittie, *Appendix to The Change of Redshift and Apparent Luminosity of Galaxies due to the Deceleration of Selected Expanding Universes.*, *ApJ* **136** (Sept., 1962) 334.

[127] S. Cristiani, G. Avila, P. Bonifacio, F. Bouchy, B. Carswell, S. D'Odorico, V. D'Odorico, B. Delabre, H. Dekker, M. Dessauges, P. Dimarcantonio, R. Garcia-Lopez, A. Grazian, M. Haehnelt, J. M. Herreros, G. Israelian, S. Levshakov, J. Liske, C. Lovis, A. Manescau, E. Martin, M. Mayor, D. Megevand, P. Molaro, M. Murphy, L. Pasquini, F. Pepe, J. Perez, D. Queloz, R. Rebolo, P. Santin, P. Shaver, P. Spanò, S. Udry, E. Vanzella, M. Viel, M. R. Zapatero, F. Zerbi, and S. Zucker, *The CODEX-ESPRESSO experiment: Cosmic dynamics, fundamental physics, planets and much more...*, *Nuovo Cimento B Serie* **122** (Sept., 2007) 1165–1170, [`arXiv:0712.4152`].

[128] C. Quercellini, L. Amendola, A. Balbi, P. Cabella, and M. Quartin, *Real-time cosmology*, *Phys. Rep.* **521** (Dec., 2012) 95–134, [`arXiv:1011.2646`].

[129] R. K. Sachs and A. M. Wolfe, *Perturbations of a Cosmological Model and Angular Variations of the Microwave Background*, *ApJ* **147** (Jan., 1967) 73.

[130] M. J. Rees and D. W. Sciama, *Large-scale Density Inhomogeneities in the Universe*, *Nature* **217** (Feb., 1968) 511–516.

[131] S. Boughn and R. Crittenden, *A correlation between the cosmic microwave background and large-scale structure in the Universe*, *Nature* **427** (Jan., 2004) 45–47, [`astro-ph/0305001`].

[132] A. J. Nishizawa, *The integrated Sachs-Wolfe effect and the Rees-Sciama effect*, *Progress of Theoretical and Experimental Physics* **2014** (June, 2014) 060000, [`arXiv:1404.5102`].

[133] Planck Collaboration, P. A. R. Ade, N. Aghanim, M. Arnaud, M. Ashdown, J. Aumont, C. Baccigalupi, A. J. Banday, R. B. Barreiro, N. Bartolo, and et al., *Planck 2015 results. XXI. The integrated Sachs-Wolfe effect*, *ArXiv e-prints* (Feb., 2015) [`arXiv:1502.01595`].

[134] G. Meylan, P. Jetzer, P. North, P. Schneider, C. S. Kochanek, and J. Wambsganss, eds., *Gravitational Lensing: Strong, Weak and Micro*, 2006.

[135] E. Barausse, S. Matarrese, and A. Riotto, *Effect of inhomogeneities on the luminosity distance-redshift relation: Is dark energy necessary in a perturbed universe?*, *Phys. Rev. D* **71** (Mar., 2005) 063537, [`astro-ph/0501152`].

[136] I. Ben-Dayan, G. Marozzi, F. Nugier, and G. Veneziano, *The second-order luminosity-redshift relation in a generic inhomogeneous cosmology*, JCAP **11** (Nov., 2012) 45, [`arXiv:1209.4326`].

[137] S. Andrianomena, C. Clarkson, P. Patel, O. Umeh, and J.-P. Uzan, *Non-linear relativistic contributions to the cosmological weak-lensing convergence*, JCAP **6** (June, 2014) 23, [`arXiv:1402.4350`].

[138] O. Umeh, C. Clarkson, and R. Maartens, *Nonlinear relativistic corrections to cosmological distances, redshift and gravitational lensing magnification: I. Key results*, Classical and Quantum Gravity **31** (Oct., 2014) 202001, [`arXiv:1207.2109`].

[139] O. Umeh, C. Clarkson, and R. Maartens, *Nonlinear relativistic corrections to cosmological distances, redshift and gravitational lensing magnification: II. Derivation*, Classical and Quantum Gravity **31** (Oct., 2014) 205001, [`arXiv:1402.1933`].

[140] K. Bolejko, C. Clarkson, R. Maartens, D. Bacon, N. Meures, and E. Beynon, *Antilensing: The Bright Side of Voids*, Physical Review Letters **110** (Jan., 2013) 021302, [`arXiv:1209.3142`].

[141] F. Nugier, *Lightcone Averaging and Precision Cosmology*, ArXiv e-prints (Sept., 2013) [`arXiv:1309.6542`].

[142] L. Hui and P. B. Greene, *Correlated fluctuations in luminosity distance and the importance of peculiar motion in supernova surveys*, Phys. Rev. D **73** (June, 2006) 123526, [`astro-ph/0512159`].

[143] C. Bonvin, R. Durrer, and M. A. Gasparini, *Fluctuations of the luminosity distance*, Phys. Rev. D **73** (Jan., 2006) 023523, [`astro-ph/0511183`].

[144] E. Di Dio and R. Durrer, *Vector and tensor contributions to the luminosity distance*, Phys. Rev. D **86** (July, 2012) 023510, [`arXiv:1205.3366`].

[145] N. Kaiser, *Weak gravitational lensing of distant galaxies*, ApJ **388** (Apr., 1992) 272–286.

[146] S. Codis, R. Gavazzi, Y. Dubois, C. Pichon, K. Benabed, V. Desjacques, D. Pogosyan, J. Devriendt, and A. Slyz, *Intrinsic alignment of simulated galaxies in the cosmic web: implications for weak lensing surveys*, MNRAS **448** (Apr., 2015) 3391–3404, [`arXiv:1406.4668`].

[147] N. E. Chisari, S. Codis, C. Laigle, Y. Dubois, C. Pichon, J. Devriendt, A. Slyz, L. Miller, R. Gavazzi, and K. Benabed, *Intrinsic alignments of galaxies in the Horizon-AGN cosmological hydrodynamical simulation*, ArXiv e-prints (July, 2015) [`arXiv:1507.07843`].

[148] N. Kaiser and G. Squires, *Mapping the dark matter with weak gravitational lensing*, ApJ **404** (Feb., 1993) 441–450.

[149] R. Tripp, *A two-parameter luminosity correction for Type IA supernovae*, A&A **331** (Mar., 1998) 815–820.

[150] M. Hicken, P. Challis, S. Jha, R. P. Kirshner, T. Matheson, M. Modjaz, A. Rest, W. M. Wood-Vasey, G. Bakos, E. J. Barton, P. Berlind, A. Bragg, C. Briceño, W. R. Brown, N. Caldwell, M. Calkins, R. Cho, L. Ciupik, M. Contreras, K.-C. Dendy, A. Dosaj, N. Durham, K. Eriksen, G. Esquerdo, M. Everett, E. Falco, J. Fernandez, A. Gaba, P. Garnavich, G. Graves, P. Green, T. Groner, C. Hergenrother, M. J. Holman, V. Hradecky, J. Huchra, B. Hutchison, D. Jerius, A. Jordan, R. Kilgard, M. Krauss, K. Luhman, L. Macri, D. Marrone, J. McDowell, D. McIntosh, B. McNamara, T. Megeath, B. Mochejska, D. Munoz, J. Muzerolle, O. Naranjo, G. Narayan, M. Pahre, W. Peters, D. Peterson, K. Rines, B. Ripman, A. Roussanova, R. Schild, A. Sicilia-Aguilar, J. Sokoloski, K. Smalley, A. Smith, T. Spahr, K. Z. Stanek, P. Barmby, S. Blondin, C. W. Stubbs, A. Szentgyorgyi, M. A. P. Torres, A. Vaz, A. Vikhlinin, Z. Wang, M. Westover, D. Woods, and P. Zhao, *CfA3: 185 Type Ia Supernova Light Curves from the CfA*, *ApJ* **700** (July, 2009) 331–357, [`arXiv:0901.4787`].

[151] M. Sako, B. Bassett, A. C. Becker, P. J. Brown, H. Campbell, R. Cane, D. Cinabro, C. B. D'Andrea, K. S. Dawson, F. DeJongh, D. L. Depoy, B. Dilday, M. Doi, A. V. Filippenko, J. A. Fischer, R. J. Foley, J. A. Frieman, L. Galbany, P. M. Garnavich, A. Goobar, R. R. Gupta, G. J. Hill, B. T. Hayden, R. Hlozek, J. A. Holtzman, U. Hopp, S. W. Jha, R. Kessler, W. Kollatschny, G. Leloudas, J. Marriner, J. L. Marshall, R. Miquel, T. Morokuma, J. Mosher, R. C. Nichol, J. Nordin, M. D. Olmstead, L. Ostman, J. L. Prieto, M. Richmond, R. W. Romani, J. Sollerman, M. Stritzinger, D. P. Schneider, M. Smith, J. C. Wheeler, N. Yasuda, and C. Zheng, *The Data Release of the Sloan Digital Sky Survey-II Supernova Survey*, *ArXiv e-prints* (Jan., 2014) [`arXiv:1401.3317`].

[152] J. Guy, M. Sullivan, A. Conley, N. Regnault, P. Astier, C. Balland, S. Basa, R. G. Carlberg, D. Fouchez, D. Hardin, I. M. Hook, D. A. Howell, R. Pain, N. Palanque-Delabrouille, K. M. Perrett, C. J. Pritchet, J. Rich, V. Ruhlmann-Kleider, D. Balam, S. Baumont, R. S. Ellis, S. Fabbro, H. K. Fakhouri, N. Fourmanoit, S. González-Gaitán, M. L. Graham, E. Hsiao, T. Kronborg, C. Lidman, A. M. Mourao, S. Perlmutter, P. Ripoche, N. Suzuki, and E. S. Walker, *The Supernova Legacy Survey 3-year sample: Type Ia supernovae photometric distances and cosmological constraints*, *A&A* **523** (Nov., 2010) A7, [`arXiv:1010.4743`].

[153] A. G. Riess, L.-G. Strolger, S. Casertano, H. C. Ferguson, B. Mobasher, B. Gold, P. J. Challis, A. V. Filippenko, S. Jha, W. Li, J. Tonry, R. Foley, R. P. Kirshner, M. Dickinson, E. MacDonald, D. Eisenstein, M. Livio, J. Younger, C. Xu, T. Dahlén, and D. Stern, *New Hubble Space Telescope Discoveries of Type Ia Supernovae at z>1: Narrowing Constraints on the Early Behavior of Dark Energy*, *ApJ* **659** (Apr., 2007) 98–121, [`astro-ph/0611572`].

[154] A. G. Riess, A. V. Filippenko, P. Challis, A. Clocchiatti, A. Diercks, P. M. Garnavich, R. L. Gilliland, C. J. Hogan, S. Jha, R. P. Kirshner, B. Leibundgut, M. M. Phillips, D. Reiss, B. P. Schmidt, R. A. Schommer, R. C. Smith, J. Spyromilio, C. Stubbs, N. B. Suntzeff, and J. Tonry, *Observational Evidence from Supernovae for an Accelerating Universe and a Cosmological Constant*, *AJ* **116** (Sept., 1998) 1009–1038, [`astro-ph/9805201`].

[155] S. Perlmutter, G. Aldering, G. Goldhaber, R. A. Knop, P. Nugent, P. G. Castro, S. Deustua, S. Fabbro, A. Goobar, D. E. Groom, I. M. Hook, A. G. Kim, M. Y. Kim, J. C. Lee, N. J. Nunes, R. Pain, C. R. Pennypacker, R. Quimby, C. Lidman, R. S. Ellis, M. Irwin, R. G. McMahon, P. Ruiz-Lapuente, N. Walton, B. Schaefer, B. J. Boyle, A. V. Filippenko, T. Matheson, A. S. Fruchter, N. Panagia, H. J. M. Newberg, W. J. Couch, and T. S. C. Project, *Measurements of Ω and Λ from 42 High-Redshift Supernovae*, ApJ **517** (June, 1999) 565–586, [astro-ph/9812133].

[156] A. Conley, J. Guy, M. Sullivan, N. Regnault, P. Astier, C. Balland, S. Basa, R. G. Carlberg, D. Fouchez, D. Hardin, I. M. Hook, D. A. Howell, R. Pain, N. Palanque-Delabrouille, K. M. Perrett, C. J. Pritchet, J. Rich, V. Ruhlmann-Kleider, D. Balam, S. Baumont, R. S. Ellis, S. Fabbro, H. K. Fakhouri, N. Fourmanoit, S. González-Gaitán, M. L. Graham, M. J. Hudson, E. Hsiao, T. Kronborg, C. Lidman, A. M. Mourao, J. D. Neill, S. Perlmutter, P. Ripoche, N. Suzuki, and E. S. Walker, *Supernova Constraints and Systematic Uncertainties from the First Three Years of the Supernova Legacy Survey*, ApJS **192** (Jan., 2011) 1, [arXiv:1104.1443].

[157] N. Kaiser and M. J. Hudson, *Kinematic Bias in Cosmological Distance Measurement*, ArXiv e-prints (Feb., 2015) [arXiv:1502.01762].

[158] T. W. B. Kibble and R. Lieu, *Average Magnification Effect of Clumping of Matter*, ApJ **632** (Oct., 2005) 718–726, [astro-ph/0412275].

[159] N. Kaiser and J. A. Peacock, *On the Bias of the Distance-Redshift Relation from Gravitational Lensing*, ArXiv e-prints (Mar., 2015) [arXiv:1503.08506].

[160] C. Bonvin, C. Clarkson, R. Durrer, R. Maartens, and O. Umeh, *Cosmological ensemble and directional averages of observables*, JCAP **7** (July, 2015) 40, [arXiv:1504.01676].

[161] I. Ben-Dayan, M. Gasperini, G. Marozzi, F. Nugier, and G. Veneziano, *Average and dispersion of the luminosity-redshift relation in the concordance model*, JCAP **6** (June, 2013) 2, [arXiv:1302.0740].

[162] I. Ben-Dayan, M. Gasperini, G. Marozzi, F. Nugier, and G. Veneziano, *Do Stochastic Inhomogeneities Affect Dark-Energy Precision Measurements?*, Physical Review Letters **110** (Jan., 2013) 021301, [arXiv:1207.1286].

[163] G. R. Bengochea and M. E. De Rossi, *Dependence on supernovae light-curve processing in void models*, Physics Letters B **733** (June, 2014) 258–264, [arXiv:1402.3167].

[164] J. Guy, P. Astier, S. Baumont, D. Hardin, R. Pain, N. Regnault, S. Basa, R. G. Carlberg, A. Conley, S. Fabbro, D. Fouchez, I. M. Hook, D. A. Howell, K. Perrett, C. J. Pritchet, J. Rich, M. Sullivan, P. Antilogus, E. Aubourg, G. Bazin, J. Bronder, M. Filiol, N. Palanque-Delabrouille, P. Ripoche, and V. Ruhlmann-Kleider, *SALT2: using distant supernovae to improve the use of type Ia supernovae as distance indicators*, A&A **466** (Apr., 2007) 11–21, [astro-ph/0701828].

[165] S. Jha, A. G. Riess, and R. P. Kirshner, *Improved Distances to Type Ia Supernovae with Multicolor Light-Curve Shapes: MLCS2k2*, *ApJ* **659** (Apr., 2007) 122–148, [`astro-ph/0612666`].

[166] G. Gamow, *The Evolution of the Universe*, *Nature* **162** (Oct., 1948) 680–682.

[167] R. A. Alpher and R. Herman, *Evolution of the Universe*, *Nature* **162** (Nov., 1948) 774–775.

[168] A. A. Penzias and R. W. Wilson, *A Measurement of Excess Antenna Temperature at 4080 Mc/s.*, *ApJ* **142** (July, 1965) 419–421.

[169] COBE collaboration (NASA). `http://aether.lbl.gov/www/projects/cobe/`.

[170] WMAP collaboration (NASA). `http://map.gsfc.nasa.gov`.

[171] Planck collaboration (ESA). `http://www.cosmos.esa.int/web/planck`.

[172] D. J. Fixsen, *The Temperature of the Cosmic Microwave Background*, *ApJ* **707** (Dec., 2009) 916–920, [`arXiv:0911.1955`].

[173] National Institute of Standards and Technology (NIST). `http://physics.nist.gov/cgi-bin/cuu/Value?bwien`.

[174] R. Durrer, *The Cosmic Microwave Background.* Cambridge University Press, Aug., 2008.

[175] Planck Collaboration, R. Adam, P. A. R. Ade, N. Aghanim, Y. Akrami, M. I. R. Alves, M. Arnaud, F. Arroja, J. Aumont, C. Baccigalupi, and et al., *Planck 2015 results. I. Overview of products and scientific results*, *ArXiv e-prints* (Feb., 2015) [`arXiv:1502.01582`].

[176] Planck Collaboration, P. A. R. Ade, N. Aghanim, M. Arnaud, M. Ashdown, J. Aumont, C. Baccigalupi, A. J. Banday, R. B. Barreiro, N. Bartolo, and et al., *Planck 2015 results. XVIII. Background geometry and topology*, *ArXiv e-prints* (Feb., 2015) [`arXiv:1502.01593`].

[177] Planck Collaboration, P. A. R. Ade, N. Aghanim, M. Arnaud, F. Arroja, M. Ashdown, J. Aumont, C. Baccigalupi, M. Ballardini, A. J. Banday, and et al., *Planck 2015 results. XX. Constraints on inflation*, *ArXiv e-prints* (Feb., 2015) [`arXiv:1502.02114`].

[178] A. Lewis and A. Challinor, *Weak gravitational lensing of the CMB*, *Phys. Rep.* **429** (June, 2006) 1–65, [`astro-ph/0601594`].

[179] Planck Collaboration, P. A. R. Ade, N. Aghanim, M. Arnaud, M. Ashdown, J. Aumont, C. Baccigalupi, A. J. Banday, R. B. Barreiro, J. G. Bartlett, and et al., *Planck 2015 results. XV. Gravitational lensing*, *ArXiv e-prints* (Feb., 2015) [`arXiv:1502.01591`].

[180] C. Clarkson, O. Umeh, R. Maartens, and R. Durrer, *What is the distance to the CMB?*, *JCAP* **11** (Nov., 2014) 36, [`arXiv:1405.7860`].

[181] C. Bonvin, C. Clarkson, R. Durrer, R. Maartens, and O. Umeh, *Do we care about the distance to the CMB? Clarifying the impact of second-order lensing*, *JCAP* **6** (June, 2015) 50, [`arXiv:1503.07831`].

[182] D. J. Eisenstein, I. Zehavi, D. W. Hogg, R. Scoccimarro, M. R. Blanton, R. C. Nichol, R. Scranton, H.-J. Seo, M. Tegmark, Z. Zheng, S. F. Anderson, J. Annis, N. Bahcall, J. Brinkmann, S. Burles, F. J. Castander, A. Connolly, I. Csabai, M. Doi, M. Fukugita, J. A. Frieman, K. Glazebrook, J. E. Gunn, J. S. Hendry, G. Hennessy, Z. Ivezić, S. Kent, G. R. Knapp, H. Lin, Y.-S. Loh, R. H. Lupton, B. Margon, T. A. McKay, A. Meiksin, J. A. Munn, A. Pope, M. W. Richmond, D. Schlegel, D. P. Schneider, K. Shimasaku, C. Stoughton, M. A. Strauss, M. SubbaRao, A. S. Szalay, I. Szapudi, D. L. Tucker, B. Yanny, and D. G. York, *Detection of the Baryon Acoustic Peak in the Large-Scale Correlation Function of SDSS Luminous Red Galaxies*, *ApJ* **633** (Nov., 2005) 560–574, [`astro-ph/0501171`].

[183] SDSS-III collaboration. `https://www.sdss3.org/index.php`.

[184] L. Anderson, É. Aubourg, S. Bailey, F. Beutler, V. Bhardwaj, M. Blanton, A. S. Bolton, J. Brinkmann, J. R. Brownstein, A. Burden, C.-H. Chuang, A. J. Cuesta, K. S. Dawson, D. J. Eisenstein, S. Escoffier, J. E. Gunn, H. Guo, S. Ho, K. Honscheid, C. Howlett, D. Kirkby, R. H. Lupton, M. Manera, C. Maraston, C. K. McBride, O. Mena, F. Montesano, R. C. Nichol, S. E. Nuza, M. D. Olmstead, N. Padmanabhan, N. Palanque-Delabrouille, J. Parejko, W. J. Percival, P. Petitjean, F. Prada, A. M. Price-Whelan, B. Reid, N. A. Roe, A. J. Ross, N. P. Ross, C. G. Sabiu, S. Saito, L. Samushia, A. G. Sánchez, D. J. Schlegel, D. P. Schneider, C. G. Scoccola, H.-J. Seo, R. A. Skibba, M. A. Strauss, M. E. C. Swanson, D. Thomas, J. L. Tinker, R. Tojeiro, M. V. Magaña, L. Verde, D. A. Wake, B. A. Weaver, D. H. Weinberg, M. White, X. Xu, C. Yèche, I. Zehavi, and G.-B. Zhao, *The clustering of galaxies in the SDSS-III Baryon Oscillation Spectroscopic Survey: baryon acoustic oscillations in the Data Releases 10 and 11 Galaxy samples*, *MNRAS* **441** (June, 2014) 24–62, [`arXiv:1312.4877`].

[185] C. Alcock and B. Paczynski, *An evolution free test for non-zero cosmological constant*, *Nature* **281** (Oct., 1979) 358.

[186] S. D. M. White, J. F. Navarro, A. E. Evrard, and C. S. Frenk, *The baryon content of galaxy clusters: a challenge to cosmological orthodoxy*, *Nature* **366** (Dec., 1993) 429–433.

[187] S. Sasaki, *A New Method to Estimate Cosmological Parameters Using the Baryon Fraction of Clusters of Galaxies*, *PASJ* **48** (Dec., 1996) L119–L122, [`astro-ph/9611033`].

[188] A. B. Mantz, S. W. Allen, R. G. Morris, D. A. Rapetti, D. E. Applegate, P. L. Kelly, A. von der Linden, and R. W. Schmidt, *Cosmology and astrophysics from relaxed galaxy clusters - II. Cosmological constraints*, *MNRAS* **440** (May, 2014) 2077–2098, [`arXiv:1402.6212`].

[189] CFHT Lensing Survey. `http://www.cfhtlens.org/astronomers/content-suitable-astronomers`.

[190] L. Fu, M. Kilbinger, T. Erben, C. Heymans, H. Hildebrandt, H. Hoekstra, T. D. Kitching, Y. Mellier, L. Miller, E. Semboloni, P. Simon, L. Van Waerbeke, J. Coupon, J. Harnois-Déraps, M. J. Hudson, K. Kuijken, B. Rowe, T. Schrabback, S. Vafaei, and M. Velander, *CFHTLenS: cosmological constraints from a combination of cosmic shear two-point and three-point correlations*, *MNRAS* **441** (July, 2014) 2725–2743, [`arXiv:1404.5469`].

[191] I. S. Gradshteyn and I. M. Ryzhik, *Table of integrals, series and products*. New York: Academic Press, 1994.

[192] B. Jain and A. Taylor, *Cross-Correlation Tomography: Measuring Dark Energy Evolution with Weak Lensing*, *Physical Review Letters* **91** (Oct., 2003) 141302, [`astro-ph/0306046`].

[193] J. P. Dietrich and J. Hartlap, *Cosmology with the shear-peak statistics*, *MNRAS* **402** (Feb., 2010) 1049–1058, [`arXiv:0906.3512`].

[194] N. Martinet, J. G. Bartlett, A. Kiessling, and B. Sartoris, *Constraining cosmology with shear peak statistics: tomographic analysis*, *ArXiv e-prints* (June, 2015) [`arXiv:1506.02192`].

[195] Euclid collaboration (ESA). `http://www.euclid-ec.org`.

[196] WFIRST collaboration (NASA). `http://wfirst.gsfc.nasa.gov`.

[197] S. Refsdal, *On the possibility of determining Hubble's parameter and the masses of galaxies from the gravitational lens effect*, *MNRAS* **128** (1964) 307.

[198] S. H. Suyu, T. Treu, S. Hilbert, A. Sonnenfeld, M. W. Auger, R. D. Blandford, T. Collett, F. Courbin, C. D. Fassnacht, L. V. E. Koopmans, P. J. Marshall, G. Meylan, C. Spiniello, and M. Tewes, *Cosmology from Gravitational Lens Time Delays and Planck Data*, *ApJL* **788** (June, 2014) L35, [`arXiv:1306.4732`].

[199] COSMOGRAIL project. `http://cosmograil.epfl.ch`.

[200] S. H. Suyu, M. W. Auger, S. Hilbert, P. J. Marshall, M. Tewes, T. Treu, C. D. Fassnacht, L. V. E. Koopmans, D. Sluse, R. D. Blandford, F. Courbin, and G. Meylan, *Two Accurate Time-delay Distances from Strong Lensing: Implications for Cosmology*, *ApJ* **766** (Apr., 2013) 70, [`arXiv:1208.6010`].

[201] S. Räsänen, K. Bolejko, and A. Finoguenov, *A new test of the FLRW metric using distance sum rule*, *ArXiv e-prints* (Dec., 2014) [`arXiv:1412.4976`].

[202] M. Biesiada, A. Piórkowska, and B. Malec, *Cosmic equation of state from strong gravitational lensing systems*, *MNRAS* **406** (Aug., 2010) 1055–1059, [`arXiv:1105.0946`].

[203] Y. B. Zel'dovich, *Observations in a Universe Homogeneous in the Mean*, *Sov. Astron. Lett.* **8** (Aug., 1964) 13.

[204] J. E. Gunn, *On the Propagation of Light in Inhomogeneous Cosmologies. I. Mean Effects*, *ApJ* **150** (Dec., 1967) 737.

[205] V. M. Dashevskii and Y. B. Zel'dovich, *Propagation of light in a nonhomogeneous nonflat universe ii, Sov. Astronom.* **8** (1965) 854.

[206] V. M. Dashevskii and V. I. Slysh, *On the Propagation of Light in a Nonhomogeneous Universe, Sov. Astronom.* **9** (Feb., 1966) 671.

[207] V. M. Dashevskii and V. I. Slysh, *On the Propagation of Light in a Nonhomogeneous Universe, Astron. Zh.* **42** (1965) 863.

[208] B. Bertotti, *The Luminosity of Distant Galaxies, Royal Society of London Proceedings Series A* **294** (Sept., 1966) 195–207.

[209] J. E. Gunn, *A Fundamental Limitation on the Accuracy of Angular Measurements in Observational Cosmology, ApJ* **147** (Jan., 1967) 61.

[210] R. Kantowski, *Corrections in the Luminosity-Redshift Relations of the Homogeneous Friedmann Models, ApJ* **155** (Jan., 1969) 89.

[211] C. C. Dyer and R. C. Roeder, *Distance-Redshift Relations for Universes with Some Intergalactic Medium, ApJL* **180** (Feb., 1973) L31.

[212] C. C. Dyer, *Observational Aspects of Locally Inhomogeneous Cosmological Models.* PhD thesis, University of Toronto (Canada), 1973.

[213] C. C. Dyer and R. C. Roeder, *Observations in Locally Inhomogeneous Cosmological Models, ApJ* **189** (Apr., 1974) 167–176.

[214] R. C. Roeder, *Apparent magnitudes, redshifts, and inhomogeneities in the universe, ApJ* **196** (Mar., 1975) 671–673.

[215] A. Einstein and E. G. Straus, *The Influence of the Expansion of Space on the Gravitation Fields Surrounding the Individual Stars, Reviews of Modern Physics* **17** (Apr., 1945) 120–124.

[216] A. Einstein and E. G. Straus, *Corrections and Additional Remarks to our Paper: The Influence of the Expansion of Space on the Gravitation Fields Surrounding the Individual Stars, Reviews of Modern Physics* **18** (Jan., 1946) 148–149.

[217] S. Weinberg, *Apparent luminosities in a locally inhomogeneous universe, ApJL* **208** (Aug., 1976) L1–L3.

[218] T. Futamase and M. Sasaki, *Light Propagation and the Distance Redshift Relation in a Realistic Inhomogeneous Universe, Phys. Rev.* **D40** (1989) 2502.

[219] P. Valageas, *Weak gravitational lensing effects on the determination of Ω_0 and Λ from SNeIa, Astron. Astrophys.* **354** (2000) 767, [`astro-ph/9904300`].

[220] A. Cooray, D. Huterer, and D. Holz, *Problems with pencils: lensing covariance of supernova distance measurements, Phys. Rev. Lett.* **96** (2006) 021301, [`astro-ph/0509581`].

[221] S. Dodelson and A. Vallinotto, *Learning from the scatter in type Ia supernovae, Phys. Rev.* **D74** (2006) 063515, [`astro-ph/0511086`].

[222] C. Bonvin, R. Durrer, and M. A. Gasparini, *Fluctuations of the luminosity distance*, *Phys. Rev.* **D73** (2006) 023523, [`astro-ph/0511183`]. [Erratum: Phys. Rev.D85,029901(2012)].

[223] N. Meures and M. Bruni, *Redshift and distances in a Lambda-CDM cosmology with non-linear inhomogeneities*, *Mon. Not. Roy. Astron. Soc.* **419** (2012) 1937, [`arXiv:1107.4433`].

[224] I. Ben-Dayan, M. Gasperini, G. Marozzi, F. Nugier, and G. Veneziano, *Backreaction on the luminosity-redshift relation from gauge invariant light-cone averaging*, *JCAP* **4** (Apr., 2012) 36, [`arXiv:1202.1247`].

[225] G. Fanizza, M. Gasperini, G. Marozzi, and G. Veneziano, *A new approach to the propagation of light-like signals in perturbed cosmological backgrounds*, *JCAP* **8** (Aug., 2015) 20, [`arXiv:1506.02003`].

[226] V. Marra, E. W. Kolb, S. Matarrese, and A. Riotto, *On cosmological observables in a swiss-cheese universe*, *Phys. Rev.* **D76** (2007) 123004, [`arXiv:0708.3622`].

[227] N. Brouzakis, N. Tetradis, and E. Tzavara, *Light Propagation and Large-Scale Inhomogeneities*, *JCAP* **0804** (2008) 008, [`astro-ph/0703586`].

[228] N. Brouzakis, N. Tetradis, and E. Tzavara, *The effect of large scale inhomogeneities on the luminosity distance*, *JCAP* **2** (Feb., 2007) 13, [`astro-ph/0612179`].

[229] T. Biswas and A. Notari, *Swiss-Cheese Inhomogeneous Cosmology and the Dark Energy Problem*, *JCAP* **0806** (2008) 021, [`astro-ph/0702555`].

[230] V. Marra, E. W. Kolb, and S. Matarrese, *Light-cone averages in a Swiss-cheese universe*, *Phys. Rev. D* **77** (Jan., 2008) 023003, [`arXiv:0710.5505`].

[231] T. Clifton and J. Zuntz, *Hubble Diagram Dispersion From Large-Scale Structure*, *Mon. Not. Roy. Astron. Soc.* **400** (2009) 2185, [`arXiv:0902.0726`].

[232] S. J. Szybka, *On light propagation in Swiss-Cheese cosmologies*, *Phys. Rev.* **D84** (2011) 044011, [`arXiv:1012.5239`].

[233] R. A. Vanderveld, E. E. Flanagan, and I. Wasserman, *Luminosity distance in 'Swiss cheese' cosmology with randomized voids: I. Single void size*, *Phys. Rev.* **D78** (2008) 083511, [`arXiv:0808.1080`].

[234] W. Valkenburg, *Swiss Cheese and a Cheesy CMB*, *JCAP* **0906** (2009) 010, [`arXiv:0902.4698`].

[235] K. Bolejko, *The effect of inhomogeneities on the distance to the last scattering surface and the accuracy of the CMB analysis*, *JCAP* **2** (Feb., 2011) 25, [`arXiv:1101.3338`].

[236] E. E. Flanagan, N. Kumar, and I. Wasserman, *Luminosity distance in Swiss cheese cosmology with randomized voids and galaxy halos*, *Phys. Rev.* **D88** (2013), no. 4 043004, [`arXiv:1207.3711`].

[237] Lavinto, M. and Räsänen, S. and Szybka, S. J., *Average expansion rate and light propagation in a cosmological Tardis spacetime*, *JCAP* **12** (Dec., 2013) 51, [arXiv:1308.6731].

[238] M. Lavinto and S. Räsänen, *CMB seen through random Swiss Cheese*, *ArXiv e-prints* (July, 2015) [arXiv:1507.06590].

[239] K. Bolejko, *The Szekeres Swiss Cheese model and the CMB observations*, *General Relativity and Gravitation* **41** (Aug., 2009) 1737–1755, [arXiv:0804.1846].

[240] K. Bolejko and M.-N. Célérier, *Szekeres Swiss-cheese model and supernova observations*, *Phys. Rev. D* **82** (Nov., 2010) 103510, [arXiv:1005.2584].

[241] A. Peel, M. A. Troxel, and M. Ishak, *Effect of inhomogeneities on high precision measurements of cosmological distances*, *Phys. Rev. D* **90** (Dec., 2014) 123536, [arXiv:1408.4390].

[242] M. A. Troxel, M. Ishak, and A. Peel, *The effects of structure anisotropy on lensing observables in an exact general relativistic setting for precision cosmology*, *JCAP* **3** (Mar., 2014) 40, [arXiv:1311.5936].

[243] J. Adamek, E. Di Dio, R. Durrer, and M. Kunz, *Distance-redshift relation in plane symmetric universes*, *Phys. Rev.* **D89** (2014), no. 6 063543, [arXiv:1401.3634].

[244] K. Bolejko and P. G. Ferreira, *Ricci focusing, shearing, and the expansion rate in an almost homogeneous Universe*, *JCAP* **1205** (2012) 003, [arXiv:1204.0909].

[245] E. V. Linder, *Averaging Inhomogeneous Universes: Volume, Angle, Line of Sight*, *ArXiv Astrophysics e-prints* (Jan., 1998) [astro-ph/9801122].

[246] S. Räsänen, *Light propagation in statistically homogeneous and isotropic dust universes*, *JCAP* **0902** (2009) 011, [arXiv:0812.2872].

[247] S. Räsänen, *Light propagation in statistically homogeneous and isotropic universes with general matter content*, *JCAP* **1003** (2010) 018, [arXiv:0912.3370].

[248] S. Räsäsnen, *Light propagation and the average expansion rate in near-FRW universes*, *Phys. Rev.* **D85** (2012) 083528, [arXiv:1107.1176].

[249] M. Gasperini, G. Marozzi, F. Nugier, and G. Veneziano, *Light-cone averaging in cosmology: formalism and applications*, *JCAP* **7** (July, 2011) 8, [arXiv:1104.1167].

[250] S. Bagheri and D. J. Schwarz, *Light propagation in the averaged universe*, *JCAP* **10** (Oct., 2014) 73, [arXiv:1404.2185].

[251] D. E. Holz and R. M. Wald, *A New method for determining cumulative gravitational lensing effects in inhomogeneous universes*, *Phys. Rev.* **D58** (1998) 063501, [astro-ph/9708036].

[252] T. Okamura and T. Futamase, *Distance-Redshift Relation in a Realistic Inhomogeneous Universe*, *Prog. Theor. Phys.* **122** (2009) 511–520, [arXiv:0905.1160].

[253] J.-P. Bruneton and J. Larena, *Observables in a lattice Universe*, *Class. Quant. Grav.* **30** (2013) 025002, [`arXiv:1208.1411`].

[254] T. Clifton and P. G. Ferreira, *Archipelagian Cosmology: Dynamics and Observables in a Universe with Discretized Matter Content*, *Phys. Rev.* **D80** (2009) 103503, [`arXiv:0907.4109`]. [Erratum: Phys. Rev.D84,109902(2011)].

[255] T. Clifton and P. G. Ferreira, *Errors in estimating $\Omega_?$ due to the fluid approximation*, *JCAP* **10** (Oct., 2009) 26, [`arXiv:0908.4488`].

[256] T. Clifton, P. G. Ferreira, and K. O'Donnell, *Improved treatment of optics in the Lindquist-Wheeler models*, *Phys. Rev. D* **85** (Jan., 2012) 023502, [`arXiv:1110.3191`].

[257] C. Clarkson, G. F. R. Ellis, A. Faltenbacher, R. Maartens, O. Umeh, and J.-P. Uzan, *(Mis-)Interpreting supernovae observations in a lumpy universe*, *Mon. Not. Roy. Astron. Soc.* **426** (2012) 1121–1136, [`arXiv:1109.2484`].

[258] G. Darmois, *Les équations de la gravitation einsteinienne*. Mémorial des sciences mathématiques, 1927.

[259] W. Israel, *Singular hypersurfaces and thin shells in general relativity*, *Nuovo Cimento B Serie* **44** (July, 1966) 1–14.

[260] W. Israel, *Singular hypersurfaces and thin shells in general relativity*, *Nuovo Cimento B Serie* **48** (Apr., 1967) 463–463.

[261] G. Lemaître, *L'Univers en expansion*, *Annales de la Société Scientifique de Bruxelles* **53** (1933) 51.

[262] J. Eisenstaedt, *Lemaître and the Schwarzschild Solution*, p. 353. 1993.

[263] V. Marra, M. Quartin, and L. Amendola, *Accurate weak lensing of standard candles. I. Flexible cosmological fits*, *Phys. Rev. D* **88** (Sept., 2013) 063004, [`arXiv:1304.7689`].

[264] M. Quartin, V. Marra, and L. Amendola, *Accurate weak lensing of standard candles. II. Measuring σ_8 with supernovae*, *Phys. Rev. D* **89** (Jan., 2014) 023009, [`arXiv:1307.1155`].

[265] L. Amendola, T. Castro, V. Marra, and M. Quartin, *Constraining the growth of perturbations with lensing of supernovae*, *MNRAS* **449** (May, 2015) 2845–2852, [`arXiv:1412.3703`].

[266] K. Kainulainen and V. Marra, *A new stochastic approach to cumulative weak lensing*, *Phys. Rev.* **D80** (2009) 123020, [`arXiv:0909.0822`].

[267] K. Kainulainen and V. Marra, *Accurate Modeling of Weak Lensing with the sGL Method*, *Phys. Rev.* **D83** (2011) 023009, [`arXiv:1011.0732`].

[268] K. Kainulainen and V. Marra, *Weak lensing observables in the halo model*, *Phys. Rev. D* **84** (Sept., 2011) 063004, [`arXiv:1101.4143`].

[269] L. Bianchi, *Sugli spazii a tre dimensioni che ammettono un gruppo continuo di movimenti (on the spaces of three dimensions that admit a continuous group of movements)*, Soc. Ital. Sci. Mem. Mat. **11** (1898) 267.

[270] G. F. R. Ellis and M. A. H. MacCallum, *A class of homogeneous cosmological models*, Communications in Mathematical Physics **12** (June, 1969) 108–141.

[271] A. Pontzen and A. Challinor, *Linearization of homogeneous, nearly-isotropic cosmological models*, Classical and Quantum Gravity **28** (Sept., 2011) 185007, [arXiv:1009.3935].

[272] A. Pontzen and A. Challinor, *Bianchi model CMB polarization and its implications for CMB anomalies*, MNRAS **380** (Oct., 2007) 1387–1398, [arXiv:0706.2075].

[273] T. Koivisto and D. F. Mota, *Anisotropic dark energy: dynamics of the background and perturbations*, JCAP **6** (June, 2008) 18, [arXiv:0801.3676].

[274] G. Marozzi and J.-P. Uzan, *Late time anisotropy as an imprint of cosmological backreaction*, Phys. Rev. D **86** (Sept., 2012) 063528, [arXiv:1206.4887].

[275] T. Damour, I. I. Kogan, and A. Papazoglou, *Nonlinear bigravity and cosmic acceleration*, Phys. Rev. D **66** (Nov., 2002) 104025, [hep-th/0206044].

[276] U. Feindt, M. Kerschhaggl, M. Kowalski, G. Aldering, P. Antilogus, C. Aragon, S. Bailey, C. Baltay, S. Bongard, C. Buton, A. Canto, F. Cellier-Holzem, M. Childress, N. Chotard, Y. Copin, H. K. Fakhouri, E. Gangler, J. Guy, A. Kim, P. Nugent, J. Nordin, K. Paech, R. Pain, E. Pecontal, R. Pereira, S. Perlmutter, D. Rabinowitz, M. Rigault, K. Runge, C. Saunders, R. Scalzo, G. Smadja, C. Tao, R. C. Thomas, B. A. Weaver, and C. Wu, *Measuring cosmic bulk flows with Type Ia supernovae from the Nearby Supernova Factory*, A&A **560** (Dec., 2013) A90, [arXiv:1310.4184].

[277] S. Appleby and A. Shafieloo, *Testing local anisotropy using the method of smoothed residuals I — methodology*, JCAP **3** (Mar., 2014) 7, [arXiv:1312.3415].

[278] S. Appleby, A. Shafieloo, and A. Johnson, *Probing Bulk Flow with Nearby SNe Ia Data*, ApJ **801** (Mar., 2015) 76, [arXiv:1410.5562].

[279] T. S. Kolatt and O. Lahav, *Constraints on cosmological anisotropy out to z = 1 from Type Ia supernovae*, MNRAS **323** (May, 2001) 859–864, [astro-ph/0008041].

[280] D. J. Schwarz and B. Weinhorst, *(An)isotropy of the Hubble diagram: comparing hemispheres*, A&A **474** (Nov., 2007) 717–729, [arXiv:0706.0165].

[281] M. Blomqvist, J. Enander, and E. Mörtsell, *Constraining dark energy fluctuations with supernova correlations*, JCAP **10** (Oct., 2010) 18, [arXiv:1006.4638].

[282] I. Antoniou and L. Perivolaropoulos, *Searching for a cosmological preferred axis: Union2 data analysis and comparison with other probes*, JCAP **12** (Dec., 2010) 12, [arXiv:1007.4347].

[283] J. Colin, R. Mohayaee, S. Sarkar, and A. Shafieloo, *Probing the anisotropic local Universe and beyond with SNe Ia data*, MNRAS **414** (June, 2011) 264–271, [arXiv:1011.6292].

[284] B. Kalus, D. J. Schwarz, M. Seikel, and A. Wiegand, *Constraints on anisotropic cosmic expansion from supernovae*, *A&A* **553** (May, 2013) A56, [`arXiv:1212.3691`].

[285] R.-G. Cai, Y.-Z. Ma, B. Tang, and Z.-L. Tuo, *Constraining the anisotropic expansion of the Universe*, *Phys. Rev. D* **87** (June, 2013) 123522, [`arXiv:1303.0961`].

[286] T. Schücker, A. Tilquin, and G. Valent, *Bianchi I meets the Hubble diagram*, *MNRAS* **444** (Nov., 2014) 2820–2836, [`arXiv:1405.6523`].

[287] B. Javanmardi, C. Porciani, P. Kroupa, and J. Pflamm-Altenburg, *Probing the Isotropy of Cosmic Acceleration Traced By Type Ia Supernovae*, *ApJ* **810** (Sept., 2015) 47, [`arXiv:1507.07560`].

[288] J. Beltrán Jiménez, V. Salzano, and R. Lazkoz, *Anisotropic expansion and SNIa: an open issue*, *Phys. Lett.* **B741** (2015) 168–177, [`arXiv:1402.1760`].

[289] C. Pitrou, J.-P. Uzan, and T. S. Pereira, *Weak lensing B modes on all scales as a probe of local isotropy*, *Phys. Rev. D* **87** (Feb., 2013) 043003, [`arXiv:1203.6029`].

[290] C. Pitrou, T. S. Pereira, and J.-P. Uzan, *Weak lensing by the large scale structure in a spatially anisotropic universe: Theory and predictions*, *Phys. Rev. D* **92** (July, 2015) 023501, [`arXiv:1503.01125`].

[291] M. A. H. MacCallum and G. F. R. Ellis, *A class of homogeneous cosmological models: II. Observations*, *Communications in Mathematical Physics* **19** (Mar., 1970) 31–64.

[292] P. T. Saunders, *Observations in homogeneous model universes*, *Month. Not. R. Astron. Soc.* **141** (1968) 427.

[293] P. T. Saunders, *Observations in some simple cosmological models with shear*, *Month. Not. R. Astron. Soc.* **142** (1969) 213.

[294] H. K. Eriksen, F. K. Hansen, A. J. Banday, K. M. Górski, and P. B. Lilje, *Asymmetries in the Cosmic Microwave Background Anisotropy Field*, *ApJ* **605** (Apr., 2004) 14–20, [`astro-ph/0307507`].

[295] K. Land and J. Magueijo, *Examination of Evidence for a Preferred Axis in the Cosmic Radiation Anisotropy*, *Physical Review Letters* **95** (Aug., 2005) 071301, [`astro-ph/0502237`].

[296] G. Hinshaw, M. R. Nolta, C. L. Bennett, R. Bean, O. Doré, M. R. Greason, M. Halpern, R. S. Hill, N. Jarosik, A. Kogut, E. Komatsu, M. Limon, N. Odegard, S. S. Meyer, L. Page, H. V. Peiris, D. N. Spergel, G. S. Tucker, L. Verde, J. L. Weiland, E. Wollack, and E. L. Wright, *Three-Year Wilkinson Microwave Anisotropy Probe (WMAP) Observations: Temperature Analysis*, *ApJS* **170** (June, 2007) 288–334, [`astro-ph/0603451`].

[297] Planck Collaboration, P. A. R. Ade, N. Aghanim, C. Armitage-Caplan, M. Arnaud, M. Ashdown, F. Atrio-Barandela, J. Aumont, C. Baccigalupi, A. J. Banday, and et al., *Planck 2013 results. XXIII. Isotropy and statistics of the CMB*, *A&A* **571** (Nov., 2014) A23, [`arXiv:1303.5083`].

[298] Planck Collaboration, P. A. R. Ade, N. Aghanim, Y. Akrami, P. K. Aluri, M. Arnaud, M. Ashdown, J. Aumont, C. Baccigalupi, A. J. Banday, and et al., *Planck 2015 results. XVI. Isotropy and statistics of the CMB*, *ArXiv e-prints* (June, 2015) [`arXiv:1506.07135`].

[299] C. Pitrou, T. S. Pereira, and J.-P. Uzan, *Predictions from an anisotropic inflationary era*, *JCAP* **4** (Apr., 2008) 4, [`arXiv:0801.3596`].

[300] M.-a. Watanabe, S. Kanno, and J. Soda, *Inflationary Universe with Anisotropic Hair*, *Phys.Rev.Lett.* **102** (2009) 191302, [`arXiv:0902.2833`].

[301] C. Caprini and L. Sorbo, *Adding helicity to inflationary magnetogenesis*, *JCAP* **10** (Oct., 2014) 56, [`arXiv:1407.2809`].

[302] PhD Tree. `http://phdtree.org/scholar/uzan-jean-philippe/`.

[303] T. Masson, "Géométrie differentielle, groupes et algèbres de lie, fibrés et connexions." Unpublished notes on differential geometry (in French), downloadable at `http://science.thilucmic.fr/spip.php?article12`, Mar., 2010.

[304] R. Aldrovandi and J. G. Pereira, *Teleparallel Gravity*. 2013.

Propagation de la lumière dans des univers inhomogènes ou anisotropes

Le modèle standard de la cosmologie est fondé sur les hypothèses d'homogénéité et d'isotropie de l'Univers. Lors de l'interprétation de la plupart des observations, ces deux hypothèses sont appliquées de façon stricte, au sens où l'on suppose que la lumière émise par des sources lointaines se propage jusqu'à nous à travers un espace-temps de Friedmann-Lemaître. L'objectif principal de cette thèse a été d'évaluer la pertinence de ces hypothèses, en particulier lorsque de très petites échelles sont mises en jeu. Après une revue détaillée des lois de l'optique géométrique en espace-temps courbe, on propose une analyse exhaustive de la propagation de la lumière à travers des modèles cosmologiques "en gruyère", conçus pour modéliser le caractère grumeleux de l'Univers à petite échelle. L'impact sur l'interprétation du diagramme de Hubble est ensuite évalué quantitativement, et s'avère être plutôt faible, en particulier grâce à la constante cosmologique. Lorsqu'appliquées aux données actuelles issues de l'observation de supernovae, les corrections associées tendent toutefois à améliorer l'accord entre les paramètre cosmologiques mesurés à partir du diagramme de Hubble d'une part, et à partir du fond diffus cosmologique d'autre part. Ceci suggère que la précision des observations cosmologiques atteinte aujourd'hui ne permet plus de négliger l'effet des petites structures sur la propagation de lumière à travers le cosmos. Un tel constat a motivé le développement d'un nouveau cadre théorique, inspiré de la physique statistique, visant à décrire ces effets avec précision. Quant à l'hypothèse d'isotropie, cette thèse aborde d'une part les conséquences potentielles d'une anisotropie à grande échelle de l'univers sur la propagation de la lumière, en résolvant de façon explicite toutes les équation de l'optique géométrique dans l'espace-temps de Bianchi I. D'autre part, on y analyse une classe de sources d'anisotropie, à savoir les modèles scalaire-vecteur pour l'inflation ou l'énergie sombre. La plupart d'entre eux ne sont pas physiquement viables.

Mots clés : cosmologie, lumière, inhomogénéité, modèles "Swiss cheese", anisotropie, Bianchi I.

Light propagation in inhomogeneous and anisotropic cosmologies

The standard model of cosmology is based on the hypothesis that the Universe is spatially homogeneous and isotropic. When interpreting most observations, this cosmological principle is applied stricto sensu: the light emitted by distant sources is assumed to propagate through a Friedmann-Lemaître spacetime. The main goal of the present thesis was to evaluate how reliable this assumption is, especially when small scales are at stake. After having reviewed the laws of geometric optics in curved spacetime, and the standard interpretation of cosmological observables, the dissertation reports a comprehensive analysis of light propagation in Swiss-cheese models, designed to capture the clumpy character of the Universe. The resulting impact on the interpretation of the Hubble diagram is quantified, and shown to be relatively small, thanks to the cosmological constant. When applied to current supernova data, the associated corrections tend however to improve the agreement between the cosmological parameters inferred from the Hubble diagram and from the cosmic microwave background. This is a hint that the effect of small-scale structures on light propagation may become non-negligible in the era of precision cosmology. This motivated the development of a new theoretical framework, based on stochastic processes, which aims at describing small-scale gravitational lensing with a better accuracy. Regarding the isotropy side of the cosmological principle, this dissertation addresses, on the one hand, the potential effect of a large-scale anisotropy on light propagation, by solving all the equations of geometric optics in the Bianchi I spacetime. On the other hand, possible sources of such an anisotropy, namely scalar-vector models for inflation or dark energy, are analysed. Most of them turn out to be excluded as physically viable theories.

Keywords: cosmology, light, inhomogeneity, Swiss-cheese models, anisotropy, Bianchi I.